Geochemical and physical properties and evolution of the lithospheric mantle beneath the Nógrád-Gömör Volcanic Field (Northern Pannonian Basin, Central Europe)

by

Nóra Liptai

Australian Research Council Centre of Excellence for Core to Crust Fluid Systems (CCFS)
& National Key Centre Geochemical Evolution and Metallogeny of Continents (GEMOC)
Department of Earth and Planetary Sciences
Faculty of Science and Engineering
Macquarie University
Sydney, Australia

Lithosphere Fluid Research Laboratory
Department of Petrology and Geochemistry
Institute of Geography and Earth Sciences
Eötvös Loránd University (ELTE)
Budapest, Hungary

A thesis submitted for the degree of Doctor of Philosophy

Macquarie University

June 2018

Table of Contents

Abstract vii

Magyar nyelvű összefoglaló ix

Declaration xi

Acknowledgements xiii

List of Figures xv

List of Tables xvii

Chapter 1. Introduction and Aims 1

Chapter 2. Geological Background 5

2.1. Structural framework and tectonic history of the Carpathian-Pannonian region 5

2.2. Neogene magmatism throughout the Carpathian-Pannonian region 9

2.3. Review of the physico-chemical properties of the upper mantle from Carpathian-Pannonian region xenoliths 11

2.4. Previous studies on the xenoliths of the Nógrád-Gömör Volcanic Field 16

Chapter 3. Structure of the Nógrád-Gömör Volcanic Field and Sample Locality Details 19

Chapter 4. Applied Techniques 22

4.1. Polarised Light Microscope 22

4.2. Electron Microprobe 22

4.3. Laser-Ablation Inductively Coupled Plasma Mass Spectrometry 22

4.4. Raman Spectroscopy 24

4.5. Focused Ion Beam - Scanning Electron Microscopy 24

4.6. Electron Backscattered Diffraction 26

4.7. Fourier-Transform Infrared Spectroscopy 29

Chapter 5. Results 31
5.1. Petrography 31
5.1.1. Texture classification 31
5.1.2. Modal compositions 34
5.2. Geochemistry of Minerals and Whole-Rocks 42
5.2.1. Mineral major-element geochemistry 42
5.2.2. Trace-element geochemistry of pyroxenes and amphibole 45
5.2.3. Whole-rock geochemistry 59
5.3. Geothermometry 61
5.4. Silicate Melt Inclusions 66
5.4.1. Petrography 66
5.4.2. Geochemistry 69
5.4.2.1. Major elements 69
5.4.2.2. Trace elements 75
5.5. Crystal Preferred Orientation 77
5.5.1. Crystal preferred orientation of the rock-forming minerals 77
5.2.2. Seismic properties 83
5.6. 'Water' Content of Nominally Anhydrous Minerals 84
5.6.1. Incorporation of 'water' in nominally anhydrous minerals 84
5.6.2. 'Water' (H_2O) content in olivine and pyroxenes in the Nógrád-Gömör xenoliths 86
Chapter 6. Discussion 90
6.1. Implications of Equilibration Temperatures 90
6.1.1. Thermal history 90
6.1.2. Estimations on the depth of origin 92
6.2. Reconstruction of Geochemical Processes 94
6.2.1. Partial melting 94
6.2.2. Imprints of metasomatic events 100
6.2.2.1. Presence and absence of amphibole 100
6.2.2.2. Implications of trace element concentrations 104
6.2.2.3. Formation of Group II xenoliths 107
6.2.2.4. Characterisation of the metasomatic agent based on silicate melt-inclusions 109

6.2.3. Geochemical evolution and tectonic context 115
6.3. Deformation History and Seismic Anisotropy in the Upper Mantle of the Nógrád-Gömör Volcanic Field 118
6.3.1. Deformation mechanisms 118
6.3.2. Interpretation of microstructures and textural evolution 122
6.3.3. Seismic properties and thickness of the anisotropic layer 129
6.3.4. Links to the tectonic evolution of the Carpathian-Pannonian region 134
6.4. Post-entrainment Processes in the Nógrád-Gömör Xenoliths 138
6.4.1. Dehydration and constraints on the original 'water' contents 138
6.4.2. Evolution of the silicate melt-inclusions 145
Chapter 7. Conclusions 148
7.1. Summary of the Presented Work 148
7.2. Synthesis and Tectonic Implications 149
References 152
Appendices A1
Appendix A: Sample Images and Description A1
Appendix B: Mineral Major- and Trace-element Analyses A29
Appendix B1 - Mineral Major-element Compositions A31
Appendix B2 - Trace-Element Compositions of Pyroxenes and Amphibole A74
Appendix B3 - Multielement Patterns of Individual Samples A110
Appendix B4 - Calculated Orthopyroxene Rare-Earth Element Contents A125
Appendix C: Crystal Preferred Orientation - Pole Figures A127
Appendix D: Publication: Liptai et al., 2017. A135

Abstract

The Nógrád-Gömör Volcanic Field (NGVF), in the northern Pannonian Basin in Central Europe, is one of five key localities where the lithospheric mantle of the Carpathian-Pannonian region can be studied using peridotite xenoliths hosted in late Miocene to Pleistocene alkali basalts. This work uses geochemical data for minerals, whole-rocks and silicate melt-inclusions, along with crystal preferred orientations and 'water' contents in nominally anhydrous mantle minerals, to interpret the geochemical and physical evolution of this mantle domain and its role in the tectonic history of the region.

Geochemical analyses revealed imprints of multiple metasomatic events, identified by Mg-numbers of olivine and REE concentration of pyroxenes, that affected a heterogeneously depleted lithospheric mantle. These events include (1) formation of Nb-poor amphibole by reaction with subduction-related volatile-bearing silicate melts/fluids, (2) metasomatism by a mafic melt of intraplate origin, resulting in enrichment of U-Th-(Nb-Ta)-LREE in clinopyroxene and formation of Nb-rich amphibole, and (3) the youngest melt-rock reaction, causing enrichment in Fe, Mn, Ti and LREE and overprinting older geochemical signatures. This latest melt was trapped as inclusions, and is similar in composition and origin (OIB-type basalt from low-degree partial melting of a garnet lherzolite) to the earlier metasomatizing melt and the host basalt.

The xenoliths display varying physical properties depending on their depth of origin: shallower (lower-temperature) layers have fine-grained textures and more dispersed crystal preferred orientation, whereas deeper layers are coarse-grained and have stronger fabrics. The latest observable deformation of the lithospheric mantle of the NGVF occurred in a dominantly transpressional regime, following the Miocene extension of the Pannonian Basin. This regime was linked to the convergence of the Adria microplate and the European platform, and produced recent mantle structures in sublithospheric layers, inferred from the observed high seismic anisotropy. Deformation effects are overprinted by annealing in all xenoliths, resulting in decreasing intragranular deformation from north to south within the NGVF. Although there is no direct correlation between fabric properties and geochemistry, annealing is most probably linked to the presence of metasomatizing melts in the upper mantle prior to entrainment of the xenoliths in the host basalt. The latest metasomatic event is detectable in higher equilibration temperatures and Fe-enrichment of xenoliths in the central part, suggesting that the heating effect of this melt was still active

during the time of sampling by the host magma.

The host basalt appears to have influenced the amount of incorporated ‘water’ in the NGVF xenoliths as they are extremely dry compared with other xenoliths from the Carpathian-Pannonian region. Lack of correlation with geochemistry or physical properties, as well as the unusually wide range of $H_2O^{cpx/opx}$, indicates loss of ‘water’ during or after ascent. The highest ‘water’ content of xenoliths is found in the only locality with pyroclastic, rather than effusive eruption, consistent with post-eruption dehydration. A small part of the xenoliths, which may have retained their original ‘water’ content, indicate a depth-related concentration distribution.

Magyar nyelvű összefoglaló

A Pannon-medence északi részén elhelyezkedő nógrád-gömöri vulkáni terület (NGVT) egyike az öt Kárpát-Pannon régióbeli lelőhelynek, ahol késő miocén – pleisztocén korú alkáli bazaltok felsőköpeny eredetű xenolitokat tartalmaznak. Dolgozatomban a terület felsőköpenyének geokémiai és fizikai fejlődéstörténetét vizsgálom a régió tektonikai folyamatainak tükrében, amelyhez a xenolitokon elvégzett komplex vizsgálatok eredményei (kőzetalkotó ásványok, teljes kőzet és szilikátolvadék-zárványok geokémiája, kristálytani orientáció, illetve a névlegesen vízmentes ásványok „víztartalma") szolgáltattak alapot.

A geokémiai elemzések alapján elmondható, hogy több különböző metaszomatikus esemény érintette a változatos mértékben kimerült köpenyrégiót. Ezek az események sorrendben a következők: (1) Nb-szegény amfibolok létrejötte egy szubdukciós eredetű, illótartalmú szilikátolvadékkal vagy fluidummal történő reakció hatására, (2) U-Th-(Nb-Ta)-könnyű RFF-gazdagodás klinopiroxénben, illetve Nb-gazdagodás amfibolban egy lemezen belüli eredetű, mafikus olvadékkal történt kölcsönhatás során, valamint (3) egy fiatal, a xenolitok csapdázódását közvetlenül megelőző metaszomatózis, amely korábbi geokémiai bélyegeket felülírva Fe-Mn-Ti- és könnyű RFF-gazdagodáshoz vezetett a kőzetalkotó ásványokban. A legutóbbi folyamathoz köthető olvadék csapdázódott a szilikátolvadék-zárványokban, és a vizsgálatok alapján mind összetételében, mind eredetét tekintve (óceáni szigetív-típusú bazalt, amely gránát lherzolit kismértékű parciális olvadásával keletkezett) a bennfoglaló bazalthoz hasonló.

A xenolitok ezen kívül származási mélységüktől függően különböző fizikai tulajdonságokkal rendelkeznek: a nagyobb mélységből származó (nagyobb egyensúlyi hőmérsékleteket mutató) minták durvább szemcsések, valamint erősebb kristálytani orientációt mutatnak, mint a kisebb egyensúlyi hőmérsékletekkel rendelkező, azaz kisebb mélységből származó xenolitok. A legutolsó deformációs esemény, amelynek nyoma a xenolitok szövetében megfigyelhető, a Pannon-medence miocén extenzióját követő transzpressziós rezsimhez köthető. Ez a tektonikai környezet az adriai mikrolemez és az európai platform konvergenciájára vezethető vissza, amely az erős szeizmikus anizotrópia alapján az asztenoszferikus köpeny felső részének struktúrájára is hatással van. A xenolitok deformációs bélyegeit egy statikus átkristályosodási folyamat részben felülírta, amely nagy valószínűséggel a felszínre szállítódás előtt a köpenyben jelenlévő

metaszomatizáló olvadékokhoz köthető. A csak a központi területet érintő legutolsó metaszomatózis a nagyobb egyensúlyi hőmérsékletekben érhető tetten, amely arra utal, hogy a kölcsönható olvadék még aktív volt a felsőköpenyben a bennfoglaló bazalt általi megmintázás idején.

A xenolitokat felszínre hozó bazalt a névlegesen vízmentes kőzetalkotó ásványok „víztartalmára" is hatással volt: a vizsgált minták szélsőségesen szárazak a Kárpát-Pannon régió más lelőhelyeihez képest. A „víztartalmak" nem mutatnak kapcsolatot sem geokémiai, sem fizikai tulajdonságokkal, azonban a klinopiroxén és ortopiroxén „víztartalmának" aránya igen változatos, amely a felszínre szállítódás során elszenvedett vízvesztésre utal. A piroklasztitokban található xenolitokra nagyobb „víztartalmak" jellemzők, mint a lávakőzetben találhatókra, amely szintén a kitörés utáni dehidratációt támasztja alá. A minták egy kis részében összefüggés mutatkozik a származási mélység és a „víztartalom" között, így ezek a xenolitok minden bizonnyal megbízhatóbban képviselik a köpeny eredeti „víztartalmát".

Declaration

This thesis is based on work carried out in the ARC Centre of Excellence for Core to Crust Fluid Systems and GEMOC National Key Centre, Department of Earth and Planetary Sciences at Macquarie University, Australia and in the Lithosphere Fluid Research Lab, Eötvös University (ELTE) in Budapest, Hungary, over the period of September 2013 to January 2018. I hereby declare that all the data and interpretations presented in this thesis are from my own work, except for information cited from published or unpublished sources, which have been acknowledged accordingly.

No part of this thesis has ever been submitted for any other degree in any university or education institute. This thesis is submitted to both Macquarie University, Australia and Eötvös Loránd University (ELTE), Hungary, under the conditions of the cotutelle agreement between these two universities for this PhD program.

Nóra Liptai
19 January 2018

Acknowledgements

First and foremost, I owe thanks to my supervisors, who had an enormous role in the preparation of this work: Csaba Szabó (Eötvös University), whose guidance and help I could always count on even at the strangest hours of the day; Sue O'Reilly and Bill Griffin (Macquarie University), who were always willing to give critical advice and polish my presenting skills, both written and oral; and to Norm Pearson, whom I unfortunately could not be in contact with as frequently as I wished, but who provided valuable help during the first difficult period of getting acquainted with the analytical methods at Macquarie University. I am grateful to all of you for the opportunity of the cotutelle PhD experience, which will definitely be one of the most important experiences in my life.

I would like to say thank you to present and former members of the Lithosphere Fluid Research Lab, Eötvös University, who in any way contributed to the compilation of this study. I received a lot of help in data interpretation from Levente Patkó, László Aradi, Márta Berkesi, Károly Hidas, István Kovács, Rita Klébesz and Zsanett Pintér. These discussions provided a lot of ideas which helped to make my thesis more complete. Furthermore, I owe thanks for assistance in analytical and field work from Ábel Szabó, Zoltán Dankházi (FIB-SEM), Réka Káldos (Raman), and Zoltán Kovács.

I received further help in facilitating or carrying out analytical work: from Dave Adams (EMPA), Will Powell (LA-ICP-MS) and Takako Satsukawa (EBSD) at Macquarie University; Anna Maria Fioretti, Raul Carampin, Orlando Vaselli and Bernardo Cesare (EMPA) at Padua, Italy; †Teresa Jeffries (LA-ICP-MS) at the Natural History Museum, London, UK; Fabrice Barou and Andréa Tommasi (EBSD) at the University of Montpellier II, France; Zoltán Zajacz (LA-ICP-MS) at ETH Zürich, Switzerland; and Judith Mihály and Csaba Németh (FTIR) at the Hungarian Academy of Science.

My PhD project was financially supported by PhD scholarships from Eötvös University and Macquarie University (iMQRES), the ARC Centre of Excellence for Core to Crust Fluid Systems (CCFS), a Marie Curie International Reintegration Grant (NAMS-230937) and a postdoctoral grant (PD101683) from the Hungarian Scientific Research Fund through István Kovács, a grant (78425) from the Hungarian Scientific Research Fund through Csaba Szabó, as well as a Synthesys Project (GB-TAF-3033) through Levente Patkó, and a Postgraduate Research Fund award from Macquarie University.

I would like to express my gratitude to the people in CCFS, whom I shared workspace with, and who made the hardest part of thesis writing more bearable and actually sometimes fun: Hadrien, Sally, Montgarri, Jinxiang, Toosin, Romain, and the rest of the ‘BD-family’.

Finally, a special thanks to everyone who kept my spirit up by constantly telling me I could do it (you were right in the end): Máté, Anthony, Hadrien, Zsani, Inès, Yoann, Levi, and last but not least, my family, who stood with me and supported me in everything from the beginning.

List of Figures

Chapter 2

Fig. 2.1. Present-day location of major tectonic units in the Carpathian-Pannonian region 6
Fig. 2.2. Schematic illustration of the tectonic evolution of the Carpathian-Pannonian region 7
Fig. 2.3. Lithospheric thickness in the Pannonian Basin and the spatial distribution of calc-alkaline volcanic rocks and xenolith-bearing late Miocene – Pleistocene alkali basalt occurrences 9
Fig. 2.4. Modal compositions and rock types of mantle xenoliths from the different localities in the Carpathian-Pannonian region 12

Chapter 3

Fig. 3.1. Spatial distribution of calc-alkaline and alkali basaltic outcrops in the Nógrád-Gömör Volcanic Field 20
Fig. 3.2. Scanned thin-section images of a typical four-phase lherzolite and a wehrlite 21

Chapter 4

Fig. 4.1. Backscattered electron image of the sample volume containing SMI3, prepared for slicing with FIB after the deposition of the Pt-layer and digging of the surrounding trenches 26

Chapter 5

Fig. 5.1. Photomicrographs of characteristic textural types among the studied Nógrád-Gömör xenoliths 33
Fig. 5.2. Comparison of modal compositions of the studied xenoliths acquired with point counting method vs. EBSD mapping 35
Fig. 5.3. Modal compositions of the xenoliths from different regions of the Nógrád-Gömör Volcanic Field 37
Fig. 5.4. Photomicrographs of characteristic microstructures in olivine 38
Fig. 5.5. Characteristic microstructures in pyroxenes 40
Fig. 5.6. Characteristic appearance of spinel, amphibole and melt pockets 41
Fig. 5.7. Major-element compositions of minerals in the NGVF xenoliths 44
Fig. 5.8. Primitive mantle-normalised multi-element diagrams for clino- and orthopyroxene 51
Fig. 5.9. Primitive mantle-normalised REE+Y patterns of clino- and orthopyroxene 52
Fig. 5.10. Multi-element and REE-Y diagrams for amphiboles in the studied xenoliths 53
Fig. 5.11. Whole-rock MgO compositions of the studied NGVF xenoliths compared to Al_2O_3, TiO_2, CaO, and Na_2O 60
Fig. 5.12. Analysed *vs* calculated light and heavy REE contents of orthopyroxene. 60
Fig. 5.13. Correlation of equilibration temperatures obtained by the application of two major-element based geothermometer 64
Fig. 5.14. Inversion diagram for calculation of equilibration T using the thermometer of Liang et al. (2013) 65
Fig. 5.15. Comparison of equilibration temperatures calculated with the REE thermometer (Liang et al., 2013) and major element-based thermometers 66
Fig. 5.16. Scanned thin section image of NFL1327 orthopyroxene-bearing wehrlite, and photomicrograph of primary silicate melt inclusions hosted in clinopyroxene 67
Fig. 5.17. Polarised-light microscope images and results of Raman spectroscopy mapping of three analysed SMIs. 67
Fig. 5.18. Characteristic Raman spectra of sulphates, apatite and CO_2 bubble 68
Fig. 5.19. BSE images of different slices of the analysed SMIs during the milling process with indications of the slice position on photomicrographs 70
Fig. 5.20. Representative SEM spectra of daughter phases with the highest modal proportion 75
Fig. 5.21. Primitive mantle-normalised multi-element and REE+Y diagrams of bulk SMIs 77

Fig. 5.22. Crystal preferred orientations of olivine and pyroxenes in representative xenoliths from the different parts of the volcanic field and different texture groups 80
Fig. 5.23. J-indices *vs* M-indices of olivine in the studied xenoliths 82
Fig. 5.24. Calculated bulk seismic properties for the Nógrád-Gömör Volcanic Field (NGVF) and the three sub-areas 83
Fig. 5.25. Average unpolarised FTIR spectra of olivine, orthopyroxene and clinopyroxene 87
Fig. 5.26. Distribution of the amount of incorporated H_2O in ortho- and clinopyroxenes 88

Chapter 6

Fig. 6.1. Estimation of depth of origin for the studied xenoliths from the three domains of the Nógrád-Gömör Volcanic Field 93
Fig. 6.2. Fractional melting model for xenoliths of Group IA, IB, IIA, IIB 96
Fig. 6.3. Fractional melting model of the studied xenoliths with the application of MgO vs FeO, Al_2O_3 and SiO_2 97
Fig. 6.4. Melting model based on MgO vs Al_2O_3 in orthopyroxene and clinopyroxene 99
Fig. 6.5. Melting curve based on Al_2O_3 in orthopyroxene vs spinel 100
Fig. 6.6. Nb vs Zr and Ti/Nb vs Zr/Nb for amphiboles in the studied xenoliths 102
Fig. 6.7. Whole-rock MgO vs Ce, Sm and Yb for the Nógrád-Gömör xenoliths 105
Fig. 6.8. $(La/Yb)_N$ vs Ti/Eu in clinopyroxenes of Group IB and IIB xenoliths 106
Fig. 6.9. MgO *vs* FeO contents of daughter clinopyroxene and amphibole in SMIs 110
Fig. 6.10. Composition of bulk SMIs and glasses, on the total alkali *vs* SiO_2 (TAS) diagram 111
Fig. 6.11. Multi-element and REE+Y diagrams of the bulk SMI compositions compared to the metasomatic amphiboles of Group IB and IIB xenoliths, and to the average host basalt 113
Fig. 6.12. Petrogenetic modelling of the origin of the melt trapped in the SMIs 114
Fig. 6.13. Schematic illustration depicting the reconstruction of metasomatic events in the upper mantle of the Nógrád-Gömör Volcanic Field 116
Fig. 6.14. Schematic illustration of the mechanism of slip systems with examples of the two most common slip systems in olivine 119
Fig. 6.15. Deformed texture with high degree of intragranular deformation and annealed texture with straight grain boundaries, triple junctions and low number of subgrain boundaries 120
Fig. 6.16. Plots of olivine BA-indices vs olivine J-indices and equilibration temperatures 123
Fig. 6.17. Plots of olivine J-indices vs mean grain size and equilibration temperatures 124
Fig. 6.18. Examples of heterogeneous olivine grain growth in pyroxene-rich and pyroxene-poor parts of annealed xenoliths 125
Fig. 6.19. Plot of grain orientation spread (GOS) vs equilibration temperatures 127
Fig. 6.20. Examples of Nb-rich amphibole grains displaying matching orientation with neighbouring clinopyroxene 128
Fig. 6.21. Illustration of the five different endmember orientations for the foliation and lineation and location of seismological stations in the vicinity of the Nógrád-Gömör Volcanic Field 131
Fig. 6.22. Directions and magnitude of the fast-polarised phase of the near-vertically propagating S-wave in the Carpathian-Pannonian region and illustration of the most favoured orientation of the foliation and lineation in the upper mantle of the Nógrád-Gömör Volcanic Field 133
Fig. 6.23. Reconstructed stages of deformation and annealing events in the Nógrád-Gömör upper mantle based on microstructural characteristics and thermal conditions 136
Fig. 6.24. 'Water' concentration ranges in ortho- and clinopyroxene from mantle xenoliths worldwide 140
Fig. 6.25. H_2O concentrations of orthopyroxene *vs* clinopyroxene in the studied xenoliths 142
Fig. 6.26. H_2O concentrations of clinopyroxene compared to Ce and $(Ce/Yb)_N$ in clinopyroxene, and to equilibration temperatures 143
Fig. 6.27. $H_2O^{cpx/opx}$ vs bulk 'water'contents of the xenoliths, in samples with 'correct' $H_2O^{cpx/opx}$ 144

List of Tables

Chapter 5

Table 1. Petrographic properties and equilibration temperatures of the studied Nógrád-Gömör xenoliths 36
Table 2. Major-element compositions of the rock forming minerals 46
Table 3. Trace element compositions of pyroxenes and amphibole 54
Table 4. Calculated whole-rock geochemical compositions 62
Table 5. Positions of CO_2 bands in the bubble of the SMIs and calculated densities 69
Table 6. Volume proportions of the identified daughter phases of the SMIs 74
Table 7. Major element compositions of amphibole, mica, clinopyroxene and glass in the SMIs analysed with FIB-SEM, and bulk compositions obtained with mass-balance calculation. 76
Table 8. Trace element compositions of the SMIs acquired with LA-ICP-MS 78
Table 9. Fabric properties and calculated seismic properties of the studied xenoliths 81
Table 10. 'Water' contents and properties of IR spectra of NAMs 89

Chapter 1. Introduction and Aims

The lithospheric mantle, in close relation with the underlying asthenospheric mantle and the overlying crust, is a key domain that accommodates a wide variety of complex physico-chemical processes, such as magmatism, melt-rock reactions, and deformation, all of which are crucial components of plate tectonics. Information about the Earth's interior can be gained by geophysical remote-sensing methods or by direct sample collection by drilling; however, the deepest drilling project to date has only penetrated about one third of the continental crust (Kola Peninsula; Kozlovsky, 1987). Petrologic and geochemical properties of lithospheric mantle rock types can be directly examined when brought the surface by tectonic processes (massif peridotites, ophiolites) and/or volcanic activity (xenoliths in asthenosphere-derived melts). Massif peridotites commonly outcrop over large areas, providing opportunity to investigate mesoscale features such as intrusive magmatic reactions (through veins, dykes), deformation processes and facies relationships on scales of metres to kilometres; however, long-term exposure can lead to extensive weathering, resulting in biased geochemical data. Xenoliths, usually hosted in mafic magmas formed by small-fraction partial melting of the mantle (alkali basalts, kimberlites, lamprophyres), can reach the surface in hours to days (e.g., O'Reilly and Griffin, 2011), which is geologically a very short time; therefore they are more likely to preserve the original, unaltered conditions of the mantle portion they are sampling. On the other hand, due to their small size, rock-type relationships and structural properties are rarely observable. Both massif peridotites and xenoliths have been subject to countless studies over the course of the past half-century. In Europe, well-documented peridotite massifs occur along Hercynian and Alpine orogenic belts (e.g., Pyrenees, Alps, Betics, Appennines); whereas xenoliths have been described and thoroughly studied from the Rhenish Massive, the Massif Central, Lower Silesia and various localities within the Carpathian-Pannonian region (see Downes, 2001 for a review).

Upper-mantle material can be studied in a number of different ways. The most widely applied methods include analyses of petrographic and geochemical characteristics, both of the whole-rocks and of the constituent phases. Earlier studies generally interpreted mantle rocks as representatives of residual material following partial melting (e.g., Frey and Green, 1974; Frey and Prinz, 1978); however, this is commonly overprinted by late processes, principally metasomatism, caused by infiltrating and reacting melts. In the past

few decades, new aspects of mantle studies have emerged, aimed at defining physical properties of the rocks such as temperature, pressure, crystal preferred orientation, and the incorporation of 'water' (as hydrogen (H)) in nominally anhydrous mantle minerals; this facilitated by the improvement in analytical instruments. Geochemical properties (coupled with geothermobarometry) are often examined separately from microfabrics, crystal preferred orientation or 'water' content; however, a limited number of integrated studies (e.g., Falus, 2004; Falus et al., 2008; Tommasi et al., 2008; 2016; Soustelle et al., 2009; 2010; 2013; Kovács et al., 2012) suggest that these properties have significant influence on each other, and thus in order to acquire the most precise picture about conditions in the upper mantle, they should be examined and interpreted in an integrated way.

The more and more widely-applied electron backscattered diffraction (EBSD) technique provides an effective way to analyse textures and microstructures (i.e., crystal preferred orientation; CPO) in a variety of rock samples. In mantle research, numerous experimental studies focus on the crystallographic behaviour of olivine, the most abundant and most easily deformed phase of the upper mantle (e.g., Carter and Avé Lallemant, 1970; Nicolas et al., 1973; Nicolas and Christensen, 1987; Mainprice and Nicolas, 1989; Zhang and Karato, 1995; Tommasi et al., 1999; 2000; Zhang et al., 2000). Formation of preferentially oriented crystal fabrics in the mantle are controlled by various factors, such as the amount and directions of stress and strain (Tommasi et al., 1999), temperature (Zhang and Karato, 1995), incorporated 'water' (Jung and Karato, 2001) and the presence of melt (Holtzman et al., 2003). The resulting large-scale structural anisotropy demonstrated in mantle minerals has a significant influence on the migration of fluids/melts (e.g., Waff and Faul, 1992), and affects the propagation of seismic waves (e.g., Ribe, 1992); hence analyses of seismic anisotropy have become a crucial part of studies focusing on mantle fabrics (see Tommasi and Vauchez, 2015 for a review).

Furthermore, over the course of the past two decades, significant developments have been achieved in the analysis of 'water' incorporation in nominally anhydrous minerals (NAMs) of the upper mantle (olivine and pyroxenes). Since the applicability of Fourier-transform infrared spectroscopy (FTIR), which is based on the light absorbance by different species of OH-bonds, has been extended to unoriented crystals (Kovács et al., 2008), it is widely used and represents a useful method to measure 'water' in small-volume or fine-grained samples, such as mantle xenoliths. The role of water in the NAMs of the mantle is well-recognised, as it affects physical properties such as melting temperature

(e.g., Green et al., 2010), rheological properties (e.g., Demouchy et al., 2012; Girard et al., 2013; Bollinger et al., 2014), electrical conductivity (e.g., Selway et al., 2014) and deformation patterns (e.g., Jung et al., 2006; Manthilake et al., 2013). On the other hand, though several studies suggest that the behaviour of H is similar to those of incompatible trace elements (e.g., Michael, 1995; Danyushevsky et al., 2000), it is still unclear how 'water' contents relate to metasomatic processes (Denis et al., 2015).

This study is part of a larger project aiming to compile a robust database on mantle material from the Carpathian-Pannonian region, combining petrologic, geochemical and physical properties from all xenolith localities within the region. The Carpathian-Pannonian region is a young back-arc basin system with a complex tectonic evolution from the early Palaeogene to recent times (see Chapter 2), and various studies have tried to constrain the role of the mantle during its geodynamic history (e.g., Falus, 2004; Szabó et al., 2004; Bali et al., 2007; Hidas et al., 2007; Falus et al., 2008; Kovács and Szabó, 2008; Kovács et al., 2012). To obtain more detailed data, analyses of large sample sets have been / are being carried out from all xenolith localities. The focus of this study is the northernmost locality, the Nógrád-Gömör Volcanic Field. Although several papers have been published on the petrographic and geochemical properties of xenoliths from this locality (Szabó and Taylor, 1994; Konečný et al., 1995; 1999), they have provided major-element geochemical compositions on small sample sets and whole-rock contents of a limited number of trace elements (Szabó and Taylor, 1994). Furthermore, while olivine CPOs were recently published for a limited number of samples from one locality (Liptai et al., 2013; Klébesz et al., 2015), the Nógrád-Gömör Volcanic Field is still the only xenolith occurrence in the Carpathian-Pannonian region where thorough analyses focusing on deformation patterns, as well as 'water' contents of both olivine and pyroxenes have not yet been reported.

The aim of this study is to present and interpret the physico-chemical properties of the lithospheric mantle beneath the NGVF, with a variety of analyses carried out on 51 xenoliths carefully selected from all localities in the volcanic field. With the large number of samples, I have been able to provide a database as accurately representative of the upper mantle portion as possible. Therefore, in this work I have examined three major aspects:

• Determination of major- and trace-element compositions with the use of electron microprobe and laser-ablation inductively-coupled-plasma mass spectrometry, in order to constrain mantle melting, metasomatic processes and geothermometry. The results of

this first part of the analyses were published by Liptai et al. (2017). Furthermore, to better characterise metasomatic processes, silicate melt inclusions (SMIs) were analysed with Raman spectroscopy and a relatively new method, focused ion beam coupled scanning electron microscopy; aimed at obtaining geochemical features of the trapped melt representing a metasomatic agent.

• Analyses of CPO of olivine and pyroxenes, using electron-backscattered diffraction, to characterise microstructures and deformation processes in the lithospheric mantle of the Nógrád-Gömör Volcanic Field, as well as calculating and interpreting seismic properties including anisotropy.

• Quantification of 'water' incorporated in the major silicate phases with the use of Fourier-transform infrared spectroscopy to characterise the hydration state of the mantle segment and possible effects on other physico-chemical properties.

With the synthesis of these data, my goal is to provide a better insight into the physico-chemical evolution of the lithospheric mantle under the northern part of the Pannonian Basin, and to contribute to a deeper understanding of how these different processes are related to each other and to the overall geodynamic evolution of the Carpathian-Pannonian region.

Chapter 2. Geological Background

2.1. Structural framework and tectonic history of the Carpathian-Pannonian region

The Carpathian-Pannonian region, located in Central Europe, consists of the Intra-Carpathian Basin System, which is framed by mountain chains (the Eastern Alps, the Carpathians and the Dinarides) formed during the late stages of the Alpine orogeny. The largest, internal part of the Intra-Carpathian Basin System is referred to as the Pannonian Basin, which is an extensional back-arc basin superimposed on two microterranes with different Mesosoic tectonostratigraphy, the ALCAPA (ALps-CArpathians-PAnnonian) and Tisza-Dacia units (Balla, 1984; Csontos, 1995; Csontos and Vörös, 2004) (Fig. 2.1). These two blocks are separated by the Mid-Hungarian Fault Zone (Csontos et al., 1992; Csontos and Nagymarosy, 1998) and have different origins based on paleobiogeography of Jurassic faunal provinces (Géczy, 1973, 1984; Vörös, 1993) and paleomagnetic data (Márton and Márton, 1978; Márton, 1997): the ALCAPA is considered to have an African affinity, whereas the Tisza-Dacia is of European origin. The ALCAPA is bordered by the Pieniny Klippen Belt in the north, the low-angle normal fault at the eastern boundary of the Tauern window in the west, and the Periadriatic-Insubric and Balaton faults in the south, the latter of which separates ALCAPA from the Mid-Hungarian Zone (Balla, 1984; Csontos, 1995; Fodor et al., 1999). The Tisza-Dacia mega-unit is located to the southeast of the Mid-Hungarian Zone, and comprises of a sequence of NE-SW directed nappe systems (Tisza), the Apuseni Mountains and Southern Carpathian units (Dacia) (Csontos et al., 1992; Balintoni, 1994; Csontos and Vörös, 2004).

The two megaunits were juxtaposed during the early Miocene, as a result of the Alpine orogeny dominated by the convergence between the Adriatic microplate and the European platform. The collision initiated transpressional stress fields and the activation of dextral strike-slip faults along the Periadriatic line during the Eocene to Oligocene (Schmid et al., 1989; Csontos et al., 1992; Fodor et al., 1992), which accommodated the onset of the ‘escape tectonics’ from late Oligocene to early Miocene (Fodor et al., 1998; 1999). This involved the eastward extrusion of the ALCAPA along the Periadriatic line (Kázmér and Kovács, 1985; Csontos et al., 1992; Fodor et al., 1999) eventually leading up to a displacement of ~4-500 km (Kovács et al., 2000). Extrusion processes require an adjacent

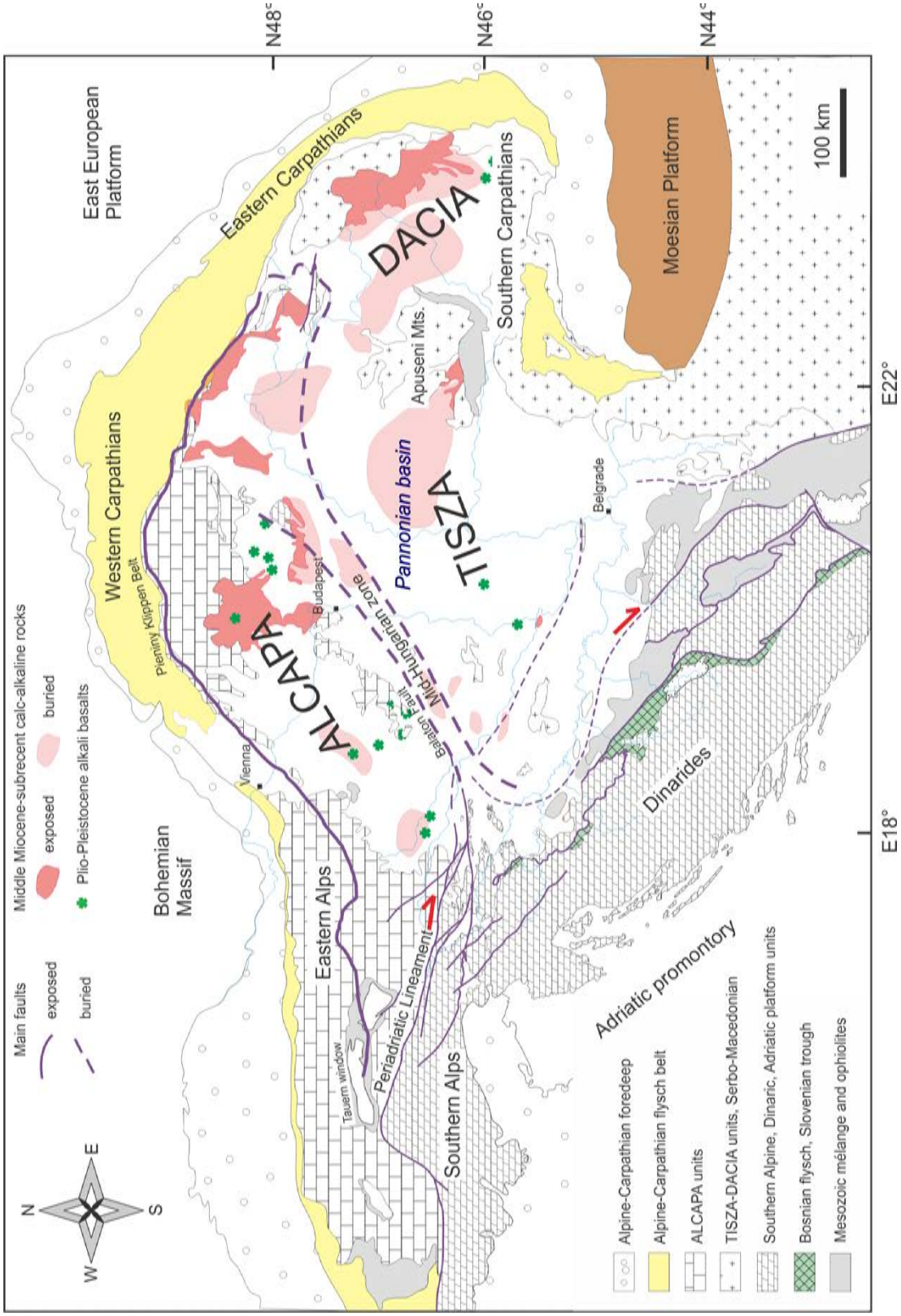

Fig. 2.1. Present-day location of major tectonic units in the Carpathian-Pannonian region (map modified after Kovács et al., 2007).

area of oceanic or thinned continental lithosphere, which is prone to subduct and thus provide space for the escaping units. From the Oligocene to the late Miocene, the ALCAPA and Tisza-Dacia units moved to the northeast into the Carpathian embayment, where the Outer Carpathian flysch basins with either oceanic or weakened continental lithosphere were subducting (Csontos, 1995), closing the Magura Ocean (Fig. 2.2). During this movement, ALCAPA rotated counter-clockwise and Tisza-Dacia rotated clockwise (Márton and Márton, 1978; Márton, 1987; Csontos et al., 1992). The escape of the microterranes (especially ALCAPA) is considered to have been promoted by an eastward asthenospheric flow (Kovács and Szabó, 2008; Kovács et al., 2012), associated with the rollback of the subduction in the eastern Carpathians. There is a debate whether the extruding ALCAPA

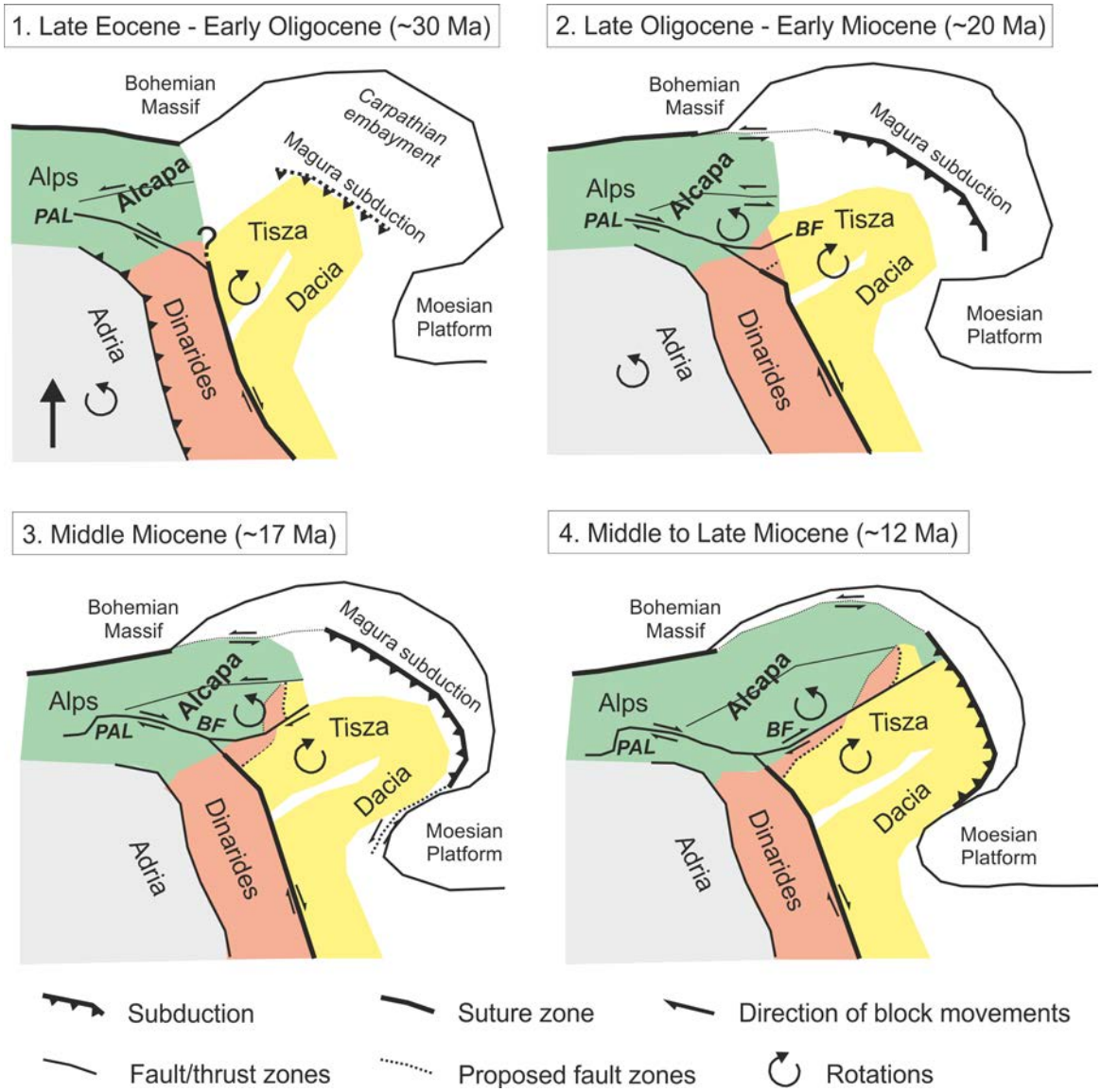

Fig. 2.2. Schematic illustration of the tectonic evolution of the Carpathian-Pannonian region since the late Eocene (modified after Kovács and Szabó, 2008).

was a crustal block only (Csontos et al., 1992; Fodor et al., 1999; Huismans et al., 2001; Horváth et al., 2006), or the whole lithosphere was involved (Willingshofer et al., 1999; Willingshofer and Cloetingh, 2003; Kovács and Szabó, 2008). Studies on mantle xenoliths revealed geochemical (e.g., Bali et al., 2007; 2008a) and deformational (e.g., Falus, 2004; Falus et al., 2008) features, which support the theory that the extrusion has affected at least part of the lithosphere; i.e., there was no decoupling between the crust and the lithospheric mantle.

From the middle Miocene, the assembled microterranes were subjected to extension divided into two major phases; first between ~17 – 14 Ma, then a second phase between ~11.5 – 8 Ma following a brief compressional episode, also known as 'tectonic inversion' (e.g., Fodor et al., 1999; Bada and Horváth, 2001; Huismans et al., 2001). The major direction of the stress field was NE-SW to ENE-WSW during the extensional period (Fodor et al., 1999), and basin formation was characterised by the activation of low-angle normal faults (e.g., Little Hungarian Plain, Tari, 1994), opening of strike-slip basins (e.g., Vienna Basin, Royden et al., 1982), and the rapid uplift of metamorphic core complexes (Tari et al., 1992). Earlier studies (e.g., Stegena et al., 1975) suggest that mantle diapirism was the main driving force for the extension, whereas later it has become more commonly accepted that the retreating subduction of the Magura ocean along the Carpathian front (Horváth, 1993; Csontos, 1995), which initiated a significant asthenosphere upwelling in the 'active phase' (Huismans et al., 2001), is responsible. Most recently, an alternative explanation has been provided by Houseman and Gemmer (2007) and Gemmer and Houseman (2007), suggesting that gravitational instability induced by the thickened crust in the collision zones led to lithospheric downwelling in the surrounding mountain belts and simultaneously, depth-variable lithosphere thinning in the Pannonian Basin. During the extension, the mantle suffered significantly greater thinning (δ = ~4–8) compared to the crust (β = ~1.5) (Royden et al., 1983; Lankreijer et al., 1995; Huismans et al., 2001). As a result, the crust and lithosphere are anomalously thin in the Pannonian Basin, having thicknesses as low as 22.5 and 60 km (Fig. 2.3), respectively, in the middle of the basin (Horváth, 1993 and references therein).

From the late Miocene (8 – 7.5 Ma), following the termination of the extension, a large-scale tectonic inversion (i.e., a change in kinematics from extensional to compressional; Horvath and Cloetingh, 1996) has dominated the geodynamics of the Carpathian-Pannonian region up until recent times (Horváth, 1995). This tectonic

environment is attributed to the push of the Adria microplate generated by its counter-clockwise rotation (Horvath and Cloetingh, 1996; Fodor et al., 2005; Bada et al., 2007; Dombrádi et al., 2010), which led to the formation of pure contractional and transpressional structures in the southwest Pannonian Basin (Fodor et al., 2005 and references therein).

2.2. Neogene magmatism throughout the Carpathian-Pannonian region

During Neogene to Quaternary times, widespread volcanic eruptions of variable chemical composition took place in the Carpathian-Pannonian region. Numerous studies have focussed on the classification of these volcanic extrusions based on their composition and/or relation to different tectonic environments (Szabó et al., 1992; Pécskay et al., 1995;

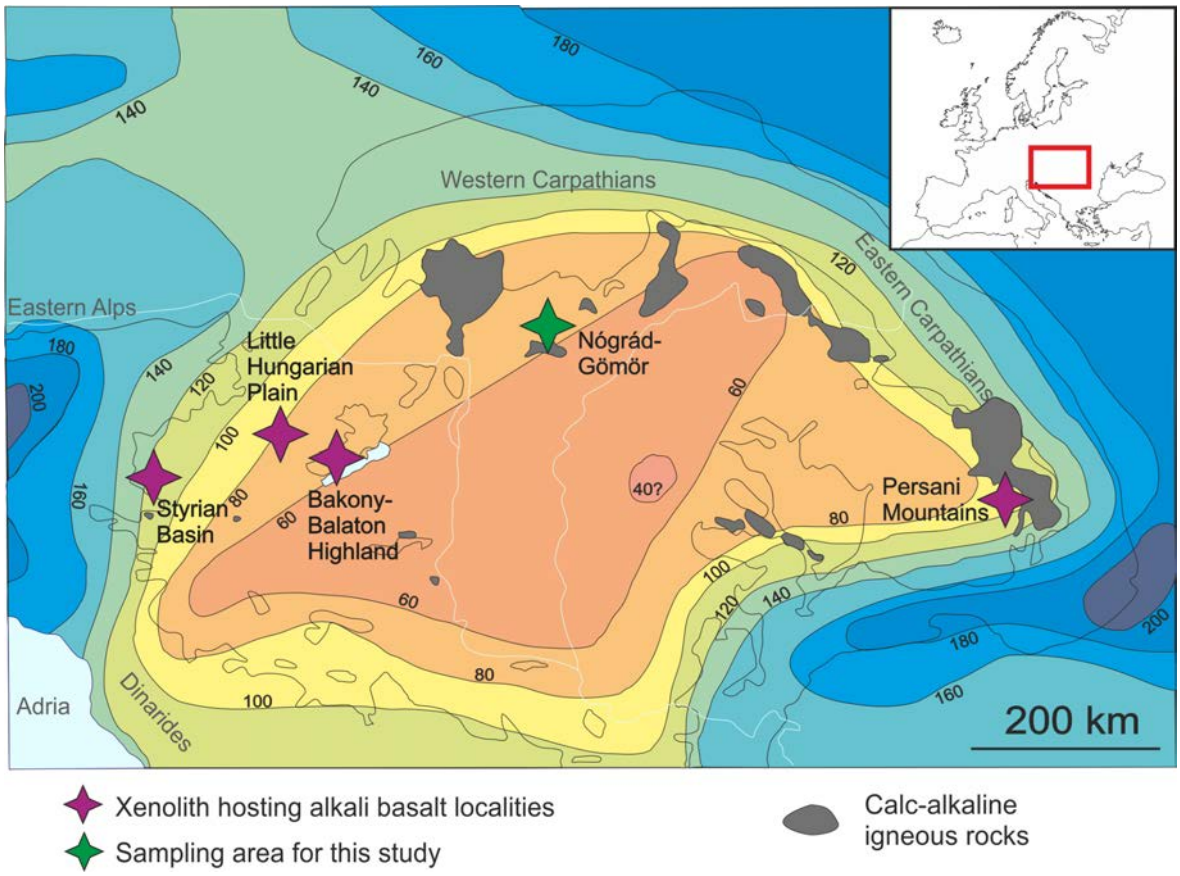

Fig. 2.3. Lithospheric thickness in the Pannonian Basin (modified after Lenkey, 1999) and the spatial distribution of calc-alkaline volcanic rocks and xenolith-bearing late Miocene – Pleistocene alkali basalt occurrences (after Szabó et al., 1992; Harangi, 2001).

Harangi, 2001; Seghedi et al., 2004; Pécskay et al., 2006; Harangi and Lenkey, 2007; Lexa et al., 2010; Seghedi and Downes, 2011). Most of the volcanic rocks are calc-alkaline, with a wide chemical range from felsic to basaltic calc-alkaline compositions, but Na- and K-alkaline and ultrapotassic volcanics are also present in smaller volumes.

The oldest of the calc-alkaline group are felsic volcanic products of rhyolitic to dacitic composition, occurring mainly in the form of tuffs and ignimbrites, widely dispersed (and mostly buried) in the Pannonian and Transylvanian Basins (Szabó et al., 1992; Pécskay et al., 1995) and minor amounts of extrusive rocks (domes and dome/flow complexes) (Lexa et al., 2010). They were formed during the early to middle Miocene (~21 – 11 Ma) in three sequences distinguishable in Hungary (e.g., Hámor et al., 1987). Due to their large spread over the region, the location of the source centres is still mostly unknown. The formation of these silicic volcanoes is attributed to the early phases of the extension. Since their isotopic composition indicates a dominance of crustal components (e.g., Seghedi et al., 2004), crustal anatexis induced by asthenosphere updoming (Lexa and Konečný, 1974, 1998), or mixing of mantle-derived and lower-crustal magmas (Harangi and Lenkey, 2007) have been proposed as a mechanism.

Intermediate calc-alkaline volcanic products spread along the inner margin of the Inner Carpathian arc, forming stratovolcanoes, domes, lava flows and subvolcanic intrusive complexes (Szabó et al., 1992; Harangi, 2001). Their chemical compositions range from basaltic andesites to rhyolites; some authors have distinguished mafic calc-alkaline (Pécskay et al., 2006), adakitic and transitional subgroups (Seghedi et al., 2004). Genesis of these volcanoes is associated with partial melting of the mantle wedge above a devolatilising subducting slab, and the ages (ranging from middle Miocene to Quaternary) decrease from the Western to the Eastern and Southern Carpathians, indicating the spatial change in the subduction (Szabó et al., 1992). Recently, it was proposed by Kovács and Szabó (2008) that calc-alkaline volcanics in the vicinity of the Western Carpathians (i.e., on the ALCAPA microterrane) were produced prior to the extrusion, from a mantle source with an inherited subduction signature. The formation of intermediate calc-alkaline magmas can also be related to late-stage back-arc extension (Lexa and Konečný, 1974, 1998). Thus, they are genetically related more to the felsic group. Seghedi et al. (2004) classified all calc-alkaline volcanites of the Carpathian-Pannonian region (including silicic ones) into one group with different subgroups based on compositional differences.

Small volumes of potassic and ultrapotassic volcanic rocks occur sporadically

as Miocene shoshonites and trachyandesites in the Styrian Basin, the Little Hungarian Plain, the Apuseni Mountains and the Southern Carpathians, and Pliocene leucitite and lamproite as two single occurrences in the southern part of the Pannonian Basin (Harangi et al., 1995b; Pécskay et al., 1995; Harangi, 2001; Seghedi and Downes, 2011). They are considered to be generated by partial melting of a K-rich metasomatized lithospheric mantle, due to the upwelling of hot asthenospheric material (Harangi et al., 1995b).

The Na-alkaline series occurs as a geochemically variable, mainly alkali basaltic and basanitic volcanic fields (Szabó et al., 1992), forming maars, tuff and cinder cones, diatremes and lava flows (Lexa et al., 2010), a buried trachyandesite volcano in the Little Hungarian Plain (Harangi et al., 1995a) and several buried formations in the Great Hungarian Plain. K-Ar dating reveals ages ranging from late Miocene to Quaternary; the oldest eruptions began in the western and central part of the Pannonian Basin (~12 - 10 Ma; Balogh et al., 1986) and the last ones occurred a few hundred thousand years ago in Central Slovakia and Persani Mountains (Balogh et al., 1981; Harangi, 2001). Genesis of the Na-alkaline volcanites is attributed to partial melting due to decompression in the upwelling asthenospheric mantle, as inferred from geochemical and isotopic studies (Embey-Isztin et al., 1993; Dobosi et al., 1995; Downes et al., 1995; Embey-Isztin and Dobosi, 1995; Harangi et al., 1995a). They contain upper-mantle xenoliths at five localities: Styrian Basin, Little Hungarian Plain, Bakony-Balaton Highland, Nógrád-Gömör, and Persani Mountains (Fig. 2.3).

2.3. Review of the physico-chemical properties of the upper mantle from Carpathian-Pannonian region xenoliths

In the last few decades, numerous studies were carried out focusing on the geochemical and deformational features of mantle xenoliths from the five localities in the Carpathian-Pannonian region. According to the review paper of Szabó et al. (2004), the xenoliths are dominantly spinel lherzolites, with subordinate amount of wehrlites, harzburgites, dunites, websterites and pyroxenites (Fig. 2.4). The ratio of ortho- and clinopyroxene varies widely among the peridotites, and modal compositions are only partly in agreement with the average European subcontinental lithospheric mantle (Downes, 1997; Szabó et al., 2004). In all localities, the xenoliths bear imprints of a complex history of partial melting and recrystallisation, metasomatism and crystal preferred orientation as

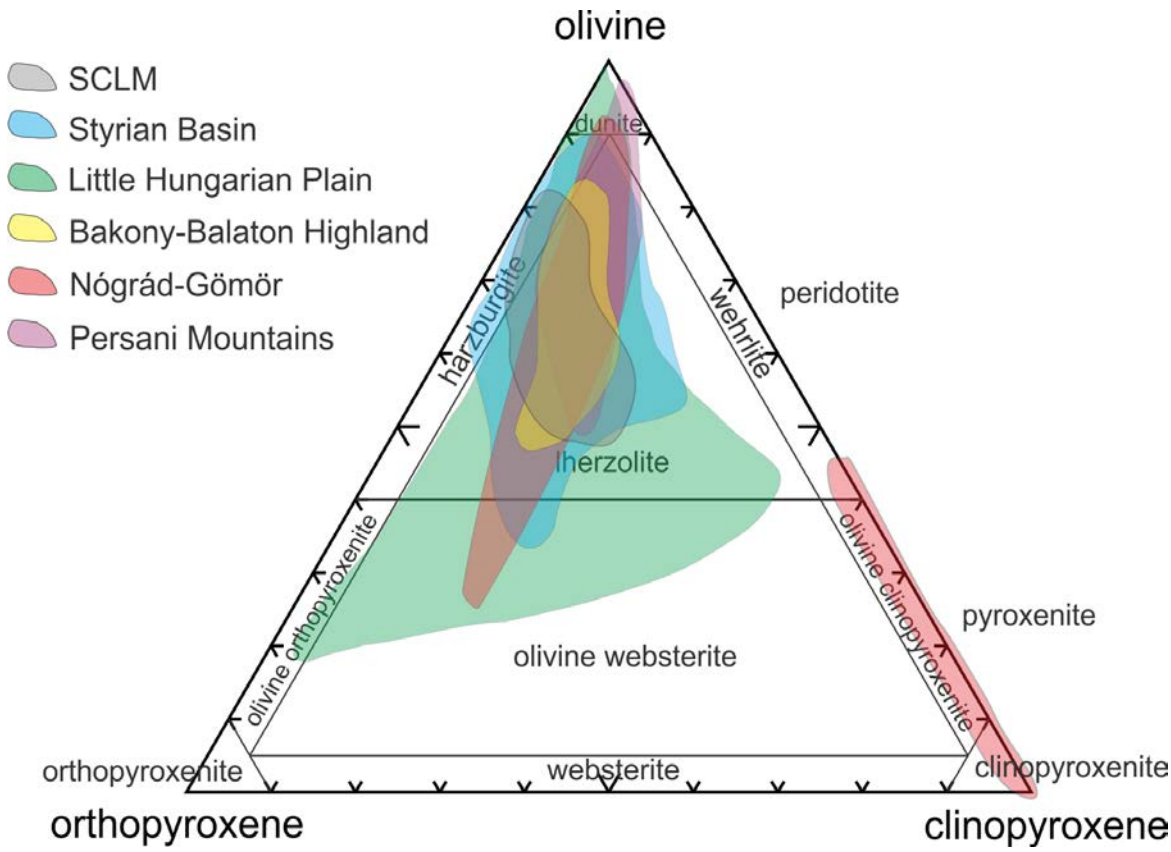

Fig. 2.4. Modal compositions and rock types of mantle xenoliths from the different localities in the Carpathian-Pannonian region using the system of Streckeisen (1975), compared to the average composition of the European subcontinental lithospheric mantle (SCLM) of Downes (1997). Figure modified after Szabó et al. (2004). Sources of the data for the different volcanic fields: Styrian Basin - Kurat et al. (1980), Vaselli et al. (1996), Aradi et al. (2017); Little Hungarian Plain - Embey-Isztin et al. (1989), Downes et al. (1992), Szabó et al. (1995); Bakony-Balaton Highland - Embey-Isztin et al. (1989); Szabó et al. (1995); Nógrád-Gömör - Szabó and Taylor (1994); Persani Mountains - Vaselli et al. (1995); Falus et al. (2008).

a result of deformation. Though xenoliths mostly originate from the spinel stability field, garnet clinopyroxenites and symplectites formed by decompression breakdown of garnet have been reported in small numbers from the Styrian Basin (Kurat, 1971; Falus et al., 2000), Little Hungarian Plain (Falus et al., 2007), Bakony-Balaton Highland (Embey-Isztin et al., 1989; Török, 1995), and Persani Mountains (Falus et al., 2000).

Textures of the spinel peridotite xenoliths, (which are generally regarded as residual upper mantle material; Szabó et al., 2004), show variable features depending on their location. On the marginal regions of the Carpathian-Pannonian region (Styrian Basin, Persani Mountains) protogranular and porphyroclastic fabrics (after classification of Mercier and Nicolas, 1975) are more dominant (Kurat et al., 1991; Vaselli et al., 1995; 1996; Coltorti et al., 2007; Falus et al., 2008), whereas in the central area of the

Pannonian Basin (Little Hungarian Plain and Bakony-Balaton Highland) porphyroclastic to equigranular, recrystallised or poikilitic textures are more abundant (Embey-Isztin, 1984; Downes et al., 1992; Hidas et al., 2007; Kovács et al., 2012; Embey-Isztin et al., 2014). In the Nógrád-Gömör area, textural types cover a wide range from frequent protogranular / coarse granular and porphyroclastic in the northern part towards porphyroclastic and equigranular and secondary-recrystallised in the southern part of the volcanic field (Szabó and Taylor, 1994; Liptai et al., 2017).

Textural types show significant correlation with chemical composition; less deformed xenoliths (i.e., protogranular, protogranular to porphyroclastic textures) have higher contents of 'basaltic elements' (Al, Ca, Na, Ti), whereas more deformed samples (equigranular and secondary-recrystallised) have more depleted characteristics (Downes et al., 1992; Szabó et al., 1995a; 1995b). The concentration of basaltic elements is usually negatively correlated with Mg contents (Downes and Vaselli, 1995), and therefore is usually interpreted as a depletion trend resulting from partial melting event(s), such as in massif peridotites at Ronda (Frey et al., 1985) or Lanzo (Bodinier, 1988), for example. On the other hand, incompatible trace elements, especially light rare earth elements in clinopyroxenes, show elevated concentrations in Carpathian-Pannonian region xenoliths with more deformed textures, compared to the less deformed ones (Downes et al., 1992). This can be explained by the metasomatic effect of an incompatible-element-rich fluid or melt, for which deformed structures can provide a more permeable pathway (Downes, 1990). Pervasive melt-rock reaction in the upper mantle could also explain depletion in basaltic major elements (Kelemen et al., 1992), and could account for the decoupling between major- and trace elements seen in mantle rocks worldwide (Frey and Green, 1974; Wilshire and Shervais, 1975).

Furthermore, xenoliths with less deformed textures in the central region of the Pannonian Basin (Little Hungarian Plain and Bakony-Balaton Highland; Fig. 2.3) tend to have higher equilibration temperatures (1050-1150°C) than those with more deformed textures (800-900°C) (Szabó et al., 1995a). Examination of crystal preferred orientation patterns (CPO) for olivine, by Falus (2004) found that the two groups have different symmetries. Xenoliths with more primitive textures and undepleted geochemical compositions have point maxima for each olivine axis, with [100] directed parallel to the lineation, and [010] parallel to the plane of foliation, whereas in xenoliths with more deformed textures, olivine [100] and [001] axes tend to show a girdle distribution in

the foliation plane with [010] axes pointing normal to this plane. The first CPO type, often referred to as 'orthorhombic', has been recognised to develop via simple shear or pure shear (Tommasi et al., 1999; 2000; Zhang et al., 2000); whereas the latter, referred to as 'axial-[010]' or '[010]-fibre', has been attributed to axial shortening or a transpressional regime (Tommasi et al., 1999), which are considered to be the main forces during collisional or extrusional tectonics. Thus, Falus (2004) proposed that in the Little Hungarian Plain and Bakony-Balaton Highland (i.e., the central part of the Pannonian Basin; Fig. 2.3), the xenoliths represent two horizontal layers of the upper mantle. Protogranular and coarse-grained porphyroclastic-textured, relatively undepleted xenoliths with orthorhombic CPO and higher equilibration temperatures originate from a deeper lithospheric domain, whereas fine-grained porphyroclastic and equigranular-textured samples represent a shallower and more strongly deformed layer.

Most recently, Kovács et al. (2012) suggested that this shallower layer bears imprints of pervasive lithospheric deformation including and post-dating the Alpine collision and extrusion, whereas the deeper layer represents a fossilised asthenospheric flow, which became part of the lithosphere during the thermal relaxation following the Miocene extension. This is supported by the inference that asthenospheric flow was a driving force for development of orthorhombic CPO as recognised by previous studies as well (Blackman et al., 2002). In the marginal parts of the Carpathian-Pannonian region, there is no evidence for the imprint of mantle flow, however, xenolith textures (grain size) still correlate well with equilibration temperatures, and thus the depth of origin (Falus et al., 2008; Aradi et al., 2017). In the Persani Mountains, this is explained by changes in the amount of deviatoric stress by depth, which is strongly linked to the convergent plate tectonics characteristic for the southeastern Carpathians (Falus et al., 2008). In the Styrian Basin, most recently Aradi et al. (2017) reported lower-temperature [010]-fibre and higher-temperature orthorhombic and [100]-fibre olivine CPOs; they proposed that despite the small distance of the locations from the centre of the basin, the major deformation forces were transpressional. However, deformation effects were extensively overprinted by annealing caused by subduction-related fluids.

Geochemical alteration in the form of enrichment of either (or both) hydrous and anhydrous phases has been described from all Carpathian-Pannonian region xenolith localities (Szabó et al., 2004). Most clinopyroxene-rich xenoliths have igneous textures with little to no deformation (Embey-Isztin et al., 1990; Kovács et al., 2004), and were

interpreted as cumulates crystallised from asthenosphere-derived mafic melts near the crust-mantle boundary (Kovács et al., 2004; Zajacz et al., 2007). Orthopyroxene-rich xenoliths (orthopyroxene-rich websterites and orthopyroxenites) occur in a small number in the Little Hungarian Plain and Bakony-Balaton Highland (Szabó et al., 1995b; Bali et al., 2007; 2008a), where the formation of secondary orthopyroxene is ascribed to reaction with an infiltrating Si-rich melt or fluid presumably originating from a subducted slab. This metasomatism also affected clinopyroxenes, resulting in U-shaped chondrite-normalised REE patterns (Bali, 2004; Bali et al., 2007).

Modal metasomatic products in the form of volatile-bearing phases such as amphibole and phlogopite occur frequently in both peridotites and pyroxenites from all over the Carpathian-Pannonian region. Amphibole, usually pargasitic in composition, is more common than phlogopite, and appears as veins or interstitial phases (Szabó et al., 2004). Their abundance shows no clear correlation to xenolith texture types in case of xenoliths from the Styrian Basin and the Persani Mountains, presumably due to the lower variability of xenolith fabrics in these localities. They tend to occur more frequently in the more deformed and recrystallised rocks in the central area of the Pannonian Basin (Szabó et al., 2004 and references therein). REE patterns of these amphiboles are usually flat (e.g., Zanetti, 1995), whereas those in xenoliths from the marginal areas show a wider compositional variety (Vaselli et al., 1995; 1996; Coltorti et al., 2007). Major- and trace-element characteristics suggest that the amphiboles were introduced by a volatile-rich melt of either subduction or asthenospheric origin (Szabó and Taylor, 1994; Vaselli et al., 1995; Coltorti et al., 2007).

Silicate melts, which occur in the form of interstitial melt pockets or inclusions in the rock-forming minerals of the xenoliths, have been the subject of several studies in the Carpathian-Pannonian region. Melt pockets, reported from the Little Hungarian Plain (Szabó et al., 1995b), Bakony-Balaton Highland (Embey-Isztin and Scharbert, 2000; Bali et al., 2002; 2008b) and Nógrád-Gömör (Szabó et al., 1996), usually contain assemblages of glass ± clinopyroxene ± spinel ± olivine ± plagioclase, and can contain carbonate, sulphide or apatite in small amount. They are only present in more deformed or recrystallised xenoliths. Major- and trace-element compositions suggest that the formation of these melt pockets can be linked to melting or breakdown of metasomatic amphibole (and possibly coexisting clinopyroxene), even when amphibole is completely absent in the xenolith; however, the effect of external melts or fluids of subductional origin cannot

be excluded (Bali et al., 2002; 2008b). Silicate melt inclusions in some metasomatized Nógrád-Gömör xenoliths, present mostly in olivines, exhibit 'andesitic' and 'basaltic' compositions (Szabó et al., 1996). However, these different compositions, as well as the accumulated melts in interstitial melt pockets may be explained with a common source. Szabó et al. (1996) proposed that the most plausible scenario is the infiltration of a subduction-related, volatile-rich silicate melt, which caused cryptic and modal metasomatism in the xenoliths, and progressive evolution of the melt during the reactions altered its composition (Szabó et al., 1996).

2.4. Previous studies on the xenoliths of the Nógrád-Gömör Volcanic Field

In the northernmost xenolith locality of the Carpathian-Pannonian region, the Nógrád-Gömör Volcanic Field, three major xenolith rock types have been found: lower crustal granulites and two, geochemically different peridotite types with upper mantle origin. Lower-crustal granulite xenoliths, which are least abundant, have been described by Kovács and Szabó (2005). These consist mainly of clinopyroxene, hornblende and plagioclase, and contain symplectites of spinel, feldspar and clinopyroxene. They are considered to having undergone granulite facies metamorphism, which corresponds to 'original' crustal depths, and then, during the Miocene extension, decompression-induced garnet breakdown and the formation of symplectites.

The upper mantle xenoliths of the Nógrád-Gömör Volcanic Field can be divided into two geochemically distinct groups (Szabó and Taylor, 1994) based on the composition of their clinopyroxenes: the Cr-diopside suite represents the olivine-rich mantle material residual after partial melting, whereas the Al-augite suite is enriched in 'basaltic' major elements and forms as cumulates crystallising directly from feeder dykes in the source zone of the host basalt (Wilshire and Shervais, 1975). Cr-diopside and Al-augite xenoliths are also referred to as group (/type) I and II, respectively (Frey and Prinz, 1978). In the Nógrád-Gömör Volcanic Field, Al-augite xenoliths have been interpreted as cumulates of a basanitic parental melt formed by ~2 % partial melting of a garnet peridotite source (Zajacz et al., 2007) and trapped in the uppermost mantle near the MOHO prior to the onset of the Plio-Pleistocene alkali basalt eruptions (Kovács et al., 2004). According to the geochemical modelling of Zajacz et al. (2007), the composition of the parental melt closely resembles

that of the host basalt. Therefore, the emplacement of the cumulates is suspected to have happened only a short time before the ascent of the xenolith hosting magma, and to be associated with melts of similar composition to that of the host lava. The cumulates also rarely contain amphibole, which was interpreted to be metasomatic product by Kovács et al. (2004). However, Zajacz et al. (2007) showed that it can be produced during the evolution of the parental melt, by resorption of previously-crystallised clinopyroxene and olivine.

The Cr-diopside or type I xenoliths of the Nógrád-Gömör Volcanic Field were first reported by Embey-Isztin (1978) and Hovorka and Fejdi (1980) from several localities from the Hungarian and Slovakian side, respectively; providing petrography and major element geochemistry of the rock forming silicates. A more detailed study was published by Szabó and Taylor (1994), providing bulk and mineral major-element compositions, as well as bulk trace-element compositions for a robust set of 22 xenoliths from seven different localities within the Nógrád-Gömör Volcanic Field. Based on modal compositions and texture types, they classified the xenoliths into two groups: (I) spinel lherzolites and spinel websterites with protogranular to porphyroclastic or equigranular textures, and (II) dunites and spinel lherzolites with secondary recrystallised textures (texture type classification of Mercier and Nicolas, 1975). The authors recognised that xenoliths with secondary recrystallised textures, which are restricted to the southernmost sampling locality, are generally depleted in 'basaltic' major elements, but contain F-rich phlogopite indicative of a volatile-rich, possibly subduction-derived metasomatic agent. The presence of amphibole and the lack of correlation between texture and rare-earth-element contents in the group I samples indicate a complex history of modal and cryptic metasomatism in the upper mantle of the Nógrád-Gömör Volcanic Field.

Inclusions of different types are common in the NGVF xenoliths, and they were subjected to several studies in the past 20 years. Sulfide inclusions have been thoroughly analysed both in the Cr-diopside (Szabó and Bodnar, 1995) and the Al-augite suite (Zajacz and Szabó, 2003). In the former case, primary sulfide inclusions are interpreted as having formed from an immiscible sulfide liquid trapped during or after partial melting of the mantle, and some during metasomatism. In the latter case, they are considered to have formed from a sulfide melt coexisting with the silicate melt inferred to be the parental melt for the cumulate xenoliths. Besides sulfide blebs, silicate melt inclusions have also been found mainly in olivines (Szabó et al., 1996), representing remnants of a

metasomatizing volatile-rich subduction-derived melt trapped at different stages of melt evolution. Different generations of fluid inclusions in several Nógrád-Gömör xenoliths, consisting mostly of CO2, have provided a valuable tool for estimating the ascension rate of the host basalt. The basalts were calculated to reach Moho depths within ~36 hours following entrainment of the xenoliths, and an additional ~1.5 hours were needed to ascend to the surface (Szabó and Bodnar, 1996). Further constraints on the geochemical properties, pressure-temperature conditions and oxygen fugacity of spinel peridotites have been provided by a number of studies, focusing only on localities from the northern side (Huraiová and Konecny, 1994; Konečný et al., 1995; 1999). These studies suggest that the upper mantle beneath southern Slovakia is moderately reduced, and bears imprints of post-extensional thermal relaxation.

Most recently, a publication reported results of olivine CPO in eight xenoliths from the southernmost locality of the NGVF (Klébesz et al., 2015), along with calculations of seismic properties and an estimate of the overall thickness of the anisotropic layer responsible for the observed SKS delay in the area. They concluded that a thickness of ~140-330 km would be required, assuming a single anisotropic layer; however, the real structure of the anisotropic body in the mantle is still unclear. Furthermore, results of S receiver-function analyses supported previous estimates of the depths to the Moho and the lithosphere-asthenosphere boundary in the region (25±5 and 65±10 km, respectively).

Chapter 3. Structure of the Nógrád-Gömör Volcanic Field and Sample Locality Details

The alkali basalts of the Nógrád-Gömör Volcanic Field range from basanite through basaltic trachyandesite to phonotephrite in composition (Dobosi et al., 1995; Harangi et al., 2015). According to Dobosi et al. (1995), trace-element and isotopic compositions suggest an OIB-type magma that has undergone significant fractionation. It is likely that the basalts originated from a common asthenospheric source, which underwent slight compositional evolution from the Miocene through the late Pliocene. The volcanic activity started out as phreatic and phreatomagmatic in the northwest in the late Miocene, when the ascending lava came in contact with fluvio-lacustrine sediments. This was followed by shifting of the eruption centres to the southwest during the Plio-Pleistocene, eventually occurring in dry-land environments due to a local updoming (Konecný et al., 1995). Volcanic forms in the NGVF include lava flows, maars, scoria cones and, due to erosional exposure, necks, dykes and diatremes (Jugovics, 1971; Konečný et al., 1999; Lexa et al., 2010). The basalts contain upper-mantle xenoliths in a belt approximately 60 km long from Podrečany in the NW to Bárna in the SE. No xenoliths have been found in the outcrops east of Fil'akovo (Fig. 3.1).

This zone of the volcanic field, where xenoliths occur, can be divided into three distinct domains (northern, central and southern parts) based on the age and spatial distribution of the host basalts. Isolated volcanic cones are characteristic in the northern and southern parts, whereas the central part consists of two basalt plateaux (Babi Hill and Medves Plateau) and one monogenetic volcano (Fil'akovo-Kerčik). Eruption ages in these domains decrease from north to south: K–Ar ages of volcanic eruptions are 6.4–4.9 Ma in the northern part, 4.0–2.5 Ma in the central part and ~2.5 Ma in the southern part (Balogh et al., 1981). The monogenetic volcano of Fil'akovo-Kerčik is older (4.0 Ma) than the two basalt plateaux forming the central part (3.0 –2.5 Ma; K. Balogh, unpublished data). U/Pb and (U–Th)/He dating yielded similar ages for the northern and central part (7.0 - 5.9 and 3.0 - 1.7 Ma, respectively; Hurai et al., 2013).

More than 300 peridotite xenoliths were collected by members of the Lithosphere Fluid Research Lab (LRG) during field trips from 2011 to 2013. The sampling sites covered all known locations in the volcanic field where upper mantle xenoliths are hosted in basalts. The 11 localities, quarries and outcrops are the following from NW to SE:

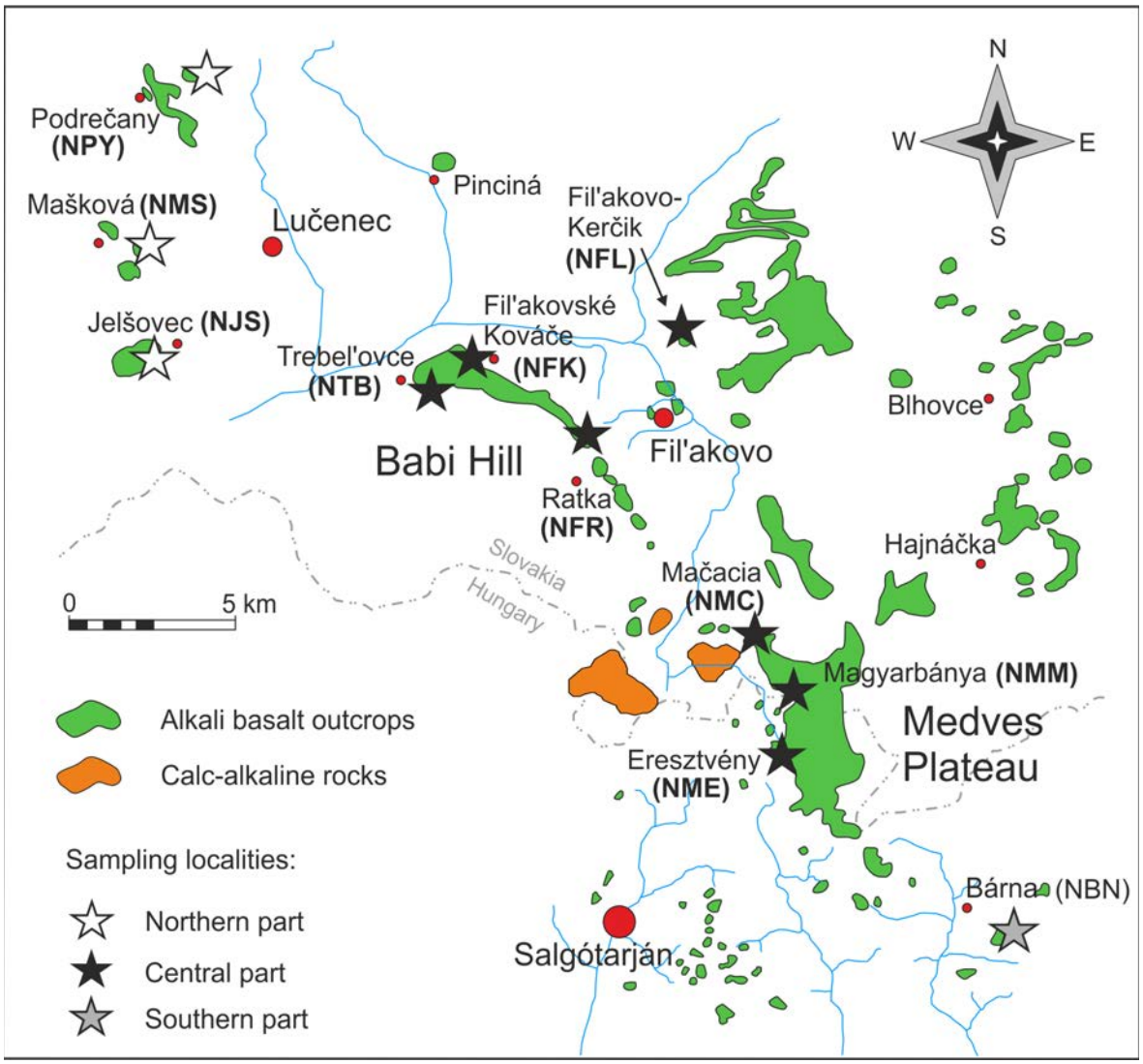

Fig. 3.1. Spatial distribution of calc-alkaline and alkali basaltic outcrops in the Nógrád-Gömör Volcanic Field, with the sampling localities marked: from NW to SE as follows: Podrečany (NPY), Mašková (NMS), Jelšovec (NJS), Trebel'ovce (NTB), Fil'akovské Kováče (NFK), Ratka (NFR), Mačacia (NMC), Magyarbánya (NMM), Eresztvény (NME) and Bárna-Nagykő (NBN).

Podrečany, Mašková, Jelšovec (northern part); Fil'akovo-Kerčik, Trebel'ovce, Fil'akovské Kováče, Ratka, Mačacia, Magyarbánya, Eresztvény (central part); and Bárna-Nagykő (southern part) (Fig. 3.1). The xenoliths occur in lavas at all localities, except for Jelšovec where they are hosted in pyroclastic deposits. Out of the collected xenoliths, polished thin sections were prepared out of over 120 samples. Since the Nógrád-Gömör xenoliths are quite small (maximum diameter is 4 cm), the most important factors for selection were size and freshness (i.e., the least possible alteration by either surface processes or reaction with the host basalt) so that the xenoliths represent compositions closest to the state of the upper mantle at the time of eruption. The selected xenoliths were subjected

to thorough petrographic examination, during which two compositionally and texturally different groups were distinguished. The lherzolitic suite generally has both ortho- and clinopyroxene, whereas the wehrlitic one lacks modal orthopyroxene, and consists of clinopyroxene-rich and olivine-rich domains on the mm-scale (Fig. 3.2). The wehrlitic group is considered as the products of reaction between an infiltrating melt and the wallrock represented by the lherzolites (Patkó et al., 2013). As this study is focused on the lherzolites and aims to constrain the physico-chemical properties of the NGVF mantle before this metasomatic event, samples for further analyses were selected from this group only. In order to adequately represent the whole upper-mantle domain beneath the NGVF, a robust set of 51 xenoliths was selected, resulting in a minimum of 3 from each location.

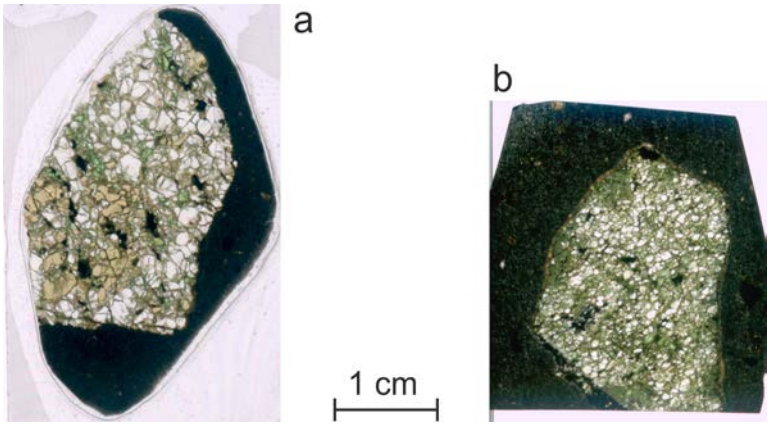

Fig. 3.2. Scanned thin-section images of a typical four-phase lherzolite (a) and a wehrlite with olivine-rich and clinopyroxene-rich patches (b).

Chapter 4. Applied Techniques

4.1. Polarised Light Microscope

Petrographic examination of the selected thin sections has been carried out in the Lithosphere Fluid Research Laboratory at Eötvös University, Budapest. I used a Nikon Eclipse LV100 POL polarised light microscope for observation of textural and microstructural features. Photomicrographs were taken with a Nikon DS-Fi1 digital camera attached to the microscope, running NIS Elements AR 2.20 digital imaging software. Thin sections of the xenoliths were digitised at 1200 dpi resolution with an HP Scanjet 2400 scanner; the scanned images were used to determine modal compositions using point-counting methods via the open source software JMicroVision developed by Nicolas Roduit (https://www.jmicrovision.com/).

4.2. Electron Microprobe

To measure concentrations of major elements in the minerals, a CAMECA SX- 50 microprobe equipped with four WDS detectors at the University of Padova (Italy), and a CAMECA SX-100 microprobe equipped with an EDS and five WDS detectors at the Geochemical Analysis Unit (GAU) of CCFS-GEMOC at Macquarie University (Sydney, Australia) were used. The accelerating voltage was 15-20 keV and the beam current was 20 nA for all analyses. For the analysed elements (Si, Ti, Al, Cr, Fe, Ni, Mn, Mg, Ca, Na, K), natural minerals and synthetic oxides were used as standards. Counting times were between 15 and 40 sec. Oxide compositions of the analysed elements were obtained following ZAF corrections.

4.3. Laser-Ablation Inductively Coupled Plasma Mass Spectrometry

Trace-element contents of orthopyroxene, clinopyroxene and amphibole in xenoliths from the northern and central part of the NGVF were determined at the Natural History Museum, (London, UK) and in the GAU at CCFS-GEMOC, Macquarie University (Sydney, Australia). At the Natural History Museum, an Agilent 7500s quadrupole inductively coupled plasma mass spectrometer equipped with an ESI New Wave Research

UP193FX laser ablation system was used. The laser beam had a wavelength of 193 nm, 3 J/cm^2 energy density at a frequency of 10 Hz and a spot size of 45 µm. The NIST-612 synthetic glass was used as an external standard, adopting the average composition determined by Pearce et al. (1997); for the internal standard ^{43}Ca was used. Evaluation of the resulting data was carried out with LAMTRACE software. At Macquarie University, I used an Agilent 7700x quadrupole ICP-MS, and the laser ablation was carried out with a Photon Machines 193 nm Excimer laser system with a frequency of 5 Hz, energy density of 9.28 J/cm^2, and 50 µm spot size. The NIST 610 synthetic glass was used as external standard and CaO previously determined by electron microprobe as the internal standard. The resulting data were evaluated using the GLITTER time-resolved software package (Griffin et al., 2008). Xenoliths from the southern part were analyzed at the Institute of Isotope Geochemistry and Mineral Resources, ETH-Zürich (Zürich, Switzerland), using a coupled ELAN 6100 DRC quadrupole mass spectrometer equipped with an ArF excimer UV laser source. Wavelength of the laser beam was 193 nm, energy density was 52 mJ/cm^2 at a frequency of 10 Hz, and the spot size was between 40 and 60 µm. For the external standard the NIST SRM 610 synthetic glass was used; data processing was carried out with the SILLS software (Guillong et al., 2008).

Trace-element concentrations of bulk silicate melt inclusions were determined at the Department of Geosciences, Virginia Tech (Blacksburg, VA, USA), with the use of an Agilent 7500ce quadrupole ICP-MS coupled with an ArF Excimer Laser system. The laser acquisition parameters were: 193 nm wavelength, ~7 - 10 J/cm^2 energy density, 5 Hz repetition rate and 24 - 32 µm spot size. The ~ 1.5 cm^3 ablation cell was fast flushed with He gas at ~ 1.2 L/min; auxiliary Ar gas flow was at 1.03 L/min. For each isotope, a 10 ms dwell time was applied. For the external standard, the NIST-612 synthetic glass was used; average Ca concentration, previously obtained by mass-balance calculation for bulk SMIs from SEM-EDX analyses, was used for internal standard. This is applicable due to the overall low variability of major-element compositions in the SMIs analysed with FIB-SEM, which allows the assumption that all primary SMIs have similar geochemical compositions. Data reduction was carried out using the AMS software of Mutchler et al. (2008).

4.4. Raman Spectroscopy

Raman-spectroscopy analyses of selected silicate melt inclusions were carried out at the Research and Instrument Core Facility of the Faculty of Science at Eötvös University, Budapest. Both point analyses of constituent phases and imaging of three whole inclusions (SMI2, SMI_R and SMI_U) were applied in order to determine the distribution of phases in the melt inclusions. The instrument used was a confocal HORIBA Labram HR spectrometer with Nd:YAG 532 nm wavelength laser excitation and 600 or 1800 grooves/mm optical grating, 50-100 µm confocal hole, 5–80 s acquisition time and a 100x long working distance objective. Laser power was 130 mW at the source and ~50 mW under the objective; the laser spot diameter was measured to be 1.35 µm and the depth resolution was 1.73 µm. The spectral resolution was 0.7 cm^{-1} at 1398.5 cm^{-1} and 0.6 cm^{-1} at 2331 cm^{-1} (defined as the measured full width at half maximum values of two neon atomic emission lines). Both mapping and analyses of individual phases (where needed) were carried out in the spectral range of 220 to 1900 cm^{-1} first and then of 2750 to 4000 cm^{-1} for detection of OH-bonds in water-bearing phases. A reference Raman spectrum was collected from the host clinopyroxene near every analysed inclusion, using the same acquisition settings, for comparison and distinction from the effect of the host on the analysed daughter phases. Each analysis was conducted at room temperature. Processing of the acquired spectra (background and peak fitting using the Gaussian-Lorentzian sum profiles) was done using the LabSpec 5.25.15 software. For phase identification, I used the databases of Frezzotti et al. (2012) and the online database of rruff.info.

4.5. Focused Ion Beam - Scanning Electron Microscopy

The FIB-SEM technique was applied to four selected silicate melt inclusions in sample NFL1327, three of which has previously been mapped with Raman microspectroscopy, to further constrain the phase composition of the inclusions and to obtain robust volume ratios and major-element compositions of the constituents. The analyses were carried out in the Research and Instrument Core Facility at Eötvös University, Budapest, with the use of an FEI Quanta 3D dual beam scanning electron microscope equipped with both secondary- and backscattered-electron detectors, along

with a silicon drift (SDD) X-ray energy dispersive (EDX) detector. Note that the recently developed SDD-EDX technique has been shown to provide the same level of precision and accuracy as wavelength dispersive spectrometer (e.g., Ritchie et al., 2012). The acceleration voltage was 10-20 keV, depending on the size of the inclusion and the elements of interest. The beam current was 0.02 – 4 nA, which facilitates the detection of major elements from carbon through oxygen to barium.

The application of FIB-SEM is a relatively new technique in studying melt- and fluid inclusions, which provides a great opportunity to combine microscopic observations with geochemical analyses on the nanoscale. The general approach of the method is to mill through the inclusion step by step with the ion beam (maintaining a constant step size to be able to more precisely calculate the volume proportions of the phases), and to carry out SEM-EDX analyses for each slice as they are exposed. The ion beam is generated from a Ga source, and besides milling, it can also be used for imaging similarly to the SEM. The method applied follows the description of Berkesi et al. (2012) and is summarised as follows. After a precise documentation of the area on the carbon-coated surface of the thin section where the selected inclusion is located, a thin platinum layer of 200-300 nm is deposited with the electron beam, in order to identify the location after subsequent tilting. The sample needs to be tilted by 52°, so that the milling ion beam is perpendicular to the surface and the electron beam is at angle. Following the tilting, an additional platinum layer of approximately 1-2 μm needs to be deposited on the sample, which protects it from abrasion by the Ga-ion beam (Wirth, 2004). This process is followed by digging trenches on three side of the sample volume containing the inclusion (Fig. 4.1), to accommodate the waste material produced by the milling. For digging the trenches, a stronger beam current is used (15-45 nA), which leads to column-like structures on the trench wall; for better imaging during exposure of the inclusion slices, a lower beam current of maximum 4 nA is needed. Based on the size of the SMIs and the expected size of the daughter minerals, the distance between the slices was 400 nm during my analyses.

Identification of the phases within the SMIs was based on: (1) previously obtained Raman spectra, if any; (2) morphology on the secondary electron images; (3) brightness on the backscattered electron images, and (4) major-element contents deducted from the EDS spectra. Due to the small size of the daughter minerals, the EDS spectra generally contain mixed signals from the analysed phase and the adjacent area (host and/or other daughter phases). A spectrum of the host was collected at every slice where daughter

phases of the SMI were analysed, for comparison and better distinction of the signals. Volume proportions of the constituent phases were determined with Amira 5.2.2 software developed by Thermo ScientificTM; the method includes defining the daughter phases on each slice, then extrapolating the areas for acquiring phase volumes between the slices, producing a 3D reconstruction of the whole SMI.

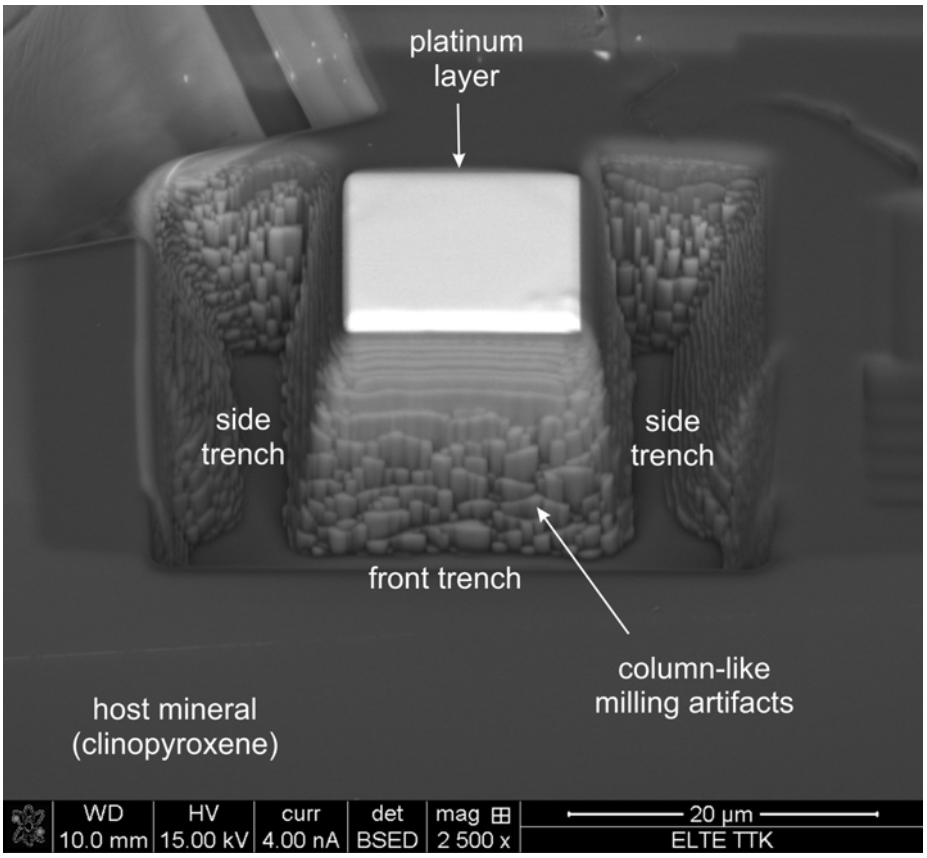

Fig. 4.1. Backscattered electron image of the sample volume containing SMI3, prepared for slicing with FIB after the deposition of the Pt-layer and digging of the surrounding trenches.

4.6. Electron Backscattered Diffraction

Crystal preferred orientation (CPO) of the rock-forming minerals was acquired by mapping the whole xenolith area (or as large area of it as possible) on the thin sections with the use of electron backscattered diffraction (EBSD) apparatus coupled with SEM. This required additional preparation including polishing with colloidal silica ('syton polishing') and carbon coating of the samples. The analyses were carried out at two laboratories. One part of the xenoliths was analysed at the Geochemical Analysis Unit at CCFS-GEMOC, Macquarie University, on a Zeiss EVO MA15 scanning electron microscope equipped with

an HKL NordlysNano EBSD detector, using AZtec analysis software (Oxford Instruments) with 20 kV accelerating voltage and a working distance between 12.5 and 25 mm. The other part of the samples was analysed at the University of Montpellier (Montpellier, France), using a JEOL JSM-5600 SEM coupled with an Oxford HKL Technology EBSD and HKL Channel 5 software package for mapping, with 17 kV accelerating voltage and 25 mm working distance. Step size for the mapping was chosen depending on the grain size, and ranged between 25 and 75 µm. Indexation rate varied between 55 and 92 %.

Post-acquisition data processing used the Tango program of HKL Channel 5 software package for all the xenoliths. The treatment followed the steps described by Soustelle et al. (2010):

1) Extrapolation applied to non-indexed pixels having 8 neighbours with identical orientation; then the extrapolation was repeated with 7, 6, then 5 identical neighbours.

2) Correction of systematic indexing errors in olivine caused by hexagonal pseudo-symmetry, which results in similar diffraction patterns for orientations differing by 60° around the [100] axis.

3) Grain recognition (grains were identified using a 15° misorientation cutoff, and subgrain boundaries using 2-15° misorientation angles) and removal of small grains with a diameter less than three times the step size.

For samples with recognisable foliation/lineation structure, oriented thin sections were prepared in a structural reference frame where lineation is directed E-W and the pole of foliation is directed N-S. For straightforward comparison of the samples, CPO data of randomly cut thin sections were rotated into this structural frame, marked by olivine [100] and [010] maxima aligning with E-W and N-S directions, respectively. Rotations were carried out using the PFch5 and ROTctf careware software of D. Mainprice (http://www.gm.univmontp2.fr/PERSO/mainprice/W_data/CareWare_Unicef_Programs/). On the pole figures, one-point-per-grain plotting was used in order to avoid overrepresentation of large grains. Crystal preferred orientation of olivine and pyroxenes was analysed in the studied xenoliths. CPO data of amphibole were insufficient due to its low abundance. Since pole figures are presented as one point per grain, a minimum of 100 grains is needed for representative and unbiased CPO (Ben Ismail and Mainprice, 1998).

To characterise fabric properties, different parameters such as the J-index, M-index, BA-index and grain orientation spread (GOS) were calculated for olivine in each xenolith, using the MTEX analysis toolbox (http://mtex-toolbox.github.io/) of Mainprice et al.

(2014) running in MATLAB (Hielscher and Schaeben, 2008). The J-index, used to describe fabric strength, is a dimensionless value, which is the volume-averaged integral of the squared orientation densities (Bunge, 1982) and ranges from 1 (random distribution) to infinity (single crystal orientation). Natural mantle peridotites exhibit J-indices between 2 and 20 (Ben Ismail and Mainprice, 1998), with a peak around 5 (Tommasi and Vauchez, 2015). The M-index (misorientation index), which is also used to characterise fabric strength, expresses the difference between the observed distribution of uncorrelated misorientation angles and that of an entirely random fabric (Skemer et al., 2005), and ranges from zero (random CPO) to 1 (single crystal). The GOS quantifies the extent of intragranular deformation, defining the average discrepancy between each measurement point and the mean orientation of the grain (Wright et al., 2011 and references therein). The GOS value for a whole xenolith is obtained by area-weighted averaging of all olivine grains. The calculation of the BA-index is based on the following equation:

$$BA = \frac{1}{2}\left(2 - \left(\frac{P_{010}}{G_{010} + P_{010}}\right) - \left(\frac{G_{100}}{G_{100} + P_{100}}\right)\right)$$

where P (point) and G (girdle) are used to characterise the shape of distribution for the [100], [010] and [001] axes of olivine and are calculated from the eigenvalues of the normalised orientation matrix (see Vollmer, 1990 for details). The BA-index ranges from 0 to 1, and distinct subranges are considered characteristic of the three most commonly observed olivine CPO. [010]-fibre symmetry (BA < 0.35) has a strong maximum of [010] axes perpendicular to the plane of foliation, whereas [100] and [001] axes are more scattered and tend to show a girdle distribution in the foliation plane, with the former usually displaying a stronger maximum subparallel to the lineation. Orthorhombic symmetry (0.35 < BA < 0.65) is characterised by strong point maxima of all three axes, with [100] having generally the highest concentrations. The [100]-fibre symmetry (BA > 0.65) displays point maxima of [100] axes parallel to the the lineation, where observable, whereas [010] and [001] axes form a girdle in a plane normal to the [100] maximum.

Seismic properties were calculated from the modal proportions and CPO data of olivine, orthopyroxene and clinopyroxene (Mainprice, 1990), using the ANISctfPC software of D. Mainprice. To avoid bias by individual samples, seismic properties of all xenoliths were averaged to obtain information as representative as possible for the subcontinental lithospheric mantle of the NGVF. To justify this, we assumed that foliation

and lineation of all samples have the same orientation, and therefore rotated CPO datasets were used for the calculations. This results in the presented seismic properties being a maximum estimate for the NGVF. During the calculations, a Voigt-Reuss-Hill averaging was applied. Elastic tensors for olivine, orthopyroxene and clinopyroxene were taken from Abramson et al. (1997), Jackson et al. (2007), and Isaak et al. (2006), respectively.

4.7. Fourier-Transform Infrared Spectroscopy

To analyse 'water' in nominally anhydrous minerals (NAMs), Fourier-transform infrared (FTIR) spectroscopy was performed on thin sections separated from the glass, in the Research Centre for Natural Sciences of the Hungarian Academy of Sciences, using a Varian FTS-60A spectrometer coupled to an UMA-600 IR microscope, and at the Geochemical Analysis Unit at CCFS, Macquarie University, using a ThermoFisher iN10 FTIR microscope. The analyses were done using unpolarised infrared light. Infrared spectra of olivine and pyroxenes were obtained between 4000 and 400 cm^{-1}, using a maximum of 100*100 μm aperture size. The samples were measured with a Globar light source, KBr beam-splitter and an MCT detector. At least 128 scans were accumulated from each spot with a 4 cm^{-1} resolution. During the measurements the sample chamber and the interferometer were constantly flushed with compressed air to reduce the background related to atmospheric moisture and carbon dioxide.

A recently developed method (Kovács et al., 2008; Sambridge et al., 2008) for unpolarised infrared light makes it possible to determine the concentration of 'water' from a small number (n>5) of unoriented anisotropic crystals with sufficient accuracy. This method may be applied for strongly anisotropic minerals such as olivine and pyroxenes only if the maximum linear unpolarised absorbance is less than 0.15, a criterion that was always met in this study. The total polarised absorbance (A_{tot}) is estimated as three times the average unpolarised integrated absorbance. The more unoriented grains that are considered for the calculation of the average integrated unpolarised absorbance (A_{tot}), the more accurate is the estimate. The A_{tot} for each NAM in each sample is obtained using the OPUS software, applying the following steps: (1) background correction using the concave rubber-band correction routine with 2 iterations and 64 baseline points; (2) averaging of spectra; (3) integration of spectral ranges of structurally bound 'water' with B-type integration. The A_{tot} is then converted to absolute concentration of 'water' (ppm,

wt %) using the calibration factors of Bell et al. (1995) for ortho- and clinopyroxene and Bell et al. (2003) for olivine. Concentration values are normalised to 1 cm thickness. The thickness of the sections was measured with a Mitutoyo analogue micrometer, which is accurate to 10 μm within the thickness range considered. Based on prior experience, the overall uncertainty in the absolute concentration of 'water' usually does not exceed 30 % (Kovács et al., 2008, 2012); however, this value can be higher in case of smaller grain numbers, or heterogeneity of mineral orientations within a sample.

Chapter 5. Results

5.1. Petrography

5.1.1. Texture classification

Textures of mantle peridotites, including the grain size, shape, distribution, orientation and relationship of the rock-forming phases can provide valuable information regarding the physical properties and processes (temperature, pressure, deformation, presence of melt and, sometimes, the history of overprints of multiple processes) of the mantle domain in question. Studies on classification of mantle rock textures (Mercier and Nicolas, 1975; Harte, 1977; Pike and Schwarzman, 1977) imply that fabrics reflect the deformation history and evolution of the upper mantle domain which the xenolith sampled. The evolution of different textures is generally regarded as being governed by recrystallisation processes, which can be dynamic or static (annealing). During dynamic recrystallisation, the strain energy of the aggregate is lowered through grain size reduction, resulting in the formation of neoblasts with little to no strain (Nicolas et al., 1973; Ross et al., 1980). After cessation of the deformation, and/or at increasing temperature, annealing can lead to grain growth and a further reduction of intragranular strain (e.g., Green et al., 1970). A subsequent deformation episode can re-start this process; and thus, a series of deformation processes can lead to a sequence of texture types representing the different stages of mantle evolution.

The widely applied texture classification of Mercier and Nicolas (1975) is based on such a sequence of deformation events. According to their system, protogranular textures represent the most pristine and undeformed mantle material. Characteristics of this texture type include relatively large grain size (~4 mm for olivine and orthopyroxene and ~1 mm for clinopyroxene and spinel), curvilinear grain boundaries, and the occurrence of spinel consistently adjacent to pyroxenes. Porphyroclastic texture, which develops from protogranular one via dynamic recrystallisation of part of the grains, displays a bimodal grain-size for olivine, orthopyroxene and rarely clinopyroxene. The coarser grains (porphyroclasts) commonly show internal strain features, curved boundaries and elongation to various extents, whereas the neoblasts are isometric, have straight grain boundaries and lack internal strain features. This texture can then evolve into the equigranular type, which

is characterised by overall fine grain size and straight boundaries joining in 120° triple junctions as a sign of textural equilibrium and annealing. Depending on whether the shape of the grains is isometric or elongated, equigranular textures were subdivided into mosaic and tabular equigranular types, respectively. According to Mercier and Nicolas (1975), annealing-induced static recrystallisation can lead to the formation of secondary versions of the described texture types, which are difficult to distinguish from the principal types by structural analysis alone.

In the Nógrád-Gömör Volcanic Field, the determination of textures is rather challenging, since the xenoliths bear imprints of both deformation and annealing. Previously, both Szabó and Taylor (1994) and Liptai et al. (2017) classified textures following the nomenclature of Mercier and Nicolas (1975). However, recent microstructural analyses have led to a slight modification in the approach of texture classification for the Nógrád-Gömör xenoliths. First, xenoliths determined as protogranular lack the presence of pyroxene-spinel clusters, as these constituents appear rather dispersed; thus, it is more accurate to use the term granular, as proposed by Lenoir et al. (2000) to distinguish from the sensu stricto protogranular texture of (Mercier and Nicolas, 1975). Second, bimodal grain size distribution is sometimes not displayed by orthopyroxene, but only by olivine, and the difference in grain size is not as striking as in the case of orthopyroxenes. However, microstructures (e.g., signs of intragranular deformation in coarser grains and the lack of them in finer-grained ones) warrant classification of these xenoliths as porphyroclastic. Grain size has a wide variability among the Nógrád-Gömör xenoliths of this study; therefore within both granular and porphyroclastic textures, a coarse- and a fine-grained subgroup was distinguished based on the area-weighted grain size, resulting in five texture types altogether: coarse granular (Fig. 5.1a-b), fine granular (Fig. 5.1c-d), coarse porphyroclastic (Fig. 5.1e-f), fine porphyroclastic (Fig. 5.1g-h), and equigranular (Fig. 5.1i-j).

Xenolith textures appear in different proportions in the different domains of the Nógrád-Gömör Volcanic Field (Table 1). Samples from localities in the northern part show dominant granular textures (62 %, consisting of 31% of both coarse and fine granular) with a smaller proportion of porphyroclastic textures (38 %, with 7 % and 31 % of coarse and fine porphyroclastic, respectively). In the central part, porphyroclastic textures are slightly more abundant (47 %, with 20 % and 27 % of coarse and fine subgroups, respectively) than granular ones (43 %, with 23 % and 20 % of coarse and fine-grained

textures, respectively), and a small proportion of equigranular textures (10 %) is also present. In the northern and central parts, both coarse- and fine-grained microstructures are observed. In the southern part, grain size is significantly smaller, and the textures are fine porphyroclastic and equigranular (50%-50%).

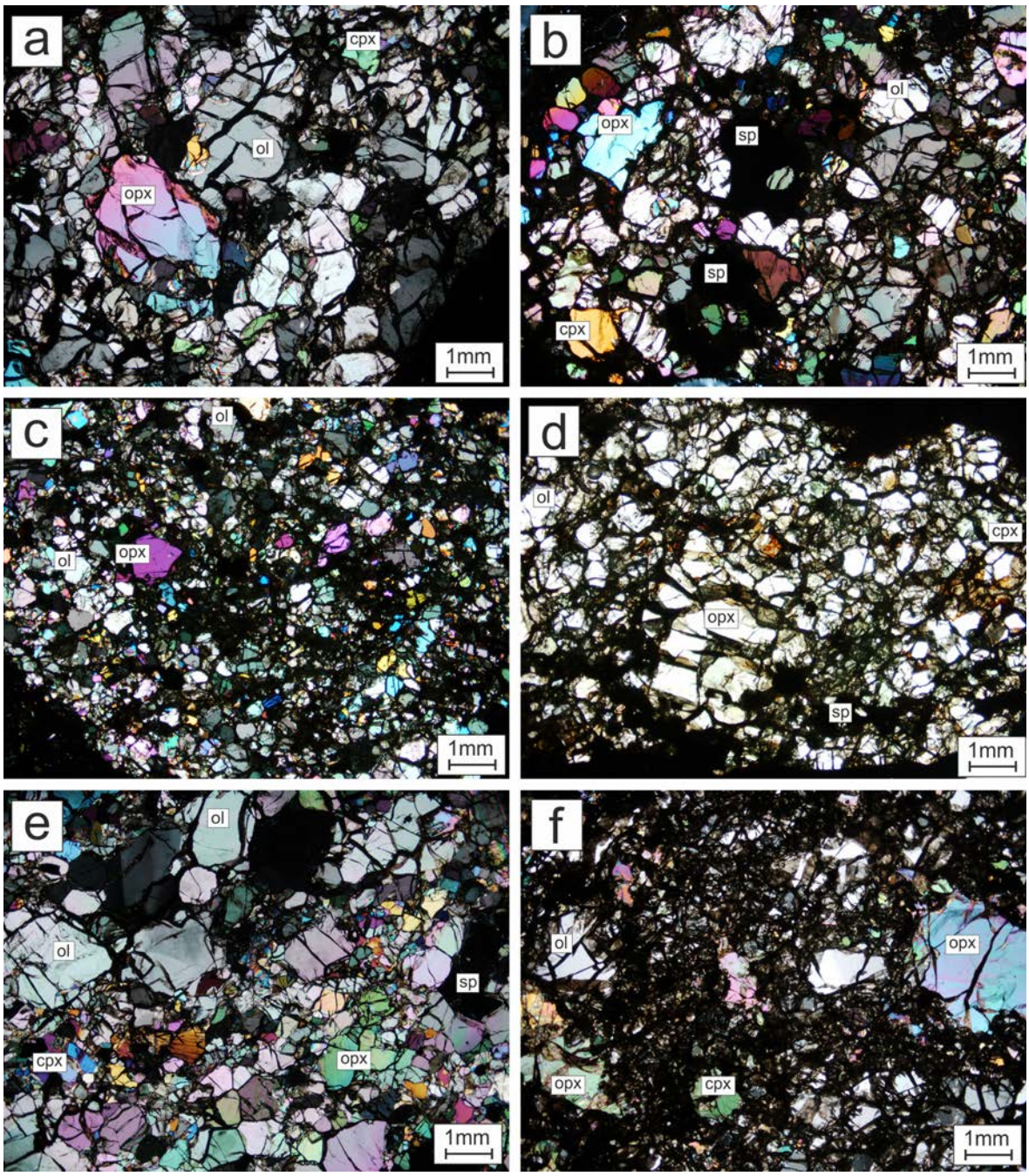

Fig. 5.1. Photomicrographs of characteristic textural types among the studied Nógrád-Gömör xenoliths. a, b – coarse granular; c, d – fine granular; e, f – coarse porphyroclastic; g, h – fine porphyroclastic; i, j – equigranular. Note that coarse and fine texture types were distinguished based on the area-weighted average grain sizes. All photos are in crossed polars transmitted light, except i, which is plane polarised.

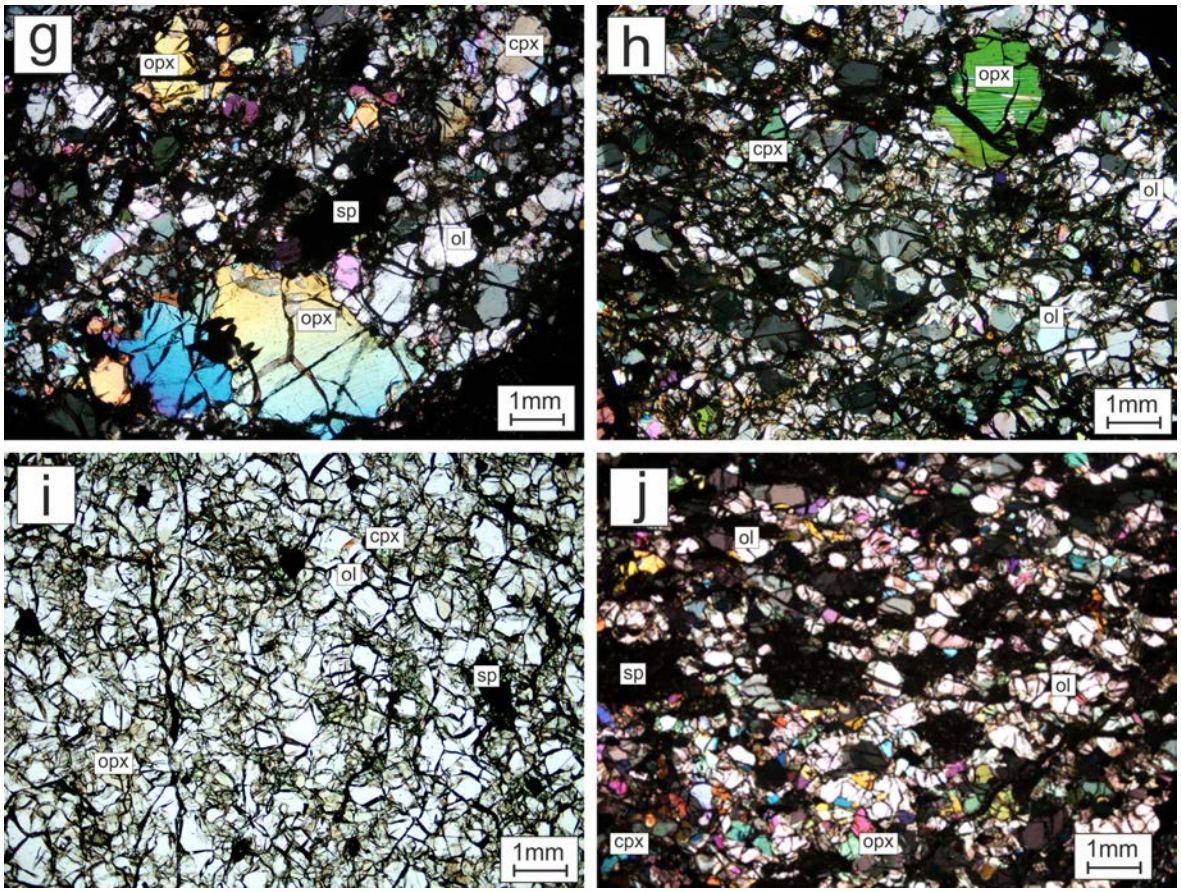

Fig. 5.1. Continued.

5.1.2. Modal compositions

In addition to point counting, modal ratios of the mineral constituents were also acquired during EBSD mapping. The results of the two methods are in good agreement (Fig. 5.2), with differences usually being around or below 5 % for olivine and pyroxenes, and reaching a maximum of 10-15 % only in a few cases. There are several reasons for these discrepancies:

• Difference in the thin-section area taken into consideration: during point counting on the scanned images the whole xenolith area was counted, whereas although EBSD analyses were aimed at analysing as much of the xenolith surface as possible, it could not reach 100 % in all of the samples due to instrumental limitations.

• Imperfect indexation: due to polishing issues, orthopyroxenes occasionally had a lower indexation rate compared to olivines, which led to underestimation of their modal proportion.

• Quality of the scanned thin-section image: if the colours of the different silicate

phases are not clearly distinguishable (e.g., the thin section is too thin), identification of the minerals becomes less precise during point counting.

Although modal compositions acquired with EBSD are generally considered to be more precise, the first two issues are present in many of the samples (see Appendix C for EBSD phase maps). Thus, modal proportions determined with point counting are accepted for further interpretation and calculations (e.g., whole-rock compositions).

The xenoliths consist of olivine, orthopyroxene, clinopyroxene and spinel, and rarely, minor amphibole. Szabó and Taylor (1994) reported phlogopite in two xenoliths, but it is completely absent in my sample set. According to the classification of rock types based on modal compositions (Streckeisen, 1975), xenoliths of this study are dominantly lherzolites, with subordinate amounts of harzburgite, dunite and wehrlite due to the variability in the ratio of ortho- and clinopyroxene (Fig. 5.3). Note that wehrlites in this sample set are still part of the 'lherzolitic' suite, as their orthopyroxene content (e.g., NFL1327; see Table 1) and/or textural features (NFL1326; see Appendix A) do not fit the 'wehrlitic' suite which, as mentioned earlier, bears clear petrographic evidence of melt/wall-rock reaction (Patkó et al., 2013). Fig. 5.3 shows that this xenolith set displays a wider compositional range than that of Szabó and Taylor (1994), and a significant part of the samples have higher olivine (and to a lesser extent, clinopyroxene) contents compared with the field of the average European sublithospheric mantle (SCLM) composition published by Downes (1997).

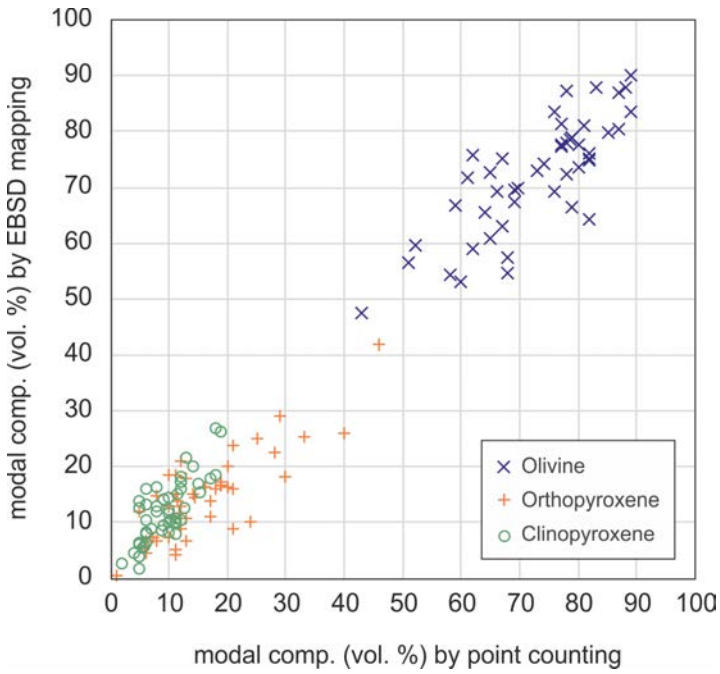

Fig. 5.2. Comparison of modal compositions of the studied xenoliths acquired with point counting method vs. EBSD mapping.

Sample	Rock name	Texture	Modal composition (%)					opx/cpx	Melt pockets*	Equilibration temperature (°C)			
			ol	opx	cpx	sp	amp			TT98	TBK90	TNG10	TREE
Northern part													
NMS1302A	lhz	fine porph	89	5	5	1		1.0	-	851	863	928	1021 ± 41
NMS1304	lhz	fine porph	80	12	6	1	1	2.0	-	829	845	921	1030 ± 29
NMS1305	lhz	fine gr	62	25	9	4		2.8	-	870	918	942	1044 ± 50
NMS1308	lhz	porph	69	20	9	2	< 1	2.2	-	861	926	930	980 ± 9
NMS1310	lhz	coarse gr	43	46	11	0		4.2	-	884	953	974	1027 ± 1
NJS1302	lhz	fine porph	73	14	11	2	< 1	1.3	-	864	962	961	1063 ± 38
NJS1304	lhz	coarse gr	80	12	5	3		2.4	-	855	944	961	1052 ± 23
NJS1306	lhz	coarse gr	66	13	17	4		0.8	< 5 %	977	1025	1043	1145 ± 2
NJS1307	lhz	coarse gr	69	17	12	2		1.4	-	947	1024	1006	1097 ± 18
NPY1301	lhz	fine gr	79	13	6	2		2.2	-	867	941	952	999 ± 17
NPY1310	lhz	fine gr	68	11	18	3		0.6	-	893	936	967	1070 ± 15
NPY1311	lhz	fine porph	60	19	19	2		1.0	-	900	944	970	1052 ± 23
NPY1314	lhz	fine gr	51	28	18	3		1.6	-	861	928	958	1040 ± 15
Central part													
NFL1302	lhz	fine gr	77	10	8	5	< 1	1.3	-	885	926	967	1031 ± 4
NFL1305	lhz	fine gr	58	29	12	1		2.4	< 5 %	904	940	971	1070 ± 56
NFL1315A	hzb	fine porph	89	8	2	1	< 1	4.0	-	862	901	969	991 ± 42
NFL1316	lhz	fine porph	82	10	5	3		2.0	-	860	892	959	965 ± 10
NFL1324	lhz	porph	52	40	5	1.5	1.5	8.0	-	896	938	991	1030 ± 39
NFL1326	wht	equi	85		12	1	2	-	-	n.a.	n.a.	n.a.	n.a.
NFL1327	wht	equi	88	1	10	1		0.1	-	925	952	1019	1112 ± 21
NFL1329	lhz	fine gr	76	12	12	1	< 1	1.0	-	889	932	965	1013 ± 10
NTB0306	lhz	fine gr	79	12	10	0.1		1.2	-	947	994	951	901 ± 1
NTB0307	lhz	fine porph	79	6	15	0.1		0.4	< 5 %	1012	1058	943	991 ± 4
NTB1124	lhz	coarse gr	62	24	12	2		2.0	-	938	993	1001	1031 ± 22
NTB1116	lhz	coarse gr	67	21	10	2		2.1	-	908	970	980	1015 ± 3
NTB1122	lhz	coarse gr	64	19	15	2		1.3	-	942	999	1044	1154 ± 32
NFK0301	lhz	porph	78	16	6	0.1		2.9	< 5 %	949	996	984	1045 ± 21
NFK1123	lhz	fine gr	61	33	5	1		6.6	-	941	985	983	1022 ± 23
NFK1108	lhz	porph	87	6	6	1		1.0	-	950	996	1044	1141 ± 23
NFK1115	lhz	equi	87	8	4	1		2.0	-	874	913	972	1028 ± 26
NFR0306	wht	coarse gr	88	1	9	2		0.1	-	922	966	1031	1080 ± 17
NFR0307	lhz	porph	79	8	10	3		0.8	-	842	869	972	962 ± 17
NFR1109	lhz	coarse gr	77	17	5	0.5		3.4	-	972	1010	1022	1056 ± 26
NFR0309	lhz	fine porph	67	19	12	2		1.6	-	883	955	977	1047 ± 25
NFR1107	lhz	porph	74	18	7	1		2.6	-	894	952	985	1021 ± 15
NMC1301	lhz	coarse gr	82	11	5	2		2.2	-	912	958	1000	1066 ± 24
NMC1309	lhz	coarse gr	78	6	14	2		0.4	-	910	942	990	1068 ± 15
NMC1322	lhz	fine porph	77	12	8	3		1.5	5 - 10 %	895	944	969	988 ± 38
NMC1336A	lhz	fine porph	68	21	8	3		2.6	< 5 %	894	961	980	1037 ± 17
NMM1126	lhz	porph	59	30	10	1		3.0	-	933	974	983	990 ± 19
NMM0318	lhz	fine porph	65	20	13	2		1.5	-	913	951	983	1071 ± 31
NMM1115	lhz	fine porph	82	10	6	2		1.7	-	865	912	957	997 ± 19
NME1122	lhz	coarse gr	78	11	11	0.5		1.0	-	916	968	968	958 ± 5
NME0528	lhz	fine gr	82	11	6	1		1.8	-	898	947	984	1059 ± 25
NME1116	lhz	porph	65	21	11	3		1.9	< 5 %	892	947	984	1027 ± 41
Southern part													
NBN0302A	lhz	fine porph	83	11	5	1		2.0	< 5 %	867	902	932	1011 ± 4
NBN0305	lhz	equi	79	15	6	0.1		2.4	-	893	912	933	1028 ± 59
NBN0311	lhz	fine porph	81	7	10	1		0.7	< 5 %	858	917	922	965 ± 28
NBN0316	lhz	equi	79	11	9	1		1.3	5 - 10 %	898	912	941	1122 ± 50
NBN0319	lhz	equi	70	16	13	1		1.3	> 10 %	886	888	941	1114 ± 51
NBN0321	lhz	fine porph	76	13	10	1		1.3	< 5 %	869	924	946	930 ± 8

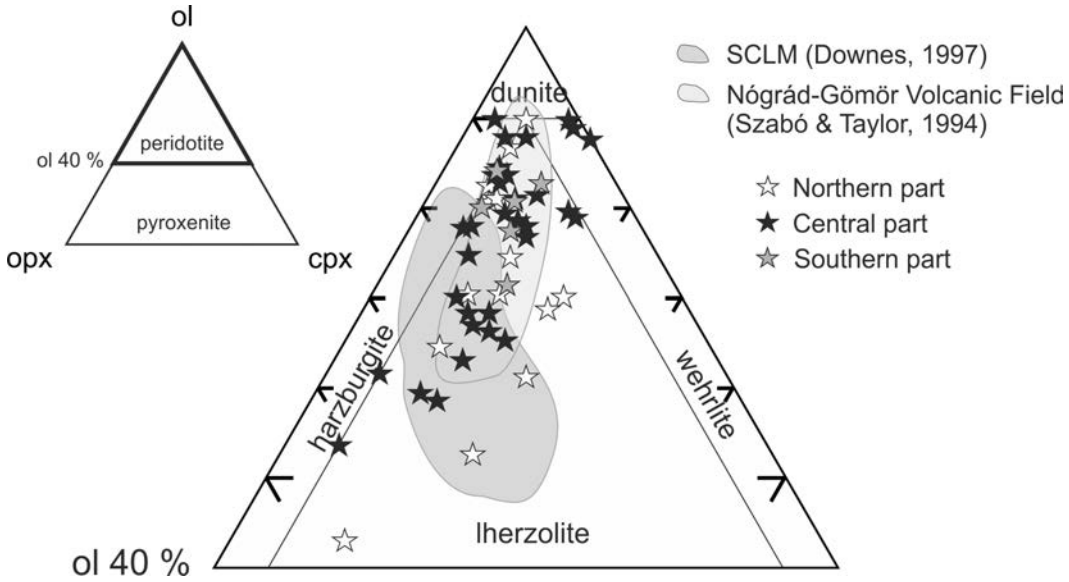

Fig. 5.3. Modal compositions of the xenoliths from different regions of the Nógrád-Gömör Volcanic Field (this study), compared to the peridotite xenoliths of Szabó and Taylor (1994) and the SCLM.

Olivine

Olivine comprises 47-90 vol. % of the studied xenoliths (Table 1). The grains are generally isometric and their size ranges from 0.1 to 1.5 mm across; some porphyroclasts reach 2-3 mm in diameter. In some xenoliths (NFL1315A, NFL1316, NMM1115, NBN032A, NBN0321), a heterogeneous distribution of olivine and pyroxenes is observed. In these samples, olivine grains tend to be larger in pyroxene-poor or pyroxene-free areas within a xenolith (Fig. 5.4a). Rarely, olivine grains are elongated up to aspect ratios of 3:1 and define a lineation (Fig. 5.4b), particularly in xenoliths from the southern part. Undulose extinction (Fig. 5.4c), a sign of high dislocation density and alignment of the grains, occurs in olivine from all studied xenoliths. In some cases, olivine contains euhedral or anhedral inclusions of spinel (Fig. 5.4d), providing evidence of grain growth (Mercier and Nicolas, 1975). However, olivine can also be included in orthopyroxene (Fig. 5.4e), which has been described in previous studies as having a poikilitic character (e.g., Frey and Prinz, 1978; Downes et al., 1992).

Table 1. Petrographic properties and equilibration temperatures of the studied Nógrád-Gömör xenoliths. Abbreviations: ol - olivine; opx - orthopyroxene; cpx - clinopyroxene; sp – spinel; lhz – lherzolite, hzb – harzburgite, wht – wehrlite; gr - granular, porph - porphyroclastic, equi – equigranular. *not included in modal compositions; n.a. - not applicable due to lack of orthopyroxene analyses; TT98 - two pyroxene method of Taylor, 1998; TBK90 - two-pyroxene method of Brey & Köhler, 1990; TNG10 - Ca-in opx method of Brey & Köhler, 1990, modified by Nimis & Grütter, 2010; TREE - REE method of Liang et al., 2013.

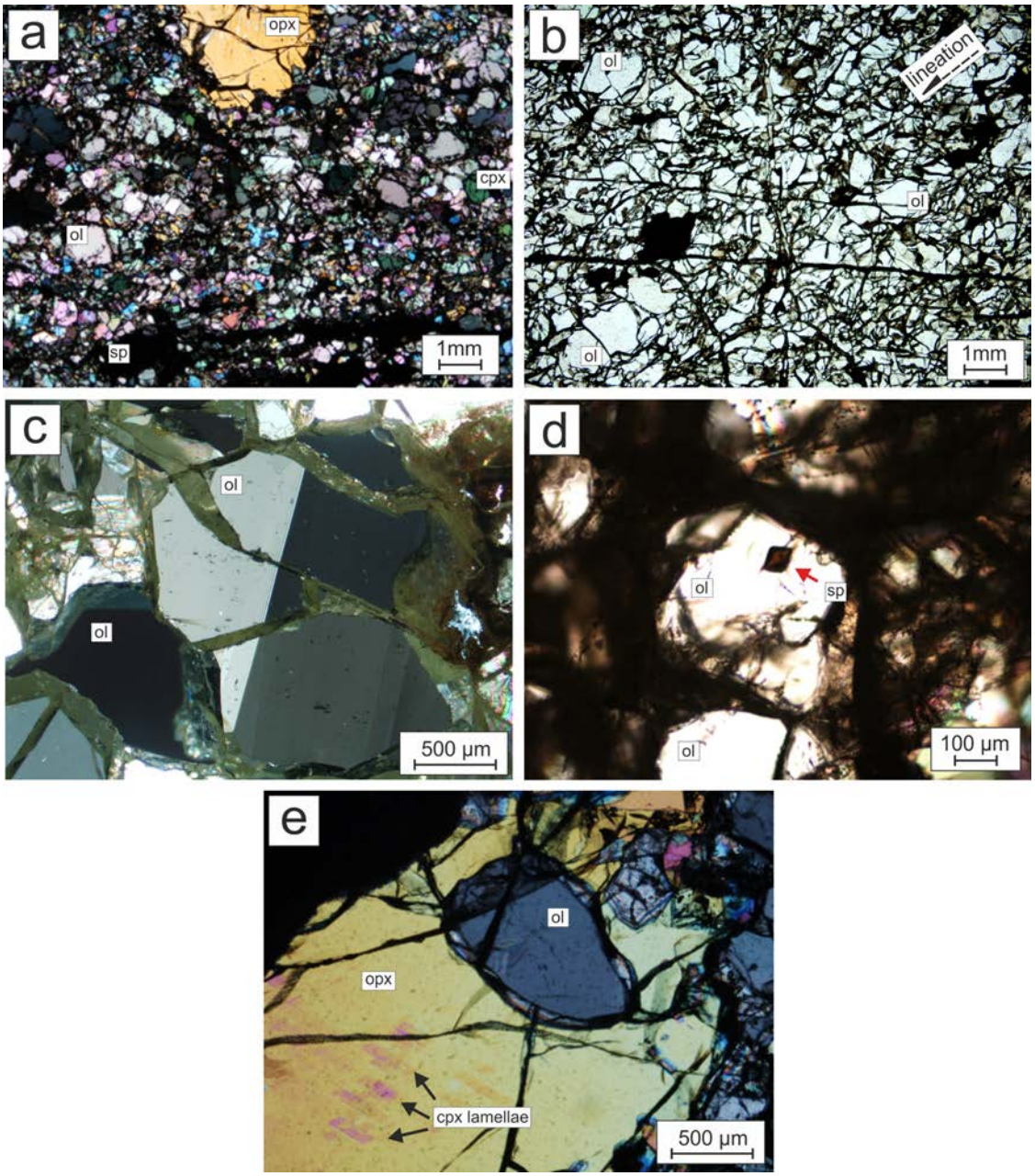

Fig. 5.4. Photomicrographs of characteristic microstructures in olivine: a – heterogeneous olivine grain size in pyroxene-rich and pyroxene-free domains in xenolith NBN032A; b – elongated olivine grains outlining lineation in xenolith NMS1304; c – undulose extinction in deformed olivine grains in xenolith NFK1108; d – spinel inclusion in olivine in xenolith NBN0311; e – olivine inclusion in orthopyroxene in xenolith NFK1123. Photos are taken under crossed polars (a, c, e), or plane-polarised (b, d) transmitted light. Abbreviations: ol – olivine, opx – orthopyroxene, cpx – clinopyroxene, sp – spinel.

Orthopyroxene

Orthopyroxene represents 1–42 vol. % of the studied xenoliths (10–25% for the majority of samples; Table 1), and is completely absent in one xenolith (NFL1326). Orthopyroxene grain sizes are similar to those of olivine, except for the porphyroclasts,

which are usually larger (up to 5–6 mm). Orthopyroxene porphyroclasts are commonly surrounded by dynamically recrystallized neoblasts. The porphyroclasts have curvilinear grain boundaries and occasionally contain clinopyroxene exsolution lamellae (Fig. 5.5a-b), as well as inclusions of spinel and/or olivine (Fig. 5.4e). Orthopyroxene neoblasts are isometric, usually between 0.1 and 0.8 mm, and have straight grain boundaries in contrast to the porphyroclasts.

Clinopyroxene

Clinopyroxene grains are smaller (50 µm to 1 mm) than orthopyroxene grains, make up 3–27 vol. %, of the xenoliths, and only rarely appear as porphyroclasts or as inclusions in poikilitic orthopyroxene (Fig. 5.5c). In xenolith NBN0311 a clinopyroxene porphyroclast contains exsolution lamellae of spinel. The opx/cpx ratio varies between 0.1 and 6.6 (Table 1); ratios below 1.5 are considered unusually clinopyroxene-rich for the average SCLM composition (Downes, 1997). One xenolith from the monogenetic volcano of Fil'akovo-Kerčik in the central part (NFL1327) contains fine-grained clinopyroxene-rich patches similar to those of the wehrlitic series, however, unlike them, it contains a small amount of orthopyroxene grains as well (Fig. 5.5d). A few xenoliths from the southern part (NBN035, NBN0311, NBN0321), as well as the above-mentioned xenolith from Fil'akovo-Kerčik (NFL1327), contain several clinopyroxene grains which host partially crystallised silicate melt inclusions.

Spinel

Spinels are mostly interstitial, slightly elongated, and may be enclosed in the silicate phases (Fig. 5.4d). Interstitial spinels usually have curved grain boundaries ('holly leaf spinel'; Fig. 5.6a). They appear in the lowest abundance, from only a trace amount up to a maximum of 3 vol. %. In some samples, the shape and distribution of spinel grains outline a lineation (Fig. 5.6b), matching the stretching lineation defined by olivine where present. Some spinel grains show a spongy, partially reacted appearance (Fig. 5.6c).

Amphibole

Amphibole is present in some of the xenoliths from two locations in the northern part (Mašková and Jelšovec) and from the monogenetic volcano of Fil'akovo-Kerčik in the central part. In the locality of Jelšovec, only one xenolith contains amphibole, as two

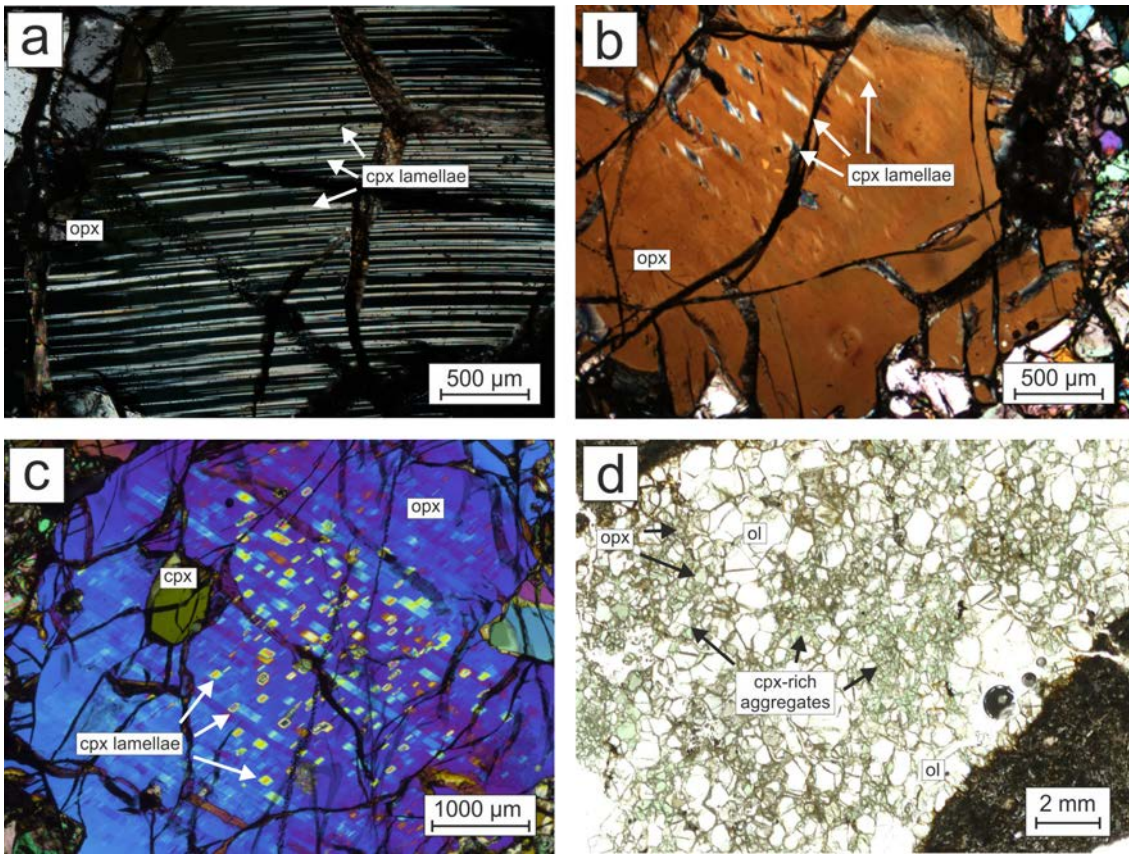

Fig. 5.5. Characteristic microstructures in pyroxenes. a, b – clinopyroxene exsolution lamellae in orthopyroxene porphyroclast in xenoliths NMC1336A and NBN032A, respectively; c – poikilitic clinopyroxene inclusion, as well as exsolution lamellae in an orthopyroxene porphyroclast in xenolith NFL1324; d – clinopyroxene-rich aggregates in an orthopyroxene-containing wehrlite (xenolith NFL1327). Photos are taken in crossed-polars transmitted light (a, b, c); part of a scanned thin section image (d). Abbreviations as in Fig. 5.4.

small grains (0.1-0.2 mm in diameter). In the remainder of the xenoliths, the amphibole abundance is also low, reaching a maximum of only 2 vol. % (Table 1). They appear interstitially (Fig. 5.6d) or form veins (Fig. 5.6e). Rarely, they are partially melted (Fig. 5.6f). There is no modal amphibole in the other localities of the central and southern part in this sample set; however, Szabó and Taylor (1994) described some xenoliths from both the central and southern part with a significant amphibole content (2-4 vol. %).

Melt pockets

Several xenoliths – mainly from the southern part – contain melt pockets with an average size of 0.5 – 1.5 mm. They are aligned subparallel to the lineation (Fig. 5.6g), where observable, and consist of glass and a secondary generation of clinopyroxene and spinel (Fig. 5.6h). Their volume proportion is estimated to be usually below 5 %, but in

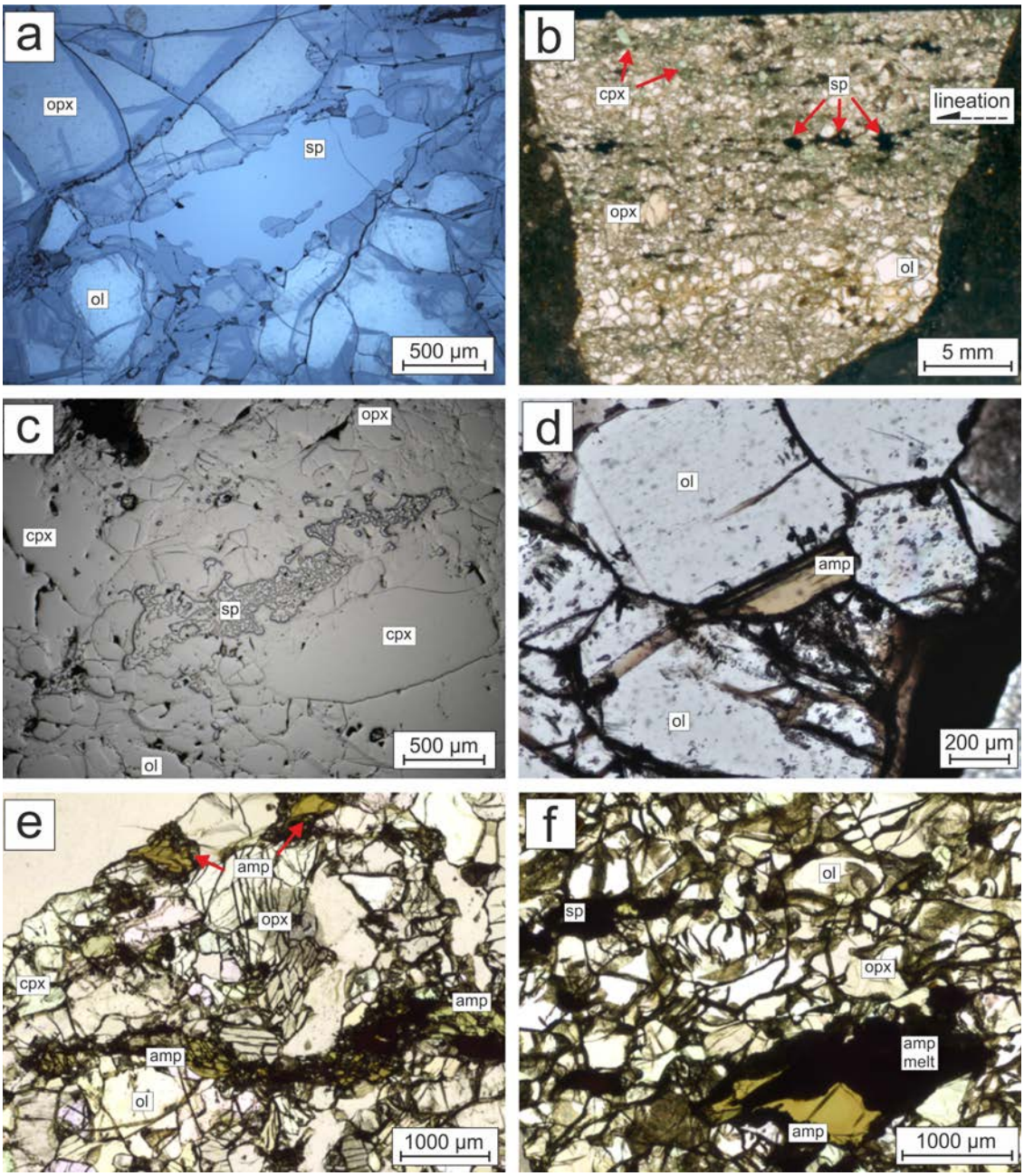

Fig. 5.6. Characteristic appearance of spinel, amphibole and melt pockets. a – 'holly leaf' shaped spinel in xenolith NMM1126 (reflected light); b – lineation outlined by distribution of spinel grains in xenolith NBN0321 (scanned thin section image); c – 'sponge-like' partially molten spinel in NBN0311 (reflected light); d – amphibole grain in an interstitial position in xenolith NFL1315A (plane-polarised transmitted light); e – amphibole veinin xenolith NFL1324 (plane-polarised transmitted light); f – partially molten amphibole in xenolith NMS1304 (plane-polarised transmitted light); g – lineation outlined by the distribution of melt pockets in xenolith NBN0319 (scanned thin section image); h – constituent phases of a melt pocket in xenolith NMC1322 (reflected light). Abbreviations: ol – olivine, opx – orthopyroxene, cpx – clinopyroxene, sp – spinel, amp – amphibole, mp – melt pocket, gl – glass.

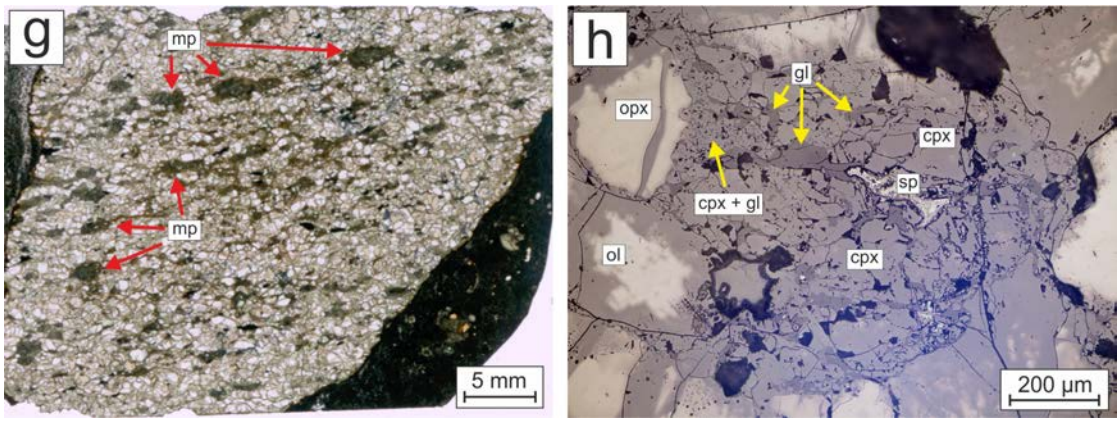

Fig. 5.6. Continued.

a few samples, it is higher (Table 1). Melt pockets were not taken into account when determining the mode of the xenoliths.

5.2. Geochemistry of Minerals and Whole-Rocks

5.2.1. Mineral major-element geochemistry

Major-element oxide compositions of olivine, orthopyroxene, clinopyroxene, spinel and amphibole are presented in Table 2. The most striking feature of these mineral major-element compositions is the variability in their Mg-number ($Mg/[Mg+Fe^{2+}]$). Mg-numbers of olivine lie between 0.85 and 0.91, with most of the xenoliths exhibiting high Mg# (0.90-0.91). However, several samples from the northern and central part show significantly lower values (between 0.85 and 0.88) (Fig. 5.7a), and six of them (NFL1326, NFL1327, NFK1115, NFR0306, NFR0307 and NFR1109) plot outside the olivine-spinel mantle array (OSMA; Arai, 1994). Note that legend on Fig. 5.7 depicts the geochemical classification carried out using criteria for both major- and trace-element compositions as detailed in 5.2.2 below. Manganese contents in olivine show a negative correlation with Mg# (Fig. 5.7b), reaching the highest values (0.23-0.26 wt%) in the xenoliths with the lowest Mg#. However, the Mn values show little variation for xenoliths with the 'normal' Mg# range (0.89-0.91).

Orthopyroxenes have CaO contents between 0.63-0.98 wt% and Al_2O_3 between 1.86-5.00 wt%. The lowest Al_2O_3 contents in orthopyroxene occur in xenoliths NMS1302A, NFL1315A, NTB0306, NFK1115, and NFR1109, which are the samples with the highest

spinel Cr# in Fig. 4a. Mg-numbers of orthopyroxene (0.86 – 0.91) correlate well with those of olivine, as well as MnO contents, which show elevated values (0.21-0.27 wt. %) in the three NFR samples mentioned above. Concentrations of Al_2O_3 generally show a broad correlation with Mg# (Fig. 5.7c), except for xenoliths with low Mg# (NFL1327, NFK1115, NFR0306, NFR0307, and NFR1109), which lie off the trend.

Al_2O_3 contents in clinopyroxene range from 2.57 to 7.64 wt%, and Na_2O contents range from 0.37 to 2.06 wt%. Xenoliths from the northern part tend to have higher concentrations of Na and Al than those from the central and southern parts. Al_2O_3 and Na_2O show a good positive correlation in most of the samples; however, one group of xenoliths defines a different trend, with decreasing Al content, while Na varies only in a narrow range (Fig. 5.7d). These xenoliths (NFL1315A, NFL1316, NTB0306, NFK1115, and NFR1109) overlap with the ones exhibiting the highest spinel Cr# (Fig. 5.7a). Equigranular xenoliths from the southern part of the study area characteristically have lower values of both elements compared with the porphyroclastic ones from the southern part. Mg-numbers of clinopyroxene vary between 0.86 and 0.94 and correlate well with those of olivine and orthopyroxene.

Spinel Cr# [Cr/(Cr+Al)] shows a wide range, from 0.06 to 0.54. Xenoliths with the highest spinel Cr# (above ~0.3) are the same ones that show the unusual Al-Na trend in clinopyroxene mentioned above, and some of them also have low olivine Mg# (Fig. 5.7a). Mg and Fe contents of spinel also display a broad range, with the highest FeO_{tot} values (20.3-24.3 wt%) occurring in xenoliths NFL1326, NFL1327, NFK1115, NFR0306 and NFR1109, which are also characterized by low Mg#. The Al-Cr trend in spinels is also demonstrated in the Al-Cr-(Ti*100) diagram (Fig. 5.7e). Furthermore, Fig. 5.7e elevated Ti contents in the xenoliths with high FeO contents and low #Mg. Variations between grains within the same xenolith are insignificant compared with differences between the average values of different samples.

Amphibole is mainly magnesio-hastingsite based on the classification of Locock (2014). The only exception is NJS1302, where the two amphibole grains are different in composition and are ferri-kaersutite and Ti-rich magnesio-hastingsite, due to their high TiO_2 content (8.09 and 4.24 wt. %, respectively) compared with the other samples, which have TiO_2 concentrations between 1.38 and 2.01 wt %. K_2O is higher in the more Cr_2O_3-rich samples: the highest values (1.13, 1.09 and 1.17 wt %) occur in the same xenoliths (NMS1304, NFL1315A and NFL1324, respectively) as the highest Cr_2O_3 concentrations

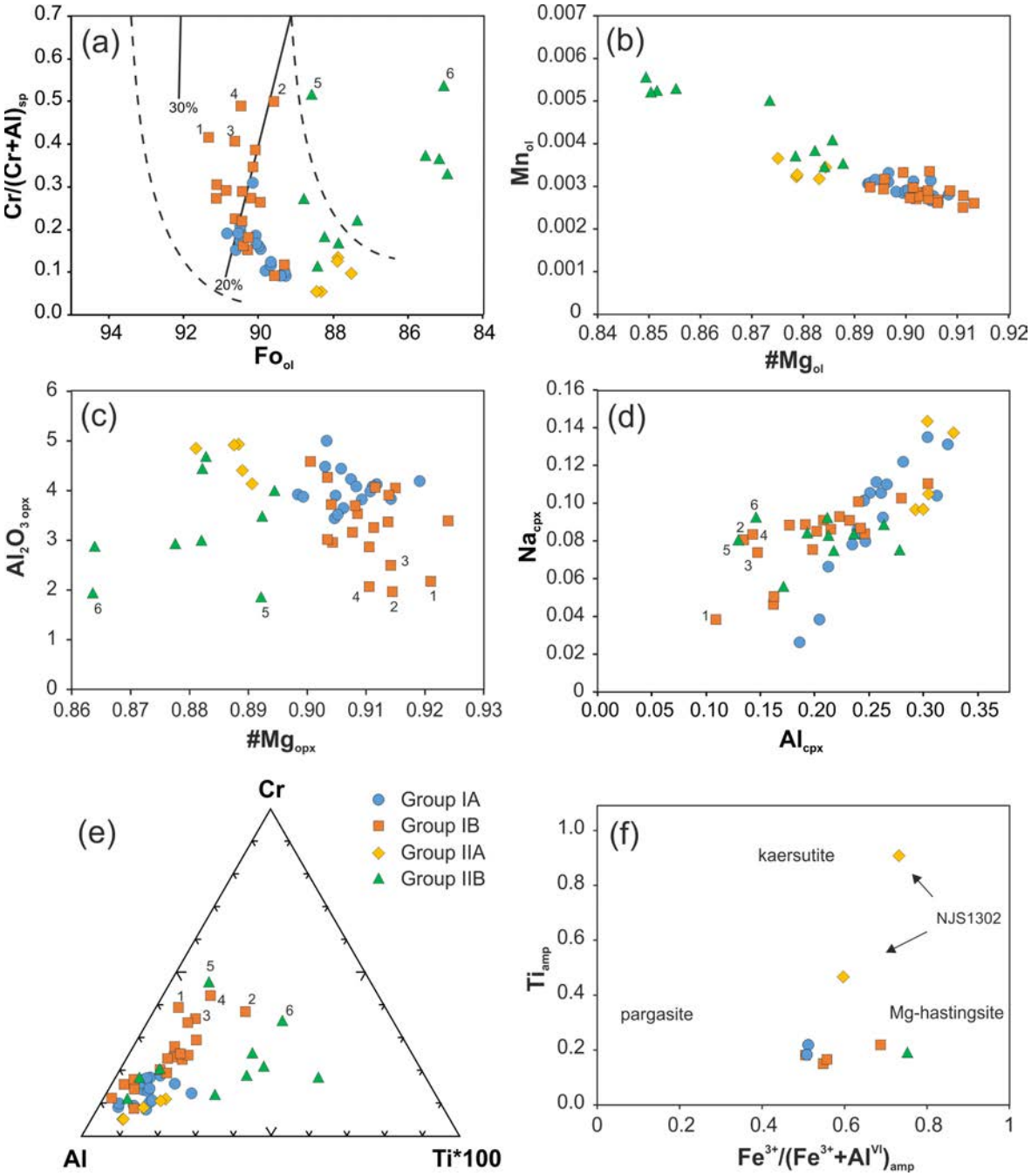

Fig. 5.7. Major-element compositions of minerals in the NGVF xenoliths. a – OSMA (olivine-spinel mantle array: forsterite contents in olivine *vs* Cr-number [Cr/(Cr+Al)] of spinel). Average composition of spinels from the upper mantle falls between the dashed lines (Arai, 1987); some Group II xenoliths plot outside this field. Solid lines represent calculated degrees of partial melting (Arai, 1994). b - Relationship of #Mg and Mn (cation numbers) in olivine, showing a positive correlation. c – Mg# *vs* Al_2O_3 in orthopyroxene. d - Al *vs* Na cation numbers in clinopyroxene. e – Al-Cr-(100*)Ti contents of spinels; f - $Fe^{3+}/(Fe^{3+}+Al^{VI})$ *vs* Ti cation numbers of amphibole, with nomenclature. Cation numbers were calculated using the spreadsheet of Locock (2014). Labelled samples: 1 - NMS1302A; 2 - NFL1315A; 3 - NFL1316; 4 - NTB0306; 5 - NFK1115; 6 - NFR1109.

(1.76, 2.18 and 2.03 wt. %, respectively). Amphibole in xenolith NJS1302 also shows lower Cr_2O_3 and higher FeO than the others. Compositional differences in the amphiboles of the distinct samples are depicted on Fig. 5.7f in terms of Fe^{3+}, Al^{VI} and Ti (follows principles of classification by Leake et al., 1997).

Since modal compositions and textural types show no visible link with geochemical characteristics, a division based on major-element geochemistry has been carried out. Based on the Mg# of olivine and pyroxenes, two major groups can be distinguished. Group I is characterized by olivine Mg# = 0.89-0.91 (usual lherzolitic mantle composition; Arai, 1994) and shows a normal mantle-depletion trend in terms of spinel Cr# and the relationship of Na and Al in clinopyroxene. Group II xenoliths have Mg# lower than 0.89, an enrichment in Fe and Mn most striking in olivine and orthopyroxene, and in some cases, elevated Ti-content in spinel. The latter xenoliths occur in the northern and central parts of the Nógrád-Gömör Volcanic Field.

5.2.2. Trace-element geochemistry of pyroxenes and amphibole

Trace-element contents of clinopyroxenes and orthopyroxenes (Table 3) were measured in order to determine if there is any signature of cryptic metasomatism and/ or partial melting processes that would provide further insights into the evolution of the SCLM beneath the area. Trace-element contents are highly variable in the xenoliths and show no obvious relationship to major-element concentrations, allowing further subdivision of Group I and II xenoliths based on trace-element compositions and REE patterns.

In general, highly incompatible trace elements, such as Ba and Pb, as well as the compatible Co and Ni show low values compared to the primitive mantle (McDonough and Sun, 1995) in both pyroxenes. The less incompatible high field strength (HFS) elements, such as Zr, Hf and Ti show negative peaks in clinopyroxene and positive peaks in orthopyroxene, whereas Nb and Ta are depleted in both pyroxenes compared to LREE, on the primitive mantle (PM) normalized multi-element diagrams (Fig. 5.8a-h). In contrast, Th and U are more enriched compared to LIL elements in almost all xenoliths. The compatible elements, particularly Sc and V, show a very narrow range in all samples.

Rare-earth elements, especially LREE, are highly variable in both Group I and Group II xenoliths. Clinopyroxene La_n/Lu_n ratios range from 0.20 (xenolith NMC1336A)

Table 2. Major-element compositions of the rock forming minerals. n.o.a. - number of analyses; n.d. - not detected.

OLIVINE

Sample	Group	n.o.a.	SiO_2	Al_2O_3	FeO	MnO	MgO	CaO	NiO	Total	Mg#
Northern part											
NMS1302A	Group IB	22	41.6	n.d.	8.47	0.13	50.1	0.05	0.40	100.70	0.91
NMS1304	Group IB	14	41.2	0.03	9.42	0.13	48.7	0.05	0.40	99.84	0.90
NMS1305	Group IB	19	41.1	0.03	10.4	0.14	48.5	0.06	0.41	100.64	0.89
NMS1308	Group IA	16	41.1	n.d.	9.60	0.14	48.8	0.05	0.41	100.13	0.90
NMS1310	Group IA	11	40.9	0.04	9.83	0.14	49.3	0.06	0.40	100.58	0.90
NJS1302	Group IIA	13	40.6	0.03	11.6	0.15	47.3	0.06	0.38	100.19	0.88
NJS1304	Group IIA	14	40.8	0.03	11.7	0.16	47.7	0.06	0.39	100.84	0.88
NJS1306	Group IIA	14	40.7	0.04	12.0	0.18	47.2	0.10	0.39	100.60	0.88
NJS1307	Group IA	12	41.0	0.03	10.4	0.15	48.5	0.09	0.40	100.62	0.89
NPY1301	Group IA	13	41.1	0.03	10.4	0.15	48.5	0.06	0.39	100.59	0.89
NPY1310	Group IIA	8	40.8	0.03	11.1	0.15	47.1	0.07	0.38	99.66	0.88
NPY1311	Group IIA	9	40.9	0.02	11.0	0.16	47.3	0.06	0.36	99.80	0.88
NPY1314	Group IA	8	40.9	0.01	10.2	0.15	48.1	0.06	0.39	99.84	0.89
Central part											
NFL1302	Group IB	14	40.9	0.12	9.41	0.14	49.1	0.06	0.41	100.07	0.90
NFL1305	Group IB	7	40.9	0.02	9.28	0.14	49.0	0.07	0.40	99.83	0.90
NFL1315A	Group IB	7	41.0	0.01	10.1	0.15	48.7	0.06	0.36	100.39	0.90
NFL1316	Group IB	8	41.4	0.04	9.13	0.13	49.5	0.07	0.40	100.70	0.91
NFL1324	Group IB	7	41.1	0.01	8.66	0.12	49.8	0.07	0.41	100.22	0.91
NFL1326	Group IIB	7	40.3	0.02	14.3	0.26	45.1	0.11	0.27	100.30	0.85
NFL1327	Group IIB	9	40.1	0.03	14.2	0.25	45.8	0.08	0.33	100.83	0.85
NFL1329	Group IA	7	40.9	0.01	9.89	0.14	48.9	0.07	0.41	100.36	0.90
NTB0306	Group IB	29	40.4	n.d.	9.46	0.16	50.4	0.07	0.39	100.91	0.90
NTB0307	Group IA	10	41.8	0.03	9.11	0.13	49.3	0.11	0.41	100.92	0.91
NTB1124	Group IA	6	40.8	0.00	9.07	0.14	50.5	0.07	0.40	100.94	0.91
NTB1116	Group IA	12	41.2	0.03	9.21	0.13	49.1	0.08	0.39	100.20	0.90
NTB1122	Group IIB	12	40.8	0.04	11.6	0.18	47.1	0.10	0.34	100.25	0.88
NFK0301	Group IB	32	40.6	0.02	9.75	0.16	49.3	0.07	0.40	100.32	0.90
NFK1123	Group IB	5	40.9	0.01	8.73	0.13	50.2	0.08	0.38	100.51	0.91
NFK1108	Group IIB	12	41.2	0.03	10.7	0.17	47.7	0.13	0.34	100.36	0.89
NFK1115	Group IIB	15	40.8	n.d.	10.9	0.20	47.4	0.06	0.39	99.83	0.89
NFR0306	Group IIB	11	39.8	0.02	13.8	0.25	45.8	0.13	0.33	100.15	0.86
NFR0307	Group IIB	9	39.9	0.03	12.1	0.24	47.0	0.14	0.33	99.78	0.87
NFR1109	Group IIB	9	40.2	0.01	14.4	0.25	45.8	0.08	0.32	101.08	0.85
NFR0309	Group IB	11	41.1	0.03	10.0	0.14	48.3	0.07	0.39	100.01	0.90
NFR1107	Group IB	12	41.3	0.03	8.85	0.14	49.3	0.07	0.40	100.08	0.91
NMC1301	Group IB	11	41.2	n.d.	9.63	0.13	49.0	0.06	0.42	100.51	0.90
NMC1309	Group IIB	9	40.9	0.03	11.4	0.18	47.8	0.06	0.40	100.76	0.88
NMC1322	Group IB	12	41.2	0.03	9.49	0.13	49.4	0.07	0.41	100.72	0.90
NMC1336A	Group IA	10	41.2	0.03	9.25	0.13	49.3	0.07	0.42	100.43	0.90
NMM1126	Group IA	6	40.7	0.01	9.41	0.15	50.2	0.08	0.42	100.98	0.90
NMM0318	Group IIB	12	41.2	0.04	11.0	0.17	47.2	0.07	0.37	100.14	0.88
NMM1115	Group IB	14	41.3	0.03	9.07	0.13	49.2	0.08	0.41	100.18	0.91
NME1122	Group IB	7	40.5	0.01	9.47	0.13	50.2	0.07	0.36	100.75	0.90
NME0528	Group IB	13	41.2	0.03	9.50	0.14	48.7	0.06	0.39	100.12	0.90
NME1116	Group IA	12	41.4	0.04	9.17	0.13	49.2	0.07	0.41	100.41	0.91
Southern part											
NBN0302A	Group IA	9	40.1	0.01	9.96	0.14	50.3	0.08	0.38	100.99	0.90
NBN0305	Group IB	11	40.4	n.d.	9.45	0.14	50.1	0.08	0.38	100.60	0.90
NBN0311	Group IA	6	39.8	n.d.	9.78	0.15	50.2	0.12	0.35	100.42	0.90
NBN0316	Group IA	6	40.5	n.d.	10.2	0.15	49.6	0.05	0.42	100.96	0.90
NBN0319	Group IA	13	40.5	n.d.	10.2	0.16	49.5	0.05	0.36	100.79	0.90
NBN0321	Group IA	9	40.2	n.d.	9.83	0.14	49.9	0.10	0.38	100.58	0.90

Table 2. Continued.

ORTHOPYROXENE													
Sample	Group	n.o.a.	SiO_2	TiO_2	Al_2O_3	Cr_2O_3	FeO	MnO	MgO	CaO	Na_2O	Total	Mg#
Northern part													
NMS1302A	Group IB	28	57.1	0.03	2.18	0.48	5.43	0.13	34.7	0.65	0.04	100.78	0.92
NMS1304	Group IB	12	56.1	0.07	2.96	0.42	6.00	0.15	33.5	0.63	0.05	99.99	0.90
NMS1305	Group IB	16	55.5	0.05	4.27	0.33	6.61	0.15	32.9	0.69	0.08	100.67	0.90
NMS1308	Group IA	10	55.8	0.08	3.65	0.49	6.07	0.14	33.2	0.65	0.07	100.24	0.91
NMS1310	Group IA	14	55.4	0.10	4.19	0.45	6.25	0.14	33.3	0.77	0.10	100.82	0.92
NJS1302	Group IIA	14	54.8	0.20	4.41	0.36	7.34	0.15	32.0	0.73	0.11	100.19	0.89
NJS1304	Group IIA	29	55.4	0.18	4.14	0.35	7.36	0.15	32.3	0.73	0.12	100.84	0.89
NJS1306	Group IIA	12	54.5	0.12	4.93	0.35	7.69	0.17	31.5	0.98	0.12	100.43	0.89
NJS1307	Group IA	14	55.0	0.16	5.00	0.36	6.56	0.15	32.4	0.86	0.14	100.64	0.90
NPY1301	Group IA	10	55.3	0.13	4.49	0.36	6.57	0.15	32.7	0.71	0.11	100.59	0.90
NPY1310	Group IIA	11	55.0	0.12	4.85	0.22	6.98	0.16	31.7	0.74	0.09	99.95	0.88
NPY1311	Group IIA	8	54.4	0.13	4.92	0.23	6.93	0.16	31.7	0.75	0.09	99.41	0.89
NPY1314	Group IA	7	54.9	0.09	4.44	0.31	6.63	0.14	32.7	0.72	0.06	100.12	0.91
Central part													
NFL1302	Group IB	11	55.4	0.07	4.07	0.43	6.03	0.14	33.2	0.75	0.07	100.24	0.91
NFL1305	Group IB	7	55.2	0.03	4.05	0.48	5.99	0.14	33.1	0.76	0.06	99.95	0.91
NFL1315A	Group IB	9	56.3	0.06	1.97	0.50	6.38	0.17	33.8	0.75	0.07	99.99	0.91
NFL1316	Group IB	10	56.7	0.05	2.50	0.55	5.85	0.14	34.1	0.73	0.05	100.72	0.91
NFL1324	Group IB	8	55.6	0.05	3.39	0.67	5.61	0.15	33.6	0.82	0.07	100.07	0.92
NFL1327	Group IIB	11	55.3	0.05	2.94	0.51	8.94	0.25	31.7	0.90	0.07	100.75	0.88
NFL1329	Group IA	12	55.5	0.06	4.23	0.36	6.30	0.15	33.0	0.74	0.07	100.48	0.91
NTB0306	Group IB	10	56.0	0.05	2.07	0.52	6.02	0.18	34.5	0.70	n.d.	100.05	0.91
NTB0307	Group IA	2	56.5	0.04	3.82	0.39	5.93	0.09	33.2	0.69	n.d.	100.67	0.91
NTB1124	Group IA	7	54.8	0.16	4.13	0.53	5.79	0.14	33.7	0.85	0.07	100.20	0.91
NTB1116	Group IA	14	55.5	0.08	4.09	0.53	5.92	0.13	33.0	0.79	0.14	100.34	0.91
NTB1122	Group IIB	11	54.7	0.25	4.69	0.48	7.44	0.18	31.6	0.98	0.08	100.41	0.88
NFK0301	Group IB	28	55.4	0.06	3.72	0.59	6.26	0.14	33.1	0.79	n.d.	100.07	0.90
NFK1123	Group IB	8	55.6	0.08	3.37	0.58	5.70	0.13	34.0	0.80	0.08	100.34	0.91
NFK1108	Group IIB	13	55.6	0.10	3.49	0.50	6.88	0.16	32.4	0.98	0.08	100.27	0.89
NFK1115	Group IIB	15	56.6	0.03	1.86	0.45	6.92	0.20	33.1	0.76	0.06	100.08	0.89
NFR0306	Group IIB	3	54.6	0.08	2.88	0.48	8.80	0.24	31.4	0.92	n.d.	99.40	0.86
NFR0307	Group IIB	2	55.0	0.01	3.01	0.39	7.70	0.21	32.4	0.75	n.d.	99.48	0.88
NFR1109	Group IIB	8	55.9	0.07	1.95	0.51	9.00	0.27	32.0	0.91	0.08	100.72	0.86
NFR0309	Group IB	16	55.1	0.14	4.59	0.32	6.43	0.15	32.5	0.78	0.09	100.22	0.90
NFR1107	Group IB	14	56.1	0.08	3.26	0.54	5.70	0.13	33.5	0.80	0.08	100.27	0.91
NMC1301	Group IB	11	56.4	0.04	2.87	0.62	6.14	0.15	33.6	0.85	0.08	100.87	0.91
NMC1309	Group IIB	8	55.3	0.05	4.01	0.47	7.23	0.18	32.3	0.81	0.08	100.57	0.89
NMC1322	Group IB	11	55.8	0.04	3.91	0.51	6.09	0.14	33.4	0.76	0.09	100.91	0.91
NMC1336A	Group IA	10	55.5	0.11	3.84	0.53	5.94	0.13	33.3	0.79	0.09	100.34	0.91
NMM1126	Group IA	6	55.1	0.06	4.08	0.47	6.02	0.13	33.6	0.79	0.09	100.29	0.91
NMM0318	Group IIB	14	55.2	0.08	4.45	0.35	7.03	0.17	31.9	0.79	0.07	100.22	0.88
NMM1115	Group IB	15	55.9	0.08	3.54	0.49	5.81	0.14	33.4	0.72	0.06	100.24	0.91
NME1122	Group IB	8	55.2	0.09	3.70	0.49	6.08	0.15	33.9	0.75	0.07	100.40	0.91
NME0528	Group IB	11	56.2	0.07	3.02	0.57	6.12	0.15	33.3	0.80	0.07	100.37	0.90
NME1116	Group IA	14	55.7	0.07	3.99	0.48	5.86	0.14	33.2	0.80	0.09	100.44	0.91
Southern part													
NBN0302A	Group IA	10	54.8	0.07	3.44	0.37	6.39	0.15	34.3	0.66	0.04	100.24	0.90
NBN0305	Group IB	13	55.3	0.07	3.16	0.43	6.16	0.14	34.2	0.66	0.03	100.09	0.91
NBN0311	Group IA	2	54.1	0.07	3.90	0.42	6.34	0.14	34.1	0.63	0.08	99.76	0.90
NBN0316	Group IA	7	54.7	0.07	3.92	0.30	6.75	0.14	33.7	0.68	0.01	100.27	0.90
NBN0319	Group IA	13	54.8	0.06	3.88	0.29	6.65	0.16	33.5	0.68	0.01	100.00	0.90
NBN0321	Group IA	9	54.6	0.09	3.52	0.41	6.31	0.13	34.0	0.69	0.04	99.85	0.91

Table 2. Continued.

CLINOPYROXENE

Sample	Group	n.o.a.	SiO_2	TiO_2	Al_2O_3	Cr_2O_3	FeO	MnO	MgO	CaO	Na_2O	Total	Mg#
Northern part													
NMS1302A	Group IB	8	54.0	0.05	2.57	0.96	2.13	0.08	17.4	23.2	0.55	100.96	0.94
NMS1304	Group IB	15	52.5	0.24	3.77	0.93	2.43	0.08	16.5	22.8	0.66	99.89	0.92
NMS1305	Group IB	20	52.2	0.27	6.59	0.77	2.80	0.09	15.3	21.2	1.47	100.75	0.91
NMS1308	Group IA	13	51.6	0.41	6.08	1.28	2.52	0.09	15.3	20.9	1.50	99.71	0.91
NMS1310	Group IA	15	51.8	0.49	6.61	1.10	2.74	0.09	15.4	20.5	1.74	100.48	0.91
NJS1302	Group IIA	11	50.8	1.16	7.64	0.93	3.10	0.08	14.3	19.8	1.95	99.84	0.89
NJS1304	Group IIA	9	51.8	0.96	7.15	0.87	3.10	0.09	14.7	20.0	2.06	100.75	0.89
NJS1306	Group IIA	14	51.2	0.51	7.13	0.72	3.86	0.11	15.3	20.0	1.49	100.31	0.88
NJS1307	Group IA	12	51.6	0.71	7.59	0.76	3.09	0.10	15.1	19.7	1.88	100.49	0.90
NPY1301	Group IA	12	52.0	0.58	7.16	0.84	2.83	0.09	14.8	20.3	1.94	100.63	0.90
NPY1310	Group IIA	9	51.7	0.56	6.86	0.43	3.08	0.10	15.1	21.1	1.38	100.23	0.90
NPY1311	Group IIA	14	51.5	0.56	7.02	0.45	3.07	0.10	15.0	21.0	1.38	100.13	0.90
NPY1314	Group IA	6	50.6	0.59	7.25	0.74	2.95	0.09	14.9	20.8	1.47	99.34	0.90
Central part													
NFL1302	Group IB	13	51.7	0.32	5.74	0.91	2.65	0.08	15.8	21.5	1.19	99.91	0.91
NFL1305	Group IB	9	51.8	0.15	5.63	0.96	2.71	0.08	15.8	21.2	1.23	99.63	0.91
NFL1315A	Group IB	9	52.7	0.15	3.12	1.39	2.71	0.09	16.6	21.5	1.14	99.53	0.92
NFL1316	Group IB	10	53.4	0.14	3.46	1.11	2.47	0.08	16.7	22.1	1.06	100.47	0.92
NFL1324	Group IB	11	52.1	0.20	4.70	1.37	2.55	0.09	16.2	21.3	1.21	99.85	0.92
NFL1326	Group IIB	10	51.4	0.38	4.92	0.93	4.15	0.12	14.9	22.0	1.17	100.02	0.86
NFL1327	Group IIB	12	52.2	0.20	4.49	1.13	4.24	0.14	15.8	21.0	1.20	100.39	0.87
NFL1329	Group IA	7	52.0	0.32	6.16	0.69	2.77	0.09	15.7	21.3	1.32	100.32	0.91
NTB0306	Group IB	9	53.1	0.11	3.32	1.25	2.65	0.09	16.7	20.8	1.18	99.19	0.92
NTB0307	Group IA	5	53.3	0.21	5.53	0.79	2.78	0.06	16.1	20.6	1.12	100.50	0.91
NTB1124	Group IA	7	51.2	0.53	5.74	1.05	2.83	0.08	16.1	21.0	1.13	99.65	0.91
NTB1116	Group IA	11	52.2	0.34	6.02	1.17	2.74	0.08	15.5	20.6	1.59	100.21	0.91
NTB1122	Group IIB	13	50.7	0.97	6.48	0.89	3.61	0.11	15.4	20.9	1.07	100.14	0.88
NFK0301	Group IB	11	52.2	0.25	5.15	1.20	2.83	0.05	15.9	20.6	1.31	99.50	0.91
NFK1123	Group IB	7	52.2	0.29	4.61	1.26	2.59	0.08	16.4	21.2	1.07	99.70	0.92
NFK1108	Group IIB	14	52.1	0.39	5.08	1.12	3.31	0.11	16.0	21.0	1.07	100.23	0.90
NFK1115	Group IIB	9	53.3	0.05	3.01	1.30	3.01	0.11	16.4	21.5	1.14	99.92	0.91
NFR0306	Group IIB	10	51.3	0.30	4.86	1.08	4.11	0.11	15.5	20.4	1.29	99.02	0.87
NFR0307	Group IIB	5	51.2	0.40	3.93	0.94	3.44	0.08	16.0	22.0	0.78	98.88	0.89
NFR1109	Group IIB	11	53.2	0.19	3.39	1.36	4.18	0.15	16.1	20.2	1.31	99.98	0.87
NFR0309	Group IB	15	51.3	0.64	7.11	0.74	2.87	0.09	15.0	20.6	1.57	100.01	0.90
NFR1107	Group IB	12	52.3	0.31	4.86	1.31	2.58	0.08	16.1	21.1	1.29	99.98	0.92
NMC1301	Group IB	12	53.0	0.11	4.13	1.41	2.80	0.08	16.4	21.2	1.26	100.36	0.91
NMC1309	Group IIB	12	52.2	0.21	5.53	0.96	3.27	0.11	15.7	21.3	1.20	100.51	0.89
NMC1322	Group IB	12	52.5	0.20	5.64	1.10	2.69	0.08	15.8	21.1	1.44	100.54	0.91
NMC1336A	Group IA	13	52.1	0.46	5.88	1.17	2.73	0.08	15.6	20.8	1.50	100.33	0.91
NMM1126	Group IA	6	51.7	0.23	5.57	0.94	2.74	0.08	16.0	21.0	1.22	99.50	0.91
NMM0318	Group IIB	12	52.2	0.34	6.19	0.71	3.09	0.11	15.4	21.2	1.27	100.43	0.90
NMM1115	Group IB	12	52.4	0.30	5.03	1.07	2.47	0.08	15.9	21.6	1.23	100.15	0.92
NME1122	Group IB	9	51.6	0.34	5.39	1.12	2.77	0.09	16.0	20.9	1.28	99.50	0.91
NME0528	Group IB	13	52.8	0.24	4.48	1.35	2.69	0.09	16.1	21.3	1.26	100.26	0.91
NME1116	Group IA	13	52.2	0.28	5.75	1.05	2.65	0.08	15.7	21.0	1.45	100.16	0.91
Southern part													
NBN0302A	Group IA	9	51.3	0.34	4.92	0.81	2.72	0.08	16.4	21.8	0.93	99.29	0.91
NBN0305	Group IB	9	52.0	0.20	3.76	0.91	2.62	0.08	16.9	22.2	0.71	99.31	0.92
NBN0311	Group IA	5	50.8	0.42	6.15	0.77	2.67	0.10	15.8	20.7	1.55	98.87	0.91
NBN0316	Group IA	7	51.2	0.33	4.73	0.50	3.04	0.08	16.7	22.4	0.54	99.57	0.91
NBN0319	Group IA	10	51.4	0.24	4.30	0.44	2.99	0.08	16.9	22.8	0.37	99.51	0.91
NBN0321	Group IA	9	50.9	0.49	5.55	0.88	2.78	0.07	16.0	21.2	1.18	99.13	0.91

Table 2. Continued.

SPINEL												
Sample		n.o.a.	TiO_2	Al_2O_3	Cr_2O_3	FeO	MnO	NiO	MgO	Total	Mg#	Cr#
Northern part												
NMS1302A	Group IB	11	0.06	33.8	36.0	13.0	0.12	0.19	17.2	100.72	0.74	0.42
NMS1304	Group IB	7	0.13	43.4	24.5	12.7	0.11	0.25	18.5	99.89	0.76	0.27
NMS1305	Group IB	15	0.03	56.3	11.2	10.9	0.10	0.39	20.9	99.98	0.81	0.12
NMS1308	Group IA	12	0.08	50.4	17.3	11.3	0.10	0.32	19.8	99.59	0.79	0.19
NMS1310	Group IA	7	0.10	52.7	14.4	11.6	0.10	0.36	20.6	100.09	0.81	0.15
NJS1302	Group IIA	6	0.20	53.8	12.5	12.5	0.09	0.37	19.7	99.38	0.78	0.14
NJS1304	Group IIA	7	0.18	55.1	11.9	12.5	0.10	0.36	20.1	100.39	0.78	0.13
NJS1306	Group IIA	6	0.14	56.4	9.14	14.2	0.12	0.41	19.9	100.44	0.78	0.10
NJS1307	Group IA	9	0.15	58.2	8.80	10.8	0.09	0.39	21.2	99.74	0.82	0.09
NPY1301	Group IA	11	0.10	57.3	9.62	11.5	0.11	0.39	20.5	99.72	0.80	0.10
NPY1310	Group IIA	9	0.09	61.0	5.30	11.3	0.09	0.40	21.4	99.83	0.82	0.06
NPY1311	Group IIA	9	0.09	60.9	5.32	11.3	0.09	0.41	21.4	99.69	0.82	0.06
NPY1314	Group IA	6	0.06	58.0	8.8	11.2	0.09	0.43	21.0	99.79	0.82	0.09
Central part												
NFL1302	Group IB	11	0.07	53.0	14.3	11.0	0.10	0.36	20.6	99.51	0.81	0.15
NFL1305	Group IB	6	0.04	52.5	15.2	11.3	0.10	0.34	20.3	100.12	0.80	0.16
NFL1315A	Group IB	7	0.27	26.9	40.3	17.4	0.17	0.17	14.9	100.46	0.66	0.50
NFL1316	Group IB	6	0.12	33.3	34.2	14.1	0.13	0.22	16.9	99.35	0.73	0.41
NFL1324	Group IB	7	0.11	40.9	27.0	13.1	0.11	0.26	18.6	100.34	0.77	0.31
NFL1326	Group IIB	6	0.49	34.5	25.5	24.3	0.23	0.22	14.4	100.04	0.62	0.33
NFL1327	Group IIB	5	0.41	33.5	29.0	21.8	0.20	0.23	14.9	100.23	0.64	0.37
NFL1329	Group IA	4	0.05	57.6	10.0	10.7	0.10	0.41	21.0	100.09	0.82	0.10
NTB0306	Group IB	6	0.13	28.0	40.2	16.0	0.30	0.19	16.1	100.75	0.71	0.49
NTB0307	Group IA	5	0.12	53.7	14.4	11.6	nd	0.39	20.5	100.72	0.80	0.15
NTB1124	Group IA	6	0.19	49.9	17.6	11.7	0.12	0.33	20.5	100.32	0.81	0.19
NTB1116	Group IA	13	0.10	49.5	18.0	11.5	0.09	0.34	20.2	99.86	0.81	0.20
NTB1122	Group IIB	10	0.39	50.0	15.2	14.3	0.11	0.33	19.1	99.75	0.76	0.17
NFK0301	Group IB	12	0.12	44.3	23.8	14.4	0.55	0.28	18.0	101.45	0.74	0.26
NFK1123	Group IB	6	0.16	43.2	24.3	12.9	0.12	0.34	19.4	100.47	0.79	0.27
NFK1108	Group IIB	4	0.49	42.4	23.8	15.7	0.13	0.27	18.2	101.29	0.74	0.27
NFK1115	Group IIB	9	0.09	24.4	39.1	20.3	0.21	0.18	13.8	98.33	0.64	0.52
NFR0306	Group IIB	6	0.95	32.4	29.0	22.6	nd	0.24	13.9	99.01	0.60	0.38
NFR0307	Group IIB	6	0.11	46.1	19.7	15.9	nd	0.29	17.1	99.18	0.70	0.22
NFR1109	Group IIB	5	0.44	22.9	39.9	24.0	0.31	0.13	12.2	99.90	0.56	0.54
NFR0309	Group IB	12	0.11	57.6	8.74	11.2	0.09	0.40	21.1	99.36	0.82	0.09
NFR1107	Group IB	8	0.17	41.1	25.4	13.3	0.11	0.26	18.7	99.23	0.78	0.29
NMC1301	Group IB	7	0.11	34.9	32.9	15.0	0.13	0.25	17.1	100.58	0.73	0.39
NMC1309	Group IIB	8	0.07	49.7	16.8	13.7	0.12	0.33	18.8	99.74	0.76	0.18
NMC1322	Group IB	8	0.05	50.8	16.8	11.3	0.11	0.35	20.1	99.76	0.80	0.18
NMC1336A	Group IA	12	0.13	48.5	19.0	12.0	0.10	0.34	19.9	100.26	0.80	0.21
NMM1126	Group IA	6	0.08	51.5	16.2	11.4	0.10	0.37	20.6	100.24	0.82	0.17
NMM0318	Group IIB	12	0.07	56.3	10.9	12.5	0.11	0.36	20.0	100.47	0.78	0.12
NMM1115	Group IB	16	0.12	47.3	20.6	11.9	0.10	0.32	19.6	100.14	0.79	0.23
NME1122	Group IB	7	0.14	47.4	20.0	12.4	0.11	0.32	19.8	100.12	0.80	0.22
NME0528	Group IB	11	0.17	37.9	30.1	14.4	0.12	0.25	17.6	100.79	0.74	0.35
NME1116	Group IA	7	0.09	50.3	17.8	11.9	0.10	0.32	20.1	100.69	0.80	0.19
Southern part												
NBN0302A	Group IA	9	0.12	51.7	15.0	11.6	0.11	0.34	20.7	99.52	0.82	0.16
NBN0305	Group IB	8	0.14	41.6	25.4	13.2	0.14	0.27	18.8	99.62	0.78	0.29
NBN0311	Group IA	2	1.08	39.8	26.7	13.3	0.15	0.21	18.2	99.43	0.75	0.31
NBN0316	Group IA	7	0.15	55.5	11.0	11.6	0.12	0.35	20.5	99.16	0.80	0.12
NBN0319	Group IA	12	0.15	54.5	11.6	12.5	0.11	0.37	20.0	99.14	0.79	0.12
NBN0321	Group IA	10	0.28	51.4	15.4	11.4	0.12	0.36	20.5	99.48	0.81	0.17

Table 2. Continued.

AMPHIBOLE																
Sample		n.o.a.	SiO_2	TiO_2	Al_2O_3	Cr_2O_3	FeO	MnO	MgO	CaO	Na_2O	K_2O	F	Cl	NiO	Total
Northern part																
NMS1304	Group IB	10	41.4	1.38	13.5	1.76	3.54	0.06	17.8	12.1	3.11	1.13	0.06	n.d.	0.13	96.01
NMS1308	Group IA	4	41.2	2.44	14.0	1.68	3.75	0.07	17.7	11.0	3.80	0.37	n.d.	n.d.	0.11	96.08
NJS1302_1	Group IIA	2	39.0	8.09	13.8	0.13	5.20	0.07	16.1	11.1	3.33	n.d.	n.d.	n.d.	n.d.	96.73
NJS1302_2	Group IIA	2	41.3	4.24	13.5	1.21	4.69	0.08	16.7	10.5	3.86	n.d.	n.d.	n.d.	0.12	96.20
Central part																
NFL1302	Group IB	2	41.6	1.68	14.4	1.38	3.79	0.07	18.0	11.3	3.82	0.48	0.06	0.03	0.16	96.66
NFL1315A	Group IB	7	42.2	2.01	12.2	2.18	4.01	0.06	18.1	11.3	3.19	1.09	0.09	0.04	0.12	96.60
NFL1324	Group IB	9	41.9	1.53	13.5	2.03	3.69	0.05	18.1	11.5	3.16	1.17	0.06	0.05	0.13	96.76
NFL1326	Group IIB	9	40.9	1.74	12.9	1.58	6.13	0.09	16.7	11.5	3.26	0.96	0.20	0.04	0.11	96.22
NFL1329	Group IA	4	41.9	1.69	14.4	1.17	4.04	0.07	17.9	11.2	3.96	0.13	n.d.	n.d.	0.14	96.47

to 12.0 (xenolith NFK1123). Since LREE-enrichment is commonly considered to indicate the effects of cryptic metasomatism, both groups have been divided into a LREE-depleted ('A') and a LREE-enriched, flat or convex upward ('B') subgroup. REE+Y patterns for clinopyroxene and orthopyroxene in these subgroups are shown in Fig. 5.9a-d and e-h, respectively. Group IA, comprising most of the xenoliths from the southern part, has very uniform clinopyroxene REE patterns (Fig. 5.9a). Group IB, on the other hand, displays an extremely wide range of LREE concentrations (La = 0.83 – 13.6 ppm), as well as HREE values (Lu = 0.056 – 0.301 ppm) (Fig. 5.9b).

The Fe-Mn-Ti-enriched Group II has a LREE-depleted subgroup (Group IIA, Fig. 5.9c) and an enriched one (Group IIB, Fig. 5.9d). The former contains only samples from the northern part, from localities Podrečany (NPY1310, NPY1311) and Jelšovec (NJS1302, NJS1304, NJS1306). It shows wide variation in the concentrations of the highly incompatible LREE, except La; two xenoliths (NJS1302, NJS1304) show considerably higher values in these elements. Group IIB consists of xenoliths from the central part, showing very similar REE patterns with different degrees of LREE enrichment. The most incompatible elements, such as Th, U, Nb and Ta, also display a wider range of values in the LREE-rich subgroups (Group IB and IIB, Fig. 5.8b, d) than the LREE-poor ones (Group IA and IIA, Fig. 5.8a, c), where they are consequently less abundant. Furthermore, the troughs of Zr and Hf in clinopyroxene are more significant in Group IB and IIB than in IA and IIA, respectively (Fig. 5.8a-d).

In contrast to the variability of trace-element contents in the xenoliths from the northern and central part, samples from the southern part have generally uniform LREE depletion in both pyroxenes (Fig. 5.9a) with the exception of NBN0305, which has flat

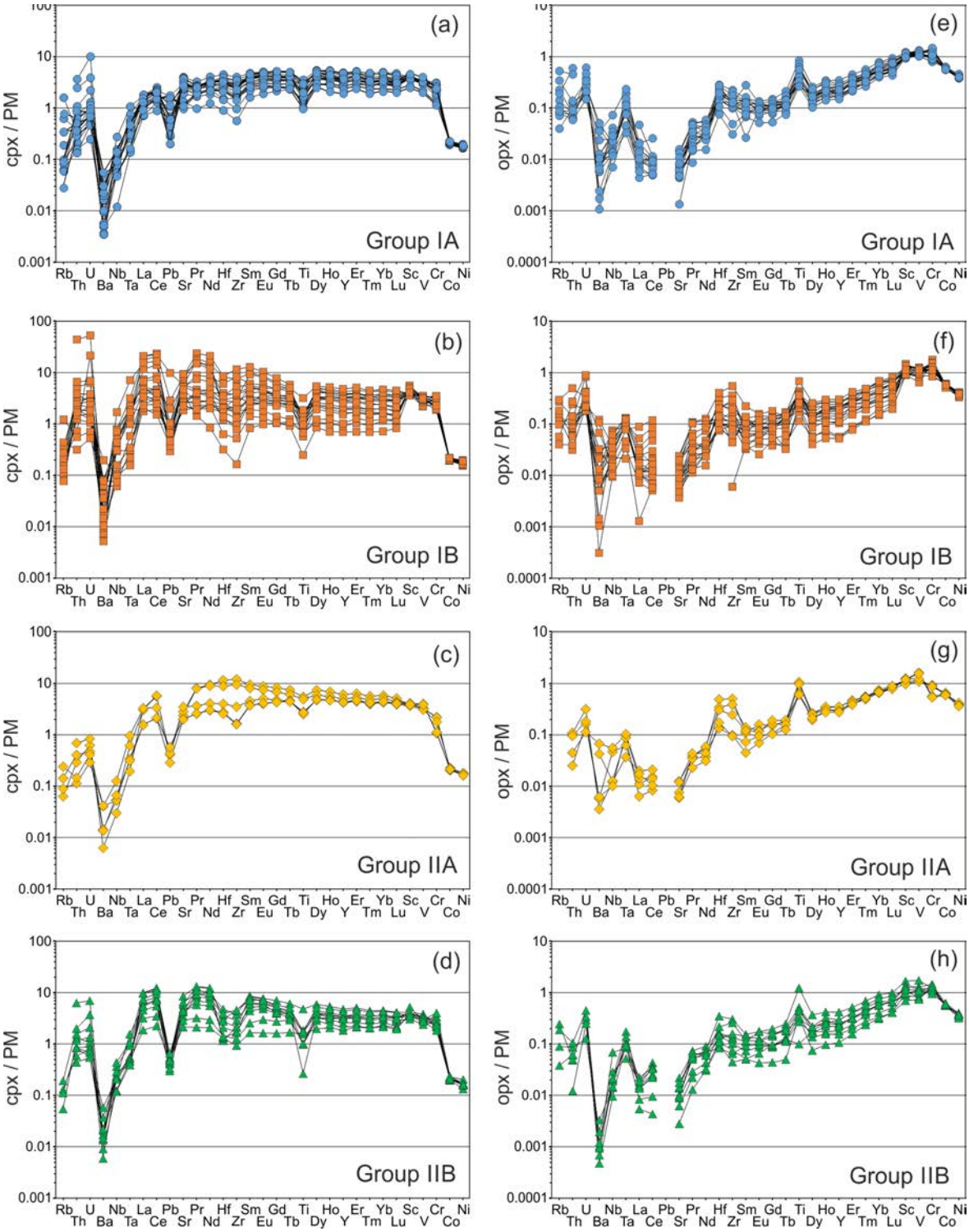

Fig. 5.8. Primitive mantle (McDonough and Sun, 1995)-normalised multi-element diagrams for clino- (a-d) and orthopyroxene (e-h) of Group IA, IB, IIA and IIB xenoliths.

patterns. Furthermore, porphyroclastic and equigranular xenoliths from the southern part have different concentrations of heavy rare earth elements in the clinopyroxenes; the latter have lower values (ΣREE = 13.79-15.88 ppm) than the former (ΣREE = 20.81-22.24 ppm).

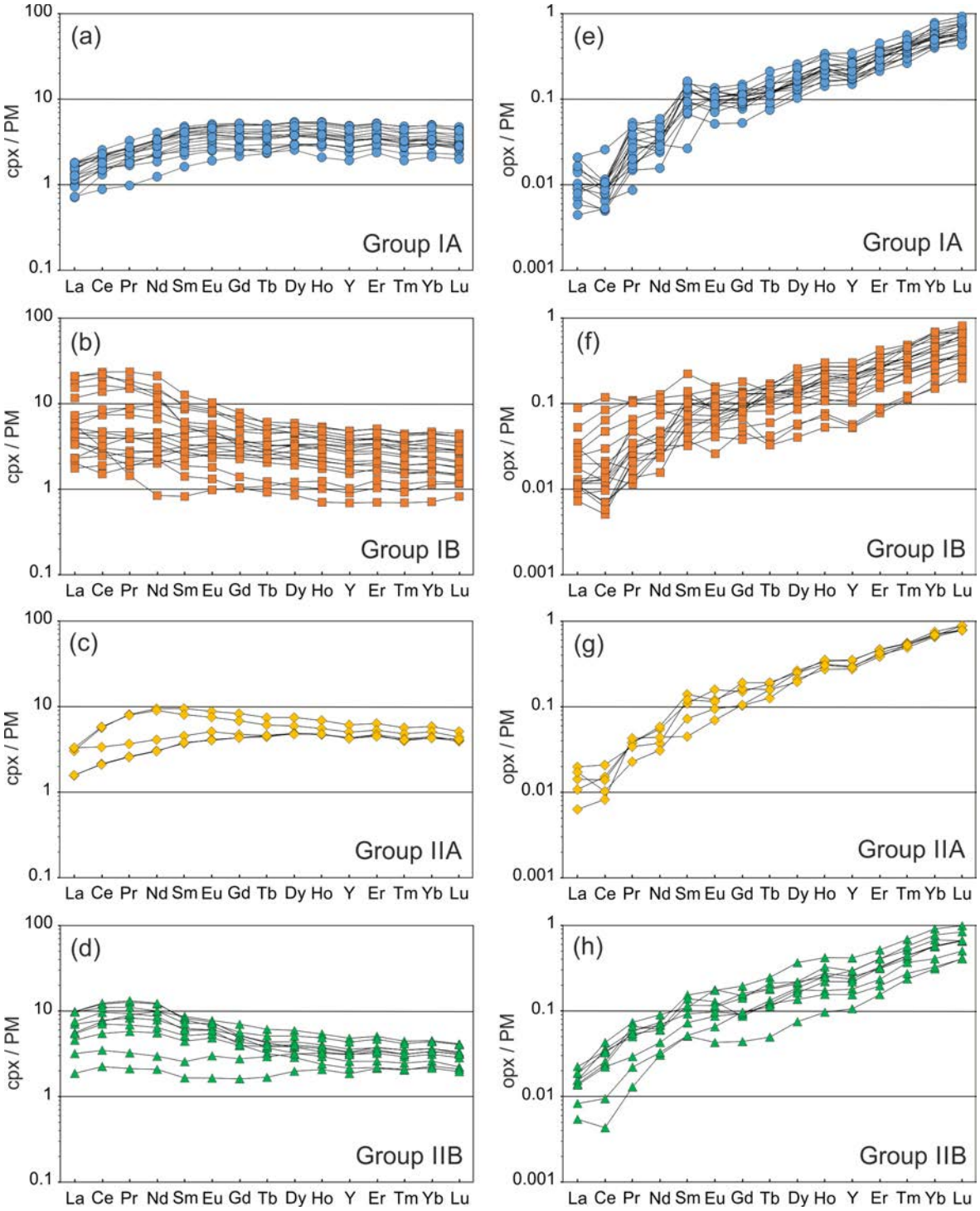

Fig. 5.9. Primitive mantle (McDonough and Sun, 1995)-normalised REE+Y patterns of clino- (a-d) and orthopyroxene (e-h) of Group IA, IB, IIA, and IIB xenoliths.

However, this correlation with REE contents and texture types is not observed in xenoliths from the northern or central parts.

Amphibole shows wide variability in the most incompatible elements, and less in the more compatible ones (Fig. 5.10a). Positive peaks are observable in Nb, Ta and Ti, whereas

Zr and Hf display slight depletion on the primitive mantle normalized multi-element diagram (Fig. 5.10a). The amphiboles are uniformly depleted in U, Th and Pb, but most of them show high Sr and Ba, except for NJS1302, which has very low Ba (1.19 ppm). Rare-earth element patterns for amphibole indicate equilibrium with coexisting clinopyroxene in each sample (Fig. 5.10b); therefore, analogous LREE-depleted and -enriched characters are both present in amphibole as well.

Multi-element and REE+Y patterns of pyroxenes and amphibole for individual samples are given in Appendix B.

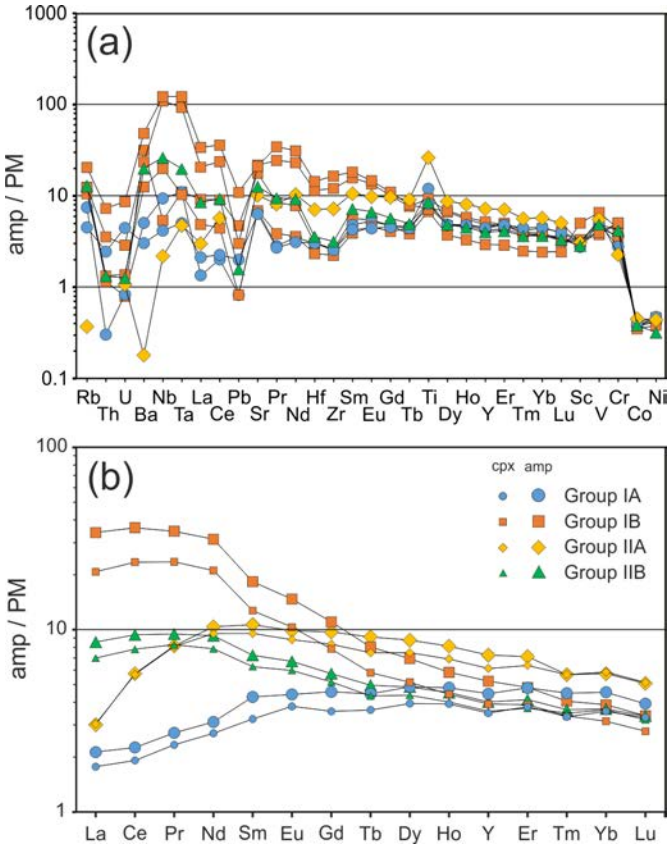

Fig. 5.10. a – Multi-element diagram for amphiboles in the studied xenoliths. b – REE - Y diagram of representative amphiboles compared to clinopyroxenes within the same xenoliths from Group IA, IB, IIA and IIB; normalising values for primitive mantle are from McDonough and Sun (1995).

Table 3. Trace element compositions of pyroxenes and amphibole. n - number of analyses; n.d. - not detected.

ORTHOPYROXENE

Sample	Group	n	Rb	Th	U	Ba	Nb	Ta	La	Ce	Pb	Sr	Pr	Nd	Hf	Zr	Sm	Eu	Gd	Tb	Ti	Dy	Ho	Y	Er	Tm	Yb	Lu	Sc	V	Cr	Co	Ni
NMS1302A	Group IB	11	0.087	0.008	0.004	0.082	0.050	0.003	0.007	0.036	0.65	0.18	0.004	0.040	0.021	1.01	0.013	0.006	0.021	0.004	139	0.039	0.011	0.23	0.038	0.008	0.066	0.017	21.9	79.6	3201	59.0	755
NMS1304	Group IB	9	n.d.	0.006	0.009	0.007	n.d.	n.d.	0.007	0.023	n.d.	0.14	0.008	0.046	0.046	0.93	0.042	0.014	0.044	0.008	448	0.072	0.020	0.51	0.073	0.016	0.12	0.028	21.5	104	2879	60.3	743
NMS1305	Group IB	6	0.163	0.011	0.004	0.152	0.045	0.005	0.013	0.033	n.d.	0.44	0.009	0.057	0.091	3.83	0.030	0.018	0.070	0.013	343	0.101	0.030	0.95	0.12	0.031	0.30	0.045	16.4	69.4	2318	62.2	774
NMS1308	Group IA	6	0.063	n.d.	n.d.	0.235	0.048	0.009	0.009	0.014	0.10	0.21	0.008	0.030	0.039	1.30	n.d.	n.d.	0.046	0.009	489	0.088	0.024	0.74	0.094	0.018	0.18	0.029	15.7	83.8	2932	60.3	757
NMS1310	Group IA	8	0.052	0.007	0.008	n.d.	0.008	0.004	0.006	0.011	n.d.	0.16	0.002	n.d.	0.050	1.47	0.038	0.012	0.066	0.014	678	0.13	0.038	1.05	0.14	0.031	0.26	0.049	18.3	100	3124	64.5	790
NJS1302	Group IIA	9	n.d.	0.002	0.003	0.038	0.031	0.002	0.007	0.025	0.051	0.12	0.010	0.069	0.139	5.34	0.045	0.024	0.082	0.018	1292	0.18	0.051	1.50	0.21	0.038	0.33	0.060	17.3	94.3	2446	65.3	755
NJS1304	Group IIA	10	n.d.	0.004	0.002	0.443	0.037	0.004	0.009	0.023	0.54	0.15	0.010	0.073	0.098	4.10	0.057	0.019	0.089	0.016	1171	0.17	0.047	1.28	0.18	0.033	0.29	0.053	15.9	89.3	2332	68.3	786
NJS1306	Group IIA	7	n.d.	0.009	0.006	0.023	0.008	0.001	0.013	0.035	n.d.	0.25	0.009	0.047	0.086	2.58	0.049	0.018	0.104	0.019	727	0.17	0.053	1.52	0.20	0.037	0.31	0.054	20.4	101	2294	65.8	818
NJS1307	Group IA	8	n.d.	n.d.	0.012	0.007	0.009	0.005	0.010	0.017	0.039	0.28	0.014	0.067	0.080	2.36	0.062	0.021	0.081	0.021	1008	0.17	0.051	1.49	0.20	0.038	0.35	0.063	19.0	109	2295	64.2	789
NPY1301	Group IA	8	0.049	0.006	0.005	0.084	0.009	0.007	0.014	0.018	0.052	0.17	0.007	0.036	0.057	1.54	0.054	0.014	0.051	0.011	781	0.13	0.037	1.14	0.15	0.028	0.33	0.057	17.0	101	2462	63.1	768
NPY1310	Group IIA	7	n.d.	0.009	n.d.	0.281	0.008	0.003	0.004	0.014	0.47	0.24	0.011	0.055	0.038	1.04	0.018	0.011	0.057	0.016	776	0.13	0.046	1.25	0.19	0.036	0.31	0.053	19.6	134	1490	65.4	744
NPY1311	Group IIA	9	n.d.	0.008	0.004	0.040	0.007	0.004	0.011	0.017	n.d.	0.12	0.006	0.039	0.049	0.99	0.030	0.015	0.057	0.013	731	0.14	0.041	1.20	0.17	0.036	0.30	0.060	19.3	128	1418	62.2	712
NPY1314	Group IA	7	n.d.	n.d.	0.010	0.012	0.005	0.002	0.007	0.017	n.d.	0.17	0.012	0.042	0.077	1.84	0.051	0.015	0.057	0.014	676	0.16	0.045	1.16	0.16	0.034	0.30	0.052	18.9	104	2287	66.0	817
NFL1302	Group IB	5	n.d.	0.006	0.004	0.214	0.025	0.003	0.008	0.021	n.d.	0.19	0.007	0.060	0.037	1.18	0.019	0.007	0.051	0.016	433	0.11	0.037	1.04	0.16	0.029	0.27	0.049	20.3	99.0	2774	62.1	775
NFL1305	Group IB	6	n.d.	0.007	n.d.	0.070	0.016	0.004	0.008	0.024	n.d.	0.15	0.003	0.034	0.069	1.88	0.014	0.010	0.042	0.013	206	0.097	0.026	0.78	0.11	0.026	0.22	0.041	19.5	92.0	3106	61.9	792
NFL1315A	Group IB	8	n.d.	0.005	0.006	0.034	0.015	0.001	0.016	0.050	0.028	0.32	0.012	0.092	0.064	2.66	0.038	0.019	0.076	0.015	370	0.14	0.034	0.94	0.12	0.024	0.19	0.035	14.7	53.3	3955	60.2	689
NFL1316	Group IB	7	n.d.	0.005	0.005	0.807	0.025	0.004	0.007	0.012	n.d.	0.18	0.003	0.020	0.032	0.86	0.025	0.009	0.037	0.003	293	0.037	0.012	0.25	0.039	0.008	0.088	0.018	24.1	93.6	3454	59.3	751
NFL1324	Group IB	4	n.d.	0.010	0.017	0.052	0.027	0.005	0.023	0.108	0.034	0.30	0.028	0.161	0.115	5.80	0.091	0.024	0.098	0.014	336	0.16	0.041	1.16	0.14	0.032	0.24	0.048	16.2	69.2	4716	62.1	812
NFL1327	Group IIB	7	n.d.	0.007	0.003	0.013	0.019	0.002	0.012	0.072	0.034	0.28	0.019	0.113	0.047	1.42	0.045	0.027	0.083	0.018	370	0.14	0.041	1.09	0.14	0.028	0.26	0.044	14.2	68.2	3314	60.5	690
NFL1329	Group IA	10	n.d.	0.011	0.007	0.016	0.009	0.001	0.004	0.009	0.035	0.091	0.009	0.037	0.056	1.37	0.011	0.015	0.053	0.011	401	0.11	0.032	0.98	0.13	0.031	0.24	0.051	18.8	93.0	2346	62.6	787
NTB0306	Group IB	11	0.081	0.003	n.d.	0.718	0.008	n.d.	0.007	0.010	0.048	0.09	0.006	n.d.	n.d.	0.06	0.015	0.004	0.026	0.003	248	0.027	0.008	0.23	0.034	0.008	0.070	0.013	15.0	69.0	3355	54.6	655
NTB0307	Group IA	5	n.d.	0.005	0.003	0.068	0.008	n.d.	n.d.	0.015	n.d.	0.10	0.004	0.045	0.030	0.51	0.031	n.d.	n.d.	0.007	318	0.070	0.021	0.65	0.097	0.022	0.19	0.034	16.0	83.5	2784	59.2	786
NTB1124	Group IA	16	0.085	0.006	0.004	0.039	0.009	0.004	0.003	0.009	0.045	0.10	0.004	0.038	0.043	1.05	0.038	0.011	0.049	0.011	858	0.12	0.033	0.93	0.13	0.027	0.23	0.041	18.9	102	3687	58.1	746
NTB1116	Group IA	7	0.136	0.006	0.006	0.260	0.011	0.006	0.011	0.015	n.d.	0.32	0.005	0.046	0.042	1.07	0.066	0.016	0.061	0.015	516	0.11	0.039	0.92	0.13	0.028	0.22	0.039	19.8	100	3495	62.4	803
NTB1122	Group IIB	6	n.d.	n.d.	0.006	0.003	0.006	0.004	0.010	0.060	n.d.	0.20	0.015	0.093	0.099	3.21	0.063	0.027	0.107	0.025	1495	0.25	0.063	1.80	0.23	0.047	0.40	0.067	27.4	143	3200	62.8	745

Table 3. Continued.

ORTHOPYROXENE

Sample	Group	n	Rb	Th	U	Ba	Nb	Ta	La	Ce	Pb	Sr	Pr	Nd	Hf	Zr	Sm	Eu	Gd	Tb	Ti	Dy	Ho	Y	Er	Tm	Yb	Lu	Sc	V	Cr	Co	Ni
NFK0301	Group IB	18	0.034	0.019	0.004	0.140	0.019	0.004	0.034	0.142	0.030	0.44	0.027	0.146	0.034	1.81	0.052	0.023	0.074	0.017	472	0.15	0.041	1.17	0.16	0.032	0.28	0.052	14.9	76.5	4112	57.2	735
NFK1123	Group IB	9	0.059	0.011	0.004	0.034	0.013	0.003	0.058	0.199	0.053	0.48	0.026	0.122	0.032	1.27	0.041	0.013	0.048	0.010	528	0.091	0.021	0.62	0.075	0.016	0.14	0.025	18.2	77.6	4111	58.1	782
NFK1108	Group IIB	6	n.d.	0.005	n.d.	0.007	0.014	0.006	0.009	0.040	0.040	0.29	0.015	0.086	0.044	1.31	n.d.	0.017	0.077	0.021	621	0.15	0.049	1.26	0.18	0.035	0.30	0.045	22.2	106	3864	66.2	789
NFK1115	Group IIB	6	0.147	0.004	0.007	0.006	0.045	0.003	0.010	0.043	0.015	0.44	0.017	0.076	0.036	1.67	0.057	0.020	0.047	0.012	121	0.12	0.026	0.78	0.10	0.025	0.18	0.034	18.7	62.6	3252	60.8	760
NFR0306	Group IIB	8	n.d.	0.004	n.d.	0.022	0.009	n.d.	0.009	0.037	n.d.	0.18	0.007	0.054	0.042	1.07	0.030	0.013	0.051	0.013	539	0.13	0.038	1.02	0.14	0.030	0.25	0.045	15.6	83.6	3518	59.2	636
NFR0307	Group IIB	13	0.054	0.007	n.d.	n.d.	0.013	n.d.	0.004	0.007	n.d.	0.06	0.003	0.038	0.028	0.47	0.021	0.007	0.024	0.005	411	0.051	0.014	0.46	0.068	0.016	0.14	0.028	15.9	90.2	2828	59.0	757
NFR1109	Group IIB	12	0.023	0.005	n.d.	n.d.	0.013	0.003	0.015	0.057	0.038	0.35	0.013	0.087	0.024	0.68	0.038	0.015	0.050	0.012	408	0.093	0.023	0.67	0.086	0.019	0.14	0.028	11.3	60.7	3606	60.9	632
NFR0309	Group IB	6	n.d.	n.d.	0.004	0.215	0.009	n.d.	0.008	0.020	0.024	0.12	0.007	0.033	0.068	2.06	0.021	0.011	0.061	0.016	831	0.17	0.045	1.30	0.19	0.033	0.30	0.055	20.9	102	2237	62.5	749
NFR1107	Group IB	7	0.096	0.005	n.d.	0.058	0.041	0.005	0.006	0.016	0.057	0.21	0.008	0.051	0.047	1.30	0.048	0.014	0.072	0.013	527	0.11	0.028	0.82	0.10	0.020	0.16	0.029	22.1	101	3750	60.2	774
NMC1301	Group IB	7	n.d.	0.003	0.004	0.009	0.030	0.005	0.018	0.080	n.d.	0.37	0.017	0.108	0.058	3.09	0.027	0.017	0.054	0.011	251	0.083	0.024	0.66	0.091	0.016	0.13	0.026	22.1	96.1	4064	64.8	820
NMC1309	Group IIB	6	n.d.	0.001	0.005	0.005	0.014	0.003	0.005	0.016	n.d.	0.12	0.006	0.041	0.031	0.79	0.021	0.010	0.053	0.011	326	0.11	0.033	0.95	0.14	0.030	0.26	0.045	21.0	100	3042	60.7	765
NMC1322	Group IB	7	0.179	0.040	0.007	0.447	0.011	n.d.	0.020	0.027	0.185	0.40	0.012	0.041	0.026	0.50	0.044	0.018	n.d.	0.012	295	0.089	0.028	0.90	0.12	0.021	0.18	0.044	18.4	85.7	3144	57.7	758
NMC1336A	Group IA	7	0.063	0.005	0.005	0.336	0.014	0.003	0.006	0.018	0.235	0.13	0.008	0.048	0.055	1.31	0.033	0.016	0.065	0.017	750	0.15	0.050	1.27	0.17	0.032	0.28	0.052	17.7	90.5	3845	63.8	844
NMM1126	Group IA	11	0.047	0.005	n.d.	0.050	0.009	0.002	0.005	0.008	n.d.	0.10	0.004	0.020	0.021	0.32	0.027	0.008	0.029	0.008	379	0.080	0.025	0.72	0.10	0.022	0.20	0.037	17.8	92.4	3475	58.9	769
NMM0318	Group IIB	8	0.114	0.008	0.009	0.008	0.010	0.005	0.012	0.055	n.d.	0.19	0.014	0.075	0.062	2.71	0.047	0.018	0.087	0.018	538	0.15	0.037	1.28	0.18	0.039	0.34	0.057	18.6	90.8	2501	62.6	723
NMM1115	Group IB	7	n.d.	0.022	0.018	0.002	0.006	0.001	0.005	0.009	n.d.	0.074	0.005	0.037	0.028	1.02	0.030	0.011	0.049	0.012	485	0.093	0.028	0.90	0.13	0.023	0.21	0.042	21.4	97.5	3396	63.0	795
NME1122	Group IB	10	0.024	0.003	n.d.	0.057	0.007	n.d.	0.007	0.012	n.d.	0.10	0.003	0.035	0.023	0.58	n.d.	0.008	0.029	0.006	457	0.058	0.017	0.45	0.067	0.013	0.11	0.021	14.9	85.0	3121	53.9	695
NME0528	Group IB	6	n.d.	0.005	0.008	0.034	0.010	0.002	0.001	0.010	0.020	0.17	0.005	0.029	0.030	0.84	0.027	0.010	0.047	0.014	438	0.095	0.032	0.82	0.12	0.023	0.20	0.039	22.3	102	3386	61.5	779
NME1116	Group IA	7	n.d.	0.010	0.004	0.158	0.017	0.003	0.013	0.043	0.037	0.27	0.012	0.074	0.044	2.19	0.052	0.019	0.075	0.012	425	0.11	0.035	0.81	0.11	0.025	0.20	0.035	18.8	89.9	3837	62.4	767
NBN0302A	Group IA	15	0.024	0.008	n.d.	0.038	0.021	n.d.	0.005	0.018	0.028	0.12	0.010	0.059	0.062	1.44	0.047	0.019	0.058	0.012	449	0.096	0.032	0.82	0.14	0.026	0.25	0.037	15.8	87.0	2531	61.4	745
NBN0305	Group IB	9	0.110	n.d.	n.d.	0.088	0.023	n.d.	0.011	0.021	0.030	0.13	0.015	n.d.	0.040	0.47	0.057	0.013	0.046	0.014	315	0.084	0.016	0.48	0.11	0.017	0.14	0.023	18.6	95.3	3003	61.0	764
NBN0311	Group IA	15	0.115	0.047	n.d.	0.039	0.027	n.d.	n.d.	0.013	0.022	0.15	0.006	0.041	0.041	1.05	0.053	0.014	0.048	0.012	455	0.096	0.029	0.81	0.14	0.024	0.25	0.043	15.1	86.7	2538	n.a.	n.a.
NBN0316	Group IA	11	0.316	0.036	n.d.	0.043	0.015	n.d.	0.031	0.019	n.d.	0.12	0.012	0.053	0.075	1.32	0.113	0.019	0.059	0.012	351	0.11	0.034	0.82	0.16	0.030	0.23	0.042	16.9	84.2	2098	64.5	763
NBN0319	Group IA	9	0.042	n.d.	n.d.	0.080	0.023	n.d.	n.d.	0.015	n.d.	0.027	0.005	n.d.	0.070	1.39	n.d.	0.013	0.042	0.012	352	0.088	0.029	0.70	0.11	0.029	0.22	0.038	16.8	85.6	2083	n.a.	n.a.
NBN0321	Group IA	14	0.206	0.011	n.d.	0.084	0.019	n.d.	0.006	0.013	0.203	0.087	0.005	0.032	0.052	1.10	0.028	0.016	0.063	0.012	537	0.10	0.033	0.75	0.11	0.021	0.19	0.037	17.1	89.6	2587	66.2	901

Table 3. Continued.

CLINOPYROXENE

Sample	Group	n	Rb	Th	U	Ba	Nb	Ta	La	Ce	Pb	Sr	Pr	Nd	Hf	Zr	Sm	Eu	Gd	Tb	Ti	Dy	Ho	Y	Er	Tm	Yb	Lu	Sc	V	Cr	Co	Ni	La_N/Lu_N	ΣREE
NMS1302A	Group IB	4	0.11	0.057	0.43	0.29	0.51	0.075	1.14	3.18	0.090	36.4	0.54	2.75	0.18	5.5	0.57	0.20	0.56	0.091	299	0.57	0.11	2.98	0.31	0.047	0.31	0.056	68.7	182	6246	21.3	350	2.13	10.4
NMS1304	Group IB	11	0.73	0.044	0.014	0.087	0.047	0.012	2.89	7.87	0.30	118	1.18	5.51	0.62	16.3	1.37	0.48	1.48	0.23	1419	1.48	0.28	7.18	0.71	0.10	0.70	0.096	70.0	250	5845	20.9	342	3.14	24.4
NMS1305	Group IB	6	0.23	0.23	0.063	0.24	0.33	0.056	4.73	14.4	0.12	100	2.25	10.2	1.72	85.8	2.47	0.88	2.59	0.44	1548	3.16	0.71	18.0	1.97	0.29	1.93	0.28	61.8	219	4913	21.0	331	1.75	46.2
NMS1308	Group IA	7	0.059	0.046	0.021	0.13	0.068	0.028	1.14	3.67	0.26	61.5	0.69	4.10	1.04	36.5	1.52	0.60	1.98	0.35	2298	2.49	0.52	13.8	1.50	0.20	1.30	0.18	60.8	248	8006	20.1	323	0.64	20.2
NMS1310	Group IA	8	0.049	0.023	0.010	0.038	0.093	0.021	1.03	3.57	n.d.	74.2	0.69	4.08	0.94	30.5	1.65	0.67	2.28	0.42	2965	2.99	0.66	17.2	1.93	0.27	1.80	0.27	68.5	272	6932	21.5	333	0.40	22.3
NJS1302	Group IIA	9	0.038	0.023	0.013	0.095	0.035	0.023	1.97	9.51	n.d.	47.5	2.06	11.9	3.27	127	3.87	1.36	4.52	0.74	6627	5.04	1.03	26.3	2.79	0.39	2.58	0.35	62.4	272	5784	21.6	320	0.59	48.1
NJS1304	Group IIA	4	0.086	0.032	0.010	0.27	0.083	0.036	2.13	9.73	0.062	56.4	2.02	11.3	2.49	100	3.29	1.16	3.72	0.60	5965	4.01	0.83	21.6	2.32	0.33	2.25	0.30	66.7	268	5687	22.0	329	0.74	44.0
NJS1306	Group IIA	7	n.d.	0.055	0.017	0.042	0.020	0.007	2.14	5.66	0.065	69.6	0.93	5.14	1.14	37.2	1.85	0.79	2.57	0.46	3051	3.29	0.71	18.6	2.03	0.27	1.91	0.27	59.3	254	4690	23.8	354	0.84	28.0
NJS1307	Group IA	6	0.059	0.017	0.011	0.024	0.10	0.020	1.16	4.26	0.042	79.4	0.83	5.06	1.28	42.3	1.95	0.79	2.83	0.50	4265	3.66	0.81	21.0	2.28	0.32	2.20	0.32	65.5	278	4912	22.7	344	0.38	26.9
NPY1301	Group IA	9	0.96	0.027	0.012	0.10	0.18	0.040	1.17	3.82	0.077	77.6	0.69	4.16	0.99	32.1	1.66	0.71	2.44	0.44	3355	3.24	0.72	18.9	2.08	0.30	2.07	0.29	64.1	270	5547	21.0	329	0.42	23.8
NPY1310	Group IIA	7	0.054	0.009	0.006	0.27	0.035	0.013	1.03	3.53	0.087	40.0	0.66	3.76	0.78	17.3	1.54	0.62	2.36	0.45	3353	3.22	0.71	18.3	1.96	0.28	1.90	0.28	66.8	327	2838	22.7	343	0.38	22.3
NPY1311	Group IIA	10	0.15	0.012	0.008	0.090	0.044	0.012	1.02	3.58	0.043	39.9	0.66	3.81	0.73	16.9	1.52	0.63	2.36	0.44	3261	3.26	0.70	18.5	2.07	0.29	1.96	0.28	62.7	319	2969	22.3	321	0.38	22.6
NPY1314	Group IA	6	n.d.	0.29	0.21	0.023	0.036	0.019	1.17	3.64	0.094	47.2	0.68	4.25	1.11	36.8	1.84	0.72	2.69	0.50	3430	3.54	0.79	20.6	2.25	0.33	2.17	0.29	62.0	263	4956	22.9	369	0.42	24.9
NFL1302	Group IB	7	0.067	0.11	0.032	0.54	0.19	0.011	2.21	5.07	0.065	50.4	0.71	3.46	0.68	20.5	1.29	0.52	1.91	0.35	1918	2.65	0.61	15.6	1.76	0.24	1.73	0.24	67.9	257	5692	21.2	341	0.95	22.7
NFL1305	Group IB	6	0.11	0.19	0.056	0.045	0.28	0.083	3.35	7.73	0.044	55.7	1.04	4.19	0.81	36.5	1.02	0.39	1.36	0.25	870	1.91	0.46	11.8	1.38	0.20	1.36	0.19	64.3	236	5873	21.1	335	1.80	24.8
NFL1315A	Group IB	7	n.d.	0.15	0.028	0.24	0.31	0.050	7.57	23.3	0.15	185	3.84	17.9	2.33	78.0	3.95	1.32	3.47	0.51	860	3.05	0.56	14.4	1.50	0.19	1.23	0.18	68.2	188	8606	20.4	302	4.36	68.6
NFL1316	Group IB	7	0.094	0.098	0.021	1.30	0.068	0.021	2.35	4.67	0.075	58.0	0.60	2.82	0.52	19.1	0.76	0.28	0.76	0.12	813	0.73	0.15	3.89	0.45	0.06	0.51	0.079	90.4	267	6970	20.2	335	3.11	14.3
NFL1324	Group IB	7	0.051	0.41	0.13	0.23	0.52	0.12	13.5	39.2	0.43	169	5.98	26.4	2.40	122	5.16	1.59	4.26	0.57	1187	3.47	0.66	16.8	1.70	0.23	1.39	0.19	60.5	179	8631	21.1	351	7.49	104
NFL1326	Group IIB	7	n.d.	0.10	0.022	0.091	0.24	0.034	4.53	13.1	0.061	96.6	2.10	9.81	1.02	30.0	2.55	0.92	2.81	0.43	2220	2.94	0.60	15.3	1.62	0.24	1.60	0.22	57.1	244	5889	21.2	259	2.18	43.4
NFL1327	Group IIB	7	n.d.	0.069	0.017	0.14	0.29	0.040	6.38	20.1	0.064	118	3.22	15.1	0.33	22.5	3.35	1.14	2.80	0.42	1209	2.54	0.50	13.4	1.40	0.20	1.37	0.19	49.6	196	6927	21.7	306	3.47	58.7
NFL1329	Group IA	7	n.d.	0.20	0.080	0.034	0.043	0.014	1.15	3.21	0.10	46.8	0.59	3.38	0.88	25.6	1.31	0.58	1.94	0.36	1815	2.65	0.58	15.0	1.65	0.23	1.57	0.22	63.7	240	4462	21.4	342	0.54	19.4
NTB0306	Group IB	8	0.13	0.30	0.054	0.41	0.040	n.d.	3.60	5.07	0.12	74.7	0.37	1.06	0.090	1.72	0.34	0.15	0.57	0.11	808	0.82	0.19	4.39	0.56	0.08	0.54	0.081	73.7	262	7253	21.5	338	4.64	13.5
NTB0307	Group IA	7	0.035	0.066	0.023	0.066	0.071	0.019	0.83	2.64	0.045	37.7	0.43	2.32	0.41	10.1	0.89	0.38	1.36	0.26	1553	2.01	0.44	11.4	1.31	0.19	1.28	0.18	61.1	255	6129	22.0	372	0.49	14.5
NTB1124	Group IA	13	0.038	0.013	0.005	0.062	0.034	0.006	0.75	2.50	0.072	48.1	0.45	2.89	0.72	17.9	1.25	0.51	1.84	0.34	3597	2.50	0.54	13.8	1.55	0.22	1.45	0.20	65.0	287	8177	23.3	374	0.40	17.0
NTB1116	Group IA	6	0.11	0.026	0.026	0.11	0.083	0.016	0.83	3.01	0.067	64.1	0.60	3.53	0.73	22.5	1.37	0.55	1.89	0.35	2070	2.53	0.57	14.5	1.51	0.22	1.47	0.19	70.5	273	7609	20.6	329	0.45	18.6
NTB1122	Group IIB	6	n.d.	0.12	0.042	0.091	0.14	0.058	3.62	12.6	0.068	68.4	2.28	12.3	1.36	39.7	3.51	1.19	3.82	0.60	5783	3.99	0.80	20.6	2.21	0.30	1.99	0.28	66.7	315	5617	23.1	332	1.35	49.5

Table 3. Continued.

CLINOPYROXENE

Sample	Group	n	Rb	Th	U	Ba	Nb	Ta	La	Ce	Pb	Sr	Pr	Nd	Hf	Zr	Sm	Eu	Gd	Tb	Ti	Dy	Ho	Y	Er	Tm	Yb	Lu	Sc	V	Cr	Co	Ni	La_N/Lu_N	ΣREE
NFK0301	Group IB	16	0.046	0.15	0.036	0.059	0.44	0.078	11.3	34.7	0.075	147	4.68	19.3	0.58	32.9	3.73	1.25	3.16	0.46	1743	3.09	0.60	15.9	1.68	0.24	1.63	0.23	59.1	230	8972	21.5	352	5.07	86.2
NFK1123	Group IB	9	n.d.	0.17	0.077	0.12	0.24	0.045	13.6	37.0	1.47	113	4.33	15.7	0.56	23.0	2.24	0.65	1.94	0.28	2011	1.75	0.35	9.03	0.95	0.13	0.89	0.12	58.3	231	9029	22.9	385	11.95	79.9
NFK1108	Group IIB	6	0.078	0.047	0.016	0.25	0.15	0.021	2.96	9.13	0.082	87.2	1.46	6.93	0.59	18.2	1.80	0.74	2.14	0.38	2010	2.58	0.54	14.0	1.54	0.21	1.49	0.21	65.0	258	7408	22.2	327	1.46	32.1
NFK1115	Group IIB	5	n.d.	0.066	0.011	0.11	0.16	0.019	6.38	20.7	0.076	170	3.36	15.4	0.85	47.1	3.21	1.03	2.67	0.37	319	2.17	0.44	11.0	1.13	0.17	1.15	0.15	84.6	238	8804	20.6	334	4.45	58.2
NFR0306	Group IIB	13	0.067	0.068	0.014	0.38	0.14	0.019	3.51	11.8	0.045	83.6	1.74	8.02	0.79	22.1	2.08	0.83	2.35	0.39	2040	2.70	0.56	14.2	1.65	0.24	1.60	0.22	63.8	281	7723	23.6	318	1.63	37.6
NFR0307	Group IIB	15	0.11	0.16	0.075	0.060	0.082	0.017	1.21	3.75	0.076	42.5	0.54	2.59	0.37	9.79	0.67	0.25	0.88	0.17	1880	1.33	0.31	7.95	0.93	0.14	1.00	0.14	61.8	274	6516	23.9	400	0.89	13.9
NFR1109	Group IIB	10	0.033	0.093	0.027	0.039	0.14	0.017	4.87	16.1	0.072	132	2.37	10.8	0.38	17.4	2.43	0.91	2.20	0.32	1184	1.92	0.36	9.20	0.95	0.14	0.95	0.13	61.2	243	10559	24.9	330	3.85	44.4
NFR0309	Group IB	6	n.d.	0.53	0.14	0.049	0.47	0.037	3.00	6.77	0.064	47.2	0.99	4.99	1.12	39.1	1.88	0.77	2.67	0.50	3825	3.66	0.77	20.6	2.23	0.30	2.06	0.30	62.5	266	5138	21.1	314	1.04	30.9
NFR1107	Group IB	6	n.d.	0.12	0.047	0.035	0.10	0.013	1.50	5.40	0.070	107	1.05	5.78	0.82	27.4	1.61	0.65	2.01	0.32	1834	2.18	0.47	11.7	1.23	0.17	1.02	0.14	82.7	284	8539	20.8	332	1.13	23.5
NMC1301	Group IB	8	n.d.	0.20	0.041	0.15	1.12	0.26	10.0	27.8	0.080	185	3.81	14.6	1.00	55.7	2.28	0.77	1.70	0.26	690	1.56	0.31	8.32	0.83	0.12	0.72	0.099	82.8	267	8910	22.2	359	10.50	64.9
NMC1309	Group IIB	8	n.d.	0.035	0.011	0.15	0.078	0.015	2.05	5.82	0.050	57.1	0.82	3.69	0.41	13.2	1.04	0.46	1.50	0.29	1235	2.12	0.48	13.2	1.48	0.21	1.49	0.21	66.7	254	6156	21.1	332	1.02	21.7
NMC1322	Group IB	8	0.13	0.15	0.037	0.54	0.29	0.068	2.59	6.61	0.14	51.4	1.01	4.81	0.35	10.3	1.21	0.41	1.53	0.28	1179	2.20	0.50	13.6	1.50	0.22	1.56	0.22	71.7	242	6893	20.1	338	1.26	24.6
NMC1336A	Group IA	7	0.050	0.086	0.045	0.032	0.008	0.005	0.46	2.19	0.16	41.8	0.55	3.95	0.94	26.1	1.77	0.74	2.68	0.49	2954	3.56	0.76	19.9	2.13	0.27	1.80	0.24	65.1	247	7565	21.2	352	0.20	21.6
NMM1126	Group IA	9	0.37	0.031	0.016	0.22	0.076	0.010	0.47	1.48	0.096	26.6	0.25	1.55	0.25	5.95	0.66	0.29	1.17	0.23	1606	1.90	0.44	11.4	1.34	0.20	1.35	0.19	65.9	265	7441	23.7	390	0.26	11.5
NMM0318	Group IIB	6	n.d.	0.50	0.14	0.097	0.19	0.014	6.27	18.4	0.10	87.4	2.80	12.5	1.11	47.9	2.91	1.11	3.06	0.50	2072	3.43	0.72	18.6	2.05	0.28	1.93	0.27	55.8	226	4815	21.9	318	2.40	56.2
NMM1115	Group IB	5	n.d.	3.48	1.06	0.063	0.070	0.008	1.31	2.54	0.055	45.4	0.47	2.98	0.58	20.2	1.17	0.49	1.73	0.31	1778	2.26	0.50	13.0	1.45	0.21	1.28	0.19	72.6	267	7089	20.5	331	0.71	16.9
NME1122	Group IB	12	0.17	0.30	0.077	0.069	0.064	0.006	2.15	4.14	0.069	45.0	0.49	2.51	0.47	13.8	0.94	0.39	1.31	0.23	2257	1.59	0.32	8.30	0.89	0.13	0.87	0.12	58.0	291	8366	23.1	382	1.82	16.1
NME0528	Group IB	7	0.080	0.13	0.025	0.096	0.20	0.063	4.38	12.4	0.10	106	1.88	8.28	0.99	41.7	2.06	0.71	2.04	0.32	1399	2.15	0.44	10.9	1.15	0.16	1.07	0.14	78.1	267	9184	20.9	324	3.18	37.2
NME1116	Group IA	6	n.d.	0.011	0.010	0.023	0.058	0.009	0.74	2.77	0.030	63.7	0.53	2.87	0.43	16.6	0.98	0.39	1.43	0.25	1648	1.97	0.44	11.7	1.30	0.19	1.31	0.19	69.9	267	7205	20.7	330	0.40	15.4
NBN0302A	Group IA	12	0.47	0.049	0.020	0.33	0.053	0.011	0.98	3.74	0.092	50.4	0.67	4.09	0.94	28.5	1.61	0.64	2.16	0.38	2067	2.55	0.53	13.7	1.52	0.21	1.53	0.20	57.8	241	6083	22.2	353	0.51	20.8
NBN0305	Group IB	9	0.26	0.025	0.011	0.51	0.049	n.d.	1.49	4.10	0.16	92.6	0.67	3.47	0.39	8.12	1.12	0.36	1.23	0.20	1166	1.29	0.26	6.53	0.76	0.11	0.71	0.10	65.8	256	6000	22.8	370	1.53	15.9
NBN0311	Group IA	18	0.20	0.040	0.013	0.15	0.098	0.017	1.01	3.58	0.031	60.6	0.62	3.73	0.81	25.9	1.50	0.63	2.16	0.41	2381	2.88	0.59	15.5	1.79	0.24	1.65	0.24	60.6	265	5966	n.a.	n.a.	0.44	21.0
NBN0316	Group IA	9	0.055	0.070	0.017	0.20	0.062	n.d.	0.65	2.50	0.27	19.7	0.45	2.86	0.63	16.7	1.13	0.48	1.55	0.29	1290	1.97	0.41	10.1	1.16	0.16	1.03	0.15	44.6	178	3287	23.4	367	0.44	14.8
NBN0319	Group IA	13	0.017	0.023	0.010	n.d.	0.031	0.006	0.61	2.58	0.23	22.4	0.48	2.73	0.61	15.2	1.06	0.43	1.41	0.24	1161	1.72	0.31	8.24	1.04	0.13	0.93	0.13	40.0	164	2971	n.a.	n.a.	0.44	13.8
NBN0321	Group IA	23	0.21	0.029	0.014	0.37	0.093	0.017	0.85	3.35	0.17	53.6	0.63	3.93	0.92	24.5	1.85	0.75	2.82	0.50	3614	3.23	0.64	15.6	1.79	0.23	1.47	0.21	75.4	329	6354	23.1	368	0.42	22.2

Table 3. Continued.

AMPHIBOLE

Sample	Group	n	Rb	Th	U	Ba	Nb	Ta	La	Ce	Pb	Sr	Pr	Nd	Hf	Zr	Sm	Eu	Gd	Tb	Ti	Dy	Ho	Y	Er	Tm	Yb	Lu	Sc	V	Cr	Co	Ni
NMS1304	Group IB	7	7.53	0.092	0.016	210	3.55	0.41	5.96	15.2	0.71	354	2.15	9.84	0.87	27.4	2.31	0.84	2.57	0.38	8139	2.52	0.49	12.7	1.27	0.17	1.07	0.17	82.0	543	11501	39.2	885
NMS1308	Group IA	3	4.51	0.024	0.017	33.6	6.21	0.41	0.87	3.38	0.12	135	0.72	4.39	0.86	26.7	1.97	0.81	2.58	0.46	14491	3.24	0.70	18.3	1.89	0.26	1.64	0.24	44.9	363	9605	39.6	812
NJS1302	Group IIA	2	n.d.	n.d.	0.017	0.94	1.04	0.069	1.26	7.15	n.d.	208	1.72	12.0	1.74	64.7	4.38	1.58	5.96	1.03	37920	6.85	1.36	34.7	3.41	0.43	2.48	0.39	54.1	539	4201	46.4	799
			0.223	n.d.	0.027	1.44	1.85	0.28	2.65	12.1	n.d.	197	2.42	14.0	2.28	87.6	4.27	1.46	4.59	0.78	25602	4.95	1.06	27.7	2.82	0.34	2.58	0.30	45.3	372	7806	48.2	928
NFL1302	Group IB	2	6.35	0.11	0.028	83.3	13.2	0.38	3.17	7.48	0.12	137	0.99	4.51	0.66	23.5	1.59	0.71	2.23	0.44	9205	3.22	0.73	19.4	2.21	0.29	1.94	0.27	53.3	414	8831	38.6	836
NFL1315A	Group IB	5	7.44	0.28	0.059	156	72.5	3.46	13.5	39.9	0.45	433	6.24	29.1	3.25	127	6.40	2.10	5.49	0.76	11278	4.49	0.83	20.9	2.10	0.26	1.64	0.22	51.8	310	13109	36.8	748
NFL1324	Group IB	7	12.3	0.58	0.18	322	80.9	4.56	22.1	60.7	1.65	424	8.79	39.1	4.10	174	7.44	2.27	6.00	0.80	8683	4.68	0.87	22.4	2.11	0.28	1.71	0.23	53.9	327	13314	39.6	914
NFL1326	Group IIB	6	7.75	0.11	0.026	132	17.4	0.74	5.55	15.7	0.24	252	2.41	11.6	1.02	33.3	2.94	1.03	3.12	0.49	10243	3.27	0.67	17.3	1.81	0.25	1.62	0.23	45.9	402	10995	40.1	625
NFL1329	Group IA	3	2.71	0.20	0.091	20.1	2.75	0.19	1.38	3.79	0.30	127	0.69	3.90	0.86	26.9	1.74	0.68	2.48	0.44	9885	3.28	0.72	19.1	2.10	0.31	2.00	0.27	50.3	406	7344	42.4	929

5.2.3. Whole-rock geochemistry

Major elements

Whole-rock major-element compositions (Table 4) were calculated from analyses of the mineral constituents using the mass-balance approach. The modal analyses may not be representative, due to the size of the xenoliths, and this uncertainty will be inherited in the calculated bulk-rock compositions; however, several conclusions can still be drawn. Contents of MgO are compared with those of the less refractory major elements in Fig. 5.11. The studied xenoliths show negative correlations between MgO and Al_2O_3, TiO_2, CaO and Na_2O (Fig. 5.11a-d, respectively), in accordance with the general pattern observed in mantle peridotites (e.g., Frey and Prinz, 1978; Boyd, 1989). The highest contents of basaltic elements and the lowest MgO contents are observed in a group of xenoliths from the northern part. In contrast, xenoliths from the southern part tend to remain on the other end of the trend, and those from the central part cover a wider range. The scattering of the data is due to the Group II xenoliths, which plot consequently to the left of the main trend, reflecting a decrease in MgO content. This is clearly linked to the lower Mg# of olivine (Fig. 5.7a, b) and orthopyroxene (Fig. 5.7c). Interestingly, whole-rock FeO contents do not seem to correlate with MgO as Group I xenoliths often show higher FeO concentrations without a decrease in MgO.

Rare-earth elements

Whole-rock trace-element contents (Table 4) have been determined by mass balance calculation. Olivine and spinel compositions have been calculated using clinopyroxene trace-element contents and mineral/melt distribution coefficients of Hart and Dunn (1993), Ionov et al. (2002) and references therein. Olivine/clinopyroxene and spinel/clinopyroxene distribution coefficients were obtained by dividing mineral/melt with cpx/melt distribution coefficients. Trace-element contents of orthopyroxene have been recalculated as well because of analytical uncertainties in the case of the most incompatible elements, which are present in very low concentrations (e.g., LREE). The reliability of the calculated concentrations is verified by good correlations between analyzed and calculated HREE contents of orthopyroxene ($R^2 = 0.85$ for Lu; Fig. 5.12).

Whole-rock REE+Y contents correlate well with clinopyroxene analyses (Table 3). Total REE+Y contents vary between 0.557 (NMS1302A) and 8.26 (NFL1324) ppm in

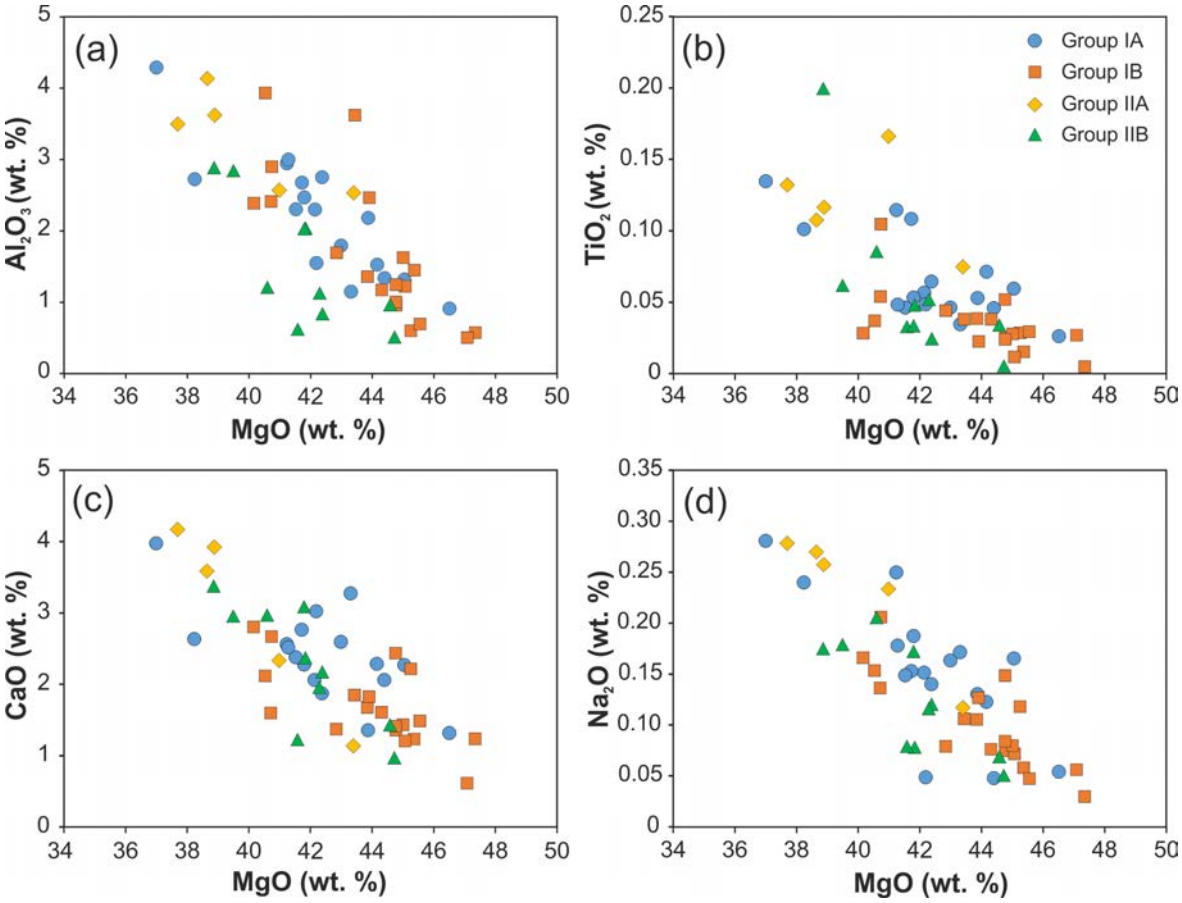

Fig. 5.11. Whole-rock MgO compositions of the studied NGVF xenoliths compared to a – Al_2O_3, b – TiO_2, c – CaO, d – Na_2O. Whole-rock compositions were calculated by mass balance from analyzed major-element components of mineral constituents (Table 4).

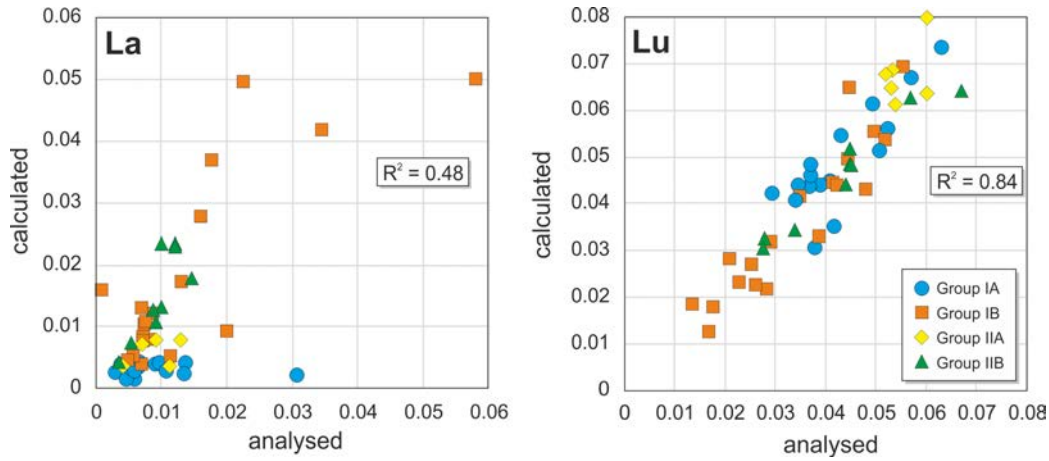

Fig. 5.12. Analysed *vs* calculated light and heavy REE (with the example of La and Lu) contents of orthopyroxene.

Group IB. Xenoliths of Group IA show a narrow range (1.27 – 3.51 ppm) in total REE+Y, whereas Groups IIA and B (2.47 – 5.67 and 1.47 – 7.78 ppm) both have significantly higher REE+Y contents. The xenoliths with the most depleted HREE (Yb < 0.1 ppm, Lu <0.015) mostly are those with the most depleted major element characteristics (highest spinel Cr#; Fig. 5.7a, Table 2).

5.3. Geothermometry

The geochemical compositions of the rock-forming minerals may allow estimation of temperature/pressure conditions in the represented upper mantle domain if there are appropriate coexisting mineral pairs. The application of geothermometers is based on cation exchange between specific minerals, if there is significant temperature dependence and, ideally, if temperature change is mostly independent of pressure. A critical factor in the reliability of geothermometers is the assumption that the coexisting phases were in equilibrium. Although there is no adequate geobarometer for the spinel peridotite field, from which the Nógrád-Gömör xenoliths all originate, there are several geothermometers based on the exchange of major elements in different rock-forming minerals, especially pyroxenes (e.g., Brey and Köhler, 1990; Witt-Eickschen and Seck, 1991; Taylor, 1998). The most widely applied of these is the two-pyroxene thermometer of Brey and Köhler (1990).

In the Nógrád-Gömör xenoliths, there is no clear petrographic signature of disequilibrium among the phases. Furthermore, there is no major geochemical variation within the grains, or between grains in the same sample, which allows the assumption that the coexisting phases were in equilibrium at the time of their entrainment. I have calculated equilibration temperatures using several methods, including the two-pyroxene thermometers of Brey and Köhler (1990) (uncertainty [σ] = 15°C) and Taylor (1998) (σ = 31°C), as well as the Ca-in-opx thermometer of Brey and Köhler (1990) with modifications applied by Nimis and Grütter (2010) (σ = 36 °C for temperatures between 900-1200 °C). The resulting equilibration temperatures are in the range of 845-1058, 829-1012 and 921-1044 °C respectively (Table 1). These values are consistent with the geothermometry c of Szabó and Taylor (1994). Xenoliths from the southern part, regardless of their texture, have lower equilibration temperatures than those from the central part (Table 1). Temperatures obtained with the two-pyroxene method of Brey and Köhler (1990) are plotted against the

Table 4. Calculated whole-rock geochemical compositions.

WHOLE ROCK

Sample	Group	SiO_2	TiO_2	Al_2O_3	Cr_2O_3	FeO	MnO	MgO	CaO	Na_2O	NiO	Th	U	Nb	Ta	La	Ce
NMS1302A	Group IB	42.5	0.00	0.58	0.43	8.05	0.12	47.3	1.24	0.03	0.37	0.003	0.022	0.039	0.004	0.059	0.17
NMS1304	Group IB	43.2	0.04	1.17	0.37	8.57	0.13	44.3	1.61	0.08	0.34	0.004	0.001	0.040	0.005	0.24	0.64
NMS1305	Group IB	44.1	0.04	3.93	0.60	8.77	0.14	40.5	2.12	0.15	0.30	0.021	0.006	0.042	0.005	0.44	1.33
NMS1308	Group IA	44.2	0.06	2.30	0.59	8.29	0.13	42.1	2.06	0.15	0.31	0.004	0.002	0.015	0.003	0.11	0.34
NMS1310	Group IA	48.8	0.10	2.73	0.34	7.42	0.13	38.2	2.63	0.24	0.23	0.003	0.001	0.014	0.002	0.12	0.40
NJS1302	Group IIA	43.0	0.17	2.57	0.40	10.12	0.14	41.0	2.33	0.23	0.31	0.003	0.001	0.006	0.003	0.22	1.08
NJS1304	Group IIA	41.8	0.07	2.53	0.44	10.80	0.15	43.4	1.14	0.12	0.34	0.002	0.000	0.007	0.002	0.11	0.51
NJS1306	Group IIA	42.6	0.11	4.13	0.53	10.15	0.16	38.6	3.59	0.27	0.30	0.009	0.003	0.004	0.001	0.37	0.98
NJS1307	Group IA	43.8	0.11	2.95	0.33	8.88	0.14	41.2	2.56	0.25	0.31	0.002	0.001	0.016	0.002	0.14	0.52
NPY1301	Group IA	42.8	0.05	2.18	0.29	9.44	0.14	43.9	1.36	0.13	0.33	0.002	0.001	0.016	0.002	0.072	0.24
NPY1310	Group IIA	43.1	0.12	3.62	0.26	9.22	0.14	38.9	3.92	0.26	0.29	0.002	0.001	0.007	0.002	0.19	0.64
NPY1311	Group IIA	44.7	0.13	3.50	0.24	8.74	0.15	37.7	4.17	0.28	0.26	0.002	0.002	0.010	0.002	0.20	0.69
NPY1314	Group IA	45.4	0.13	4.29	0.49	7.91	0.14	37.0	3.97	0.28	0.25	0.052	0.037	0.008	0.003	0.21	0.67
NFL1302	Group IB	41.2	0.04	3.62	0.83	8.61	0.13	43.4	1.85	0.11	0.35	0.009	0.003	0.035	0.001	0.18	0.43
NFL1305	Group IB	45.9	0.03	2.39	0.42	7.56	0.13	40.2	2.80	0.17	0.27	0.023	0.007	0.043	0.010	0.41	0.95
NFL1315A	Group IB	41.2	0.03	0.50	0.49	9.88	0.15	47.1	0.61	0.06	0.34	0.003	0.001	0.088	0.005	0.18	0.56
NFL1316	Group IB	42.3	0.02	1.45	1.14	8.62	0.13	45.4	1.23	0.06	0.34	0.005	0.001	0.006	0.001	0.12	0.25
NFL1324	Group IB	46.8	0.05	2.41	0.78	7.13	0.13	40.7	1.60	0.14	0.27	0.030	0.009	1.26	0.075	1.04	3.00
NFL1326	Group IIB	41.2	0.09	1.21	0.41	12.98	0.24	40.6	2.97	0.21	0.24	0.015	0.003	0.38	0.019	0.66	1.91
NFL1327	Group IIB	41.1	0.02	0.84	0.41	13.27	0.24	42.4	2.18	0.12	0.30	0.007	0.002	0.036	0.004	0.65	2.05
NFL1329	Group IA	43.5	0.05	1.80	0.23	8.67	0.13	43.0	2.59	0.16	0.33	0.023	0.009	0.009	0.002	0.14	0.38
NTB0306	Group IB	43.5	0.03	0.60	0.24	8.41	0.16	45.3	2.22	0.12	0.32	0.030	0.005	0.005	0.000	0.37	0.52
NTB0307	Group IA	44.4	0.03	1.15	0.19	7.97	0.12	43.3	3.28	0.17	0.33	0.010	0.004	0.013	0.003	0.13	0.41
NTB1124	Group IA	44.6	0.11	2.68	0.62	7.59	0.13	41.7	2.76	0.15	0.28	0.002	0.001	0.005	0.001	0.092	0.31
NTB1116	Group IA	44.5	0.05	2.47	0.59	7.92	0.13	41.8	2.28	0.19	0.30	0.003	0.003	0.011	0.002	0.085	0.31
NTB1122	Group IIB	44.1	0.20	2.89	0.53	9.68	0.17	38.9	3.38	0.17	0.25	0.019	0.006	0.026	0.009	0.55	1.92
NFK0301	Group IB	43.7	0.02	0.96	0.20	8.80	0.15	44.8	1.36	0.07	0.31	0.009	0.002	0.038	0.005	0.67	2.07
NFK1123	Group IB	45.9	0.04	1.69	0.47	7.44	0.13	42.8	1.37	0.08	0.27	0.009	0.004	0.021	0.002	0.71	1.96
NFK1108	Group IIB	42.3	0.03	0.96	0.38	10.12	0.17	44.6	1.43	0.07	0.31	0.003	0.001	0.013	0.001	0.18	0.57
NFK1115	Group IIB	42.2	0.01	0.51	0.48	10.37	0.19	44.7	0.97	0.05	0.35	0.003	0.000	0.011	0.001	0.27	0.88
NFR0306	Group IIB	40.2	0.05	1.13	0.70	13.05	0.23	42.3	1.96	0.12	0.29	0.006	0.001	0.016	0.002	0.32	1.08
NFR0307	Group IIB	41.0	0.05	2.04	0.75	11.00	0.21	41.8	2.37	0.08	0.27	0.016	0.008	0.011	0.002	0.12	0.38
NFR1109	Group IIB	43.1	0.03	0.62	0.38	12.92	0.25	41.6	1.23	0.08	0.26	0.005	0.001	0.011	0.001	0.25	0.85
NFR0309	Group IB	44.2	0.10	2.90	0.32	8.51	0.14	40.7	2.67	0.21	0.29	0.063	0.017	0.071	0.004	0.37	0.83
NFR1107	Group IB	44.3	0.04	1.36	0.44	7.88	0.13	43.8	1.68	0.11	0.32	0.008	0.003	0.011	0.001	0.11	0.39
NMC1301	Group IB	42.7	0.01	1.22	0.80	9.01	0.13	45.1	1.20	0.07	0.36	0.010	0.002	0.090	0.014	0.52	1.46
NMC1309	Group IIB	42.5	0.03	2.03	0.50	10.03	0.17	41.8	3.09	0.17	0.33	0.005	0.002	0.013	0.002	0.29	0.83
NMC1322	Group IB	42.6	0.02	2.47	0.65	8.59	0.13	43.9	1.83	0.13	0.35	0.012	0.003	0.032	0.006	0.21	0.55
NMC1336A	Group IA	43.8	0.06	2.75	0.80	8.11	0.12	42.4	1.87	0.14	0.32	0.007	0.004	0.001	0.000	0.038	0.18
NMM1126	Group IA	45.7	0.05	2.30	0.41	7.75	0.14	41.5	2.38	0.15	0.28	0.003	0.002	0.010	0.001	0.048	0.15
NMM0318	Group IIB	44.6	0.06	2.84	0.38	9.23	0.16	39.5	2.96	0.18	0.28	0.065	0.018	0.031	0.002	0.83	2.44
NMM1115	Group IB	42.6	0.03	1.63	0.53	8.41	0.12	45.0	1.43	0.08	0.35	0.21	0.064	0.006	0.001	0.081	0.16
NME1122	Group IB	43.3	0.05	1.25	0.29	8.42	0.13	44.8	2.44	0.15	0.29	0.034	0.009	0.009	0.001	0.24	0.47
NME0528	Group IB	43.2	0.02	1.00	0.48	8.77	0.14	44.8	1.42	0.08	0.34	0.008	0.001	0.018	0.004	0.27	0.77
NME1116	Group IA	44.4	0.05	3.00	0.00	7.84	0.13	41.3	2.52	0.18	0.29	0.001	0.001	0.008	0.001	0.083	0.31
NBN0302A	Group IA	42.1	0.03	0.91	0.18	9.18	0.14	46.5	1.32	0.05	0.33	0.003	0.001	0.004	0.001	0.055	0.21
NBN0305	Group IB	43.1	0.03	0.70	0.16	8.52	0.14	45.6	1.49	0.05	0.32	0.002	0.001	0.004	0.000	0.093	0.26
NBN0311	Group IA	41.5	0.06	1.32	0.39	8.81	0.14	45.0	2.27	0.17	0.29	0.004	0.001	0.013	0.002	0.11	0.38
NBN0316	Group IA	42.3	0.05	1.34	0.20	9.14	0.14	44.4	2.06	0.05	0.34	0.006	0.001	0.007	0.000	0.058	0.22
NBN0319	Group IA	43.6	0.05	1.55	0.19	8.65	0.15	42.2	3.02	0.05	0.27	0.003	0.001	0.005	0.001	0.079	0.33
NBN0321	Group IA	42.7	0.07	1.53	0.31	8.68	0.13	44.2	2.29	0.12	0.31	0.003	0.001	0.012	0.002	0.087	0.34

Table 4. Continued.

WHOLE ROCK																		
Sample	Pb	Sr	Pr	Nd	Hf	Zr	Sm	Eu	Gd	Tb	Ti	Dy	Ho	Er	Tm	Yb	Lu	ΣREE
NMS1302A	0.005	1.85	0.028	0.14	0.014	0.44	0.030	0.011	0.030	0.005	25.1	0.032	0.006	0.019	0.003	0.021	0.004	0.56
NMS1304	0.026	10.7	0.095	0.44	0.065	1.73	0.11	0.038	0.12	0.019	233	0.13	0.026	0.068	0.010	0.072	0.011	2.02
NMS1305	0.012	9.14	0.21	0.94	0.21	10.3	0.23	0.083	0.26	0.045	270	0.34	0.081	0.24	0.037	0.27	0.043	4.55
NMS1308	0.025	5.74	0.065	0.38	0.13	4.40	0.14	0.057	0.20	0.036	373	0.26	0.057	0.17	0.025	0.17	0.027	2.05
NMS1310	-	8.27	0.078	0.46	0.14	4.30	0.19	0.078	0.29	0.055	644	0.41	0.099	0.31	0.049	0.36	0.059	2.96
NJS1302	-	5.47	0.23	1.35	0.46	17.7	0.44	0.15	0.53	0.088	1120	0.61	0.13	0.36	0.052	0.37	0.052	5.67
NJS1304	0.003	2.87	0.11	0.59	0.20	8.06	0.17	0.061	0.21	0.034	633	0.24	0.052	0.16	0.024	0.18	0.026	2.47
NJS1306	0.011	11.9	0.16	0.89	0.23	7.32	0.32	0.14	0.45	0.081	701	0.59	0.13	0.38	0.052	0.38	0.055	4.97
NJS1307	0.005	9.60	0.10	0.62	0.19	6.28	0.24	0.097	0.36	0.064	767	0.48	0.11	0.32	0.048	0.35	0.053	3.51
NPY1301	0.005	4.73	0.043	0.26	0.090	2.89	0.10	0.044	0.16	0.030	381	0.23	0.053	0.16	0.025	0.19	0.029	1.64
NPY1310	0.016	7.24	0.12	0.69	0.16	3.58	0.28	0.11	0.44	0.084	776	0.61	0.14	0.38	0.056	0.39	0.060	4.18
NPY1311	0.008	7.62	0.13	0.73	0.16	3.67	0.29	0.12	0.47	0.088	822	0.66	0.15	0.44	0.063	0.45	0.066	4.54
NPY1314	0.017	8.55	0.12	0.78	0.23	7.64	0.34	0.13	0.51	0.096	905	0.70	0.16	0.48	0.073	0.51	0.073	4.86
NFL1302	0.006	4.21	0.060	0.29	0.076	2.27	0.11	0.044	0.16	0.031	278	0.24	0.056	0.17	0.024	0.18	0.027	2.00
NFL1305	0.006	6.75	0.13	0.51	0.12	5.45	0.13	0.048	0.18	0.033	173	0.27	0.068	0.21	0.032	0.24	0.037	3.24
NFL1315A	0.004	4.30	0.092	0.43	0.12	4.09	0.094	0.032	0.090	0.014	63.2	0.088	0.018	0.052	0.007	0.053	0.009	1.72
NFL1316	0.004	2.95	0.031	0.15	0.042	1.53	0.040	0.015	0.042	0.007	83.2	0.043	0.009	0.030	0.004	0.038	0.006	0.78
NFL1324	0.050	15.0	0.45	1.99	0.27	12.6	0.39	0.12	0.36	0.051	312	0.33	0.069	0.20	0.029	0.20	0.031	8.26
NFL1326	0.012	16.7	0.30	1.43	0.17	5.07	0.37	0.13	0.40	0.062	521	0.43	0.087	0.24	0.035	0.24	0.032	6.32
NFL1327	0.007	11.9	0.33	1.54	0.042	2.88	0.34	0.12	0.29	0.043	152	0.26	0.052	0.15	0.021	0.15	0.021	6.01
NFL1329	0.013	5.55	0.070	0.40	0.13	3.69	0.16	0.069	0.24	0.044	300	0.33	0.075	0.22	0.031	0.23	0.034	2.41
NTB0306	0.013	7.54	0.037	0.11	0.012	0.22	0.034	0.016	0.060	0.011	115	0.090	0.021	0.065	0.010	0.070	0.011	1.42
NTB0307	0.007	5.80	0.066	0.36	0.074	1.81	0.14	0.059	0.21	0.041	283	0.32	0.072	0.21	0.031	0.22	0.031	2.30
NTB1124	0.009	5.82	0.056	0.35	0.11	2.67	0.15	0.064	0.24	0.044	695	0.34	0.077	0.23	0.035	0.24	0.035	2.27
NTB1116	0.007	6.47	0.061	0.36	0.097	2.91	0.14	0.057	0.20	0.039	347	0.29	0.069	0.19	0.030	0.21	0.030	2.08
NTB1122	0.011	10.3	0.35	1.88	0.24	7.06	0.54	0.18	0.60	0.096	1232	0.65	0.13	0.39	0.055	0.38	0.056	7.78
NFK0301	0.005	8.51	0.28	1.15	0.051	2.87	0.22	0.075	0.20	0.030	189	0.21	0.044	0.13	0.021	0.15	0.024	5.28
NFK1123	0.084	5.77	0.23	0.83	0.048	1.88	0.12	0.035	0.12	0.018	275	0.13	0.028	0.085	0.013	0.10	0.016	4.40
NFK1108	0.005	5.30	0.091	0.43	0.053	1.63	0.11	0.046	0.14	0.025	192	0.17	0.037	0.11	0.016	0.12	0.017	2.06
NFK1115	0.003	6.93	0.14	0.65	0.060	3.31	0.14	0.043	0.12	0.017	25.5	0.10	0.022	0.061	0.010	0.071	0.010	2.53
NFR0306	0.004	7.58	0.16	0.74	0.093	2.61	0.19	0.076	0.22	0.036	245	0.25	0.053	0.16	0.023	0.16	0.023	3.49
NFR0307	0.008	4.29	0.055	0.26	0.047	1.26	0.068	0.026	0.091	0.018	277	0.14	0.034	0.11	0.016	0.12	0.018	1.47
NFR1109	0.004	6.71	0.12	0.57	0.031	1.40	0.13	0.049	0.13	0.019	124	0.12	0.024	0.069	0.011	0.083	0.013	2.43
NFR0309	0.008	5.71	0.12	0.61	0.17	5.81	0.23	0.095	0.34	0.064	702	0.49	0.11	0.32	0.046	0.33	0.051	4.00
NFR1107	0.005	7.59	0.076	0.42	0.083	2.74	0.12	0.048	0.15	0.026	236	0.18	0.041	0.11	0.017	0.11	0.016	1.82
NMC1301	0.004	9.44	0.20	0.77	0.081	4.47	0.12	0.041	0.093	0.015	68.9	0.093	0.020	0.055	0.008	0.056	0.008	3.45
NMC1309	0.007	8.04	0.12	0.52	0.068	2.21	0.15	0.065	0.21	0.042	220	0.31	0.071	0.22	0.033	0.23	0.034	3.13
NMC1322	0.012	4.16	0.083	0.40	0.038	1.13	0.10	0.034	0.13	0.024	160	0.20	0.047	0.15	0.023	0.17	0.025	2.13
NMC1336A	0.014	3.38	0.045	0.33	0.11	2.87	0.15	0.062	0.24	0.045	451	0.34	0.076	0.23	0.031	0.22	0.033	2.01
NMM1126	0.010	2.69	0.025	0.16	0.034	0.77	0.068	0.031	0.13	0.026	290	0.23	0.056	0.18	0.029	0.22	0.033	1.38
NMM0318	0.013	11.4	0.37	1.65	0.18	7.58	0.39	0.15	0.42	0.071	405	0.49	0.11	0.32	0.046	0.33	0.050	7.66
NMM1115	0.004	2.76	0.029	0.19	0.053	1.81	0.073	0.030	0.11	0.021	191	0.15	0.036	0.11	0.017	0.11	0.018	1.13
NME1122	0.008	4.99	0.055	0.28	0.065	1.91	0.11	0.044	0.15	0.026	343	0.19	0.039	0.11	0.017	0.12	0.018	1.86
NME0528	0.006	6.44	0.12	0.52	0.090	3.75	0.13	0.045	0.13	0.022	147	0.15	0.032	0.088	0.013	0.093	0.013	2.39
NME1116	0.003	7.07	0.059	0.32	0.061	2.31	0.11	0.045	0.17	0.031	300	0.25	0.058	0.18	0.027	0.20	0.032	1.87
NBN0302A	0.005	2.77	0.038	0.23	0.080	2.40	0.091	0.036	0.13	0.023	201	0.16	0.035	0.11	0.016	0.12	0.018	1.27
NBN0305	0.010	5.65	0.042	0.22	0.036	0.73	0.070	0.023	0.081	0.014	126	0.091	0.019	0.061	0.009	0.067	0.010	1.05
NBN0311	0.003	6.29	0.065	0.39	0.11	3.40	0.16	0.066	0.23	0.044	334	0.32	0.066	0.21	0.029	0.20	0.031	2.29
NBN0316	0.025	1.73	0.040	0.26	0.073	1.94	0.10	0.043	0.14	0.027	169	0.19	0.041	0.12	0.017	0.12	0.018	1.39
NBN0319	0.031	2.84	0.062	0.35	0.094	2.34	0.14	0.055	0.19	0.032	207	0.24	0.044	0.15	0.020	0.15	0.023	1.86
NBN0321	0.018	5.41	0.065	0.40	0.12	3.15	0.19	0.077	0.30	0.053	536	0.36	0.073	0.21	0.028	0.19	0.029	2.40

modified Ca-in-opx method provided by Nimis and Grütter (2010) in Fig. 5.13. The linear correlation generally supports equilibrium, with a few outliers (NTB0306, NTB0307, and NFR0307), where significant differences between the temperatures suggest a lack of chemical equilibrium between ortho- and clinopyroxene. Although there is no correlation between calculated temperatures and geochemical features, it can be observed that Group IIB xenoliths have slightly higher temperatures compared to the rest of the samples (Fig. 5.13; Table 1).

Besides thermometers based on major element cation exchange, the transfer of trace elements can also be taken into account. Liang et al. (2013) recently proposed a geothermometer based on the temperature dependence of REE+Y partitioning between ortho- and clinopyroxene. An advantage of this method is that REE+Y are treated as a group during the calculations, and since least-squares inversion is used on the partitioning data, any disequilibrium caused by analytical uncertainties or secondary/metasomatic processes can be recognised and excluded. The partition coefficient between ortho- and clinopyroxene for trace element *i* ($D_i^{opx/cpx}$) is calculated using the following equation: $\ln D_i^{opx/cpx} = A_i + B_i/T$, where A_i and B_i are functions of pyroxene composition and the ionic radius of element *i* (Liang et al., 2013 and references therein). $D_i^{opx/cpx}$ was calibrated with the use of pyroxene-melt partitioning experimental data of Sun and Liang (2012) and Yao et al. (2012).

In the Nógrád-Gömör xenoliths, where orthopyroxene has low LREE contents, linear regressions of only the HREE were considered because of the larger analytical

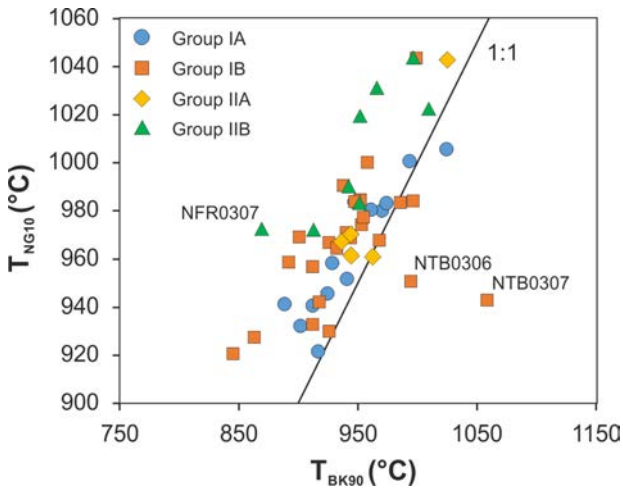

Fig. 5.13. Correlation of equilibration temperatures obtained by the application of two major-element based geothermometer. BK90 – Two-pyroxene method of Brey and Köhler (1990); NG10 – Ca-in-opx method of Brey and Köhler (1990) modified by Nimis and Grütter (2010).

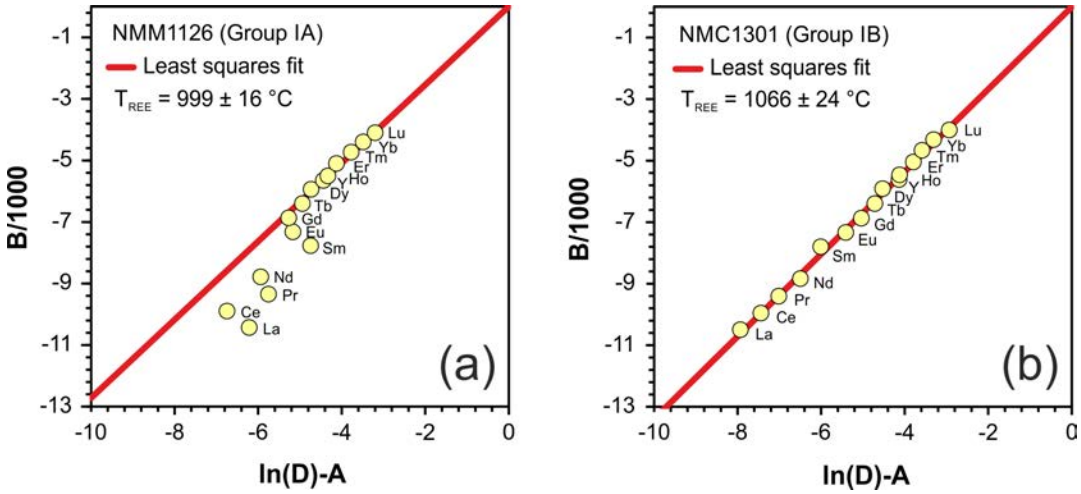

Fig. 5.14. Inversion diagram for calculation of equilibration T using the thermometer of Liang et al. (2013), based on the temperature dependence of REE partitioning between ortho- and clinopyroxene. The calculation is based on the equation $\ln D_i^{opx/cpx} = A_i + B_i/T$, where A_i and B_i are coefficients determined by pyroxene composition and ionic radii for elements i. In the inversion diagram, the slope of the linear regression is correlated with the temperature; in the case of ideal pyroxene equilibrium, LREE and HREE fall on the same line. a - Representative inversion diagram for a sample with apparent pyroxene disequilibrium in LREE owing to low concentrations in opx (NMM1126, Group IA). b - Representative inversion diagram of a sample with LREE-equilibrated pyroxenes (NMC1301, Group IB).

uncertainties for LREE (an example is shown in Fig. 5.14a). In the case of xenoliths with high LREE concentrations (i.e. the most enriched samples of Group IB and IIB), these elements could be taken into account and the good correlation verifies that the pyroxenes of the metasomatized xenoliths are in equilibrium (Fig. 5.14b). Thus, the standard deviation could be reduced for the individual xenoliths (1–59 °C; see Table 1 for individual samples).

REE temperatures of the studied xenoliths range from 930 to 1154 °C (Table 1); the only exception is NTB0306, which yields 901 °C. However, this sample has already been shown to lack pyroxene equilibrium from the calculations above for major element-based thermometers (Fig. 5.13). For the rest of the xenoliths, REE temperatures appear to be higher by an average of 100 °C than temperatures obtained with the two-pyroxene method of Brey and Köhler (1990) (Fig. 5.15a), and by an average of 50 °C compared with the Ca-in-opx method of Nimis and Grütter (2010) (Fig. 5.15b).

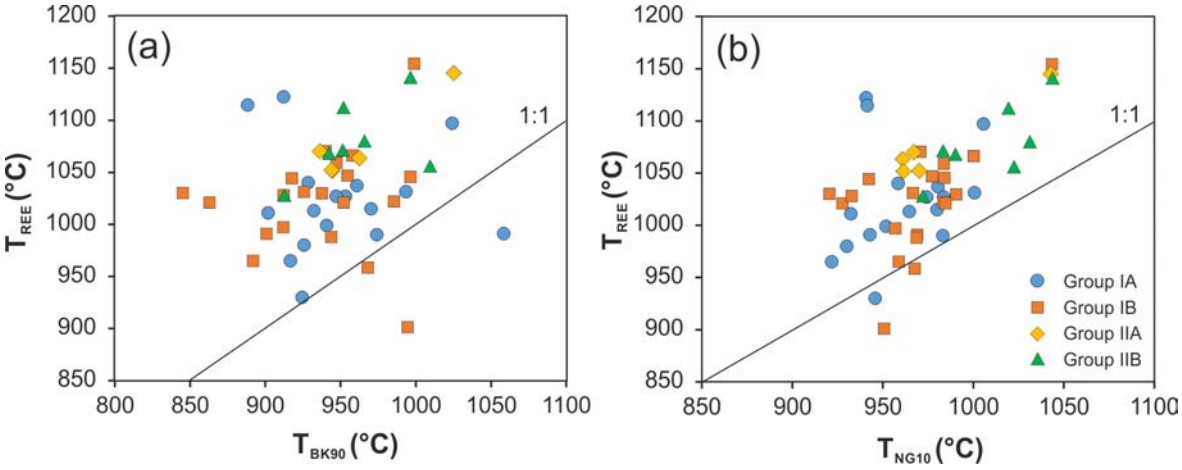

Fig. 5.15. Comparison of equilibration temperatures calculated with the REE thermometer (Liang et al., 2013) and major element-based thermometers: a - two-pyroxene method of Brey and Köhler (1990); b - Ca-in-opx method as revisited by Nimis and Grütter (2010).

5.4. Silicate Melt Inclusions

5.4.1. Petrography

Primary silicate melt inclusions (SMIs) are abundant in clinopyroxene and are also present in olivine in xenoliths of the wehrlite suite (Patkó, 2014), but they are extremely rare in the lherzolite suite. One xenolith from the monogenetic volcano of Fil'akovo-Kerčik (NFL1327), which is clinopyroxene-rich but not orthopyroxene-free (Fig. 5.16a), contains a few clinopyroxene grains which host primary SMIs (Fig. 5.16b). The SMIs are randomly distributed within the grain, usually have negative crystal shapes, and range from 5 to 20 µm in diameter. They are partially crystallised, and in a polarised light microscope, a gas bubble, glass and several daughter phases are observable (Fig. 5.17).

2D Raman mapping in a plane of the maximum dimensions of the inclusions, these allowed identification of daughter phases in three selected SMIs (Fig. 5.17). All three SMIs contain apatite and a volatile-bearing mineral (either amphibole or mica). Besides these, sulphates such as anhydrite and barite were found in SMI_2 and a clinopyroxene daughter phase with a spectrum slightly differing from the host was identified in SMI_R. Characteristic Raman spectra of apatite, sulphates and the CO_2-bubble are depicted in Fig. 5.18, along with the reference spectrum of the host clinopyroxene.

The gas bubble in all three analysed SMIs proved to consist of CO_2; the key evidence for it is the two highest-intensity peaks, the so-called Fermi diad (Fermi, 1931). The bands

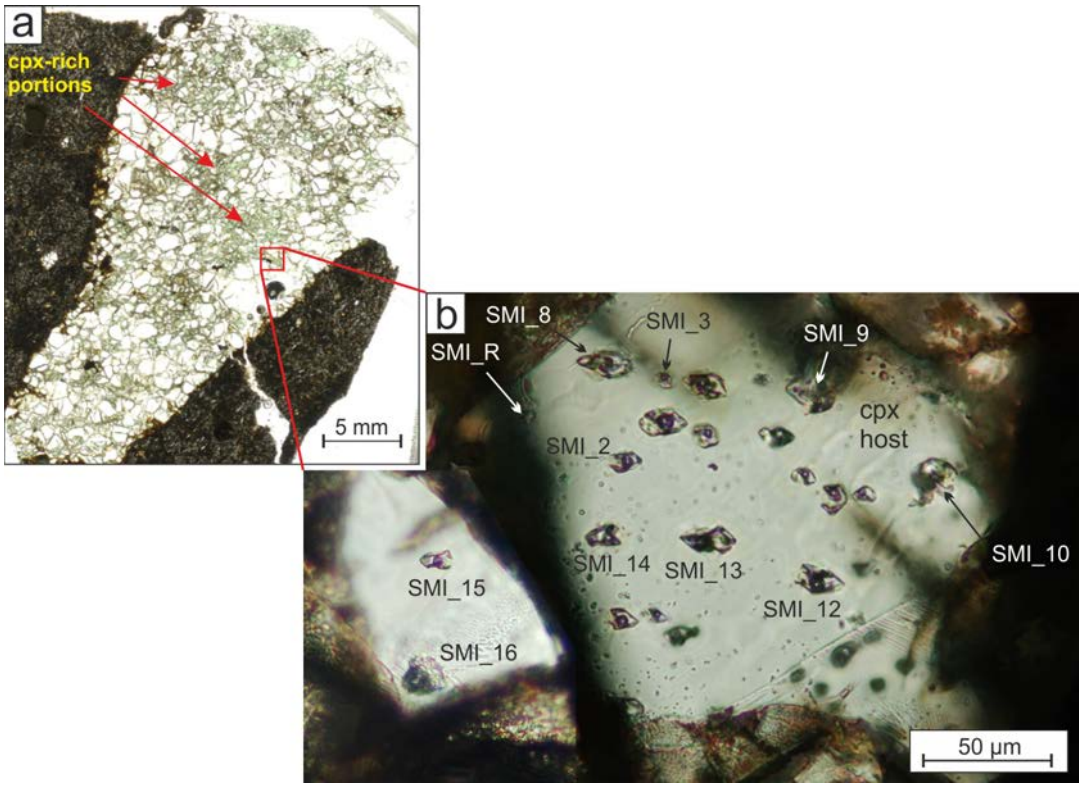

Fig. 5.16. a – Scanned thin section image of NFL1327 orthopyroxene-bearing wehrlite with distinguishable clinopyroxene- and olivine-rich parts. b - Primary silicate melt inclusions hosted in clinopyroxene in the NFL1327 wehrlite.

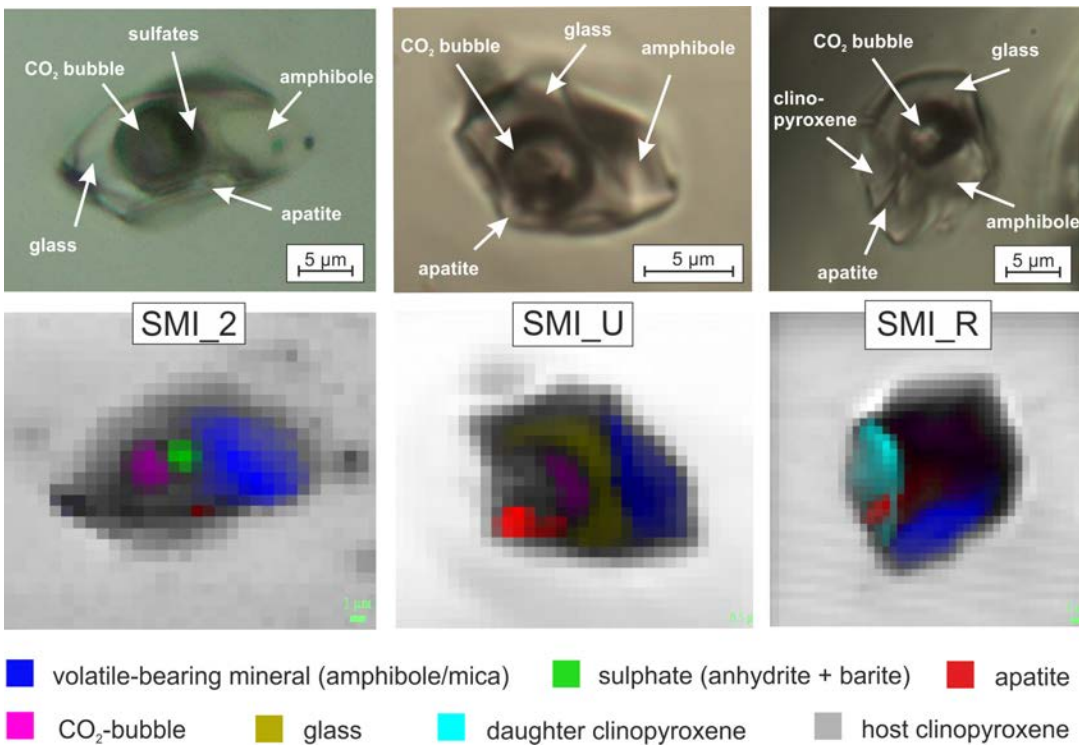

Fig. 5.17. Polarised-light microscope images and results of Raman spectroscopy mapping of three analysed SMIs.

of the Fermi diad appear at 1283.45 – 1387.01, 1284.72 – 1388.31, and 1284.7 – 1388.28 cm^{-1} in SMI_2, SMI_R and SMI_U, respectively (Table 5). The shift in the peaks has been recognized as a function of the CO_2 density (Rosso and Bodnar, 1995). There are several experimentally developed densimeters which can be used to calculate the density of the CO_2-bubble. In this study, the equations of Fall et al. (2011) and Wang et al. (2011) were used. Since the peak shifts are very similar in the three inclusions, the resulting densities (0.375 - 0.389 and 0.355 – 0.369 g/cm^3 with the two densimeters; Table 5) are almost identical.

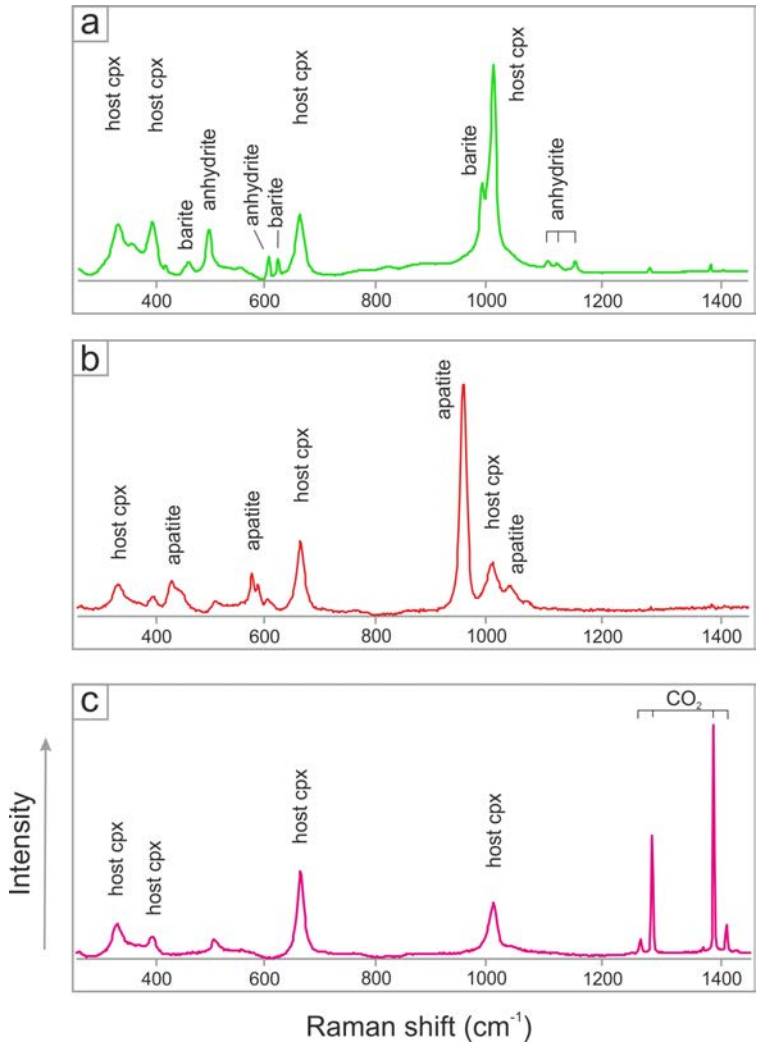

Fig. 5.18. Characteristic Raman spectra of sulphates (a), apatite (b) and CO_2 bubble (c).

FIB-slicing and subsequent SEM-EDX analyses of the melt inclusions supported the presence of daughter minerals identified with Raman spectroscopy, and revealed further daughter phases, (sometimes two or more distinct grains of the same phase, as described below) which were too small to detect with Raman. The largest volatile-bearing

Table 5. Positions of CO_2 bands (Fermi diad) in the bubble of the SMIs analysed with Raman spectroscopy and calculated densities based on the densimeters of Fall et al. (2011) and Wang et al. (2011).

Inclusion	Position of CO_2 bands (Fermi diad)		Δ Fermi diad	CO_2 density (g/cm^3)	
	upper band	lower band		Fall et al., 2011	Wang et al., 2011
SMI_2	1283.45	1387.01	103.56	0.375	0.355
SMI_R	1284.72	1388.31	103.59	0.389	0.369
SMI_U	1284.70	1388.28	103.58	0.384	0.364

mineral was identified as amphibole by the EDS spectra in three out of four analysed SMIs (SMI_2, SMI_3, and SMI_R; Fig. 5.19a-d); in SMI_3, two distinct amphibole grains are present (Fig. 5.19b). Mica is present in all four SMIs, appearing next to or very near the gas bubble. SMI_U contains two distinct mica flakes (Fig. 5.19d). Spinel and apatite are present in all four SMIs. Sulfide blebs were detected in SMI_R and SMI_U, and sulphates (anhydrite ± barite) in SMI_R, SMI_2 and SMI_3. Note that in SMI_R, both sulfide and sulphate daughter phases are present (Fig. 5.19c). Distinction of daughter clinopyroxenes was difficult due to their similarity in composition to the host clinopyroxene; however, irregularities in the shape of the inclusion (Fig. 5.19a, c) and SEM spectra yielding slightly different compositions could be used. It is highly likely that the modal proportions of the daughter clinopyroxenes are far underestimated.

Volume proportions acquired with the Amira 5.2.2 software have been converted into weight proportions and are shown in Table 6. The modal compositions of the SMIs are quite similar to one another. Glass makes up roughly half of the inclusions with 45-52 wt%. Amphibole and mica show a little wider modal range, being present in 25-39 and 0.2-1.2 wt%, except for SMI_U, where mica is more abundant (9.9 wt%) than amphibole (8.4 wt%). Daughter clinopyroxenes were determined to make up 9-24 wt% of the inclusions. Spinel, apatite, sulfide, anhydrite and barite (where present) are in very low amounts, usually below 2 wt% but no higher than 3.3 wt%.

5.4.2. Geochemistry

5.4.2.1. Major elements

Robust major-element compositions were acquired from SEM spectra for the most abundant daughter phases (Table 7; representative spectra are shown in Fig. 5.20). In the

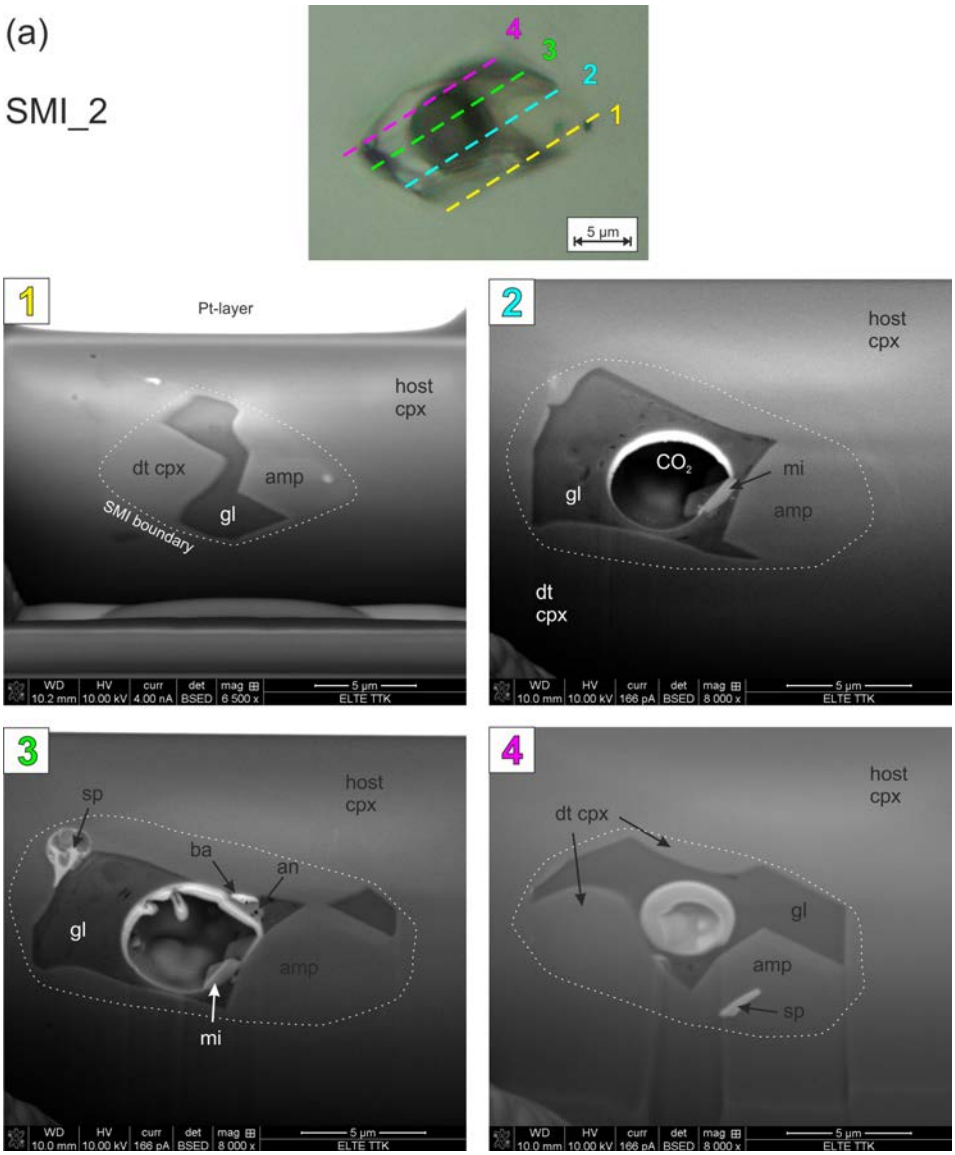

Fig. 5.19. BSE images of different slices of the analysed SMIs during the milling process with indications of the slice position on photomicrographs. a – SMI_2; b – SMI_3; c - SMI_R d - SMI_U. Abbreviations: dt cpx – daughter clinopyroxene, amp – amphibole, mi – mica, gl – glass, ap – apatite, sp – spinel, su – sulfide, an – anhydrite, ba - barite

case of volatile-bearing phases (amphibole, mica, glass) compositions were corrected to add up to a lower total to count for the volatile content. Total values for amphibole and glass were taken from clinopyroxene-hosted SMIs in wehrlites described by Patkó (2014), and for mica, from the olivine-hosted SMIs of Nógrád-Gömör xenoliths of Szabó and Taylor (1994) and Szabó et al. (1996). Spinel compositions were corrected by omitting oxides (SiO_2, CaO, Na_2O, K_2O) expected to be present only in surrounding silicate phases and glass. The resulting compositions are very similar among the four melt inclusions, as described below.

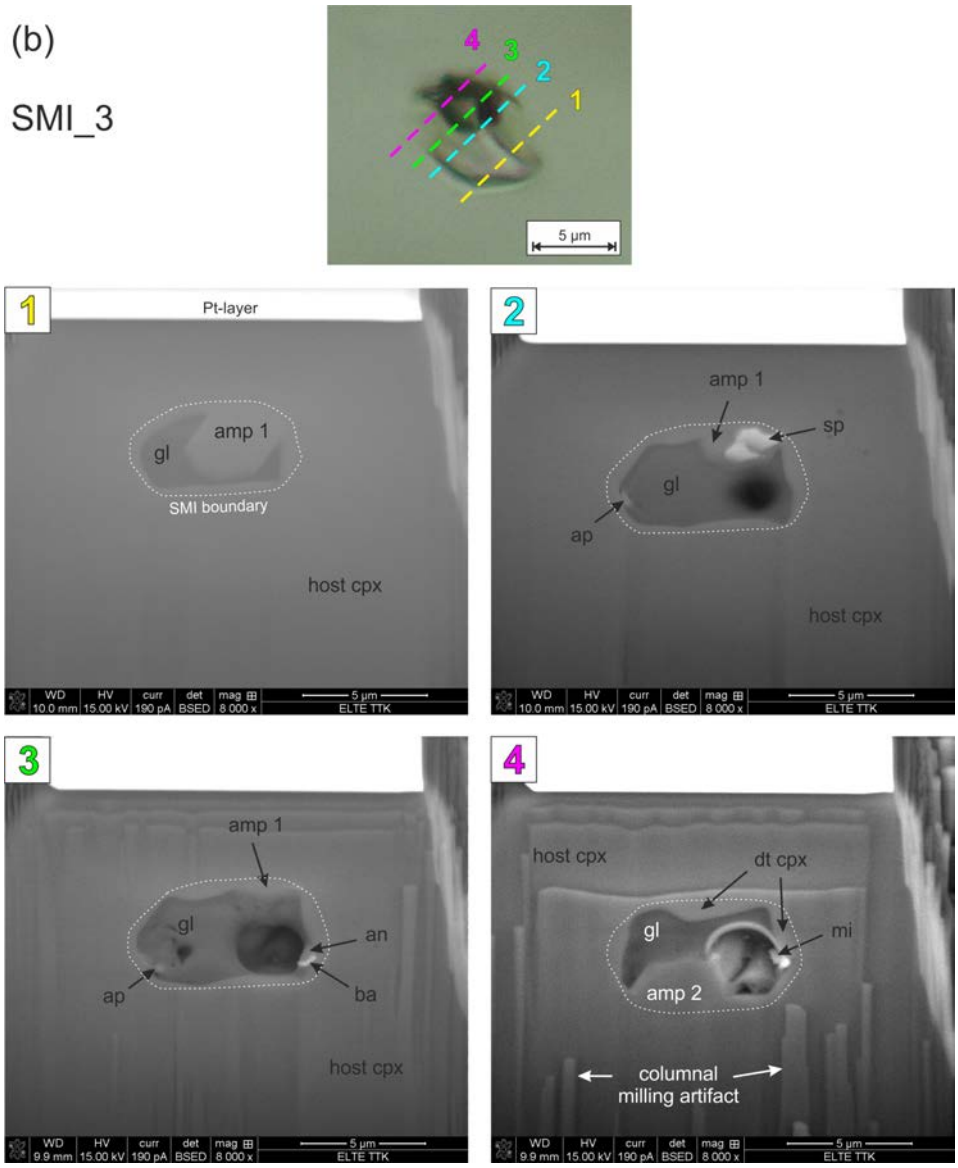

Fig. 5.19. Continued.

Clinopyroxene

Although daughter clinopyroxene was generally difficult to distinguish from the host, several analyses in SMI_2 and SMI_R revealed slightly different major-element compositions. This difference is observable as an increase in FeO (8.5-9.5 wt%) and Al_2O_3 (5.6-6.1 wt%) at the expense of MgO (10.4-11.3 wt%), whereas in the host clinopyroxene, FeO and Al_2O_3 are lower, and MgO higher (5.8-6.4, 4.1-4.9 and 11.9-14.2 wt%, respectively).

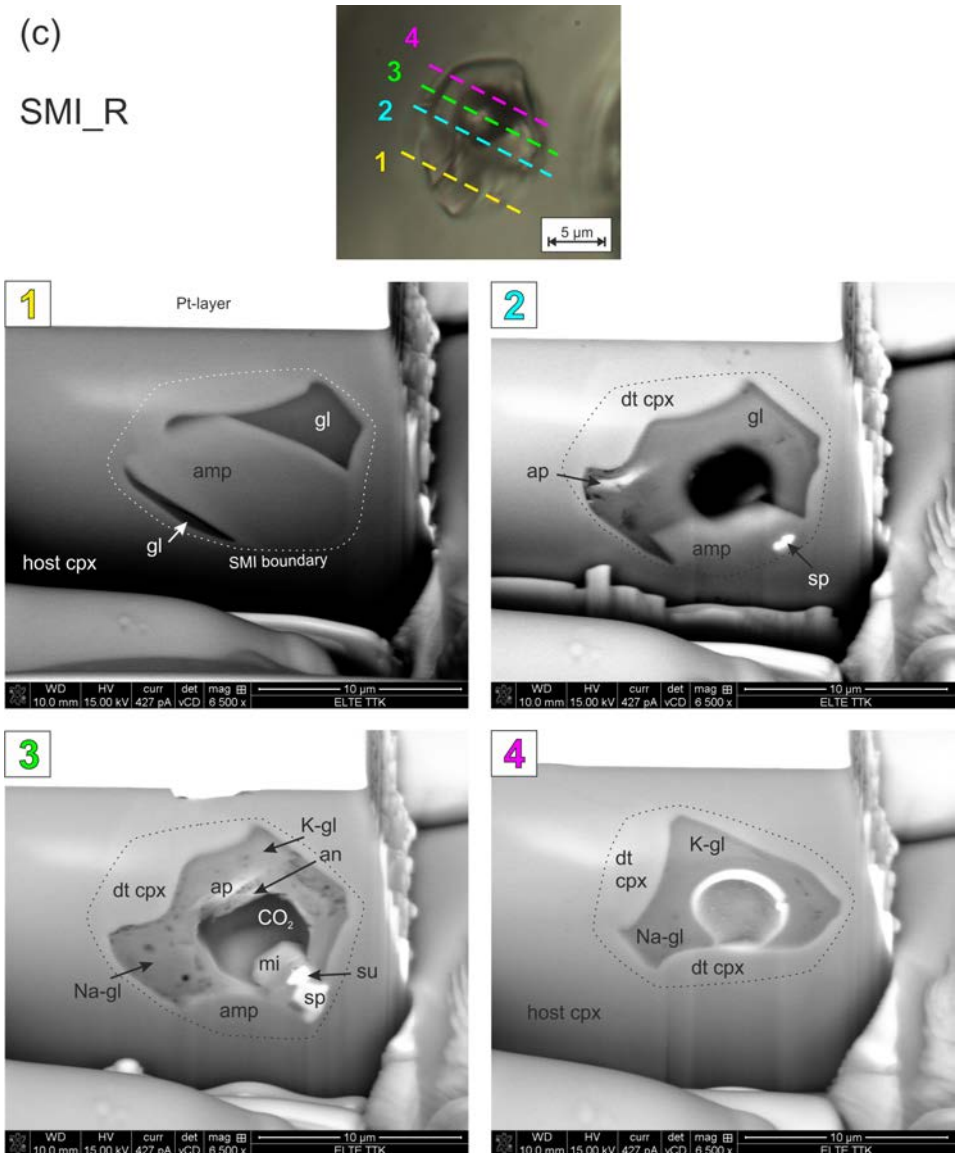

Fig. 5.19. Continued.

Amphibole

Amphibole shows very little compositional variability among the different SMIs. They are strikingly enriched in FeO (12.3-14.8 wt%) and TiO_2 (3.48-6.95 wt%) compared to amphiboles in most lherzolites of the NGVF suite. However, they are consistent with the observed Fe- and Ti- enrichment in the rock-forming minerals of Group IIB xenoliths. Furthermore, amphiboles in the SMIs have slightly lower SiO_2, Al_2O_3, MgO and Na_2O but higher CaO contents compared to the amphiboles of the xenoliths, and with the use of the spreadsheet of Locock (2014), they can be classified as Ti-rich magnesio-hastingsite and ferri-kaersutite.

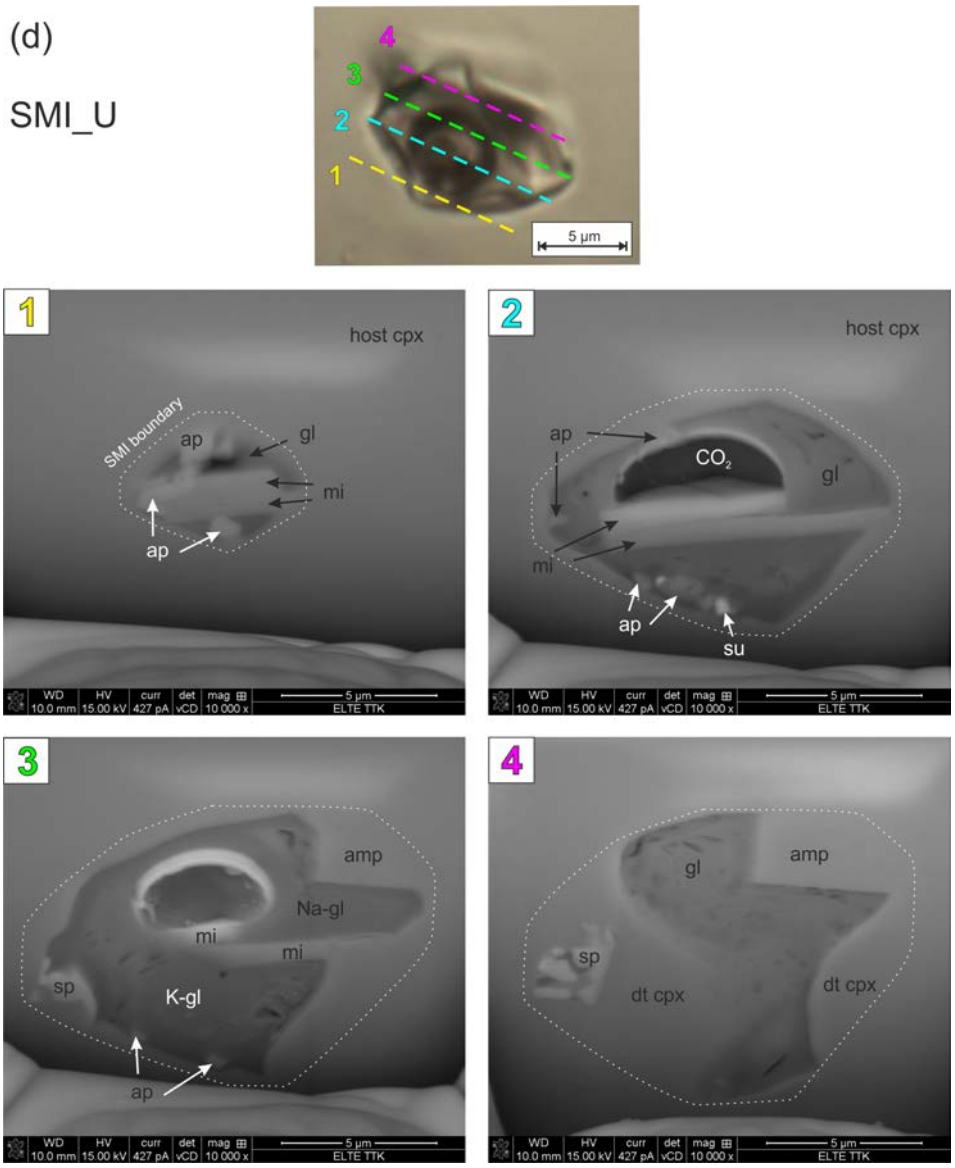

Fig. 5.19. Continued.

Mica

Due to their small grain size (see images of Fig. 5.19), the composition of mica varies on a wider range, and the analyses most likely have larger errors than those of clinopyroxene, amphibole or glass. However, the enrichment in FeO and the depletion of MgO is very strong, compared to mica (phlogopite) in the melt inclusions of NGVF xenoliths described by Szabó et al. (1996).

Glass

Glass is not entirely homogeneous; even on the BSE images of several slices, numerous dark spots, possibly sub-micron-sized bubbles, are observed (e.g., Fig. 5.19.c, d).

Table 6. Volume proportions of the identified daughter phases of the SMIs. * mineral densities for volume to weight conversion: clinopyroxene (diopside), amphibole (pargasite), mica (average), spinel (hercynite), sulfide (pyrrhotite), anhydrite, barite: webmineral.com; CO_2: see Fermi diad calculations in Table 5; glass: Stolper and Walker, 1980.

	Modal proportions wt % (v/v %)*							
Daughter phase	SMI_2		SMI_3		SMI_R		SMI_U	
	wt %	v/v %	wt %	v/v %	wt %	v/v %	wt %	v/v %
Clinopyroxene	16	12	9.2	7.0	24	19	23	19
Amphibole	33	28	39	32	25	22	8.4	7.5
Mica	0.53	0.47	0.17	0.15	1.3	1.2	9.9	9.4
Glass	45	43	48	46	45	45	52	53
Apatite	-		0.51	0.41	0.61	0.5	2.2	1.9
Spinel	2.4	1.6	1.4	0.93	1.5	0.99	3.3	2.3
Sulfide	-		-		0.32	0.18	0.33	0.2
Anhydrite	0.22	0.19	0.16	0.14	0.13	0.12	-	
Barite	0.16	0.09	0.18	0.11	-		-	
CO_2 bubble	2.1	14	1.9	13	1.73	12	1	7.3

Although the analyses did not identify the nature of these inhomogeneities, they revealed major differences in the Na/K ratio of the glass. In most analyses the glass appears to be K-rich, but several areas in SMI_2, SMI_R and SMI_U show Na-rich compositions, with Na_2O contents reaching 7.2-15.9 wt% (Table 7). These Na-rich areas also have lower SiO_2-contents (52.0-59.6 wt%). Similar compositional variability was reported by Szabó et al. (1996) in glasses of melt inclusions from the southern part of the NGVF. Furthermore, in SMI_U, the glass also has a slightly elevated iron content (FeO = 2.3-3.4 wt%).

Spinel

Spinels are dominantly iron-rich, with a small proportion of chromium and aluminium. In SMI_U, the spinel is richer in aluminium and more depleted in iron (Table 7).

Whole SMI

Major-element compositions of the whole SMIs were calculated by mass balance using the composition of individual phases comprising more than 1 wt% of the inclusion (glass, clinopyroxene, amphibole, ± mica, spinel, apatite; Table 6). The resulting compositions vary in a narrow range among the four SMIs. SiO_2 contents vary between 51.7 and 53.2 wt%, and FeO contents are between 6.6-8.4 wt%, which is significantly higher than those described by Szabó et al. (1996) from NGVF inclusions, and closer to

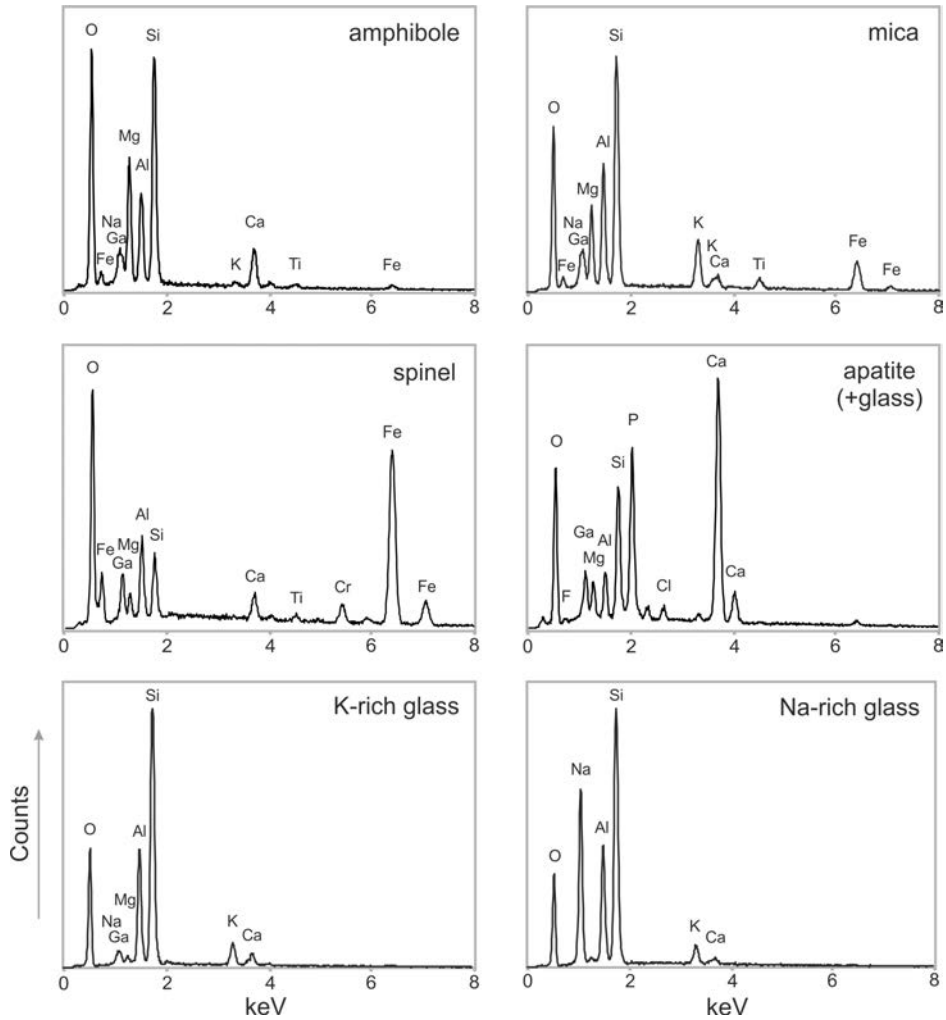

Fig. 5.20. Representative SEM spectra of daughter phases with the highest modal proportion.

the values reported by Zajacz et al. (2007) for melt inclusions trapped in mafic cumulate xenoliths in the Nógrád-Gömör Volcanic Field. Apart from the high FeO, the SMI compositions are in good agreement with those found in wehrlite xenoliths from the Nógrád-Gömör Volcanic Field (Patkó, 2014).

5.4.2.2. Trace elements

Trace-element contents of 8 further SMIs in clinopyroxenes of sample NFL1327 were acquired by LA-ICP-MS analysis (Table 8). The compositions are quite similar for all 8 inclusions. Although there is a little variability in the more compatible elements, they produce relatively homogeneous patterns when normalised to a primitive-mantle composition (McDonough and Sun, 1995) (Fig. 5.21). The SMIs are enriched in incompatible elements such as Rb, Ba, Nb and Ta (3.52 – 33.9, 117 – 530, 19.6 – 86.7

and 0.92 – 4.56 ppm, respectively); the concentrations are significantly higher than those in the host clinopyroxene of xenolith NFL1327 (Table 3). On the other hand, U and Th have negative anomalies (Fig. 5.21a), although their concentrations (0.047 – 0.18 and 0.14 – 0.65 ppm) are similar to those in the host clinopyroxenes (i.e., Group IIB, Table 3). Another negative peak is seen at Hf, whereas Zr is less depleted. There is a continuous

Table 7. Major element compositions of amphibole, mica, clinopyroxene and glass in the SMIs analysed with FIB-SEM, and bulk compositions obtained with mass-balance calculation.

	Clinopyroxene						**Amphibole**					**Mica**			
	SMI_2		SMI_3	SMI_R		SMI_U	SMI_2	SMI_3		SMI_R	SMI_U	SMI_2	SMI_3	SMI_R	SMI_U
	daughter	host	host	daughter	host	host		amp1	amp2						
n	3	3	6	6	5	2	4	2	3	7	1	5	3	2	6
SiO_2	50.19	53.03	49.44	45.98	49.01	49.05	39.66	37.87	39.66	38.49	38.51	34.24	41.53	35.85	35.90
TiO_2	1.75	1.09	1.08	1.34	1.15	1.10	3.48	5.23	4.88	3.89	6.95	0.00	1.45	3.33	3.93
Al_2O_3	5.59	4.78	4.08	6.05	4.23	4.19	10.55	10.09	10.09	11.36	10.37	11.14	9.04	10.54	14.17
Cr_2O_3			1.36		1.55					0.76				3.36	
FeO	8.50	2.76	5.81	9.51	6.44	6.18	14.79	14.75	12.27	12.82	12.38	33.82	25.60	29.14	21.11
MgO	11.34	13.91	12.56	10.38	11.93	11.89	11.64	10.80	11.27	11.55	10.98	2.93	3.82	1.73	7.85
CaO	22.14	24.01	25.11	25.64	25.47	26.60	13.64	15.43	15.84	15.34	15.08	5.19	10.27	7.17	2.37
Na_2O	1.66	1.15	0.79	1.03	0.76	0.87	2.25	1.74	2.13	1.75	1.82	1.84	0.93	0.58	2.53
K_2O				0.49		0.30	1.50	1.59	1.37	1.55	1.40	7.34	3.86	4.81	8.64
Total	101.17	99.64	100.23	100.41	100.54	100.16	97.5	97.5	97.5	97.5	97.5	96.5	96.5	96.5	96.5

	Spinel				**Glass**							**Whole SMI**			
	SMI_2	SMI_3	SMI_R	SMI_U	SMI_2		SMI_3	SMI_R		SMI_U		SMI_2	SMI_3	SMI_R	SMI_U
					K-rich	Na-rich	K-rich	Krich	Na-rich	Krich	Na-rich				
n	4	1	6	1	9	1	3	8	4	7	1				
SiO_2					66.50	59.61	65.50	63.61	52.02	62.39	57.81	53.23	52.90	51.71	52.08
TiO_2	1.92	3.74	1.79									1.53	2.11	1.40	1.26
Al_2O_3	7.09	9.54	5.77	43.68	20.26	18.56	18.40	20.30	17.43	18.87	17.63	14.29	13.70	14.28	14.96
Cr_2O_3	11.39	6.33	5.80	3.30								0.27	0.20	0.32	0.11
FeO	79.60	80.38	86.63	47.21					1.65	2.34	3.40	8.36	6.57	7.24	7.50
MgO				5.81	0.81	0.66	1.61	1.12	0.84	1.56	1.48	6.22	6.38	6.02	5.55
CaO					1.67	1.55	2.81	2.80	2.74	3.12	2.09	9.06	9.95	11.52	10.61
Na_2O					3.40	12.02	2.97	2.10	15.91	1.28	7.23	2.65	2.36	1.71	1.31
K_2O					2.86	3.10	4.21	5.57	4.92	5.95	5.85	1.87	2.68	3.24	4.29
P_2O_5															0.91
F_2O															0.02
Cl_2O															0.04
Total	100.00	100.00	100.00	100.00	95.5	95.5	95.5	95.5	95.5	95.5	95.5	97.48	96.86	97.44	98.63

depletion from the light towards the heavy REE, with the former showing concentrations about one order of magnitude higher than the host clinopyroxene (Fig. 5.21b). The most compatible elements (Sc to Ni) show the greatest depletion, similar to the pattern of the host (Fig. 5.8d).

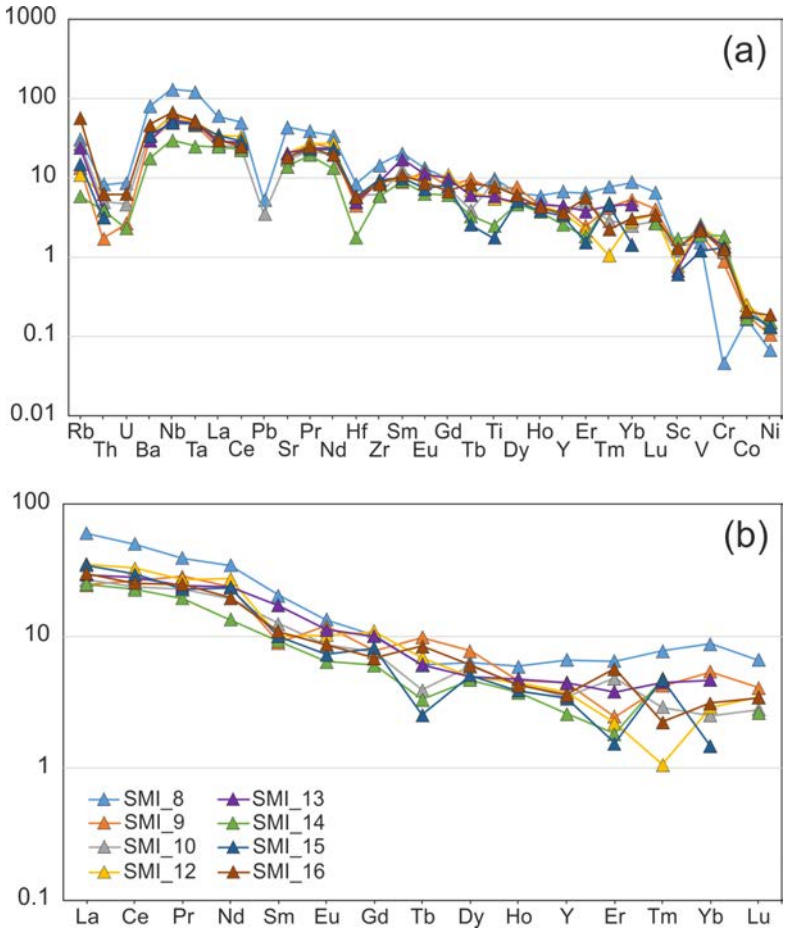

Fig. 5.21. Primitive mantle (McDonough and Sun, 1995)-normalised multi-element (a) and REE+Y (b) diagrams of bulk SMIs analysed by LA-ICP-MS.

5.5. Crystal Preferred Orientation

5.5.1. Crystal preferred orientation of the rock-forming minerals

<u>Olivine</u>

Pole figures of both olivine and pyroxenes of representative xenoliths are depicted on Fig. 5.22; for pole figures of all xenoliths, see Appendix C. In the Nógrád-Gömör xenoliths, olivine shows all three of the most widespread crystal preferred orientation (CPO) types, namely ([100]-fibre, [010]-fibre and orthorhombic, described from the

Table 8. Trace element compositions of the SMIs acquired with LA-ICP-MS.

	SMI_8	SMI_9	SMI_10	SMI_12	SMI_13	SMI_14	SMI_15	SMI_16
Rb	18.5	7.95	16.2	6.46	14.4	3.52	9.06	33.9
Th	0.65	0.14	0.40	0.50	0.32	0.31	0.25	0.50
U	0.18	0.054	0.095	n.d.	n.d.	0.047	n.d.	0.13
Ba	530	193	232	228	194	117	227	311
Nb	86.7	33.4	41.0	39.7	36.1	19.6	32.2	44.1
Ta	4.56	1.74	2.00	1.87	1.81	0.92	1.78	1.93
La	39.1	15.9	17.2	22.8	18.9	16.1	22.4	19.3
Ce	83.8	44.1	39.3	55.1	46.7	37.8	49.4	42.4
Pb	0.79	n.d.	0.52	n.d.	n.d.	n.d.	n.d.	n.d.
Sr	865	338	338	407	405	278	367	364
Pr	9.88	7.20	5.71	6.82	6.09	4.91	5.83	6.29
Nd	43.0	29.9	24.3	34.1	29.6	16.7	29.0	24.4
Hf	2.38	1.26	1.68	1.41	1.41	0.51	1.64	1.61
Zr	152	97.3	64.7	96.4	90.9	61.0	99.5	88.5
Sm	8.27	3.62	5.04	4.03	6.96	3.73	4.07	4.39
Eu	2.05	1.84	1.32	1.58	1.74	0.99	1.12	1.33
Gd	5.49	4.23	4.13	5.93	5.46	3.28	4.44	3.73
Tb	0.60	0.97	0.39	0.68	0.60	0.33	0.25	0.83
Ti	12034	8563	10722	6544	7069	3043	2112	9445
Dy	4.27	5.20	3.99	3.34	3.31	3.14	3.41	4.06
Ho	0.88	0.69	0.65	0.67	0.71	0.56	0.58	0.63
Y	28.6	19.2	15.1	16.1	19.0	11.1	14.6	15.5
Er	2.86	1.08	2.10	0.96	1.67	0.80	0.68	2.49
Tm	0.52	0.29	0.20	0.07	0.30	0.32	0.32	0.15
Yb	3.87	2.38	1.11	1.28	2.06	n.d.	0.65	1.38
Lu	0.45	0.28	0.19	0.23	n.d.	0.18	n.d.	0.23
Sc	22.4	22.0	19.3	12.8	11.1	27.5	9.94	20.8
V	127	161	214	200	191	156	98	179
Cr	120	2309	3032	4049	3610	4856	3493	3270
Co	17.5	19.7	26.0	26.6	21.0	18.1	21.7	22.0
Ni	134	209	254	297	267	298	260	369

lithospheric mantle worldwide (see Tommasi and Vauchez, 2015 for a review). Most of the Nógrád-Gömör xenoliths do not have straightforward CPO types, instead, they have transitional symmetries with a dominant character (as reflected in BA-indices; Table 9). In xenoliths where lineation is observable, [100] axes of olivine have a cluster maximum parallel to the lineation (A-type orthorhombic and [100]-fibre), or spread in a girdle in the plane of foliation, usually with a weak maximum parallel to the lineation ([010]-fibre). [010] axes tend to cluster normal to the plane of foliation (orthorhombic and [010]-fibre), or distribute in a girdle in a plane normal to the [100] direction ([001]-fibre). In contrast, [001] axes either form a weak girdle in a plane normal to the [100] directions ([100]-fibre),

or have a weak maximum normal to the lineation in the foliation plane, or show random distributions.

The distribution of CPO types is slightly different for each domain within the volcanic field. In the northern part, most of the xenoliths show [010]-fibre symmetries with BA-indices lower than 0.35 (Table 9), with the exceptions of NMS1304 (BA = 0.66) and NJS1304 (BA =0.45). In the central part, the orthorhombic type is the dominant CPO symmetry, shown by 17 xenoliths, followed by [010]-fibre (12 xenoliths); there is only one sample with [100]-fiber symmetry (NFK0301; BA = 0.75). In the southern part, xenoliths cover a wide range of BA-index and display a texture-dependent distinction: fine-porphyroclastic-textured xenoliths tend to have lower BA-indices (0.09-0.44) than equigranular ones (0.59-0.70). This correlation between texture and CPO symmetry was previously observed by Liptai et al. (2013). For the other localities, no clear correlation is observable between texture type and CPO symmetry. However, it can generally be established that granular- and porphyroclastic-textured xenoliths tend to show [010]-fibre and orthorhombic symmetries with lower BA-indices, whereas equigranular-textured ones have rather higher BA-indices (orthorhombic and [100]-fibre symmetries).

The J-indices of olivine, were also calculated on the basis of one point per grain (Table 9). It represents the strength of fabric in a dimensionless value, ranging from 1 (random orientation distribution) to infinity (single crystal) (Bunge, 1982). Since the J-index may be biased by low numbers of analysed grains, it was compared with the M-index, which is independent of this factor (Fig. 5.23). The M-index expresses the distribution of uncorrelated misorientation angles compared to a randomly oriented fabric, and ranges from zero (random fabric) to 1 (single crystal) (Skemer et al., 2005). The correlation of the J- and M-indices is rather poor ($R^2 = 0.56$), however, there are only three outlier xenoliths (NTB1122, NTB1124, NMM1126), which show a significant discrepancy between their J- and M-indices. This can be explained by the low number of analysed grains, which distorts the calculation and results in too high J-indices. Omitting these samples gives a much stronger correlation coefficient ($R^2 = 0.80$) (Fig. 5.23), suggesting that for the rest of the xenoliths, these two parameters are consistent, and the J-index is a valid expression of the fabric strength. In the northern and central parts, J-indices have a similar range (2.1-4.8 and 2.4-4.4, respectively; Table 9), except for the above-mentioned outliers. In the southern part, olivine J-indices range from 1.6 to 2.3, which is clearly lower than the values in the northern and central part. Furthermore, equigranular-textured

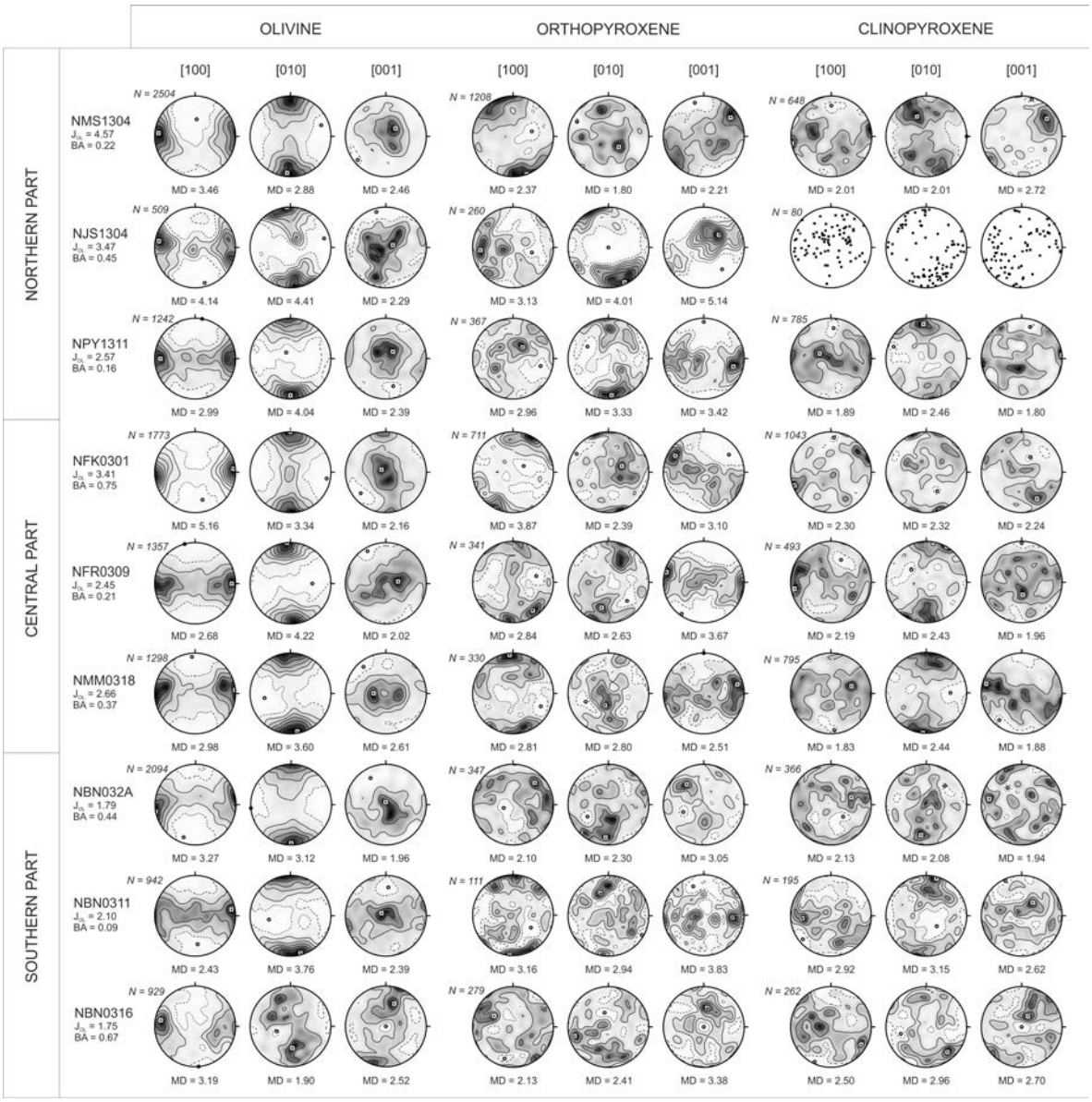

Fig. 5.22. Crystal preferred orientations of olivine and pyroxenes in representative xenoliths from the different parts of the volcanic field and different texture groups. Pole figures are lower hemisphere, equal area projections, contoured at 0.5 multiples of uniform distribution. Maximum and minimum densities are indicated with a black square and a white circle, respectively; dashed line marks the lowest-value (0.5) contour. For CPO plots of all xenoliths studied, see Appendix C.

xenoliths from the southern part appear to show slightly lower J-indices (1.6-1.8) than fine-porphyroclastic ones (1.8-2.3).

Orthopyroxene

Orthopyroxene CPOs are generally weaker and show more scattered patterns than those for olivines (Fig. 5.22). They sometimes show strong clustering in random directions, which can be explained by scattered indexation of large grains, or an increased number

Table 9. Fabric properties acquired with EBSD-analyses and calculated seismic properties. n.g. – number of grains, g.s. – mean grain size (area-weighted; µm), AVp – P-wave anisotropy, AVs – S-wave anisotropy.

Sample	n.g.	Properties of olivine					Seismic properties				
		g.s.	J-index	M-index	BA-index	GOS	Max. Vp (km/s)	Min. Vp (km/s)	AVp (%)	Max. AVs (%)	Min. AVs (%)
NMS1302A	5340	672	4.6	0.249	0.22	3.2	8.74	7.83	11.0	7.55	0.37
NMS1304	5977	701	2.8	0.123	0.66	2.2	8.65	8.03	7.40	5.19	0.10
NMS1305	3608	730	2.3	0.098	0.20	2.7	8.43	7.98	5.50	4.09	0.10
NMS1308	7753	697	2.6	0.130	0.29	3.0	8.53	7.97	6.80	5.22	0.12
NMS1310	3349	803	3.7	0.150	0.33	2.6	8.35	8.01	4.10	4.17	0.06
NJS1302	5654	686	2.1	0.095	0.26	2.2	8.53	7.94	7.10	4.31	0.19
NJS1304	2081	805	3.5	0.149	0.45	2.6	8.62	7.89	8.80	5.81	0.06
NJS1306	1341	1215	4.8	0.183	0.23	2.2	8.50	7.91	7.30	4.68	0.17
NJS1307	3443	1003	4.3	0.182	0.26	3.2	8.56	7.91	7.90	5.50	0.17
NPY1301	3254	643	3.0	0.129	0.27	2.9	8.55	7.93	7.60	4.85	0.12
NPY1310	1701	657	2.6	0.068	0.16	2.1	8.41	7.95	5.60	3.55	0.19
NPY1311	6051	596	2.4	0.103	0.19	2.3	8.42	7.92	6.10	4.06	0.06
NPY1314	3266	550	2.8	0.128	0.23	2.2	8.48	7.97	6.20	4.54	0.21
NFL1302	2119	718	2.6	0.109	0.27	2.0	8.59	7.96	7.60	5.76	0.06
NFL1305	1979	610	2.8	0.120	0.41	1.4	8.36	7.99	4.60	4.43	0.10
NFL1315A	2953	669	3.8	0.175	0.46	1.8	8.84	7.92	11.0	7.99	0.29
NFL1316	3006	633	2.5	0.111	0.42	1.6	8.58	8.01	6.90	5.15	0.06
NFL1324	4486	999	4.3	0.185	0.36	2.4	8.56	7.87	8.40	5.47	0.35
NFL1326	3850	956	3.1	0.140	0.49	1.5	8.70	7.98	8.70	5.43	0.29
NFL1327	2624	744	3.0	0.157	0.34	1.5	8.72	7.95	9.30	6.07	0.06
NFL1329	5458	498	2.4	0.117	0.28	1.3	8.54	7.96	7.00	5.28	0.15
NTB0306	2021	665	2.5	0.088	0.53	1.4	8.60	8.03	6.70	5.28	0.19
NTB0307	3007	507	2.4	0.084	0.27	2.3	8.51	8.02	6.90	3.97	0.04
NTB1124	422	1253	6.0	0.147	0.39	1.3	8.69	7.97	8.60	6.08	0.21
NTB1116	1945	863	4.4	0.183	0.62	1.6	8.76	7.95	9.80	6.48	0.12
NTB1122	1083	1156	4.9	0.111	0.20	1.4	8.48	8.03	5.40	3.87	0.12
NFK0301	5691	981	3.4	0.167	0.75	2.1	8.80	8.02	9.30	6.13	0.39
NFK1123	678	724	4.0	0.168	0.45	1.4	8.70	8.06	7.70	5.81	0.20
NFK1108	3972	1249	3.6	0.181	0.43	2.3	8.81	7.95	10.20	6.64	0.51
NFK1115	4320	678	3.0	0.144	0.54	1.4	8.74	7.97	9.20	6.62	0.16
NFR1109	1272	844	3.4	0.148	0.33	1.5	8.71	7.95	9.00	6.58	0.16
NFR0309	4443	552	2.4	0.116	0.21	1.9	8.46	7.96	6.00	4.32	0.08
NFR1107	2152	1054	3.6	0.144	0.44	2.4	8.55	7.98	6.80	5.12	0.15
NMC1301	3690	1177	3.7	0.169	0.32	2.0	8.64	7.93	8.50	6.81	0.25
NMC1309	1779	1150	4.3	0.155	0.12	2.3	8.56	7.86	8.50	6.66	0.21
NMC1322	4672	773	2.6	0.123	0.25	2.2	8.59	7.95	7.70	5.51	0.15
NMC1336A	5049	669	2.6	0.102	0.40	1.7	8.44	8.00	5.30	3.99	0.04
NMM1126	485	895	6.1	0.184	0.60	2.1	8.69	7.93	9.20	6.85	0.27
NMM0318	5047	592	2.7	0.136	0.37	1.7	8.52	7.99	6.40	4.91	0.14
NMM1115	3875	488	3.1	0.143	0.29	1.6	8.62	7.95	8.10	5.02	0.27
NME1122	857	1094	4.3	0.135	0.34	2.0	8.69	7.97	8.70	6.49	0.25
NME1116	4267	723	3.2	0.143	0.35	1.9	8.57	7.95	7.60	4.99	0.12
NME0528	3379	1003	3.2	0.148	0.49	1.8	8.66	7.93	8.80	6.12	0.27
NBN0302A	3717	479	1.8	0.061	0.44	1.3	8.60	8.06	6.60	4.45	0.08
NBN0305	5828	562	1.8	0.061	0.59	1.2	8.55	8.08	5.60	4.00	0.14
NBN0311	1704	509	2.1	0.075	0.09	1.6	8.51	8.00	6.10	4.42	0.08
NBN0316	2044	618	1.7	0.039	0.67	1.3	8.52	8.15	4.50	3.18	0.08
NBN0319	7166	500	1.6	0.049	0.70	1.1	8.51	8.13	4.60	2.92	0.04
NBN0321	1407	567	2.3	0.069	0.17	1.3	8.54	8.05	6.00	4.96	0.10

of neoblasts around a porphyroclast that have similar orientation. In oriented samples, orthopyroxene [001] axes are characterised by a distribution parallel to or at a low angle to the lineation, similarly to olivine [100] axes, and [100] axes of orthopyroxene are often normal to the foliation plane. This link between olivine and orthopyroxene CPO is present in the randomly cut xenoliths as well, where orthopyroxene axes show clearly observable maxima; this suggests that CPO patterns of all xenoliths have the same relationship with the foliation and lineation. This justifies rotation of the samples into a common reference frame defined by the lineation (E-W) and the pole of foliation (N-S). In xenoliths where [001] and [100] axes of orthopyroxene do not follow olivine [100] and [010] axes, respectively, orthopyroxene axes are either scattered (e.g., NTB6, NMM1115), or [100] and [001] axes show similar maxima to olivine [100] and [001], respectively (NFK1115, NBN035, NBN0319; see Appendix C).

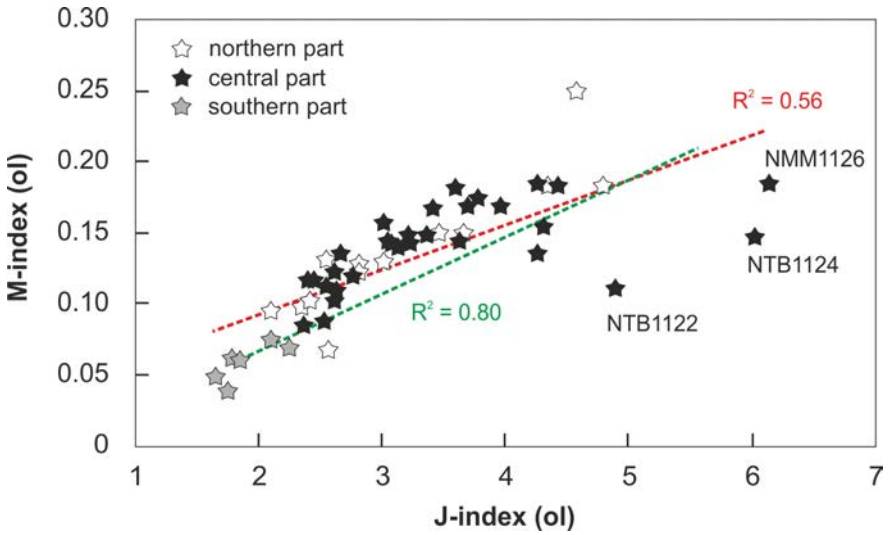

Fig. 5.23. J-indices *vs* M-indices of olivine in the studied xenoliths. The high correlation (after excluding the three outliers for reasons detailed in the text) verifies the reliability of these parameters as representations of the fabric strength.

Clinopyroxene

Clinopyroxene axes are even more dispersed than orthopyroxene axes; in the majority of the xenoliths, no clear CPO is observable (Fig. 5.22; Appendix C). Where there is, it tends to reflect major concentration directions similar to those of orthopyroxene, with [001] axes corresponding to or being at a small angle to olivine [100] maxima (e.g., NMS1304, NPY1311, NFK0301, NMM0318; Fig 5.22). In a few xenoliths, weak clinopyroxene orientations seem to show directions of [100] and [010] axes similar to

olivine [100] and [010] axes, respectively (NPY1311, NFR0309, NMM0318; Fig. 5.22). These also correspond to orthopyroxene [001] and [100] axes (i.e., the lineation and the direction normal to the plane of foliation).

5.2.2. Seismic properties

Seismic properties of individual xenoliths (Table 9) share similar characteristics, which are presented in pole figures averaged for the whole NGVF (Fig. 5.24). The P-wave propagation is fastest in the direction close to the strongest concentrations of olivine [100]

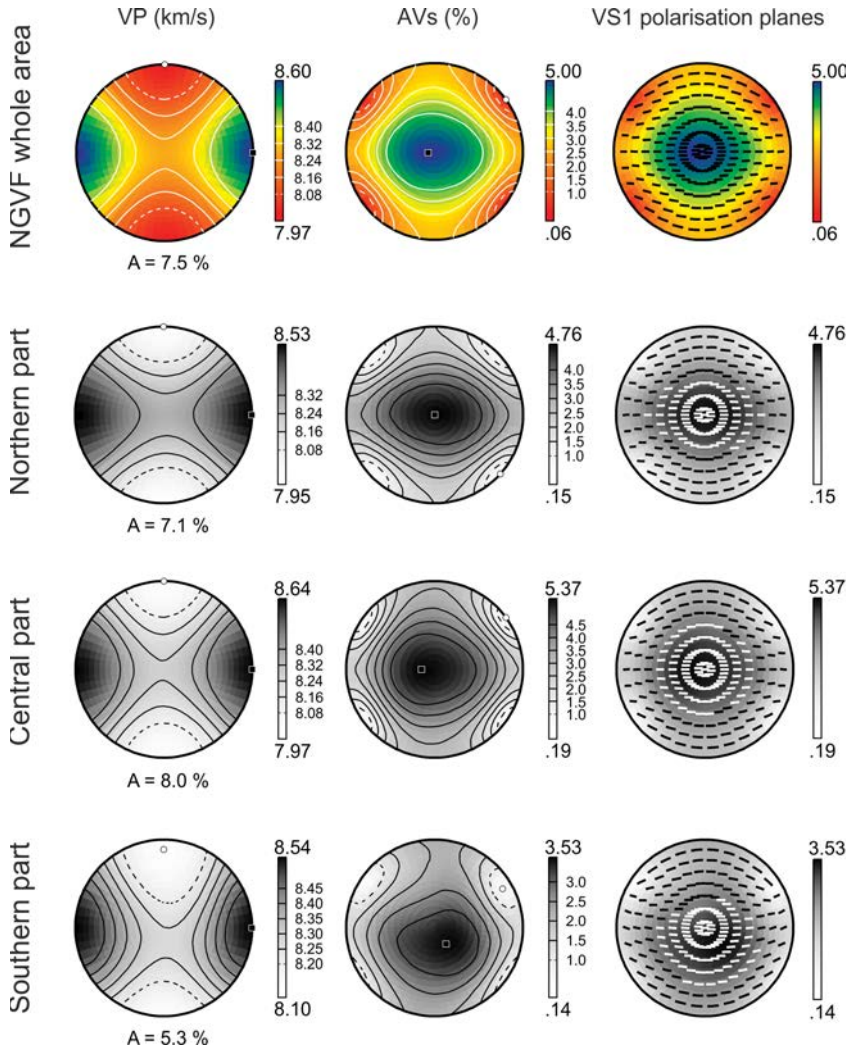

Fig. 5.24. Calculated bulk seismic properties for the Nógrád-Gömör Volcanic Field (NGVF) and the three sub-areas in lower-hemisphere equal- area stereographic projections. V_P, V_{S1} and V_{S2} are the 3D distributions of P-wave, fast and slow S-wave velocities, respectively; AVs is the 3D distribution of the polarisation anisotropy of S-waves due to S-wave splitting; V_{S1} (fast S-wave) polarisation planes are displayed as a function of the orientation of the incoming wave relative to the structural framework of the samples.

axes, i.e., the direction of the lineation, and slowest to a direction normal to the foliation plane (olivine [010] maxima in xenoliths with orthorhombic and [010]-fibre symmetries). The calculated P-wave velocities vary within a narrow range (8.58 – 7.98 km/s on average). The fast split S-wave (S1) is polarized in a plane that contains the propagation direction and the lineation. The maximum S-wave anisotropy, ranging between 2.92 and 7.99 % and averaging 4.91 %, is directed in the plane of foliation, perpendicular to the lineation.

Seismic properties were calculated for each of the three sub-areas of the Nógrád-Gömör Volcanic Field as well. The velocities and fastest directions of P-waves are in very good agreement, as well as the S1 polarisation directions. There is, however, a slight difference between the maximum S-wave anisotropies among the distinct domains: the central part shows the highest degree (5.37 %) and the southern part shows the lowest (3.53 %), while the anisotropy in the northern part falls in the middle (4.76 %) (Fig. 5.24).

5.6. 'Water' Content of Nominally Anhydrous Minerals

5.6.1. Incorporation of 'water' in nominally anhydrous minerals

'Water' in the mantle can occur in several forms, such as H_2O (e.g., as a fluid phase), OH^- as structurally bound in volatile-bearing minerals such as amphibole or mica, or H^+ incorporated in nominally anhydrous minerals (NAMs) in the mantle (such as olivine and pyroxenes) by substitution in tetra- or octahedral crystal sites (e.g., Berry et al., 2005). Hence 'water' in NAMs generally refers to H^+ in the crystal structure, forming OH-bonds which allow detectability with infrared spectroscopy. The different substitutional types and peak positions in the infrared spectra are well-known for olivine, and have been described as follows:

• Si-substitution: four H atoms occupy a tetrahedral site (Lemaire et al., 2004; Walker et al., 2007), yielding peaks around 3613, 3580, 3567 and 3480 cm^{-1} on the infrared spectrum. Recently it was shown that this substitution can also occur with H^+ coupled to boron in a tetrahedral site, resulting in absorption bands at 3704, 3598 and 3525 cm^{-1} (Ingrin et al., 2014). In the mantle environment, where olivine generally coexists with one or more pyroxenes, silica activity is buffered and therefore Si-vacancies are expected to be too low in abundance to significantly influence H^+ storage (e.g., Demouchy and

Bolfan-Casanova, 2016).

• Mg-substitution: two H atoms substitute for a divalent cation in octahedral positions (Lemaire et al., 2004; Berry et al., 2005; Walker et al., 2007), producing absorption peaks at 3220 and 3160 cm^{-1}.

• 'Ti-clinohumite' substitution: a Ti^{4+} occupies an octahedral site instead of a divalent cation, and the resulting charge imbalance is relieved by two H^+ substituting for Si^{4+} in a neighbouring tetrahedral site (Berry et al., 2005; Berry et al., 2007b; Walker et al., 2007). This results in absorption peaks at around 3572 and 3525 cm^{-1}.

• Trivalent cation substitution: a trivalent cation (e.g., Al^{3+}) and an H^+ occupy two octahedral sites, with absorption peaks appearing between 3400 and 3300 cm^{-1} on the infrared spectrum (Berry et al., 2007a; Blanchard et al., 2017).

Alternatively, H^+ may be present in olivine interstitially (Ingrin et al., 2013), associated with Fe^{3+} (Mackwell and Kohlstedt, 1990), or as molecular H_2 in reduced conditions (Yang et al., 2016).

In the case of pyroxenes, H^+ can be incorporated in tetrahedral- and octahedral sites as well (e.g., Sundvall and Stalder, 2011; Balan et al., 2013). However, the links between substitution types and absorption peaks seem to be more complex than in olivine due to the wider compositional variety. In synthetic orthoenstatite, two major bands are observed at 3360 and 3070 cm^{-1} (Stalder and Skogby, 2002; Stalder, 2004), and two at 3690 and 3590 cm^{-1} for samples synthesized at lower silica activity and higher pressure (e.g., Stalder et al., 2012). Balan et al. (2013) proposed that the former bands are associated with two H atoms substituting for Mg^{2+} at the M2 site, whereas the latter bands can be linked to a Si vacancy filled by two H^+ and a Mg^{2+} located either within the tetrahedron or in an interstitial position. In both orthopyroxene and clinopyroxene, the amount of Al or other trivalent cations is positively correlated with incorporated H^+, as together they can substitute for a tetrahedral Si^{4+} or two octahedral Mg^{2+} (e.g., Stalder and Skogby, 2002; Stalder, 2004; Férot and Bolfan-Casanova, 2012). Nevertheless, even though Al has an influence on the incorporation of H^+ in pyroxenes, it appears that the coupling of the two is not common (Stalder, 2004).

5.6.2. 'Water' (H_2O) content in olivine and pyroxenes in the Nógrád-Gömör xenoliths

Olivine

Olivine displays no sign of structurally bound water in most of the xenoliths. Small absorption peaks are observable in the four xenoliths from Jelšovec (NJS1302, NJS1304, NJS1306, NJS1307) at around 3572 and 3525 cm^{-1} (Fig. 5.25), associated with Ti-clinohumite type substitution (Berry et al., 2005; 2007b). The calculated 'water' contents (values are given as H_2O weight ppm) are 0.7 – 2.2 ppm (Table 10) for these four xenoliths. Extremely small absorption peaks are present in another 5 of the xenoliths (NTB0307, NFK0301, NFK1123, NFR0306 and NBN0311) at approximately the same wavenumbers; however, these absorption bands are too small to yield a significant H_2O content.

Orthopyroxene

Orthopyroxenes have major absorption bands in the ranges of 3600-3570, 3530-3510 and 3430-3420 cm^{-1}, with weaker ones around 3250-3200 cm^{-1} (Table 10; Fig. 5.25). The first band range appears to result from the overlapping of three peaks at ~3595, ~3580 and ~3570; usually only one or two of them are observable in a given spectrum. These band ranges are well known from both natural (e.g., Falus et al., 2008; Bonadiman et al., 2009; Sundvall and Stalder, 2011; Denis et al., 2013) and experimental (Kovács et al., 2012b) orthopyroxenes, but their exact substitution assignments are still not clear. However, the relative intensities of the three major bands are not homogeneous for all samples, although in most cases, the first band is the most intense (Fig. 5.25). Besides the bands of structurally-bound water in orthopyroxene, additional peaks are present occasionally at 3690-3670 (NTB0306, NTB0307, NFK1115, NFR0307, and NBN0311) and 3630-3620 (NTB0307 and NFR0307) cm^{-1}. The calculated amount of H_2O varies over a broad range, from completely dry (NPY1301, NPY1310, NPY1311, NPY1314, NFL1315A, NFR0306, NME0528, NME1116) up to a maximum of 147 ppm (NFR0307), with the majority falling below 40 ppm (Fig. 5.26, Table 10). There is no observed correlation between water content and the sampling localities of the xenoliths, although it can be observed that xenoliths of the southern part have lower 'water' contents, whereas the higher amounts of incorporated water appear in samples from the northern and central parts (Fig. 5.26).

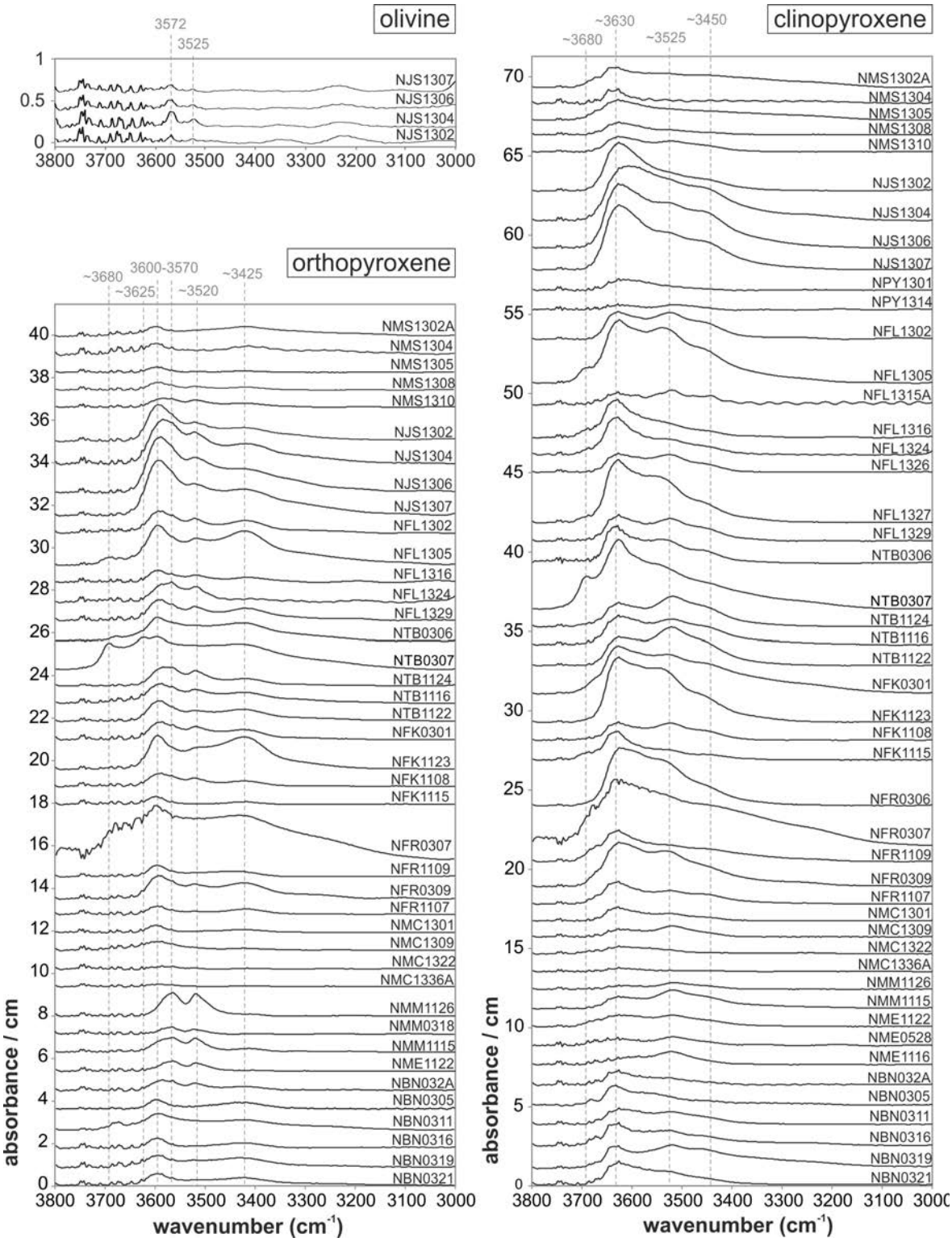

Fig. 5.25. Average unpolarised FTIR spectra of olivine (a), orthopyroxene (b) and clinopyroxene (c) of the Nógrád-Gömör xenoliths, normalised to 1 cm^{-1}. Wavenumbers of major absorption bands are contained in Table 10.

Clinopyroxene

Clinopyroxene has main absorption bands at 3640-3620, 3530-3520 and ~3450 cm^{-1}, but a weaker band may appear at 3590 and 3250 cm^{-1} as well (Table 10, Fig. 5.25). The intensity of the three main bands varies similarly to those of the orthopyroxenes; in the majority of the xenoliths, the first peak is the biggest, but in some cases, the second one is more prominent (Fig. 5.25). These bands are all believed to represent structurally bound H in clinopyroxene (e.g., Sundvall and Stalder, 2011; Kovács et al., 2012b). However, in some cases extra bands are observable at ~3680 cm^{-1}. Although clinopyroxene is the most H_2O-rich NAM, several Nógrád-Gömör samples have extremely low amounts (below 20 ppm in NMS1304, NPY1314, and NMC1336A). The total range varies between 11 and 481 ppm (Table 10), with the majority of the values below 150 ppm (Fig. 5.26), and three xenoliths (NPY1310, NPY1311, NMM0318) have completely dry clinopyroxenes. Xenoliths from the southern part are the most H_2O-poor, with water content of clinopyroxenes below 100 ppm; samples from the northern and central parts cover a wider range (Fig. 5.26). Sample NMM0318 is quite unusual, with clinopyroxene dryer than the coexisting orthopyroxene. For the rest of the xenoliths with measurable H_2O contents, the ratio of water in the clinopyroxene *vs* orthopyroxene varies between 1 and 10, with a few exceptions (NMS1302A, NMS1305, NFL1316, NFK1115, NFR1109, NMC1322). In these exceptions the ratio of H_2O content in clinopyroxene *vs* orthopyroxene is greater than 10 (Table 10).

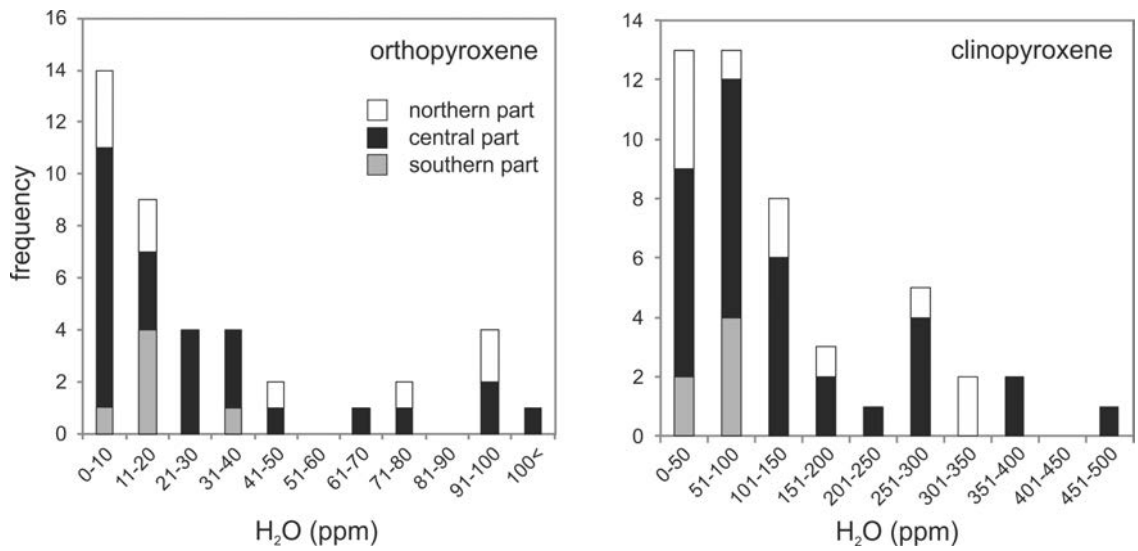

Fig. 5.26. Distribution of the amount of incorporated H_2O in ortho- and clinopyroxenes in the Nógrád-Gömör xenoliths.

Table 10. 'Water' contents and properties of IR spectra of NAMs. Int. r. – integration range; *hydrous lamella, 'weak band; grey highlight indicates $H_2O^{cpx/opx} < 4$.

Sample	Thickness (μm)	OLIVINE			ORTHOPYROXENE			CLINOPYROXENE			Bulk rock H_2O (ppm)	H_2O cpx/opx
		Int. r.: 3583-3505 cm^{-1}			Int. r.: 3740-3020 cm^{-1}			Int. r.: 3765-3000 cm^{-1}				
		n	A_{unpol}	H_2O (ppm)	n	A_{unpol}	H_2O (ppm)	n	A_{unpol}	H_2O (ppm)		
NMS1302A	260				6	0.42	3	4	8.68	140	7.2	42.6
NMS1304	95				4	0.71	15	5	0.42	19	2.9	1.2
NMS1305	275				7	0.39	3	6	7.36	112	10.8	38.9
NMS1308	275				5	0.92	7	3	3.15	48	5.7	7.1
NMS1310	280				4	1.54	11	5	4.44	67	12.4	6.0
NJS1302	200	10	0.043	1.21	7	4.60	46	6	7.90	166	25.6	3.6
NJS1304	170	8	0.067	2.22	6	6.13	73	4	13.24	327	26.9	4.5
NJS1306	185	11	0.023	0.70	6	8.29	91	5	15.04	342	70.3	3.8
NJS1307	225	11	0.028	0.70	6	10.93	98	6	15.10	282	51.0	2.9
NPY1301	135				6	-	-	6	1.08	34	2.0	-
NPY1310	180				3	-	-	4	-	-	-	-
NPY1311	170				7	-	-	6	-	-	-	-
NPY1314	205				5	-	-	5	0.94	19	3.5	-
NFL1302	230				5	3.75	33	4	8.16	149	15.2	4.5
NFL1305	335				4	15.77	95	4	28.71	360	70.8	3.8
NFL1315A	110				7	-	-	2	1.51	58	1.2	-
NFL1316	255				6	1.18	9	2	7.40	122	7.0	13.0
NFL1324	125				5	1.01	16	4	2.44	82	10.6	5.0
NFL1326	150				-	-	-	7	3.08	86	10.4	-
NFL1327	200				-	-	-	6	12.60	265	26.5	-
NFL1329	155				6	2.31	30	6	4.49	122	17.5	4.0
NTB0306	270				4	8.32	62	8	7.77	121	19.3	1.9
NTB0307	250				6	11.45	93	3	23.11	388	64.8	4.2
NTB1124	310				15	3.55	23	11	9.31	126	20.7	5.4
NTB1116	300				7	4.39	30	7	11.63	163	22.5	5.5
NTB1122	250				6	3.98	32	6	11.19	188	34.3	5.8
NFK0301	260				4	3.48	27	5	16.40	265	19.5	9.8
NFK1123	220				9	8.00	74	4	15.67	299	39.2	4.1
NFK1108	200				7	1.46	15	7	3.85	81	5.7	5.5
NFK1115	180				7	0.38	4	7	3.80	89	3.9	20.6
NFR0306	270				-	-	-	6	16.61	258	23.3	-
NFR0307	210				3	15.22	147	5	24.04	481	59.8	3.3
NFR1109	255				10	1.11	9	5	8.81	145	8.7	16.6
NFR0309	210				7	4.57	44	6	11.80	236	36.7	5.4
NFR1107	220				5	1.06	10	6	5.06	97	8.5	9.9
NMC1301	250				7	0.65	5	6	2.49	42	2.7	7.9
NMC1309	175				6	0.58	7	5	1.76	42	6.3	6.3
NMC1322	155				7	0.08	1	6	0.72	19	1.7	18.0
NMC1336A	220				6	0.16	1	6	0.56	11	1.2	7.2
NMM1126	190				3	2.34	25	5	1.67	37	11.2	1.5
NMM0318	210				12	0.41	4	7	-	-	0.9	0.0
NMM1115	240				4	1.72	14	3	3.84	67	5.5	4.6
NME1122	220				2	0.84	8	5	3.31	63	7.8	8.2
NME0528	180				2	-	-	3	1.63	38	2.3	-
NME1116	230				6	-	-	6	2.63	48	5.3	-
NBN0302A	125				24	0.57	9	5	1.27	43	3.3	4.6
NBN0305	145				10	0.72	10	5	1.58	46	4.2	4.6
NBN0311	335				8	5.13	31	4	5.68	71	9.6	2.3
NBN0316	160				17	0.82	10	9	2.71	71	7.3	6.9
NBN0319	160				11	1.01	13	10	3.59	94	13.9	7.4
NBN0321	180				11	1.12	13	9	3.76	88	10.4	7.0

Chapter 6. Discussion

6.1. Implications of Equilibration Temperatures

6.1.1. Thermal history

Calculated equilibration temperatures can provide information about the thermal conditions of the mantle depth sampled by the xenoliths. In addition to temperatures at the time of sampling by the host magma, the application of different thermometers may give further insight into the thermal history of the mantle domain, provided that detectable changes have occurred on a geologically short time scale. This is based on the different diffusional behavior of the different elements used by the thermometers. However, there are several factors which can influence the validity of the temperature estimates. One of these is the presence of melts in the mantle, as indicated by melt pockets in some xenoliths (Table 1; Fig. 5.6g, h).

The formation of melt pockets may be explained by 1) reaction of the peridotite xenolith and the host basalt during ascent to the surface, 2) melting of anhydrous phases (e.g., Huebner and Turnock, 1980), 3) breakdown of volatile-bearing phases as a result of increasing temperature prior to ascent (e.g., Stosch and Seck, 1980), and 4) reaction with a migrating silicate melt in the mantle (Bali et al., 2002; 2008b). In the case of the Nógrád-Gömör xenoliths, the large size of the melt pockets (1-2 mm; Fig. 5.6g, h) and the lack of definite connection between them (Fig. 5.5g) suggests *in situ* melting at depth, because ascent of the host magma was relatively rapid (i.e., ~36 hours to the MOHO and an additional ~1.5 hours to the surface; Szabó and Bodnar, 1996). The fact that clinopyroxenes in xenoliths from the southern part of the area, which contain the most melt pockets, (Table 1), are generally depleted in incompatible elements (Table 3; Appendix B), and the lack of any visible sign of melt percolation, also argue against melt-wall-rock reaction. On the other hand, the presence of melt pockets can bring into question the validity of the equilibration temperatures calculated with major element-based thermometers. The two-pyroxene and Ca-in-opx methods rely on Ca-contents of pyroxenes and part of the Ca may go into the melt pockets as it becomes incompatible at elevated temperatures (e.g., Witt and Seck, 1987). Furthermore, temperature data under 900 °C are slightly below the values previously reported from the Carpathian-Pannonian region (e.g.,

Bali et al., 2002). Therefore, equilibration temperatures calculated with thermometers based on major-element exchange should be considered as minimum values.

The distribution of REE in pyroxenes can provide further insight into this matter. For the continental upper mantle, which is thermally well equilibrated and usually did not undergo thermal variations shortly before sampling by the host magma, major elements and REE thermometers are expected to be in agreement. However, the diffusion rates of the trivalent REE are slower than those of the divalent cations in mantle silicates (Van Orman et al., 2001; Cherniak and Liang, 2007), and in the case of a high cooling rate, the closure temperature for REE diffusion will be higher than for the major elements. Hence, the REE-based thermometer is thought to give sub-solidus temperatures, whereas major element-based thermometers provide the temperature of the latest thermal equilibration (Liang et al., 2013). A discrepancy between the two values is characteristic of abyssal peridotites (e.g., Marchesi et al., 2016), as cooling rates in the lower oceanic crust are around 10^{-1} – 10^{-5}°C/yr (Coogan et al., 2002; VanTongeren et al., 2008), in contrast to xenoliths from the continental mantle, which are assumed to have equilibrated over longer geological time.

In the case of the studied Nógrád-Gömör xenoliths, there is an average difference of ~ 50-100 °C between temperature values (Table 1) calculated with thermometers based on the REE (Liang et al., 2013) and major elements. This suggests that major thermal changes have affected the upper mantle prior to the entrainment of the xenoliths in the host basalt. REE distributions in pyroxenes record a higher-temperature environment, which was followed by cooling and late stage re-equilibration recorded by the major-element thermometers. This cooling event beneath the whole Carpathian-Pannonian region is supported by other studies carried out on mantle xenoliths from Little Hungarian Plain, Bakony-Balaton Highland and Persani Mountains (Fig. 2.3): Embey-Isztin et al. (2001) and Falus et al. (2008) detected a cooling defined by compositional differences between the cores and rims of porphyroclasts, and Falus et al. (2007) presented temperature differences based on exsolution lamellae in pyroxenes. The estimated extent of cooling is ~40-50 °C in the Persani Mountains (Falus et al., 2008) and ~100-150 °C in the Little Hungarian Plain (Falus et al., 2007). These rates are consistent with the temperature gap detected in the Nógrád-Gömör xenoliths and thus support the record of thermal evolution in the Carpathian-Pannonian region.

In the Nógrád-Gömör Volcanic Field, higher temperatures can also induce melting of amphibole, which has a solidus T of ~ 1050-1100 °C depending on the composition

and H_2O content of the peridotite (Green et al., 2010), over a wide range of pressures (~30 - 90 km; Niida and Green, 1999). The breakdown of amphibole could explain the more common presence of melt pockets most in xenoliths from the southern part of the study area (Table 1). This is also consistent with earlier observations on the modal abundance of amphibole in xenoliths from the southern part (Szabó and Taylor, 1994), despite its absence in the present sample set. Furthermore, heating induced by extension and asthenospheric upwelling in the Pannonian Basin (Horváth, 1993; Csontos, 1995) could have affected the southern part more than the northern and central parts, because it is closer to the centre of the extensional basin (Fig. 2.3). In the central part (except for the Fil'akovo-Kerčik locality), the rarity of amphibole in xenoliths can be due to lower initial abundance, or to an additional heating factor, such as melts ascending from greater depths.

6.1.2. Estimations on the depth of origin

To better understand the geochemical and physical conditions of the upper mantle beneath the volcanic field, it is necessary to locate the approximate depth from which xenoliths are derived. Ideally, the application of geobarometers would provide the best estimates for the depth of origin. However, as mentioned above, existing geobarometers for lherzolites are based on the presence of coexisting garnet: therefore constraining pressure, and thus depth, in the spinel stability field is more challenging.

A possible method is using the appropriate geotherms of the study area and converting equilibration temperatures to depth, depending on the shape of the curve. Such a method was used to give a robust estimation on the depth of origin for xenoliths from Bakony-Balaton Highland and Little Hungarian Plain (Kovács et al., 2012a) and Styrian Basin (Aradi et al., 2017) in the Carpathian-Pannonian region. However, there are no precisely calculated geotherm curves for the Nógrád-Gömör Volcanic Field. For xenoliths from the Little Hungarian Plain and Bakony-Balaton Highland, Kovács et al. (2012a) used geotherms calculated for Cenozoic lithosphere and modified it based on the appropriate heat flow value for the central part of the Pannonian Basin (Lenkey et al., 2002). However, relying on heat flow only for determining mantle geotherms has a very high uncertainty. The locus of the conductive crustal geotherm depends on the heat production and thermal conductivity of all the rocks in the crustal column, properties that are rarely known. In addition, the lithospheric mantle geotherms in regions with significant recent basaltic

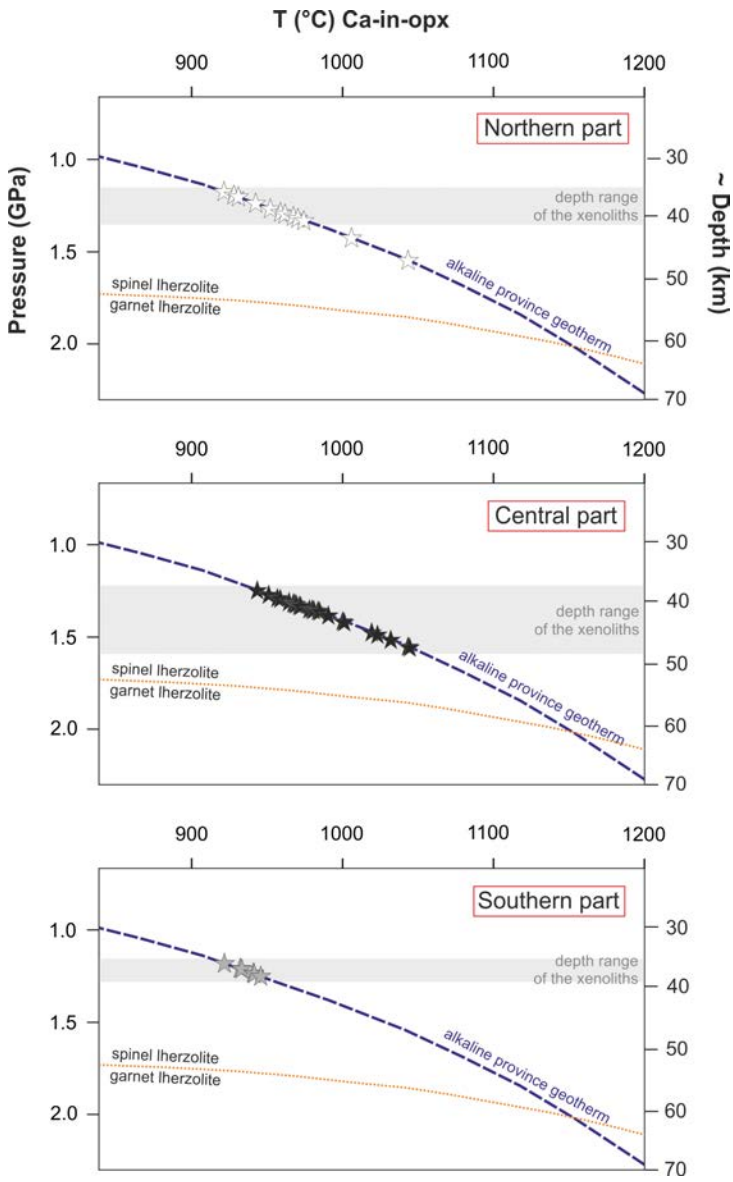

Fig. 6.1. Estimation of depth of origin for the studied xenoliths from the three domains of the Nógrád-Gömör Volcanic Field, using the alkaline-province geotherm of (Jones et al., 1983). The equilibration temperatures were obtained with the corrected Ca-in-opx thermometer of Nimis and Grütter (2010). Spinel lherzolite to garnet lherzolite transformation curve (Fo_{90} composition) is taken from O'Reilly et al. (1997), based on the work of O'Neill (1981).

activity are not simply conductive, but are advective, as the ascent of basalts and intrusions at density discontinuities result in a convex-upward inflected geotherm (Griffin and O'Reilly, 1987; O'Reilly and Griffin, 2006). An alternative approach to inferring the depth sampled by xenoliths is to refer xenolith temperature estimates to the empirical 'alkaline-province' geotherm of Jones et al. (1983). This has been shown to be generally consistent for mantle xenoliths hosted in alkali basalts in active Cenozoic areas worldwide including southeastern Australia (Griffin et al., 1984; O'Reilly and Griffin, 1985), or South China (Yu

et al., 2003). The studied xenoliths from the different areas of the Nógrád-Gömör Volcanic Field are plotted on Fig. 6.1. The temperatures used are calculated with the Ca-in-opx method of Brey and Köhler (1990) as modified by Nimis and Grütter (2010), as these are considered to represent more recent conditions than the REE thermometer as discussed above. Note that due to uncertainties within the equilibration temperatures (see Chapter 5.3) the resulting estimations should be considered as approximate depth values where the local geotherm cannot be constructed precisely, and/or where unambiguous geophysical data are not available.

As a consequence of different ranges in the equilibration temperatures, xenoliths from the distinct parts of the Nógrád-Gömör Volcanic Field show on average slightly different estimated depths of origin. Samples from the southern and northern parts (apart from two outliers with high temperatures) indicate shallower depths of origin (~35-40 km) than that for xenoliths from the central part (~40-50 km) (Fig. 6.1), and the total depth range is around 15 km. However, as mentioned earlier, the increased temperature range in the central part may be due to other processes, such as late heating. This question is further discussed in Chapter 6.3.

6.2. Reconstruction of Geochemical Processes

Major- and trace-element contents of xenoliths from the upper mantle can provide valuable clues concerning the geochemical characteristics of the sampled mantle domain(s) and of the events that caused changes in the modal and/or chemical composition. These processes commonly result in depletion of the incompatible elements by melt extraction during partial melting, or enrichment of these components by metasomatism produced by reaction with fertile melts/fluids. The variability in the major- and trace-element compositions in the Nógrád-Gömör xenoliths suggests several that major geochemical processes affected the upper mantle beneath the region. This section discusses the reconstruction of these processes based on the analysed mineral and calculated bulk-rock compositions.

6.2.1. Partial melting

In residual mantle material, represented by some xenoliths, determination of the

degree of partial melting is usually challenging due to overprinting by late geochemical (i.e., metasomatism) and/or physical (deformation, recrystallisation) processes. Thus, the best indicators for melt extraction are elements which are less affected by subsequent metasomatic events.

In the Nógrád-Gömör Volcanic Field, partial melting can be traced as either (or both) a change in major-element compositions, such as increased spinel Cr# (Arai, 1994), and depletion of rare-earth elements, especially LREE. These attributes have been described both in peridotite massifs (e.g., Bodinier et al., 1988) and mantle xenoliths hosted in alkali basalts (e.g., Frey and Green, 1974; Downes et al., 1992), and are interpreted as reflecting partial melting of an originally fertile mantle by extraction of basaltic melts (e.g., Frey and Prinz, 1978). However, there are several examples showing that LREE-poor compositions can also result from metasomatic reaction with a large fraction of basaltic melt (e.g., Van der Wal and Bodinier, 1996; Bedini et al., 1997; Le Roux et al., 2007).

A common trend towards moderate depletion is seen in some Nógrád-Gömör xenoliths in the OSMA diagram (Fig. 5.7a), and the estimated degree of partial melting is around 20 %. This value generally corresponds to partial melting degrees previously proposed for the Nógrád-Gömör Volcanic Field by Szabó and Taylor (1994) and Konečný et al. (1995; 1999). However, in order to achieve more precise values regarding the degree of melting, several models can be used, based on major- element contents of rock-forming minerals (Upton et al., 2011; Faccini et al., 2013) or whole-rock samples (Walter, 2003; Herzberg, 2004), HREE (Norman, 1998; Niu, 2004) or Cr# of spinel in equilibrium with clinopyroxene (Hellebrand et al., 2001). Several of these models are applied and compared for the Nógrád-Gömör xenoliths as described below.

The HREE display a wide compositional range in clinopyroxenes (e.g. Yb = 0.31–2.58 ppm; Table 3) and also in calculated bulk-rock compositions (Yb = 0.02–0.51 ppm; Table 4), and there is some variability within each of the four xenolith groups. The degree of partial melting compared with a PM (primitive mantle) source (Sun and McDonough, 1989) has been estimated using the melting curves of Niu (2004) for bulk-rock fractional modelling (Fig. 6.2a–d). Model parameters and distribution coefficients for this model have been summarised by Niu and Hékinian (1997). Because of the sensitivity of the LREE to metasomatic events, only HREE were used to determine the amounts of melt extraction. Groups IA and IIA show partial melting degrees of ~ 5 – 20 % (except for NPY1314, which has a PM composition) and < 5 – 15 %, respectively (Fig. 6.2a, c).

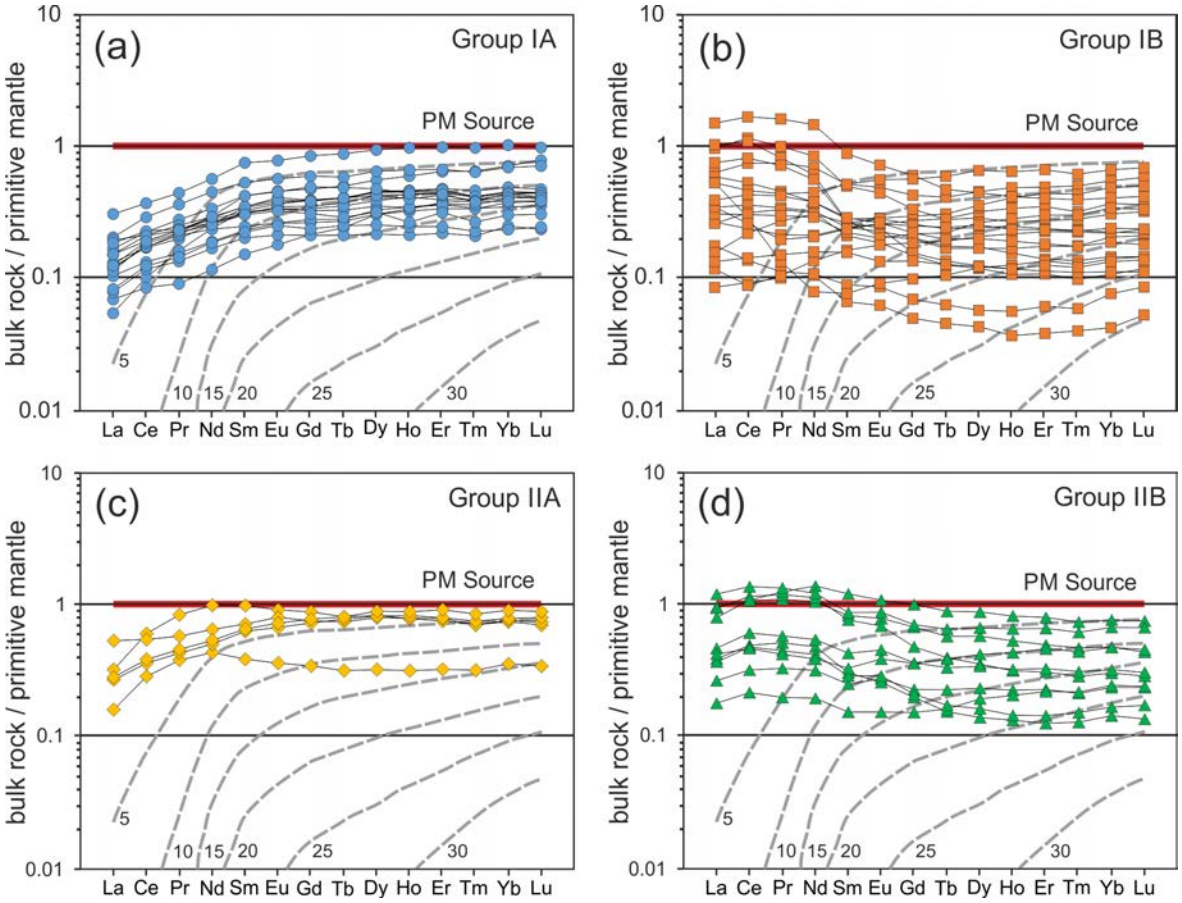

Fig. 6.2. Fractional melting model for xenoliths of Group IA, IB, IIA, IIB (a-d, respectively). Fractional melting curves and PM source are taken from Niu (2004) and references therein. Whole-rock REE (Table 4) have been calculated by mass balance, using the analysed data for pyroxenes and concentrations for olivine and spinel calculated with the use of mineral/melt partition coefficients of Hart and Dunn (1993) and Ionov et al. (2002).

Groups IB and IIB, however, display a wider range of partial melting (~ 5 – 30 % and 5 – 25 %, respectively; Fig. 6.2b and d). The high variability in melting degree in all groups suggests that partial melting has affected the mantle volumes represented by the xenoliths independently of their classification or locality, and therefore is likely to have occurred before any metasomatic overprint. Xenoliths of Group IIA show the lowest amount of melt extraction (< 5 %), and therefore they represent the most fertile upper mantle domain in the Nógrád-Gömör Volcanic Field (Fig. 6.2c). The fertile character of this group is also supported by major-element contents, such as low spinel Cr# (Fig. 5.7a), high orthopyroxene Al_2O_3 (Fig. 5.7c), and high clinopyroxene Na and Al contents (Fig. 5.7d). These geochemical features are characteristic of only Podrečany and Jelšovec in the northern part. Group IIA xenoliths are unique to this locality, and they make up the majority of xenoliths from these two locations (Fig. 3.1).

To further constrain the amount of melt extraction, the relationships of major elements in whole-rock compositions, as well as in individual phases, were examined. The bulk compositions of the Nógrád-Gömör xenoliths (Table 3) are plotted on the fractional melting and pressure grids of Herzberg (2004) (Fig. 6.3). The source material for this melting model is a fertile peridotite described by Walter (1998), which was obtained by extracting 1 % mid-ocean ridge basalt (MORB) melt from the PM (McDonough and Sun, 1995). The model also takes initial and final melting pressures into consideration. The FeO

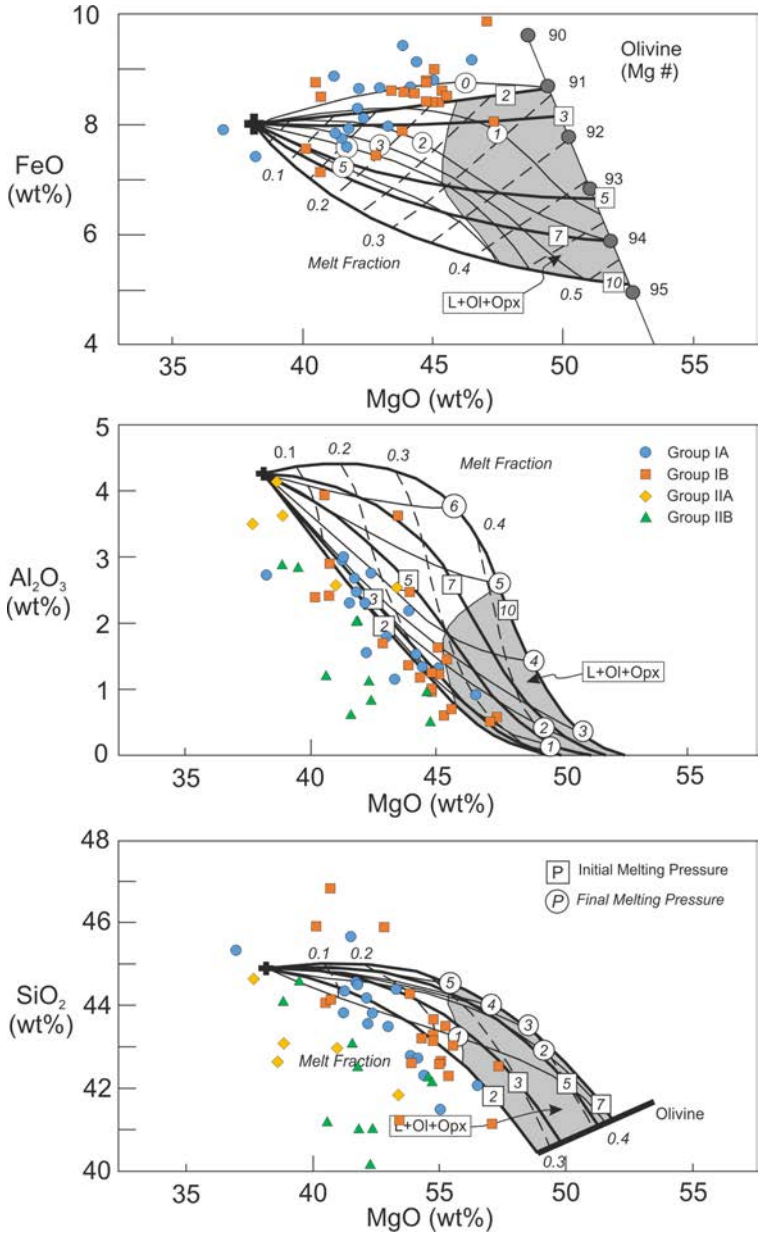

Fig. 6.3. Fractional melting model of the studied xenoliths with the application of MgO vs FeO (a), Al_2O_3 (b) and SiO_2 (c). Melt fraction, initial and final melting pressure curves (in GPa) are taken from Herzberg (2004); melting source is a fertile peridotite with a composition given by Walter (1998). Light grey field represents the composition of a residual harzburgite. Lines with numbers 90-95 on (a) stand for Mg# of olivine. In (a), only Group IA and IB are plotted owing to the high Fe contents of Group IIA and IIB.

content of the Nógrád-Gömör xenoliths spreads over a wide range (7.13 – 13.27 wt%; Table 4), and because of the high FeO concentrations of Group II xenoliths, these samples are not plotted on Fig. 6.3a.

Group IA and IB xenoliths show no correlation between MgO and FeO, and elevated FeO often accompanies elevated MgO, so that the olivine Mg# of these xenoliths does not fall below 'average' values (89-90; Table 2). This feature is characteristic of the Nógrád-Gömör mantle. However, most of the samples falling on the grid, plot around or on the dashed lines representing 0.1–0.2 (0.3) fractions of melt extraction; the initial melting pressures (bold lines) tend to be higher than the final pressures (fine lines). Group II xenoliths are also plotted on the grid based on MgO vs Al_2O_3 (Fig. 6.3b). Group IIB xenoliths fall consistently towards lower MgO contents compared with Group I xenoliths, as shown also on Fig. 5.11a, reflecting enrichment of Fe at the expense of Mg, also observed in Mg# values; Fig. 5.7a–c, Table 2). Groups IA and IB plot consistently between 0.1 and 0.3 melt extraction fraction, with initial melting pressures of 2-3 GPa on average and final melting pressures usually at or below 2 GPa. Some xenoliths plot above the grids (Fig. 6.3c) because of high (> 45 wt %) bulk SiO_2 contents. This can be explained by a high pyroxene mode; for example, large orthopyroxene porphyroclasts in a small xenolith, which is true of several Nógrád-Gömör samples (Table 1). The highest degree of partial melting is recorded in Group IB xenoliths, consistent with the model of Niu (2004), where the lowest HREE contents occur in Group IB and indicate up to 30% partial melting (Fig. 6.2b). However, such high degrees of melt extraction are not consistent with the Mg-numbers and the relatively high amount of clinopyroxene in the xenoliths (Table 1), as clinopyroxene would be no longer present under these conditions (marked by the grey field in Fig. 6.3a-c).

To avoid possible errors caused by uncertainties in the modal composition, empirical melting curves based on the major-element contents of pyroxenes (and spinel) can be used, such as those of Upton et al. (2011) and Faccini et al. (2013). Theoretical melting curve for orthopyroxene was obtained by Faccini et al. (2013) with a PM starting composition (McDonough and Sun, 1995) and mass balance calculation using progressive melting residua derived from the experimental results of Herzberg (2004). MgO vs Al_2O_3 in orthopyroxene (Fig. 6.4a) shows a good correlation for Group I xenoliths, with melting degrees ranging between ~ 9 – 20 % for Group IA and ~ 11 – 26 % for Group IB. Group II xenoliths shift towards lower MgO values with increased FeO contents (as discussed

above), but the difference in the degree of melt extraction is well defined (~ 7 – 12 % for Group IIA and ~ 8 – 20 % for IIB). Slightly lower values appear on the MgO vs. Al_2O_3 melting curve for clinopyroxene (Fig. 6.4b), which was calculated by Upton et al. (2011) using the same PM source and the equations of Workman and Hart (2005). Note that the melting curve terminates at 25 %, which is considered to be the point of complete clinopyroxene consumption. Most of the xenoliths show melting degrees below 20 %, with Group IB having the widest range and Group IIA showing the most fertile characteristics. On the plot of Al_2O_3 in orthopyroxene *vs* spinel (Fig. 6.5), the distinct groups generally show similar ranges as on Fig. 6.4a; Group IA shows a slightly narrower range (~ 8 – 14 %) and the Group IIB maximum rises to ~ 23 %. The xenoliths with the highest degrees of melting (NMS1302A, NFL1315A, NFL1316, NTB0306, NFK1115, NFR1109) on all three major element melting models correspond to those with the highest spinel Cr# in Fig. 5.7a.

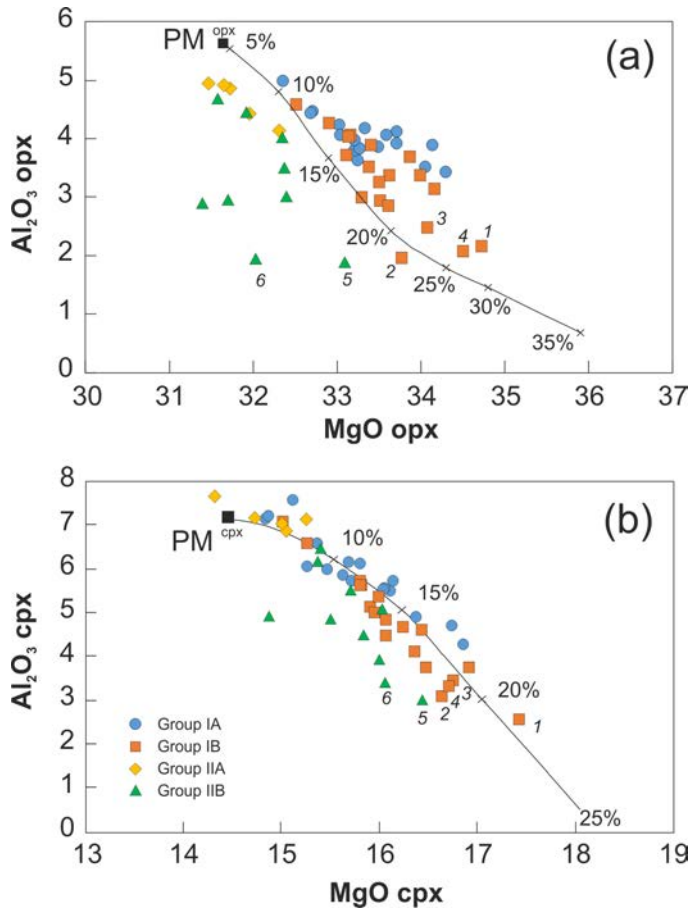

Fig. 6.4. Melting model based on MgO vs Al_2O_3 in orthopyroxene (a) and clinopyroxene (b). Melting curves are taken from the calculation of Faccini et al. (2013) and Upton et al. (2011); primitive mantle (PM) compositions (black squares) were calculated by mass balance using the major element and modal compositions of McDonough and Sun (1995) for the spinel stability field. Labelled xenoliths: 1 – NMS1302A; 2 – NFL1315A; 3 – NFL1316; 4 – NTB0306; 5 – NFK1115; 6 – NFR1109.

This group is among the most depleted xenoliths from the European SCLM (see Downes, 2001 for a review); similarly high partial melting degrees were reported in xenoliths from Eastern Serbia (Cvetkovic et al., 2007).

In summary, whereas the degrees of melting calculated with methods based on REE (Fig. 6.2) and major elements (Fig. 6.3 – 6.5) are generally in agreement, the methods using calculated bulk-rock compositions have slightly higher uncertainty. Therefore, the partial melting degrees based on the analysed compositions of mineral phases are more preferred; these suggest a maximum of ~ 23 – 25 % of melt extraction, shown by Group IB and IIB xenoliths (Fig. 6.4, 6.5) and a minimum of ~ 7 – 10 % for the most fertile xenoliths, i.e. Group IIA (Fig. 6.4, 6.5). This implies that subsequent metasomatic events, on which the group classification is based, affected an already heterogeneously-depleted mantle domain under the Nógrád-Gömör Volcanic Field.

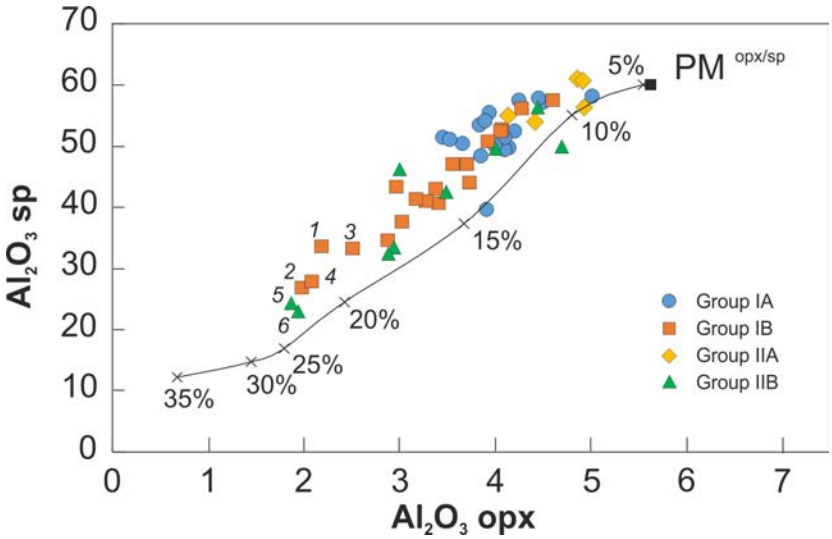

Fig. 6.5. Melting curve based on Al_2O_3 in orthopyroxene vs spinel (Faccini et al., 2013). Primitive mantle (PM) composition (black square) was calculated by mass balance using the major element and modal compositions of McDonough and Sun (1995) for the spinel stability field. Labelled xenoliths: 1 – NMS1302A; 2 – NFL1315A; 3 – NFL1316; 4 – NTB0306; 5 – NFK1115; 6 – NFR1109.

6.2.2. Imprints of metasomatic events

6.2.2.1. Presence and absence of amphibole

The most common, but not exclusive, products of modal metasomatism are volatile-bearing phases such as amphibole and phlogopite. Pargasitic amphibole occurs widely

in upper mantle peridotites, and is an important reservoir for volatiles and incompatible trace elements such as Rb, Ba, Nb and Ta. Experimental studies reveal that amphibole is stable up to 2.5 – 3.0 GPa at subsolidus conditions, and to temperatures of 950 – 1000 °C under water-saturated and to 1025 – 1150 °C under water-undersaturated conditions, depending on peridotite composition (e.g., Green, 1973; Mengel and Green, 1989; Wallace and Green, 1991; Niida and Green, 1999). In the studied Nógrád-Gömör xenoliths, amphibole occurs in several samples from the northern part and one location in the central part, and amphibole has been reported from the southern part by Szabó and Taylor (1994). They found the amphiboles to be homogeneously pargasitic in composition, regardless of sampling locality; this was verified by re-calculation using the spreadsheet of Locock (2014). Amphiboles analysed in this study, however, were found to be mostly magnesio-hastingsitic in composition, using the same calculation method. As the main difference between these two sets of amphibole compositions is based on the ratio and distribution of Fe^{2+} and Fe^{3+}, which cannot be determined by microprobe analyses alone, the calculation for the cations in each position depends heavily on the concentrations of other major elements in the amphibole. There are differences in SiO_2, Al_2O_3 and total abundances between this study and that of Szabó and Taylor (1994), where these values are higher by 1 – 2 % on average. Thus, it is likely that the discrepancy in the classification is due to analytical differences.

Szabó and Taylor (1994) suggested that volatile-bearing minerals (amphibole and traces of phlogopite) are products of a reaction with a K_2O-rich, H_2O- (and possibly F-) bearing subduction-related silicate melt. The presence of such melts is supported by a study of melt inclusions in Nógrád-Gömör xenoliths by Szabó et al. (1996). However, both amphibole and phlogopite can be precipitated from melts of different origins (Pilet et al., 2011). Coltorti et al. (2007a) reported compositional differences in HFSE such as Nb, Zr and Ti between amphiboles in suprasubduction and intraplate environments, which can be used to discriminate between amphiboles of different metasomatic origins. These compositional differences are based on the ratio of Nb to other HFSE, as Nb can be retained in the subducting slab, and thus is in low concentrations in subduction-related melts (Foley et al., 2000; Schmidt et al., 2004). It can then reappear in intraplate magmas that may contain contributions from older subducted slabs (McDonough, 1991; Fitton, 1995; Rudnick et al., 2000). Amphiboles in the Nógrád-Gömör xenoliths show a wide range of Nb contents (Table 3). The relationship between Nb and Zr (Fig. 6.6a) and ratios

of Ti/Nb and Zr/Nb (Fig. 6.6b) were used to constrain the crystallization environment of the amphiboles in the studied xenoliths, along with unpublished data of Szabó and Zajacz from the Nógrád-Gömör Volcanic Field (Mašková, Fil'akovo-Kerčik and Bárna; Fig. 3.1). Group IA and IIA amphiboles (and NMS1304 of Group IB) have lower Nb contents and thus plot in the suprasubduction field, whereas most Group IB and IIB amphiboles plot in or next to the intraplate field due to their higher Nb contents. Because Group IA and IIA xenoliths are LREE-depleted, they are considered to have been unaffected by the metasomatic events that enriched LREE in Group IB and IIB. This suggests that amphiboles of the former group were independent of the LREE-enriching metasomatism, and they were originally formed via volatile-rich fluids/melts related to a subducting slab. Based on the REE patterns of Group IA and IIA amphiboles (Fig. 5.10b), this slab-related fluid/melt must have been depleted in LREE and Nb-Ta to be able to produce amphibole

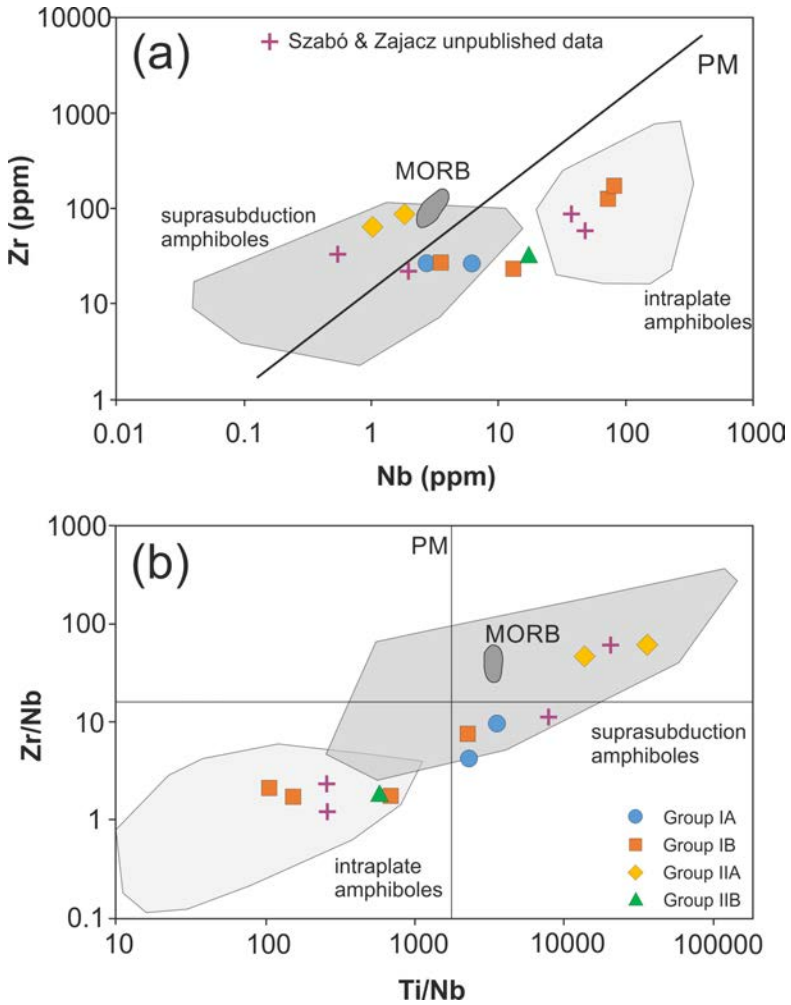

Fig. 6.6. Nb vs Zr (a) and Ti/Nb vs Zr/Nb (b) for amphiboles in the studied xenoliths and several previously unpublished analyses from the Nógrád-Gömör Volcanic Field (+ signs). Fields for suprasubduction and intraplate origins are from Coltorti et al. (2007). PM values are from McDonough and Sun (1995).

with the same trace element signature. Such depleted amphiboles have been reported from the Carpathian-Pannonian region previously, at the Kapfenstein locality in the Styrian Basin; however, these amphiboles grew at the expense of primary (LREE-enriched) clinopyroxene and spinel (Coltorti et al., 2007b), or possibly crystallized from the residual melt of a metasomatizing agent (Vaselli et al., 1996).

As for amphiboles in Group IB and IIB xenoliths, their probable intraplate origin suggests the impact of melts generated later, during or after the formation of the Pannonian Basin. These amphiboles, including the two unpublished ones, are all exclusively from the Fil'akovo-Kerčik locality (Fig. 3.1; Table 1). They either were formed by intraplate, LREE-enriched melts that reacted with the rest of the rock forming minerals, or formed originally in a suprasubduction environment, but were later metasomatized by intraplate melts. However, the latter is less likely because of the lack of any textural evidence of subsequent alteration, such as melting at the rims of the amphiboles. Therefore, it is proposed that amphiboles in Group IB and IIB were formed during reaction with a silicate melt of intraplate origin, and this mechanism was dominant at Fil'akovo-Kerčik, a locality slightly older than and spatially separated from the plateaux of the central part (Fig. 3.1). The strong similarity in the REE patterns of clinopyroxene and amphibole suggests that this melt probably also caused cryptic metasomatism in the pyroxenes. In addition to the LREE, enrichment of Rb, Nb and Ta is also characteristic of intraplate amphiboles, as well as of Group IB and IIB clinopyroxenes (compared with Group IA and IIA; see Fig. 5.8 and Table 3) suggesting that the metasomatizing agent was also enriched in these elements.

In the studied sample set, amphibole is basically absent in xenoliths from localities on the two large basalt plateaux of the central part (Fig. 3.1), although it has been reported previously by Szabó and Taylor (1994), in lower abundance compared to the northern and southern part. A possible explanation for this phenomenon is that amphibole has been completely reacted out by heating during asthenosphere upwelling (see Chapter 2.1), or by infiltrating metasomatizing melts, as will be discussed below. In this case, the low abundance of melt pockets (Table 1) in the central part would suggest that amphibole was originally not as common in the central part. These observations, along with the small size of the xenoliths, substantially decrease the chance of finding modal amphibole.

6.2.2.2. Implications of trace element concentrations

Variations in the distribution of REE contents in the studied xenoliths (Fig. 5.9a-h) show that the upper mantle beneath the Nógrád-Gömör Volcanic Field has undergone metasomatic transformation by a basaltic silicate melt to various extents. The character and degree of metasomatism is different for the distinct groups. Groups IA and IIA have REE patterns (Fig. 5.9a, c) characteristic of depleted MORB mantle observed in 'unmetasomatized' orogenic peridotites (e.g., Bodinier and Godard, 2003). Therefore, they are assumed to represent the 'original' geochemical composition of the mantle beneath the Nógrád-Gömör Volcanic Field, which was later overprinted by LREE-enriching metasomatism, the effects of which appear in the xenoliths of Group IB. The variations in representative light to heavy REE (Ce, Sm and Yb on Fig. 6.7a-c, respectively) with bulk-rock MgO content are associated with the extent of depletion. The correlation is very poor for highly incompatible LREE (i.e., Ce, Fig. 6.7a), but is strong for the less incompatible HREE (i.e., Yb, Fig. 6.7c). Thus, it can be concluded that metasomatic processes mostly affected the LREE whereas HREE were left generally unchanged, implying that the melt reacting with the wall rock was LREE-enriched. Several other incompatible elements also are enriched in Group IB clinopyroxenes, such as U and Th, with ranges of 0.01-1.06 ppm and 0.03-3.5 ppm, respectively (Table 3), compared to concentrations in Group IA which are lower by roughly an order of magnitude (0.005-0.21 and 0.01-0.29 ppm for U and Th, respectively; Fig. 5.8). Group IIA has U-Th contents in a similar range, whereas Group IIB is only slightly more enriched (0.01-0.14 and 0.04-0.50 ppm, respectively). Similar patterns can be observed for Nb and Ta: Group IB has wide concentration ranges and maxima as high as 1.1 ppm Nb and 0.26 ppm Ta, an order of magnitude higher than concentrations in the other groups (Fig. 5.8b). This suggests that Group IB xenoliths were affected by a melt rich in U-Th-Nb-Ta-LREE, which had no significant effect on major elements. Enrichment of Nb and Ta is characteristic for amphiboles of intraplate origin (Fig. 6.6), and therefore it was assumed that these elements were present in high concentrations in the amphibole-forming metasomatizing melt. Consequently, the metasomatism of Group IB xenoliths was probably related to this intraplate mafic melt, although extensive amphibole formation only occurred at the Fil'akovo-Kerčik locality in the central part (Fig. 3.1; Table 1). On the other hand, Group IIB xenoliths show a different geochemical character, namely the enrichment of several "basaltic" major elements (Fe,

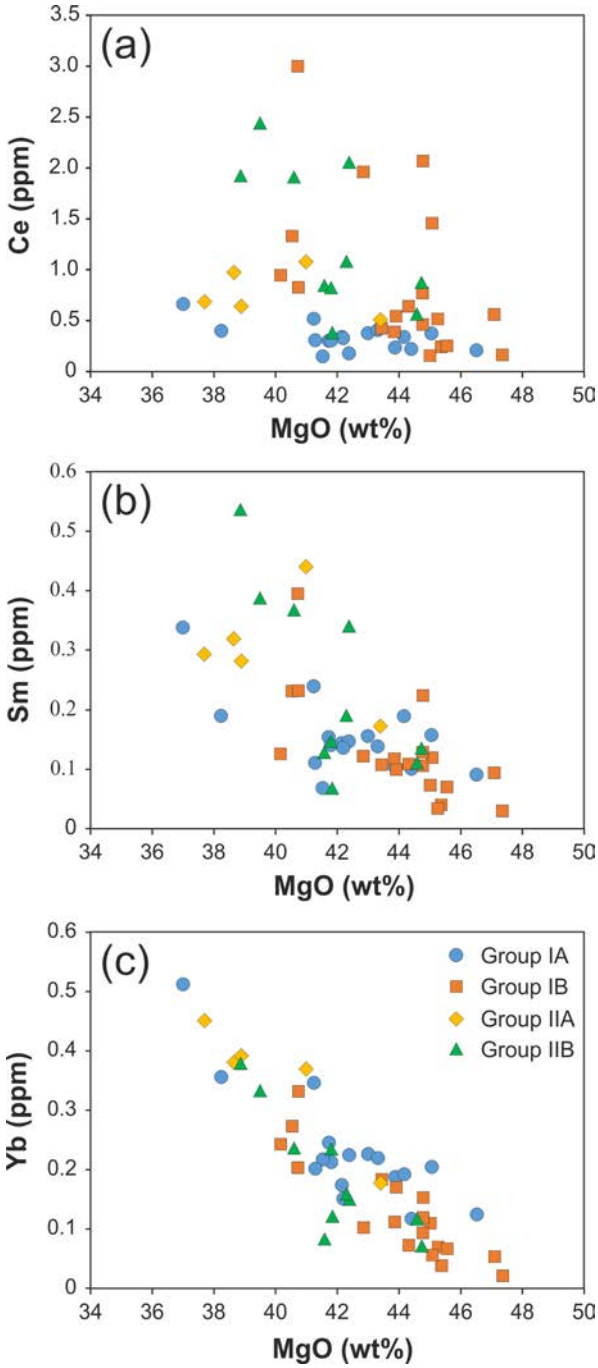

Fig. 6.7. Whole-rock MgO vs Ce (a), Sm (b) and Yb (c) for the Nógrád-Gömör xenoliths. Whole-rock MgO was calculated by mass balance from modal and analysed major-element compositions. Whole-rock REE were calculated by mass balance, using analysed data for pyroxenes and concentrations for olivine and spinel calculated using mineral/melt partition coefficients from Hart and Dunn (1993) and Ionov et al. (2002). Calculated whole-rock concentrations are reported in Table 4.

Mn, Ti) (Fig. 5.7a, b, e) as well as LREE (Fig. 5.9d), indicating a different metasomatic agent. Xenoliths of this group are also only present in the central part (Fig. 3.1), which suggests a metasomatic process different in chemistry and/or extent, as will be discussed further below.

Group IB xenoliths are present in almost all Nógrád-Gömör locations (Table 1). This group is variably enriched in LREE (Fig. 5.9b), which is attributed to reaction with a small melt fraction (or the late stage of a percolating large melt fraction) leading to more fractionated REE patterns (Van der Wal and Bodinier, 1996). It is assumed that

metasomatic processes affected the upper mantle to different degrees, even on a cm-scale (e.g., Bodinier et al., 1990; O'Reilly and Griffin, 2013). Based on the REE patterns of Group IB clinopyroxenes (Fig. 5.9b) and the presence of mafic melts in the mantle under the Nógrád-Gömör Volcanic Field, such as the host basalt, a mafic melt is assumed to have been the metasomatic agent. However, some Group IB xenoliths have very high LREE/HREE (LaN/LuN >5; Table 3) along with low Ti/Eu (Fig. 6.8), suggesting the effect of carbonatitic melts (Coltorti et al., 1999). A carbonatitic component is further supported by slightly elevated Na contents in clinopyroxene in some Group IB (and IIB) xenoliths (Fig. 5.7d), as well as by the presence of CO_2 fluid inclusions in Nógrád-Gömör xenoliths (Konecna, 1990; Szabó and Bodnar, 1996). However, other geochemical features, such as the lack of significant depletion in HFSE compared to REE, indicate that metasomatism cannot be explained only by carbonatitic melt. High LREE/HREE proportions can be a result of geochemical fractionation of metasomatizing silicate melt percolating through the wall-rock (e.g., Bodinier et al., 1990; Rivalenti et al., 2004), and thus xenoliths with such

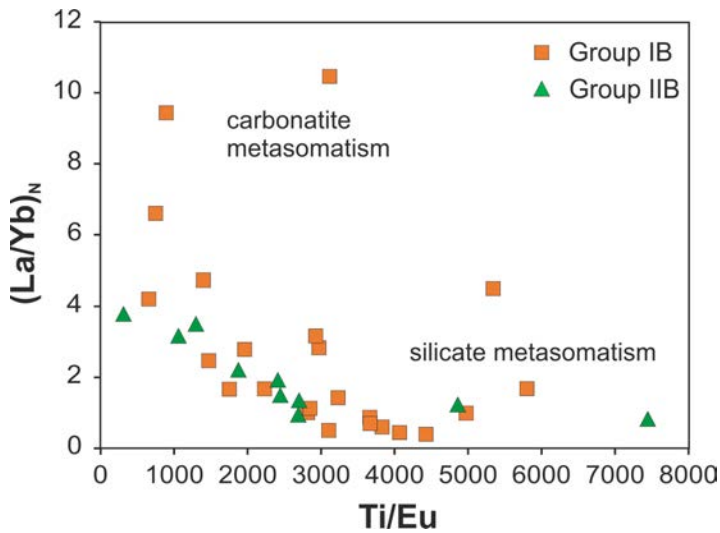

Fig. 6.8. $(La/Yb)_N$ vs Ti/Eu in clinopyroxenes of Group IB and IIB xenoliths, which show imprints of cryptic metasomatism. Areas of silicate and carbonatite metasomatism are from Coltorti et al. (1999).

REE contents can be the products of reaction with a highly evolved melt. Furthermore, as several studies (e.g., Zanetti et al., 1999; Bodinier et al., 2004) have pointed out, fractionation of a hydrous silicate melt during reactive porous flow can result in a carbonatitic residual melt, which leaves carbonatitic imprints in the metasomatized wall rock. For Group IB xenoliths, it is therefore assumed that the dominant metasomatizing agent was a silicate melt, possibly with a small amount of carbonatite component, which

can account for enrichment of LREE without affecting major elements (Mg, Ca) or modal compositions significantly (Rudnick et al., 1993).

The heterogeneous distribution of metasomatic patterns in the studied xenoliths indicates that melt migration occurred selectively, leaving volumes of the mantle domain partially or completely unaltered (e.g., Wilshire et al., 1980). Such localized melt percolation can be achieved if the lithosphere beneath the Nógrád-Gömör Volcanic Field contains a dense network of ductile shear zones that channelize melt percolation and reaction with the peridotite wallrock (Irving, 1980; Wilshire et al., 1980). Alternatively, dunitic lithologies, which also occur as xenoliths in the Nógrád-Gömör Volcanic Field (Szabó and Taylor, 1994; Konečný et al., 1995; 1999a; this study), may act as porous conduits for percolating melts (Kelemen et al., 1997; Liang et al., 2010). It is clear that sampling by the host basalt must have been less selective, as segments depleted in LREE, and thus presumably not affected by this metasomatic event, were sampled as well (i.e., Group IA and IIA).

6.2.2.3. Formation of Group II xenoliths

Group II xenoliths are characterized by increased Fe contents, and thus low Mg# (Fig. 5.7a-c). However, subgroups IIA and IIB differ in both major- and trace-element distribution (see Fig. 5.7, 5.8, 5.9 and Table 2). The Fe-rich nature of Group IIA is accompanied by high concentrations of other “basaltic” elements, such as Al, Na (Fig. 5.7d), Ca (Fig. 5.11c) and Ti (Fig. 5.11b), and they are on the low Cr#-end of the OSMA field (Fig. 5.7a). Furthermore, they have relatively high HREE concentrations (Fig. 5.9c). These attributes suggest that Group IIA xenoliths represent a generally more fertile mantle segment than the other groups, due to a lesser extent of partial melting (most of the xenoliths show ~5% melt extraction; Fig. 6.4, 6.5). This fertile mantle is present only beneath the northern part, as all Group IIA xenoliths are from either Podrečany or Jelšovec (Fig. 3.1; Table 1).

Group IIB xenoliths, however, show no significant increase in Na, Al or Ca (Fig. 5.7d, 5.11a and c, respectively). Furthermore, they show a continuous increase in both light and heavy REE, and have distribution patterns very similar to each other (Fig. 5.9d), suggesting that their REE contents were produced by the same process, alongside enrichment in Fe, Mn and Ti. Reactions of peridotite wall-rock with a percolating mafic

silicate melt resulting in such geochemical signatures has been observed widely in both orogenic peridotites and mantle xenoliths (Bodinier et al., 1990; Peslier et al., 2002a; Ionov et al., 2005; Raffone et al., 2009; Kourim et al., 2014). It is likely that this metasomatism overprinted the effects of any previous melting or metasomatism. The geochemical characteristics suggest that the host alkali basalt is a possible candidate for the reacting melt (Dobosi et al., 1995). However, the metasomatism is inferred to have happened *prior* to the entrainment and ascent of the xenoliths, for several reasons. *First*, alkali basalts in the Nógrád-Gömör Volcanic Field ascended very rapidly (Szabó and Bodnar, 1996). *Second*, geochemical evidence of reaction between the xenoliths and the host basalt has not been observed as major- and trace-element compositions are homogeneous within single samples (i.e., there is no change from the centre towards the contact with the basalt). *Third*, clinopyroxene-rich cumulate xenoliths, which are also present in the Nógrád-Gömör Volcanic Field, have been interpreted as having crystallized from basaltic melts propagating through the upper mantle and being trapped near the MOHO (Kovács et al., 2004; Zajacz et al., 2007), supporting the presence of basaltic melts in the upper mantle before eruption of the host basalt.

The key to the formation of this group may be a group of wehrlitic xenoliths, found only in the central part of the Nógrád-Gömör Volcanic Field (Patkó et al., 2013). These xenoliths show similar geochemical characteristics to Group IIB: low #Mg, moderate enrichment in Fe, Mn and LREE in clinopyroxenes and slight Ti-enrichment in spinel. The wehrlitic group differs petrographically from the lherzolites since they contain aggregates of secondary olivine, clinopyroxene and spinel, and no modal orthopyroxene. Patkó et al. (2013) suggest that these xenoliths are the products of reaction between basaltic melt and wall-rock, to form clinopyroxene at the expense of orthopyroxene. Such a process, resulting in modal enrichment in a metasomatic phase that was already present in the assemblage, is known as stealth metasomatism (O'Reilly and Griffin, 2013). It is therefore proposed that Group IIB xenoliths are also related to this process, although the modal change in pyroxenes was incomplete. The modal ratio of ortho- to clinopyroxene ranges from 0 to 3.4 with only three xenoliths at or above 1.5 (Table 1), which suggests that some clinopyroxenes are the product of stealth metasomatism, even though this is not obvious from their petrography (the very nature of stealth metasomatism). Furthermore, Group IIB xenoliths only appear in the central part (Table 1) together with the wehrlite xenoliths. No wehrlitic signature was found in samples of the northern and southern parts of the

Nógrád-Gömör Volcanic Field, suggesting that this process was localized in the central part and was independent of the metasomatism that affected Group IB xenoliths.

6.2.2.4. Characterisation of the metasomatic agent based on silicate melt-inclusions

The geochemical (especially trace-element) compositions of the xenoliths can provide insights on the properties of metasomatizing melts that reacted with them in the mantle, but primary silicate melt inclusions (SMIs; Fig. 5.16) offer the most precise constraints on the compositions of such melts, because they are considered to represent the melt at the instant of entrapment at mantle conditions (e.g., Schiano et al., 1992; 2000; Frezzotti, 2001). A major condition of this approach is that the trapped melt droplet remains isolated, i.e., behaves as a closed system and evolves independently from the host (e.g., Roedder, 1984). This condition can occur because of the large elastic modulus of the host minerals, which may prevent chemical re-equilibration of the inclusion at low pressure during and after ascent to the surface (Schiano and Bourdon, 1999). However, diffusion may still occur to different extents for different elements, depending on the concentrations and diffusion coefficients of the given element in the host mineral. Therefore, the elements most likely to retain their original concentrations in the melt inclusion are those that are least compatible with the host (Qin et al., 1992).

The primary SMIs found in clinopyroxenes in xenolith NFL1327 preserve key information regarding the metasomatizing melt that affected the represented mantle domain. This xenolith is part of Group IIB, which is associated with the reaction responsible for the formation of the wehrlite suite as well (Patkó et al., 2013). Since that process involved the increase of modal clinopyroxene, which also is the host mineral of the SMIs in xenolith NFL1327, the most plausible interpretation is that they represent the melt linked to the wehrlite formation, i.e., the last metasomatic event before entrainment by the host basalt.

The most striking compositional feature of the daughter minerals (i.e., clinopyroxene, amphibole, mica and spinel) in the SMIs (Table 7), is their enrichment in FeO. FeO content appears to be the best geochemical tool to distinguish daughter clinopyroxene from the host clinopyroxene; the former contains significantly higher amounts than the latter (Fig. 6.9a; Table 7). The high FeO concentrations in mica result in annite-like compositions.

This is strikingly different from the phlogopites described from SMIs found in the southern part of the Nógrád-Gömör Volcanic Field by Szabó et al. (1996); however, those inclusions have been interpreted to have a different genesis (see Chapter 2.3). Furthermore, minor FeO is detectable in the glass of SMI_R and SMI_U (Table 7) as well. Overall, these compositions agree well with the Fe-rich nature of the metasomatizing melt forming Group IIB xenoliths. However, it needs to be noted that the accompanying Mn- and Ti-enrichment observed in the rock-forming silicates and spinel (Fig. 5.7a, b, e), respectively, is not reflected in the composition of the SMIs. This may be because Mn is only present in very low amounts and was below detection limit with SEM-EDX, and enrichment of Ti may not be that dominant, as it only occurred in spinel, but not in clinopyroxene of the Group IIB xenoliths (Fig. 5.7e).

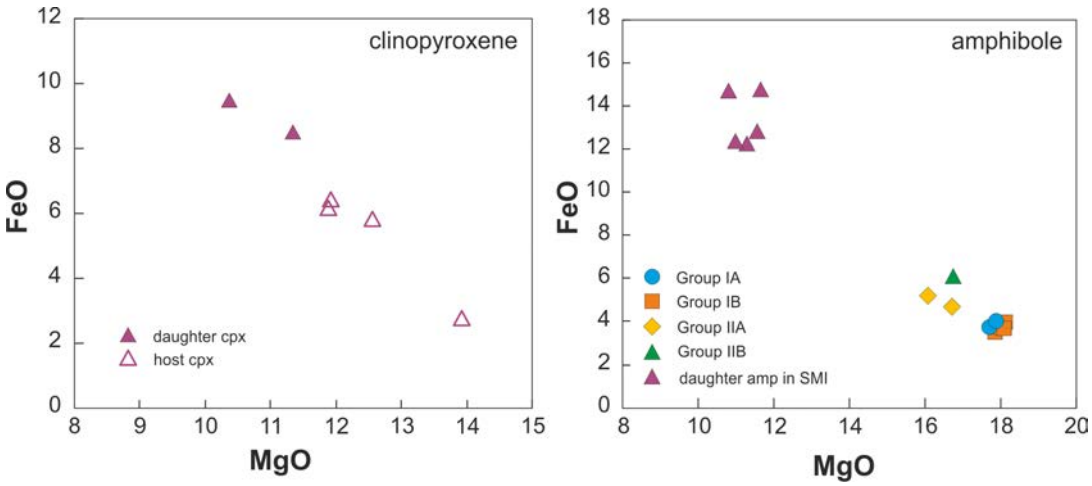

Fig. 6.9. MgO *vs* FeO contents of daughter clinopyroxene (a) and amphibole (b) in SMIs. Daughter clinopyroxene is compared to the composition of the host grain (Table 7) and daughter amphibole to the amphiboles in xenoliths of different groups (Table 2).

Bulk compositions, both for the four SMIs analysed with FIB-SEM and the eight additional ones analysed with LA-ICP-MS, show generally low alkali contents along with a variability in SiO_2, which puts them in compositional fields ranging across basaltic andesite and trachyandesite through basalt to picrobasalt and basanite on the TAS-diagram (Le Bas et al., 1986) (Fig. 6.10a). Interestingly, the SMIs with compositions acquired by mass balance calculation have much less variability than those obtained by LA-ICP-MS, which show lower SiO_2 and total alkali contents. The higher compositional variability compared to FIB-SEM analyses, and the general consideration that LA-ICP-MS has lower accuracy for major elements, would suggest that a basaltic andesite/trachyandesite – basalt composition is the best estimate for the trapped melt. This differs slightly from the

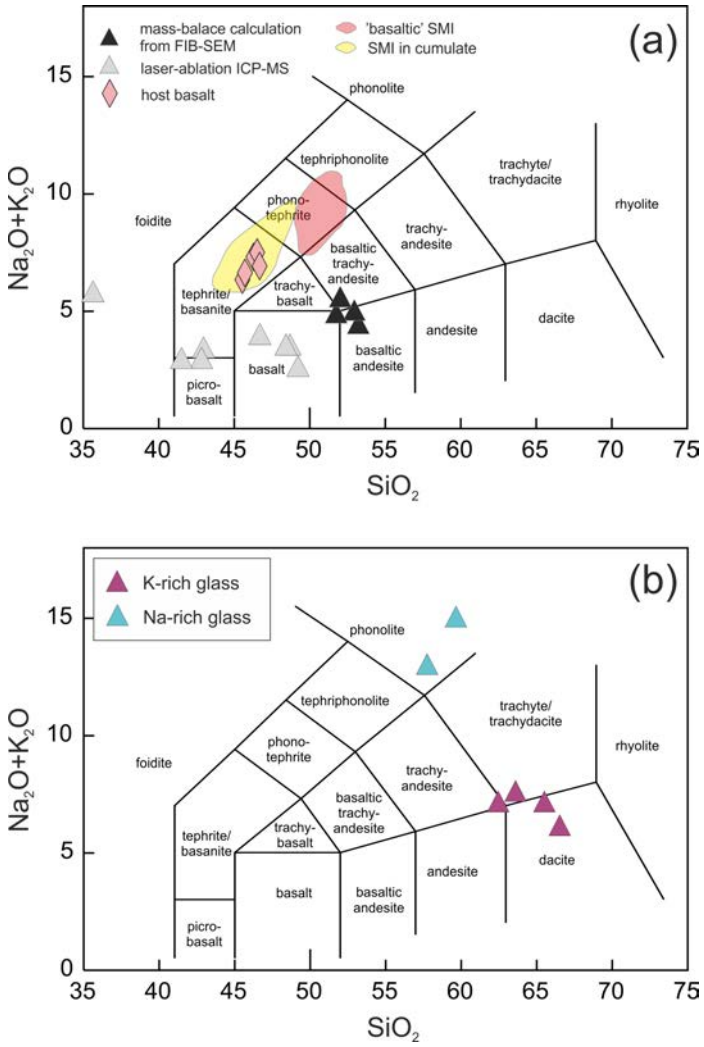

Fig. 6.10. a - Composition of bulk SMIs acquired with both LA-ICP-MS and mass balance calculations from major-element analyses with FIB-SEM, on the total alkali *vs* SiO_2 (TAS) diagram (Le Bas et al., 1986). Compositions of Nógrád-Gömör basalts (Embey-Isztin et al., 1993; Dobosi et al., 1995) are plotted, with fields for compositions of SMIs found in cumulates (Zajacz et al., 2007) and 'basaltic' SMI in olivine from the southern part (Szabó et al., 1996). b – Compositions of K-rich and Na-rich glasses in the analysed SMIs on the total alkali *vs* SiO2 (TAS) diagram.

composition of the host basalt (Fig. 6.10a), which is a basanite with higher total alkali and lower SiO_2 content, and an overall limited variability among the different localities of the Nógrád-Gömör Volcanic Field (Embey-Isztin et al., 1993; Dobosi et al., 1995; Dobosi and Jenner, 1999). This observed compositional difference supports the earlier conclusion that the melt responsible for the metasomatism of Group IIB xenoliths is generally similar to the host basalt, but with slight geochemical differences. The production of basaltic melts with small changes in composition depending on their age throughout the Nógrád-Gömör Volcanic Field has been previously observed by Dobosi et al. (1995). The changes they found were present dominantly in trace elements (Zr, Nb), and, to a lesser extent, SiO_2

and total alkali content. Furthermore, the melt represented by the SMIs probably had a different evolution, as it has been resident in the upper mantle and reacting with the wall rock instead of undergoing a quick ascent like the host magma. However, constraining this evolution is challenging. From a study of SMIs in olivines in cumulate xenoliths from the Nógrád-Gömör Volcanic Field, Zajacz et al. (2007) found that they were absent from the cores of olivine grains; consequently, their composition represents a melt evolution stage where a certain proportion of olivine had already crystallised. To obtain a more precise estimate of the parental melt composition, they proposed that analysed bulk SMI data need to be corrected, by adding ~ 15 % olivine. In case of the SMIs of this study, they appear to be distributed throughout the whole grains in which they occur (Fig. 5.16b), thus allowing the assumption that their composition accurately represents the melt which crystallised the host clinopyroxene.

To better characterise the parental melt, the trace-element compositions of the SMIs need to be more closely examined. Although the compositions of the individual inclusions are generally in good agreement with one another, there is an unusual fluctuation in some of the HREE concentrations (e.g., Tb, Er, Tm, Yb; Fig. 5.21). This can very likely be explained by analytical uncertainties due to low counts of these elements during ablation; similarly to LREE contents in orthopyroxene of the Nógrád-Gömör xenoliths, as mentioned earlier (see Chapter 5.2.2; Fig. 5.12). To identify SMIs with reliable REE patterns, Y contents were compared to Yb, using the general approach that the Y/Yb ratio is approximately 10 in mantle environment. SMIs with too low or too high Y/Yb (7.4 and 22.6 for SMI_8 and SMI_15; as well as SMI_14 without detectable Yb content) were omitted from further comparisons (Fig. 5.21, Table 8).

The trace-element patterns of the SMIs are compared with the compositions of possible melts in the upper mantle of the Nógrád-Gömör Volcanic Field and with those of amphiboles in Group IB and IIB xenoliths i.e., amphiboles with intraplate origin (see Chapter 6.2.2) in Figures 6.11a and b. For the incompatible elements, SMI compositions usually fall between the most enriched amphiboles in Group IB, and in the Group IIB xenoliths. Note that the Group IIB xenolith that contains amphibole is a different sample from the one containing the SMIs. Several elements (U, Th, Nb, Ta) are even more abundant in the amphibole of the most enriched Group IB xenoliths (NFL1315A, NFL1324) than in the SMI, whereas REE+Y patterns show a good agreement. However, in equilibrium, amphibole/melt partitioning of these trace elements would not allow

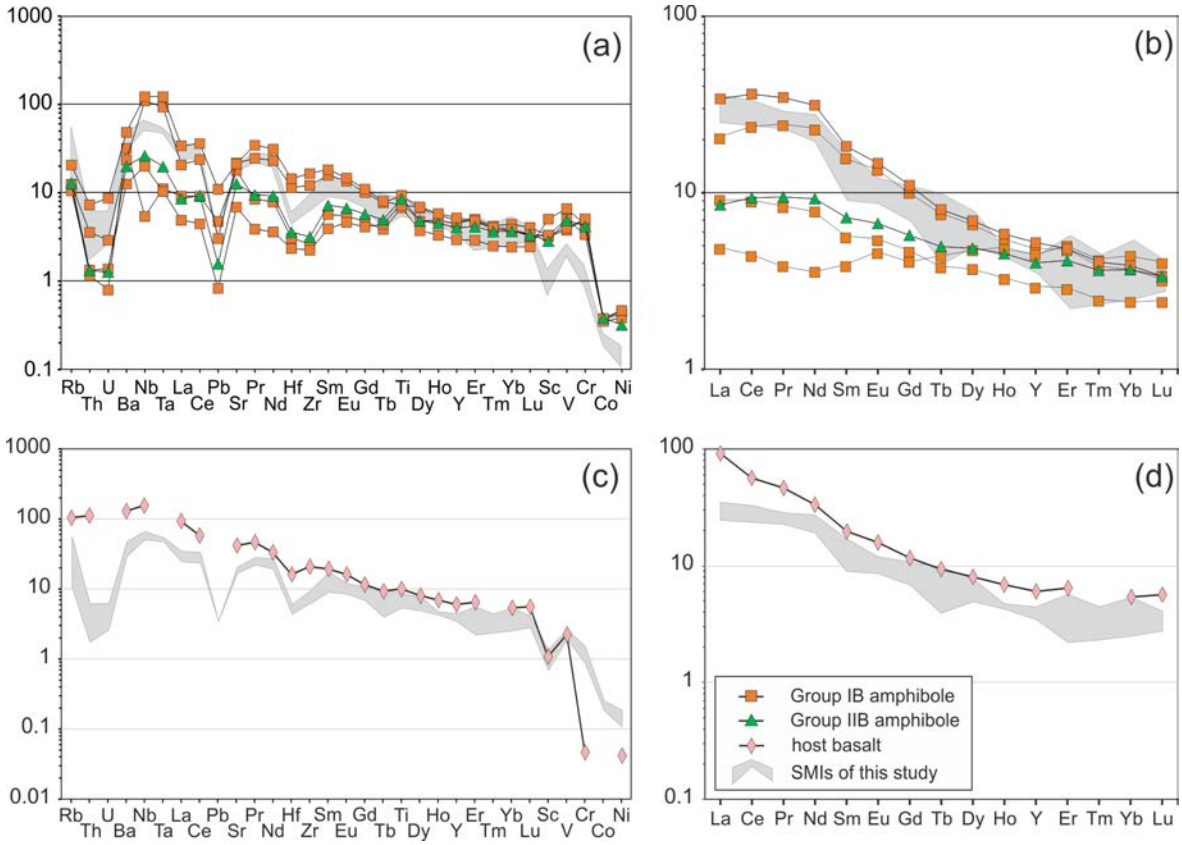

Fig. 6.11. a, b – Multi-element and REE+Y diagrams of the bulk SMI compositions compared to the metasomatic amphiboles of Group IB and IIB xenoliths; c, d – compared to the average host basalt (Dobosi and Jenner, 1999). Concentrations are normalised to primitive mantle (McDonough and Sun, 1995).

them to be more enriched in amphibole compared to the melt as the relevant distribution coefficients are less than 1 (Adam and Green, 1994; LaTourrette et al., 1995; Dalpé and Baker, 2000). Based on concentrations and the element distribution pattern (Fig. 6.11a-b), amphibole in the Group IIB xenolith is probably more likely to have crystallized from the same melt, i.e., the agent associated with wehrlite formation. This melt appears to be of OIB character, like the host basalt (Dobosi et al., 1995), but slightly less fertile (Fig. 6.11c and d) as shown by lower concentrations of Th (U), Nb (Ta), La, Ce, Hf and Zr in the SMIs. The high contents of incompatible trace elements in the host basalt may be explained by fractionation of olivine and clinopyroxene, which affected this melt (Embey-Isztin et al., 1993; Dobosi et al., 1995; Zajacz et al., 2007), whereas the SMIs seem to have trapped a more primitive melt.

To constrain the origin of this melt, the equilibrium melting model of Zajacz et al. (2007) was applied to the studied SMI compositions (Fig. 6.12). This model is based on calculations of Nb and Y in the partial melts for spinel lherzolite and garnet lherzolite

sources with different modal clinopyroxene/garnet ratios. Bulk source compositions were determined using the primitive mantle composition of McDonough and Sun (1995) and mineral-melt partition coefficients from garnet lherzolite melting experiments at pressures between 2.8 – 3.2 GPa by Salters et al. (2002). Based on the model, Nb is a good indicator for the degree of partial melting, and Y can generally be used to indicate the presence of garnet in the source. Furthermore, these elements are in high enough abundance in the SMIs to be analysed with satisfactory reliability, and they are considered insensitive to potential fluid metasomatism in the source. Based on this model (Fig. 6.12), the melt trapped in the SMIs was produced by ~ 2 % melting of a garnet lherzolite source, with a clinopyroxene/garnet ratio of ~ 1. This source appears to be slightly more garnet-rich than the calculated parental melt composition of the cumulate xenoliths of the Nógrád-Gömör Volcanic Field (Zajacz et al., 2007) and the average composition of the host basalt (Fig. 6.12). However, the latter is already modified due to olivine and clinopyroxene fractionation (Dobosi et al., 1995), as described above. In summary, the geochemical characteristics of the melt represented by the SMIs point to an OIB-type intraplate magma, of similar origin to other basaltic melts present in the region, but with small differences in the source composition, and possibly in the degree of partial melting.

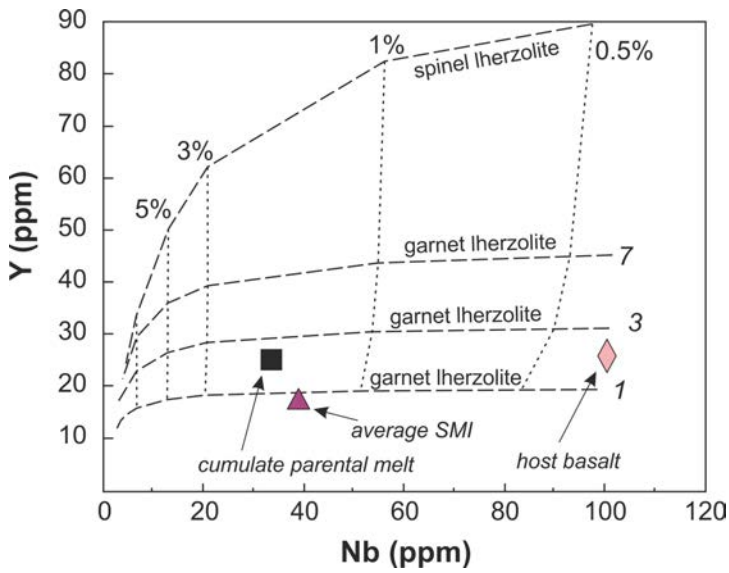

Fig. 6.12. Petrogenetic modelling of the origin of the melt trapped in the SMIs (Zajacz et al., 2007). Dashed lines represent modelled compositions of partial melts from spinel- and garnet lherzolite, respectively, with primitive-mantle composition. Numbers in italic refer to the clinopyroxene/garnet ratio in the source region. Dotted lines represent the degree of partial melting expressed in percentage. Average composition of the host basalt (pink diamond) (Dobosi and Jenner, 1999) and the calculated parental melt composition for the cumulates (black square) (Zajacz et al., 2007) are plotted for comparison.

6.2.3. Geochemical evolution and tectonic context

Based on the geochemical results discussed above, a relative order of geochemical events and a scenario for mantle evolution can be proposed in relation to the tectonic situation and history of the Nógrád-Gömör Volcanic Field (Fig. 6.13). Metasomatic events overprint the effects of partial melting, interpreted as the earliest traceable event in the history of the upper mantle of the studied area. The oldest metasomatic products in the Nógrád-Gömör xenoliths are inferred to be the Nb-poor amphiboles of Group IA (present in all three sub-areas) and IIA xenoliths (northern part), which show characteristics suggesting a suprasubduction origin (depleted HFSE, especially Nb). However, the origin of the metasomatizing fluid is difficult to determine in the current tectonic environment of the Carpathian-Pannonian region. Geophysical studies (Szafián and Horváth, 2006; Tašárová et al., 2009) have found that subduction of the European plate under the ALCAPA microplate either was not developed beneath the entire Western Carpathians or was later overprinted by collision tectonics between the two blocks. As Kovács and Szabó (2008) proposed, the most fitting explanation for a subduction environment near the mantle domain of the Nógrád-Gömör Volcanic Field is outside the Carpathian-Pannonian region, in the Alpine collision zone, before the extrusion of the ALCAPA microplate and the formation of the Pannonian Basin. This explanation implies that the lithospheric mantle was involved in the extrusion and subsequent movement of the microplate, as suggested by studies of deformed mantle xenoliths from the Carpathian-Pannonian region (Falus, 2004; Hidas et al., 2007). It is therefore suggested that the upper mantle of the ALCAPA microplate inherited its geochemical characteristics from a former subduction environment. Subduction-related geochemical imprints (positive anomalies of Ba and Sr, and U-shaped REE patterns) have been reported in xenoliths from other locations of the ALCAPA microplate, such as the Styrian Basin (Coltorti et al., 2007b) and the Bakony-Balaton Highland (e.g., Downes et al., 1992; Bali et al., 2007). Although these characteristics have not been found in the xenoliths of this study, volatile-rich melt inclusions reported previously from the Nógrád-Gömör Volcanic Field have been interpreted as remnants of a subduction-related silicate melt (Szabó et al., 1996). This, along with the presence of Nb-poor amphibole, suggests than event where a fluid or a volatile-bearing melt affected the upper mantle beneath the whole Nógrád-Gömör region (Stage 1 in Fig. 6.13).

The formation of Nb-poor amphiboles in Group IA and IIA xenoliths was followed

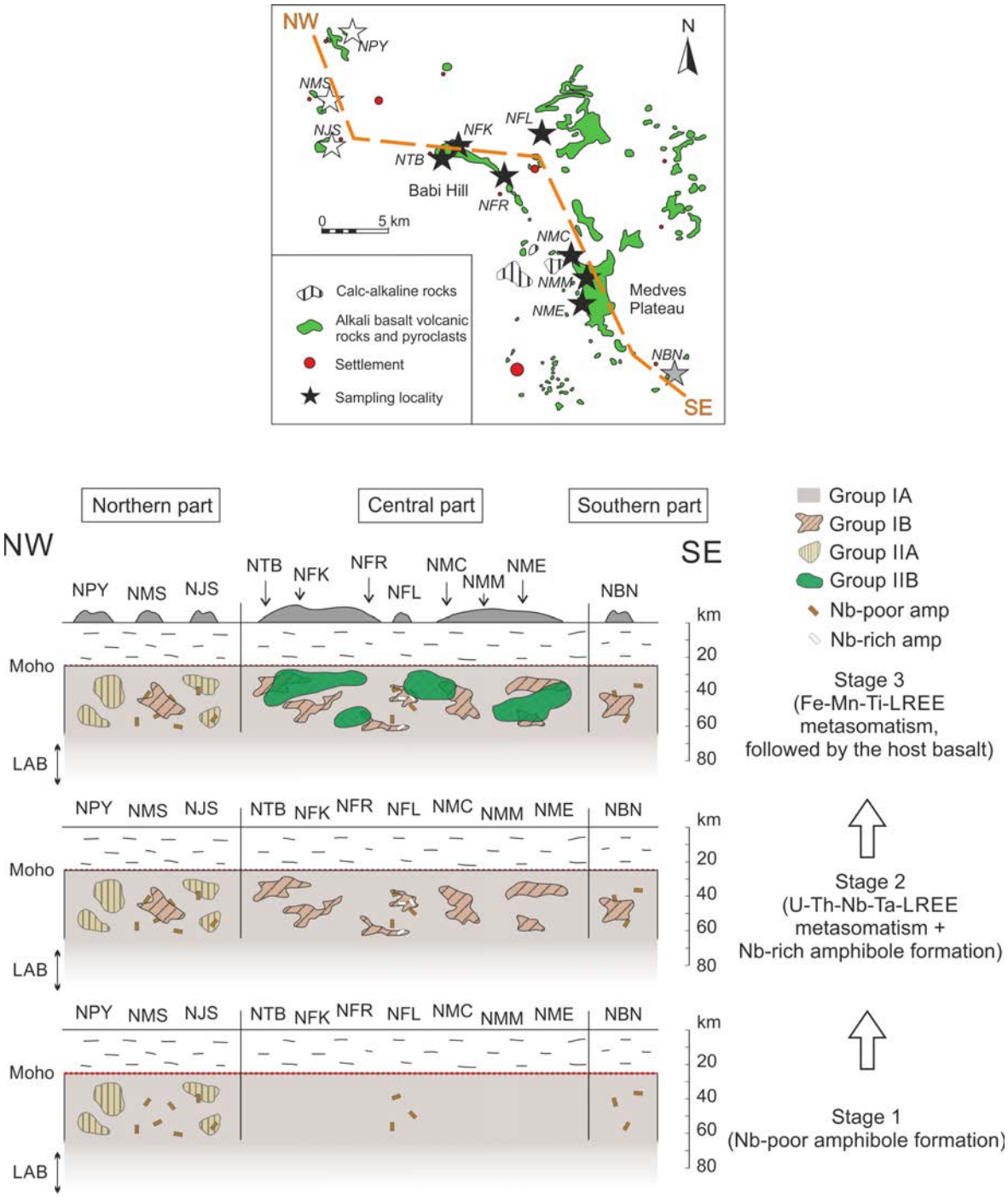

Fig. 6.13. Schematic illustration depicting the reconstruction of metasomatic events in the upper mantle of the Nógrád-Gömör Volcanic Field, on a section from NW to SE and involving all xenolith sampling localities (see map above). Stage 1 - formation of Nb-poor amphibole via reaction with a subduction-related fluid (or volatile-rich melt); Stage 2 - U–Th–LREE enrichment in clinopyroxenes and formation of Nb-rich amphiboles only in the Fil'akovo-Kerčik locality; Stage 3 - Fe–Mn–enrichment in olivine and pyroxenes, Ti–enrichment in spinel and LREE–enrichment in clinopyroxene in selected domains beneath the central part. Depth of Moho and minimum lithosphere–asthenosphere boundary (LAB) in the Nógrád-Gömör Volcanic Field are taken from Klébesz et al. (2015). For abbreviations of the sampling sites see Fig. 3.1.

by extensive metasomatism causing varying enrichment in U–Th–LREE and local amphibole formation in the mantle beneath the whole area, represented by Group IB xenoliths. Nb–Ta enrichment in these amphiboles and clinopyroxenes suggests that this metasomatic agent was an intraplate basaltic melt (Coltorti et al., 2007a). Such basaltic magmas could have been generated by decompression melting during the Miocene extension and asthenosphere upwelling throughout the Carpathian-Pannonian region (Embey-Isztin et al., 1993), following the juxtaposition of the ALCAPA and Tisza-Dacia blocks (Csontos, 1995) (Fig. 2.1.). Although the alkali basaltic volcanism followed the period of extension, generation of these melts probably occurred during the extension; part of them did not reach the surface, but interacted with mantle peridotites. As Group IB xenoliths are found in all sub-areas of the Nógrád-Gömör Volcanic Field, this metasomatic event had to occur before the oldest eruptions of xenolith-bearing basalts in the northern part (7 - 6.5 Ma; Balogh et al., 1981; Hurai et al., 2013), but presumably after the onset of the extension (~20 - 17 Ma; Konecný et al., 2002; Horváth et al., 2006). As discussed above, REE-based equilibration temperatures of the studied xenoliths are considerably higher than those obtained by major element based methods (Table 1); this discrepancy was interpreted as a record of heating by the asthenospheric upwelling. As this temperature difference is recognized in Group IB xenoliths, which were influenced by U–Th–(Nb–Ta)–LREE metasomatism, this second metasomatism is likely to have occurred before cooling to the closure temperature for diffusion of the major cations used in the two-pyroxene and Ca-in-opx thermometers. These xenoliths are found in all three sub-areas of the Nógrád-Gömör Volcanic Field (Stage 2 in Fig. 6.13), but Nb-rich amphiboles formed during this phase are present in only one locality (Fil'akovo-Kerčik; see Fig. 3.1).

The youngest geochemical process is the third metasomatism, caused by another basaltic melt, also with a composition close to that of the host basalts, causing the enrichment in Fe–Mn–Ti and LREE observed in Group IIB xenoliths. This event affected the mantle domain of only the central part of the Nógrád-Gömör Volcanic Field, and overprinted any previous geochemical characteristics (Stage 3 in Fig. 6.13). This melt was trapped and preserved in SMIs in clinopyroxenes of Group IIB xenoliths, and its composition reflects low-degree (~ 2 %) partial melting of a garnet-lherzolite source. Based on the major- and trace-element characteristics of rock-forming minerals of Group IIB xenoliths and the SMIs, this youngest metasomatic process is most likely linked to the formation of the wehrlite suite.

6.3. Deformation History and Seismic Anisotropy in the Upper Mantle of the Nógrád-Gömör Volcanic Field

6.3.1. Deformation mechanisms

Under upper mantle conditions (high-moderate pressure and temperature and relatively coarse grain-size), the most common deformation mechanism is dislocation creep (e.g., Green and Radcliffe, 1972). Dislocation creep is a form of intracrystalline deformation in which lattice defects move within the crystal in order to minimise stress, eventually forming subgrain boundaries (Passchier and Trouw, 1996 and references therein). The presence of a large number of similar dislocations in one crystal causes the lattice to be slightly misoriented, which appears in the polarised microscope as undulose extinction under crossed polars. The dislocation creep can be characterised by the crystal plane on which it is moving and the direction of the movement, which together define the active slip system (Fig. 6.14). Strongly developed CPO is generally considered as microstructural evidence for deformation via dislocation creep (Mercier and Nicolas, 1975). The dominant slip system during mantle deformation is heavily dependent on physical properties such as temperature, stress, strain, incorporated 'water', the presence of melts/fluids, etc., as discussed further below.

The mantle xenolith suite of the Nógrád-Gömör Volcanic Field displays generally clearly defined CPOs (Fig. 5.28) and intermediate fabric strength (J_{OL} = 1.6-4.9; Table 9), with abundant signs of intracrystalline deformation mainly in olivine, such as undulatory extinction (Fig. 5.4c), grain elongation (Fig. 5.4b) and subgrain boundaries (Fig. 6.15a) which are often perpendicular to the elongation direction, and parallel to the lineation. These features are consistent with deformation via dislocation creep. The strong orientation of olivine [100] axes in most xenoliths indicates that [100]-direction slip was dominant during the deformation. Orthopyroxene [001] axes cluster around the direction parallel to, or at a small angle to, olivine [100] axes, which suggests coeval deformation of olivine and orthopyroxene with a dominant [001]-direction slip (e.g., Soustelle et al., 2010; Soustelle and Manthilake, 2017).

Most Nógrád-Gömör xenoliths display [010]-fibre and orthorhombic CPO patterns, and only a few samples have [100]-fibre symmetries (Appendix C). There is no correlation between equilibration temperatures and CPO patterns, and based on olivine BA-indices,

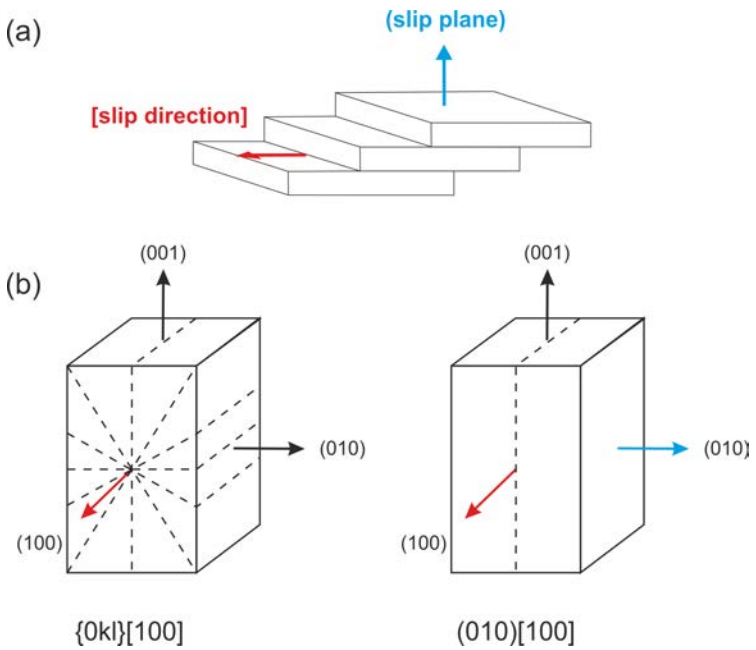

Fig. 6.14. a – Schematic illustration of the mechanism of slip systems. b – Examples of the two most common slip systems in olivine: (010)[100] and (0kl)[100] (see text for further explanation). Figure modified after Falus (2004).

the xenoliths show a continuous distribution between the different symmetries. This suggests that no distinct deformation event can be linked to the distinct CPO types. Orthorhombic and [100]-fibre symmetries, characterised by the [100] axes being more strongly oriented than [010] or [001], are linked to the activation of (0kl)[100] slip systems. The [100]-fibre pattern develops via activation of the [100] glide on multiple planes (Fig. 6.14) at high temperatures (Zhang and Karato, 1995; Bystricky et al., 2000; Hansen et al., 2014), under a simple shear or transtensional deformation regime (Tommasi et al., 1999). However, there is no evidence for high temperatures or textural differences in xenoliths with the [100]-fibre pattern, and their BA-indices do not significantly exceed orthorhombic ones (Fig. 6.16). Therefore, it is suggested that the major effect forming these symmetries can be attributed to a transtensional component in the complex deformation regime of the mantle region. Orthorhombic CPO is associated with the dominance of (010)[100] slip system (Fig. 6.14) via simple shear, pure shear, or the combination of these (Tommasi et al., 1999; 2000). Furthermore, it has been interpreted as forming during asthenospheric flow (Blackman et al., 2002; Kovács et al., 2012a). Although it was shown in the central part of the Pannonian Basin that coarse-grained, high-temperature xenoliths represent a newly accreted lithospheric, deeper mantle portion (Kovács et al., 2012a), in the Nógrád-Gömör Volcanic Field there is no evidence for a distinct layer with such an origin.

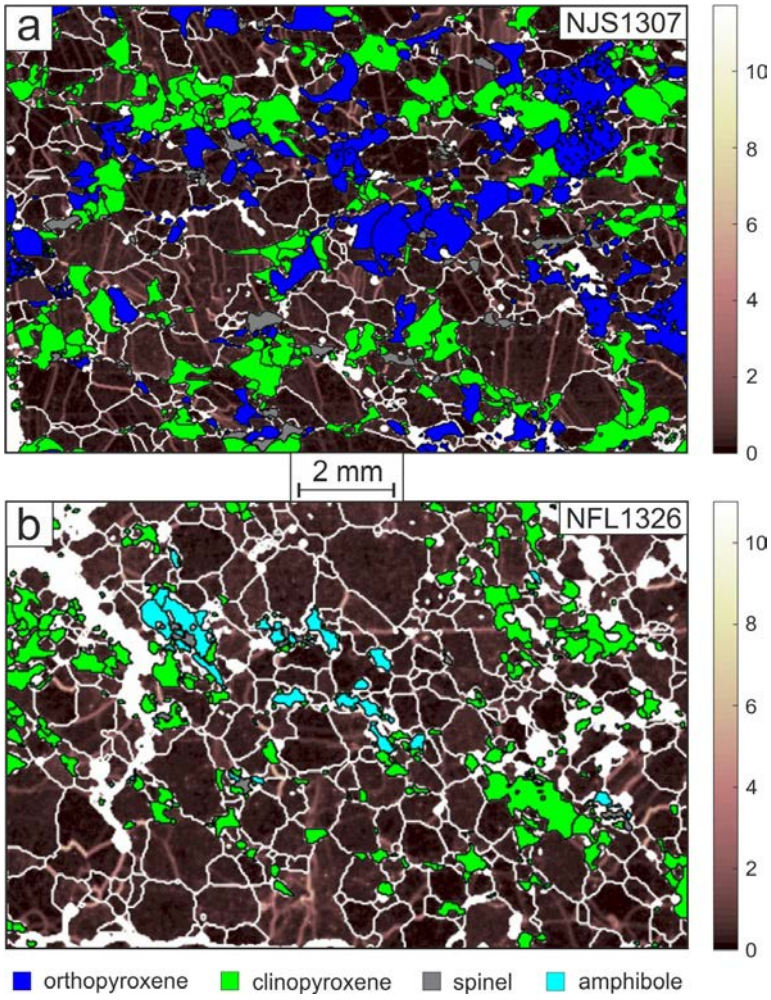

Fig. 6.15. a - Deformed texture with high degree of intragranular deformation (abundant subgrain boundaries) in xenolith NJS1307. b – Annealed texture with straight grain boundaries, triple junctions and low number of subgrain boundaries in xenolith NFL1326. EBSD maps are kernel average misorientation (KAM) '2' (Wright et al., 2011) maps for olivine, depicting the average misorientation between a measurement point and the nearest and 2nd nearest neighbours. The average misorientation is expressed in degrees and displayed on a colour scale next to the maps. Since this mapping method reveals local misorientations within grains, it can effectively be applied to show intragranular orientation heterogeneities, i.e., subgrain boundaries.

Among the studied xenoliths, [010]-fibre symmetries (Fig. 5.28) have a high abundance (~ 50 %; Table 9) compared with the proportion of this type worldwide, which is less than 15 % in the database of Ben Ismail and Mainprice (1998). This CPO-type can develop under a range of conditions. Axial compression under experimental conditions on dunitic aggregates led to the formation of [010]-fibre CPO, via the activation of the low temperature (110)[001] slip system (Carter and Avé Lallemant, 1970; Nicolas et al., 1973). However, the experimentally-achieved CPOs are characterised by the [001] axes showing stronger concentrations compared to [100]. In naturally deformed peridotites with [010]-fibre symmetries, [001] axes are usually more dispersed than [100]. Numerical

modelling by Tommasi et al. (1999) suggested that at high temperatures but low strain rates, [100] is the dominant slip direction, which could account for the [010]-fibre pattern either via axial shortening or transpression.

Even though [010]-fibre symmetries have been described from a range of different tectonic environments, such as peridotite massifs (e.g., Vauchez and Garrido, 2001; Le Roux et al., 2007; Soustelle et al., 2009), cratonic (e.g., Vauchez et al., 2005; Baptiste et al., 2012) and off-cratonic xenoliths (e.g., Vonlanthen et al., 2006; Zaffarana et al., 2014; Kourim et al., 2015), the rarity of these pattern suggests that axial shortening and transpression are not common mechanisms in the upper mantle (Tommasi et al., 1999). However, it the most likely explanation for the dominance of [010]-fibre symmetries in the Nógrád-Gömör Volcanic Field, as similar conclusions were drawn for xenoliths in the Styrian Basin (Aradi et al., 2017), the Little Hungarian Plain and the Bakony-Balaton Highland (Kovács et al., 2012a) (Fig. 2.3), suggesting it is a general feature in the upper mantle of the Carpathian-Pannonian region. The [010]-fibre pattern can also form via simultaneous activation of [100] and [001] glide at high pressure or stress (Vauchez et al., 2005), such as at greater mantle depths (below ~ 250 km), where [001] slip transitionally becomes dominant over the [100] direction (Mainprice et al., 2005). In the Nógrád-Gömör Volcanic Field, xenoliths with [010]-fibre symmetries do not show any textural evidence of having been exposed to higher stress than the rest of the sample suite; in fact, based on equilibration temperatures (Table 1), the xenoliths are inferred to come from a narrow depth range (Fig. 6.1). Alternatively, deformation in the presence of melt also can lead to [010]-fibre CPO (Holtzman et al., 2003; Soustelle et al., 2009; Higgie and Tommasi, 2012). This possibility cannot be excluded straightforwardly as there is evidence for multiple metasomatic events in the mantle of the Nógrád-Gömör Volcanic Field through subduction-related volatile-rich melts and mafic melts of intraplate origin (see Chapter 6.2; Liptai et al., 2017). However, constraining the effect of these melts is difficult as their exact spatial distribution is not known. On the other hand, [010]-fibre type xenoliths are not strongly represented in the 'metasomatized' groups (Group IB and IIB), i.e., a significant part of the xenoliths with this CPO type shows no evidence of having been in contact with a metasomatizing melt. This would suggest that the melts present in the Nógrád-Gömör mantle (Fig. 6.13) most likely had only minimal effects on the deformation, if any.

In conclusion, since the xenoliths display a rather transitional distribution between [010]-fibre and orthorhombic (and [100]-fibre) symmetries (Fig. 6.28; Appendix C)

instead of clustering into groups. It is likely that the variety of CPO types observable in the Nógrád-Gömör mantle is the result of a mixture of deformation regimes, with a dominant transpressional component; transtensional and/or shearing regimes also were active to some extent.

6.3.2. Interpretation of microstructures and textural evolution

Since the BA-index is a good indicator for a more precise determination of CPO-type (Mainprice et al., 2014), it is often correlated with other physical properties, such as the fabric strength (J-index) or equilibration temperature. In natural peridotites, the correlation with J-index is usually very poor (Mainprice et al., 2014; Kourim et al., 2015; Hidas et al., 2016), but there is a positive correlation with equilibration temperatures in xenoliths from the Styrian Basin (Aradi et al., 2017). In the Nógrád-Gömör Volcanic Field, BA-indices do not show clear correlation with either the fabric strength or the equilibration temperatures (Fig. 6.16a, b), although a slight difference is observable in the distribution of CPO patterns among the three domains of the Nógrád-Gömör Volcanic Field (as described in Chapter 5.5). Note that CPO symmetries are also independent of the observed textural types (Fig. 6.16c, d).

However, there is a strong positive correlation between fabric strength, grain size and equilibration temperatures, associated with different xenolith textures. Coarse-granular and porphyroclastic-textured xenoliths have (on average) higher fabric strength and higher equilibration temperatures than fine-granular, fine-porphyroclastic and equigranular-textured ones (Fig. 6.17a, b). It is not uncommon that fine-grained mantle rocks exhibit weaker fabrics, as during dynamic recrystallization, CPO usually disperses. Although fine-grained peridotites are sometimes associated with higher equilibration temperatures than coarse-grained ones (e.g., Kourim et al., 2015), in the Nógrád-Gömör Volcanic Field the positive correlation between J-index and temperature indicates the opposite (Fig. 6.17b). On the other hand, the correlation is only present for temperatures acquired with major-element based thermometers. For temperatures calculated with the thermometer of Liang et al. (2013) based on REE-distribution between ortho- and clinopyroxene, J-indices are much more scattered (Fig. 6.17c). Since REE-based equilibrium temperatures are interpreted to represent older, hotter mantle conditions, presumably linked to the Miocene extension and asthenospheric uplift (see Chapter 6.1; Liptai et al., 2017), this

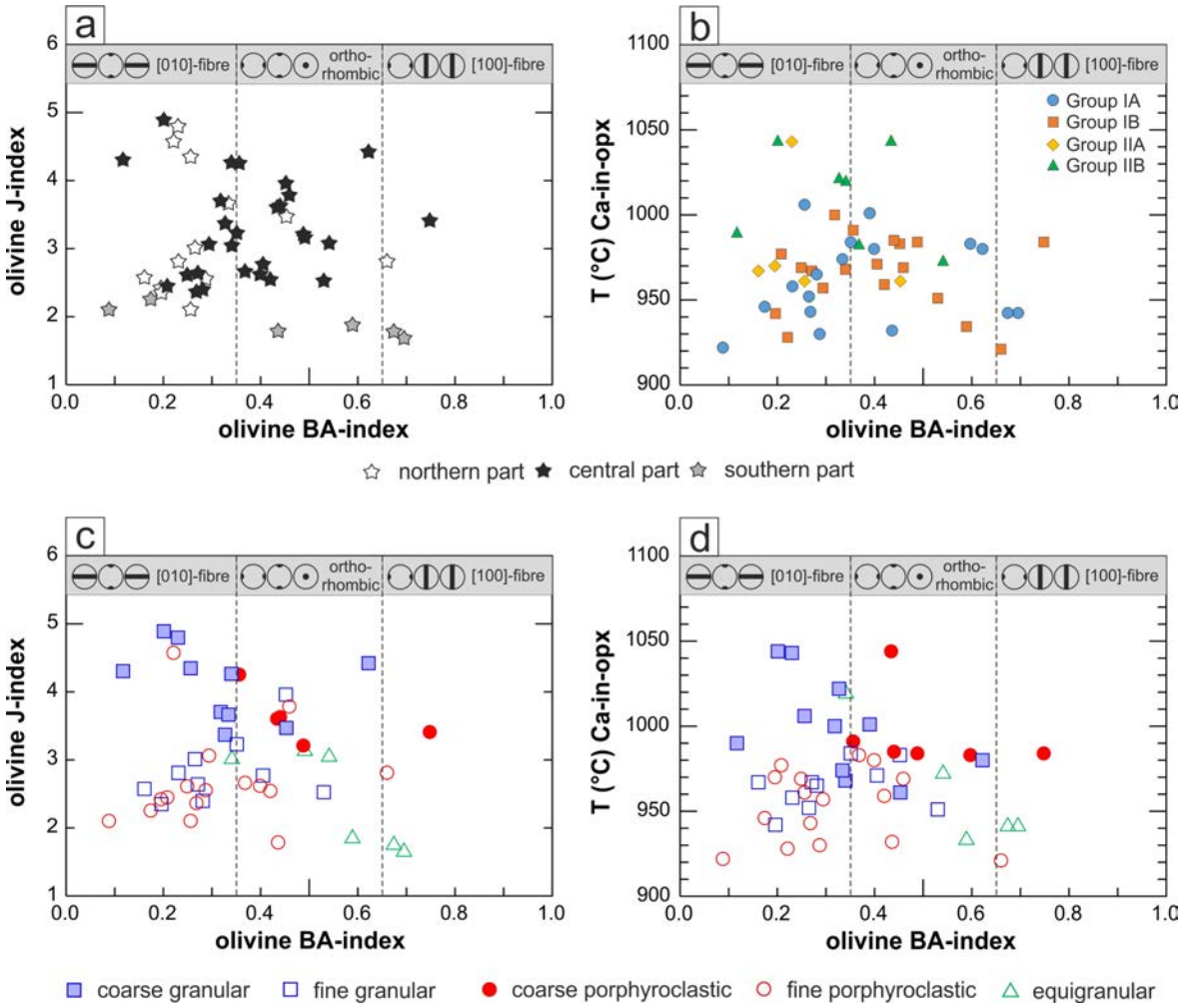

Fig. 6.16. Plots of olivine BA-indices vs olivine J-indices and equilibration temperatures calculated with the Ca-in-opx thermometer of Brey and Köhler (1990) modified by Nimis and Grütter (2010). Legends based on sampling locality (a), geochemical groups (b) and xenoliths textures (c, d).

would indicate that the last deformation process resulting in the observed fabric strengths postdates the extension.

Based on equilibration temperatures acquired with the major element-based thermometers, (Table 1) the xenoliths originate from ~40-55 km depth (Fig. 6.1), with fine-grained types representing a shallower mantle domain than coarse-grained xenoliths. Such correlations between grain size/texture type and depth of origin have previously been recognized in other xenolith suites in the Carpathian-Pannonian region (Falus et al., 2008; Kovács et al., 2012a; Aradi et al., 2017), although they were given different tectonic interpretations (see Chapter 6.3.4). In the Nógrád-Gömör Volcanic Field, it is suggested that these temperature values reflect post-extensional cooling, and therefore represent domains with different depths of origin. This vertical distinction is present in each sub-area, except for the southern part, where all xenoliths seem to represent the shallower,

fine-grained domain. The northern, and especially the central part, has a much wider range in both temperature and grain size (Tables 1; 9).

Alongside the clear indication of deformation effects mentioned earlier, the lesser occurrence of subgrains and intragranular deformation (Fig. 6.15b), and the overall near-equilibrium texture (i.e., straight grain boundaries and triple junctions) in the majority of the xenoliths indicate post-kinematic annealing. This process partially restored crystal structures (i.e., decreased intragranular deformation) while preserving the CPO and weakening fabric strength (e.g., Vauchez and Garrido, 2001; Tommasi et al., 2008). Further evidence for annealing is the grain growth of olivine, observable in several xenoliths by well-distinguished olivine-rich and pyroxene-rich parts (Fig. 6.18). In the olivine-rich

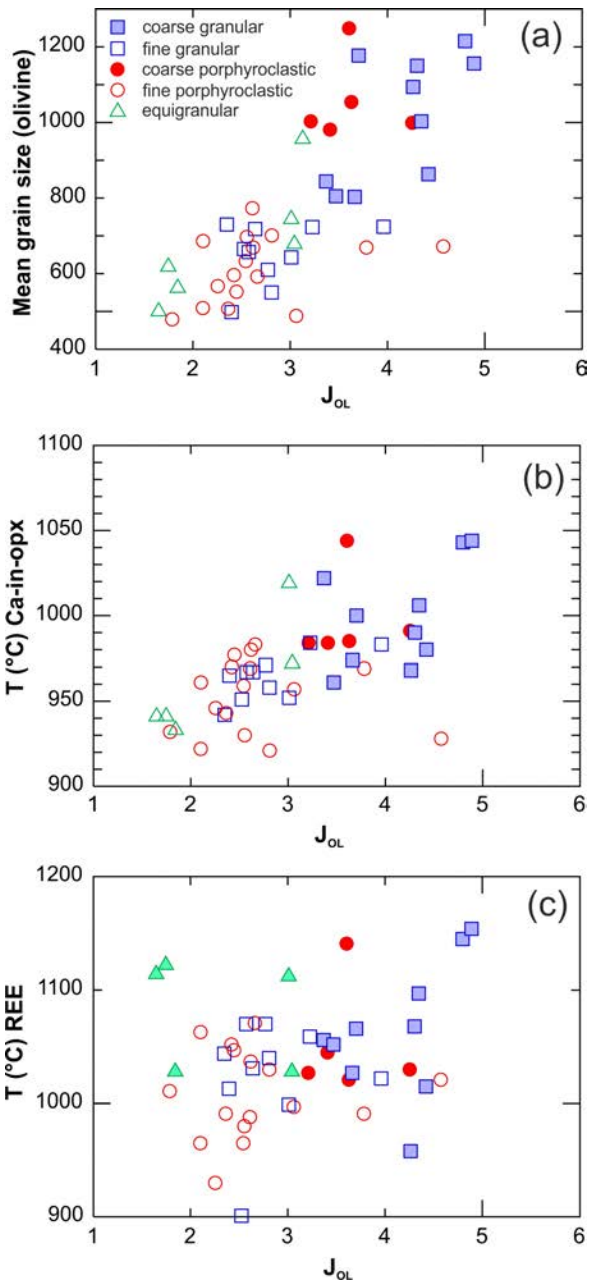

Fig. 6.17. Plots of olivine J-indices vs mean grain size (a), and equilibration temperatures calculated with the Ca-in-opx thermometer of Brey and Köhler (1990) modified by Nimis and Grütter (2010) (b), and with the REE-thermometer of Liang et al. (2013) (c).

parts, olivine grains show larger size with significantly less intragranular deformation compared to those xenoliths where signs of annealing are less obvious. On the other hand, olivines in pyroxene-rich domains are smaller due to the effect of pinning, which is the effect of second phases, in this case pyroxenes, preventing grain growth (Herwegh et al., 2011). Heterogeneous olivine grain size due to pinning can result in strain localisation upon deformation: as the grain size decreases, the deformation mechanism may switch from dislocation to diffusion creep, creating a weakened zone that promotes the formation of mylonites (e.g., Drury et al., 1991; Karato and Wu, 1993; Jaroslow et al., 1996; Vissers et al., 1997; Linckens et al., 2011). In the smaller olivine grains of the studied samples, there is almost no sign of intragranular deformation, whereas the larger ones tend to retain some. This is because the larger the grain is, the less chance there is for all intragranular deformation to be erased during annealing. It is suggested that the present grain-size heterogeneity is a consequence of static recrystallisation. This supports that the annealing process was subsequent to the deformation. Common melt pockets in xenoliths of the southern part of the Nógrád-Gömör Volcanic Field (Fig. 5.6g, h; Table 1), and in lower

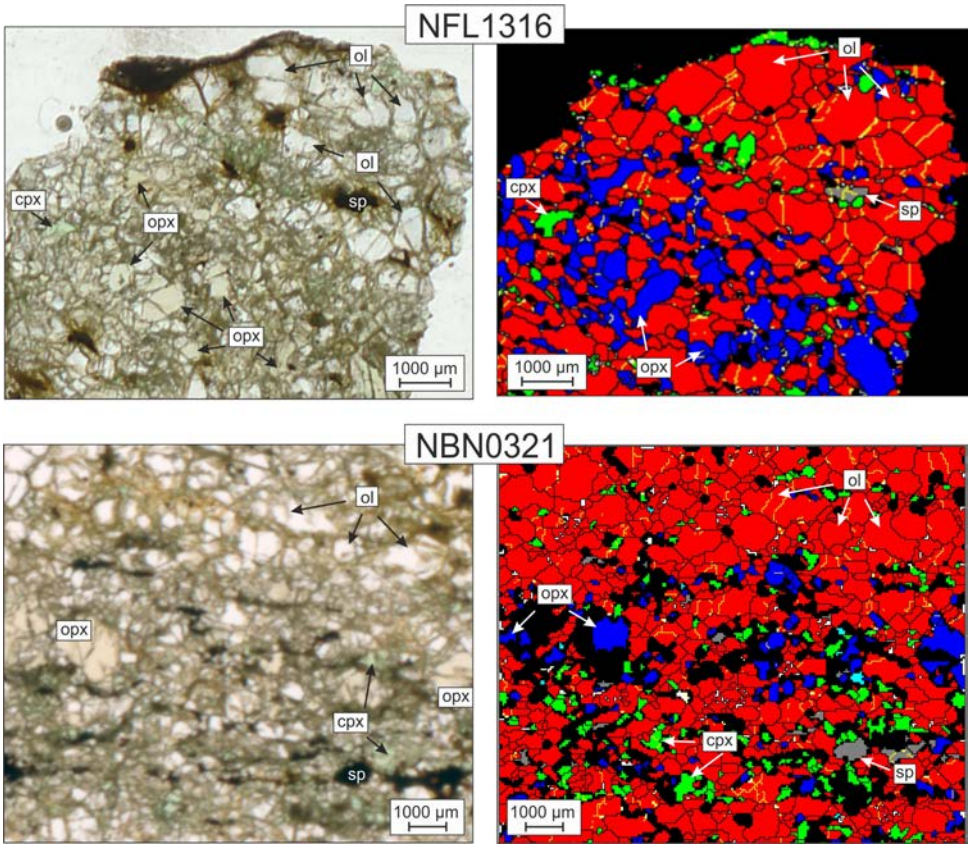

Fig. 6.18. Examples of heterogeneous olivine grain growth in pyroxene-rich and pyroxene-poor parts of annealed xenoliths (NFL1316, NBN0321), with scanned thin section images on the left and EBSD phase maps on the right.

abundance, the northern and central part, which were interpreted as reflecting *in situ* melting of amphiboles (see Chapter 6.2.2; Liptai et al., 2017) further support intensive heating.

The combined effect of deformation and annealing is responsible for the average grain orientation spread (GOS; see Chapter 4.6) observed in the xenoliths, since the amount of intragranular deformation increases during exposure to stress, while annealing usually counteracts these processes by eliminating dislocations. Although GOS values do not seem to correlate with different texture types in the Nógrád-Gömör Volcanic Field, they show a clear distinction among the different sub-areas (Fig. 6.19), decreasing from the northern part towards the southern. The lack of correlation with textural type can be explained by the difficulty of textural classification, since annealing-induced grain growth can lead to apparent bimodal distributions of grain sizes. It is very likely that part of the porphyroclastic-textured xenoliths has been affected by that, and therefore texture types should not be regarded as straightforward indicators of deformation in the Nógrád-Gömör Volcanic Field. The areal distribution of the GOS values reflects different deformation-annealing histories for the three parts, and may record different degrees of original deformation that affected the distinct mantle domains, prior to annealing.

There are a few possibilities for the cause of annealing effects in the xenoliths. One of these is the extension and accompanying asthenospheric uplift in the Miocene, which acted as a significant source of heat (e.g., Embey-Isztin et al., 2001). However, as mentioned earlier, the correlation of fabric strength and equilibration temperatures acquired with REE- and major-element-based thermometers (Fig. 6.17b, c) suggests that the deformation resulting in the observed J-indices postdates the extensional phase. The microstructures of the annealed xenoliths indicate that the annealing followed the deformation, and therefore it could not have been caused by the extension. Another possible candidate for the heat source are melts percolating through the upper mantle prior to entrainment by the host basalt. Melt-induced annealing was described in recent studies from a number of xenolith suites such as the Eastern Betics in SE Iberia (Rampone et al., 2010; Hidas et al., 2016), the Hoggar swell in Algeria (Kourim et al., 2015) or the Styrian Basin in the western Carpathian-Pannonian region (Aradi et al., 2017), where microstructural or geochemical evidence (e.g., amphibole formation) points to melt-rock interaction.

In the Nógrád-Gömör Volcanic Field, microstructural evidence for melt-induced

annealing is scarce. However, as shown by the geochemical results, several distinct metasomatic events have affected the upper mantle beneath the area (see Chapter 6.2 and Liptai et al., 2017). These metasomatic events include (1) formation of Nb-poor amphiboles presumably due to interaction with subduction-related fluids/melts; (2) reaction

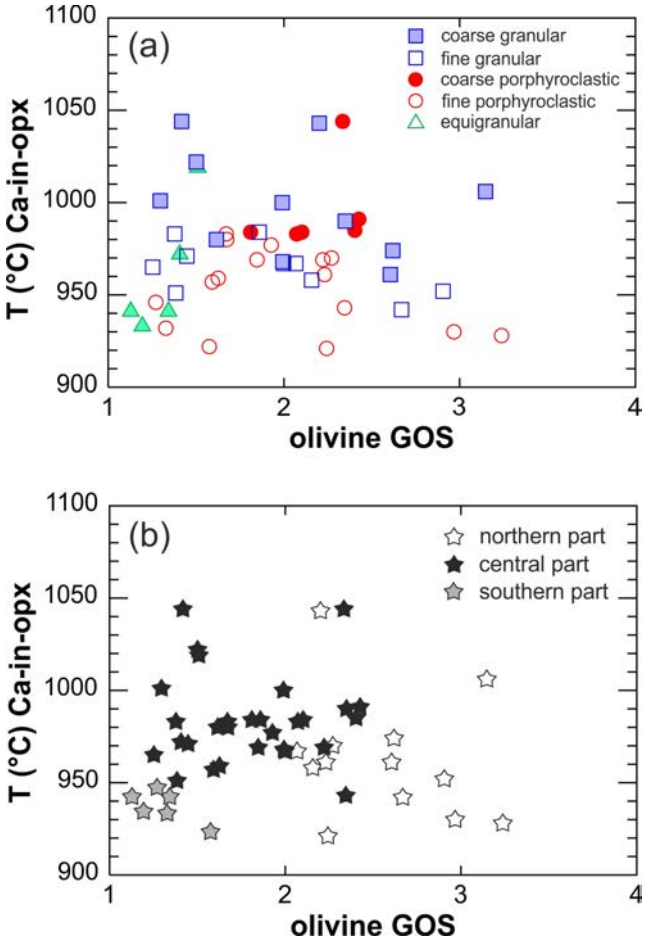

Fig. 6.19. Plot of grain orientation spread (GOS) vs equilibration temperatures calculated with the Ca-in-opx thermometer of Brey and Köhler (1990) modified by Nimis and Grütter (2010). Legend based on xenoliths textures (a) and sampling locality (b).

with a mafic melt of intraplate origin, resulting in the formation of Nb-rich amphiboles and enrichment of U-Th-Nb-Ta-LREE in clinopyroxenes; (3) reaction with an intraplate melt of slightly different composition, resulting in the enrichment of Fe and Mn in olivine and pyroxenes, Ti in spinel and LREE in pyroxenes. This later process is assumed to be also linked to the formation of the wehrlitic xenolith suite in the central part (Patkó et al., 2013) (Fig. 6.13). The first of these metasomatic events is considered to be older than the Miocene extension; however, the last two involve melts which are assumed to have been percolating in the upper mantle of the Nógrád-Gömör Volcanic Field after the extension but prior to eruption of the host basalt. The second metasomatic event appears to be

more widespread, affecting the upper mantle under all three parts of the Nógrád-Gömör Volcanic Field. Evidence for this metasomatism mostly appears only in geochemical compositions there are no petrographic signs except for the Nb-rich amphiboles, which are present only in a few xenoliths, almost exclusively at the Fil'akovo-Kerčik locality (Fig. 3.1). Nevertheless, most of these amphiboles tend to have CPO that matches those of adjacent pyroxenes (Fig. 6.20). Such a microstructural relationship between amphibole and clinopyroxene has been described by Kaczmarek and Tommasi (2011) from the Lanzo orogenic peridotite (Italy), Kourim et al. (2015) from the Hoggar swell (Algeria) and Aradi et al. (2017) from the Styrian Basin, and has been interpreted as amphibole crystallization on a pre-existing, deformed clinopyroxene during late-stage modal metasomatism. Consequently, the Nb-rich amphiboles in the Nógrád-Gömör Volcanic Field support the presence and thus the heating effect of metasomatizing melts that infiltrated the upper mantle subsequently or at a late stage of previous deformation.

The third and youngest metasomatic event, responsible for the formation of Group IIB xenoliths, was only active under the central part, as indicated by the lack of xenoliths carrying a wehrlitic signature in the northern and southern parts (Fig. 3.1; 3.2). The presence of a reacting melt under the central part shortly before the eruption of the host basalt can explain the increased range of temperatures observed in the xenoliths from the central part (Fig. 6.19). Thus, it is likely that annealing in the SCLM of the Nógrád-Gömör

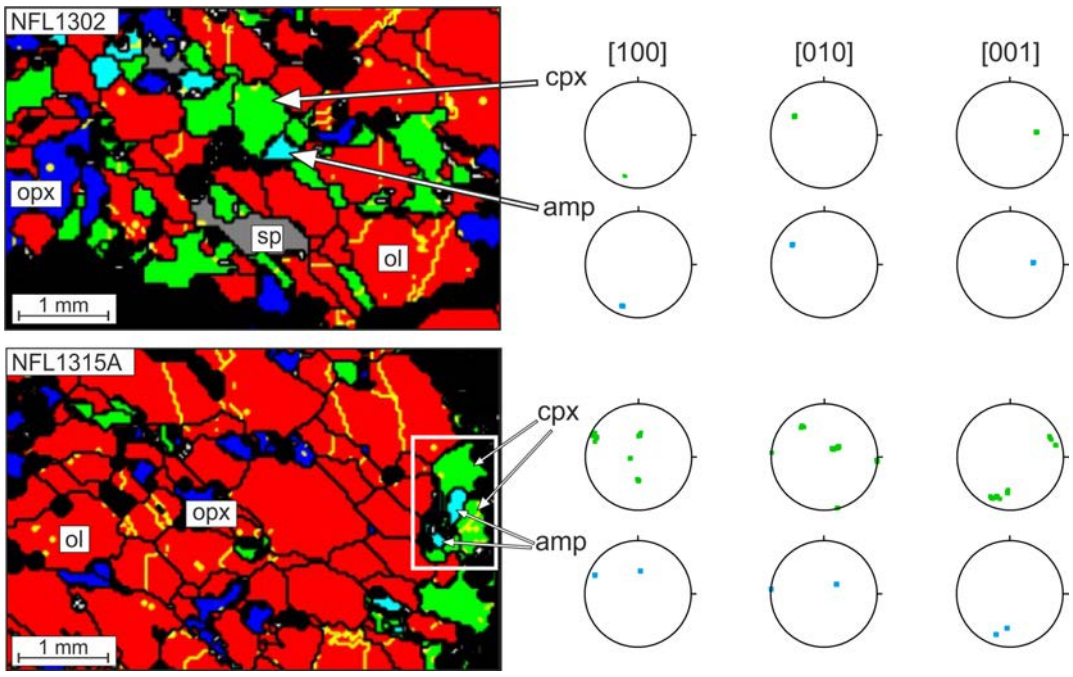

Fig. 6.20. Examples of Nb-rich amphibole grains displaying matching orientation with neighbouring clinopyroxene in xenoliths NFL1302 and NFL1315A.

Volcanic Field is the result of the heating effect of percolating and reacting melts; which was followed by cooling in the northern and southern parts. In contrast, in the central part, xenoliths retained higher equilibration temperatures due to the shorter time between wehrlite formation and entrainment by the host basalt. Note that in this case, equilibration temperatures of xenoliths from the central part cannot be regarded as indicators for greater depth of origin (Fig. 6.1). It is more probable that these xenoliths represent similar mantle depths as the northern and southern parts, and the elevated temperatures are the result of the presence of melt shortly before, or even during, their entrainment by the host magma.

6.3.3. Seismic properties and thickness of the anisotropic layer

Seismic anisotropy in the upper mantle is generally considered to result from the elastic anisotropy of the dominant mineral phases, namely olivine and pyroxenes (e.g., Nicolas and Christensen, 1987). Mantle anisotropy thus indicates that olivine, the most abundant constituent of the upper mantle, has a coherent orientation on a large scale (tens to hundreds of kilometres) as a result of active or past deformation events (e.g., Nicolas and Christensen, 1987; Silver and Chan, 1991; Vauchez and Nicolas, 1991; Savage, 1999; Silver et al., 1999). Upon reaching and passing through an anisotropic layer, shear (S) waves split into two components polarised perpendicularly and travelling at different velocities, resulting in delay times observable on the surface (e.g., Crampin et al., 1984). The delay time is usually constrained by the combined effect of the thickness of the anisotropic layer and the magnitude of the anisotropy.

The presence of a clear CPO in the lithospheric mantle of the Nógrád-Gömör Volcanic Field indicates that at least part of the SKS splitting is accumulated in the anisotropic upper mantle (e.g., Tommasi and Vauchez, 2015). Using the seismic property data of the xenolith suite in this study, the thickness of the anisotropic layer under the Nógrád-Gömör Volcanic Field can be estimated, assuming a single layer with homogeneous orientation for the foliation and lineation. Since the measured delay time between fast and slow polarized S-waves depends on the orientation of the foliation and lineation, five endmember cases have been proposed by Baptiste and Tommasi (2014) for the optimal calculation (Fig. 6.21a): horizontal foliation and lineation (case 1), vertical foliation and horizontal lineation (case 2), vertical foliation and lineation (case 3), 45° dipping foliation and lineation (case 4), 45° dipping foliation and horizontal lineation

(case 5). For the calculations, a ~1.3 s delay time was used, based on observations at three seismological stations closest to the Nógrád-Gömör Volcanic Field (Fig. 6.21b). The thickness of the anisotropic layer (T) is given by the following equation:

$$T = 100dt * \frac{Vs}{AVs}$$

where dt is the delay time, Vs is the average velocity of the fast and slow S-waves, and AVs is the S-wave anisotropy expressed in percentage. For determining Vs and AVs, propagation directions for case 1-5 were taken from Baptiste and Tommasi (2014) (Fig. 6.21a).

The calculated thicknesses of the anisotropic layer are 224, 125, 281, 1260, and 177 km for cases 1-5, respectively. Considering that the global average maximum depth where CPO-induced seismic anisotropy is strong is estimated to be ~250 km (Mainprice et al., 2005), the thickness estimate acquired by assuming case 4 (45° dipping foliation and lineation) is too high to be accepted as realistic. The rest of the values are all slightly higher than the corresponding thicknesses calculated by Klébesz et al. (2015). However, they used xenoliths only from the southern part of the Nógrád-Gömör Volcanic Field (Fig. 3.1), while this study involves a more representative, hence more robust sample set, including all three sub-areas of the volcanic field, and the average seismic properties are weighted by xenolith size.

An important factor in considering thickness values such as those presented by Klébesz et al. (2015) is that they are ignore crustal contributions to Vs delay times. However, Barruol and Mainprice (1993) estimated that on average, a delay time of 0.1-0.2 s is accumulated in 10 km of crustal rocks. Taking a ~25 km thick crust for the Nógrád-Gömör Volcanic Field (Klébesz et al., 2015), this would indicate that 0.25 – 0.50 s of the observed delay time is a crustal contribution. Recalculating the thickness of the anisotropic mantle layer using delay times of 0.8-1.05 s, the values are 138-181, 77-101, 173-227, 775-1017, and 109-143 km for cases 1-5, respectively. These results still significantly exceed the thickness of the lithospheric mantle beneath the Nógrád-Gömör Volcanic Field, which is estimated to be ~40 ± 10 km (based on Moho and lithosphere-asthenosphere boundary depth of Klébesz et al., 2015). Consequently, a major contribution from the sublithospheric mantle (37-187 km), with the same structure, is required to produce the observed delay times. The presence of a sublithospheric anisotropic layer under the Carpathian-Pannonian region, which produces uniform SKS directions despite the complex crustal structures

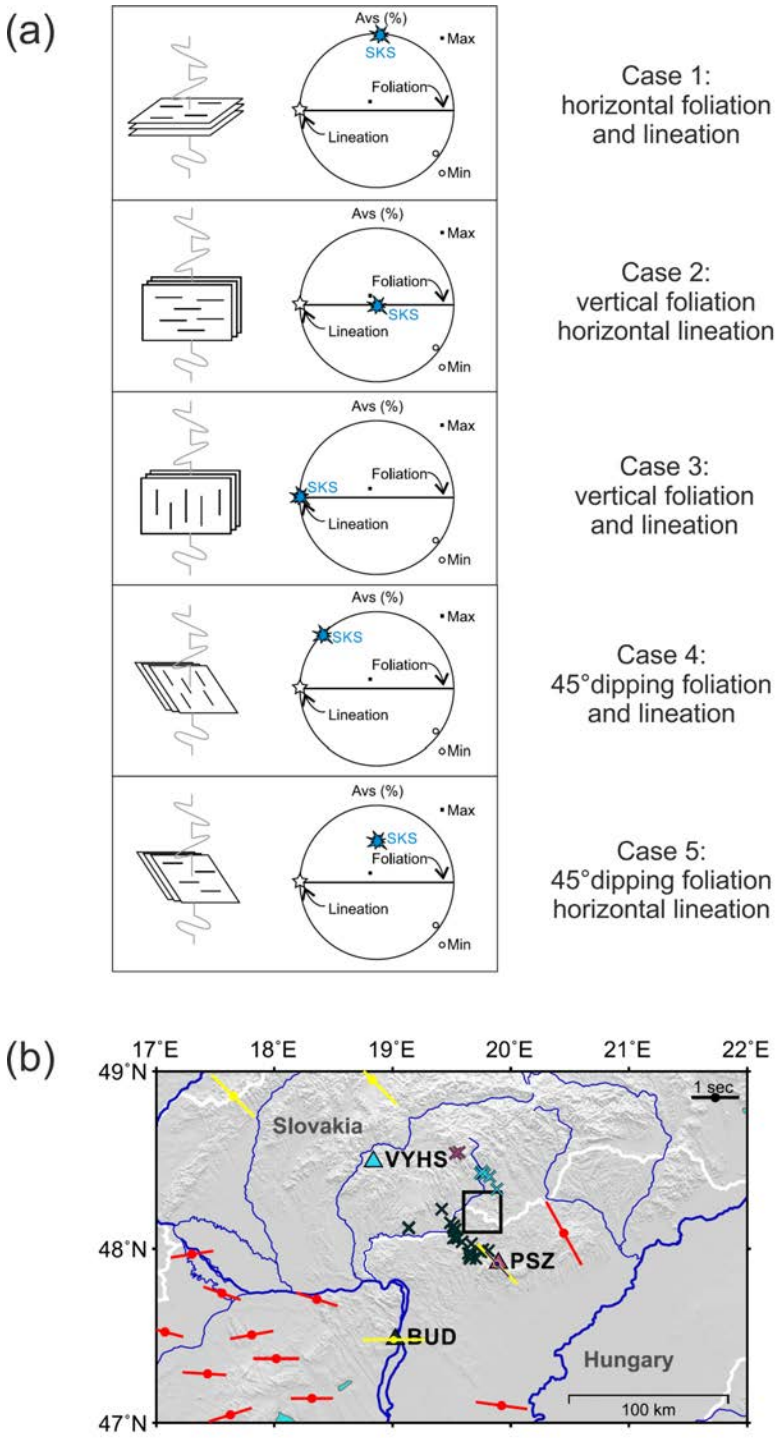

Fig. 6.21. a - Illustration of the five different endmember orientations for the foliation and lineation (Baptiste and Tommasi, 2014) indicating SKS directions on the pole figure of AVs (S-wave anisotropy). Figure modified after Klébesz et al. (2015). b – Location of seismological stations (triangles) in the vicinity of the Nógrád-Gömör Volcanic Field (black square): BUD—MTA CSFK Geodetic and Geophysical Institute, Hungary; PSZ—GEOFON Global Seismic Network, GFZ, Germany and MTA CSFK Geodetic and Geophysical Institute, Hungary; VYHS—Geophysical Institute, Slovak Academy of Sciences, Slovakia. Several examples of the magnitude and direction of fast-polarised phase of the near-vertically propagating S-wave are also shown; see Fig. 6.22 for a more detailed map. Figure from Klébesz et al. (2015).

of the region, has been proposed by Qorbani et al. (2016), and it is supported by seismic properties of upper mantle xenoliths in the Carpathian-Pannonian region (Kovács et al., 2012a; Klébesz et al., 2015; Aradi et al., 2017). We suggest that the xenoliths of this study further prove the presence of anisotropy in the sublithospheric mantle.

This discrepancy between the assumed lithospheric thickness and the calculated thickness of the anisotropic layer in the Carpathian-Pannonian region raises some questions. Due to the different rheological properties, it is questionable whether the asthenosphere can have the same structures as the lithosphere, producing a single and uninterrupted anisotropic layer. Geophysical methods used to constrain the depth of the lithosphere-asthenosphere boundary (LAB), such as receiver functions (Klébesz et al., 2015), detect surfaces marking changes in physical properties which affect seismic wave velocity. However, such changes may result from different mantle compositions as well, e.g., the transition from the spinel to garnet facies, or a decrease in the modal proportion of olivine if the deeper layer has a different bulk composition – e.g. if it is more fertile. In this case, the mantle segment below the detected LAB depth may still be part of the lithosphere, formed by subcretion of former asthenosphere. This would be consistent with the observed uniform anisotropy, but the deeper parts would differ from shallower layers in composition and/or tectonic history. An example of such a scenario is the proposed upper mantle model of Kovács et al. (2012a) for the central part of the Pannonian Basin (see section 6.3.4 below). Nevertheless, it has been shown that deformation-induced preferred orientation can be present at asthenospheric depths (Mainprice et al., 2005 and references therein). In the Carpathian-Pannonian region, present-day stress fields resulting from the tectonic inversion and compression starting in the late Miocene, caused by the convergence of the Adria microplate and the European platform (Bada et al., 2007), could account for the presence of anisotropy in both the lithosphere and the uppermost asthenosphere.

The fast-polarized S-wave direction in the vicinity of the Nógrád-Gömör Volcanic Field is oriented NW-SE based on recent geophysical data (Stuart et al., 2007; Dando et al., 2011; Qorbani et al., 2016) as depicted on Fig. 6.22a. This is consistent with the above-mentioned present-day tectonics in the Carpathian-Pannonian region. For maximum anisotropy, the average lineation in the anisotropic mantle layer would be subparallel to this NW-SE direction. This excludes the possibility of case 3 (vertical foliation and lineation); which leaves the options of horizontal, vertical, or dipping foliation. Horizontal foliation would require the thickest anisotropic layer, whereas vertical orientation

would require the thinnest to produce the observed 1.3 s delay time. In the case of the Nógrád-Gömör Volcanic Field, both options would require a significant asthenospheric contribution, similar to what was established for the SCLM beneath Styrian Basin (Aradi

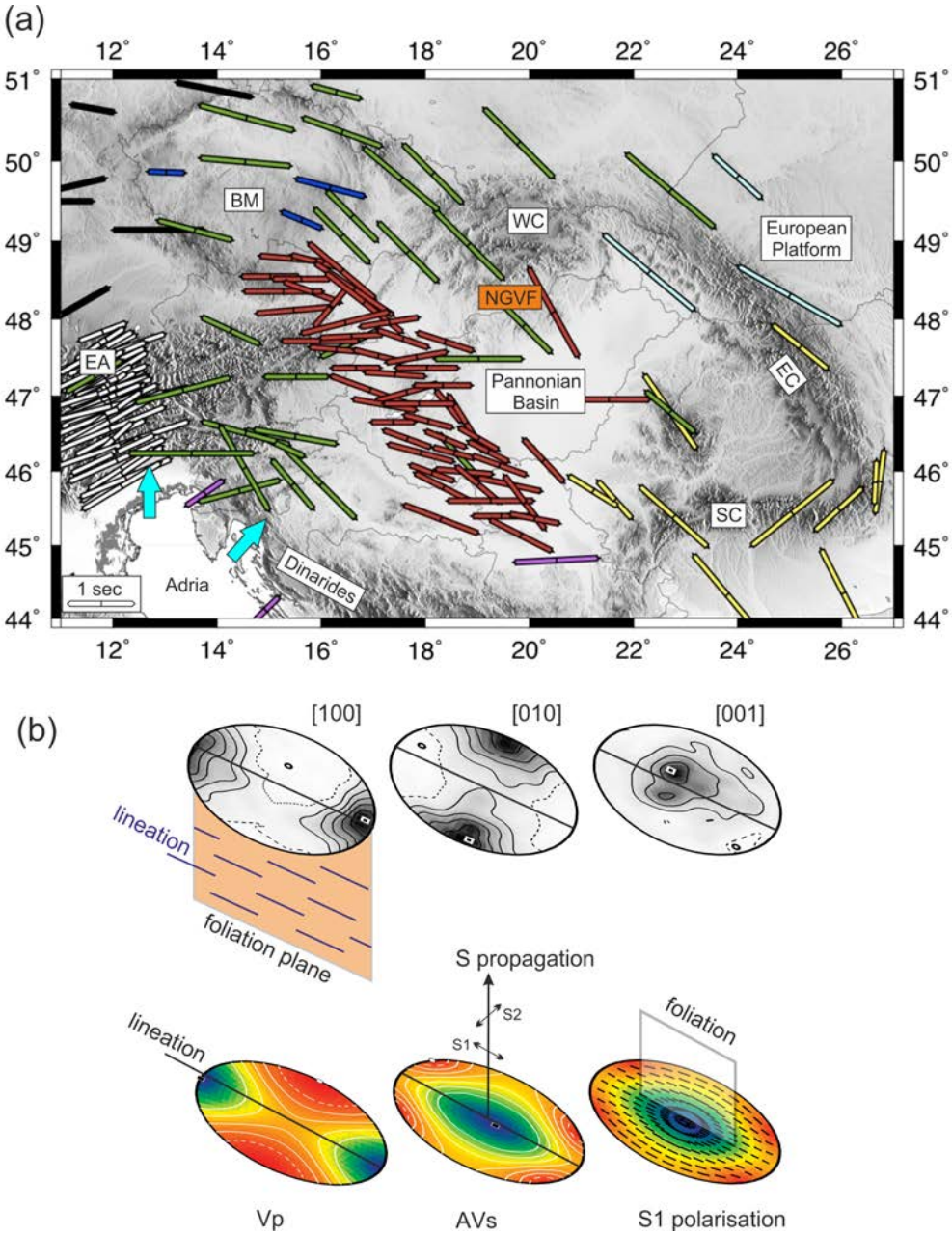

Fig. 6.22. a – Directions and magnitude (expressed in seconds referring to delay time) of the fast-polarised phase of the near-vertically propagating S-wave in the Carpathian-Pannonian region (Stuart et al., 2007; Dando et al., 2011; Kovács et al., 2012). Different colours represent data from different studies; see references under Fig. 5 of Kovács et al. (2012). Blue arrows indicate the pushing directions caused by the indentation and slight rotation of the Adria microplate (Horváth et al., 2006). Abbreviations: EA – Eastern Alps, BM – Bohemian Massif, WC – Western Carpathians, EC – Eastern Carpathians, SC – Southern Carpathians. b – Illustration of the most favoured orientation of the foliation and lineation in the upper mantle of the Nógrád-Gömör Volcanic Field, using a representative CPO pole figure group and pole figures of seismic properties average for the entire Nógrád-Gömör sample set.

et al., 2017) and the central region of the Pannonian Basin (Little Hungarian Plain and Bakony-Balaton Highland; Kovács et al., 2012a). However, for the Persani Mountains on the eastern margin of the Carpathian-Pannonian region, Falus et al. (2008) concluded that assuming vertical foliation, observed delay times (~1 s) could entirely be attributed to the lithospheric mantle. If a single layer with specific orientation is assumed, subvertical foliation is the more favoured option (Fig. 6.22b). This would be more consistent with the present-day stress field as the eruption of the xenolith-hosting alkali basalts took place (6.4 - 2.5 Ma; Balogh et al., 1981) after the change from extensional to compressional regime (~8 Ma; e.g., Horvath and Cloetingh, 1996). Furthermore, vertical foliation could better accommodate the vertical migration of melts (Waff and Faul, 1992; Tommasi et al., 2008) such as the basalts hosting the xenoliths. It could also be a plausible explanation for the clearly NW-SE oriented distribution of the xenolith- hosting basalt formations on the surface (Fig. 3.1). However, it cannot be excluded that the orientation / dipping angle of the foliation varies with different depths, as in large-scale shear- zone systems (e.g., Vauchez et al., 2012).

6.3.4. Links to the tectonic evolution of the Carpathian-Pannonian region

Both geochemical and crystallographic data on the studied xenoliths suggest that the upper mantle beneath the Nógrád-Gömör Volcanic Field has a complex Neogene history. It is difficult to provide a full reconstruction of the different metasomatic and deformation events, due to the overprinting of different signatures. However, using previous constraints on the tectonic evolution of the Carpathian-Pannonian region and the results of studies on other Carpathian-Pannonian region xenoliths, a tentative model can be proposed for the mantle segment of the Nógrád-Gömör Volcanic Field (Fig. 6.23).

The last major deformation occurred during or following the extension. Since the BA-indices and CPO-types indicate various deformation regimes, which do not directly correlate with other textural properties, it is suggested that this is the result of a complex deformation event. Microstructural features indicating annealing are present in xenoliths from all Nógrád-Gömör localities, suggesting that annealing affected the upper mantle under the entire area. Since there is no straightforward correlation between the amount of intragranular deformation and the fabric strength / grain size, it is likely that the former is a local character of the Nógrád-Gömör Volcanic Field, and the latter is a general feature

for the whole Carpathian-Pannonian region. This is supported by studies on xenoliths from the other parts of the region (Persani Mountains, Bakony-Balaton Highland, Styrian Basin; Falus et al., 2008; Kovács et al., 2012a; Aradi et al., 2017). However, the tectonic environment is different for these xenolith occurrences, and it is important to constrain the geodynamic situation of the Nógrád-Gömör Volcanic Field compared to these volcanic fields.

In the central part of the Pannonian Basin (Little Hungarian Plain and Bakony-Balaton Highland), Kovács et al. (2012a) described a shallower layer with fine-grained porphyroclastic- and equigranular-textured xenoliths showing [010]-fibre CPO, and a deeper layer with coarse-grained porphyroclastic xenoliths showing orthorhombic symmetries. The former group was interpreted to represent the uppermost part of the lithospheric mantle of the ALCAPA microplate, which was deformed during the Alpine collision and extrusion, whereas the latter group was suggested to be the remnant of the east-west directed asthenospheric flow associated with the Miocene extension. These xenoliths became part of the lower lithospheric layer during the post-extensional thermal relaxation (Kovács et al., 2012a), an interpretation which is supported by their fertile geochemical composition as well. The affiliation with the asthenospheric flow is further supported by seismic data, as fast-polarised S-wave directions for the near-vertically propagating SKS phase outline a general east-west direction in the central part of the Pannonian Basin (Stuart et al., 2007; Dando et al., 2011; see Fig. 5. of Kovács et al., 2012a). In the marginal zones of the Pannonian Basin such as the Styrian Basin and the Persani Mountains, the rate of extension, and thus the asthenospheric uplift, had significantly less effect on the upper mantle; therefore, xenoliths with coarse-grained microstructures cannot be interpreted as fossil asthenosphere (Falus et al., 2008; Aradi et al., 2017). Xenoliths from the Styrian Basin provide evidence for a major deformation event in a transpressional regime (Aradi et al., 2017), which is in agreement with recent geodynamics in the western Carpathian-Pannonian region, i.e., the NE-directed subduction and rotation of the Adria microplate (Bada et al., 2007; Qorbani et al., 2016). In the Persani Mountains, convergent plate tectonics (subduction/collision) dominated the deformation processes in the lithospheric mantle (Csontos, 1995; Matenco et al., 2007; Falus et al., 2008). Both of these marginal areas show petrographic and geochemical evidence of percolating subduction-related fluids/melts (Vaselli et al., 1995; Vaselli et al., 1996; Falus et al., 2008; Aradi et al., 2017).

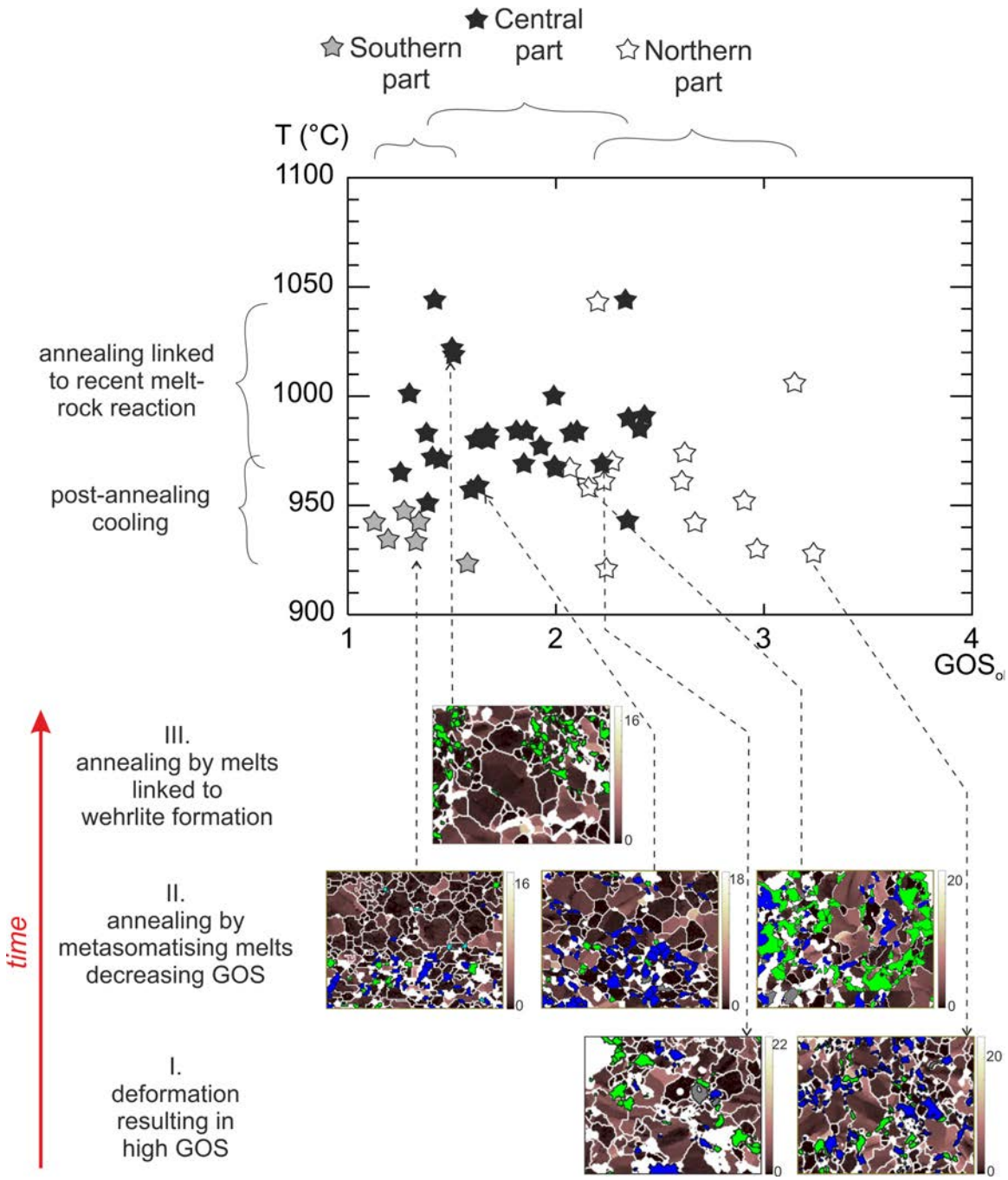

Fig. 6.23. Reconstructed stages of deformation and annealing events in the Nógrád-Gömör upper mantle based on microstructural characteristics and thermal conditions. I. – deformation in a dominantly transpressional regime, leading to strong intragranular deformation manifested in high grain orientation spread (GOS); II. – annealing linked to the heating effect of percolating metasomatizing mafic melts in the upper mantle, resulting in grain growth and the decrease of intragranular deformation. III. – annealing in the central part of the Nógrád-Gömör Volcanic Field, linked to the formation of the wehrlite suite and causing Fe-Mn-Ti-LREE-metasomatism in some central-part lherzolites (Group IIB) shortly before the eruption of the host basalt. EBSD maps showing the transformation from deformed to annealed textures are 'mis-to-mean' (M2M; Wright et al., 2011) maps for olivine, where the colour scale indicates the deviation of each measurement point from the average orientation of the grain. Note that the maximum value on the colour bar decreases from the deformed samples towards the more annealed ones. Colours of mineral phases other than olivine are the same as in Fig. 6.15.

In the Nógrád-Gömör Volcanic Field, there is no sign of any recent subduction environment, except for the scarce Nb-poor amphiboles (Fig. 6.6), which were interpreted as modal metasomatic products of a subduction-related fluid/melt based on the work of Coltorti et al. (2007a) (see Chapter 6.2.2). However, these were suggested to be the imprint of an older subduction event, predating the extrusion of the ALCAPA microplate (Kovács and Szabó, 2008; Liptai et al., 2017). Furthermore, the presence of a 'lithospherised' mantle layer similar to the central part of the Pannonian Basin is not corroborated either, as CPO patterns do not seem to correlate with depth, and there is no evidence for E-W fast-polarisation directions. The wide variety of CPO patterns depicted by BA-indices (Fig. 5.28) suggests mixed deformation regimes, among which transpression is likely the most dominant, given the high abundance of [010]-fibre symmetries compared to the world average (Ben Ismail and Mainprice, 1998). This can probably be attributed to the effect of the convergence of the rotating Adria block and the European plate (e.g., Horvath and Cloetingh, 1996; Fodor et al., 1999; Horváth et al., 2006; Bada et al., 2007). A transpressional stress field was also suggested to have played a major role in the deformation of the shallower lithospheric layer in the central part of the Pannonian Basin (Kovács et al., 2012a) and can explain the high abundance of [010]-fibre symmetries in the Styrian Basin (Aradi et al., 2017). This, along with recent measurements of fast SKS splitting directions, further supports the interpretation that in the upper mantle of the Nógrád-Gömör Volcanic Field, the most probable orientation of the foliation is vertical, and lineation is most likely NW-SE directed in accordance with fast polarisation directions (Fig. 6.22).

Although the age of the xenolith-hosting basalts in the Nógrád-Gömör Volcanic Field is young (~ 6.4 – 2.5 Ma; Balogh et al., 1981), it is unclear how well the xenoliths correspond to the present-day upper mantle. As the ages decrease from the northern towards the southern part, any ongoing deformation since the Miocene might be expected to be detectable as an increase in deformation microstructure in xenoliths hosted by younger basalts. However, xenoliths from the youngest basalts (i.e., the southern part) show rather more annealed and less deformed characters (triple junctions, grain growth and low fabric strength e.g., Fig. 6.18) compared to those from the northern and central parts, even considering the fine-grained xenoliths from the shallowest lithospheric mantle. Furthermore, olivine GOS values also decrease from the north to the south (Fig. 6.19). Since GOS reflects the combined effects of the degree of deformation and annealing, this is

likely due to local differences in the influence of these two major physical processes among the three domains of the volcanic field.

Since annealed microstructures appear to overprint deformation in the xenoliths, it is suggested to have taken place after the onset of compressional tectonics (~8 Ma; e.g., Horvath and Cloetingh, 1996). Although intraplate mafic melts are inferred to be generated by the decompression during extension (Embey-Isztin et al., 1993), the eruption ages of the host basalts suggest that melt percolation and reaction with the peridotite wall-rock was possible during convergent tectonics. The time gap between the active extensional phase and the ascent of asthenospheric melts may be explained by mantle convectional patterns, as proposed by numerical models of Balázs et al. (2017). However, heating by these melts must have happened considerably prior to entrapment as low equilibration temperatures in the northern and southern parts suggest cooling and are more likely to represent depths of origin at the time of entrapment. Trepmann et al. (2013) showed that annealing microstructures in natural peridotites can be produced on a scale of tens to tens of thousands of years. The ascent of the host basalt can be regarded as instantaneous in geological terms (O'Reilly and Griffin, 2011), and this was verified by Szabó and Bodnar (1996) for the Nógrád-Gömör Volcanic Field with the study of CO_2 inclusions and spinel zonation; the resulting ~36 hours of ascent to the surface from mantle depths excludes any annealing effect from the host. Finally, as discussed in Chapter 6.2.2.3, the most recent annealing event is assumed to be a reaction associated with the formation of wehrlites (Patkó et al., 2013; Liptai et al., 2017), as this is restricted to the central part only, where equilibrium temperatures cover a significantly higher range (Fig. 6.23). The fact that central-part xenoliths retained these high temperatures suggests that the melt/wall-rock reaction linked to wehrlite formation was still occurring during the time of host basalt eruptions in the central part of the Nógrád-Gömör Volcanic Field.

6.4. Post-entrainment Processes in the Nógrád-Gömör Xenoliths

6.4.1. Dehydration and constraints on the original 'water' contents

The amount of incorporated 'water' in nominally anhydrous minerals (NAMs) has recently come into focus from a number of studies aimed at the behaviour of 'water' in mantle rocks (e.g., Mackwell and Kohlstedt, 1990; Bell and Rossman, 1992b; Peslier et

al., 2002b; 2010; Grant et al., 2007; Bonadiman et al., 2009; Green et al., 2010; Sundvall and Stalder, 2011; Férot and Bolfan-Casanova, 2012; Kovács et al., 2012b; Demouchy and Bolfan-Casanova, 2016). The significance of NAMs as a reservoir for water is due to their large proportion in the mantle; they are estimated to hold more than the mass of the Earth's oceans (e.g., Peslier et al., 2017). It has been shown that even small amounts of incorporated 'water' can affect rheology and other physical properties of the mantle, e.g., weaken olivine (e.g., Mackwell et al., 1985; Demouchy et al., 2012), decrease solidus temperature (e.g., Green et al., 2010) and, especially when present in high concentrations, influence the activation of particular slip systems during olivine deformation (Jung and Karato, 2001; Jung et al., 2006). As detailed in Chapter 5.6, 'water' can be present in different forms in mantle rocks and minerals – in fluid phase, structurally bound in volatile-bearing minerals, or as H^+ as substitution in tetra- or octahedral positions in NAMs. The geochemical relevance of 'water' has been investigated in numerous studies, based on the general observation that H behaves as an incompatible element during mineral-melt partitioning. More precisely, H was found to behave in a similar way to LREE (e.g., Ce) in terms of incompatibility (e.g., Michael, 1995; Danyushevsky et al., 2000). Although there is evidence for 'water' content being associated with fluid-related metasomatism in xenoliths from the Kaapvaal and Siberian cratons (Bell and Rossman, 1992a; Peslier et al., 2012; Doucet et al., 2014), studies on off-cratonic xenoliths have found no clear correlation between the concentrations of H and other incompatible trace elements affected by metasomatism (e.g., Yang et al., 2008; Xia et al., 2010; Denis et al., 2015; Hao et al., 2016).

Experimental studies on the capacity of mantle minerals for 'water' storage between 1 and 4 GPa and 1000-1380 °C showed that olivine, orthopyroxene and clinopyroxene can incorporate up to 30-140, 233-1840, and 332-2000 ppm H_2O, respectively (Aubaud et al., 2004; Hauri et al., 2006; Kovács et al., 2012b). Mantle xenoliths from off-cratonic lithosphere, which represent the lower end of this pressure-temperature range, show generally low values: 0-79, 5-460 and 5-1080 ppm for olivine, orthopyroxene and clinopyroxene, respectively (e.g., Bell and Rossman, 1992b; Peslier et al., 2002b; Grant et al., 2007; Yang et al., 2008; Bonadiman et al., 2009; Xia et al., 2010; Yu et al., 2011; 2013; Pintér et al., 2015). However, the Nógrád-Gömör xenoliths seem to be quite dry even compared with these concentrations (Fig. 6.24), as the majority of the xenoliths have no 'water' in olivine, and less than 40 ppm for orthopyroxene and 200 ppm for clinopyroxene

(Fig. 5.26; Table 10). These concentration ranges are similar to those reported from xenoliths from the North China Craton (Yang et al., 2008; Xia et al., 2010; 2013) (Fig. 6.24). These 'water' contents are even considerably lower than values reported in xenoliths from other localities within the Carpathian-Pannonian region (Falus et al., 2008; Aradi et al., 2017). However, it must be noted that these occurrences (Styrian Basin and Persani Mountains, Fig. 2.3) are located in the marginal regions of the Carpathian-Pannonian region, where the upper mantle has been affected by subduction-related processes.

The dryness of olivine in xenoliths hosted in basaltic lavas has recently been discovered to result from dehydration during ascent or slow cooling after eruption, as suggested by profiles in olivine grains showing decreasing 'water' contents from the core towards the rim (Demouchy et al., 2006; Peslier and Luhr, 2006; Denis et al., 2013; Peslier et al., 2015). Even though these magmas reached the surface in a matter of hours to days, as discussed earlier, H has a very high diffusion rate (e.g., Kohlstedt and Mackwell, 1998; Demouchy and Mackwell, 2003; Ingrin and Blanchard, 2006; Padrón-Navarta et al., 2014), which facilitates effective 'water' loss in such short time periods. In the Nógrád-Gömör xenoliths, the extremely 'water'-poor olivines can most likely be explained with post-entrapment dehydration. The only four xenoliths where small amount of 'water' is

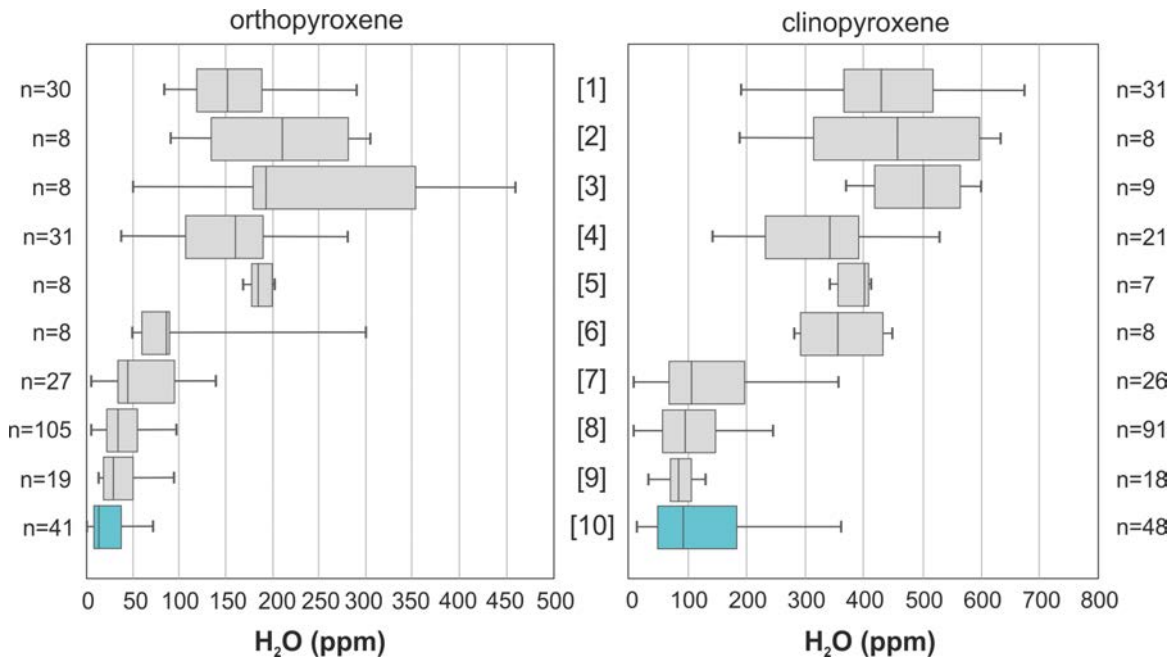

Fig. 6.24. 'Water' concentration ranges in ortho- and clinopyroxene from mantle xenoliths worldwide, in a box-whiskers diagram (without the outliers). Numbered studies are: [1] Aradi et al. (2017); [2] Falus et al. (2008); [3] Bell and Rossman (1992); [4] Peslier et al. (2002); [5] Grant et al. (2007); [6] Pintér et al. (2015); [7] Yang et al. (2008); [8] Xia et al. (2010); [9] Xia et al. (2013); [10] this study.

detectable, are from the same locality: Jelšovec (northern part, Fig. 3.1). Furthermore, this is the only locality where the xenoliths are hosted in pyroclastics and not in lava flows; although the amount of water in olivine in these samples (0.7 – 2.2 ppm) is still very low. This suggests that dehydration does not only take place during ascent, but also following eruption, as there is a better chance of retaining some 'water' in olivines in rapidly-cooling pyroclasts compared to slowly-cooling lava flows. This is supported by the observed difference in the diffusivity of H depending on the cooling rate in olivine-hosted melt inclusions in tephra samples (Lloyd et al., 2013).

Pyroxenes are generally considered to be better indicators than olivine of the original 'water' content of the mantle. This is because of: the slower diffusion rate of H in pyroxenes (Stalder and Skogby, 2003; Ingrin and Blanchard, 2006), their homogeneous 'water' concentrations even when coexisting olivine shows diffusion profiles (Denis et al., 2013; Hao et al., 2016), and consistency with the generally observed H_2O partitioning between ortho- and clinopyroxene ($D^{cpx/opx} = \sim 2 - 3$; Grant et al., 2007; Bonadiman et al., 2009; Sundvall and Stalder, 2011; Warren and Hauri, 2014). The 'water' contents of ortho- vs clinopyroxene for the Nógrád-Gömör xenoliths are plotted on Fig 6.25. Interestingly, the xenoliths show a very wide variability, with the majority displaying high cpx/opx ratios. Only three xenoliths (NJS1307, NTB0306, NBN0311) have ratios consistent with the empirical partition values. This apparent lack of equilibrium between pyroxenes, and the fact that it is consistently clinopyroxene that shows higher 'water' contents (even to extremes such as 40 times more than orthopyroxene; NMS1302A, NMS1305; Table 10) suggests that orthopyroxene may also not retain its original, mantle-environment 'water' content. This is in agreement with a recent study by Tian et al. (2017), who found dehydration profiles in orthopyroxene from peridotite xenoliths. Furthermore, water loss has recently been described from clinopyroxene megacrysts in basaltic lavas as well, implying that slow cooling on the surface (~20 minutes spent above H^+ closure temperature) can result in significant differences compared to clinopyroxes in the pyroclast host (Lloyd et al., 2016). Thus, the question arises, which xenoliths in the Nógrád-Gömör sample set, if any, represent reliable 'water' contents representative of the original upper-mantle conditions?

As a first approach, samples with cpx/opx H_2O ratios matching or close to the empirical equilibrium partition value range were selected (i.e., $D^{cpx/opx} = 1.2 – 4.0$) for further comparisons. This subgroup contains nine xenoliths (NMS1304, NJS1302,

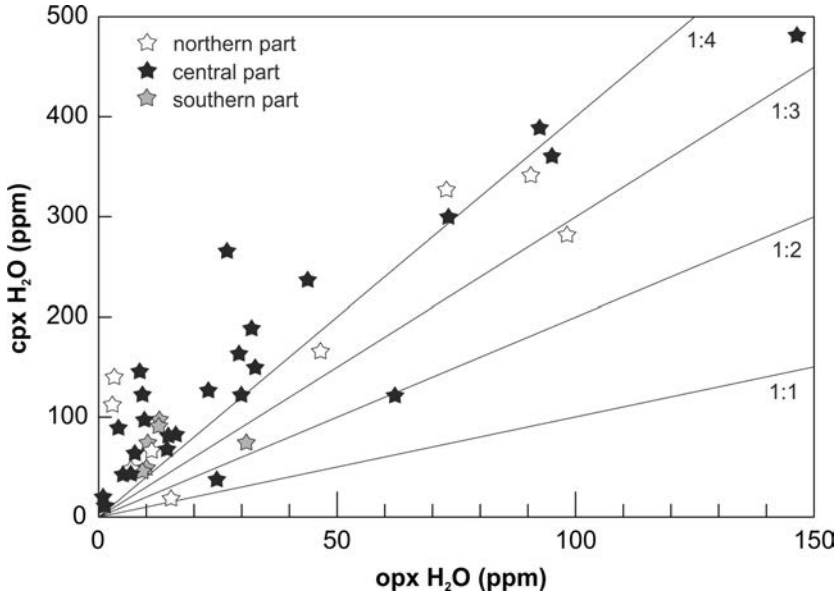

Fig. 6.25. H_2O concentrations of orthopyroxene *vs* clinopyroxene in the studied xenoliths.

NJS1306, NJS1307, NFL1305, NTB0306, NFR0307, NMM1126, NBN0311; Table 10), which are considered more likely to have retained their original 'water' contents. This is due to the observation that H^+ diffusion has a different rate in ortho- and clinopyroxene (Ingrin and Blanchard, 2006; Tian et al., 2017), and thus dehydration would lead to the distortion of H_2O partitioning between the pyroxenes. Note that three out of the four xenoliths from Jelšovec (the sampling locality with pyroclastitic host rocks) fall within the above proposed group, and the fourth one has $D^{cpx/opx} = 4.5$, not much higher than the maximum of the chosen range. Investigation of possible relationships between 'water' content and deformational characteristics is not applicable to the Nógrád-Gömör xenolith set, because the latter are most dominantly influenced by the behaviour of olivine, and, as established earlier, olivine has lost its original 'water' content in almost all studied xenoliths. The amount of incorporated 'water' does not seem to be linked to any metasomatic process either, as there is no correlation between clinopyroxene H_2O content and the concentration of the similarly incompatible Ce or the ratio of Ce/Yb (as an indicator for metasomatism) (Fig. 6.26a, b), neither for the whole sample set nor for the group of xenoliths with the 'reliable" $H_2O^{cpx/opx}$.

On the other hand, when compared with equilibration temperatures, this xenolith group yields a good correlation; xenoliths with higher temperatures are more 'water'-rich, whereas 'water'-poor samples have lower temperatures (Fig. 6.26c). Since higher equilibration temperatures are generally considered to represent greater depths of origin,

this correlation suggests that the deeper upper mantle portion has somewhat higher 'water' contents than shallower layers. However, as discussed earlier (Chapter 6.3.2), equilibration temperatures calculated with major- element-based thermometers are likely to have been affected by annealing during the latest metasomatic event linked to Fe-enrichment in xenoliths from the central part of the area. Interestingly, the correlation between clinopyroxene H_2O content and equilibration temperature is also seen when using REE-based thermometer (Fig. 6.26d), which supports an increase in the water content with depth. Note that the two outliers, NTB0306 and NFR0307 were previously found to be unreliable for the application of two-pyroxene thermometers due to possible pyroxene disequilibrium (Fig. 5.13). Such a correlation has not been observed in the other Carpathian-Pannonian region localities where 'water' contents of xenoliths were studied (Persani Mountains and Styrian Basin; Falus et al., 2008; Aradi et al., 2017); however, these locations are both in marginal regions of the basin system. In the central part of the

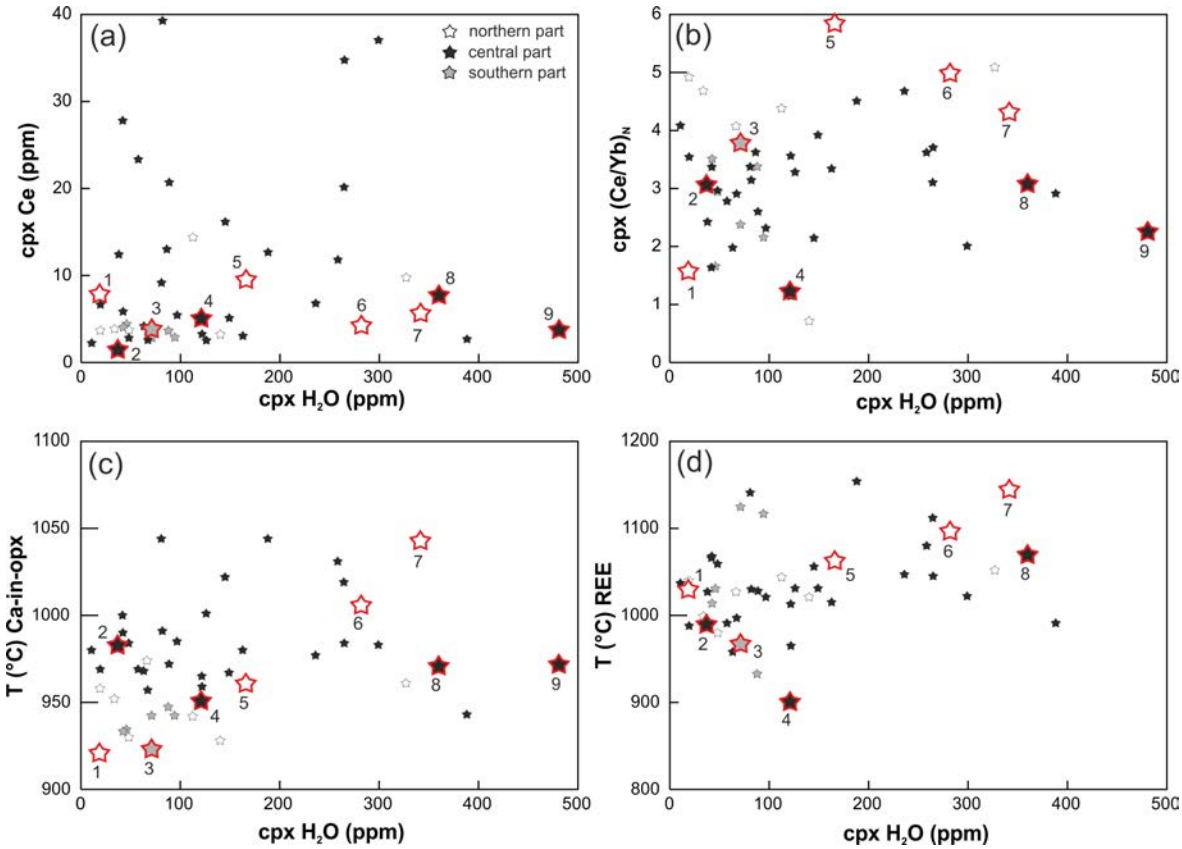

Fig. 6.26. H_2O concentrations of clinopyroxene compared to Ce (a) and $(Ce/Yb)_N$ (b) in clinopyroxene, $T_{Ca\text{-}in\text{-}opx}$ (Brey and Köhler, 1990; Nimis and Grütter, 2010) (c) and T_{REE} (Liang et al., 2013) (d). Numbered large symbols with red outline indicate xenoliths with 'correct' $H_2O^{cpx/opx}$ (see text for further details): 1 – NMS1304, 2 – NMM1126, 3 – NBN0311, 4 – NTB0306, 5 – NJS1302, 6 – NJS1307, 7 – NJS1306, 8 – NFL1305, 9 – NFR0307.

Pannonian Basin (Little Hungarian Plain and Bakony-Balaton Highland; Kovács et al., 2012a) the two upper mantle layers, showing differences in grain size and fabric strength like those in the Nógrád-Gömör Volcanic Field, were also found to have lower 'water' contents in the shallower domain and higher ones in the deeper (Kovács et al., 2013). This implies that the vertical distinction in both fabric and hydration state is a characteristic feature for the upper mantle of the central part of the Carpathian-Pannonian region. Furthermore, as shown in Chapter 6.1, REE-based temperatures are inferred to represent older, hotter mantle conditions, which were reached during the Miocene extension and accompanying asthenosphere uplift. This suggests that the original 'water' contents of the Nógrád-Gömör mantle have not changed significantly at least since the time of the extension, and were not affected by cooling, annealing or the overall metasomatism caused by the percolating basaltic melts.

The bulk water content of these xenoliths, calculated using mass balance methods and analysed water content of the mineral constituents (excluding amphibole), varies over a wide range (from 2.9 ppm in NMS1304 to 71 ppm in NFL1305; Table 10). When plotting bulk-rock water contents against $H_2O^{cpx/opx}$ (Fig. 6.27), a positive correlation is observed shown only by these xenoliths (for comparison, xenoliths with $H_2O^{cpx/opx}$ between 4 – 6 were plotted as well). This suggests an interesting observation, namely the higher the total 'water' content, the more likely this 'water' is to be partitioned into clinopyroxene compared to orthopyroxene. However, such a correlation has not been described in other xenoliths, and it is difficult to verify whether it is coincidental or not.

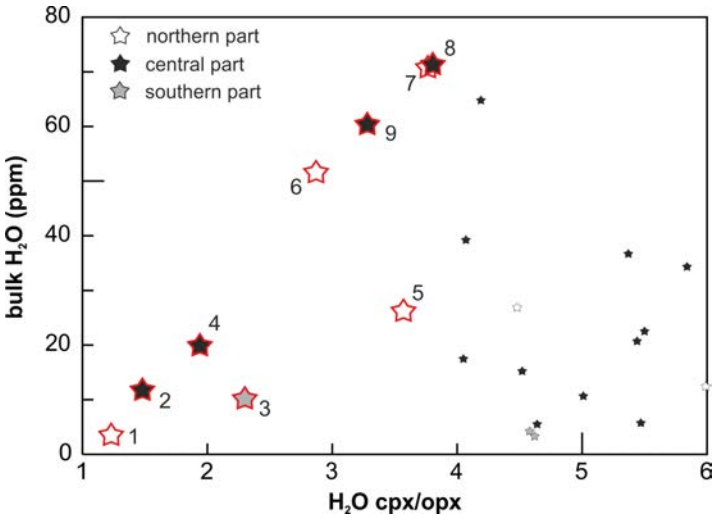

Fig. 6.27. $H_2O^{cpx/opx}$ vs bulk 'water'contents of the xenoliths, in samples with 'correct' $H_2O^{cpx/opx}$ (see text for further details). Xenoliths with $H_2O^{cpx/opx}$ between 4 and 6 are plotted for comparison. Numbered symbols are the same as in Fig. 6.26.

In summary, the anomalously low 'water' contents of the Nógrád-Gömör xenoliths can most likely be explained by extensive 'water' loss during ascent to the surface, and possibly, during post-eruption cooling, which affected olivine, most orthopyroxene and possibly a large proportion of the clinopyroxene as well. Xenoliths hosted in pyroclastics are the most likely to represent the original 'water' content of the mantle. The possibly original 'water' contents, based on their H_2O ratio in clino- and orthopyroxene, observed in a small group of the xenolith set, points to a 'water' distribution increasing with depth, a characteristic feature of the Nógrád-Gömör upper mantle, which remained unaffected by the metasomatizing melts.

6.4.2. Evolution of the silicate melt-inclusions

The phase assemblage (the appearance, modal ratio and compositions of daughter phases) in a silicate-melt inclusion (SMI), is highly dependent on the cooling history of the host rock. Very fast cooling ('quenching') results in a single glass phase (± volatile bubble), whereas slow cooling can allow complete crystallisation (e.g., Roedder, 1984). The SMIs in the studied Nógrád-Gömör xenolith are partially crystallised (Fig. 5.16b), suggesting that after entrapment, slow cooling dominated the environment represented by the xenoliths, allowing precipitation of most of the daughter minerals. The beginning of the crystallisation is in many cases a non-equilibrium process; due to heterogeneous nucleation on the inclusion wall, it is only the host mineral that crystallises, even if the melt is saturated with other phases (e.g., Frezzotti et al., 1991). In the studied samples, this means that daughter clinopyroxene is probably the first to crystallise. This precipitation eventually leads to an increase of volatiles in the residual melt, allowing the onset of crystallisation of volatile-bearing daughter phases (Frezzotti, 2001) such as amphibole, apatite and mica. The presence of glass in the SMIs indicates that a fast cooling phase interrupted the crystallisation process, which is interpreted to have occurred during and after ascent to the surface.

The calculated densities of the CO_2-bubbles yield very similar values in all three SMIs analysed with Raman spectroscopy (Table 5), suggesting that the results are reliable, and the inclusions share not only a common origin, but similar post-entrapment processes as well. This is supported by petrographic observations, including the similarity of the daughter phase assemblages, and the consistent volume ratio of the gas bubble (7 - 14

v/v %; Table 6). The densities of the CO_2-bubbles fall in the relatively low-density range (< 1 g/cm^3; e.g., Frezzotti and Touret, 2014), which is considered to represent ~ 0.1 – 0.3 GPa pressure, corresponding to ~ 2 – 7 km depth, where the CO_2-bubble formed. This depth range typically represents the last stages of magma ascent, shortly before eruption, and devolatilisation of the glass took place when volatile saturation was reached (e.g., Frezzotti, 2001). There is no sign of decrepitation around the SMIs, which would produce a decrease in the CO_2 density. However, the glass is not completely homogeneous in any of the SMIs (see Chapter 5.4). The lack of homogeneity is evidenced as numerous dark spots observable on BSE images (Fig. 5.19c, d). Analyses on these spots did not reveal any compositional characteristic that distinguished the spots from the surrounding glass. Given their dark colour, the spots may represent tiny gas bubbles that froze in the glass before they could merge with the main CO_2 bubble. In this case, the calculated densities may be less precise. Furthermore, estimations of depth, based on the CO_2 density, usually needs to be considered as minimum values, for several reasons. Isochores are generally determined assuming that the original composition was pure CO_2, which is commonly not accurate (e.g., Andersen and Neumann, 2001). Furthermore, some fluid loss may occur by diffusion, through nanofractures, or by reaction with the enclosing glass (Viti and Frezzotti, 2000; Berkesi et al., 2012).

The presence of certain phases in the SMIs of this study, suggests that the original composition of the volatile bubble was not exclusively CO_2. Crystals growing inside the bubble can be interpreted as having formed during a late crystallisation process, following the exsolution of the volatiles from the residual melt. In the Nógrád-Gömör inclusions, anhydrite and barite (where present) are always located on the boundary between the bubble and the glass (Fig. 5.19a-d). Although they appear to have been grown at the expense of the glass, Frezzotti and Touret (2014) suggested that anhydrite can form during the latest stages of ascent. The close association with barite (Fig. 5.19a, b) implies a common genesis. Sulphur is known to be a common component in the volatile phase of mantle fluids (e.g., Andersen et al., 1984; Andersen and Neumann, 2001), and it can explain the crystallisation of these minerals, as the glass contains sufficient amounts of both Ca (Table 7) and Ba (Table 8, Fig. 5.21a).

In addition to sulphates, mica also appears on the boundary between the gas bubble and the glass (Fig. 5.19a-d), with the exception of SMI_U, where only one of the two mica flakes is in contact with the bubble (Fig. 5.19d). In all four SMIs, mica appears to

grow partly inside the bubble. This allows the assumption that mica also formed at a late stage, following the exsolution of the volatile phase. Furthermore, mica may contain a significant amount of OH in the mineral structure. Although this could not be determined during the FIB-SEM analyses, the lack of detected F and Cl in mica may suggests that its volatile content consists of OH, which could have come from the bubble. Alternatively, the presence of anhydrite itself may support the H_2O-content of the volatile phase, as the solubility of $CaSO_4$ in water increases with the amount of NaCl in the system (Newton and Manning, 2004), which could also lead to anhydrite precipitation during cooling.

The crystallisation of late phases may be linked to the chemical heterogeneity of the glass in the SMIs, detected by FIB-SEM analyses by variation in alkali contents (Table 7). Although K_2O contents vary only moderately (2.9 – 6.0 wt %), Na_2O changes on a much wider scale (1.3 – 15.9 wt %; Table 7). Therefore, the total alkali content is more influenced by the abundance of Na than K. This results in Na-rich glass compositions distinctly separate from K-rich glass on the TAS-diagram: the former produce phonolitic compositions, whereas the latter plot in the dacite/trachyte fields (Fig. 6.10b). These compositions are consistent with those of glasses in SMIs in xenoliths of the wehrlitic suite (Patkó, 2014 and unpublished data), although the compositional range for such glasses in the wehrlitic suite is only observed *among* individual SMIs, rather than *within* single inclusions. However, if crystallisation of mica occurred during the late stage of the eruption, it may have sequestered elements such as Si, Al and K from the residual melt (locally enriching it in Na), which, with fast cooling, would not allow restoration of homogeneity before reaching closure temperature (e.g., Newcombe et al., 2014). This could be a possible explanation for the compositional difference between Na-rich and K-rich ('original') glass domains, and for the observation that in the former, the elevated Na_2O contents are always accompanied by a slight decrease in SiO_2, Al_2O_3 and K_2O compared to the latter (Table 7).

Chapter 7. Conclusions

7.1. Summary of the Presented Work

In this study, detailed analytical work has been carried out on peridotite xenoliths from the Nógrád-Gömör Volcanic Field, one of the key localities in the Carpathian-Pannonian region where the lithospheric upper mantle can be studied as xenoliths hosted by late Miocene-Pleistocene alkali basalts. In the Nógrád-Gömör Volcanic Field, a lherzolitic and a wehrlitic xenolith suite was distinguished based on petrographic observations (i.e., texture and modal characteristics). The focus of this study is the lherzolite suite, and a robust geochemical and physical dataset was obtained for 51 such xenoliths. This is the first work which presents mineral trace-element contents, modal and geochemical composition of silicate melt-inclusions hosted in clinopyroxenes of metasomatised xenoliths, determination of crystal preferred orientation in mantle silicates, and 'water' contents of the nominally anhydrous mantle silicates from this region. The results allow detailed interpretations of the geochemical and deformation processes that affected the studied upper mantle domain.

The xenoliths of the lherzolite suite show broad geochemical heterogeneity, which is the result of a sequence of partial-melting and metasomatic processes. The lithospheric mantle domain displays various extents of depletion, revealing degrees of partial melting between ~ 7 - 25 %. This was overprinted by three distinct metasomatic events. The oldest one, detectable by the presence of Nb-poor and LREE-depleted amphibole, is linked to a subduction-related fluid. Subsequently, the peridotite wallrock came into contact with two distinct mafic melts of intraplate origin, similar to, but slightly different from, the compositional range of the host alkali basalts. The first of these is associated with extensive enrichment in incompatible trace elements (U-Th-Nb-Ta-LREE) in clinopyroxene, as well as the formation of Nb-rich amphibole. The second and youngest reaction led to Fe- and Mn- enrichment in olivine and pyroxenes, Ti-enrichment in spinel, and elevated LREE contents in clinopyroxene and to some extent in orthopyroxene. This geochemical signature suggests that the metasomatising melt is the same that is inferred to have played the main role in the formation of the wehrlitic rocks in the xenolith suite from the Nógrád-Gömör Volcanic Field. Detailed geochemical analyses of the silicate melt-inclusions revealed them to have trapped this latest reacting melt. Its bulk composition suggests that it

was produced by very low-degree melting of a garnet lherzolite source. The distribution of wehrlitic xenoliths indicates that this metasomatic event was restricted to the central part of the volcanic field.

Physical properties, such as fabric strength, grain size, crystal preferred orientation patterns and calculated equilibration temperatures display heterogeneities present both vertically and horizontally in the studied mantle portion. On the one hand, fine-grained and weakly oriented xenoliths represent shallower layers, whereas those that are coarse-grained and e with strong preferred orientation originated from greater depths. On the other hand, the amount of intragranular deformation, which is a combined result of deformational and annealing processes, is greatest in the northern part and decreases towards the central and southern parts. Based on the observed crystal preferred orientation symmetries, the latest deformation recorded in olivine fabrics occurred in a dominantly transpressional regime. Calculated high seismic anisotropies in the Nógrád-Gömör mantle indicate that the deformed mantle section extends below the lithosphere. Annealing of the xenoliths, subsequent to the deformation, was caused by heat from the percolating metasomatising melts and increase in ambient mantle temperature immediately prior to entrainment and ascent in the host magma.

Compared with mantle studies worldwide, the Nógrád-Gömör xenoliths have extremely low amounts of incorporated 'water', which show no correlation with metasomatic events. The dry characteristics and the unbalanced H_2O ratio of clino- and orthopyroxene are attributed to dehydration processes during ascent to the surface or during post-eruption cooling. This is supported by the observation that xenoliths hosted in rapidly cooled pyroclastic rocks have consistently high 'water' contents. Xenoliths with $H_2O^{cpx/opx}$ around world-average values are the best indicators for the original 'water' content in the upper mantle. Their correlation with equilibration temperatures suggests that the amount of incorporated 'water' increases with depth, a feature which appears to be unaffected by the latest metasomatic events.

7.2. Synthesis and Tectonic Implications

Although physical properties and geochemical processes are considered to be closely related to one another, the correlation between them is often not that straightforward. In natural samples, this is mostly due to the fact that the effects of multiple processes

have overprinted one another. Furthermore, the major recorder of deformation events is olivine, whereas metasomatism is usually best tracked in pyroxenes and amphibole, that are more capable of incorporating incompatible elements. The reconstruction of the link between these processes is even more difficult in the case of xenoliths, where the spatial relationships of the samples are typically not known. However, there are now some constraints on how these different processes are connected in the Nógrád-Gömör Volcanic Field.

The key link is the equilibration temperature, which has twofold significance: firstly, it can indicate (at least relatively) depth of origin for the xenoliths, and secondly, it may record different episodes of changes in temperature conditions, i.e., annealing and/or cooling. In the Nógrád-Gömör Volcanic Field, it was found that shallower mantle layers have smaller grain-sizes, lower fabric strength, and lower water contents than deeper layers. Although these layers are not geochemically distinct, some of the metasomatic events that influenced wall-rock compositions were found to have occurred only shortly before the eruption of the host basalt. These late metasomatic processes are indirectly linked to equilibration temperatures. During the residence time of these melts, annealing was the dominant process rather than active deformation; hence melt percolation was post-kinematic rather than syn-kinematic, and affected the whole mantle column with the pre-existing vertical heterogeneity, independently of depth.

The reconstructed thermal, deformational and metasomatic processes can be linked to late stages of the Neogene tectonic evolution of the region. The oldest trackable metasomatism, which suggests a subduction-related environment, is most likely to have occurred prior to the ALCAPA extrusion and the *sensu stricto* formation of the Pannonian Basin. The extension and asthenospheric uplift in the Miocene had two major effects on the lithospheric mantle of the Nógrád-Gömör Volcanic Field. Firstly, it resulted in the generation of a series of mafic melts through decompression melting, and these melts later infiltrated the studied mantle region and/or sampled it during their ascent to the surface. Secondly, it left a paleo-temperature signature recorded by the REE-based thermometer. The extension was followed by a change to a compressional/transpressional regime in the late Miocene through to recent times, resulting from the convergence between the Adria microplate and the European platform. This is the major tectonic factor that dominated the evolution of the latest mantle deformation processes, which had already developed before the onset of metasomatism by the intraplate mafic melts. Finally, in the central part of the

volcanic field, the petrographic and geochemical evidence presented in this work points to the conclusion that the melt-rock reaction associated with the formation of the wehrlite suite may have been still active at the time the host basalt erupted.

References

Abramson, E.H., Brown, J.M., Slutsky, L.J., Zaug, J., 1997. The elastic constants of San Carlos olivine to 17 GPa. Journal of Geophysical Research: Solid Earth 102, 12253-12263.

Adam, J., Green, T., 1994. The effects of pressure and temperature on the partitioning of Ti, Sr and REE between amphibole, clinopyroxene and basanitic melts. Chemical Geology 117, 219-233.

Andersen, T., Neumann, E.-R., 2001. Fluid inclusions in mantle xenoliths. Lithos 55, 301-320.

Andersen, T., O'Reilly, S.Y., Griffin, W.L., 1984. The trapped fluid phase in upper mantle xenoliths from Victoria, Australia: implications for mantle metasomatism. Contributions to Mineralogy and Petrology 88, 72-85.

Aradi, L.E., Hidas, K., Kovács, I.J., Tommasi, A., Klébesz, R., Garrido, C.J., Szabó, C., 2017. Fluid-Enhanced Annealing in the Subcontinental Lithospheric Mantle Beneath the Westernmost Margin of the Carpathian-Pannonian Extensional Basin System. Tectonics doi:10.1002/2017TC004702.

Arai, S., 1994. Characterization of spinel peridotites by olivine-spinel compositional relationships: Review and interpretation. Chemical Geology 113, 191-204.

Aubaud, C., Hauri, E.H., Hirschmann, M.M., 2004. Hydrogen partition coefficients between nominally anhydrous minerals and basaltic melts. Geophysical Research Letters 31, doi:10.1029/2004GL021341.

Bada, G., Horváth, F., 2001. On the structure and tectonic of the Pannonian Basin and surrounding orogens. Acta Geologica Hungarica 44, 301-327.

Bada, G., Horváth, F., Dövényi, P., Szafián, P., Windhoffer, G., Cloetingh, S., 2007. Present-day stress field and tectonic inversion in the Pannonian basin. Global and Planetary Change 58, 165-180.

Balan, E., Blanchard, M., Yi, H., Ingrin, J., 2013. Theoretical study of OH-defects in pure enstatite. Physics and Chemistry of Minerals 40, 41-50.

Balázs, A., Burov, E., Matenco, L., Vogt, K., Francois, T., Cloetingh, S., 2017. Symmetry during the syn- and post-rift evolution of extensional back-arc basins: The role of inherited orogenic structures. Earth and Planetary Science Letters 462, 86-98.

Bali, E., Falus, G., Szabó, C., Peate, D.W., Hidas, K., Török, K., Ntaflos, T., 2007. Remnants of boninitic melts in the upper mantle beneath the central Pannonian Basin? Mineralogy and Petrology 90, 51-72.

Bali, E., Szabó, C., Vaselli, O., Török, K., 2002. Significance of silicate melt pockets in upper mantle xenoliths from the Bakony-Balaton Highland Volcanic Field, Western Hungary. Lithos 61, 79-102.

Bali, E., Zajacz, Z., Kovács, I., Szabó, C., Halter, W., Vaselli, O., Török, K., Bodnar, R.J., 2008a. A quartz-bearing orthopyroxene-rich websterite xenolith from the Pannonian Basin, Western Hungary: evidence for release of quartz-saturated melts from a subducted slab. Journal of Petrology 49, 421-439.

Bali, E., Zanetti, A., Szabó, C., Peate, D., Waight, T., 2008b. A micro-scale investigation of melt production and extraction in the upper mantle based on silicate melt pockets in ultramafic xenoliths from the Bakony–Balaton Highland Volcanic Field (Western Hungary). Contributions to Mineralogy and Petrology 155, 165-179.

Balintoni, I., 1994. Structure of the Apuseni mountains. Romanian Journal of Tectonics and Regional Geology 75, 9-14.

Balla, Z., 1984. The Carpathian loop and Pannonian Basin: a kinematic analysis. Geophysical Transactions 30, 313-355.

Balogh, K., Árva-Sós, E., Pécskay, Z., 1986. K/Ar dating of post Sarmatian alkali basaltic rocks in Hungary. Acta Mineralogie et Petrographie Szeged 28, 75-93.

Balogh, K., Mihaliková, A., Vass, D., 1981. Radiometric dating of basalts in southern and central Slovakia. Západné Karpaty, séria Geológia 7, 113-126.

Baptiste, V., Tommasi, A., 2014. Petrophysical constraints on the seismic properties of the Kaapvaal craton mantle root. Solid Earth Discuss. 5, 963-1005.

Baptiste, V., Tommasi, A., Demouchy, S., 2012. Deformation and hydration of the lithospheric mantle beneath the Kaapvaal craton, South Africa. Lithos 149, 31-50.

Barruol, G., Mainprice, D., 1993. A quantitative evaluation of the contribution of crustal rocks to the shear-wave splitting of teleseismic SKS waves. Physics of the Earth and Planetary Interiors 78, 281-300.

Bedini, R., Bodinier, J.-L., Dautria, J.-M., Morten, L., 1997. Evolution of LILE-enriched small melt fractions in the lithospheric mantle: a case study from the East African Rift. Earth and Planetary Science Letters 153, 67-83.

Bell, D.R., Ihinger, P.D., Rossman, G.R., 1995. Quantitative analysis of trace OH in garnet and pyroxenes. American Mineralogist 80, 465-474.

Bell, D.R., Rossman, G.R., 1992a. The distribution of hydroxyl in garnets from the subcontinental mantle of southern Africa. Contributions to Mineralogy and Petrology 111, 161-178.

Bell, D.R., Rossman, G.R., 1992b. Water in Earth's mantle: The role of nominally anhydrous minerals. Science 255, 1391-1397.

Bell, D.R., Rossman, G.R., Maldener, J., Endisch, D., Rauch, F., 2003. Hydroxide in olivine: a quantitative determination of the absolute amount and calibration of the IR spectrum. Journal of Geophysical Research: Solid Earth (1978–2012) 108, doi:10.1029/2001JB000679.

Ben Ismail, W., Mainprice, D., 1998. An olivine fabric database: an overview of upper mantle fabrics and seismic anisotropy. Tectonophysics 296, 145-157.

Berkesi, M., Guzmics, T., Szabó, C., Dubessy, J., Bodnar, R.J., Hidas, K., Ratter, K., 2012. The role of CO2-rich fluids in trace element transport and metasomatism in the lithospheric mantle beneath the Central Pannonian Basin, Hungary, based on fluid inclusions in mantle xenoliths. Earth and Planetary Science Letters 331, 8-20.

Berry, A.J., Hermann, J., O'Neill, H.S., Foran, G.J., 2005. Fingerprinting the water site in mantle olivine. Geology 33, 869-872.

Berry, A.J., O'Neill, H.S.C., Hermann, J., Scott, D.R., 2007a. The infrared signature of water associated with trivalent cations in olivine. Earth and Planetary Science Letters 261, 134-142.

Berry, A.J., Walker, A.M., Hermann, J., O'Neill, H.S.C., Foran, G.J., Gale, J.D., 2007b. Titanium substitution mechanisms in forsterite. Chemical Geology 242, 176-186.

Blackman, D.K., Wenk, H.-R., Kendall, J.M., 2002. Seismic anisotropy of the upper mantle 1. Factors that affect mineral texture and effective elastic properties. Geochemistry, Geophysics, Geosystems 3, 1-24.

Blanchard, M., Ingrin, J., Balan, E., Kovács, I.J., Withers, A.C., 2017. Effect of iron and trivalent cations on OH defects in olivine. American Mineralogist 102, 302-311.

Bodinier, J.-L., Godard, M., 2003. Orogenic, ophiolitic, and abyssal peridotites. Treatise on geochemistry 2, 568.

Bodinier, J.-L., Menzies, M.A., Shimizu, N., Frey, F.A., McPherson, E., 2004. Silicate, hydrous and carbonate metasomatism at Lherz, France: contemporaneous derivatives of silicate melt–harzburgite reaction. Journal of Petrology 45, 299-320.

Bodinier, J.-L., 1988. Geochemistry and petrogenesis of the Lanzo peridotite body, western Alps. Tectonophysics 149, 67-88.

Bodinier, J.-L., Dupuy, C., Dostal, J., 1988. Geochemistry and petrogenesis of Eastern Pyrenean peridotites. Geochimica et Cosmochimica Acta 52, 2893-2907.

Bodinier, J.-L., Vasseur, G., Vernières, J., Dupuy, C., Fabries, J., 1990. Mechanisms of mantle metasomatism: geochemical evidence from the Lherz orogenic peridotite. Journal of Petrology 31, 597-628.

Bollinger, C., Raterron, P., Cordier, P., Merkel, S., 2014. Polycrystalline olivine rheology in dislocation creep: Revisiting experimental data to 8.1 GPa. Physics of the Earth and Planetary Interiors 228, 211-219.

Bonadiman, C., Hao, Y., Coltorti, M., Dallai, L., Faccini, B., Huang, Y., Xia, Q., 2009. Water contents of pyroxenes in intraplate lithospheric mantle. European Journal of Mineralogy 21, 637-647.

Boyd, F.R., 1989. Compositional distinction between oceanic and cratonic lithosphere. Earth and Planetary Science Letters 96, 15-26.

Brey, G.P., Köhler, T., 1990. Geothermobarometry in four-phase lherzolites II. New thermobarometers, and practical assessment of existing thermobarometers. Journal of Petrology 31, 1353-1378.

Bunge, H., 1982. Texture analysis in materials science. Butterworth, London.

Bystricky, M., Kunze, K., Burlini, L., Burg, J.-P., 2000. High shear strain of olivine aggregates: rheological and seismic consequences. Science 290, 1564-1567.

Carter, N.L., Avé Lallemant, H.G., 1970. High temperature flow of dunite and peridotite. Bulletin of the Geological Society of America 81, 2181-2202.

Cherniak, D.J., Liang, Y., 2007. Rare earth element diffusion in natural enstatite. Geochimica et Cosmochimica Acta 71, 1324-1340.

Coltorti, M., Bonadiman, C., Faccini, B., Grégoire, M., O'Reilly, S.Y., Powell, W., 2007a.

Amphiboles from suprasubduction and intraplate lithospheric mantle. Lithos 99, 68-84.

Coltorti, M., Bonadiman, C., Faccini, B., Ntaflos, T., Siena, F., 2007b. Slab melt and intraplate metasomatism in Kapfenstein mantle xenoliths (Styrian Basin, Austria). Lithos 94, 66-89.

Coltorti, M., Bonadiman, C., Hinton, R., Siena, F., Upton, B., 1999. Carbonatite metasomatism of the oceanic upper mantle: evidence from clinopyroxenes and glasses in ultramafic xenoliths of Grande Comore, Indian Ocean. Journal of Petrology 40, 133-165.

Coogan, L.A., Jenkin, G.R., Wilson, R.N., 2002. Constraining the cooling rate of the lower oceanic crust: a new approach applied to the Oman ophiolite. Earth and Planetary Science Letters 199, 127-146.

Crampin, S., Chesnokov, E.M., Hipkin, R.G., 1984. Seismic anisotropy — the state of the art: II. Geophysical Journal International 76, 1-16.

Csontos, L., 1995. Tertiary tectonic evolution of the Intra-Carpathian area: a review. Acta Vulcanologica 7, 1-13.

Csontos, L., Nagymarosy, A., 1998. The Mid-Hungarian line: a zone of repeated tectonic inversions. Tectonophysics 297, 51-71.

Csontos, L., Nagymarosy, A., Horvath, F., Kovac, M., 1992. Tertiary evolution of the Intra-Carpathian area: A model. Tectonophysics 208, 221-241.

Csontos, L., Vörös, A., 2004. Mesozoic plate tectonic reconstruction of the Carpathian region. Palaeogeography Palaeoclimatology Palaeoecology 210, 1-56.

Cvetkovic, V., Lazarov, M., Downes, H., Prelevic, D., 2007. Modification of the subcontinental mantle beneath East Serbia: Evidence from orthopyroxene-rich xenoliths. Lithos 94, 90-110.

Dalpé, C., Baker, D.R., 2000. Experimental investigation of large-ion-lithophile-element-, high-field-strength-element-and rare-earth-element-partitioning between calcic amphibole and basaltic melt: the effects of pressure and oxygen fugacity. Contributions to Mineralogy and Petrology 140, 233-250.

Dando, B.D.E., Stuart, G.W., Houseman, G.A., Hegedüs, E., Brückl, E., Radovanović, S., 2011. Teleseismic tomography of the mantle in the Carpathian–Pannonian region of central Europe. Geophysical Journal International 186, 11-31.

Danyushevsky, L.V., Eggins, S.M., Falloon, T.J., Christie, D.M., 2000. H2O abundance in depleted to moderately enriched mid-ocean ridge magmas; Part I: incompatible behaviour, implications for mantle storage, and origin of regional variations. Journal of Petrology 41, 1329-1364.

Demouchy, S., Bolfan-Casanova, N., 2016. Distribution and transport of hydrogen in the lithospheric mantle: A review. Lithos 240, 402-425.

Demouchy, S., Jacobsen, S.D., Gaillard, F., Stern, C.R., 2006. Rapid magma ascent recorded by water diffusion profiles in mantle olivine. Geology 34, 429-432.

Demouchy, S., Mackwell, S., 2003. Water diffusion in synthetic iron-free forsterite. Physics and Chemistry of Minerals 30, 486-494.

Demouchy, S., Tommasi, A., Barou, F., Mainprice, D., Cordier, P., 2012. Deformation of olivine in torsion under hydrous conditions. Physics of the Earth and Planetary Interiors 202, 56-70.

Denis, C.M.M., Demouchy, S., Shaw, C.S., 2013. Evidence of dehydration in peridotites from Eifel Volcanic Field and estimates of the rate of magma ascent. Journal of Volcanology and Geothermal Research 258, 85-99.

Denis, C.M.M., Alard, O., Demouchy, S., 2015. Water content and hydrogen behaviour during metasomatism in the uppermost mantle beneath Ray Pic volcano (Massif Central, France). Lithos 236-237, 256-274.

Dobosi, G., Fodor, R.V., Goldberg, S.A., 1995. Late-Cenozoic alkali basalt magmatism in Northern Hungary and Slovakia: petrology, source compositions and relationship to tectonics. 7, 199-207.

Dobosi, G., Jenner, G., 1999. Petrologic implications of trace element variation in clinopyroxene megacrysts from the Nograd volcanic province, north Hungary: a study by laser ablation microprobe-inductively coupled plasma-mass spectrometry. Lithos 46, 731-749.

Dombrádi, E., Sokoutis, D., Bada, G., Cloetingh, S., Horváth, F., 2010. Modelling recent deformation of the Pannonian lithosphere: lithospheric folding and tectonic topography. Tectonophysics 484, 103-118.

Doucet, L.S., Peslier, A.H., Ionov, D.A., Brandon, A.D., Golovin, A.V., Goncharov, A.G., Ashchepkov, I.V., 2014. High water contents in the Siberian cratonic mantle linked to metasomatism: An FTIR study of Udachnaya peridotite xenoliths. Geochimica et Cosmochimica Acta 137, 159-187.

Downes, H., 1990. Shear zones in the upper mantle—relation between geochemical enrichment and deformation in mantle peridotites. Geology 18, 374-377.

Downes, H., 1997. Shallow continental lithospheric mantle heterogeneity—petrological constraints, in: Fuchs, K. (Ed.), Upper Mantle Heterogeneities from Active and Passive Seismology. Springer, pp. 295-308.

Downes, H., 2001. Formation and Modification of the Shallow Sub-continental Lithospheric Mantle: a Review of Geochemical Evidence from Ultramafic Xenolith Suites and Tectonically Emplaced Ultramafic Massifs of Western and Central Europe. Journal of Petrology 42, 233-250.

Downes, H., Embey-Isztin, A., Thirlwall, M.F., 1992. Petrology and geochemistry of spinel peridotite xenoliths from the western Pannonian Basin (Hungary): evidence for an association between enrichment and texture in the upper mantle. Contributions to Mineralogy and Petrology 109, 340-354.

Downes, H., Seghedi, I., Szakacs, A., Dobosi, G., James, D.E., Vaselli, O., Rigby, I.J., Ingram, G.A., Rex, D., Pecskay, Z., 1995. Petrology and geochemistry of late Tertiary/Quaternary mafic alkaline volcanism in Romania. Lithos 35, 65-81.

Downes, H., Vaselli, O., 1995. The lithospheric mantle beneath the Carpathian-Pannonian Region: a review of trace element and isotopic evidence from ultramafic xenoliths. Acta Vulcanologica 7, 219-230.

Drury, M.R., Vissers, R.L., Van der Wal, D., Strating, E.H.H., 1991. Shear localisation in

upper mantle peridotites. Pure and Applied Geophysics 137, 439-460.

Embey-Isztin, A., 1978. On the petrology of spinel lherzolite nodules in basaltic rocks from Hungary and Auvergne, France. Annales Historico-Naturales Musei Nationalis Hungarici 70, 27-44.

Embey-Isztin, A., 1984. Texture types and their relative frequencies in ultramafic and mafic xenoliths from Hungarian alkali basaltic rocks. Annales Historico-Naturales Musei Nationalis Hungarici 76, 27-42.

Embey-Isztin, A., Dobosi, G., 1995. Mantle source characteristics for Miocene-Pleistocene alkali basalts, Carpathian-Pannonian Region: a review of trace elements and isotopic composition., in: Downes, H., Vaselli, O. (Eds.), Neogene and related volcanism in the Carpatho-Pannonian Region. Acta Vulcanologica, pp. 155-166.

Embey-Isztin, A., Dobosi, G., Altherr, R., Meyer, H.P., 2001. Thermal evolution of the lithosphere beneath the western Pannonian Basin: evidence from deep-seated xenoliths. Tectonophysics 331, 285-306.

Embey-Isztin, A., Dobosi, G., Bodinier, J.-L., Bosch, D., Jenner, G., Pourtales, S., Bruguier, O., 2014. Origin and significance of poikilitic and mosaic peridotite xenoliths in the western Pannonian Basin: geochemical and petrological evidences. Contributions to Mineralogy and Petrology 168, 1-16.

Embey-Isztin, A., Downes, H., James, D.E., Upton, B.G.J., Dobosi, G., Ingram, G.A., Harmon, R.S., Scharbert, H.G., 1993. The petrogenesis of Pliocene alkaline volcanic rocks from the Pannonian Basin, Eastern Central Europe. Journal of Petrology 34, 317-343.

Embey-Isztin, A., Scharbert, H., Dietrich, H., Poultidis, H., 1990. Mafic granulites and clinopyroxenite xenoliths from the Transdanubian Volcanic Region (Hungary): implications for the deep structure of the Pannonian Basin. Mineralogical Magazine 54, 463-483.

Embey-Isztin, A., Scharbert, H.G., 2000. Glasses in peridotite xenoliths from the western Pannonian basin. Annales Historico-Naturales Musei Nationalis Hungarici 92, 5-20.

Embey-Isztin, A., Scharbert, H.G., Dietrich, H., Poultidis, H., 1989. Petrology and geochemistry of peridotite xenoliths in alkali basalts from the Transdanubian Volcanic Region, West Hungary. Journal of Petrology 30, 79-105.

Faccini, B., Bonadiman, C., Coltorti, M., Grégoire, M., Siena, F., 2013. Oceanic material recycled within the sub-Patagonian lithospheric mantle (Cerro del Fraile, Argentina). Journal of Petrology 54, 1211-1258.

Fall, A., Tattitch, B., Bodnar, R.J., 2011. Combined microthermometric and Raman spectroscopic technique to determine the salinity of H2O–CO2–NaCl fluid inclusions based on clathrate melting. Geochimica et Cosmochimica Acta 75, 951-964.

Falus, G., 2004. Microstructural analysis of upper mantle peridotites: their application in understanding mantle processes during the formation of the Intra-Carpathian Basin System. Lithosphere Fluid Research Lab, Eötvös Loránd University, Budapest, p. 163.

Falus, G., Szabó, C., Kovács, I., Zajacz, Z., Halter, W., 2007. Symplectite in spinel lherzolite xenoliths from the Little Hungarian Plain, Western Hungary: A key for

understanding the complex history of the upper mantle of the Pannonian Basin. Lithos 94, 230-247.

Falus, G., Szabó, C., Vaselli, O., 2000. Mantle upwelling within the Pannonian Basin: evidence from xenolith lithology and mineral chemistry. Terra Nova 12, 295-302.

Falus, G., Tommasi, A., Ingrin, J., Szabó, C., 2008. Deformation and seismic anisotropy of the lithospheric mantle in the southeastern Carpathians inferred from the study of mantle xenoliths. Earth and Planetary Science Letters 272, 50-64.

Fermi, E., 1931. Über den Ramaneffekt des Kohlendioxyds. Zeitschrift für Physik 71, 250-259.

Férot, A., Bolfan-Casanova, N., 2012. Water storage capacity in olivine and pyroxene to 14 GPa: Implications for the water content of the Earth's upper mantle and nature of seismic discontinuities. Earth and Planetary Science Letters 349, 218-230.

Fitton, J.G., 1995. Coupled molybdenum and niobium depletion in continental basalts. Earth and Planetary Science Letters 136, 715-721.

Fodor, L., Bada, G., Csillag, G., Horváth, E., Ruszkiczay-Rüdiger, Z., Palotás, K., Síkhegyi, F., Timár, G., Cloetingh, S., Horváth, F., 2005. An outline of neotectonic structures and morphotectonics of the western and central Pannonian Basin. Tectonophysics 410, 15-41.

Fodor, L., Csontos, L., Bada, G., Györfi, I., Benkovics, L., 1999. Tertiary tectonic evolution of the Pannonian basin system and neighbouring orogens: a new synthesis of palaeostress data., in: Durand, B., Jolivet, L., F., H., Séranne, M. (Eds.), The Mediterranean Basins: Tertiary Extension within the Alpine Orogen. - Geological Society, London, Special Publications, pp. 295-334.

Fodor, L., Jelen, B., Márton, E., Skaberne, D., Čar, J., Vrabec, M., 1998. Miocene-Pliocene tectonic evolution of the Slovenian Periadriatic fault: Implications for Alpine-Carpathian extrusion models. Tectonics 17, 690-709.

Fodor, L., Magyari, Á., Kázmér, M., Fogarasi, A., 1992. Gravity-flow dominated sedimentation on the Buda paleoslope (Hungary): Record of Late Eocene continental escape of the Bakony unit. Geologische Rundschau 81, 695-716.

Foley, S.F., Barth, M.G., Jenner, G.A., 2000. Rutile/melt partition coefficients for trace elements and an assessment of the influence of rutile on the trace element characteristics of subduction zone magmas. Geochimica et Cosmochimica Acta 64, 933-938.

Frey, F.A., Green, D.H., 1974. The mineralogy, geochemistry and origin of Iherzolite inclusions in Victorian basanites. Geochimica et Cosmochimica Acta 38, 1023-1059.

Frey, F.A., Prinz, M., 1978. Ultramafic inclusions from San Carlos, Arizona: petrologic and geochemical data bearing on their petrogenesis. Earth and Planetary Science Letters 38, 129-176.

Frey, F.A., Suen, C.J., Stockman, H.W., 1985. The Ronda high temperature peridotite: geochemistry and petrogenesis. Geochimica et Cosmochimica Acta 49, 2469-2491.

Frezzotti, M.-L., 2001. Silicate-melt inclusions in magmatic rocks: applications to petrology. Lithos 55, 273-299.

Frezzotti, M.-L., Touret, J.L., 2014. CO_2, carbonate-rich melts, and brines in the mantle.

Geoscience Frontiers 5, 697-710.

Frezzotti, M.L., De Vivo, B., Clocchiatti, R., 1991. Melt-mineral-fluid interactions in ultramafic nodules from alkaline lavas of Mount Etna (Sicily, Italy): Melt and fluid inclusion evidence. Journal of Volcanology and Geothermal Research 47, 209-219.

Frezzotti, M.L., Tecce, F., Casagli, A., 2012. Raman spectroscopy for fluid inclusion analysis. Journal of Geochemical Exploration 112, 1-20.

Géczy, B., 1973. Plate tectonics and paleogeography in the East-Mediterranean Mesozoic. Acta Geol. Hung 17, 421-428.

Géczy, B., 1984. Provincialism of Jurassic ammonites: examples from Hungarian faunas. Acta Geologica Hungarica 27, 379-389.

Gemmer, L., Houseman, G.A., 2007. Convergence and extension driven by lithospheric gravitational instability: evolution of the Alpine–Carpathian–Pannonian system. Geophysical Journal International 168, 1276-1290.

Girard, J., Chen, J., Raterron, P., Holyoke, C.W., 2013. Hydrolytic weakening of olivine at mantle pressure: Evidence of [100](010) slip system softening from single-crystal deformation experiments. Physics of the Earth and Planetary Interiors 216, 12-20.

Grant, K., Ingrin, J., Lorand, J.P., Dumas, P., 2007. Water partitioning between mantle minerals from peridotite xenoliths. Contributions to Mineralogy and Petrology 154, 15-34.

Green, D., 1973. Experimental melting studies on a model upper mantle composition at high pressure under water-saturated and water-undersaturated conditions. Earth and Planetary Science Letters 19, 37-53.

Green, D.H., Hibberson, W.O., Kovács, I., Rosenthal, A., 2010. Water and its influence on the lithosphere-asthenosphere boundary. Nature 467, 448-451.

Green, H., Griggs, D., Christie, J., 1970. Syntectonic and annealing recrystallization of fine-grained quartz aggregates, in: Paulitsch, P. (Ed.), Experimental and Natural Rock Deformation. Springer Verlag, Berlin, pp. 272-335.

Green, H., Radcliffe, S., 1972. Deformation processes in the upper mantle, in: Heard, H.C., Borg, I.Y., Carter, N.L., Raleigh, C.B. (Eds.), Flow and fracture of rocks. AGU, Washington D. C., pp. 139-156.

Griffin, W., O'Reilly, S.Y., 1987. Is the continental Moho the crust-mantle boundary? Geology 15, 241-244.

Griffin, W., Powell, W., Pearson, N., O'Reilly, S., 2008. GLITTER: data reduction software for laser ablation ICP-MS. Laser Ablation-ICP-MS in the earth sciences. Mineralogical Association of Canada short courses 40, 204-207.

Griffin, W.L., Wass, S.Y., Hollis, J.D., 1984. Ultramafic Xenoliths from Bullenmerri and Gnotuk Maars, Victoria, Australia: Petrology of a Sub-Continental Crust-Mantle Transition. Journal of Petrology 25, 53-87.

Guillong, M., Meier, D., Allan, M., Heinrich, C., Yardley, B., 2008. SILLS: a MATLAB-based program for the reduction of laser ablation ICP-MS data of homogeneous materials and inclusions. Mineralogical Association of Canada short courses 40, 328-333.

Hámor, G., Ravasz-Baranyai, L., Halmai, J., Balogh, K., Árva-Sós, E., 1987. Dating of Miocene acid and intermediate volcanic activity in Hungary. Ann Hung Geol Inst 70, 149-154.

Hansen, L.N., Zhao, Y.-H., Zimmerman, M.E., Kohlstedt, D.L., 2014. Protracted fabric evolution in olivine: Implications for the relationship among strain, crystallographic fabric, and seismic anisotropy. Earth and Planetary Science Letters 387, 157-168.

Hao, Y.T., Xia, Q.K., Jia, Z.B., Zhao, Q.C., Li, P., Feng, M., Liu, S.C., 2016. Regional heterogeneity in the water content of the Cenozoic lithospheric mantle of Eastern China. Journal of Geophysical Research: Solid Earth 121, 517-537.

Harangi, S., 2001. Neogene to Quaternary volcanism of the Carpathian-Pannonian Region - A review. Acta Geologica Hungarica 44, 223-258.

Harangi, S., Jankovics, M.É., Sági, T., Kiss, B., Lukács, R., Soós, I., 2015. Origin and geodynamic relationships of the Late Miocene to Quaternary alkaline basalt volcanism in the Pannonian basin, eastern–central Europe. International Journal of Earth Sciences 104, 2007-2032.

Harangi, S., Lenkey, L., 2007. Genesis of the Neogene to Quaternary volcanism in the Carpathian-Pannonian region: Role of subduction, extension, and mantle plume, in: Beccaluva, L., Bianchini, G., Wilson, M. (Eds.), Special Paper 418: Cenozoic Volcanism in the Mediterranean Area, pp. 67-92.

Harangi, S., Vaselli, O., Tonarini, S., Szabó, C., Harangi, R., Coradossi, N., 1995a. Petrogenesis of Neogene extension-related alkaline volcanic rocks of the Little Hungarian Plain Volcanic Field (Western Hungary). in: Downes, H., Vaselli, O. (Eds.), Neogene and related magmatism in the Carpatho-Pannonian Region. Acta Vulcanologica, pp. 173-187.

Harangi, S., Wilson, M., Tonarini, S., 1995b. Petrogenesis of Neogene potassic volcanic rocks in the Pannonian Basin. Acta Vulcanologica 7, 125-134.

Hart, S.R., Dunn, T., 1993. Experimental cpx/melt partitioning of 24 trace elements. Contributions to Mineralogy and Petrology 113, 1-8.

Harte, B., 1977. Rock Nomenclature with Particular Relation to Deformation and Recrystallisation Textures in Olivine-Bearing Xenoliths. The Journal of Geology 85, 279-288.

Hauri, E.H., Gaetani, G.A., Green, T.H., 2006. Partitioning of water during melting of the Earth's upper mantle at H_2O-undersaturated conditions. Earth and Planetary Science Letters 248, 715-734.

Hellebrand, E., Snow, J.E., Dick, H.J., Hofmann, A.W., 2001. Coupled major and trace elements as indicators of the extent of melting in mid-ocean-ridge peridotites. Nature 410, 677-681.

Herwegh, M., Linckens, J., Ebert, A., Berger, A., Brodhag, S., 2011. The role of second phases for controlling microstructural evolution in polymineralic rocks: A review. Journal of Structural Geology 33, 1728-1750.

Herzberg, C., 2004. Partial melting below the Ontong Java Plateau, in: Fitton, J.G., Mahoney, J.J., Wallace, P.J., Saunders, A.D. (Eds.), Origin and Evolution of the Ontong Java Plateau. The Geological Society of London, London, pp. 179-183.

Hidas, K., Falus, G., Szabó, C., Szabó, P.J., Kovács, I., Földes, T., 2007. Geodynamic implications of flattened tabular equigranular textured peridotites from the Bakony-Balaton Highland Volcanic Field (Western Hungary). Journal of Geodynamics 43, 484-503.

Hidas, K., Konc, Z., Garrido, C.J., Tommasi, A., Vauchez, A., Padrón-Navarta, J.A., Marchesi, C., Booth-Rea, G., Acosta-Vigil, A., Szabó, C., Varas-Reus, M.I., Gervilla, F., 2016. Flow in the western Mediterranean shallow mantle: Insights from xenoliths in Pliocene alkali basalts from SE Iberia (eastern Betics, Spain). Tectonics 35, 2657-2676.

Hielscher, R., Schaeben, H., 2008. A novel pole figure inversion method: specification of the MTEX algorithm. Journal of Applied Crystallography 41, 1024-1037.

Higgie, K., Tommasi, A., 2012. Feedbacks between deformation and melt distribution in the crust–mantle transition zone of the Oman ophiolite. Earth and Planetary Science Letters 359, 61-72.

Holtzman, B.K., Kohlstedt, D.L., Zimmerman, M.E., Heidelbach, F., Hiraga, T., Hustoft, J., 2003. Melt Segregation and Strain Partitioning: Implications for Seismic Anisotropy and Mantle Flow. Science 301, 1227-1230.

Horváth, F., 1993. Towards a mechanical model for the formation of the Pannonian basin. Tectonophysics 226, 333-357.

Horváth, F., 1995. Phases of compression during the evolution of the Pannonian Basin and its bearing on hydrocarbon exploration. Marine and Petroleum Geology 12, 837-844.

Horváth, F., Bada, G., Szafián, P., Tari, G., Ádám, A., Cloetingh, S., 2006. Formation and deformation of the Pannonian Basin: constraints from observational data. Geological Society, London, Memoirs 32, 191-206.

Horvath, F., Cloetingh, S., 1996. Stress-induced late-stage subsidence anomalies in the Pannonian basin. Tectonophysics 266, 287-300.

Houseman, G.A., Gemmer, L., 2007. Intra-orogenic extension driven by gravitational instability: Carpathian-Pannonian orogeny. Geology 35, 1135-1138.

Hovorka, D., Fejdi, P., 1980. Spinel peridotite xenoliths in the West Carpathian late cenozoic alkali basalts and their tectonic significance. Bulletin of Volcanology 43, 95-106.

Huebner, J., Turnock, A., 1980. The melting relations at 1 bar of pyroxenes composed largely of Ca-, Mg-, and Fe-bearing components. American Mineralogist 65, 225-271.

Huismans, R.S., Podladchikov, Y.Y., Cloetingh, S., 2001. Dynamic modeling of the transition from passive to active rifting, application to the Pannonian basin. Tectonics 20, 1021-1039.

Hurai, V., Danišík, M., Huraiová, M., Paquette, J.-L., Ádám, A., 2013. Combined U/Pb and (U–Th)/He geochronometry of basalt maars in Western Carpathians: implications for age of intraplate volcanism and origin of zircon metasomatism. Contributions to Mineralogy and Petrology 166, 1235-1251.

Huraiová, M., Konecny, P., 1994. Pressure-temperature conditions and oxidation state of the upper mantle in southern Slovakia. Acta Geologica Hungarica 37, 29-39.

Ingrin, J., Blanchard, M., 2006. Diffusion of hydrogen in minerals. Reviews in Mineralogy and Geochemistry 62, 291-320.

Ingrin, J., Kovács, I.J., Deloule, E., Balan, E., Blanchard, M., Kohn, S.C., Hermann, J., 2014. Identification of hydrogen defects linked to boron substitution in synthetic forsterite and natural olivine. American Mineralogist 99, 2138-2141.

Ingrin, J., Liu, J., Depecker, C., Kohn, S.C., Balan, E., Grant, K.J., 2013. Low-temperature evolution of OH bands in synthetic forsterite, implication for the nature of H defects at high pressure. Physics and Chemistry of Minerals 40, 499-510.

Ionov, D.A., Bodinier, J.-L., Mukasa, S.B., Zanetti, A., 2002. Mechanisms and sources of mantle metasomatism: major and trace element compositions of peridotite xenoliths from Spitsbergen in the context of numerical modelling. Journal of Petrology 43, 2219-2259.

Ionov, D.A., Chanefo, I., Bodinier, J.-L., 2005. Origin of Fe-rich lherzolites and wehrlites from Tok, SE Siberia by reactive melt percolation in refractory mantle peridotites. Contributions to Mineralogy and Petrology 150, 335-353.

Irving, A.J., 1980. Petrology and geochemistry of composite ultramafic xenoliths in alkalic basalts and implications for magmatic processes within the mantle. American Journal of Science 280, 389-426.

Isaak, D.G., Ohno, I., Lee, P.C., 2006. The elastic constants of monoclinic single-crystal chrome-diopside to 1,300 K. Physics and Chemistry of Minerals 32, 691-699.

Jackson, J.M., Sinogeikin, S.V., Bass, J.D., 2007. Sound velocities and single-crystal elasticity of orthoenstatite to 1073 K at ambient pressure. Physics of the Earth and Planetary Interiors 161, 1-12.

Jaroslow, G., Hirth, G., Dick, H., 1996. Abyssal peridotite mylonites: implications for grain-size sensitive flow and strain localization in the oceanic lithosphere. Tectonophysics 256, 17-37.

Jones, A.P., Smith, J.V., Dawson, J.B., Hansen, E.C., 1983. Metamorphism, Partial Melting, and K-Metasomatism of Garnet-Scapolite-Kyanite Granulite Xenoliths from Lashaine, Tanzania. The Journal of Geology 91, 143-165.

Jugovics, L., 1971. Észak-magyarországi-Salgótarján környéki-bazaltterületek (North Hungarian basaltic areas in the vicinty of Salgótarján). Annual report of the Geological Institute of Hungary (1968), 145-165.

Jung, H., Karato, S.-I., 2001. Water-induced fabric transitions in olivine. Science 293, 1460-1463.

Jung, H., Katayama, I., Jiang, Z., Hiraga, T., Karato, S.-I., 2006. Effect of water and stress on the lattice-preferred orientation of olivine. Tectonophysics 421, 1-22.

Kaczmarek, M.-A., Tommasi, A., 2011. Anatomy of an extensional shear zone in the mantle, Lanzo massif, Italy. Geochemistry, Geophysics, Geosystems 12, doi:10.1029/2011GC003627.

Karato, S.-i., Wu, P., 1993. Rheology of the upper mantle: a synthesis. Science 260, 771-778.

Kázmér, M., Kovács, S., 1985. Permian-Paleogene paleogeography along the eastern part

of the Insubric-Periadriatic lineament system: evidence for continental escape of the Bakony-Drauzug Unit. Acta Geologica Hungarica 28, 71-84.

Kelemen, P., Hirth, G., Shimizu, N., Spiegelman, M., Dick, H., 1997. A review of melt migration processes in the adiabatically upwelling mantle beneath oceanic spreading ridges. Philosophical Transactions of the Royal Society of London. Series A: Mathematical, Physical and Engineering Sciences 355, 283-318.

Kelemen, P.B., Dick, H.J., Quick, J.E., 1992. Formation of harzburgite by pervasive melt/rock reaction in the upper mantle. Nature 358, 635-641.

Klébesz, R., Gráczer, Z., Szanyi, G., Liptai, N., Kovács, I., Patkó, L., Pintér, Z., Falus, G., Wesztergom, V., Szabó, C., 2015. Constraints on the thickness and seismic properties of the lithosphere in an extensional setting (Nógrád-Gömör Volcanic Field, Northern Pannonian Basin). Acta Geodaetica et Geophysica 50, 133-149.

Kohlstedt, D.L., Mackwell, S.J., 1998. Diffusion of hydrogen and intrinsic point defects in olivine. Zeitschrift für physikalische Chemie 207, 147-162.

Konecna, M., 1990. Fluidne inkluzie a termodynamicke pod mienky vzniku xenolitov spinelovych lherzolitov v alka lickych bazaltoch juzneho Slovenska. Mineralia Slovaca 22, 555-564.

Konečný, P., Huraiová, M., Bielik, M., 1999a. P-T-X-fO_2 conditions in upper mantle: evidence from lherzolitic xenoliths hosted by Plio-Pleistocene alkali basalts. Geolines 9, 59-66.

Konečný, P., Konečný, V., Lexa, J., Huraiová, M., 1995. Mantle xenoliths in alkali basalts of Southern Slovakia. Acta Vulcanologica 7, 241-248.

Konecný, V., Kovác, M., Lexa, J., Šefara, J., 2002. Neogene evolution of the Carpatho-Pannonian region: an interplay of subduction and back-arc diapiric uprise in the mantle. EGU Stephan Mueller Special Publication Series 1, 105-123.

Konečný, V., Lexa, J., Balogh, K., 1999b. Neogene-Quaternary alkali basalt volcanism in central and southern Slovakia (Western Carpathians). Geolines 9, 67-75.

Konecný, V., Lexa, J., Balogh, K., Konecný, P., 1995. Alkali basalt volcanism in Southern Slovakia: volcanic forms and time evolution. Acta Vulcanologica 7, 167-171.

Kourim, F., Bodinier, J.-L., Alard, O., Bendaoud, A., Vauchez, A., Dautria, J.-M., 2014. Nature and evolution of the lithospheric mantle beneath the Hoggar Swell (Algeria): a record from mantle xenoliths. Journal of Petrology 55, 2249-2280.

Kourim, F., Vauchez, A., Bodinier, J.-L., Alard, O., Bendaoud, A., 2015. Subcontinental lithosphere reactivation beneath the Hoggar swell (Algeria): Localized deformation, melt channeling and heat advection. Tectonophysics 650, 18-33.

Kovács, I., Falus, G., Stuart, G., Hidas, K., Szabó, C., Flower, M.J., Hegedűs, E., Posgay, K., Zilahi-Sebess, L., 2012a. Seismic anisotropy and deformation patterns in upper mantle xenoliths from the central Carpathian–Pannonian region: Asthenospheric flow as a driving force for Cenozoic extension and extrusion? Tectonophysics 514-517, 168-179.

Kovács, I., Falus, G., Szabó, C., Kiss, J., Fancsik, T., Hegedűs, E., Pintér, Z., 2013. Integrated geological and geophysical probing of lithospheric dynamics in a young

extensional basin (Carpathian-Pannonian Region). Mineralogical Magazine 77, 1504.

Kovács, I., Green, D.H., Rosenthal, A., Hermann, J., O'Neill, H.S.C., Hibberson, W.O., Udvardi, B., 2012b. An experimental study of water in nominally anhydrous minerals in the upper mantle near the water-saturated solidus. Journal of Petrology 53, 2067-2093.

Kovács, I., Hermann, J., O'Neill, H.S.C., Gerald, J.F., Sambridge, M., Horváth, G., 2008. Quantitative absorbance spectroscopy with unpolarized light: Part II. Experimental evaluation and development of a protocol for quantitative analysis of mineral IR spectra. American Mineralogist 93, 765-778.

Kovács, I., Szabó, C., 2005. Petrology and geochemistry of granulite xenoliths beneath the Nógrád-Gömör Volcanic Field, Carpathian-Pannonian Region (N-Hungary/S-Slovakia). Mineralogy and Petrology 85, 269-290.

Kovács, I., Szabó, C., 2008. Middle Miocene volcanism in the vicinity of the Middle Hungarian zone: Evidence for an inherited enriched mantle source. Journal of Geodynamics 45, 1-17.

Kovács, I., Zajacz, Z., Szabó, C., 2004. Type-II xenoliths and related metasomatism from the Nógrád-Gömör Volcanic Field, Carpathian-Pannonian region (northern Hungary–southern Slovakia). Tectonophysics 393, 139-161.

Kovács, S., Szederkényi, T., Haas, J., Hámor, G., Nagymarosy, A., 2000. Tectonostratigraphic terranes in the pre-Neogene basement of the Hungarian part of the Pannonian area. Acta Geologica Hungarica 43, 225-328.

Kozlovsky, Y.A., 1987. The superdeep well of the Kola Peninsula. Springer Verlag, Berlin-Heidelberg.

Kurat, G., 1971. Granat-Spinell-Websterit und Lherzolith aus dem Basalttuff von Kapfenstein, Steiermark. Tschermaks mineralogische und petrographische Mitteilungen 16, 192-214.

Kurat, G., Embey-Isztin, A., Kracher, A., Scharbert, H.G., 1991. The upper uantle beneath Kapfenstein and the Transdanubian Volcanic Region, E-Austria and W-Hungary - a comparison. Mineralogy and Petrology 44, 21-38.

Lankreijer, A., Kováč, M., Cloetingh, S., Pitoňák, P., Hlôška, M., Biermann, C., 1995. Quantitative subsidence analysis and forward modelling of the Vienna and Danube basins: thin-skinned versus thick-skinned extension. Tectonophysics 252, 433-451.

LaTourrette, T., Hervig, R.L., Holloway, J.R., 1995. Trace element partitioning between amphibole, phlogopite, and basanite melt. Earth and Planetary Science Letters 135, 13-30.

Le Bas, M.J., Le Maitre, R.W., Streckeisen, A., Zanettin, B., 1986. A chemical classification of volcanic rocks based on the total alkali-silica diagram. Journal of Petrology 27, 745-750.

Le Roux, V., Bodinier, J.-L., Tommasi, A., Alard, O., Dautria, J.-M., Vauchez, A., Riches, A., 2007. The Lherz spinel lherzolite: refertilized rather than pristine mantle. Earth and Planetary Science Letters 259, 599-612.

Leake, B.E., Woolley, A.R., Arps, C.E.S., Brich, W.D., Gilbert, M.C., Grice, J.D.,

Hawthorne, F.C., Kato, A., Kisch, H.J., G., K.V., Kees, L., Laird, J., Mandarino, J.A., Maresch, W.V., Nickel, E.H., Rock, N.M.S., Schumacher, J.C., Smith, D.C., Stephenson, N.C.N., Ungaretti, L., Whittaker, E.J.W., Youzhi, G., 1997. Nomenclature of amphiboles: report of the subcommittee on amphiboles of the International Mineralogical Assiciation, Commission on new minerals and mineral names. The Canadian Mineralogist 35, 219-246.

Lemaire, C., Kohn, S., Brooker, R., 2004. The effect of silica activity on the incorporation mechanisms of water in synthetic forsterite: a polarised infrared spectroscopic study. Contributions to Mineralogy and Petrology 147, 48-57.

Lenkey, L., Dövényi, P., Horváth, F., Cloetingh, S., 2002. Geothermics of the Pannonian Basin and its bearing on the neotectonics. EGU Stephan Mueller Special Publications Series 3, 29-40.

Lenoir, X., Garrido, C.J., Bodinier, J.-L., Dautria, J.-M., 2000. Contrasting lithospheric mantle domains beneath the Massif Central (France) revealed by geochemistry of peridotite xenoliths. Earth and Planetary Science Letters 181, 359-375.

Lexa, J., Konečný, V., 1974. The Carpathian Volcanic Arc: a discussion. Acta Geologica Hungarica 18, 279-294.

Lexa, J., Konečný, V., 1998. Geodynamic aspects of the Neogene to Quaternary volcanism, in: Rakús, M. (Ed.), Geodynamic development of the Western Carpathians. Geological Survey of Slovak Republik, Bratislava, pp. 219-240.

Lexa, J., Seghedi, I., Németh, K., Szakács, A., Konečný, V., Pécskay, Z., Fülöp, A., Kovacs, M., 2010. Neogene-Quaternary Volcanic forms in the Carpathian-Pannonian Region: a review. Central European Journal of Geosciences 2, 207-270.

Liang, Y., Schiemenz, A., Hesse, M.A., Parmentier, E.M., Hesthaven, J.S., 2010. High-porosity channels for melt migration in the mantle: Top is the dunite and bottom is the harzburgite and lherzolite. Geophysical Research Letters 37, doi:10.1029/2010GL044162.

Liang, Y., Sun, C., Yao, L., 2013. A REE-in-two-pyroxene thermometer for mafic and ultramafic rocks. Geochimica et Cosmochimica Acta 102, 246-260.

Linckens, J., Herwegh, M., Müntener, O., Mercolli, I., 2011. Evolution of a polymineralic mantle shear zone and the role of second phases in the localization of deformation. Journal of Geophysical Research: Solid Earth 116, doi:10.1029/2010JB008119.

Liptai, N., Jung, H., Park, M., Szabó, C., 2013. Olivine orientation study on upper mantle xenoliths from Bárna-Nagykő, Nógrád-Gömör Volcanic Field (Northern Pannonian Basin, Hungary). Bulletin of the Hungarian Geological Society (in Hungarian with English abstract) 143, 371-382.

Liptai, N., Patkó, L., Kovács, I.J., Hidas, K., Pintér, Z., Jeffries, T., Zajacz, Z., O'Reilly, S.Y., Griffin, W.L., Pearson, N.J., Szabó, C., 2017. Multiple Metasomatism beneath the Nógrád–Gömör Volcanic Field (Northern Pannonian Basin) Revealed by Upper Mantle Peridotite Xenoliths. Journal of Petrology 58, 1107-1144.

Lloyd, A.S., Ferriss, E., Ruprecht, P., Hauri, E.H., Jicha, B.R., Plank, T., 2016. An assessment of clinopyroxene as a recorder of magmatic water and magma ascent rate. Journal of Petrology 57, 1865-1886.

Lloyd, A.S., Plank, T., Ruprecht, P., Hauri, E.H., Rose, W., 2013. Volatile loss from melt inclusions in pyroclasts of differing sizes. Contributions to Mineralogy and Petrology 165, 129-153.

Locock, A.J., 2014. An Excel spreadsheet to classify chemical analyses of amphiboles following the IMA 2012 recommendations. Computers & Geosciences 62, 1-11.

Mackwell, S., Kohlstedt, D., Paterson, M., 1985. The role of water in the deformation of olivine single crystals. Journal of Geophysical Research: Solid Earth 90, 11319-11333.

Mackwell, S.J., Kohlstedt, D.L., 1990. Diffusion of hydrogen in olivine: Implications for water in the mantle. Journal of Geophysical Research: Solid Earth 95, 5079-5088.

Mainprice, D., 1990. A FORTRAN program to calculate seismic anisotropy from the lattice preferred orientation of minerals. Computers & Geosciences 16, 385-393.

Mainprice, D., Bachmann, F., Hielscher, R., Schaeben, H., 2014. Descriptive tools for the analysis of texture projects with large datasets using MTEX: strength, symmetry and components. Geological Society, London, Special Publications 409, 251-271.

Mainprice, D., Nicolas, A., 1989. Development of shape and lattice preferred orientations: application to the seismic anisotropy of the lower crust. Journal of Structural Geology 11, 175-189.

Mainprice, D., Tommasi, A., Couvy, H., Cordier, P., Frost, D.J., 2005. Pressure sensitivity of olivine slip systems and seismic anisotropy of Earth's upper mantle. Nature 433, 731-733.

Manthilake, M., Miyajima, N., Heidelbach, F., Soustelle, V., Frost, D., 2013. The effect of aluminum and water on the development of deformation fabrics of orthopyroxene. Contributions to Mineralogy and Petrology 165, 495-505.

Marchesi, C., Garrido, C.J., Proenza, J.A., Hidas, K., Varas-Reus, M.I., Butjosa, L., Lewis, J.F., 2016. Geochemical record of subduction initiation in the sub-arc mantle: Insights from the Loma Caribe peridotite (Dominican Republic). Lithos 252, 1-15.

Márton, E., 1987. Palaeomagnetism and tectonics in the Mediterranean region. Journal of Geodynamics 7, 33-57.

Márton, E., 1997. Paleomagnetic aspects of plate tectonics in the Carpatho-Pannonian region. Mineralium Deposita 32, 441-445.

Márton, E., Márton, P., 1978. Tectonic implications of a new palaeomagnetic result from the Jurassic of the Transdanubian Central Mountains. Tectonophysics 45, T1-T6.

Matenco, L., Bertotti, G., Leever, K., Cloetingh, S., Schmid, S.M., Tărăpoancă, M., Dinu, C., 2007. Large-scale deformation in a locked collisional boundary: Interplay between subsidence and uplift, intraplate stress, and inherited lithospheric structure in the late stage of the SE Carpathians evolution. Tectonics 26, doi:10.1029/2006TC001951.

McDonough, W., 1991. Partial melting of subducted oceanic crust and isolation of its residual eclogitic lithology. Philosophical Transactions of the Royal Society of London A: Mathematical, Physical and Engineering Sciences 335, 407-418.

McDonough, W.F., Sun, S.-S., 1995. The composition of the Earth. Chemical Geology 120,

223-253.

Mengel, K., Green, D., 1989. Stability of amphibole and phlogopite in metasomatized peridotite under water-saturated and water-undersaturated conditions, in: Ross, J. (Ed.), Kimberlites and related rocks. Geological Society of Australia, pp. 571-581.

Mercier, J.C.C., Nicolas, A., 1975. Textures and fabrics of upper mantle peridotites as illustrated by xenoliths from basalts. Journal of Petrology 16, 454-487.

Michael, P., 1995. Regionally distinctive sources of depleted MORB: Evidence from trace elements and H_2O. Earth and Planetary Science Letters 131, 301-320.

Mutchler, S., Fedele, L., Bodnar, R.J., 2008. Analysis Management System (AMS) for reduction of laser ablation ICPMS data, in: Sylvester, P. (Ed.), Laser-Ablation-ICPMS in the Earth Sciences: Current Practices and Outstanding Issues. Mineralogical Association of Canada, Vancouver, BC, pp. 318-327.

Newcombe, M. E:, Fabbrizio, A., Zhang, Y., Ma, C., Le Voyer, M., Guan, Y., Eiler, J. M., Saal, A. E., Stolper, E. M., 2014. Chemical zonation in olivine-hosted melt inclusions. Contributions to Mineralogy and Petrology, 168:1030.

Newton, R.C., Manning, C.E., 2004. Solubility of anhydrite, CaSO4, in NaCl–H2O solutions at high pressures and temperatures: applications to fluid–rock interaction. Journal of Petrology 46, 701-716.

Nicolas, A., Boudier, F., Boullier, A., 1973. Mechanisms of flow in naturally and experimentally deformed peridotites. American Journal of Science 273, 853-876.

Nicolas, A., Christensen, N.I., 1987. Formation of Anisotropy in Upper Mantle Peridotites-A Review, in: Fuchs, K., Froidevaux, C. (Eds.), Composition, structure and dynamics of the lithosphere-asthenosphere system (Geodynamics Series), pp. 111-123.

Niida, K., Green, D., 1999. Stability and chemical composition of pargasitic amphibole in MORB pyrolite under upper mantle conditions. Contributions to Mineralogy and Petrology 135, 18-40.

Nimis, P., Grütter, H., 2010. Internally consistent geothermometers for garnet peridotites and pyroxenites. Contributions to Mineralogy and Petrology 159, 411-427.

Niu, Y., 2004. Bulk-rock major and trace element compositions of abyssal peridotites: implications for mantle melting, melt extraction and post-melting processes beneath mid-ocean ridges. Journal of Petrology 45, 2423-2458.

Niu, Y., Hékinian, R., 1997. Basaltic liquids and harzburgitic residues in the Garrett Transform: a case study at fast-spreading ridges. Earth and Planetary Science Letters 146, 243-258.

Norman, M.D., 1998. Melting and metasomatism in the continental lithosphere: laser ablation ICPMS analysis of minerals in spinel lherzolites from eastern Australia. Contributions to Mineralogy and Petrology 130, 240-255.

O'Reilly, S.Y., Griffin, W., 2013. Mantle metasomatism, in: Harlov, D.E., Austrheim, H. (Eds.), Metasomatism and the Chemical Transformation of Rock. Springer, pp. 471-533.

O'Reilly, S.Y., Griffin, W.L., 1985. A xenolith-derived geotherm for southeastern Australia

and its geophysical implications. Tectonophysics 111, 41-63.

O'Reilly, S.Y., Griffin, W.L., 2006. Imaging global chemical and thermal heterogeneity in the subcontinental lithospheric mantle with garnets and xenoliths: Geophysical implications. Tectonophysics 416, 289-309.

O'Reilly, S.Y., Griffin, W.L., 2011. Rates of magma ascent: Constraints from mantle-derived xenoliths, in: Dosseto, A., Turner, S., Van Orman, J. (Eds.), Timescales of Magmatic Processes. Wiley-Blackwell, pp. 116-124.

Padrón-Navarta, J.A., Hermann, J., O'Neill, H.S.C., 2014. Site-specific hydrogen diffusion rates in forsterite. Earth and Planetary Science Letters 392, 100-112.

Passchier, C., Trouw, R., 1996. Microtectonics: Springer Verlag. Berlin, Germany, 289.

Patkó, L., 2014. Reconstruction of metasomatic processes in the upper mantle of the Nógrád-Gömör Volcanic Field based on wehrlite xenoliths (in Hungarian with English abstract). Eötvös University, Budapest, p. 83.

Patkó, L., Aradi, L., Liptai, N., Bodnar, R., Fedele, L., Kovács, Z., Cesare, B., Vaselli, O., Fioretti, A., Jeffries, T., 2013. Wehrlitization processes within the upper mantle beneath the Northern Pannonian Basin (Hungary). Mineralogical Magazine 77, 1934.

Pearce, N.J., Perkins, W.T., Westgate, J.A., Gorton, M.P., Jackson, S.E., Neal, C.R., Chenery, S.P., 1997. A compilation of new and published major and trace element data for NIST SRM 610 and NIST SRM 612 glass reference materials. Geostandards Newsletter 21, 115-144.

Pécskay, Z., Lexa, J., A., S., Balogh, K., Seghedi, I., Konečny, V., Kovács, M., Márton, E., Kaliciak, M., Széky-Fux, V., Póka, T., Gyarmati, P., Edelstein, O., Rosu, E., Zec, B., 1995. Space and time distribution of Neogene-Quartenary volcanism in the Carpatho-Pannonian Region. Acta Vulcanologica 7, 15-28.

Pécskay, Z., Lexa, J., Szakács, A., Seghedi, I., Balogh, K., Konečny, V., Zelenka, T., Kovac, M., Póka, T., Fülöp, A., Márton, E., Panaiotu, C., Cvetkovič, V., 2006. Geochronology of Neogene magmatism in the Carpathian arc and intra-Carpathian area. Geologica Carpathica 57, 511-530.

Peslier, A., Woodland, A., Bell, D., Lazarov, M., Lapen, T., 2012. Metasomatic control of water contents in the Kaapvaal cratonic mantle. Geochimica et Cosmochimica Acta 97, 213-246.

Peslier, A.H., Bizimis, M., Matney, M., 2015. Water disequilibrium in olivines from Hawaiian peridotites: Recent metasomatism, H diffusion and magma ascent rates. Geochimica et Cosmochimica Acta 154, 98-117.

Peslier, A.H., Francis, D., Ludden, J., 2002a. The lithospheric mantle beneath continental margins: melting and melt–rock reaction in Canadian Cordillera xenoliths. Journal of Petrology 43, 2013-2047.

Peslier, A.H., Luhr, J.F., 2006. Hydrogen loss from olivines in mantle xenoliths from Simcoe (USA) and Mexico: mafic alkalic magma ascent rates and water budget of the sub-continental lithosphere. Earth and Planetary Science Letters 242, 302-319.

Peslier, A.H., Luhr, J.F., Post, J., 2002b. Low water contents in pyroxenes from spinel-peridotites of the oxidized, sub-arc mantle wedge. Earth and Planetary Science Letters

201, 69-86.

Peslier, A.H., Schönbächler, M., Busemann, H., Karato, S.-I., 2017. Water in the Earth's Interior: Distribution and Origin. Space Science Reviews 212, 743-810.

Peslier, A.H., Woodland, A.B., Bell, D.R., Lazarov, M., 2010. Olivine water contents in the continental lithosphere and the longevity of cratons. Nature 467, 78.

Pike, J.N., Schwarzman, E., 1977. Classification of textures in ultramafic xenoliths. The Journal of Geology 85, 49-61.

Pilet, S., Baker, M. B., Müntener, O., Stolper, E. M., 2011. Monte Carlo simulations of metasomatic enrichment in the lithosphere and implications for the source of alkaline basalts. Journal of Petrology 52, 1415-1442.

Pintér, Z., Patkó, L., Djoukam, J.F.T., Kovács, I., Tchouankoue, J.P., Falus, G., Konc, Z., Tommasi, A., Barou, F., Mihály, J., 2015. Characterization of the sub-continental lithospheric mantle beneath the Cameroon volcanic line inferred from alkaline basalt hosted peridotite xenoliths from Barombi Mbo and Nyos Lakes. Journal of African Earth Sciences 111, 170-193.

Qin, Z., Lu, F., Anderson, A.T., 1992. Diffuse reequilibration of melt and fluid inclusions. American Mineralogist 77, 565-576.

Qorbani, E., Bokelmann, G., Kovács, I., Horváth, F., Falus, G., 2016. Deformation in the asthenospheric mantle beneath the Carpathian-Pannonian Region. Journal of Geophysical Research: Solid Earth 121, 6644-6657.

Raffone, N., Chazot, G., Pin, C., Vannucci, R., Zanetti, A., 2009. Metasomatism in the lithospheric mantle beneath Middle Atlas (Morocco) and the origin of Fe-and Mg-rich wehrlites. Journal of Petrology 50, 197-249.

Rampone, E., Vissers, R.L.M., Poggio, M., Scambelluri, M., Zanetti, A., 2010. Melt Migration and Intrusion during Exhumation of the Alboran Lithosphere: the Tallante Mantle Xenolith Record (Betic Cordillera, SE Spain). Journal of Petrology 51, 295-325.

Ribe, N.M., 1992. On the relation between seismic anisotropy and finite strain. Journal of Geophysical Research: Solid Earth 97, 8737-8747.

Ritchie, N.W., Newbury, D.E., Davis, J.M., 2012. EDS measurements of X-ray intensity at WDS precision and accuracy using a silicon drift detector. Microscopy and Microanalysis 18, 892-904.

Rivalenti, G., Zanetti, A., Mazzucchelli, M., Vannucci, R., Cingolani, C.A., 2004. Equivocal carbonatite markers in the mantle xenoliths of the Patagonia backarc: the Gobernador Gregores case (Santa Cruz Province, Argentina). Contributions to Mineralogy and Petrology 147, 647-670.

Roedder, E., 1984. Fluid inclusions. Mineralogical Society of America.

Ross, J.V., Lallemant, H.G.A., Carter, N.L., 1980. Stress dependence of recrystallized-grain and subgrain size in olivine. Tectonophysics 70, 39-61.

Rosso, K.M., Bodnar, R.J., 1995. Microthermometric and Raman spectroscopic detection limits of CO_2 in fluid inclusions and the Raman spectroscopic characterization of CO_2. Geochimica et Cosmochimica Acta 59, 3961-3975.

Royden, L.H., Horváth, F., Burchfiel, B.C., 1982. Transform faulting, extension and subduction in the Carpathian-Pannonian region. Geological Society of America Bullettin 93, 717-725.

Royden, L.H., Horváth, F., Nagymarosy, A., Stegena, L., 1983. Evolution of the Pannonian basin system. 2. Subsidence and thermal history. Tectonophysics 2, 91-137.

Rudnick, R.L., Barth, M., Horn, I., McDonough, W.F., 2000. Rutile-bearing refractory eclogites: missing link between continents and depleted mantle. Science 287, 278-281.

Rudnick, R.L., McDonough, W.F., Chappell, B.W., 1993. Carbonatite metasomatism in the northern Tanzanian mantle: petrographic and geochemical characteristics. Earth and Planetary Science Letters 114, 463-475.

Salters, V.J., Longhi, J.E., Bizimis, M., 2002. Near mantle solidus trace element partitioning at pressures up to 3.4 GPa. Geochemistry, Geophysics, Geosystems 3, 1-23.

Sambridge, M., Gerald, J.F., Kovács, I., O'Neill, H.S.C., Hermann, J., 2008. Quantitative absorbance spectroscopy with unpolarized light: Part I. Physical and mathematical development. American Mineralogist 93, 751-764.

Savage, M., 1999. Seismic anisotropy and mantle deformation: what have we learned from shear wave splitting? Reviews of Geophysics 37, 65-106.

Schiano, P., Bourdon, B., 1999. On the preservation of mantle information in ultramafic nodules: glass inclusions within minerals versus interstitial glasses. Earth and Planetary Science Letters 169, 173-188.

Schiano, P., Clocchiatti, R., Bourdon, B., Burton, K., Thellier, B., 2000. The composition of melt inclusions in minerals at the garnet–spinel transition zone. Earth and Planetary Science Letters 174, 375-383.

Schiano, P., Clocchiatti, R., Joron, J., 1992. Melt and fluid inclusions in basalts and xenoliths from Tahaa Island, Society Archipelago: evidence for a metasomatized upper mantle. Earth and Planetary Science Letters 111, 69-82.

Schmid, S., Aebli, H., Heller, F., Zingg, A., 1989. The role of the Periadriatic Line in the tectonic evolution of the Alps. Geological Society, London, Special Publications 45, 153-171.

Schmidt, M., Dardon, A., Chazot, G., Vannucci, R., 2004. The dependence of Nb and Ta rutile–melt partitioning on melt composition and Nb/Ta fractionation during subduction processes. Earth and Planetary Science Letters 226, 415-432.

Seghedi, I., Downes, H., 2011. Geochemistry and tectonic development of Cenozoic magmatism in the Carpathian–Pannonian region. Gondwana Research 20, 655-672.

Seghedi, I., Downes, H., Szakacs, A., Mason, P.R.D., Thirlwall, M.F., Rosu, E., Pecskay, Z., Marton, E., Panaiotu, C., 2004. Neogene-Quaternary magmatism and geodynamics in the Carpathian-Pannonian region: a synthesis. Lithos 72, 117-146.

Selway, K., Yi, J., Karato, S.-I., 2014. Water content of the Tanzanian lithosphere from magnetotelluric data: Implications for cratonic growth and stability. Earth and Planetary Science Letters 388, 175-186.

Silver, P., Mainprice, D., Ben Ismaïl, W., Tommasi, A., Barruol, G., 1999. Mantle structural

geology from seismic anisotropy, in: Fei, Y., Bertka, C.M., Mysen, B.O. (Eds.), Mantle petrology: Field observations and high pressure experimentation: A tribute to Francis R. (Joe) Boyd. The Geochemical Society, Washington, pp. 79-103.

Silver, P.G., Chan, W.W., 1991. Shear wave splitting and subcontinental mantle deformation. Journal of Geophysical Research: Solid Earth 96, 16429-16454.

Skemer, P., Katayama, I., Jiang, Z., Karato, S.-i., 2005. The misorientation index: Development of a new method for calculating the strength of lattice-preferred orientation. Tectonophysics 411, 157-167.

Soustelle, V., Manthilake, G., 2017. Deformation of olivine-orthopyroxene aggregates at high pressure and temperature: Implications for the seismic properties of the asthenosphere. Tectonophysics 694, 385-399.

Soustelle, V., Tommasi, A., Bodinier, J.-L., Garrido, C., Vauchez, A., 2009. Deformation and reactive melt transport in the mantle lithosphere above a large-scale partial melting domain: the Ronda Peridotite Massif, Southern Spain. Journal of Petrology 50, 1235-1266.

Soustelle, V., Tommasi, A., Demouchy, S., Franz, L., 2013. Melt-rock interactions, deformation, hydration and seismic properties in the sub-arc lithospheric mantle inferred from xenoliths from seamounts near Lihir, Papua New Guinea. Tectonophysics 608, 330-345.

Soustelle, V., Tommasi, A., Demouchy, S., Ionov, D., 2010. Deformation and fluid–rock interaction in the supra-subduction mantle: microstructures and water contents in peridotite xenoliths from the Avacha Volcano, Kamchatka. Journal of Petrology 51, 363-394.

Stalder, R., 2004. Influence of Fe, Cr and Al on hydrogen incorporation in orthopyroxene. European Journal of Mineralogy 16, 703-711.

Stalder, R., Prechtel, F., Ludwig, T., 2012. No site-specific infrared absorption coefficients for OH-defects in pure enstatite. European Journal of Mineralogy 24, 465-470.

Stalder, R., Skogby, H., 2002. Hydrogen incorporation in enstatite. European Journal of Mineralogy 14, 1139-1144.

Stalder, R., Skogby, H., 2003. Hydrogen diffusion in natural and synthetic orthopyroxene. Physics and Chemistry of Minerals 30, 12-19.

Stegena, L., Géczy, B., Horváth, F., 1975. Late Cenozoic evolution of the Pannonian basin. Tectonophysics 26, 71-90.

Stosch, H.-G., Seck, H., 1980. Geochemistry and mineralogy of two spinel peridotite suites from Dreiser Weiher, West Germany. Geochimica et Cosmochimica Acta 44, 457-470.

Streckeisen, A., 1975. To each plutonic rock its proper name. Earth Science Reviews 12, 1-33.

Stuart, G., Houseman, G., Dando, B., Hegedus, E., Brueckl, E., Radovanovic, S., Falus, G., Kovacs, A., Hausmann, H., Brisbourne, A., 2007. Understanding extension within a convergent orogen: Initial results from the Carpathian Basins Seismic Project, AGU Fall Meeting Abstracts.

Sun, C., Liang, Y., 2012. Distribution of REE between clinopyroxene and basaltic melt along a mantle adiabat: effects of major element composition, water, and temperature. Contributions to Mineralogy and Petrology 163, 807-823.

Sun, S.-S., McDonough, W.F., 1989. Chemical and isotopic systematics of oceanic basalts: implications for mantle composition and processes. Geological Society, London, Special Publications 42, 313-345.

Sundvall, R., Stalder, R., 2011. Water in upper mantle pyroxene megacrysts and xenocrysts: A survey study. American Mineralogist 96, 1215-1227.

Szabó, C., Bodnar, R., 1995. Chemistry and origin of mantle sulfides in spinel peridotite xenoliths from alkaline basaltic lavas, Nógrád-Gömör Volcanic Field, northern Hungary and southern Slovakia. Geochimica et Cosmochimica Acta 59, 3917-3927.

Szabó, C., Bodnar, R., 1996. Changing magma ascent rates in the Nógrád-Gömör Volcanic Field Northern Hungary/Southern Slovakia: Evidence from CO_2-rich fluid inclusions in metasomatized upper mantle xenoliths. Petrology 4, 221-230.

Szabó, C., Bodnar, R.J., Sobolev, A.V., 1996. Metasomatism associated with subduction-related, volatile-rich silicate melt in the upper mantle beneath the Nógrád-Gömör volcanic field, northern Hungary/southern Slovakia; evidence from silicate melt inclusions. European Journal of Mineralogy 8, 881-899.

Szabó, C., Falus, G., Zajacz, Z., Kovács, I., Bali, E., 2004. Composition and evolution of lithosphere beneath the Carpathian–Pannonian Region: a review. Tectonophysics 393, 119-137.

Szabó, C., Harangi, S., Csontos, L., 1992. Review of Neogene and Quaternary volcanism of the Carpathian-Pannonian region. Tectonophysics 208, 243-256.

Szabó, C., Harangi, S., Vaselli, O., Downes, H., 1995a. Temperature and oxygen fugacity in peridotite xenoliths from the Carpathian–Pannonian Region. Acta Vulcanologica 7, 231-239.

Szabó, C., Taylor, L.A., 1994. Mantle petrology and geochemistry beneath the Nógrád-Gömör Volcanic Field, Carpathian-Pannonian Region. International Geology Review 36, 328-358.

Szabó, C., Vaselli, O., Vannucci, R., Bottazzi, P., Ottolini, L., Coradossi, N., Kubovics, I., 1995b. Ultramafic xenoliths from the Little Hungarian Plain (Western Hungary): a petrologic and geochemical study. Acta Vulcanologica 7, 249-264.

Szafián, P., Horváth, F., 2006. Crustal structure in the Carpatho-Pannonian region: insights from three-dimensional gravity modelling and their geodynamic significance. International Journal of Earth Sciences 95, 50-67.

Tari, G., Horvath, F., Rumpler, J., 1992. Styles of extension in the Pannonian Basin. Tectonophysics 208, 203-219.

Tašárová, A., Afonso, J.C., Bielik, M., Götze, H.J., Hók, J., 2009. The lithospheric structure of the Western Carpathian–Pannonian Basin region based on the CELEBRATION 2000 seismic experiment and gravity modelling. Tectonophysics 475, 454-469.

Taylor, W., 1998. An experimental test of some geothermometer and geobaro-meter formulations for upper mantle peridotites with application to the thermobarometry of fertile

lherzolite and garnet websterite. Neues Jahrbuch für Mineralogie-Abhandlungen 172, 381-408.

Tian, Z.-Z., Liu, J., Xia, Q.-K., Ingrin, J., Hao, Y.-T., Christophe, D., 2017. Water concentration profiles in natural mantle orthopyroxenes: A geochronometer for long annealing of xenoliths within magma. Geology 45, 87-90.

Tommasi, A., Baptiste, V., Vauchez, A., Holtzman, B., 2016. Deformation, annealing, reactive melt percolation, and seismic anisotropy in the lithospheric mantle beneath the southeastern Ethiopian rift: Constraints from mantle xenoliths from Mega. Tectonophysics 682, 186-205.

Tommasi, A., Mainprice, D., Canova, G., Chastel, Y., 2000. Viscoplastic self-consistent and equilibrium-based modeling of olivine lattice preferred orientations: Implications for the upper mantle seismic anisotropy. Journal of Geophysical Research: Solid Earth 105, 7893-7908.

Tommasi, A., Tikoff, B., Vauchez, A., 1999. Upper mantle tectonics: three-dimensional deformation, olivine crystallographic fabrics and seismic properties. Earth and Planetary Science Letters 168, 173-186.

Tommasi, A., Vauchez, A., 2015. Heterogeneity and anisotropy in the lithospheric mantle. Tectonophysics 661, 11-37.

Tommasi, A., Vauchez, A., Ionov, D.A., 2008. Deformation, static recrystallization, and reactive melt transport in shallow subcontinental mantle xenoliths (Tok Cenozoic volcanic field, SE Siberia). Earth and Planetary Science Letters 272, 65-77.

Török, K., 1995. Garnet breakdown reaction and fluid inclusions in a garnet-clinopyroxenite xenolith from Szentbékkálla (Balaton-Highland, Western Hungary). Acta Vulcanologica 7, 285-290.

Trepmann, C.A., Renner, J., Druiventak, A., 2013. Experimental deformation and recrystallization of olivine – processes and timescales of damage healing during postseismic relaxation at mantle depths. Solid Earth 4, 423-450.

Upton, B.G.J., Downes, H., Kirstein, L.A., Bonadiman, C., Hill, P.G., Ntaflos, T., 2011. The lithospheric mantle and lower crust–mantle relationships under Scotland: a xenolithic perspective. Journal of the Geological Society 168, 873-886.

Van der Wal, D., Bodinier, J.-L., 1996. Origin of the recrystallisation front in the Ronda peridotite by km-scale pervasive porous melt flow. Contributions to Mineralogy and Petrology 122, 387-405.

Van Orman, J.A., Grove, T.L., Shimizu, N., 2001. Rare earth element diffusion in diopside: influence of temperature, pressure, and ionic radius, and an elastic model for diffusion in silicates. Contributions to Mineralogy and Petrology 141, 687-703.

VanTongeren, J.A., Kelemen, P.B., Hanghøj, K., 2008. Cooling rates in the lower crust of the Oman ophiolite: Ca in olivine, revisited. Earth and Planetary Science Letters 267, 69-82.

Vaselli, O., Downes, H., Thirlwall, M.F., Dobosi, G., Coradossi, N., Seghedi, I., Szakács, A., Vannucci, R., 1995. Ultramafic xenoliths in Plio-Pleistocene alkali basalts from the eastern Transylvanian Basin: depleted mantle enriched by vein metasomatism. Journal of Petrology 36, 23-53.

Vaselli, O., Downes, H., Thirlwall, M.F., Vannucci, R., Coradossi, N., 1996. Spinel-peridotite xenoliths from Kapfenstein (Graz Basin, Eastern Austria): A geochemical and petrological study. Mineralogy and Petrology 57, 23-50.

Vauchez, A., Dineur, F., Rudnick, R., 2005. Microstructure, texture and seismic anisotropy of the lithospheric mantle above a mantle plume: insights from the Labait volcano xenoliths (Tanzania). Earth and Planetary Science Letters 232, 295-314.

Vauchez, A., Garrido, C.J., 2001. Seismic properties of an asthenospherized lithospheric mantle: constraints from lattice preferred orientations in peridotite from the Ronda massif. Earth and Planetary Science Letters 192, 235-249.

Vauchez, A., Nicolas, A., 1991. Mountain building: strike-parallel motion and mantle anisotropy. Tectonophysics 185, 183-201.

Vauchez, A., Tommasi, A., Mainprice, D., 2012. Faults (shear zones) in the Earth's mantle. Tectonophysics 558, 1-27.

Vissers, R., Drury, M., Newman, J., Fliervoet, T., 1997. Mylonitic deformation in upper mantle peridotites of the North Pyrenean Zone (France): implications for strength and strain localization in the lithosphere. Tectonophysics 279, 303-325.

Viti, C., Frezzotti, M.-L., 2000. Re-equilibration of glass and CO_2 inclusions in xenolith olivine: A TEM study. American Mineralogist 85, 1390-1396.

Vollmer, F.W., 1990. An application of eigenvalue methods to structural domain analysis. Geological Society of America Bulletin 102, 786-791.

Vonlanthen, P., Kunze, K., Burlini, L., Grobety, B., 2006. Seismic properties of the upper mantle beneath Lanzarote (Canary Islands): Model predictions based on texture measurements by EBSD. Tectonophysics 428, 65-85.

Vörös, A., 1993. Jurassic microplate movements and brachiopod migrations in the western part of the Tethys. Palaeogeography, Palaeoclimatology, Palaeoecology 100, 125-145.

Waff, H.S., Faul, U.H., 1992. Effects of crystalline anisotropy on fluid distribution in ultramafic partial melts. Journal of Geophysical Research: Solid Earth 97, 9003-9014.

Walker, A., Hermann, J., Berry, A.J., O'Neill, H.S.C., 2007. Three water sites in upper mantle olivine and the role of titanium in the water weakening mechanism. Journal of Geophysical Research: Solid Earth 112.

Wallace, M., Green, D., 1991. The effect of bulk rock composition on the stability of amphibole in the upper mantle: implications for solidus positions and mantle metasomatism. Mineralogy and Petrology 44, 1-19.

Walter, M.J., 1998. Melting of garnet peridotite and the origin of komatiite and depleted lithosphere. Journal of Petrology 39, 29-60.

Walter, M.J., 2003. Melt extraction and compositional variability in mantle lithosphere, in: Turekian, K.K., Holland, H.D. (Eds.), Treatise on geochemistry. Elsevier, Amsterdam, pp. 363-394.

Wang, X., Chou, I.M., Hu, W., Burruss, R.C., Sun, Q., Song, Y., 2011. Raman spectroscopic measurements of CO_2 density: Experimental calibration with high-pressure optical cell (HPOC) and fused silica capillary capsule (FSCC) with application to fluid

inclusion observations. Geochimica et Cosmochimica Acta 75, 4080-4093.

Warren, J.M., Hauri, E.H., 2014. Pyroxenes as tracers of mantle water variations. Journal of Geophysical Research: Solid Earth 119, 1851-1881.

Willingshofer, E., Cloetingh, S., 2003. Present-day lithospheric strength of the Eastern Alps and its relationship to neotectonics. Tectonics 22, doi:10.1029/2002TC001463.

Willingshofer, E., van Wees, J.D., Cloetingh, S.A.P.L., Neubauer, F., 1999. Thermomechanical consequences of Cretaceous continent-continent collision in the eastern Alps (Austria): Insights from two-dimensional modeling. Tectonics 18, 809-826.

Wilshire, H., Pike, J.N., Meyer, C., Schwarzman, E., 1980. Amphibole-rich veins in lherzolite xenoliths, Dish Hill and Deadman Lake, California. American Journal of Science 280, 576-593.

Wilshire, H., Shervais, J., 1975. Al-augite and Cr-diopside ultramafic xenoliths in basaltic rocks from western United States. Physics and Chemistry of the Earth 9, 257-272.

Wirth, R., 2004. Focused Ion Beam (FIB): A novel technology for advanced application of micro- and nanoanalysis in geosciences and applied mineralogy. European Journal of Mineralogy 16, 863-876.

Witt-Eickschen, G., Seck, H., 1991. Solubility of Ca and Al in orthopyroxene from spinel peridotite: an improved version of an empirical geothermometer. Contributions to Mineralogy and Petrology 106, 431-439.

Witt, G., Seck, H., 1987. Temperature history of sheared mantle xenoliths from the West Eifel, West Germany: evidence for mantle diapirism beneath the Rhenish Massif. Journal of Petrology 28, 475-493.

Workman, R.K., Hart, S.R., 2005. Major and trace element composition of the depleted MORB mantle (DMM). Earth and Planetary Science Letters 231, 53-72.

Wright, S.I., Nowell, M.M., Field, D.P., 2011. A review of strain analysis using electron backscatter diffraction. Microscopy and Microanalysis 17, 316-329.

Xia, Q.-K., Hao, Y.-T., Liu, S.-C., Gu, X.-Y., Feng, M., 2013. Water contents of the Cenozoic lithospheric mantle beneath the western part of the North China Craton: Peridotite xenolith constraints. Gondwana Research 23, 108-118.

Xia, Q.-K., Hao, Y., Li, P., Deloule, E., Coltorti, M., Dallai, L., Yang, X., Feng, M., 2010. Low water content of the Cenozoic lithospheric mantle beneath the eastern part of the North China Craton. Journal of Geophysical Research: Solid Earth 115, doi:10.1029/2009JB006694.

Yang, X.-Z., Xia, Q.-K., Deloule, E., Dallai, L., Fan, Q.-C., Feng, M., 2008. Water in minerals of the continental lithospheric mantle and overlying lower crust: a comparative study of peridotite and granulite xenoliths from the North China Craton. Chemical Geology 256, 33-45.

Yang, X., Keppler, H., Li, Y., 2016. Molecular hydrogen in mantle minerals. Geochemical Perspectives Letters 2, 160-168.

Yao, L., Sun, C., Liang, Y., 2012. A parameterized model for REE distribution between low-Ca pyroxene and basaltic melts with applications to REE partitioning in low-Ca

pyroxene along a mantle adiabat and during pyroxenite-derived melt and peridotite interaction. Contributions to Mineralogy and Petrology 164, 261-280.

Yu, J.-H., O'Reilly, S.Y., Griffin, W.L., Xu, X., Zhang, M., Zhou, X., 2003. The thermal state and composition of the lithospheric mantle beneath the Leizhou Peninsula, South China. Journal of Volcanology and Geothermal Research 122, 165-189.

Yu, Y., Xu, X.-S., Griffin, W.L., O'Reilly, S.Y., Xia, Q.-K., 2011. H_2O contents and their modification in the Cenozoic subcontinental lithospheric mantle beneath the Cathaysia block, SE China. Lithos 126, 182-197.

Zaffarana, C., Tommasi, A., Vauchez, A., Grégoire, M., 2014. Microstructures and seismic properties of south Patagonian mantle xenoliths (Gobernador Gregores and Pali Aike). Tectonophysics 621, 175-197.

Zajacz, Z., Kovács, I., Szabó, C., Halter, W., Pettke, T., 2007. Evolution of mafic alkaline melts crystallized in the uppermost lithospheric mantle: a melt inclusion study of olivine-clinopyroxenite xenoliths, northern Hungary. Journal of Petrology 48, 853-883.

Zajacz, Z., Szabó, C., 2003. Origin of sulfide inclusions in cumulate xenoliths from Nógrád–Gömör Volcanic Field, Pannonian Basin (north Hungary/south Slovakia). Chemical Geology 194, 105-117.

Zanetti, A., 1995. Trace element composition and crystal-chemistry of mantle amphiboles from the Pannonian and Eastern Transylvanian Basins: Implications for enrichment events in the lithospheric mantle. Acta Vulcanologica 7, 265-276.

Zanetti, A., Mazzucchelli, M., Rivalenti, G., Vannucci, R., 1999. The Finero phlogopite-peridotite massif: an example of subduction-related metasomatism. Contributions to Mineralogy and Petrology 134, 107-122.

Zhang, S., Karato, S.-I., 1995. Lattice preferred orientation of olivine aggregates deformed in simple shear. Nature 375, 774-777.

Zhang, S., Karato, S.-I., Gerald, J.F., Faul, U.H., Zhou, Y., 2000. Simple shear deformation of olivine aggregates. Tectonophysics 316, 133-152.

Appendices

Appendix A: Sample Images and Description

Thin-section photos are scanned plane-polarised images; electron backscattered diffraction (EBSD) maps use artificial colours for the different phases and subgrain boundaries.

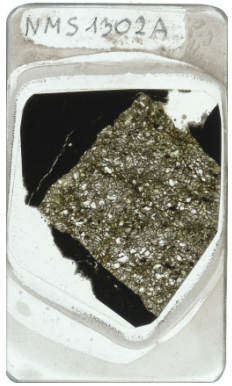

2 cm

NMS1302A

Texture: fine porphyroclastic

Phase assemblage: ol+opx+cpx+sp

Lineation is outlined by elongated olivine grains

2 cm

NMS1304

Texture: fine porphyroclastic

Phase assemblage: ol+opx+cpx+sp+amp

Lineation is outlined by elongated olivine grains and the distribution of spinel and amphibole.

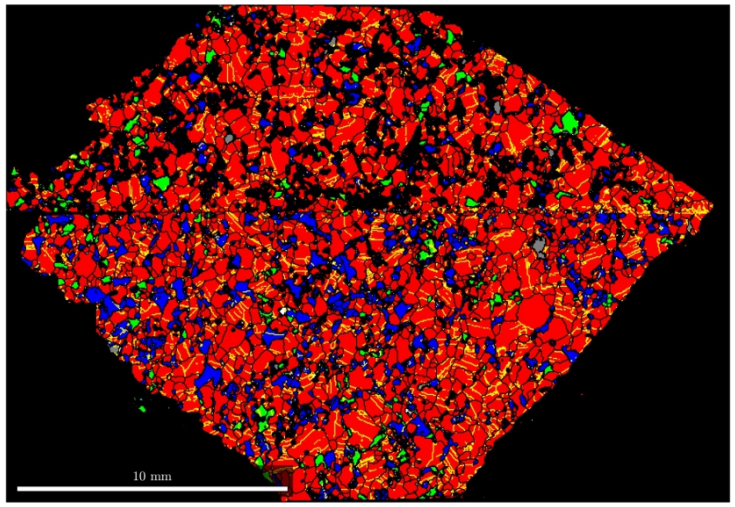

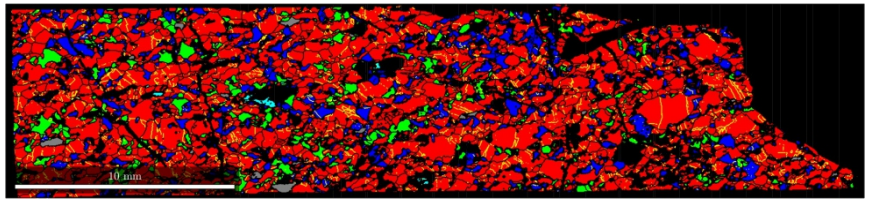

olivine orthopyroxene clinopyroxene spinel amphibole yellow lines - subgrain boundaries

NMS1305

Texture: fine granular

Phase assemblage:
ol+opx+cpx+sp

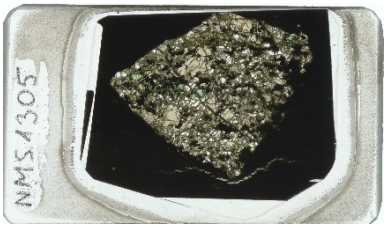

2 cm

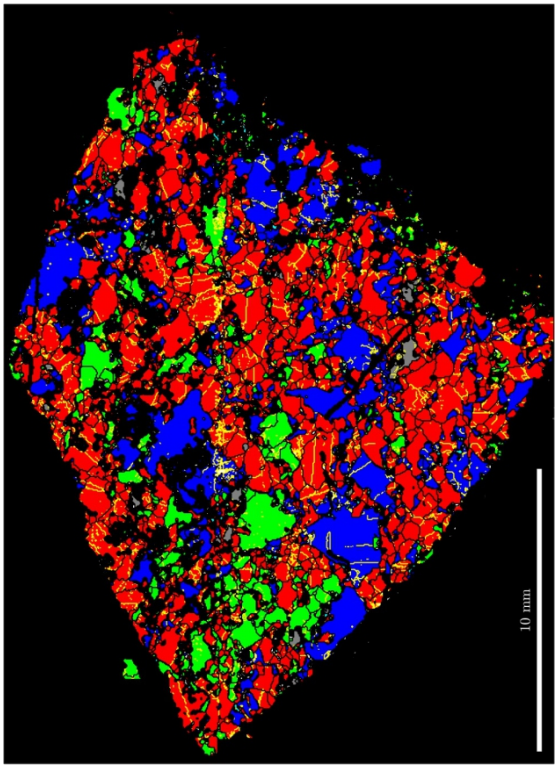

NMS1308

Texture: porphyroclastic

Phase assemblage:
ol+opx+cpx+sp+amp

Lineation is outlined by elongated olivine grains. Subgrain boundaries are perpendicular to the elongation.

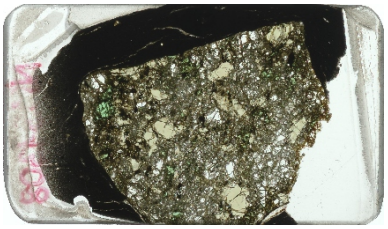

2 cm

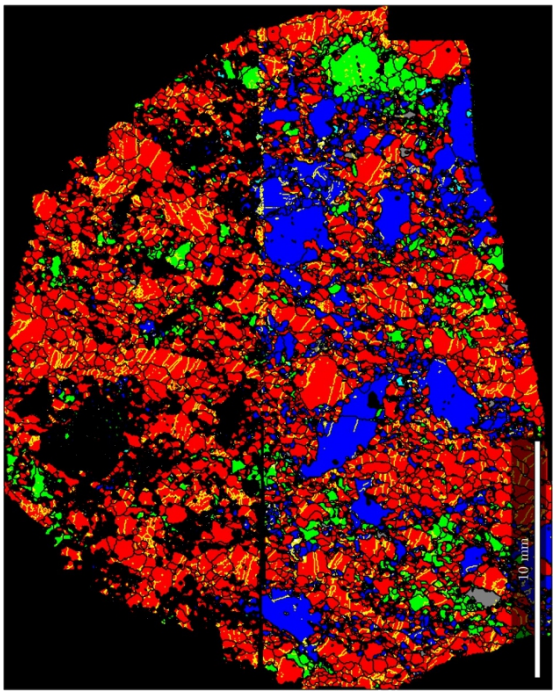

olivine orthopyroxene clinopyroxene spinel amphibole yellow lines - subgrain boundaries

2 cm

NMS1310

Texture: coarse granular

Phase assemblage:
ol+opx+cpx+sp

Pyroxene-rich modal composition.

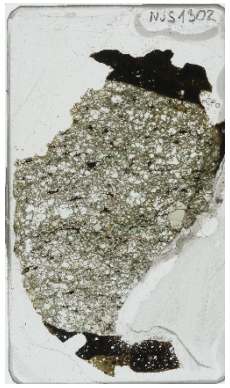

2 cm

NJS1302

Texture: fine porphyroclastic

Phase assemblage:
ol+opx+cpx+sp+amp

Amphibole is only present as two small grains. Lineation is slightly outlined by elongated olivine grains.

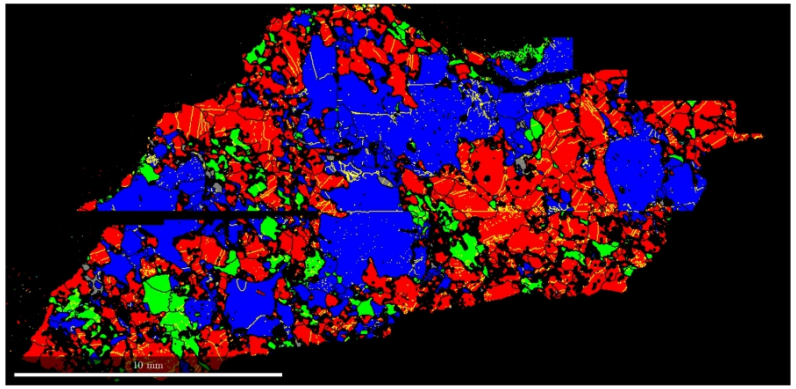

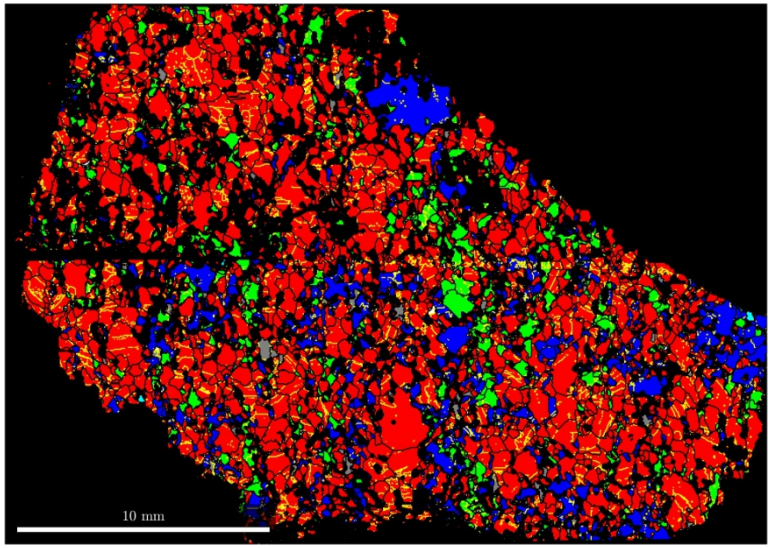

olivine orthopyroxene clinopyroxene spinel amphibole yellow lines - subgrain boundaries

NJS1304

Texture: coarse granular

Phase assemblage:
ol+opx+cpx+sp

Orthopyroxene-rich modal composition.

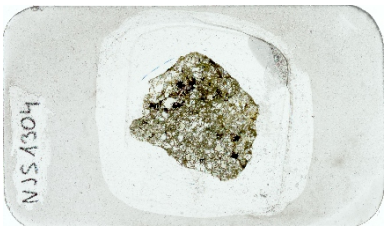

2 cm

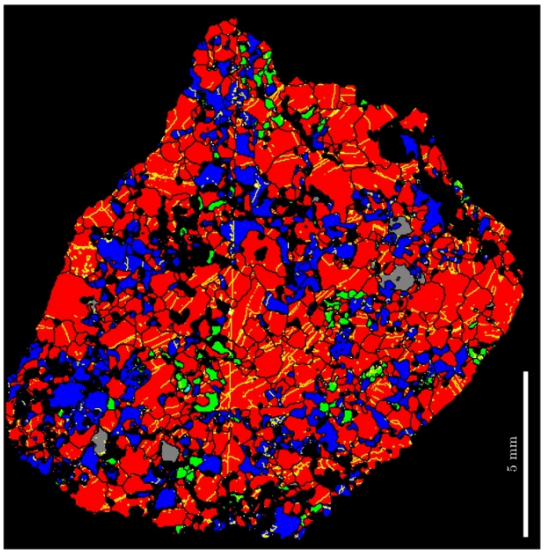

NJS1306

Texture: coarse granular

Phase assemblage:
ol+opx+cpx+sp

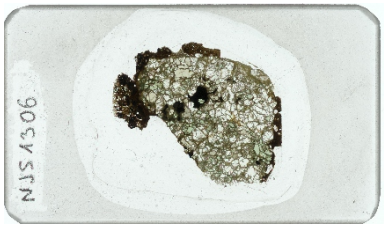

2 cm

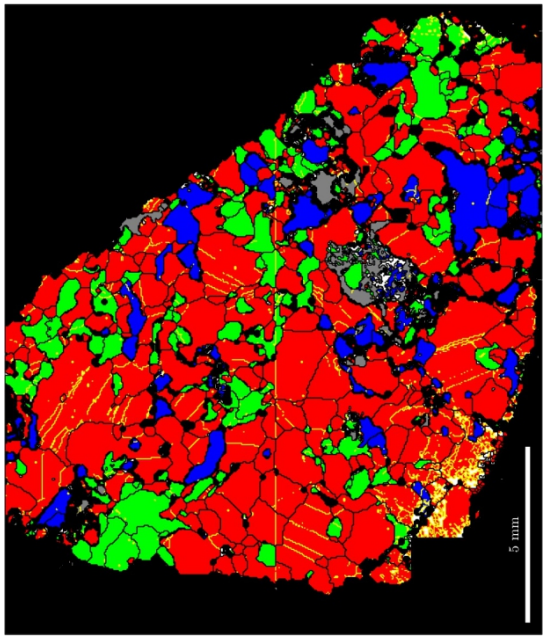

olivine
orthopyroxene
clinopyroxene
spinel
amphibole
yellow lines - subgrain boundaries

NJS1307

Texture: coarse granular

Phase assemblage:
ol+opx+cpx+sp

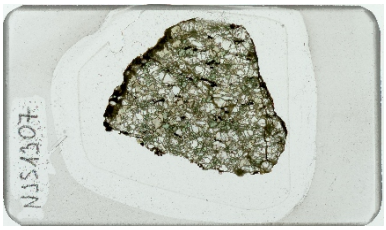

2 cm

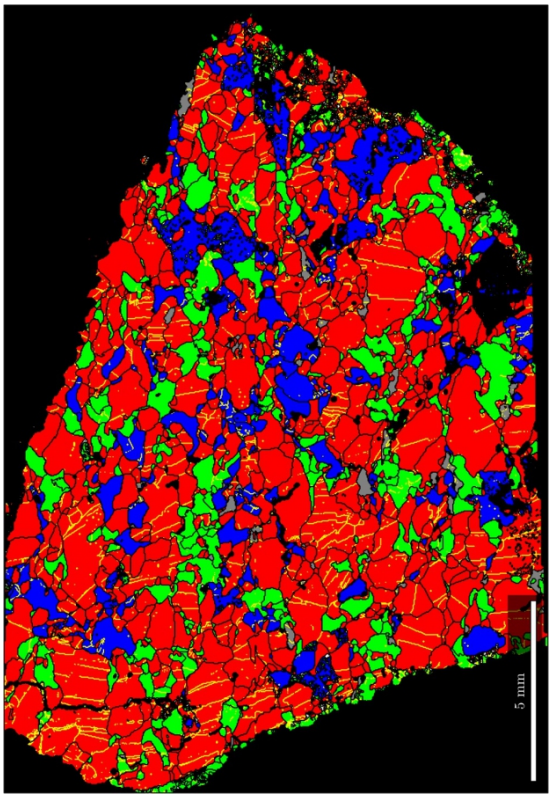

NPY1301

Texture: fine granular

Phase assemblage:
ol+opx+cpx+sp

2 cm

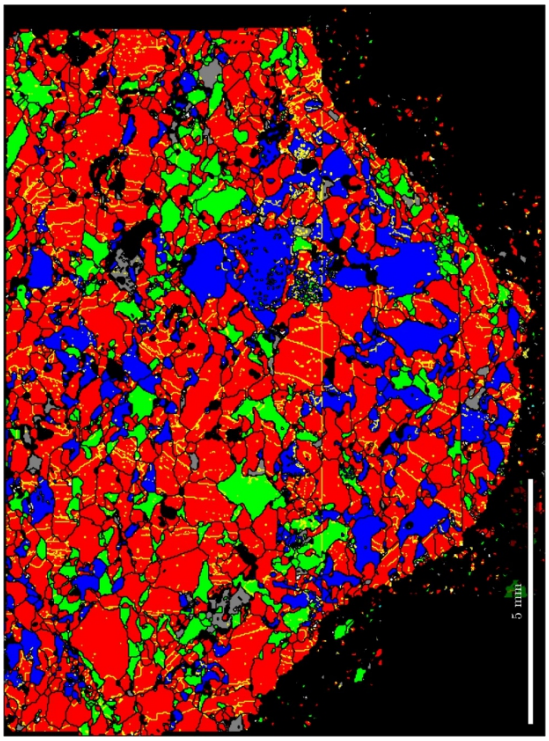

olivine orthopyroxene clinopyroxene spinel amphibole yellow lines - subgrain boundaries

NPY1310

Texture: fine granular

Phase assemblage:
ol+opx+cpx+sp

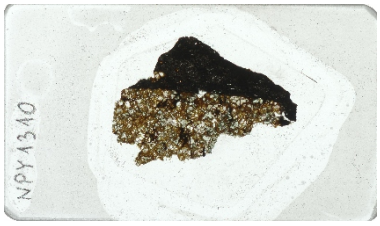

2 cm

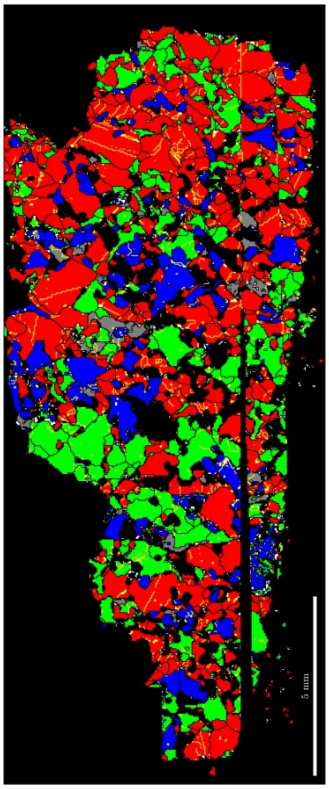

NPY1311

Texture: fine porphyroclastic

Phase assemblage:
ol+opx+cpx+sp

Lineation is outlined by elongated olivine grains and pyroxene-spinel distribution.

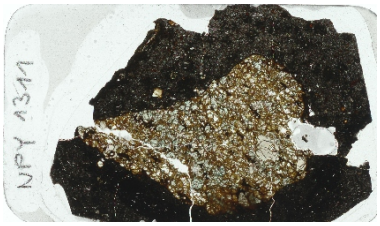

2 cm

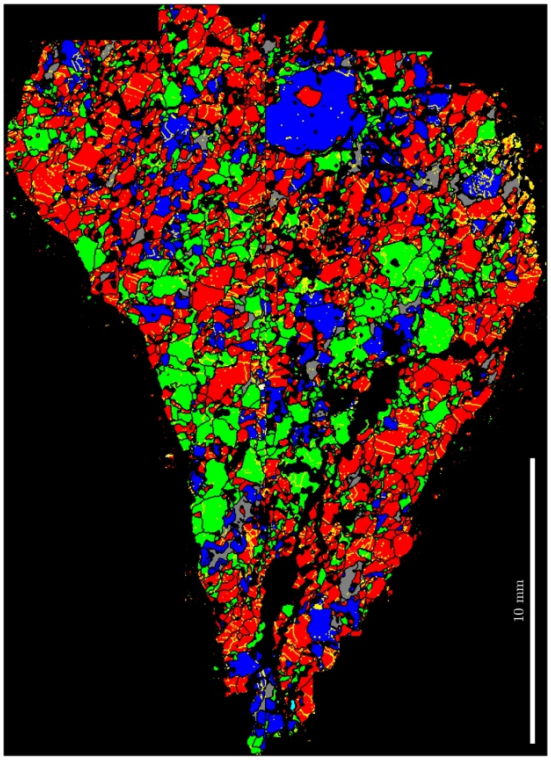

olivine ■ orthopyroxene ■ clinopyroxene ■ spinel ■ amphibole ■ yellow lines - subgrain boundaries

NPY1314

Texture: fine granular

Phase assemblage:
ol+opx+cpx+sp

2 cm

NFL1302

Texture: fine granular

Phase assemblage:
ol+opx+cpx+sp+amp

Lineation is outlined by
elongated olivine grains.

2 cm

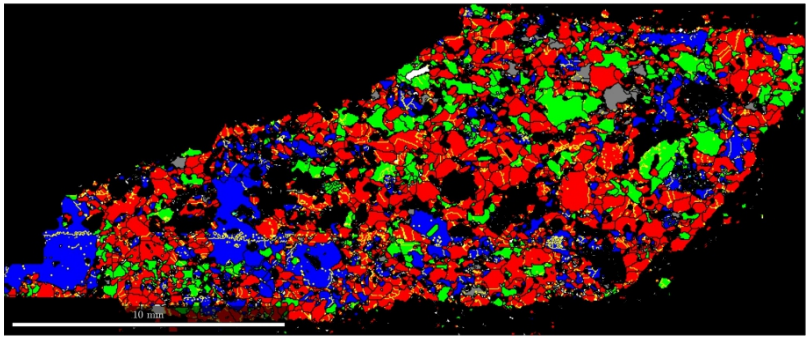

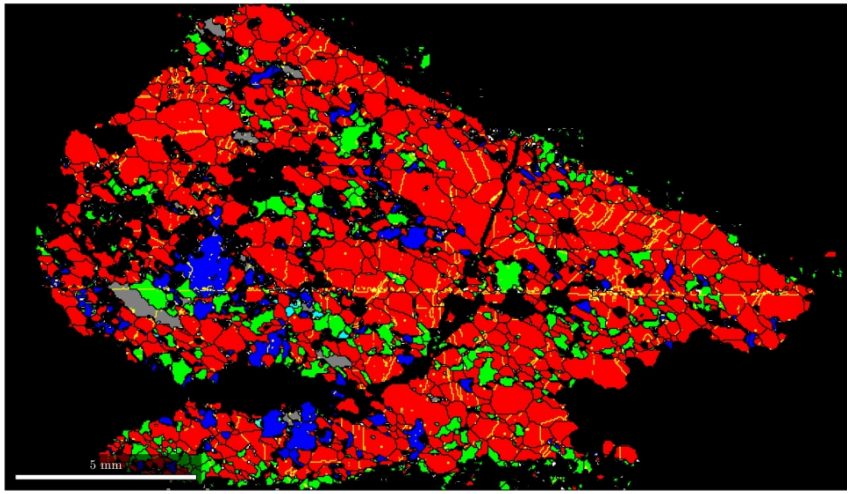

olivine orthopyroxene clinopyroxene spinel amphibole yellow lines - subgrain boundaries

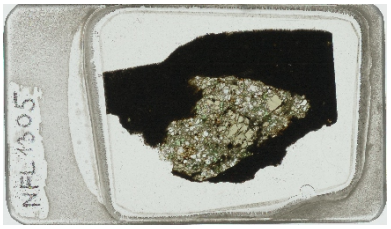

2 cm

NFL1305

Texture: fine granular

Phase assemblage:
ol+opx+cpx+sp

Orthopyroxene porphyroclasts, but olivine grains are evenly sized and have slightly curved boundaries.

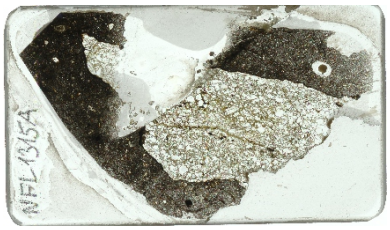

2 cm

NFL1315A

Texture: fine porphyroclastic

Phase assemblage:
ol+opx+cpx+sp+amp

Few amphibole grains are present. Olivine grain size differs in pyroxene-rich and pyroxene-poor parts.

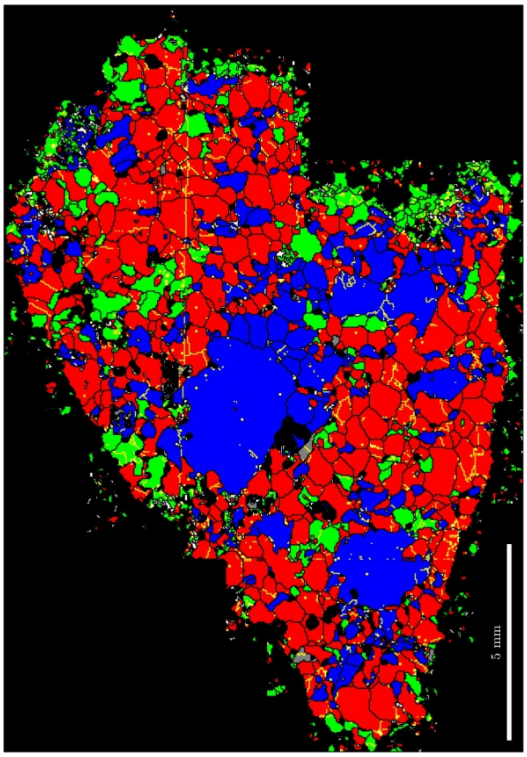

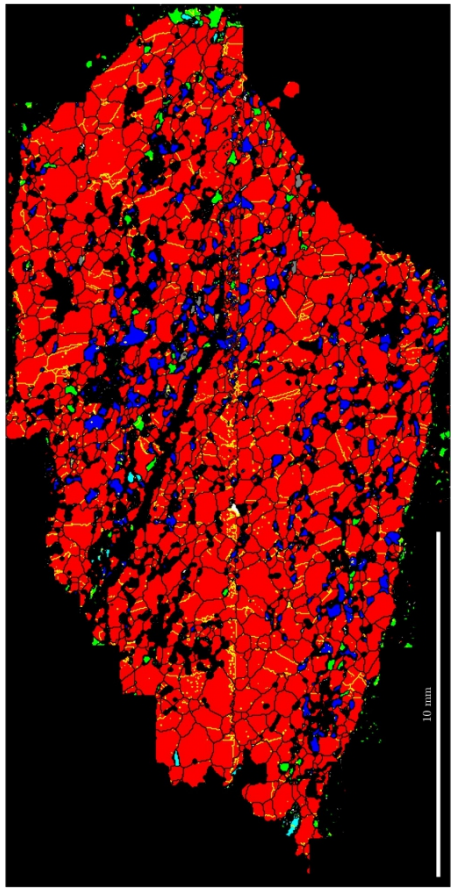

olivine ■ orthopyroxene ■ clinopyroxene ■ spinel ■ amphibole ■ yellow lines - subgrain boundaries

NFL1316

Texture: fine porphyroclastic

Phase assemblage: ol+opx+cpx+sp

Olivine grain size differs in pyroxene-rich and pyroxene-poor parts.

2 cm

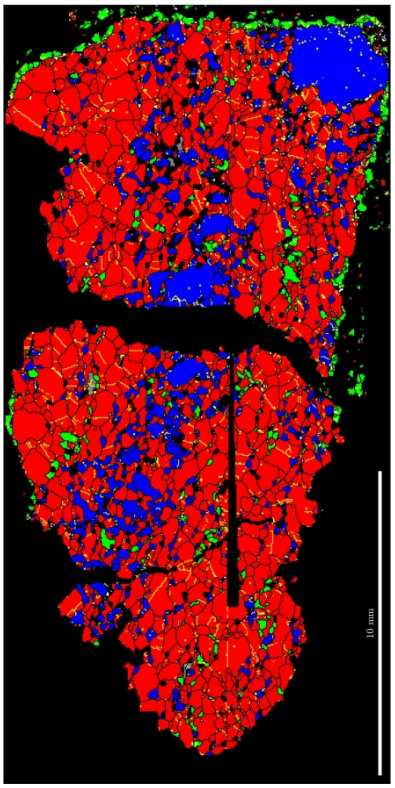

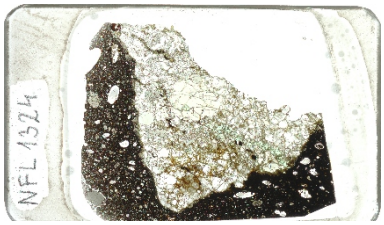

NFL1324

Texture: porphyroclastic

Phase assemblage: ol+opx+cpx+sp+amp

Vein-like appearance of amphibole and clinopyroxene; poikilitic orthopyroxene porphyroclast.

2 cm

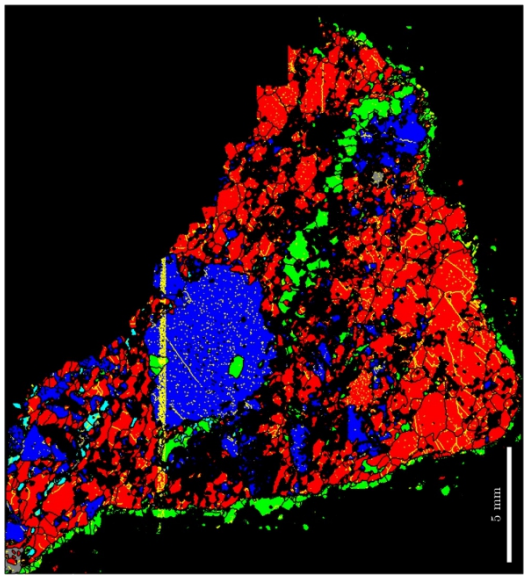

olivine orthopyroxene clinopyroxene spinel amphibole yellow lines - subgrain boundaries

2 cm

NFL1326

Texture: equigranular

Phase assemblage:
ol+cpx+sp+amp

The only xenolith without orthopyroxene, but with a texture matching the lherzolitic suite.

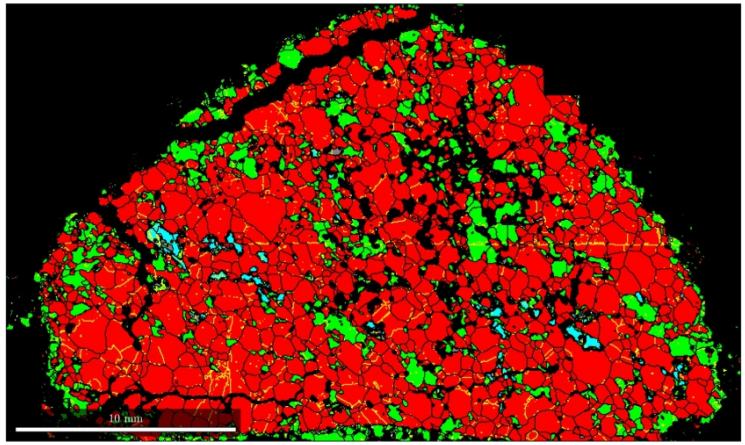

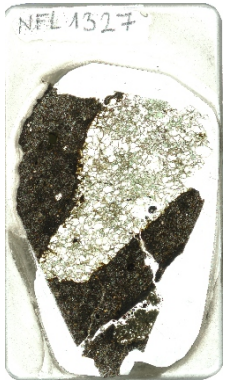

2 cm

NFL1327

Texture: equigranular

Phase assemblage:
ol+opx+cpx+sp

The only xenolith with a texture similar to the wehlite suite, but contains a small amount of orthopyroxene. Clinopyroxene grains contain silicate melt-inclusions.

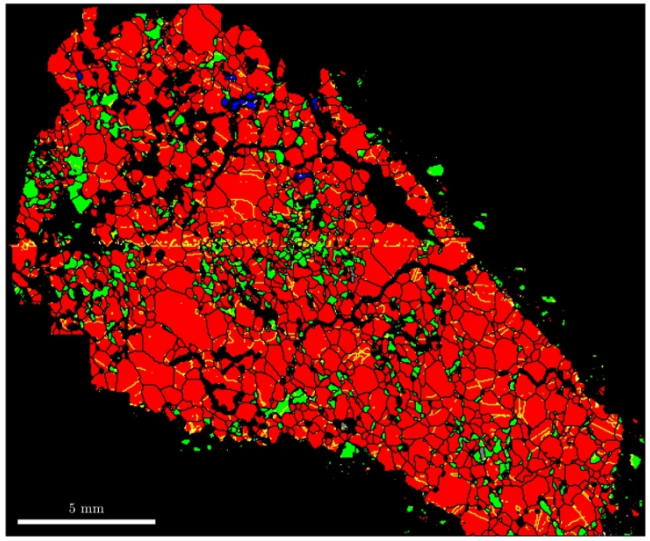

olivine orthopyroxene clinopyroxene spinel amphibole yellow lines - subgrain boundaries

NTB0306

Texture: fine granular

Phase assemblage:
ol+opx+cpx+sp

2 cm

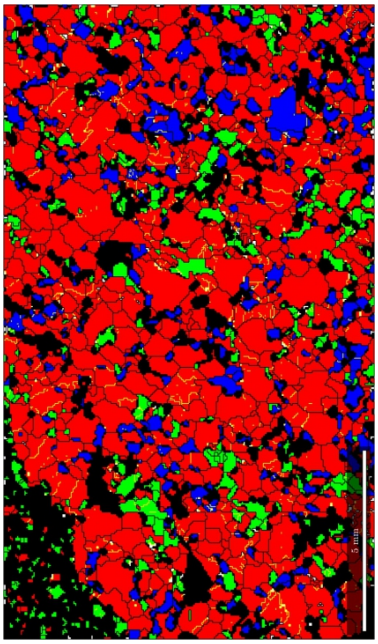

NFL1329

Texture: fine granular

Phase assemblage:
ol+opx+cpx+sp+amp

Small amount of
amphibole is present.

2 cm

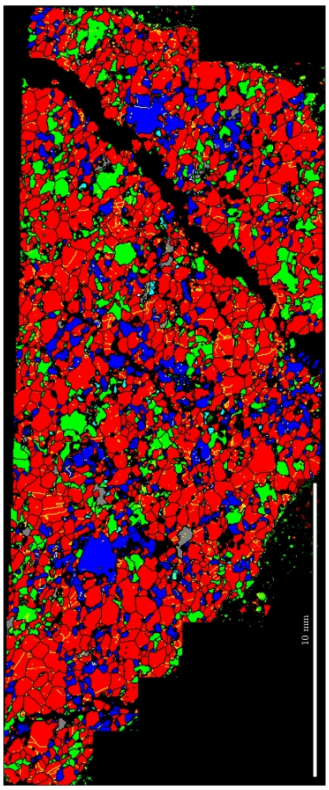

olivine orthopyroxene clinopyroxene spinel amphibole yellow lines - subgrain boundaries

NTB0307

Texture: fine porphyroclastic

Phase assemblage: ol+opx+cpx+sp

2 cm

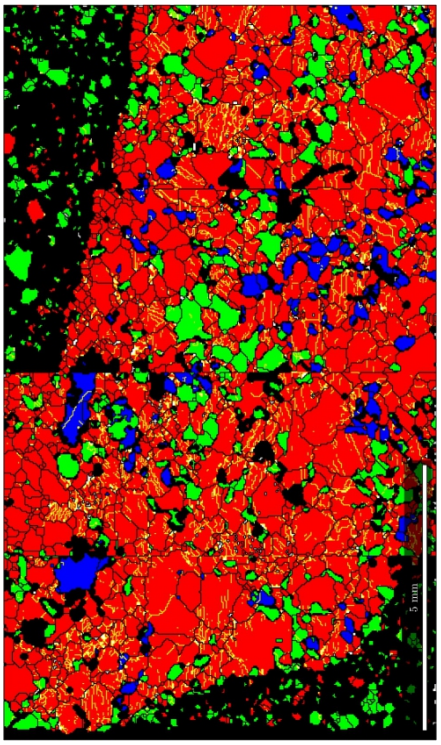

NTB1124

Texture: coarse granular

Phase assemblage: ol+opx+cpx+sp

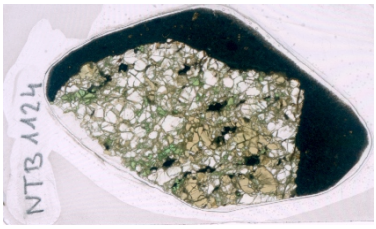

2 cm

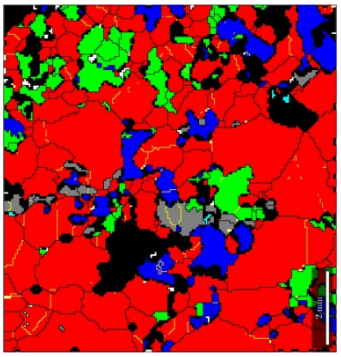

olivine orthopyroxene clinopyroxene spinel amphibole yellow lines - subgrain boundaries

NTB1122

Texture: coarse granular

Phase assemblage:
ol+opx+cpx+sp

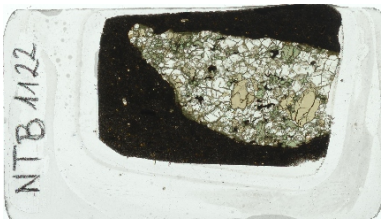

2 cm

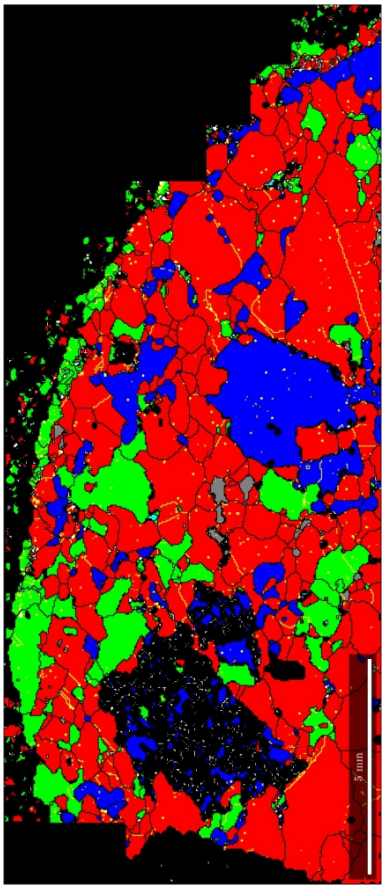

NTB1116

Texture: coarse granular

Phase assemblage:
ol+opx+cpx+sp

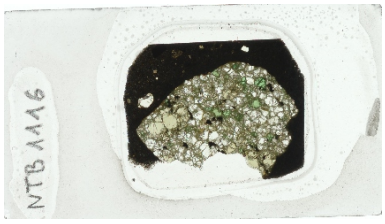

2 cm

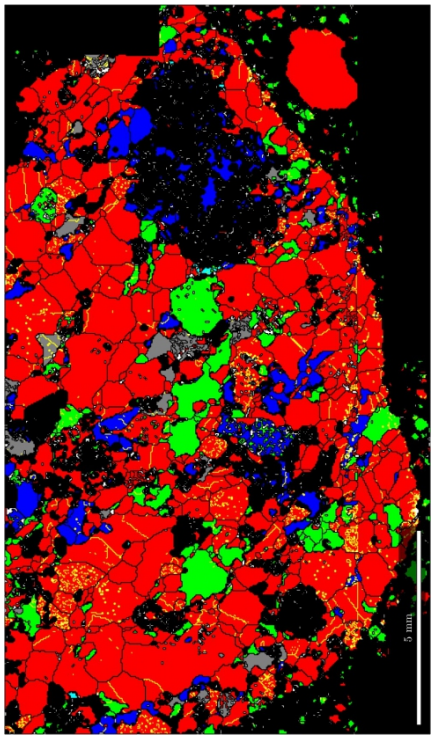

olivine
orthopyroxene
clinopyroxene
spinel
amphibole
yellow lines - subgrain boundaries

NFK0301

Texture: porphyroclastic

Phase assemblage:
ol+opx+cpx+sp

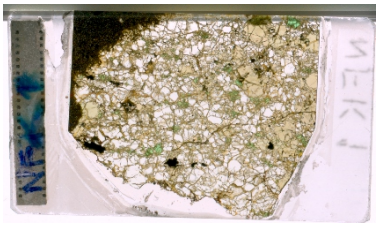

2 cm

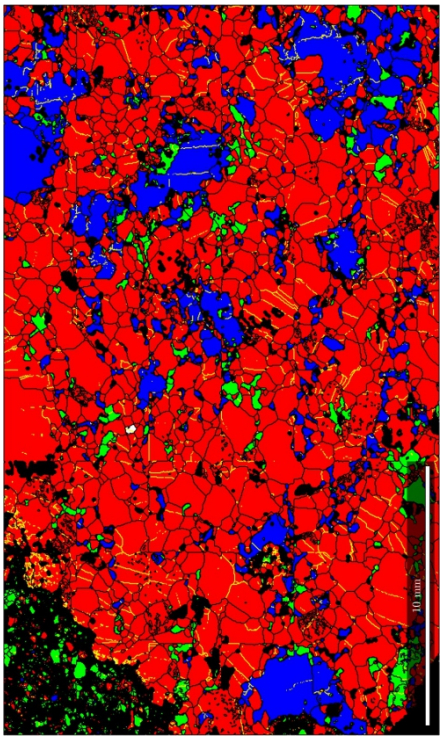

NFK1123

Texture: fine granular

Phase assemblage:
ol+opx+cpx+sp

Poikilitic character in
orthopyroxene porphyroxene porphyroclast.

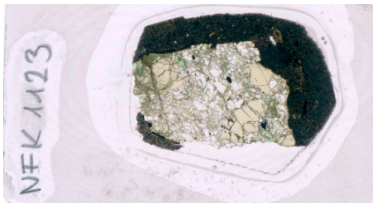

2 cm

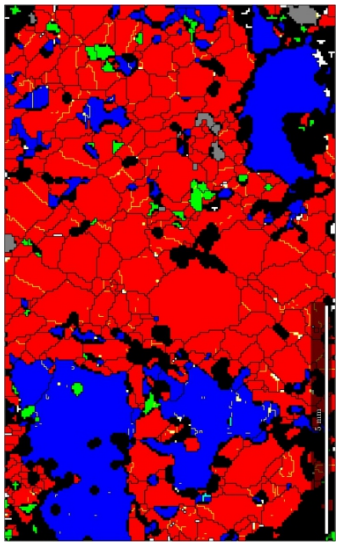

olivine orthopyroxene clinopyroxene spinel amphibole yellow lines - subgrain boundaries

2 cm

NFK1108

Texture: porphyroclastic

Phase assemblage:
ol+opx+cpx+sp

Olivine grain size differs in pyroxene-rich and pyroxene-poor parts.

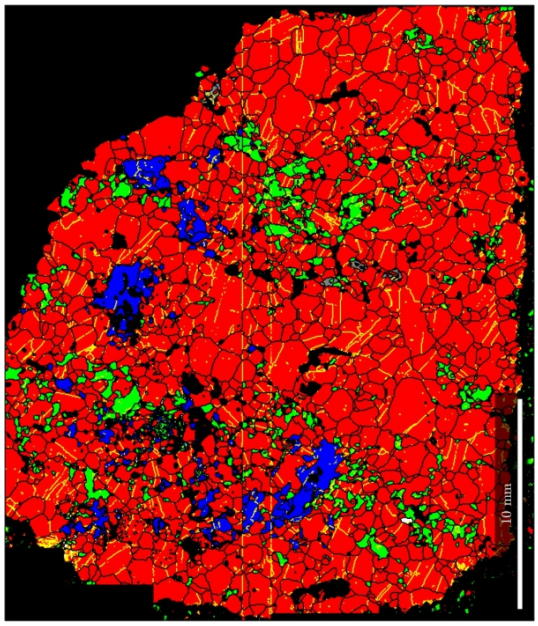

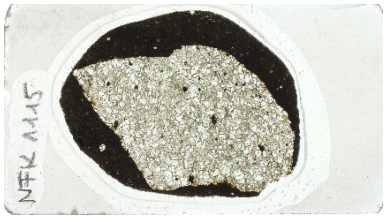

2 cm

NFK1115

Texture: equigranular

Phase assemblage:
ol+opx+cpx+sp

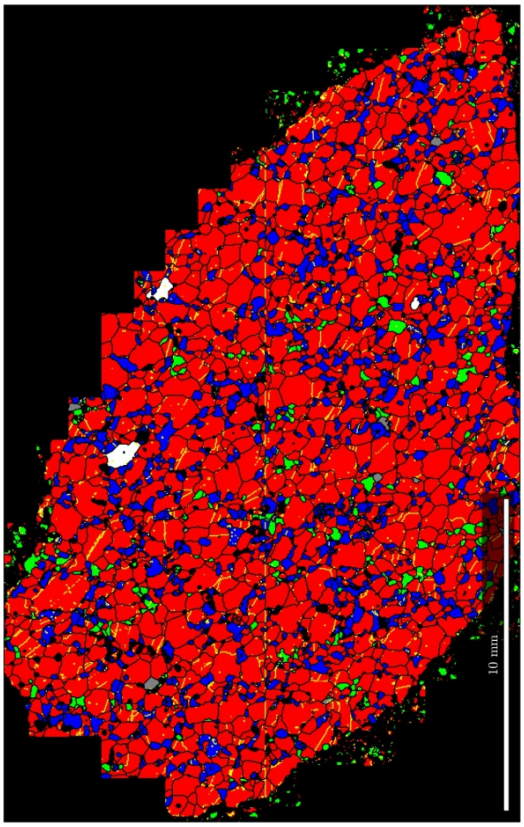

olivine
orthopyroxene
clinopyroxene
spinel
amphibole
yellow lines - subgrain boundaries

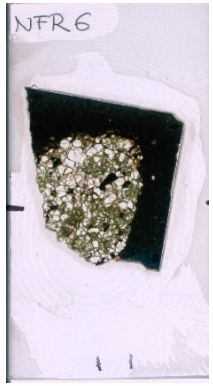

2 cm

NFR0306

Texture: coarse granular

Phase assemblage:
ol+opx+cpx+sp

Orthopyroxene-containing wehrlite

No EBSD analyses were carried out on this sample due to technical issues.

2 cm

NFR0307

Texture: porphyroclastic

Phase assemblage:
ol+opx+cpx+sp

No EBSD analyses were carried out on this sample due to technical issues.

olivine orthopyroxene clinopyroxene spinel amphibole yellow lines - subgrain boundaries

NFR1109

Texture: coarse granular

Phase assemblage:
ol+opx+cpx+sp

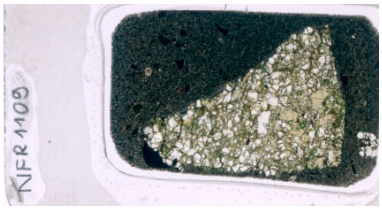

2 cm

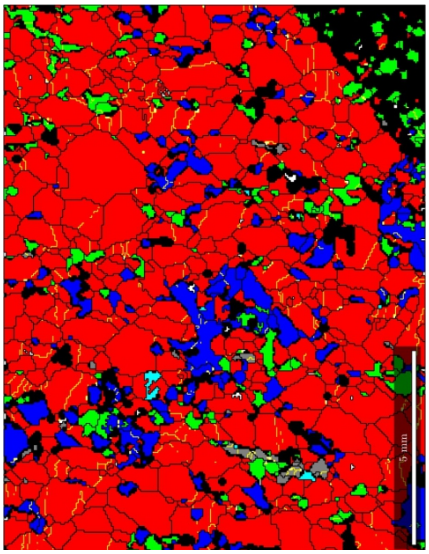

NFR0309

Texture: fine porphyroclastic

Phase assemblage:
ol+opx+cpx+sp

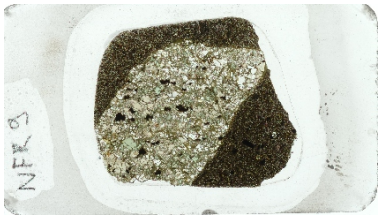

2 cm

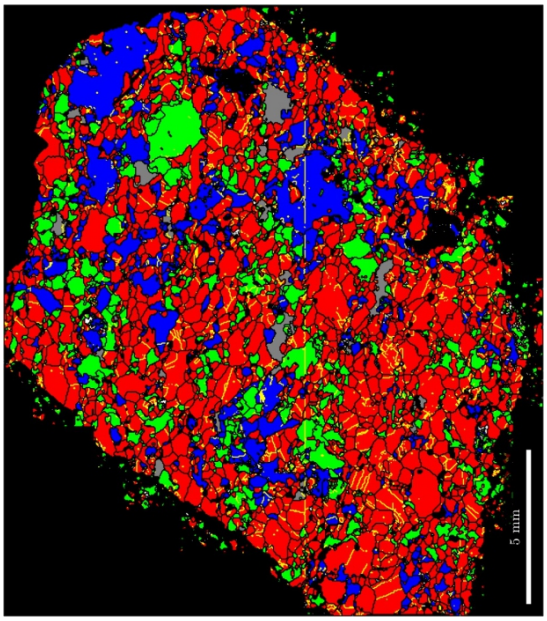

olivine orthopyroxene clinopyroxene spinel amphibole yellow lines - subgrain boundaries

NFR1107

Texture: porphyroclastic

Phase assemblage:
ol+opx+cpx+sp

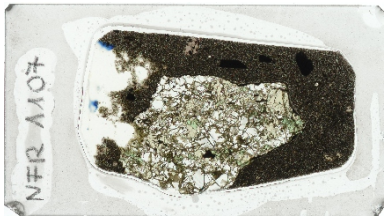

2 cm

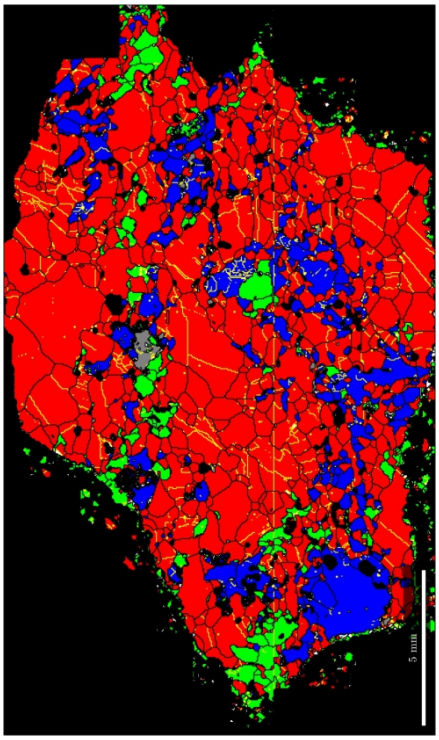

NMC1301

Texture: coarse granular

Phase assemblage:
ol+opx+cpx+sp

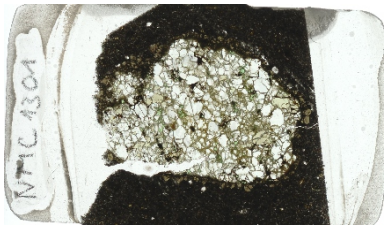

2 cm

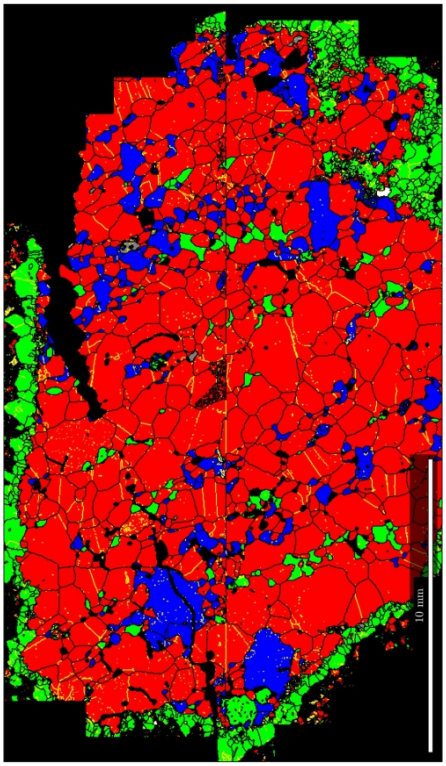

olivine
orthopyroxene
clinopyroxene
spinel
amphibole
yellow lines - subgrain boundaries

NMC1322

Texture: fine porphyroclastic

Phase assemblage:
ol+opx+cpx+sp

Abundant melt pockets.

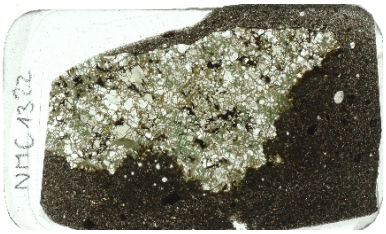

2 cm

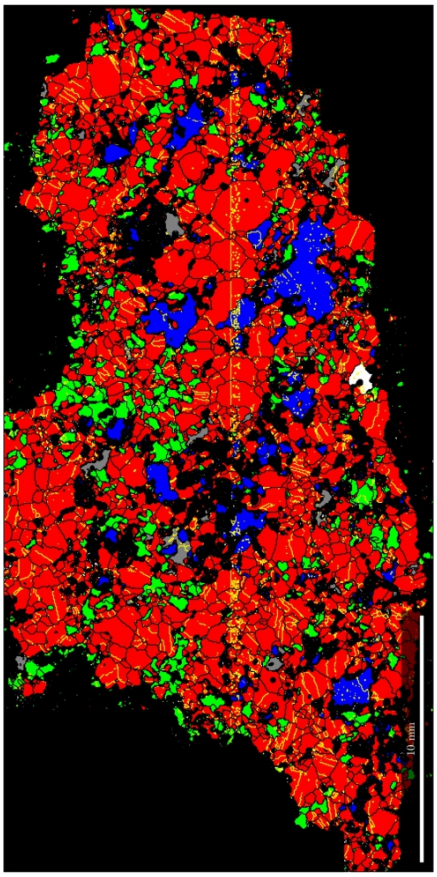

NMC1309

Texture: coarse granular

Phase assemblage:
ol+opx+cpx+sp

Clinopyroxene-rich modal composition.

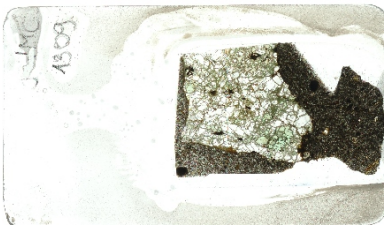

2 cm

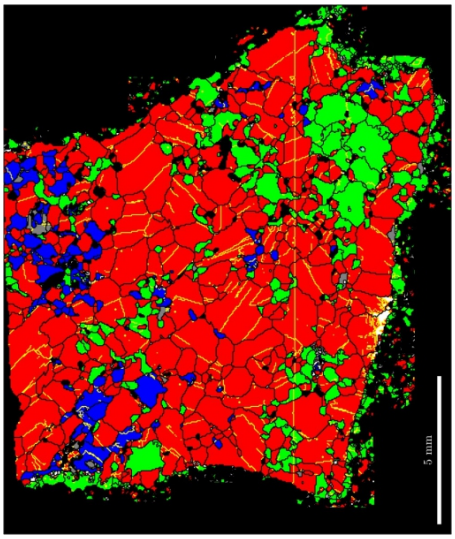

olivine orthopyroxene clinopyroxene spinel amphibole yellow lines - subgrain boundaries

NMC1336A

Texture: fine porphyroclastic

Phase assemblage: ol+opx+cpx+sp

Lineation is outlined by spinel distribution and elongated olivine grains.

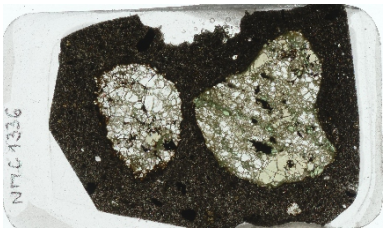

2 cm

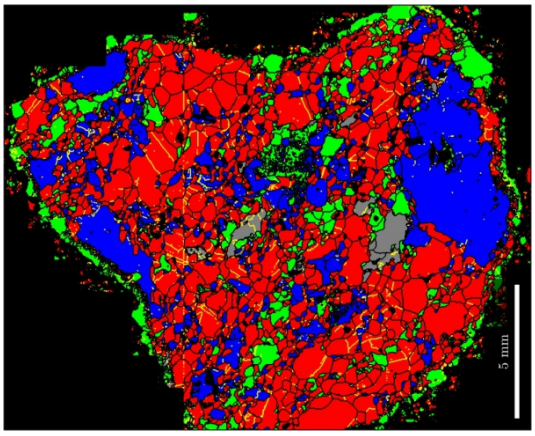

NMM1126

Texture: porphyroclastic

Phase assemblage: ol+opx+cpx+sp

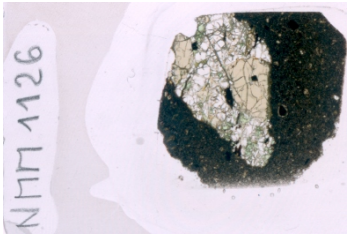

2 cm

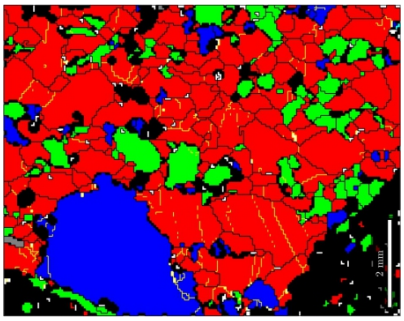

olivine orthopyroxene clinopyroxene spinel amphibole yellow lines - subgrain boundaries

2 cm

NMM0318

Texture: fine porphyroclastic

Phase assemblage: ol+opx+cpx+sp

Minor amount of amphibole, revealed only by EBSD mapping.

2 cm

NMM1115

Texture: fine porphyroclastic

Phase assemblage: ol+opx+cpx+sp

Lineation outlined by spinel distribution.

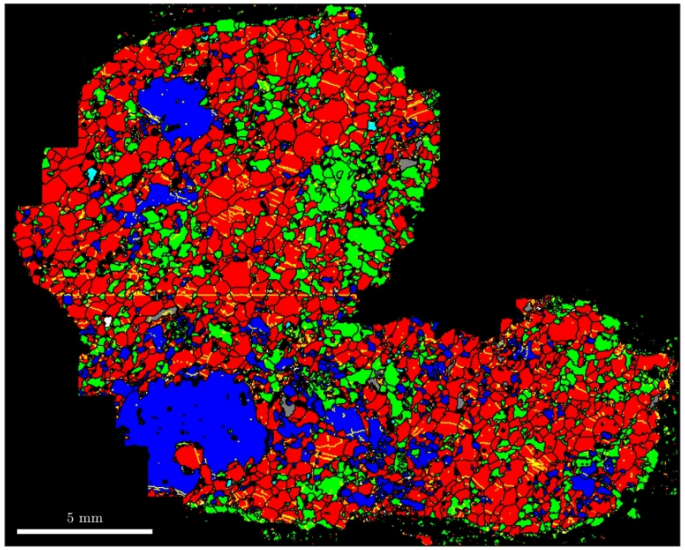

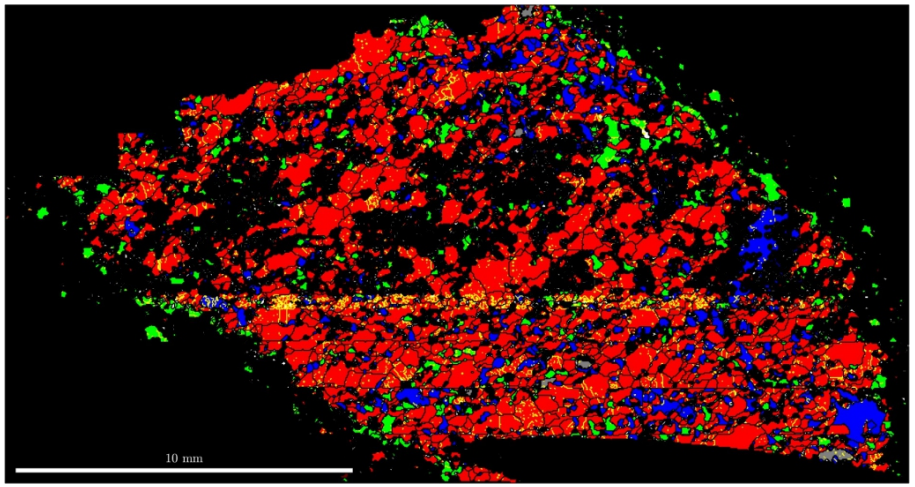

olivine orthopyroxene clinopyroxene spinel amphibole yellow lines - subgrain boundaries

NME1116

Texture: porphyroclastic

Phase assemblage:
ol+opx+cpx+sp

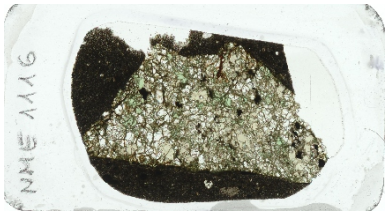

2 cm

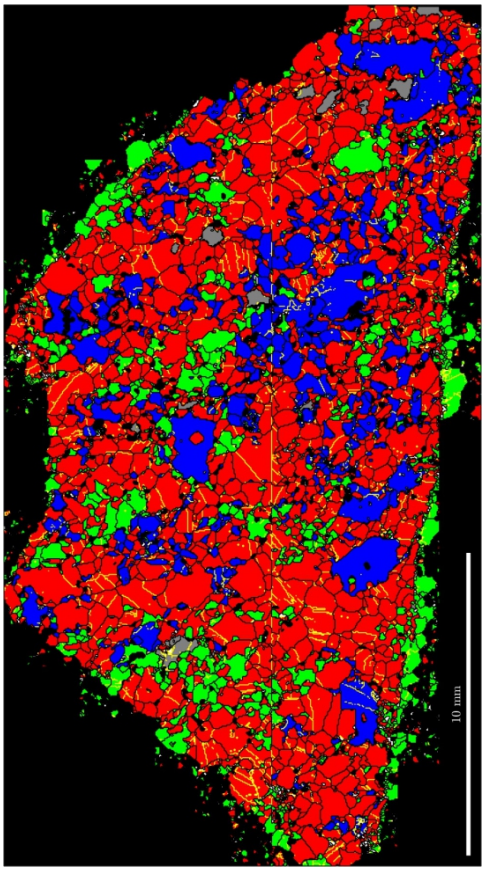

NME1122

Texture: coarse granular

Phase assemblage:
ol+opx+cpx+sp

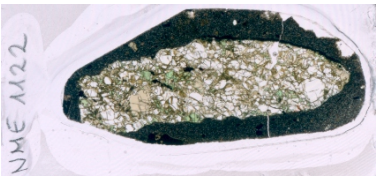

2 cm

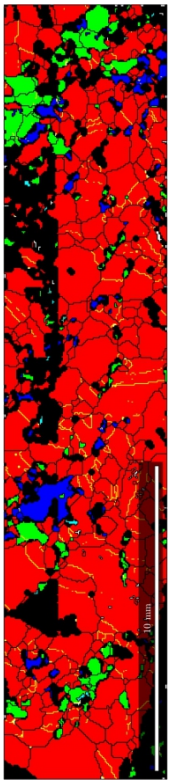

olivine
orthopyroxene
clinopyroxene
spinel
amphibole
yellow lines - subgrain boundaries

NME0528

Texture: fine granular

Phase assemblage:
ol+opx+cpx+sp

Olivine grain size differs in pyroxene-rich and pyroxene-poor parts.

2 cm

NBN0302A

Texture: fine porphyroclastic

Phase assemblage:
ol+opx+cpx+sp

Lineation outlined by spinel and melt pocket distribution. Olivine grain size differs in pyroxene-rich and pyroxene-poor parts.

2 cm

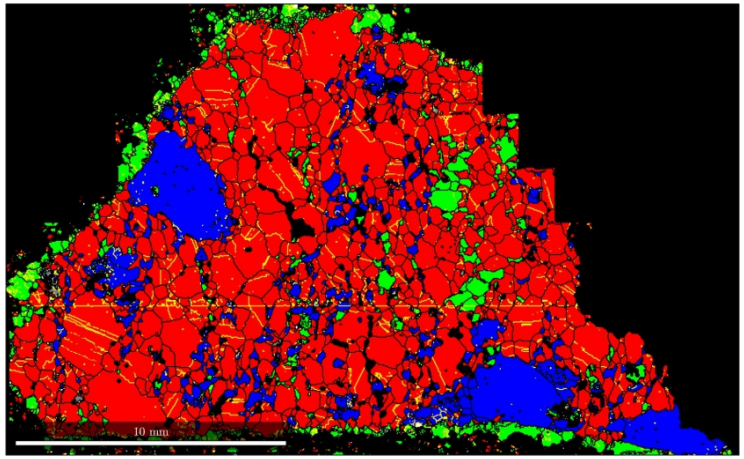

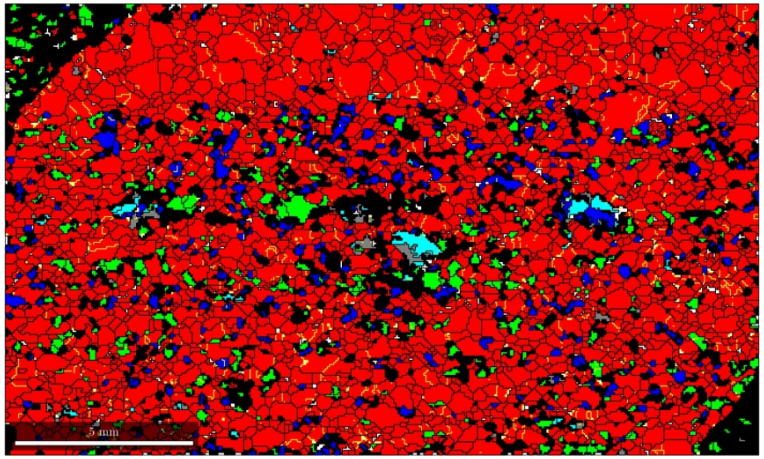

olivine orthopyroxene clinopyroxene spinel amphibole yellow lines - subgrain boundaries

NBN0305

Texture: equigranular

Phase assemblage: ol+opx+cpx+sp

Lineation outlined by spinel distribution.

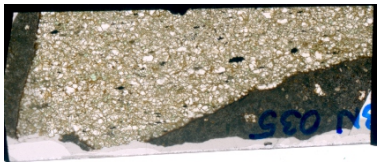

2 cm

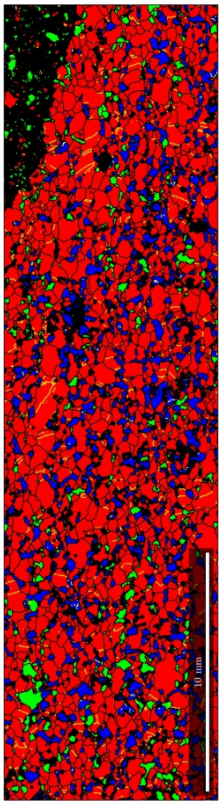

NBN0311

Texture: fine porphyroclastic

Phase assemblage: ol+opx+cpx+sp

Lineation outlined by spinel and melt pocket distribution.

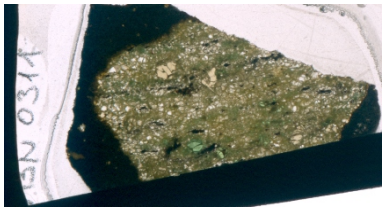

2 cm

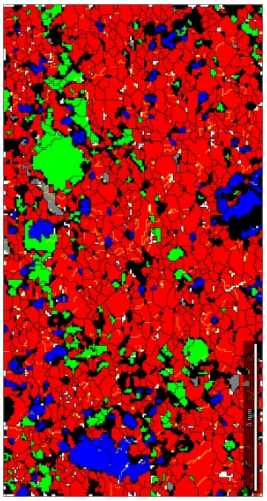

olivine | orthopyroxene | clinopyroxene | spinel | amphibole | yellow lines - subgrain boundaries

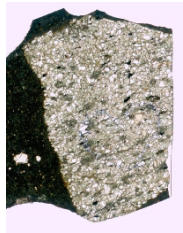

NBN0316

Texture: equigranular

Phase assemblage:
ol+opx+cpx+sp

Lineation outlined by
spinel distribution.

NBN0319

Texture: equigranular

Phase assemblage:
ol+opx+cpx+sp

Lineation outlined by spinel
and melt pocket distribution.

2 cm

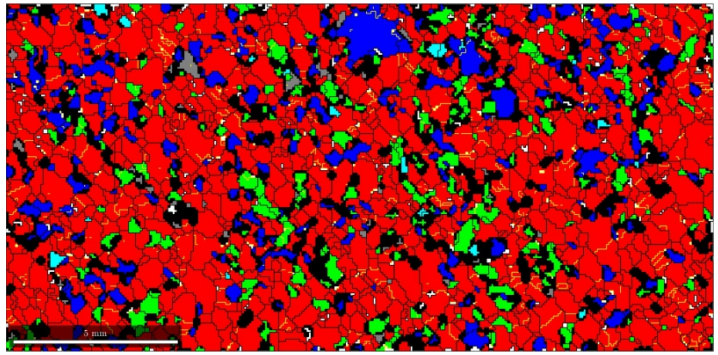

2 cm

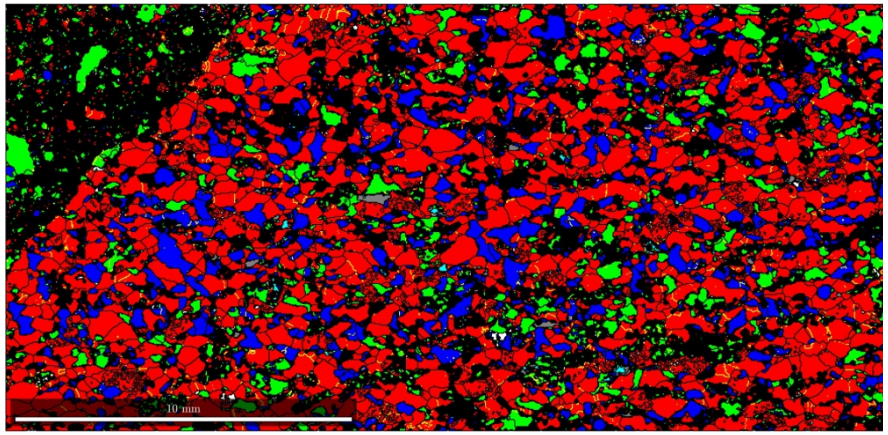

olivine orthopyroxene clinopyroxene spinel amphibole yellow lines - subgrain boundaries

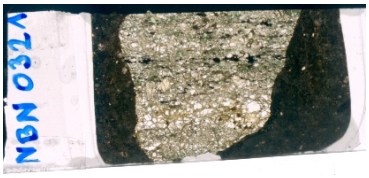

NBN0321

Texture: fine porphyroclastic

Phase assemblage: ol+opx+cpx+sp

Lineation outlined by spinel distribution. Olivine grain size differs in pyroxene-rich and pyroxene-poor parts.

2 cm

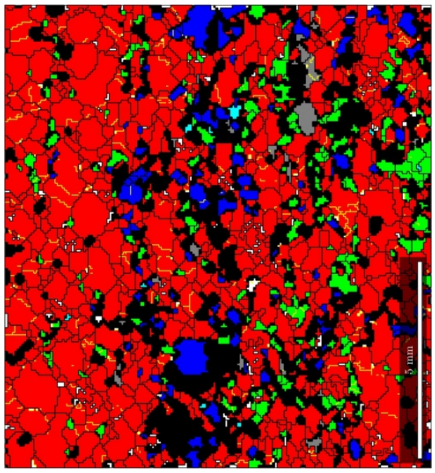

olivine | orthopyroxene | clinopyroxene | spinel | amphibole | yellow lines - subgrain boundaries

Appendix B: Mineral Major- and Trace-element Analyses

Appendix B1 - Mineral Major-element Compositions

OLIVINE

Sample	SiO_2	Al_2O_3	FeO	MnO	MgO	CaO	NiO
NMS1302A	41.4		8.44	0.15	50.2	0.05	0.39
	41.8		8.36	0.11	50.0	0.06	0.40
	41.8		8.34	0.12	50.0	0.05	0.39
	41.5		8.43	0.12	50.0	0.06	0.39
	41.7		8.51	0.15	50.2	0.03	0.41
	41.9		8.56	0.12	50.1	0.04	0.40
	41.8		8.48	0.13	50.2	0.04	0.42
	41.7		8.31	0.15	49.9	0.04	0.37
	41.4		8.52	0.13	49.9	0.04	0.41
	41.3		8.34	0.14	49.9	0.05	0.39
	42.0		8.43	0.12	49.9	0.03	0.39
	41.7		8.53	0.14	50.1	0.05	0.40
	41.7		8.48	0.09	50.1	0.05	0.39
	41.3		8.52	0.14	50.2	0.05	0.45
	41.2		8.52	0.13	50.2	0.05	0.40
	41.1		8.48	0.12	50.2	0.04	0.44
	41.5		8.65	0.12	50.3	0.06	0.41
	41.2		8.56	0.13	50.2	0.05	0.39
	41.4		8.51	0.12	50.1	0.06	0.39
	41.6		8.47	0.14	50.1	0.05	0.43
	41.8		8.53	0.12	50.1	0.05	0.43
	41.6		8.46	0.10	50.0	0.06	0.41
NMS1304	41.5		9.42	0.12	48.6	0.05	0.39
	41.4		9.52	0.14	48.6	0.04	0.37
	41.1		9.54	0.15	48.8	0.05	0.44
	40.5		9.44	0.11	48.8	0.05	0.41
	41.0		9.46	0.11	48.6	0.06	0.39
	41.1		9.35	0.13	48.8	0.06	0.37
	41.4		9.36	0.15	48.7	0.05	0.39
	41.5		9.39	0.14	48.7	0.05	0.41
	41.2		9.42	0.14	48.7	0.07	0.40
	40.8		9.42	0.11	48.5	0.06	0.39
	41.0		9.38	0.13	48.6	0.05	0.39
	41.2		9.34	0.13	48.7	0.04	0.43
	41.1	0.03	9.53	0.12	48.7	0.05	0.42
	41.3	0.03	9.35	0.14	48.7	0.05	0.41
NMS1305	41.1		10.5	0.15	48.5	0.06	0.38
	40.7		10.3	0.15	48.5	0.06	0.36
	41.2		10.4	0.13	48.6	0.06	0.43
	41.1		10.3	0.17	48.7	0.07	0.44
	40.9		10.4	0.12	48.6	0.06	0.42
	41.0	0.03	10.2	0.15	48.6	0.06	0.41
	41.2		10.4	0.14	48.5	0.06	0.39
	41.0		10.3	0.16	48.5	0.06	0.39
	41.2		10.3	0.12	48.7	0.05	0.43
	41.2		10.4	0.15	48.6	0.04	0.39
	41.4		10.5	0.14	48.6	0.06	0.44
	41.1		10.4	0.13	48.6	0.06	0.39
	40.7		10.3	0.14	48.6	0.05	0.38
	40.9		10.4	0.16	48.5	0.05	0.40
	41.1		10.4	0.17	48.5	0.05	0.42
	41.7		10.3	0.13	48.4	0.06	0.42
	41.3		10.4	0.14	48.6	0.06	0.43
	41.4		10.5	0.15	48.5	0.05	0.45
	41.2		10.3	0.13	48.4	0.06	0.39

OLIVINE

Sample	SiO_2	Al_2O_3	FeO	MnO	MgO	CaO	NiO
NMS1308	40.9		9.60	0.15	48.8	0.06	0.39
	41.3		9.54	0.14	48.8	0.06	0.40
	41.1		9.64	0.12	48.9	0.06	0.40
	41.3		9.58	0.15	48.7	0.04	0.39
	41.2		9.65	0.13	48.9	0.05	0.38
	41.4		9.62	0.14	48.7	0.04	0.41
	40.9		9.56	0.14	48.8	0.05	0.40
	40.9		9.55	0.14	48.9	0.05	0.44
	40.8		9.60	0.17	48.9	0.06	0.42
	41.3		9.66	0.15	48.9	0.06	0.40
	41.2		9.64	0.13	48.7	0.05	0.42
	41.2		9.49	0.15	48.9	0.06	0.43
	41.2		9.59	0.13	48.9	0.06	0.40
	40.8		9.47	0.13	48.8	0.05	0.40
	41.1		9.73	0.14	48.9	0.06	0.40
	41.0		9.61	0.14	49.0	0.05	0.40
NMS1310	40.6		9.76	0.15	49.2	0.06	0.40
	40.6		9.84	0.13	49.3	0.06	0.40
	41.5		9.78	0.13	49.5	0.06	0.41
	40.7		9.88	0.12	49.4	0.06	0.38
	40.9		9.85	0.12	49.5	0.06	0.38
	41.0		9.92	0.15	49.4	0.05	0.45
	41.3		9.82	0.16	49.3	0.05	0.41
	40.8		9.83	0.13	49.3	0.05	0.39
	41.0		9.73	0.14	49.1	0.05	0.40
	40.6	0.04	9.89	0.15	48.9	0.07	0.37
	40.6		9.83	0.13	49.3	0.06	0.41
NJS1302	40.2		11.7	0.17	47.2	0.07	0.40
	40.2		11.9	0.15	47.3	0.06	0.39
	40.5		11.7	0.15	47.4	0.05	0.37
	41.1		11.8	0.13	47.3	0.06	0.41
	40.3	0.03	11.6	0.15	47.2	0.06	0.38
	41.0	0.03	11.6	0.14	47.1	0.06	0.38
	40.9	0.03	11.7	0.16	47.4	0.06	0.40
	40.7	0.03	11.6	0.20	47.2	0.04	0.35
	41.2		11.5	0.13	47.3	0.07	0.36
	40.3		11.7	0.15	47.4	0.06	0.40
	40.5		11.5	0.16	47.2	0.07	0.36
	41.0	0.04	11.6	0.15	47.3	0.06	0.41
	40.7	0.03	11.5	0.16	47.4	0.05	0.36
NJS1304	40.7		11.7	0.16	47.6	0.05	0.39
	40.5		11.7	0.16	47.7	0.06	0.36
	40.9		11.6	0.15	47.8	0.07	0.39
	41.1		11.7	0.13	47.7	0.07	0.38
	41.0	0.03	11.7	0.19	47.7	0.06	0.37
	40.3		11.7	0.17	47.6	0.05	0.37
	41.0		11.9	0.16	47.8	0.07	0.41
	40.6	0.04	11.6	0.16	47.9	0.07	0.42
	40.8		11.8	0.15	47.7	0.05	0.37
	41.0		11.6	0.17	47.4	0.05	0.41
	40.9	0.03	11.8	0.15	47.8	0.06	0.37
	40.4	0.03	11.9	0.14	47.9	0.08	0.42
	41.1		11.7	0.16	47.9	0.06	0.42
	40.5		11.8	0.15	47.8	0.06	0.40

OLIVINE

Sample	SiO_2	Al_2O_3	FeO	MnO	MgO	CaO	NiO
NJS1306	39.8	0.04	12.3	0.18	47.1	0.11	0.36
	40.9		12.7	0.20	46.8	0.09	0.39
	40.7		12.4	0.18	46.8	0.09	0.41
	40.6	0.06	12.4	0.19	46.7	0.09	0.41
	41.0	0.04	12.4	0.18	47.0	0.09	0.41
	40.8		11.9	0.17	47.6	0.10	0.40
	41.2	0.03	11.6	0.18	47.6	0.09	0.41
	40.6		11.6	0.16	47.4	0.10	0.32
	40.9	0.04	11.7	0.17	47.3	0.10	0.41
	40.4		11.5	0.16	47.4	0.09	0.37
	40.9		11.9	0.16	47.4	0.09	0.34
	40.7	0.04	12.0	0.16	47.4	0.09	0.36
	40.5	0.03	11.9	0.18	47.3	0.10	0.38
	40.8		11.9	0.18	47.5	0.10	0.43
NJS1307	40.8	0.03	10.5	0.18	48.4	0.07	0.39
	40.9	0.03	10.5	0.16	48.5	0.09	0.38
	40.8		10.5	0.18	48.5	0.08	0.44
	41.6	0.03	10.4	0.18	48.3	0.09	0.38
	40.8	0.03	10.3	0.14	48.5	0.09	0.42
	40.7	0.03	10.4	0.13	48.5	0.08	0.36
	41.1		10.4	0.12	48.5	0.08	0.35
	41.3		10.4	0.13	48.7	0.10	0.38
	41.1		10.4	0.13	48.7	0.09	0.43
	41.2		10.4	0.16	48.8	0.08	0.41
	41.2		10.5	0.14	48.5	0.08	0.39
	40.9		10.4	0.12	48.6	0.10	0.41
NPY1301	41.2	0.03	10.4	0.14	48.3	0.06	0.39
	41.2		10.4	0.13	48.3	0.06	0.35
	40.6		10.3	0.14	48.5	0.07	0.42
	41.4		10.4	0.15	48.5	0.06	0.35
	41.2		10.3	0.13	48.6	0.07	0.37
	40.9		10.3	0.15	48.4	0.07	0.39
	41.4		10.3	0.17	48.8	0.08	0.40
	41.1		10.5	0.14	48.5	0.05	0.42
	41.3		10.4	0.18	48.5	0.06	0.41
	41.2		10.4	0.15	48.6	0.06	0.41
	41.5		10.4	0.14	48.5	0.05	0.37
	41.4		10.3	0.15	48.5	0.05	0.38
	40.4		10.4	0.16	48.6	0.05	0.38
NPY1310	41.2		11.0	0.15	47.2	0.06	0.43
	40.8		11.1	0.17	47.0	0.06	0.36
	40.9		11.1	0.15	47.1	0.07	0.34
	41.0	0.03	11.1	0.14	47.1	0.08	0.35
	40.9	0.03	11.3	0.13	47.1	0.06	0.36
	40.5		11.0	0.16	47.1	0.07	0.39
	40.5		11.2	0.17	47.2	0.07	0.40
	40.8		11.2	0.14	47.2	0.07	0.40
NPY1311	40.8		11.0	0.15	47.1	0.05	0.36
	40.6		11.0	0.18	47.2	0.06	0.37
	40.5		11.1	0.17	47.5	0.07	0.39
	41.2		11.0	0.15	47.2	0.06	0.38
	40.9		11.0	0.19	47.3	0.06	0.35
	40.9		11.0	0.15	47.3	0.07	0.38
	40.9		10.9	0.14	47.3	0.07	0.34
	40.9		10.9	0.18	47.2	0.06	0.33
	41.0	0.02	11.3	0.17	47.7	0.07	0.37

OLIVINE

Sample	SiO_2	Al_2O_3	FeO	MnO	MgO	CaO	NiO
NPY1314	41.2	-0.01	10.3	0.15	48.1	0.07	0.38
	41.2		10.2	0.17	48.3	0.06	0.36
	40.7	0.01	10.3	0.15	47.9	0.07	0.41
	40.7	0.02	10.2	0.12	48.2	0.07	0.38
	40.6	-0.01	10.1	0.14	48.0	0.05	0.40
	41.2	0.03	10.2	0.16	47.9	0.07	0.43
	41.4		10.0	0.18	48.3	0.05	0.37
	40.4	0.02	9.92	0.14	48.2	0.05	0.40
NFL1302	41.3		9.36	0.16	49.3	0.07	0.41
	40.4		9.39	0.13	49.2	0.05	0.40
	41.2		9.43	0.15	49.1	0.07	0.42
	41.1		9.39	0.15	49.1	0.05	0.46
	40.7		9.40	0.13	49.0	0.07	0.41
	41.1		9.39	0.12	49.0	0.07	0.39
	40.9		9.41	0.13	49.1	0.06	0.40
	41.1		9.36	0.12	49.1	0.07	0.38
	41.0		9.46	0.15	49.2	0.06	0.41
	41.0	0.03	9.51	0.13	49.2	0.06	0.37
	41.0		9.45	0.17	49.0	0.03	0.41
	41.2		9.47	0.11	48.9	0.07	0.41
	40.3	0.30	9.39	0.13	49.0	0.06	0.40
	40.7	0.03	9.35	0.15	49.2	0.08	0.41
NFL1305	40.9	0.03	9.30	0.14	49.0	0.07	0.37
	40.5	0.02	9.35	0.15	49.1	0.07	0.37
	40.7	0.01	9.20	0.13	48.8	0.07	0.41
	41.1	0.01	9.25	0.14	49.0	0.05	0.39
	41.0	0.03	9.29	0.12	49.0	0.07	0.42
	40.6	0.01	9.28	0.15	49.2	0.07	0.40
	41.2	0.02	9.30	0.13	49.2	0.06	0.41
NFL1315A	40.9	0.02	10.0	0.15	48.9	0.05	0.40
	41.5	0.01	10.0	0.15	48.6	0.05	0.39
	40.9		10.2	0.15	48.9	0.04	0.35
	40.9	0.01	10.0	0.16	48.6	0.06	0.34
	40.9	0.01	10.1	0.17	48.6	0.07	0.33
	41.1	0.03	10.2	0.15	48.6	0.06	0.34
	40.9	0.01	10.1	0.14	48.6	0.07	0.36
NFL1316	41.6	0.04	9.28	0.13	49.4	0.09	0.41
	41.9		9.14	0.14	49.6	0.06	0.40
	41.4	0.03	9.18	0.14	49.4	0.07	0.39
	40.9		9.21	0.13	49.5	0.06	0.37
	41.7		9.04	0.12	49.6	0.06	0.40
	41.3		9.11	0.12	49.6	0.07	0.41
	41.1		9.08	0.13	49.6	0.08	0.45
	41.5		9.00	0.13	49.5	0.07	0.37
NFL1324	41.1	0.01	8.66	0.12	49.6	0.06	0.41
	41.8	0.02	8.68	0.12	49.8	0.06	0.42
	41.0	0.01	8.50	0.13	49.7	0.06	0.40
	41.2	0.02	8.63	0.13	49.8	0.06	0.40
	40.8	0.01	8.71	0.10	49.9	0.07	0.41
	41.1		8.72	0.13	50.1	0.07	0.45
	40.9		8.74	0.12	49.9	0.08	0.40
NFL1326	40.2	0.01	14.2	0.28	44.9	0.11	0.28
	39.6	0.02	14.4	0.25	45.3	0.11	0.27
	40.5	0.01	14.3	0.26	45.2	0.11	0.23
	40.5	0.02	14.3	0.25	45.0	0.12	0.28
	40.3	0.02	14.1	0.24	45.3	0.12	0.30
	40.6	0.02	14.3	0.28	45.1	0.10	0.27
	40.3	0.03	14.2	0.28	45.1	0.12	0.27

OLIVINE

Sample	SiO_2	Al_2O_3	FeO	MnO	MgO	CaO	NiO
NFL1327	40.1		14.4	0.27	45.8	0.08	0.34
	39.9		14.5	0.25	45.8	0.07	0.37
	40.0		14.5	0.22	45.8	0.08	0.34
	39.8		14.3	0.26	45.9	0.08	0.33
	40.2		14.2	0.22	45.8	0.07	0.33
	40.4	0.03	14.1	0.26	45.8	0.09	0.29
	40.3		14.0	0.26	45.8	0.08	0.33
	40.2		14.1	0.24	45.9	0.07	0.35
	39.9		14.1	0.26	45.9	0.09	0.29
NFL1329	41.0		9.76	0.14	48.9	0.07	0.39
	40.9	0.01	10.0	0.12	48.9	0.07	0.43
	40.9		10.0	0.13	48.7	0.06	0.38
	40.8	0.03	9.95	0.13	48.9	0.08	0.40
	41.4	0.02	9.83	0.14	49.1	0.06	0.43
	40.7	0.01	9.78	0.15	49.0	0.06	0.41
	41.0	0.02	9.88	0.16	48.9	0.06	0.42
NTB0306	40.4		9.72	0.15	50.4	0.05	0.41
	40.4		9.41	0.12	50.3	0.07	0.36
	40.3	0.00	9.53	0.18	50.3	0.06	0.36
	40.2		9.56	0.16	50.6	0.08	0.27
	40.6	0.00	9.40	0.20	50.2	0.06	0.38
	40.4	0.01	9.14	0.23	50.5	0.08	0.42
	40.6		9.37	0.18	50.1	0.08	0.49
	40.4	0.01	9.57	0.16	50.4	0.08	0.47
	40.4		9.55	0.15	50.3	0.07	0.39
	40.7		9.36	0.09	50.4	0.06	0.32
NTB0307	42.2	0.03	9.23	0.14	49.6	0.08	0.44
	42.1	0.04	9.11	0.14	49.3	0.09	0.40
	41.4	0.04	9.35	0.12	49.5	0.08	0.44
	41.8	0.04	8.93	0.12	49.3	0.11	0.44
	41.6	0.02	9.09	0.13	49.0	0.09	0.36
	42.0	0.02	9.03	0.14	49.2	0.11	0.38
	41.7	0.03	9.02	0.13	49.0	0.19	0.38
NTB1124	40.7		9.06	0.15	50.5	0.07	0.40
	40.8		9.19	0.12	50.2	0.08	0.38
	40.7		9.17	0.19	50.5	0.08	0.34
	40.8	0.00	8.96	0.10	50.5	0.09	0.42
	40.8		8.89	0.10	50.6	0.06	0.39
	40.8	0.01	9.18	0.14	50.5	0.06	0.43
NTB1116	41.3		9.34	0.14	49.2	0.09	0.36
	40.7	0.03	9.13	0.11	49.2	0.08	0.36
	41.4		9.25	0.13	49.2	0.07	0.37
	41.3	0.03	9.12	0.15	48.9	0.07	0.39
	40.8		9.27	0.13	49.1	0.08	0.43
	41.3		9.17	0.12	49.2	0.07	0.41
	41.4		9.21	0.13	49.1	0.06	0.42
	41.4		9.20	0.15	49.1	0.07	0.39
	41.3		9.13	0.15	49.0	0.07	0.40
	41.3		9.21	0.14	49.2	0.08	0.39
	41.2		9.26	0.11	49.2	0.09	0.41
	41.6		9.28	0.11	49.1	0.10	0.39

OLIVINE

Sample	SiO_2	Al_2O_3	FeO	MnO	MgO	CaO	NiO
NTB1122	40.7	0.03	11.7	0.17	47.2	0.09	0.29
	40.7		11.7	0.21	47.3	0.11	0.34
	40.8		11.6	0.18	47.1	0.09	0.38
	40.7		11.6	0.20	47.1	0.10	0.34
	40.8		11.7	0.18	47.0	0.10	0.34
	41.3		11.7	0.16	47.0	0.09	0.33
	40.6		11.6	0.17	47.1	0.11	0.34
	40.8		11.6	0.18	47.2	0.10	0.35
	40.8	0.03	11.6	0.16	47.2	0.07	0.36
	41.1		11.4	0.18	47.0	0.10	0.33
	41.1		11.7	0.15	47.1	0.09	0.30
	40.6	0.05	11.5	0.19	47.3	0.11	0.37
NFK0301	41.0	0.02	9.62	0.15	49.3	0.08	0.41
	40.1	0.02	9.59	0.16	49.3	0.05	0.38
	41.0	0.01	9.79	0.17	49.2	0.06	0.41
	39.6	0.01	9.85	0.14	49.4	0.08	0.40
	40.9	0.02	9.78	0.15	49.4	0.07	0.39
	40.7	0.02	9.88	0.17	49.4	0.08	0.42
	40.3	0.01	9.85	0.15	49.4	0.07	0.39
	40.9	0.02	9.85	0.16	49.4	0.07	0.39
	40.5	0.02	9.67	0.17	49.2	0.06	0.40
	40.9	0.02	9.83	0.16	49.3	0.06	0.39
	40.4	0.02	9.84	0.16	49.0	0.07	0.39
	40.6	0.01	9.90	0.16	48.8	0.06	0.36
	40.6	0.02	9.74	0.13	48.9	0.07	0.38
	41.0	0.02	9.85	0.18	49.2	0.05	0.37
	40.9	0.02	9.78	0.14	49.1	0.05	0.40
	40.6	0.00	9.66	0.15	49.1	0.05	0.38
	40.7	0.01	9.84	0.18	49.1	0.06	0.42
	40.6	0.02	9.76	0.13	48.1	0.05	0.40
	40.9	0.02	9.76	0.13	48.0	0.05	0.38
	40.7	0.02	9.77	0.14	49.1	0.07	0.43
	40.6	0.02	9.84	0.15	49.2	0.08	0.42
	40.1	0.01	9.78	0.19	49.3	0.05	0.40
	40.9	0.02	9.80	0.15	49.3	0.07	0.44
	41.0	0.01	9.61	0.15	49.3	0.04	0.45
	40.9	0.02	9.64	0.16	48.8	0.06	0.41
	41.2	0.01	9.67	0.17	48.9	0.07	0.36
	41.3	0.02	9.84	0.17	49.0	0.06	0.37
	40.3	0.02	9.99	0.18	49.1	0.07	0.43
	41.3	0.01	9.73	0.14	48.9	0.07	0.38
NFK1123	40.8	0.00	8.59	0.15	50.3	0.09	0.42
	40.2	0.00	11.2	0.31	48.6	0.11	0.35
	40.9	0.02	8.75	0.09	50.4	0.06	0.38
	40.9		8.93	0.15	50.4	0.07	0.39
	40.9	0.01	8.76	0.14	50.0	0.11	0.37
	41.0	0.01	8.60	0.15	50.1	0.08	0.32
NFK1108	41.6	0.03	10.7	0.17	47.5	0.11	0.33
	41.2	0.03	10.9	0.15	47.9	0.11	0.32
	41.0		10.8	0.16	47.8	0.09	0.35
	41.6		10.7	0.17	47.7	0.13	0.36
	41.2		10.7	0.16	47.6	0.13	0.33
	40.7	0.03	10.8	0.18	47.7	0.12	0.35
	40.9	0.03	10.6	0.17	47.8	0.12	0.34
	41.1		10.7	0.18	47.6	0.13	0.30
	41.7	0.03	11.0	0.18	47.6	0.15	0.35
	41.5	0.03	10.8	0.17	47.7	0.12	0.36
	40.8		10.6	0.18	47.7	0.15	0.35
	41.2		10.7	0.17	47.8	0.14	0.36

OLIVINE

Sample	SiO_2	Al_2O_3	FeO	MnO	MgO	CaO	NiO
NFK1115	40.7		11.4	0.20	47.3	0.06	0.37
	40.5		11.2	0.18	47.4	0.06	0.40
	41.0		11.1	0.19	47.3	0.05	0.36
	40.8		11.0	0.21	47.1	0.06	0.35
	40.8		11.0	0.21	47.2	0.05	0.37
	40.4		11.0	0.21	47.5	0.06	0.40
	40.9		10.8	0.19	47.6	0.06	0.40
	41.2		10.9	0.20	47.4	0.05	0.33
	40.9		10.8	0.19	47.7	0.05	0.39
	40.8		10.7	0.17	47.5	0.05	0.38
	41.3		10.7	0.19	47.5	0.05	0.42
	40.7		10.7	0.18	47.6	0.06	0.41
	40.8		10.8	0.19	47.8	0.04	0.42
	40.6		10.7	0.19	47.6	0.08	0.40
	41.0		10.9	0.23	47.4	0.07	0.41
NFR0306	39.7	0.01	13.6	0.25	46.1	0.11	0.30
	39.5	0.01	14.0	0.25	45.8	0.12	0.32
	39.5	0.03	13.8	0.25	45.7	0.13	0.34
	39.6	0.01	13.8	0.26	45.6	0.12	0.32
	39.8	0.03	14.1	0.26	45.6	0.24	0.33
	40.3	0.02	13.6	0.24	46.5	0.12	0.34
	39.7	0.02	14.0	0.25	45.8	0.10	0.32
	39.8	0.01	13.9	0.24	45.6	0.10	0.36
	39.3		13.9	0.27	45.4	0.11	0.27
	39.9	0.02	13.4	0.23	45.7	0.13	0.35
	40.1	0.02	13.8	0.26	45.7	0.12	0.33
NFR0307	40.1	0.04	11.2	0.25	47.6	0.17	0.33
	40.0	0.02	11.9	0.20	47.0	0.06	0.38
	39.8	0.00	12.3	0.24	47.1	0.07	0.29
	39.5	0.03	12.2	0.24	47.1	0.07	0.35
	39.6	0.01	12.9	0.27	46.2	0.09	0.35
	39.7	0.03	12.7	0.24	46.5	0.06	0.35
	40.2	0.05	12.6	0.27	46.7	0.24	0.28
	40.2	0.08	12.0	0.21	46.7	0.35	0.31
	40.3	0.02	11.3	0.22	47.7	0.16	0.31
NFR1109	40.1	0.00	14.1	0.20	46.1	0.09	0.35
	39.9		14.5	0.24	45.8	0.09	0.31
	40.1		14.1	0.24	46.0	0.07	0.31
	40.4	0.01	14.1	0.25	45.7	0.11	0.32
	39.8	0.02	14.3	0.31	46.5	0.09	0.33
	40.3	0.02	14.7	0.25	45.8	0.07	0.34
	40.2		14.5	0.26	45.4	0.09	0.33
	40.5	0.02	14.6	0.26	45.5	0.06	0.27
	40.4		14.6	0.23	45.5	0.06	0.31
NFR0309	41.0	0.04	9.95	0.14	48.2	0.07	0.37
	40.6		9.99	0.15	48.2	0.06	0.41
	40.6		9.90	0.15	48.2	0.08	0.37
	41.8		10.1	0.12	48.4	0.08	0.41
	40.9		10.1	0.14	48.2	0.08	0.35
	41.2	0.03	10.0	0.15	48.2	0.07	0.38
	41.1		10.1	0.14	48.3	0.05	0.37
	41.7		10.1	0.14	48.1	0.08	0.41
	40.8		10.1	0.16	48.3	0.06	0.38
	41.3	0.03	9.96	0.14	48.3	0.06	0.40
	41.1	0.03	10.1	0.12	48.5	0.07	0.42

OLIVINE

Sample	SiO_2	Al_2O_3	FeO	MnO	MgO	CaO	NiO
NFR1107	41.4		8.99	0.14	49.4	0.05	0.38
	41.2		8.89	0.13	49.3	0.08	0.38
	41.3	0.03	8.67	0.14	49.1	0.05	0.41
	40.9		9.01	0.15	49.3	0.07	0.42
	41.1		8.76	0.13	49.4	0.08	0.36
	41.3		8.79	0.16	49.4	0.07	0.41
	41.2		8.85	0.16	49.4	0.07	0.38
	41.4	0.03	8.86	0.12	49.1	0.07	0.38
	41.3		8.78	0.11	49.5	0.07	0.42
	41.5		8.89	0.16	49.4	0.08	0.41
	41.1		8.80	0.12	49.3	0.08	0.37
	41.5		8.87	0.16	49.4	0.07	0.43
NMC1301	41.3		9.62	0.12	49.3	0.06	0.46
	41.1		9.72	0.16	49.1	0.07	0.42
	41.3		9.73	0.12	49.3	0.06	0.40
	41.1		9.66	0.14	49.1	0.07	0.40
	40.8		9.56	0.14	49.2	0.06	0.41
	41.0		9.65	0.12	49.2	0.06	0.40
	41.1		9.64	0.15	49.1	0.07	0.45
	41.6		9.57	0.14	48.8	0.07	0.40
	41.7		9.54	0.12	48.9	0.05	0.45
	41.7		9.58	0.13	48.8	0.05	0.39
	40.9		9.61	0.11	48.8	0.06	0.39
NMC1309	41.0		11.2	0.19	47.7	0.07	0.39
	41.1		11.4	0.19	47.7	0.06	0.41
	40.4		11.5	0.17	47.9	0.07	0.41
	41.2		11.3	0.18	47.7	0.06	0.41
	40.7		11.5	0.17	47.9	0.06	0.42
	41.4	0.03	11.5	0.19	47.8	0.07	0.36
	41.1		11.3	0.16	47.8	0.06	0.36
	40.6		11.4	0.20	47.9	0.08	0.40
	40.9		11.3	0.21	47.7	0.05	0.40
NMC1322	41.1		9.34	0.13	49.3	0.06	0.41
	41.4		9.37	0.12	49.5	0.06	0.40
	40.9		9.34	0.12	49.4	0.06	0.39
	41.1		9.27	0.14	49.6	0.05	0.43
	41.4	0.03	9.39	0.14	49.5	0.07	0.44
	41.6		9.66	0.13	49.4	0.07	0.42
	41.0		9.66	0.13	49.4	0.08	0.41
	41.1		9.62	0.13	49.2	0.08	0.38
	41.2	0.03	9.57	0.17	49.4	0.06	0.41
	40.9	0.03	9.60	0.13	49.5	0.07	0.43
	41.3		9.55	0.14	49.2	0.06	0.41
	41.2		9.49	0.13	49.4	0.06	0.42
NMC1336A	41.2		9.28	0.13	49.3	0.06	0.43
	41.3		9.29	0.11	49.4	0.07	0.42
	41.3		9.19	0.13	49.3	0.07	0.42
	40.7		9.22	0.13	49.3	0.06	0.42
	41.4		9.30	0.13	49.4	0.06	0.42
	41.5		9.30	0.12	49.2	0.07	0.43
	41.3		9.27	0.13	49.2	0.07	0.38
	40.9		9.24	0.13	49.4	0.06	0.45
	41.0	0.03	9.25	0.14	49.4	0.06	0.42
	41.4	0.03	9.12	0.14	49.4	0.07	0.39

OLIVINE

Sample	SiO_2	Al_2O_3	FeO	MnO	MgO	CaO	NiO
NMM1126	40.7	0.02	9.41	0.15	50.3	0.10	0.41
	40.6	0.02	9.37	0.14	50.4	0.08	0.41
	40.6		9.46	0.13	49.9	0.09	0.44
	40.7	0.03	9.34	0.19	50.2	0.07	0.46
	40.5	0.00	9.61	0.12	50.5	0.08	0.38
	40.8		9.29	0.17	50.1	0.07	0.40
NMM0318	41.4		11.1	0.16	47.2	0.07	0.36
	41.3		11.0	0.16	47.2	0.07	0.37
	41.4		10.9	0.14	47.2	0.07	0.42
	40.9		11.0	0.17	47.3	0.07	0.38
	41.8		11.0	0.15	47.2	0.06	0.32
	41.7	0.04	11.1	0.16	47.3	0.06	0.37
	41.2		11.1	0.16	47.4	0.08	0.38
	40.9		10.8	0.17	47.1	0.06	0.39
	41.0		11.1	0.16	47.2	0.06	0.40
	41.3		11.1	0.20	47.4	0.07	0.35
	40.5		11.1	0.16	47.3	0.06	0.40
	41.1		11.0	0.20	47.3	0.08	0.35
NMM1115	41.2		9.11	0.13	49.0	0.06	0.41
	41.1		9.11	0.14	49.2	0.06	0.43
	41.3		9.02	0.12	49.1	0.07	0.38
	41.6	0.03	9.08	0.09	49.2	0.08	0.40
	41.0		8.89	0.16	49.2	0.10	0.37
	41.4		9.05	0.13	49.2	0.10	0.43
	41.6		9.07	0.13	49.1	0.08	0.46
	41.3		9.04	0.12	49.2	0.09	0.39
	41.7		9.11	0.14	49.3	0.08	0.42
	41.0		9.09	0.10	49.2	0.06	0.40
	41.5		9.03	0.12	49.1	0.09	0.40
	40.9		9.05	0.13	49.1	0.09	0.41
	41.1		9.19	0.12	49.3	0.08	0.40
	41.4		9.15	0.14	49.2	0.10	0.39
NME1122	40.3		9.44	0.13	50.4	0.09	0.36
	40.6	0.01	9.57	0.15	50.1	0.08	0.36
	40.5	0.02	9.42	0.12	50.1	0.05	0.33
	40.5		9.29	0.12	50.1	0.07	0.30
	40.3	0.03	9.46	0.12	50.3	0.05	0.40
	40.5	0.00	9.64	0.15	50.2	0.09	0.39
	40.5	0.01	9.43	0.12	50.4	0.07	0.39
NME0528	41.2		9.52	0.14	48.8	0.07	0.39
	41.4		9.60	0.14	48.7	0.07	0.41
	41.2		9.54	0.17	48.8	0.06	0.39
	41.4		9.50	0.15	48.7	0.06	0.36
	41.5		9.49	0.14	48.7	0.05	0.38
	40.9		9.47	0.15	48.7	0.07	0.40
	41.1		9.50	0.13	48.9	0.06	0.35
	41.3		9.40	0.13	48.6	0.06	0.38
	41.3		9.36	0.15	48.8	0.06	0.41
	41.2	0.03	9.50	0.12	48.8	0.06	0.35
	41.0		9.49	0.15	48.7	0.06	0.44
	41.5		9.50	0.16	48.8	0.06	0.40
	41.0		9.59	0.13	48.7	0.08	0.38

OLIVINE

Sample	SiO_2	Al_2O_3	FeO	MnO	MgO	CaO	NiO
NME1116	41.5		9.28	0.11	49.1	0.07	0.41
	41.1		9.20	0.15	49.2	0.08	0.43
	41.1		9.17	0.14	49.1	0.07	0.40
	41.1		9.09	0.15	49.4	0.06	0.42
	41.4	0.03	9.06	0.13	49.2	0.07	0.37
	41.3		9.31	0.15	49.3	0.07	0.37
	41.6		9.06	0.12	49.1	0.06	0.38
	41.6	0.04	9.07	0.14	49.2	0.06	0.39
	41.5		9.20	0.14	49.3	0.07	0.44
	41.7		9.18	0.14	49.1	0.06	0.42
	42.0		9.14	0.12	49.2	0.07	0.43
	41.1		9.24	0.12	49.2	0.06	0.41
NBN0302A	40.1		10.1	0.15	50.3	0.08	0.35
	40.0		9.84	0.11	50.2	0.07	0.44
	40.2	0.00	10.1	0.14	50.5	0.06	0.38
	39.9	0.03	9.82	0.12	50.3	0.08	0.37
	40.3		9.77	0.15	50.3	0.09	0.42
	40.0		10.1	0.16	50.0	0.08	0.37
	40.1	0.02	9.71	0.17	50.2	0.11	0.35
	40.0		10.2	0.15	50.2	0.09	0.40
	40.1	0.01	10.0	0.11	50.3	0.05	0.37
NBN0305	40.4		9.33	0.13	50.0	0.09	0.37
	40.1	0.01	9.52	0.09	50.3	0.07	0.41
	40.7		9.29	0.18	49.9	0.04	0.37
	40.2		9.38	0.18	50.4	0.10	0.45
	40.6		9.63	0.17	50.3	0.07	0.42
	40.2		9.31	0.12	50.1	0.11	0.34
	40.4		9.46	0.14	50.0	0.09	0.37
	40.4	0.00	9.17	0.11	50.1	0.06	0.42
	40.4		9.58	0.11	50.4	0.05	0.37
	40.6		9.57	0.16	49.7	0.09	0.33
	40.4		9.68	0.18	49.7	0.13	0.35
NBN0311	39.5		9.79	0.19	50.2	0.12	0.39
	39.7		9.72	0.16	50.3	0.13	0.33
	40.1		9.91	0.17	50.1	0.12	0.29
	39.2		9.83	0.14	50.1	0.13	0.33
	39.8		9.81	0.14	50.2	0.11	0.36
	40.3		9.65	0.09	50.6	0.10	0.39
NBN0316	40.4		10.0	0.15	49.6	0.06	0.38
	40.4		10.2	0.13	49.9	0.06	0.43
	40.7	0.01	10.3	0.14	49.3	0.06	0.41
	40.5	0.00	10.1	0.16	49.6	0.07	0.40
	40.5		10.3	0.18	49.6	0.04	0.46
	40.6	0.00	10.3	0.16	49.7	0.05	0.43
NBN0319	40.6		10.2	0.18	49.5	0.04	0.35
	40.7		10.1	0.16	49.8	0.06	0.40
	40.7	0.02	10.2	0.19	49.5	0.05	0.41
	40.0	0.00	10.2	0.19	49.5	0.07	0.34
	40.6	0.01	10.4	0.15	49.4	0.06	0.37
	40.4		10.2	0.16	49.5	0.04	0.28
	40.7		10.2	0.14	49.6	0.06	0.45
	40.7		9.99	0.18	49.5	0.03	0.40
	40.3		10.2	0.17	49.7	0.06	0.38
	40.1		10.2	0.15	49.8	0.03	0.34
	40.3		10.2	0.18	49.3	0.03	0.38
	40.4		10.2	0.14	49.3	0.05	0.35
	40.4	0.02	10.0	0.15	49.3	0.05	0.30

OLIVINE

Sample	SiO_2	Al_2O_3	FeO	MnO	MgO	CaO	NiO
NBN0321	39.8		9.73	0.11	49.5	0.10	0.40
	40.2		10.2	0.16	49.8	0.09	0.36
	40.2		9.88	0.17	50.0	0.11	0.35
	40.5	0.02	9.97	0.11	50.5	0.04	0.42
	40.6		10.0	0.16	50.3	0.08	0.36
	40.0	0.00	9.54	0.11	49.8	0.10	0.37
	40.5		9.80	0.13	49.8	0.13	0.42
	40.0		9.72	0.16	49.9	0.16	0.38
	39.9		9.67	0.16	49.6	0.12	0.38

ORTHOPYROXENE

Sample	SiO_2	TiO_2	Al_2O_3	Cr_2O_3	FeO	MnO	MgO	CaO	Na_2O
NMS1302A	57.6		2.16	0.44	5.46	0.15	34.7	0.66	
	57.0		2.10	0.45	5.40	0.11	34.9	0.66	
	57.2		2.17	0.43	5.47	0.13	34.8	0.66	
	56.9		2.11	0.47	5.37	0.16	34.6	0.64	
	57.4	0.03	2.12	0.46	5.49	0.16	34.9	0.63	
	57.3	0.03	2.16	0.48	5.48	0.13	34.8	0.64	0.04
	56.3		2.40	0.57	5.41	0.13	34.6	0.70	
	57.2		2.31	0.49	5.46	0.12	34.7	0.67	
	57.3	0.03	2.11	0.45	5.44	0.11	34.7	0.66	
	57.3		2.15	0.44	5.37	0.13	34.6	0.66	
	57.1		2.26	0.50	5.42	0.15	34.7	0.65	
	57.2		2.23	0.50	5.37	0.13	34.6	0.65	0.04
	56.9		2.21	0.46	5.38	0.12	34.7	0.65	
	56.4		2.22	0.47	5.46	0.12	34.8	0.66	
	57.5	0.03	2.12	0.44	5.45	0.14	34.7	0.63	
	56.8		2.14	0.48	5.45	0.14	34.5	0.68	
	57.1		2.20	0.47	5.39	0.16	34.7	0.66	
	56.9		2.16	0.61	5.37	0.14	34.8	0.65	0.05
	56.7	0.03	2.17	0.48	5.43	0.12	34.8	0.65	
	57.3		2.13	0.46	5.46	0.13	34.8	0.65	
	57.5		1.97	0.43	5.46	0.16	34.9	0.64	
	56.7	0.03	2.27	0.51	5.37	0.13	34.7	0.66	
	56.7		2.26	0.42	5.41	0.14	34.8	0.64	
	57.3		2.22	0.48	5.51	0.14	34.8	0.65	0.04
	57.2		2.16	0.48	5.51	0.12	34.6	0.66	
	56.8	0.03	2.19	0.51	5.38	0.12	34.8	0.63	0.04
	57.8		2.11	0.48	5.37	0.13	34.6	0.65	
	57.4	0.03	2.12	0.46	5.41	0.12	34.5	0.64	
NMS1304	56.4	0.06	2.83	0.42	5.90	0.14	33.5	0.64	
	56.6	0.07	2.87	0.44	6.08	0.13	33.5	0.64	
	56.0	0.08	3.24	0.44	6.03	0.15	33.4	0.62	0.05
	56.0	0.07	2.94	0.43	5.99	0.16	33.5	0.62	
	56.3	0.06	3.04	0.44	6.00	0.15	33.4	0.61	
	56.2	0.07	3.04	0.43	5.95	0.15	33.4	0.63	
	56.0	0.07	2.83	0.41	5.97	0.14	33.5	0.62	
	56.5	0.07	2.83	0.38	6.05	0.15	33.7	0.64	0.05
	55.8	0.07	2.93	0.42	6.09	0.15	33.5	0.63	
	55.8	0.07	2.93	0.43	6.03	0.15	33.6	0.63	
	55.9	0.07	3.09	0.42	5.95	0.18	33.6	0.62	0.05
	56.2	0.07	2.94	0.41	5.93	0.13	33.6	0.65	0.04
NMS1305	54.8	0.09	4.83	0.37	6.69	0.14	32.7	0.71	0.08
	54.4	0.08	4.83	0.41	6.61	0.17	32.6	0.77	0.11
	55.1	0.04	4.27	0.37	6.55	0.14	32.9	0.71	0.06
	55.0	0.07	4.49	0.42	6.55	0.16	32.8	0.69	0.06
	55.6	0.04	4.40	0.35	6.69	0.16	32.9	0.67	0.12
	55.3	0.04	4.24	0.32	6.61	0.16	33.0	0.66	0.07
	55.7	0.04	4.30	0.32	6.63	0.15	32.8	0.68	0.09
	56.1	0.03	4.08	0.31	6.57	0.15	32.9	0.68	0.10
	55.3	0.03	4.27	0.34	6.59	0.15	32.9	0.66	0.09
	56.2		4.21	0.32	6.55	0.14	33.0	0.67	0.08
	56.5	0.03	3.91	0.31	6.63	0.16	33.1	0.66	0.11
	55.5	0.04	3.98	0.31	6.61	0.16	32.9	0.69	0.08
	55.9	0.03	3.98	0.28	6.50	0.16	32.8	0.71	0.08
	56.1	0.03	4.09	0.30	6.68	0.16	32.9	0.67	0.07
	55.4		4.23	0.30	6.62	0.14	32.9	0.65	0.06
	55.5		4.21	0.29	6.68	0.14	33.0	0.68	0.08

ORTHOPYROXENE

Sample	SiO_2	TiO_2	Al_2O_3	Cr_2O_3	FeO	MnO	MgO	CaO	Na_2O
NMS1308	55.6	0.07	3.83	0.50	6.18	0.13	33.2	0.68	0.07
	56.2	0.06	3.40	0.46	6.07	0.13	33.4	0.65	0.06
	55.6	0.05	3.41	0.45	5.99	0.17	33.4	0.65	0.05
	55.8	0.10	3.85	0.51	6.03	0.12	33.1	0.65	0.06
	55.9	0.07	3.49	0.46	6.12	0.14	33.3	0.69	0.09
	55.3	0.12	3.98	0.57	6.09	0.15	33.1	0.64	0.07
	55.3	0.09	3.81	0.49	6.04	0.14	33.2	0.64	0.08
	56.1	0.06	3.21	0.36	6.02	0.13	33.4	0.65	0.06
	56.5	0.09	3.71	0.51	6.05	0.13	33.2	0.65	0.06
	55.6	0.08	3.80	0.55	6.07	0.13	33.2	0.63	0.05
NMS1310	55.5	0.10	3.93	0.42	6.13	0.16	33.4	0.76	0.08
	55.2	0.09	4.01	0.46	6.25	0.13	33.3	0.78	0.11
	55.6	0.09	4.20	0.41	6.27	0.15	33.3	0.77	0.09
	55.6	0.10	3.94	0.40	6.27	0.14	33.5	0.78	0.12
	54.9	0.10	4.21	0.46	6.27	0.14	33.1	0.78	0.11
	55.6	0.12	4.37	0.47	6.26	0.12	33.3	0.74	0.12
	55.0	0.10	4.10	0.44	6.23	0.15	33.5	0.78	0.11
	55.5	0.10	4.30	0.44	6.23	0.16	33.4	0.77	0.11
	55.2	0.13	4.51	0.51	6.23	0.14	33.1	0.82	0.14
	55.9	0.09	4.06	0.43	6.31	0.12	33.4	0.77	0.09
	55.2	0.11	4.41	0.48	6.22	0.14	33.2	0.76	0.11
	55.4	0.11	4.34	0.51	6.27	0.15	33.2	0.78	0.10
	55.8	0.10	4.15	0.42	6.30	0.12	33.5	0.77	0.09
	55.3	0.10	4.17	0.46	6.26	0.14	33.4	0.75	0.08
NJS1302	54.3	0.19	4.30	0.34	7.30	0.17	32.2	0.75	0.11
	54.9	0.23	4.91	0.38	7.39	0.14	31.8	0.73	0.09
	54.2	0.24	4.87	0.44	7.28	0.14	31.9	0.72	0.08
	54.9	0.16	3.89	0.28	7.36	0.16	32.1	0.70	0.08
	55.3	0.18	4.15	0.30	7.47	0.14	32.1	0.75	0.12
	54.5	0.22	4.70	0.36	7.41	0.15	31.7	0.77	0.11
	55.2	0.21	4.18	0.32	7.44	0.16	32.0	0.71	0.11
	55.2	0.19	4.15	0.33	7.31	0.17	32.0	0.72	0.10
	54.7	0.23	4.55	0.39	7.43	0.13	31.9	0.76	0.14
	55.1	0.20	4.43	0.35	7.39	0.14	31.9	0.70	0.11
	55.2	0.21	4.61	0.36	7.34	0.15	31.9	0.71	0.14
	55.0	0.19	4.20	0.36	7.21	0.14	32.0	0.74	0.10
	54.8	0.19	4.27	0.43	7.17	0.12	32.1	0.70	0.13
	54.6	0.21	4.49	0.42	7.19	0.16	31.9	0.73	0.09

ORTHOPYROXENE

Sample	SiO_2	TiO_2	Al_2O_3	Cr_2O_3	FeO	MnO	MgO	CaO	Na_2O
NJS1304	55.3	0.19	4.25	0.36	7.35	0.15	32.3	0.73	0.13
	55.2	0.19	4.19	0.40	7.42	0.17	32.2	0.73	0.10
	55.2	0.16	3.92	0.35	7.29	0.13	32.3	0.74	0.13
	55.6	0.17	4.25	0.34	7.29	0.12	32.3	0.71	0.14
	55.4	0.19	3.91	0.33	7.29	0.16	32.3	0.72	0.10
	55.0	0.17	4.05	0.38	7.35	0.17	32.2	0.72	0.11
	55.8	0.18	4.07	0.35	7.49	0.15	32.4	0.72	0.08
	55.3	0.19	4.27	0.35	7.28	0.16	32.2	0.73	0.10
	55.2	0.20	4.18	0.36	7.38	0.17	32.2	0.73	0.13
	55.7	0.17	4.11	0.31	7.34	0.12	32.3	0.74	0.14
	54.9	0.19	4.36	0.37	7.30	0.11	32.3	0.69	0.11
	55.5	0.19	4.40	0.34	7.40	0.16	32.2	0.77	0.15
	55.3	0.20	4.27	0.37	7.36	0.14	32.3	0.74	0.14
	55.7	0.21	4.34	0.37	7.41	0.14	32.2	0.72	0.11
	55.5	0.16	4.06	0.33	7.32	0.15	32.4	0.70	0.11
	55.1	0.16	4.04	0.32	7.43	0.15	32.4	0.77	0.12
	56.1	0.19	4.00	0.33	7.44	0.16	32.4	0.76	0.10
	55.9	0.17	3.87	0.33	7.26	0.15	32.5	0.74	0.09
	55.0	0.16	4.06	0.32	7.41	0.16	32.3	0.74	0.11
	55.6	0.16	4.19	0.31	7.39	0.16	32.3	0.72	0.14
	55.7	0.17	4.00	0.32	7.41	0.14	32.5	0.71	0.10
	55.0	0.16	4.05	0.33	7.30	0.16	32.4	0.77	0.10
	55.4	0.18	4.21	0.35	7.41	0.13	32.3	0.71	0.14
	55.4	0.16	3.96	0.33	7.28	0.13	32.4	0.74	0.11
	55.2	0.16	4.19	0.39	7.41	0.15	32.3	0.75	0.12
	55.5	0.17	4.12	0.32	7.46	0.16	32.3	0.74	0.14
	55.6	0.17	4.17	0.37	7.37	0.17	32.2	0.77	0.13
	55.6	0.18	4.30	0.36	7.37	0.14	32.2	0.74	0.13
	55.0	0.17	4.28	0.40	7.30	0.13	32.3	0.73	0.11
NJS1306	54.3	0.12	4.87	0.34	7.94	0.19	31.3	0.98	0.13
	54.8	0.12	4.86	0.37	8.04	0.18	31.6	0.88	0.11
	54.1	0.11	4.93	0.35	7.80	0.22	31.2	0.97	0.11
	54.3	0.11	4.90	0.33	7.92	0.17	31.3	1.02	0.11
	54.3	0.11	4.93	0.35	7.97	0.13	31.2	1.01	0.10
	54.2	0.12	5.04	0.36	7.45	0.17	31.4	1.04	0.13
	54.7	0.11	4.98	0.36	7.45	0.15	31.5	1.02	0.09
	54.7	0.11	4.81	0.31	7.47	0.16	31.8	0.97	0.11
	54.5	0.13	4.96	0.35	7.50	0.16	31.6	0.97	0.13
	54.8	0.13	5.04	0.37	7.55	0.17	31.5	0.89	0.15
	55.0	0.11	4.92	0.38	7.58	0.14	31.6	0.95	0.15
	54.3	0.12	4.97	0.36	7.57	0.16	31.7	1.01	0.17
NJS1307	54.9	0.15	4.93	0.36	6.61	0.14	32.5	0.85	0.17
	54.5	0.17	5.09	0.37	6.72	0.15	32.3	0.87	0.11
	54.7	0.15	4.99	0.35	6.61	0.13	32.3	0.86	0.13
	55.1	0.17	4.95	0.38	6.47	0.16	32.4	0.85	0.17
	54.9	0.16	5.04	0.36	6.52	0.17	32.4	0.87	0.17
	54.5	0.17	5.29	0.42	6.51	0.16	32.1	0.84	0.16
	55.3	0.15	4.85	0.32	6.56	0.15	32.4	0.90	0.13
	55.1	0.15	4.83	0.33	6.50	0.15	32.2	0.92	0.13
	55.3	0.14	4.82	0.32	6.48	0.16	32.2	0.88	0.14
	55.0	0.16	5.06	0.32	6.63	0.16	32.2	0.89	0.15
	55.0	0.15	4.99	0.37	6.57	0.15	32.5	0.83	0.15
	54.5	0.15	5.00	0.35	6.51	0.12	32.5	0.82	0.13
	55.6	0.15	5.08	0.36	6.62	0.11	32.4	0.84	0.12
	55.0	0.16	5.11	0.37	6.51	0.14	32.4	0.85	0.13

ORTHOPYROXENE

Sample	SiO_2	TiO_2	Al_2O_3	Cr_2O_3	FeO	MnO	MgO	CaO	Na_2O
NPY1301	54.5	0.12	4.91	0.45	6.52	0.14	32.3	0.79	0.13
	55.1	0.13	4.61	0.43	6.61	0.14	32.4	0.75	0.08
	55.4	0.12	4.50	0.32	6.61	0.12	32.6	0.69	0.11
	55.6	0.12	4.77	0.41	6.61	0.15	32.7	0.71	0.15
	55.2	0.12	4.21	0.28	6.65	0.17	32.9	0.69	0.12
	55.2	0.14	4.38	0.33	6.56	0.17	32.9	0.68	0.13
	55.3	0.14	4.50	0.34	6.53	0.13	32.7	0.71	0.12
	55.8	0.13	4.48	0.39	6.52	0.15	32.8	0.67	0.09
	55.5	0.11	4.06	0.30	6.52	0.15	33.0	0.68	0.11
	55.3	0.12	4.43	0.32	6.53	0.15	32.7	0.72	0.06
NPY1310	55.3	0.12	4.73	0.21	7.14	0.16	31.9	0.73	0.09
	54.4	0.12	4.95	0.25	7.06	0.17	31.7	0.74	0.13
	54.6	0.12	4.84	0.19	6.95	0.15	31.7	0.74	0.08
	54.7	0.12	5.00	0.27	6.94	0.16	31.6	0.73	0.06
	54.7	0.12	5.15	0.26	6.96	0.15	31.4	0.75	0.08
	54.8	0.12	4.93	0.22	6.99	0.19	31.8	0.73	0.09
	54.9	0.11	4.74	0.17	7.03	0.18	31.7	0.75	0.09
	55.3	0.11	4.52	0.17	6.85	0.15	32.0	0.76	0.07
	55.6	0.11	4.69	0.17	6.96	0.15	31.8	0.75	0.10
	55.2	0.13	4.95	0.24	6.97	0.15	31.8	0.76	0.07
	55.1	0.11	4.87	0.25	6.88	0.14	31.8	0.75	0.11
NPY1311	54.7	0.14	5.02	0.26	7.02	0.17	31.7	0.76	0.10
	54.9	0.12	4.68	0.19	7.02	0.14	31.8	0.75	0.09
	55.0	0.13	4.86	0.19	7.04	0.14	32.0	0.72	0.09
	55.3	0.12	4.72	0.20	6.92	0.19	31.8	0.72	0.06
	54.8	0.11	4.61	0.18	7.05	0.15	32.0	0.75	0.08
	54.5	0.12	5.00	0.23	6.89	0.18	32.1	0.74	0.08
	53.3	0.14	4.96	0.27	6.67	0.15	30.5	0.78	0.08
	53.3	0.12	5.49	0.30	6.83	0.17	31.3	0.77	0.11
NPY1314	55.4	0.08	4.40	0.30	6.82	0.15	33.1	0.71	0.06
	54.9	0.10	4.66	0.37	6.68	0.13	32.6	0.70	0.07
	54.9	0.08	4.42	0.31	6.66	0.15	32.5	0.76	0.06
	54.8	0.09	4.57	0.30	6.60	0.15	32.6	0.68	0.04
	54.8	0.09	4.00	0.28	6.61	0.12	32.7	0.78	0.04
	54.9	0.10	4.19	0.26	6.51	0.16	32.8	0.71	0.09
	54.8	0.12	4.85	0.37	6.54	0.14	32.5	0.72	0.06
NFL1302	55.0	0.06	3.98	0.44	6.06	0.17	33.3	0.73	0.08
	55.4	0.07	4.06	0.42	6.08	0.12	33.1	0.74	0.05
	55.3	0.06	4.02	0.40	6.13	0.14	33.1	0.73	0.07
	56.0	0.07	3.92	0.43	6.04	0.13	33.2	0.77	0.07
	55.5	0.06	4.05	0.41	6.00	0.15	33.3	0.79	0.09
	55.4	0.07	4.11	0.42	5.96	0.17	33.3	0.73	0.09
	55.3	0.06	4.11	0.42	5.89	0.15	33.1	0.74	0.09
	55.5	0.09	4.21	0.44	6.09	0.09	33.0	0.75	0.05
	55.4	0.07	4.10	0.47	5.99	0.15	33.0	0.75	0.04
	55.5	0.07	4.09	0.43	6.02	0.15	33.1	0.78	0.07
	55.5	0.07	4.07	0.43	6.09	0.14	33.1	0.72	0.07
NFL1305	55.2	0.04	4.21	0.49	6.03	0.17	33.0	0.79	0.08
	55.4	0.03	3.89	0.46	6.02	0.15	33.2	0.75	0.06
	55.5	0.02	3.91	0.45	5.91	0.13	33.2	0.75	0.05
	54.8	0.04	4.15	0.51	6.03	0.13	33.1	0.78	0.07
	55.4	0.04	4.01	0.44	6.01	0.12	33.1	0.74	0.05
	55.4	0.03	3.93	0.47	5.93	0.14	33.2	0.74	0.07
	54.9	0.03	4.26	0.52	5.99	0.16	33.1	0.75	0.07

ORTHOPYROXENE

Sample	SiO_2	TiO_2	Al_2O_3	Cr_2O_3	FeO	MnO	MgO	CaO	Na_2O
NFL1315A	56.1	0.04	1.92	0.50	6.42	0.18	33.9	0.76	0.07
	56.7	0.06	1.92	0.45	6.34	0.19	33.9	0.77	0.06
	56.4	0.06	1.94	0.47	6.51	0.15	33.9	0.74	0.06
	56.0	0.07	1.99	0.53	6.25	0.18	33.5	0.74	0.09
	56.0	0.05	2.00	0.51	6.37	0.15	33.8	0.72	0.06
	56.4	0.06	2.04	0.50	6.40	0.18	33.7	0.73	0.07
	56.6	0.06	1.95	0.48	6.33	0.16	33.7	0.76	0.07
	56.1	0.05	1.99	0.50	6.43	0.15	33.7	0.75	0.06
	56.1	0.06	1.98	0.52	6.35	0.15	33.8	0.79	0.06
NFL1316	56.5	0.05	2.50	0.58	5.91	0.15	34.1	0.71	0.06
	57.2	0.04	2.41	0.53	5.91	0.17	33.9	0.73	0.07
	56.3	0.05	2.52	0.59	6.05	0.14	34.0	0.74	0.05
	56.7	0.06	2.54	0.53	5.92	0.15	33.9	0.78	0.06
	56.5	0.04	2.55	0.51	5.76	0.11	34.2	0.75	0.04
	56.2	0.05	2.49	0.62	5.75	0.14	34.2	0.71	0.05
	56.9	0.04	2.48	0.53	5.77	0.13	34.2	0.74	0.05
	56.4	0.06	2.48	0.54	5.75	0.15	33.9	0.77	0.06
	57.1	0.04	2.49	0.53	5.88	0.13	34.3	0.70	0.03
	57.2	0.03	2.50	0.52	5.75	0.13	34.2	0.68	0.05
NFL1324	56.0	0.05	3.40	0.58	5.50	0.13	33.6	0.85	0.09
	55.3	0.06	3.25	0.59	5.64	0.14	33.7	0.81	0.06
	55.8	0.05	3.23	0.53	5.62	0.13	33.6	0.81	0.09
	55.9	0.04	3.55	0.81	5.56	0.13	33.4	0.82	0.07
	55.3	0.04	3.61	0.83	5.61	0.17	33.5	0.80	0.07
	54.9	0.04	3.75	0.89	5.68	0.15	33.5	0.83	0.05
	55.8	0.05	3.19	0.56	5.68	0.16	33.9	0.80	0.07
	55.8	0.06	3.16	0.56	5.62	0.15	33.8	0.80	0.07
NFL1327	54.7	0.06	2.90	0.50	8.95	0.27	31.6	0.89	0.07
	55.2	0.05	2.88	0.51	8.95	0.27	31.6	0.88	0.09
	55.7	0.05	2.93	0.53	8.89	0.25	31.7	0.89	0.06
	55.7	0.05	2.88	0.47	9.05	0.27	31.9	0.89	0.06
	55.9	0.05	2.86	0.49	8.93	0.26	31.7	0.88	0.04
	55.5	0.06	2.95	0.52	8.88	0.24	31.6	0.91	0.07
	54.8	0.04	2.88	0.48	9.02	0.26	31.8	0.92	0.06
	55.0	0.05	2.95	0.51	8.91	0.22	31.6	0.91	0.07
	54.8	0.05	2.94	0.48	8.92	0.25	31.8	0.92	0.05
	55.6	0.05	3.05	0.56	8.84	0.24	31.7	0.88	0.09
	55.5	0.06	3.07	0.51	9.00	0.25	31.7	0.89	0.07
NFL1329	54.8	0.06	4.61	0.36	6.37	0.14	32.8	0.73	0.08
	55.3	0.05	4.28	0.34	6.35	0.15	33.2	0.73	0.07
	55.3	0.06	3.98	0.32	6.34	0.15	33.1	0.74	0.05
	55.6	0.06	4.16	0.35	6.31	0.15	33.0	0.73	0.05
	55.2	0.06	4.36	0.31	6.31	0.13	33.0	0.73	0.06
	55.4	0.06	4.40	0.35	6.29	0.15	33.0	0.79	0.06
	55.6	0.05	4.33	0.36	6.36	0.14	33.0	0.73	0.08
	55.5	0.05	4.17	0.37	6.20	0.15	33.0	0.72	0.07
	55.5	0.07	4.02	0.35	6.25	0.14	33.2	0.74	0.07
	55.8	0.08	4.10	0.38	6.29	0.17	33.2	0.78	0.08
	55.9	0.08	4.05	0.39	6.27	0.16	32.9	0.72	0.05
	55.5	0.09	4.34	0.41	6.24	0.15	32.9	0.78	0.08
NTB0306	55.7	0.08	2.22	0.76	6.24	0.23	34.6	0.75	
	56.2	0.06	2.01	0.50	5.78	0.15	34.7	0.68	
	55.7	0.09	2.11	0.51	5.85	0.19	34.4	0.72	
	56.2	0.05	1.93	0.44	5.93	0.19	34.4	0.70	
	56.3	0.08	1.87	0.49	5.88	0.19	34.5	0.68	
	55.7	0.02	2.32	0.59	6.27	0.20	33.9	0.78	
	56.2	0.03	2.10	0.49	5.99	0.19	34.5	0.72	
	56.0	0.04	2.16	0.43	6.15	0.17	34.6	0.65	
	56.0	0.04	2.03	0.49	5.98	0.13	34.6	0.67	
	56.3	0.06	1.97	0.48	6.12	0.18	34.6	0.70	

ORTHOPYROXENE

Sample	SiO_2	TiO_2	Al_2O_3	Cr_2O_3	FeO	MnO	MgO	CaO	Na_2O
NTB0307	56.5	0.04	3.87	0.39	5.92	0.09	33.3	0.68	
	56.5	0.04	3.78	0.39	5.93	0.10	33.1	0.70	
NTB1124	55.0	0.17	4.16	0.54	5.82	0.10	33.6	0.80	
	55.2	0.15	4.08	0.55	5.81	0.14	33.7	0.87	
	54.8	0.17	4.01	0.57	5.76	0.11	33.6	0.83	
	54.8	0.15	4.25	0.51	5.77	0.12	33.4	0.88	
	54.7	0.13	4.16	0.50	5.75	0.17	33.9	0.84	
	54.6	0.15	4.04	0.51	5.86	0.18	33.9	0.86	
	54.8	0.18	4.21	0.53	5.73	0.15	33.7	0.83	
NTB1116	55.3	0.09	4.22	0.58	5.98	0.14	33.1	0.79	0.11
	56.0	0.08	3.83	0.55	5.93	0.14	33.2	0.79	0.09
	54.9	0.09	4.13	0.55	5.91	0.13	32.9	0.78	0.10
	55.8	0.08	4.11	0.52	5.95	0.12	33.2	0.80	0.13
	55.8	0.08	3.87	0.49	5.98	0.13	33.3	0.77	0.09
	55.6	0.09	4.23	0.61	5.89	0.14	33.1	0.78	0.10
	55.6	0.08	4.35	0.50	5.84	0.12	32.3	0.80	0.54
	55.4	0.08	4.17	0.55	5.97	0.15	33.1	0.75	0.11
	55.4	0.07	3.91	0.47	6.01	0.14	33.2	0.79	0.11
	55.6	0.07	4.07	0.52	5.79	0.14	33.1	0.81	0.14
	55.4	0.07	3.87	0.49	5.95	0.13	33.2	0.77	0.09
	55.5	0.07	4.23	0.52	5.84	0.15	32.6	0.81	0.12
	55.6	0.07	4.03	0.50	5.99	0.11	33.2	0.79	0.10
	55.7	0.10	4.17	0.56	5.91	0.13	32.9	0.78	0.08
NTB1122	53.9	0.26	4.87	0.47	7.41	0.19	31.4	1.01	0.07
	54.8	0.25	4.89	0.50	7.44	0.17	31.5	1.00	0.07
	54.9	0.24	4.52	0.50	7.45	0.20	31.7	0.95	0.08
	55.0	0.27	4.50	0.49	7.48	0.17	31.7	0.95	0.07
	55.0	0.25	4.50	0.47	7.39	0.19	31.7	0.98	0.08
	55.1	0.24	4.57	0.50	7.48	0.17	31.6	0.99	
	54.3	0.25	4.60	0.47	7.48	0.18	31.6	0.97	0.08
	54.2	0.26	4.89	0.48	7.42	0.15	31.5	0.98	0.08
	54.6	0.23	5.09	0.47	7.39	0.18	31.5	0.98	0.07
	55.1	0.22	4.61	0.47	7.38	0.17	31.5	0.97	0.07
	54.4	0.23	4.57	0.49	7.50	0.17	31.7	0.99	0.10

ORTHOPYROXENE

Sample	SiO_2	TiO_2	Al_2O_3	Cr_2O_3	FeO	MnO	MgO	CaO	Na_2O
NFK0301	55.5	0.06	3.73	0.55	6.16	0.12	33.1	0.81	
	55.7	0.05	3.37	0.48	6.28	0.13	33.5	0.75	
	55.1	0.05	4.04	0.70	6.25	0.16	33.1	0.83	
	55.1	0.05	3.96	0.64	6.27	0.10	33.0	0.83	
	55.2	0.07	3.91	0.65	6.41	0.14	33.3	0.78	
	55.4	0.06	3.93	0.62	6.29	0.16	33.2	0.89	
	55.2	0.07	3.96	0.66	6.39	0.12	33.1	0.85	
	56.0	0.06	3.50	0.48	6.29	0.14	33.5	0.78	
	55.4	0.06	3.83	0.57	6.23	0.16	33.4	0.77	
	55.3	0.06	3.69	0.56	6.22	0.16	33.3	0.76	
	55.2	0.07	3.64	0.56	6.26	0.16	33.2	0.79	
	56.0	0.07	3.60	0.57	6.33	0.13	33.2	0.77	
	55.3	0.07	4.08	0.73	6.33	0.13	32.8	0.81	
	55.7	0.07	3.81	0.63	6.31	0.12	33.1	0.76	
	55.9	0.08	3.59	0.54	6.29	0.17	33.0	0.81	
	55.4	0.05	3.20	0.44	6.24	0.14	31.6	0.76	
	55.1	0.06	3.55	0.54	6.17	0.15	31.9	0.73	
	55.3	0.07	3.60	0.52	6.22	0.14	33.1	0.78	
	56.0	0.07	3.62	0.55	6.27	0.15	33.1	0.79	
	55.3	0.07	4.02	0.70	6.32	0.13	32.7	0.81	
	55.2	0.06	3.70	0.58	6.27	0.16	33.1	0.81	
	55.5	0.06	3.79	0.63	6.28	0.13	33.1	0.78	
	55.6	0.08	3.64	0.55	6.27	0.16	33.0	0.79	
	55.3	0.06	3.49	0.54	6.14	0.12	33.1	0.81	
	55.4	0.06	3.50	0.58	6.12	0.12	33.0	0.87	
	55.1	0.07	3.93	0.68	6.16	0.14	33.2	0.80	
	55.2	0.07	3.64	0.60	6.17	0.14	33.3	0.77	
	54.9	0.06	3.85	0.66	6.27	0.14	33.4	0.76	
NFK1123	55.8	0.06	3.43	0.60	5.52	0.13	33.7	0.74	
	55.4	0.08	3.28	0.59	5.84	0.12	34.2	0.80	
	55.5	0.09	3.46	0.66	5.65	0.13	34.0	0.78	
	55.6	0.06	3.33	0.47	5.77	0.11	34.0	0.81	
	55.9	0.11	3.44	0.63	5.72	0.12	34.1	0.82	
	55.7	0.08	3.24	0.54	5.52	0.12	33.9	0.79	
	55.3	0.09	3.42	0.59	5.85	0.15	33.9	0.82	
	55.7	0.10	3.38	0.56	5.75	0.14	34.1	0.83	
NFK1108	55.2	0.10	3.98	0.54	7.09	0.17	32.3	0.87	0.07
	55.2	0.07	3.63	0.50	6.90	0.15	32.6	0.87	0.08
	55.6	0.10	3.50	0.46	6.79	0.17	32.4	0.86	0.10
	56.2	0.08	3.33	0.48	6.77	0.15	32.6	0.87	0.11
	55.9	0.09	3.43	0.46	6.79	0.17	32.5	0.88	0.09
	55.8	0.16	3.11	0.48	6.81	0.14	32.1	1.43	0.08
	55.6	0.09	3.67	0.54	6.98	0.19	32.4	0.86	0.06
	55.7	0.10	3.62	0.49	6.96	0.14	32.4	0.84	0.05
	55.9	0.09	3.10	0.51	6.92	0.18	32.2	1.20	0.08
	55.7	0.10	3.70	0.49	7.02	0.16	32.4	0.91	0.07
	55.2	0.08	3.61	0.51	6.94	0.17	32.5	0.85	0.11
	55.0	0.07	3.84	0.55	6.77	0.15	32.4	0.85	0.09
	55.9	0.11	2.83	0.53	6.70	0.18	32.2	1.47	0.08

ORTHOPYROXENE

Sample	SiO_2	TiO_2	Al_2O_3	Cr_2O_3	FeO	MnO	MgO	CaO	Na_2O
NFK1115	56.6		1.84	0.44	7.24	0.18	33.1	0.75	0.04
	56.1		1.96	0.46	7.12	0.23	33.2	0.77	0.07
	57.2		1.82	0.46	6.99	0.21	33.1	0.80	0.05
	56.4		1.77	0.41	7.03	0.23	33.2	0.77	0.05
	56.6		1.92	0.49	7.01	0.18	33.0	0.76	0.07
	56.4	0.03	1.85	0.44	6.95	0.19	32.9	0.76	0.05
	56.5	0.03	1.87	0.40	6.91	0.22	33.0	0.77	0.10
	56.6		1.84	0.47	6.91	0.18	33.1	0.74	0.05
	56.6	0.03	1.92	0.49	6.91	0.18	33.0	0.77	0.04
	56.6		1.84	0.42	6.83	0.21	33.1	0.75	0.08
	56.2	0.03	1.90	0.41	6.70	0.20	33.0	0.75	0.06
	56.5		1.99	0.47	6.85	0.19	33.3	0.75	0.06
	57.2		1.76	0.41	6.79	0.20	33.2	0.75	0.08
	56.7		1.86	0.48	6.75	0.22	33.2	0.75	0.06
	57.1		1.83	0.45	6.77	0.20	33.1	0.75	0.07
NFR0306	54.2	0.08	2.89	0.48	8.79	0.25	31.3	0.91	
	54.7	0.08	2.98	0.49	8.53	0.22	31.3	0.92	
	55.0	0.08	2.78	0.46	9.08	0.26	31.5	0.95	
NFR0307	55.0	0.01	2.94	0.38	7.81	0.21	32.5	0.77	
	55.0	0.01	3.07	0.39	7.60	0.21	32.3	0.74	
NFR1109	55.5	0.06	1.99	0.58	9.07	0.32	32.1	0.92	
	55.9	0.07	1.85	0.59	9.02	0.30	32.2	0.90	
	56.2	0.05	1.99	0.51	8.96	0.25	32.0	0.91	
	55.9	0.07	1.99	0.51	8.77	0.27	32.3	0.92	
	55.9	0.08	2.10	0.55	8.96	0.22	31.9	0.89	
	55.5	0.06	1.95	0.47	8.92	0.25	32.2	0.90	
	56.1	0.08	1.89	0.46	9.10	0.29	31.9	0.90	
	56.1	0.07	1.82	0.42	9.17	0.26	31.7	0.90	
NFR0309	54.9	0.12	4.50	0.31	6.40	0.14	32.6	0.78	0.10
	55.4	0.14	4.53	0.31	6.47	0.16	32.6	0.78	0.06
	55.6	0.12	4.52	0.34	6.49	0.16	32.5	0.75	0.06
	55.0	0.14	4.55	0.35	6.44	0.14	32.5	0.81	0.12
	54.7	0.15	4.75	0.34	6.38	0.15	32.4	0.77	0.07
	55.3	0.15	4.64	0.36	6.44	0.14	32.3	0.83	0.10
	55.2	0.15	4.73	0.34	6.54	0.17	32.3	0.76	0.12
	55.5	0.15	4.64	0.31	6.45	0.14	32.4	0.79	0.09
	54.4	0.13	4.67	0.30	6.43	0.14	32.5	0.81	0.06
	55.8	0.12	4.48	0.32	6.35	0.15	32.5	0.74	0.09
	55.3	0.12	4.49	0.36	6.38	0.16	32.7	0.75	0.10
	54.7	0.14	4.67	0.33	6.49	0.17	32.7	0.80	0.11
	55.6	0.13	4.54	0.32	6.43	0.17	32.6	0.75	0.11
	54.7	0.14	4.46	0.27	6.35	0.13	32.6	0.78	0.06
	54.8	0.13	4.52	0.29	6.39	0.12	32.5	0.78	0.11
NFR1107	55.2	0.13	4.70	0.32	6.47	0.18	32.5	0.74	0.11
	56.0	0.08	3.37	0.54	5.72	0.14	33.5	0.79	
	56.0	0.07	3.30	0.56	5.75	0.12	33.4	0.79	0.05
	56.1	0.07	3.24	0.54	5.70	0.13	33.5	0.78	0.10
	56.0	0.09	3.02	0.51	5.73	0.13	33.5	0.81	0.11
	56.2	0.10	3.25	0.50	5.74	0.13	33.6	0.80	0.09
	56.8	0.07	3.20	0.54	5.60	0.11	33.6	0.78	0.09
	56.3	0.08	3.27	0.52	5.68	0.15	33.4	0.81	0.09
	55.6	0.09	3.31	0.53	5.63	0.13	33.4	0.82	0.07
	56.0	0.09	3.31	0.57	5.77	0.14	33.5	0.81	0.06
	56.0	0.09	3.19	0.54	5.75	0.12	33.5	0.79	0.09
	56.1	0.08	3.27	0.56	5.78	0.15	33.7	0.81	0.08
	55.7	0.09	3.36	0.57	5.63	0.15	33.6	0.80	0.07
	56.2	0.08	3.28	0.56	5.60	0.14	33.4	0.78	0.08
	56.3	0.09	3.26	0.52	5.65	0.13	33.6	0.83	0.08

ORTHOPYROXENE

Sample	SiO_2	TiO_2	Al_2O_3	Cr_2O_3	FeO	MnO	MgO	CaO	Na_2O
NMC1301	56.3	0.04	2.94	0.65	6.28	0.16	34.1	0.85	0.05
	56.4	0.03	2.93	0.64	6.27	0.14	34.4	0.87	0.07
	56.1	0.03	2.97	0.57	6.16	0.17	33.7	0.84	0.07
	56.8		2.84	0.61	6.01	0.17	33.4	0.95	0.11
	56.4		2.86	0.66	6.14	0.15	33.5	0.87	0.08
	57.3	0.03	2.88	0.61	6.11	0.12	33.6	0.90	0.10
	56.1	0.04	2.74	0.63	6.09	0.14	33.5	0.86	0.08
	56.7	0.04	2.78	0.59	6.15	0.14	33.5	0.83	0.08
	55.7	0.04	2.80	0.62	6.13	0.15	33.4	0.79	0.08
	56.2	0.03	2.93	0.61	6.15	0.13	33.4	0.80	0.07
	56.6	0.04	2.88	0.62	6.06	0.14	33.4	0.78	0.07
NMC1309	55.2	0.05	3.90	0.45	7.25	0.20	32.5	0.78	0.08
	55.3	0.05	4.12	0.49	7.31	0.20	32.3	0.81	0.10
	55.1	0.05	4.07	0.50	7.17	0.17	32.3	0.81	0.05
	55.0	0.04	3.70	0.45	7.20	0.18	32.4	0.79	0.09
	55.2	0.03	3.89	0.45	7.18	0.19	32.4	0.80	0.07
	55.2	0.06	4.22	0.45	7.33	0.18	32.4	0.83	0.06
	55.7	0.05	4.08	0.44	7.12	0.14	32.2	0.83	0.10
	55.7	0.06	4.06	0.49	7.30	0.18	32.4	0.85	0.10
NMC1322	56.1	0.04	3.99	0.51	5.97	0.14	33.3	0.74	0.09
	55.4	0.05	4.22	0.60	6.01	0.15	33.2	0.77	0.13
	56.0	0.04	4.11	0.52	6.00	0.15	33.2	0.79	0.11
	55.8	0.05	3.69	0.44	6.03	0.14	33.5	0.72	0.07
	55.8	0.04	3.92	0.53	6.06	0.13	33.5	0.73	0.08
	55.8	0.03	3.85	0.51	6.12	0.13	33.3	0.77	0.06
	55.6	0.05	4.04	0.53	6.14	0.16	33.2	0.78	0.09
	55.9	0.06	3.84	0.53	6.09	0.14	33.3	0.76	0.08
	56.0	0.03	3.83	0.48	6.26	0.14	33.8	0.76	0.13
	56.3	0.04	3.52	0.46	6.18	0.16	33.7	0.72	0.10
	55.7	0.05	3.99	0.53	6.09	0.15	33.4	0.80	0.10
NMC1336A	55.4	0.12	3.84	0.54	6.00	0.14	33.3	0.79	0.10
	55.2	0.13	4.02	0.56	5.87	0.13	32.9	0.78	0.07
	55.6	0.12	3.90	0.60	5.92	0.12	33.0	0.81	0.11
	55.4	0.13	3.92	0.59	5.81	0.13	33.2	0.81	0.09
	55.5	0.10	3.74	0.49	6.06	0.13	33.4	0.75	0.09
	55.6	0.10	3.89	0.52	5.92	0.10	33.4	0.79	0.10
	55.7	0.12	3.83	0.54	6.03	0.15	33.3	0.80	0.09
	56.3	0.08	3.53	0.46	6.03	0.11	33.5	0.77	0.10
	55.3	0.11	3.89	0.53	5.86	0.15	33.3	0.80	0.10
	55.4	0.11	3.79	0.49	5.91	0.14	33.3	0.77	0.09
NMM1126	55.3	0.07	3.89	0.44	6.01	0.14	33.7	0.84	
	54.9	0.06	4.31	0.44	5.91	0.13	33.2	0.82	
	54.9	0.06	4.16	0.50	6.08	0.15	33.5	0.72	
	55.0	0.07	4.09	0.52	5.98	0.12	33.5	0.80	
	55.2	0.06	3.89	0.40	6.03	0.13	33.8	0.82	
	54.9	0.05	4.17	0.51	6.10	0.14	33.8	0.76	

ORTHOPYROXENE

Sample	SiO_2	TiO_2	Al_2O_3	Cr_2O_3	FeO	MnO	MgO	CaO	Na_2O
NMM0318	54.7	0.09	4.34	0.30	7.02	0.17	32.1	0.78	0.10
	55.9	0.06	4.08	0.34	7.11	0.15	32.0	0.78	0.06
	55.8	0.08	4.30	0.36	7.01	0.16	32.0	0.76	0.09
	55.0	0.07	4.33	0.33	7.07	0.19	32.0	0.79	0.08
	55.3	0.07	4.26	0.35	7.01	0.18	31.9	0.81	0.09
	55.1	0.08	4.48	0.37	7.01	0.17	32.0	0.76	0.08
	55.7	0.08	4.43	0.32	7.04	0.19	32.0	0.78	0.06
	55.5	0.09	4.52	0.38	7.11	0.17	32.0	0.77	0.07
	54.9	0.07	4.47	0.35	6.96	0.18	31.8	0.77	0.03
	54.5	0.08	4.72	0.36	6.93	0.16	31.8	0.77	0.07
	55.2	0.08	4.49	0.33	6.96	0.16	31.9	0.82	0.08
	55.7	0.07	4.51	0.31	7.16	0.19	31.8	0.85	0.05
	54.9	0.07	4.42	0.36	7.05	0.16	32.1	0.81	0.07
	55.2	0.13	4.91	0.39	7.04	0.18	31.8	0.83	0.06
NMM1115	55.9	0.08	3.49	0.45	5.76	0.14	33.5	0.71	0.05
	55.8	0.06	3.46	0.42	5.76	0.14	33.4	0.69	0.04
	55.1	0.09	3.58	0.46	5.72	0.14	33.5	0.76	0.03
	56.4	0.09	3.60	0.45	5.87	0.14	33.4	0.69	0.09
	55.6	0.09	3.67	0.47	5.80	0.16	33.4	0.70	0.04
	55.5	0.07	3.48	0.48	5.86	0.13	33.5	0.69	0.07
	55.4	0.08	4.04	0.43	5.95	0.15	32.3	0.84	0.04
	56.2	0.08	3.43	0.47	5.75	0.15	33.4	0.70	0.09
	56.0	0.08	3.28	0.43	5.84	0.16	33.7	0.70	0.08
	56.7	0.06	3.27	0.48	5.75	0.15	33.6	0.75	0.06
	56.2	0.07	3.47	0.50	5.78	0.13	33.4	0.78	0.06
	55.8	0.07	3.63	0.58	5.83	0.13	33.4	0.70	0.08
	56.2	0.07	3.52	0.57	5.88	0.12	33.4	0.69	0.08
	55.9	0.09	3.57	0.59	5.81	0.12	33.5	0.72	0.06
	56.2	0.07	3.60	0.59	5.77	0.15	33.4	0.72	0.04
NME1122	55.2	0.09	3.87	0.51	6.15	0.14	34.0	0.71	
	55.3	0.09	3.70	0.47	6.12	0.19	34.0	0.70	
	55.1	0.10	3.57	0.46	6.01	0.17	34.0	0.75	
	55.4	0.06	3.60	0.53	6.10	0.12	34.0	0.78	
	54.9	0.08	3.73	0.41	6.19	0.12	33.8	0.78	
	55.3	0.11	3.68	0.52	6.05	0.14	33.7	0.80	
	55.2	0.11	3.62	0.52	5.89	0.17	33.8	0.76	
	55.2	0.05	3.81	0.52	6.11	0.13	33.6	0.73	
NME0528	55.9	0.07	3.35	0.75	6.10	0.14	33.0	0.79	0.06
	55.8	0.10	3.38	0.72	6.16	0.17	33.0	0.82	0.09
	56.4	0.08	2.90	0.51	6.04	0.15	33.6	0.76	0.07
	56.4	0.07	2.92	0.57	6.08	0.15	33.3	0.87	0.07
	56.0	0.07	2.87	0.53	6.19	0.15	33.4	0.79	0.07
	57.0	0.06	2.97	0.54	6.14	0.16	33.3	0.77	0.07
	56.3	0.07	2.84	0.52	6.00	0.13	33.4	0.81	0.09
	55.7	0.08	3.11	0.59	6.15	0.13	33.2	0.79	0.06
	56.4	0.07	2.87	0.51	6.15	0.15	33.4	0.80	0.07
	56.0	0.06	2.97	0.49	6.14	0.13	33.3	0.77	0.09

ORTHOPYROXENE

Sample	SiO_2	TiO_2	Al_2O_3	Cr_2O_3	FeO	MnO	MgO	CaO	Na_2O
NME1116	55.7	0.06	3.99	0.43	5.92	0.12	33.2	0.78	0.11
	55.8	0.07	3.91	0.50	5.88	0.15	33.1	0.77	0.10
	56.0	0.08	4.08	0.46	5.90	0.14	33.4	0.79	0.11
	55.6	0.06	4.19	0.52	5.95	0.12	33.2	0.76	0.14
	55.6	0.07	3.99	0.49	5.87	0.13	33.3	0.80	0.09
	55.8	0.07	3.88	0.48	5.77	0.15	33.3	0.81	0.08
	55.5	0.07	4.07	0.49	5.82	0.15	33.1	0.76	0.09
	56.0	0.06	4.07	0.51	5.86	0.14	33.1	0.83	0.07
	56.0	0.08	4.05	0.49	5.86	0.12	33.3	0.80	0.08
	55.8	0.06	4.14	0.48	5.87	0.17	33.0	0.81	0.08
	55.8	0.08	3.94	0.46	5.82	0.11	33.2	0.87	0.05
	56.0	0.07	3.52	0.43	5.80	0.14	33.5	0.78	0.09
	55.3	0.08	4.04	0.49	5.93	0.16	33.1	0.82	0.10
	55.2	0.06	3.96	0.49	5.82	0.14	33.2	0.79	0.07
NBN0302A	54.7	0.07	3.42	0.39	6.26	0.13	34.4	0.67	0.01
	55.1	0.05	3.36	0.34	6.39	0.13	34.5	0.66	0.02
	54.7	0.07	3.39	0.42	6.35	0.16	34.3	0.65	0.04
	54.9	0.08	3.68	0.30	6.45	0.17	34.3	0.65	0.06
	54.9	0.06	3.51	0.31	6.39	0.18	34.3	0.70	0.01
	54.9	0.06	3.48	0.32	6.38	0.13	34.1	0.65	0.05
	54.8	0.08	3.31	0.42	6.52	0.17	34.2	0.64	0.03
	54.6	0.04	3.55	0.38	6.43	0.17	34.2	0.65	0.05
	55.0	0.06	3.48	0.47	6.51	0.14	34.3	0.63	0.04
	54.7	0.09	3.27	0.37	6.25	0.16	34.3	0.67	0.04
NBN0305	55.4	0.08	2.80	0.49	6.36	0.11	34.7	0.67	0.04
	55.2	0.08	2.91	0.43	6.06	0.16	34.2	0.65	0.04
	55.1	0.06	2.89	0.44	6.09	0.10	34.5	0.70	0.03
	55.6	0.07	2.95	0.45	6.32	0.17	34.1	0.60	
	55.2	0.07	2.84	0.43	6.18	0.16	34.3	0.66	0.05
	55.3	0.05	2.81	0.44	6.03	0.16	34.0	0.65	0.04
	55.3	0.06	3.12	0.50	5.98	0.17	34.1	0.66	0.02
	55.3	0.07	2.91	0.44	6.16	0.13	34.6	0.66	0.02
	55.6	0.05	2.93	0.38	6.02	0.14	34.6	0.67	0.01
	55.5	0.06	2.94	0.47	6.07	0.11	34.2	0.67	0.01
	55.2	0.08	3.94	0.40	6.23	0.16	33.4	0.66	0.06
	54.8	0.06	3.94	0.33	6.27	0.12	33.9	0.64	0.05
	55.1	0.08	4.10	0.44	6.34	0.16	33.5	0.66	0.06
NBN0311	54.6	0.07	3.60	0.40	6.31	0.14	34.4	0.63	0.07
	53.5	0.08	4.21	0.44	6.37	0.13	33.8	0.63	0.08
NBN0316	54.8	0.07	3.81	0.29	6.76	0.12	33.9	0.72	
	54.8	0.10	4.08	0.34	6.68	0.14	33.6	0.71	0.04
	54.5	0.08	3.91	0.27	6.86	0.19	33.6	0.67	
	54.6	0.07	3.86	0.29	6.73	0.17	33.8	0.64	0.02
	55.0	0.05	4.01	0.26	6.79	0.13	33.8	0.66	
	54.4	0.06	3.88	0.33	6.72	0.14	33.5	0.67	0.00
	54.8	0.08	3.89	0.32	6.73	0.11	33.8	0.68	
NBN0319	54.9	0.03	3.85	0.24	6.43	0.18	33.5	0.67	
	54.7	0.08	4.01	0.29	6.79	0.19	33.5	0.63	
	54.9	0.05	3.81	0.25	6.70	0.15	33.6	0.64	0.01
	54.8	0.08	3.90	0.31	6.61	0.16	33.4	0.68	0.02
	54.9	0.07	3.83	0.32	6.73	0.12	33.3	0.75	
	54.4	0.06	3.79	0.32	6.73	0.16	33.6	0.71	0.01
	54.7	0.07	4.01	0.33	6.61	0.16	33.5	0.71	0.00
	54.6	0.05	4.07	0.25	6.40	0.15	33.5	0.67	0.02
	54.5	0.07	4.01	0.29	6.53	0.16	33.4	0.68	0.02
	55.2	0.07	3.66	0.24	6.70	0.16	33.5	0.66	
	54.7	0.07	3.84	0.32	6.70	0.20	33.6	0.68	0.01
	54.9	0.04	3.84	0.30	6.81	0.14	33.3	0.68	0.05
	55.1	0.06	3.77	0.33	6.69	0.14	33.5	0.65	0.02

ORTHOPYROXENE

Sample	SiO_2	TiO_2	Al_2O_3	Cr_2O_3	FeO	MnO	MgO	CaO	Na_2O
NBN0321	54.8	0.07	3.32	0.38	6.30	0.14	34.2	0.68	0.03
	54.4	0.10	3.60	0.42	6.29	0.12	33.9	0.70	0.03
	54.6	0.10	3.46	0.44	6.41	0.12	34.4	0.68	0.03
	55.2	0.06	3.38	0.43	6.46	0.12	34.0	0.65	0.03
	55.0	0.10	3.43	0.37	6.24	0.16	34.0	0.71	0.02
	55.3	0.07	3.12	0.41	6.37	0.13	34.3	0.67	0.08
	54.6	0.10	3.72	0.38	6.31	0.14	34.1	0.69	0.05
	54.4	0.11	3.79	0.40	6.21	0.09	33.9	0.69	0.03
	53.4	0.13	3.87	0.44	6.22	0.16	33.6	0.72	0.03

CLINOPYROXENE

Sample	SiO_2	TiO_2	Al_2O_3	Cr_2O_3	FeO	MnO	MgO	CaO	Na_2O
NMS1302A	53.6	0.04	2.81	1.10	2.15	0.08	17.3	23.1	0.52
	53.9	0.06	2.62	1.01	2.14	0.07	17.3	23.2	0.56
	54.1		2.62	0.98	2.11	0.09	17.4	23.2	0.54
	54.5	0.05	2.34	0.81	2.21	0.07	17.6	23.1	0.53
	54.9	0.06	2.44	0.86	2.14	0.06	17.5	23.3	0.52
	53.3	0.05	2.57	0.90	2.19	0.07	17.5	23.4	0.57
	53.7	0.05	2.70	1.18	2.04	0.07	17.3	23.3	0.62
	53.8	0.07	2.45	0.86	2.07	0.09	17.4	23.3	0.55
NMS1304	52.0	0.26	4.17	0.99	2.59	0.06	16.3	22.7	0.69
	52.7	0.25	3.91	0.90	2.47	0.07	16.5	22.9	0.64
	52.4	0.26	4.10	0.98	2.44	0.10	16.4	22.9	0.70
	52.4	0.26	3.85	0.99	2.34	0.09	16.4	22.8	0.68
	53.2	0.24	3.63	0.83	2.54	0.08	16.4	22.9	0.68
	52.5	0.26	3.84	1.03	2.34	0.10	16.5	22.9	0.63
	52.2	0.25	3.79	1.04	2.32	0.09	16.5	22.8	0.66
	52.7	0.24	3.68	1.02	2.37	0.09	16.6	22.8	0.68
	52.5	0.25	3.84	0.95	2.49	0.08	16.5	22.7	0.66
	52.1	0.25	3.94	1.06	2.48	0.08	16.4	22.6	0.64
	52.5	0.23	3.53	0.82	2.49	0.09	16.5	22.9	0.69
	52.4	0.21	3.47	0.74	2.42	0.09	16.7	23.0	0.60
	53.1	0.24	3.64	0.80	2.46	0.07	16.5	22.9	0.67
	52.6	0.22	3.64	0.91	2.46	0.09	16.4	22.8	0.65
	52.1	0.23	3.52	0.85	2.30	0.09	16.5	23.0	0.59
NMS1305	52.2	0.28	6.46	0.73	2.79	0.10	15.4	21.5	1.44
	51.8	0.40	7.03	0.79	2.87	0.09	15.0	21.2	1.62
	52.4	0.27	6.39	0.73	2.84	0.09	15.4	21.4	1.46
	52.7	0.23	6.11	0.72	2.77	0.10	15.6	21.4	1.32
	53.1	0.22	5.64	0.73	2.66	0.09	15.7	21.5	1.36
	52.8	0.21	5.90	0.72	2.71	0.09	15.8	21.4	1.37
	52.1	0.24	6.63	0.83	2.77	0.08	15.2	21.2	1.45
	52.5	0.18	5.82	0.84	2.73	0.10	15.7	21.6	1.40
	52.2	0.22	6.26	0.66	2.87	0.09	15.4	21.2	1.41
	52.1	0.31	6.94	0.75	2.81	0.09	15.2	21.0	1.55
	52.1	0.31	6.99	0.84	2.72	0.09	15.0	21.1	1.42
	51.6	0.36	7.04	0.81	2.85	0.11	14.9	21.1	1.49
	52.4	0.33	6.92	0.79	2.82	0.11	15.1	21.2	1.51
	52.6	0.15	6.09	0.78	2.87	0.09	15.5	21.3	1.46
	51.9	0.40	7.49	0.86	2.78	0.10	14.7	21.2	1.53
	52.0	0.14	6.19	0.76	2.72	0.11	15.5	21.3	1.36
	52.4	0.14	6.43	0.79	2.75	0.08	15.4	21.3	1.49
	52.5	0.18	6.35	0.74	2.80	0.08	15.3	21.3	1.47
	52.2	0.42	7.61	0.78	2.97	0.09	14.8	20.9	1.64
	51.5	0.41	7.53	0.77	2.94	0.09	14.8	20.5	1.70
NMS1308	50.7	0.45	6.67	1.43	2.54	0.10	15.0	20.6	1.63
	51.9	0.42	6.56	1.45	2.55	0.08	15.0	20.4	1.76
	51.5	0.47	6.59	1.44	2.55	0.10	15.1	20.3	1.73
	51.2	0.42	6.37	1.36	2.54	0.10	15.1	21.0	1.41
	51.8	0.37	5.85	1.14	2.54	0.08	15.4	21.1	1.45
	51.8	0.34	5.95	1.33	2.58	0.08	15.3	20.9	1.49
	52.5	0.39	5.75	1.10	2.60	0.09	15.5	21.2	1.42
	51.5	0.44	5.99	1.31	2.51	0.08	15.3	21.1	1.43
	52.0	0.43	6.14	1.34	2.49		15.2	21.2	1.48
	52.0	0.40	5.69	1.10	2.53	0.08	15.4	20.9	1.37
	51.6	0.42	6.28	1.29	2.51	0.09	15.1	20.9	1.54
	51.6	0.34	5.37	1.15	2.42	0.10	15.6	21.2	1.33
	51.3	0.41	5.89	1.23	2.44	0.09	15.3	21.2	1.40

CLINOPYROXENE

Sample	SiO_2	TiO_2	Al_2O_3	Cr_2O_3	FeO	MnO	MgO	CaO	Na_2O
NMS1310	51.9	0.49	6.59	1.07	2.71	0.09	15.3	20.8	1.54
	51.5	0.51	6.75	1.07	2.72	0.07	15.3	20.6	1.82
	52.1	0.47	6.30	0.98	2.71	0.09	15.5	20.5	1.67
	51.4	0.47	6.48	1.12	2.73	0.07	15.4	20.6	1.73
	51.8	0.42	6.29	1.04	2.70	0.12	15.4	20.7	1.71
	51.6	0.50	6.61	1.03	2.80	0.08	15.4	20.5	1.63
	51.9	0.49	6.82	1.17	2.77	0.10	15.2	20.2	1.89
	52.3	0.50	6.35	1.09	2.72	0.09	15.6	20.7	1.86
	52.0	0.50	6.76	1.13	2.75	0.09	15.3	20.4	1.68
	51.6	0.49	6.65	1.09	2.78	0.09	15.3	20.5	1.78
	52.0	0.49	6.79	1.23	2.71	0.09	15.2	20.3	1.81
	51.4	0.49	6.88	1.17	2.75	0.07	15.2	20.3	1.78
	52.1	0.51	6.49	1.11	2.78	0.08	15.4	20.5	1.65
	52.2	0.50	6.88	1.20	2.72	0.10	15.2	20.3	1.88
	51.8	0.49	6.53	1.07	2.76	0.09	15.5	20.6	1.72
NJS1302	51.1	1.01	7.18	0.76	3.24	0.08	14.8	20.1	1.83
	51.6	1.13	7.60	0.87	3.06	0.08	14.3	20.1	1.93
	50.7	1.15	7.73	0.89	3.11	0.07	14.3	19.9	1.93
	50.4	1.29	8.03	0.95	3.09	0.06	14.2	19.4	2.13
	50.6	1.16	7.59	0.91	3.10	0.08	14.3	19.8	1.89
	50.8	1.05	7.31	0.90	3.09	0.09	14.5	20.0	1.85
	50.4	1.12	7.55	0.87	3.05	0.08	14.5	19.9	1.91
	50.8	1.25	7.78	0.96	3.16	0.08	14.2	19.7	2.09
	50.6	1.28	8.01	1.09	3.08	0.08	14.0	19.8	1.99
	50.9	1.15	7.50	1.03	3.05	0.11	14.2	19.6	1.92
	51.1	1.18	7.81	1.04	3.08	0.10	14.2	19.6	1.99
NJS1304	51.6	1.13	7.72	1.01	3.10	0.09	14.4	19.7	2.16
	52.0	0.86	6.59	0.77	3.02	0.09	14.8	20.1	1.98
	52.1	0.93	6.93	0.82	3.14	0.10	14.9	20.2	1.95
	51.6	0.94	7.15	0.92	3.12	0.05	14.7	20.1	2.01
	52.1	0.94	7.14	0.85	3.09	0.11	14.8	19.9	2.00
	51.2	1.06	7.56	0.92	3.14	0.06	14.7	20.0	2.15
	51.5	0.92	7.02	0.86	3.08	0.09	14.9	20.1	2.11
	52.1	0.95	7.22	0.84	3.12	0.09	14.6	19.8	2.12
	51.8	0.93	7.04	0.84	3.11	0.09	14.8	20.2	2.02
NJS1306	51.3	0.47	6.98	0.72	3.98	0.12	15.3	20.0	1.47
	50.5	0.47	7.07	0.70	4.02	0.09	15.3	19.9	1.40
	50.5	0.49	6.92	0.69	4.06	0.10	15.3	20.0	1.45
	51.6	0.45	6.96	0.67	3.95	0.12	15.4	20.0	1.44
	51.5	0.45	7.08	0.75	3.98	0.12	15.2	19.9	1.46
	51.7	0.51	7.04	0.66	3.75	0.10	15.3	20.0	1.57
	51.5	0.59	7.07	0.73	3.78	0.11	15.3	20.1	1.50
	51.3	0.53	7.25	0.75	3.69	0.10	15.2	20.1	1.48
	51.2	0.49	7.09	0.70	3.71	0.08	15.4	19.9	1.57
	50.9	0.49	7.08	0.70	3.88	0.11	15.4	19.9	1.45
	51.3	0.55	7.35	0.72	3.86	0.12	15.1	19.9	1.44
	51.5	0.51	7.14	0.78	3.83	0.11	15.2	20.0	1.46
	51.3	0.61	7.47	0.79	3.74	0.08	15.2	20.0	1.59
	51.1	0.54	7.32	0.74	3.79	0.13	15.1	20.1	1.61

CLINOPYROXENE

Sample	SiO_2	TiO_2	Al_2O_3	Cr_2O_3	FeO	MnO	MgO	CaO	Na_2O
NJS1307	51.3	0.72	7.60	0.76	3.10	0.08	15.1	19.5	1.93
	51.2	0.71	7.56	0.74	3.03	0.10	15.1	19.8	1.87
	52.0	0.74	7.83	0.78	3.09	0.10	14.9	19.7	1.96
	51.1	0.73	7.79	0.80	3.05	0.08	15.0	19.7	1.86
	51.9	0.73	7.66	0.80	3.02	0.09	15.0	19.8	1.87
	52.0	0.69	7.37	0.70	3.16	0.11	15.2	19.5	1.82
	51.6	0.71	7.54	0.76	3.13	0.11	15.1	19.7	1.90
	51.7	0.69	7.49	0.76	3.22	0.11	15.3	19.5	1.82
	51.9	0.70	7.52	0.79	3.06	0.10	15.2	19.7	1.94
	51.0	0.69	7.56	0.73	3.07	0.10	15.2	19.6	1.86
	51.5	0.70	7.73	0.84	3.05	0.10	15.1	19.7	1.90
	52.1	0.69	7.45	0.70	3.09	0.10	15.3	19.6	1.82
NPY1301	52.1	0.55	6.88	0.90	2.82	0.10	14.9	20.4	1.91
	51.7	0.56	6.99	0.91	2.84	0.09	14.9	20.3	1.92
	52.5	0.60	7.02	0.77	2.82	0.05	14.9	20.5	1.90
	52.2	0.59	7.35	0.92	2.85	0.08	14.7	20.2	2.01
	52.2	0.55	7.44	0.91	2.87	0.09	14.7	20.3	1.85
	51.8	0.61	7.36	0.93	2.80	0.08	14.7	20.3	1.90
	51.8	0.59	7.27	0.82	2.87	0.10	14.8	20.3	2.00
	51.9	0.64	6.88	0.71	2.84	0.10	15.0	20.4	1.87
	52.6	0.60	6.92	0.77	2.82	0.11	15.1	20.5	1.84
	51.7	0.54	7.23	0.81	2.83	0.11	14.9	20.0	1.96
	52.2	0.56	7.19	0.86	2.76	0.12	14.8	20.4	2.02
	51.9	0.54	7.35	0.80	2.88	0.08	14.7	20.1	2.05
NPY1310	51.9	0.54	6.71	0.42	3.11	0.10	15.2	21.1	1.34
	51.7	0.56	6.85	0.41	3.01	0.12	15.1	21.1	1.36
	51.8	0.56	6.54	0.42	3.10	0.11	15.2	21.1	1.47
	51.8	0.59	6.93	0.42	3.07	0.07	15.0	21.2	1.32
	51.3	0.55	6.74	0.43	3.09	0.08	15.1	21.1	1.35
	50.9	0.60	6.91	0.47	3.07	0.07	15.0	21.1	1.36
	52.2	0.57	6.88	0.44	3.07	0.11	15.0	21.1	1.38
	51.6	0.54	7.15	0.46	3.08	0.11	14.9	21.0	1.42
	51.9	0.53	7.03	0.42	3.08	0.10	14.9	21.0	1.39
NPY1311	51.5	0.57	7.31	0.49	3.14	0.06	14.9	20.9	1.39
	51.6	0.56	7.41	0.48	3.09	0.11	14.8	20.8	1.43
	51.2	0.58	7.20	0.52	3.04	0.08	15.0	20.9	1.52
	51.1	0.61	7.46	0.48	2.98	0.11	14.8	20.9	1.37
	52.1	0.52	6.60	0.45	3.15	0.07	15.1	21.1	1.36
	51.3	0.57	7.17	0.50	3.05	0.09	14.9	21.1	1.40
	51.3	0.56	7.19	0.44	3.03	0.12	14.9	21.1	1.32
	51.7	0.57	6.94	0.43	3.07	0.10	15.1	21.1	1.39
	51.6	0.56	6.81	0.45	3.10	0.09	15.2	21.1	1.24
	51.6	0.56	6.93	0.46	2.99	0.12	14.9	20.9	1.42
	52.0	0.53	6.63	0.42	3.10	0.09	15.1	21.0	1.45
	50.9	0.56	7.10	0.45	3.02	0.09	15.0	21.0	1.35
	51.6	0.56	6.94	0.41	3.10	0.10	15.1	21.0	1.33
	52.0	0.53	6.58	0.35	3.09	0.10	15.4	21.0	1.33
NPY1314	50.8	0.60	7.24	0.71	2.99	0.10	14.7	20.5	1.52
	50.5	0.56	6.99	0.69	2.95	0.12	15.0	21.1	1.36
	50.7	0.64	7.63	0.79	2.92	0.08	14.5	20.4	1.57
	50.2	0.63	7.56	0.79	2.95	0.08	14.7	20.4	1.64
	50.8	0.49	6.66	0.68	2.96	0.07	15.3	21.3	1.34
	50.5	0.63	7.39	0.79	2.91	0.09	15.0	21.0	1.37

CLINOPYROXENE

Sample	SiO_2	TiO_2	Al_2O_3	Cr_2O_3	FeO	MnO	MgO	CaO	Na_2O
NFL1302	51.7	0.36	5.90	0.93	2.69	0.09	15.8	21.2	1.19
	51.8	0.34	5.73	0.90	2.72	0.08	15.8	21.2	1.24
	51.8	0.34	5.74	0.90	2.74	0.09	15.9	21.2	1.26
	51.7	0.35	6.11	1.07	2.63	0.08	15.5	21.4	1.23
	51.6	0.32	5.67	0.86	2.57	0.10	15.9	21.7	1.08
	51.3	0.31	5.72	0.92	2.67	0.09	15.8	21.8	1.12
	52.2	0.30	5.64	0.84	2.59	0.08	15.8	21.6	1.15
	51.4	0.31	5.76	0.87	2.62	0.07	15.9	21.5	1.18
	52.1	0.36	5.82	0.95	2.73	0.10	15.8	21.2	1.27
	51.9	0.30	5.55	0.84	2.57	0.09	15.8	21.6	1.15
	51.8	0.32	5.80	0.98	2.65	0.09	15.7	21.4	1.24
	51.5	0.29	5.63	0.89	2.63	0.07	15.9	21.5	1.14
	51.8	0.31	5.59	0.93	2.60	0.06	15.8	21.7	1.22
NFL1305	51.7	0.15	5.43	0.88	2.78	0.11	15.9	20.9	1.27
	51.3	0.19	5.94	1.06	2.73	0.09	15.6	21.1	1.27
	51.7	0.16	5.73	1.00	2.73	0.07	15.8	21.4	1.31
	51.8	0.14	5.39	0.90	2.61	0.06	15.9	21.4	1.20
	52.5	0.15	5.70	0.91	2.69	0.08	15.7	21.3	1.12
	51.5	0.15	5.65	0.98	2.73	0.07	15.9	21.1	1.29
	51.9	0.12	5.52	1.00	2.62	0.09	15.8	21.6	1.11
	52.1	0.14	5.42	0.93	2.74	0.07	15.9	21.4	1.18
	51.5	0.19	5.93	0.95	2.72	0.09	15.8	21.1	1.31
NFL1315A	52.6	0.17	3.28	1.41	2.75	0.11	16.6	21.4	1.18
	52.8	0.14	3.10	1.30	2.71	0.09	16.7	21.6	1.11
	52.9	0.11	3.11	1.39	2.72	0.11	16.7	21.5	1.16
	52.6	0.15	3.18	1.55	2.71	0.10	16.6	21.6	1.15
	53.4	0.08	3.01	1.37	2.70	0.10	16.7	21.3	1.19
	52.8	0.19	3.28	1.41	2.75	0.11	16.6	21.5	1.20
	52.5	0.17	3.05	1.31	2.72	0.06	16.7	21.7	1.03
	52.6	0.18	3.01	1.38	2.67	0.08	16.6	21.7	1.19
	52.0	0.18	3.03	1.38	2.70	0.08	16.6	21.7	1.03
NFL1316	53.7	0.13	3.44	1.03	2.42	0.08	16.7	21.8	1.18
	53.3	0.14	3.37	1.20	2.52	0.09	16.8	22.1	1.16
	53.0	0.14	3.53	1.13	2.58	0.08	16.7	21.9	1.10
	52.8	0.15	3.56	1.10	2.38	0.05	16.6	22.2	1.01
	52.8	0.17	3.66	1.18	2.58	0.08	16.9	21.9	0.93
	53.4	0.13	3.44	1.11	2.57	0.08	16.6	21.9	1.06
	53.5	0.14	3.42	1.03	2.46	0.09	16.9	22.2	1.01
	53.6	0.13	3.36	1.14	2.40	0.09	16.8	22.2	1.00
	53.8	0.13	3.41	1.10	2.41	0.07	16.8	22.2	1.01
	53.5	0.14	3.37	1.09	2.42	0.06	16.8	22.2	1.09
NFL1324	51.9	0.23	4.66	1.28	2.48	0.08	16.2	21.6	1.15
	52.4	0.22	4.80	1.26	2.54	0.10	16.0	21.3	1.19
	51.6	0.21	4.77	1.34	2.49	0.08	16.1	21.6	1.24
	52.2	0.19	4.53	1.36	2.56	0.10	16.4	21.5	1.08
	51.5	0.14	4.97	1.78	2.56	0.09	16.1	20.9	1.39
	52.0	0.19	4.67	1.26	2.59	0.09	16.3	21.1	1.27
	52.2	0.21	4.43	1.22	2.55	0.12	16.4	21.7	1.11
	52.3	0.19	4.77	1.39	2.62	0.07	16.2	21.1	1.23
	52.4	0.21	4.69	1.30	2.54	0.09	16.3	21.3	1.26
	52.6	0.18	4.67	1.48	2.52	0.08	16.3	21.3	1.18
	52.3	0.20	4.76	1.36	2.60	0.07	16.3	21.3	1.17

CLINOPYROXENE

Sample	SiO_2	TiO_2	Al_2O_3	Cr_2O_3	FeO	MnO	MgO	CaO	Na_2O
NFL1326	51.4	0.39	4.82	0.92	4.08	0.13	15.0	22.1	1.14
	50.9	0.38	5.03	0.84	4.15	0.12	14.7	21.9	1.24
	51.5	0.38	4.71	0.91	4.14	0.13	14.9	22.0	1.14
	51.6	0.34	4.49	0.89	4.15	0.11	15.2	22.0	1.12
	51.6	0.37	4.81	0.98	4.13	0.11	15.0	22.0	1.20
	51.3	0.39	4.88	0.92	4.09	0.14	14.9	22.2	1.24
	52.1	0.38	4.70	0.88	4.18	0.11	14.9	22.1	1.06
	51.5	0.41	5.42	1.01	4.31	0.11	14.7	22.0	1.22
	50.9	0.42	5.47	1.00	4.12	0.12	14.7	22.2	1.18
	51.4	0.36	4.84	0.94	4.15	0.12	14.8	22.1	1.14
NFL1327	51.5	0.29	4.44	1.08	4.21	0.14	15.8	21.6	1.00
	51.7	0.25	4.46	1.05	4.25	0.14	15.8	21.5	1.05
	52.1	0.22	4.29	1.10	4.32	0.17	15.9	21.1	1.22
	52.1	0.18	4.74	1.13	4.32	0.15	15.7	20.5	1.31
	52.0	0.20	4.65	1.17	4.29	0.17	15.8	20.8	1.25
	52.4	0.19	4.50	1.10	4.17	0.14	15.9	21.0	1.22
	53.1	0.18	4.59	1.16	4.21	0.14	15.8	20.8	1.30
	52.7	0.18	4.24	1.14	4.16	0.13	16.0	21.0	1.19
	52.2	0.16	4.73	1.16	4.02	0.13	15.7	21.0	1.28
	52.3	0.19	4.24	1.13	4.39	0.14	16.0	20.9	1.18
	52.1	0.17	4.55	1.15	4.29	0.14	15.8	20.8	1.25
	51.8	0.18	4.50	1.13	4.22	0.14	15.9	20.8	1.09
NFL1329	51.7	0.29	6.17	0.65	2.70	0.05	15.6	21.5	1.23
	51.8	0.31	6.28	0.66	2.84	0.09	15.7	21.0	1.43
	51.5	0.31	6.31	0.61	2.77	0.12	15.6	21.3	1.37
	51.8	0.31	6.09	0.71	2.76	0.09	15.7	21.4	1.24
	51.9	0.32	6.14	0.67	2.82	0.07	15.7	21.2	1.38
	52.7	0.34	5.99	0.74	2.76	0.12	15.8	21.1	1.34
	52.4	0.35	6.13	0.79	2.74	0.12	15.6	21.4	1.24
NTB0306	53.1	0.12	3.25	1.29	2.51	0.05	16.5	20.7	1.18
	52.9	0.07	3.04	1.10	2.67	0.12	16.8	20.8	1.11
	53.1	0.04	3.30	1.16	2.65	0.10	16.8	21.0	1.12
	53.5	0.12	3.09	1.18	2.63	0.07	16.9	20.7	1.07
	53.3	0.10	3.55	1.27	2.62	0.09	16.4	20.6	1.27
	53.1	0.12	3.14	1.32	2.65	0.10	16.7	21.0	1.13
	53.0	0.14	3.26	1.47	2.63	0.09	16.6	21.1	1.17
	53.1	0.16	3.60	0.91	2.79	0.07	16.8	20.8	1.29
	52.9	0.13	3.61	1.56	2.70	0.09	16.6	20.5	1.29
NTB0307	52.9	0.22	5.94	0.79	2.52	0.06	15.9	20.8	1.20
	53.6	0.20	5.33	0.80	2.92	0.06	16.4	20.8	1.09
	53.1	0.21	5.49	0.81	2.66	0.04	16.0	20.7	1.10
	52.8	0.22	5.78	0.78	2.70	0.06	15.9	20.9	1.11
	54.1	0.19	5.14	0.75	3.11	0.10	16.4	19.9	1.11
NTB1124	51.2	0.51	5.58	1.02	2.85	0.07	16.2	21.1	1.06
	51.2	0.50	5.77	1.14	2.74	0.10	16.0	20.8	1.14
	51.0	0.54	5.85	1.02	2.75	0.12	16.1	21.0	1.15
	51.3	0.54	5.69	1.02	2.84	0.04	16.1	21.1	1.22
	51.3	0.50	5.56	1.01	2.96	0.08	16.1	20.8	1.11
	51.2	0.51	5.78	1.10	2.93	0.10	16.2	21.0	1.10
	51.1	0.59	5.93	1.06	2.74	0.06	16.2	20.9	1.12

CLINOPYROXENE

Sample	SiO_2	TiO_2	Al_2O_3	Cr_2O_3	FeO	MnO	MgO	CaO	Na_2O
NTB1116	52.3	0.30	5.79	1.22	2.79	0.07	15.6	20.6	1.51
	52.1	0.35	6.09	1.32	2.74	0.09	15.4	20.4	1.64
	51.7	0.36	6.23	1.14	2.79	0.07	15.4	20.5	1.58
	51.9	0.36	6.20	1.04	2.81	0.06	15.4	20.4	1.54
	52.1	0.36	5.97	1.17	2.73	0.08	15.4	20.5	1.46
	52.3	0.35	6.02	1.10	2.69	0.08	15.5	20.7	1.61
	52.0	0.36	6.12	1.31	2.75	0.09	15.4	20.4	1.73
	52.7	0.33	5.79	1.11	2.77	0.10	15.6	20.7	1.66
	52.7	0.33	6.00	1.19	2.71	0.06	15.5	20.8	1.48
	52.5	0.37	6.13	1.17	2.67	0.10	15.5	20.7	1.67
	52.0	0.32	5.89	1.09	2.71	0.07	15.6	20.7	1.58
NTB1122	50.8	0.90	6.32	0.85	3.60	0.11	15.4	21.0	1.11
	50.4	0.98	6.53	0.86	3.67	0.11	15.5	20.7	1.15
	50.4	0.99	6.65	0.83	3.61	0.12	15.4	20.8	1.06
	50.2	0.99	6.48	0.91	3.61	0.11	15.4	20.9	1.10
	50.5	1.04	6.85	0.88	3.63	0.10	15.2	20.8	1.09
	51.2	0.93	6.31	0.92	3.69	0.09	15.6	20.8	1.03
	51.1	0.92	6.21	0.89	3.55	0.13	15.6	20.8	1.04
	50.6	0.99	6.43	0.93	3.56	0.11	15.4	20.9	1.02
	50.8	0.99	6.40	0.91	3.63	0.10	15.3	20.9	1.03
	51.0	0.97	6.45	0.86	3.64	0.11	15.4	20.9	1.03
	50.4	0.97	6.57	0.92	3.54	0.10	15.3	21.0	1.02
	51.0	0.96	6.45	0.92	3.59	0.09	15.4	20.9	1.12
	51.1	0.95	6.53	0.88	3.61	0.10	15.4	21.0	1.09
NFK0301	51.9	0.24	5.29	1.36	2.83	0.05	15.8	20.5	1.32
	52.1	0.26	5.19	1.32	2.85	0.07	15.9	20.6	1.35
	52.6	0.23	5.04	1.11	2.84	0.06	16.0	20.7	1.26
	52.4	0.26	5.18	1.22	2.82	0.03	15.9	20.5	1.34
	52.3	0.25	5.32	1.20	2.79	0.05	15.9	20.6	1.34
	52.4	0.25	5.03	1.12	2.83	0.04	16.0	20.8	1.29
	51.9	0.24	5.01	1.09	2.86	0.06	16.1	20.6	1.31
	52.1	0.25	5.31	1.26	2.87	0.06	15.9	20.5	1.29
	51.7	0.24	5.22	1.30	2.81	0.04	15.7	20.7	1.29
	52.0	0.24	5.20	1.26	2.84	0.04	16.1	20.5	1.34
	52.0	0.24	5.24	1.24	2.75	0.08	15.9	20.8	1.35
NFK1123	51.8	0.35	4.86	1.30	2.58	0.08	16.4	21.5	1.07
	52.1	0.30	4.64	1.37	2.64	0.06	16.3	21.2	1.02
	51.9	0.31	4.54	1.27	2.46	0.10	16.4	21.3	1.00
	52.5	0.30	4.56	1.19	2.62	0.12	16.6	21.4	1.06
	52.4	0.24	4.70	1.17	2.51	0.08	16.4	21.2	1.05
	52.0	0.31	4.72	1.10	2.60	0.08	16.2	21.1	1.03
	52.5	0.22	4.25	1.44	2.72	0.07	16.8	20.5	1.25
NFK1108	51.9	0.31	4.99	1.08	3.24	0.09	15.9	21.3	1.13
	53.0	0.38	4.35	1.16	3.56	0.12	17.2	20.0	1.09
	51.7	0.32	5.02	1.06	3.18	0.10	15.9	21.2	1.07
	51.7	0.99	5.86	1.24	3.49	0.12	16.1	20.0	1.15
	52.4	0.41	4.76	1.05	3.37	0.10	16.3	20.9	1.00
	51.8	0.34	5.02	1.20	3.19	0.11	15.9	21.5	1.02
	52.0	0.34	5.21	1.17	3.26	0.12	15.7	21.4	1.08
	52.4	0.32	4.98	1.09	3.25	0.09	15.9	21.5	1.02
	52.3	0.30	5.25	1.21	3.21	0.10	15.8	21.3	1.11
	51.9	0.33	5.30	1.08	3.19	0.12	15.7	21.3	1.09
	51.7	0.33	5.36	1.08	3.18	0.10	15.6	21.3	1.10
	51.6	0.33	5.05	1.17	3.21	0.12	15.7	21.4	1.09
	52.9	0.39	4.91	0.99	3.47	0.12	16.4	20.7	0.93
	51.8	0.38	5.06	1.11	3.49	0.10	16.3	20.8	1.03

CLINOPYROXENE

Sample	SiO_2	TiO_2	Al_2O_3	Cr_2O_3	FeO	MnO	MgO	CaO	Na_2O
NFK1115	52.6	0.04	3.09	1.40	3.11	0.12	16.4	21.6	1.20
	53.2	0.05	2.98	1.34	3.04	0.09	16.4	21.5	1.15
	53.3	0.07	2.99	1.38	3.09	0.13	16.5	21.5	1.15
	53.0	0.07	3.02	1.12	3.07	0.11	16.5	21.4	1.02
	53.9	0.04	2.98	1.30	3.00	0.13	16.4	21.5	1.14
	53.0	0.05	3.25	1.48	3.00	0.12	16.2	21.5	1.22
	53.5	0.05	3.17	1.13	2.97	0.09	16.5	21.4	1.14
	54.1	0.04	2.71	1.24	2.85	0.12	16.6	21.8	1.09
	53.3	0.05	2.94	1.28	2.98	0.10	16.5	21.7	1.17
NFR0306	51.6	0.32	5.16	0.99	4.14	0.12	15.5	20.6	1.33
	51.3	0.30	4.90	0.93	4.01	0.12	15.7	20.5	1.28
	51.3	0.29	4.78	0.97	4.04	0.11	15.5	20.5	1.35
	51.3	0.27	4.53	1.02	4.20	0.11	15.6	20.5	1.23
	50.8	0.32	5.02	1.13	4.07	0.13	15.4	20.4	1.32
	50.8	0.29	4.84	1.20	4.14	0.06	15.4	20.3	1.30
	51.5	0.31	4.95	1.21	4.11	0.09	15.4	20.3	1.33
	51.1	0.33	5.00	1.18	4.08	0.11	15.3	20.3	1.26
	51.8	0.25	4.47	1.02	4.12	0.12	15.8	20.4	1.23
	51.7	0.36	5.00	1.12	4.17	0.12	15.6	20.3	1.31
NFR0307	51.5	0.27	4.09	0.92	3.51	0.11	17.4	20.5	0.74
	50.4	0.66	4.88	1.17	2.94	0.03	15.4	23.4	0.57
	51.5	0.33	3.46	0.85	3.71	0.08	15.8	22.1	0.86
	51.4	0.37	3.73	0.94	3.46	0.08	15.8	22.1	0.89
	51.4	0.36	3.47	0.83	3.57	0.09	15.7	22.1	0.85
NFR1109	53.4	0.17	3.43	1.31	4.13	0.16	16.2	20.4	1.37
	53.4	0.18	3.32	1.26	4.35	0.14	16.4	20.1	1.29
	53.3	0.19	3.26	1.45	4.04	0.14	16.2	20.2	1.30
	53.3	0.18	3.48	1.52	4.26	0.13	15.9	20.3	1.31
	53.0	0.19	3.60	1.30	4.09	0.14	15.9	20.2	1.35
	53.3	0.16	3.62	1.17	4.11	0.20	15.9	20.1	1.31
	53.3	0.17	3.53	1.33	4.07	0.15	15.7	20.1	1.25
	53.0	0.21	3.22	1.33	4.27	0.13	16.2	20.1	1.28
	53.0	0.22	3.20	1.37	4.19	0.13	16.1	20.2	1.26
	53.0	0.19	3.33	1.48	4.18	0.16	16.0	19.9	1.36
	52.7	0.22	3.34	1.44	4.31	0.17	16.0	20.3	1.34
NFR0309	51.2	0.64	7.19	0.75	3.00	0.10	15.0	20.5	1.60
	51.2	0.64	7.14	0.79	2.93	0.09	15.2	20.2	1.61
	51.5	0.62	6.88	0.68	2.88	0.09	15.2	20.8	1.63
	51.4	0.66	7.25	0.72	2.89	0.07	14.9	20.5	1.55
	50.9	0.65	6.98	0.72	2.90	0.09	15.0	20.7	1.57
	51.8	0.63	6.73	0.75	2.71	0.10	15.1	20.9	1.47
	51.1	0.64	7.66	0.82	2.96	0.11	14.8	20.2	1.68
	51.2	0.58	7.84	0.83	2.96	0.12	14.6	20.3	1.69
	51.0	0.64	7.29	0.75	2.80	0.08	15.0	20.6	1.48
	51.2	0.72	7.31	0.68	2.87	0.07	14.8	20.7	1.55
	51.5	0.64	6.81	0.73	2.86	0.07	15.1	20.7	1.61
	51.3	0.65	7.02	0.67	2.85	0.08	15.1	20.8	1.58
	51.3	0.64	6.90	0.72	2.73	0.09	15.0	20.9	1.49
	52.1	0.63	6.79	0.69	2.95	0.10	15.1	20.9	1.54
	51.4	0.62	6.92	0.76	2.82	0.08	15.1	20.9	1.50

CLINOPYROXENE

Sample	SiO_2	TiO_2	Al_2O_3	Cr_2O_3	FeO	MnO	MgO	CaO	Na_2O
NFR1107	52.3	0.31	5.01	1.35	2.67	0.08	16.0	21.0	1.36
	52.1	0.34	4.92	1.43	2.60	0.07	16.0	21.2	1.31
	52.1	0.29	4.80	1.47	2.61	0.09	16.1	20.9	1.36
	52.6	0.30	4.72	1.35	2.54	0.10	16.1	21.2	1.28
	52.6	0.32	4.92	1.31	2.53	0.07	16.1	21.3	1.30
	52.3	0.33	4.99	1.22	2.65	0.08	16.1	21.0	1.40
	52.4	0.32	4.81	1.31	2.51	0.08	16.1	21.1	1.31
	52.0	0.30	4.77	1.30	2.52	0.09	16.1	21.2	1.23
	52.6	0.32	4.91	1.20	2.47	0.06	16.1	21.2	1.18
	52.7	0.30	4.68	1.26	2.66	0.08	16.1	21.4	1.26
	52.2	0.30	4.89	1.26	2.59	0.07	16.0	21.1	1.28
	52.1	0.30	4.85	1.22	2.62	0.05	16.0	21.3	1.26
NMC1301	53.1	0.10	4.20	1.44	2.87	0.09	16.6	21.3	1.38
	53.5	0.12	4.27	1.43	2.85	0.08	16.4	21.3	1.26
	53.1	0.12	4.19	1.35	2.75	0.09	16.4	21.3	1.23
	53.0	0.12	4.11	1.44	2.79	0.10	16.2	21.2	1.24
	52.9	0.11	4.10	1.38	2.81	0.08	16.4	21.2	1.23
	53.2	0.10	4.06	1.45	2.82	0.08	16.4	21.1	1.32
	52.5	0.12	4.18	1.36	2.77	0.07	16.3	21.0	1.24
	52.4	0.11	4.18	1.38	2.74	0.08	16.4	21.0	1.23
	53.0	0.11	4.10	1.40	2.79	0.06	16.3	21.3	1.20
	53.1	0.11	4.12	1.44	2.79	0.08	16.3	21.2	1.28
	53.0	0.11	4.03	1.44	2.77	0.09	16.4	21.4	1.20
	53.1	0.13	4.08	1.43	2.83	0.07	16.3	21.2	1.30
NMC1309	52.4	0.21	5.63	1.00	3.25	0.10	15.5	21.5	1.20
	52.4	0.24	5.67	0.89	3.36	0.11	15.7	21.1	1.25
	52.5	0.22	5.64	0.94	3.30	0.09	15.7	21.3	1.22
	52.0	0.20	5.40	0.97	3.30	0.13	15.7	21.2	1.15
	52.4	0.20	5.42	0.96	3.19	0.11	15.8	21.4	1.19
	52.2	0.18	5.18	0.90	3.22	0.10	16.0	21.4	1.19
	52.7	0.20	5.41	0.91	3.26	0.12	15.8	21.3	1.15
	51.8	0.20	5.31	0.96	3.25	0.11	15.9	21.5	1.21
	52.0	0.21	5.58	0.93	3.27	0.10	15.6	21.4	1.22
	52.1	0.22	5.73	1.02	3.28	0.10	15.6	21.3	1.17
	51.8	0.22	5.64	1.04	3.32	0.09	15.6	21.3	1.16
	51.9	0.20	5.72	1.04	3.26	0.13	15.5	21.2	1.23
NMC1322	52.8	0.20	5.69	1.11	2.59	0.06	15.8	21.1	1.55
	52.1	0.18	5.71	1.05	2.59	0.08	15.9	21.2	1.47
	52.3	0.20	5.64	1.06	2.64	0.08	15.8	21.1	1.40
	52.3	0.20	5.59	1.06	2.66	0.10	15.9	21.0	1.35
	52.4	0.20	5.74	1.05	2.67	0.09	15.8	21.0	1.47
	52.2	0.20	5.78	1.31	2.69	0.06	15.6	21.1	1.44
	52.8	0.19	5.74	1.15	2.75	0.07	15.7	21.1	1.39
	52.3	0.21	5.65	1.11	2.75	0.08	15.8	21.1	1.45
	52.9	0.19	5.54	1.06	2.83	0.06	15.8	21.0	1.54
	52.9	0.21	5.59	1.02	2.75	0.05	15.9	21.0	1.51
	52.8	0.19	5.49	1.10	2.65	0.08	15.9	21.3	1.35
	52.3	0.18	5.56	1.06	2.74	0.09	15.8	21.0	1.38

CLINOPYROXENE

Sample	SiO_2	TiO_2	Al_2O_3	Cr_2O_3	FeO	MnO	MgO	CaO	Na_2O
NMC1336A	52.3	0.35	5.55	1.17	2.76	0.08	15.7	20.9	1.43
	52.0	0.40	5.69	1.21	2.71	0.08	15.5	21.0	1.45
	51.8	0.48	5.93	1.19	2.81	0.10	15.7	20.5	1.60
	52.5	0.37	5.36	1.09	2.68	0.07	15.8	21.0	1.48
	51.9	0.46	5.80	1.16	2.74	0.06	15.7	21.0	1.41
	52.0	0.51	6.04	1.15	2.76	0.08	15.6	20.6	1.50
	52.2	0.51	6.08	1.18	2.77	0.09	15.6	20.5	1.71
	52.3	0.48	5.99	1.21	2.73	0.10	15.6	20.7	1.49
	51.5	0.47	5.98	1.18	2.64	0.08	15.6	20.8	1.49
	52.2	0.47	5.94	1.26	2.70	0.08	15.5	21.0	1.45
	51.8	0.52	6.10	1.19	2.75	0.07	15.5	21.0	1.49
	52.1	0.51	6.02	1.13	2.70	0.07	15.6	20.8	1.48
	52.4	0.50	5.96	1.10	2.77	0.08	15.6	20.7	1.58
NMM1126	51.3	0.24	5.67	0.91	2.75	0.07	16.0	20.9	1.26
	51.7	0.24	5.59	1.01	2.77	0.12	15.9	20.9	1.25
	51.6	0.24	5.64	1.03	2.75	0.06	15.8	20.9	1.15
	52.1	0.22	5.31	0.78	2.73	0.06	16.3	21.0	1.20
	51.8	0.21	5.56	1.00	2.78	0.10	16.0	21.0	1.17
	51.8	0.23	5.64	0.91	2.68	0.09	16.1	20.9	1.26
NMM0318	52.2	0.33	5.87	0.67	3.11	0.11	15.6	21.2	1.23
	51.6	0.33	6.30	0.75	3.18	0.12	15.4	20.9	1.35
	52.7	0.37	6.37	0.73	3.16	0.11	15.3	21.0	1.35
	51.9	0.33	6.06	0.68	3.08	0.09	15.4	21.3	1.18
	51.8	0.36	6.29	0.71	3.02	0.14	15.3	21.1	1.32
	52.2	0.34	6.20	0.77	3.19	0.11	15.4	21.0	1.24
	52.0	0.34	6.00	0.69	3.09	0.11	15.4	21.3	1.21
	52.3	0.35	6.09	0.70	3.05	0.10	15.3	21.3	1.24
	53.0	0.36	6.28	0.71	3.15	0.12	15.4	21.2	1.28
	51.9	0.34	6.26	0.77	3.00	0.10	15.2	21.5	1.17
	52.3	0.33	6.31	0.67	3.06	0.11	15.3	21.3	1.30
	52.0	0.32	6.23	0.65	3.03	0.08	15.4	21.3	1.33
NMM1115	52.6	0.31	5.22	0.99	2.49	0.07	15.9	21.5	1.20
	51.9	0.32	5.30	1.02	2.47	0.09	15.9	21.7	1.25
	52.8	0.31	5.10	1.05	2.48	0.11	16.0	21.5	1.22
	52.2	0.29	4.98	1.18	2.42	0.07	15.9	21.5	1.28
	52.1	0.32	5.08	1.15	2.41	0.09	15.8	21.6	1.32
	52.8	0.29	4.99	1.13	2.50	0.06	15.9	21.6	1.19
	52.9	0.27	5.03	1.05	2.44	0.07	16.0	21.6	1.27
	52.3	0.30	5.01	1.03	2.48	0.10	15.9	21.6	1.20
	52.4	0.29	4.78	0.93	2.49	0.08	16.1	21.7	1.18
	52.5	0.28	5.00	1.16	2.48	0.08	16.0	21.5	1.19
	52.3	0.30	4.88	1.07	2.47	0.07	15.9	21.8	1.18
	52.6	0.30	4.94	1.10	2.46	0.07	16.0	21.5	1.26
NME1122	51.9	0.31	5.14	1.18	2.72	0.07	16.3	20.7	1.28
	51.6	0.34	5.36	1.08	2.78	0.12	16.1	20.9	1.27
	51.4	0.37	5.53	1.19	2.79	0.07	16.0	20.8	1.31
	51.9	0.30	5.16	0.94	2.76	0.05	16.2	20.8	1.26
	51.8	0.34	5.42	1.13	2.71	0.12	15.9	21.0	1.21
	51.8	0.28	5.33	1.20	2.76	0.09	15.9	21.1	1.24
	51.5	0.36	5.57	1.16	2.80	0.10	16.0	20.8	1.30
	51.4	0.37	5.43	1.17	2.67	0.10	15.7	21.1	1.37
	51.5	0.41	5.56	1.07	2.96	0.08	15.8	20.7	1.32

CLINOPYROXENE

Sample	SiO_2	TiO_2	Al_2O_3	Cr_2O_3	FeO	MnO	MgO	CaO	Na_2O
NME0528	52.5	0.23	4.65	1.41	2.71	0.08	16.0	21.1	1.33
	53.3	0.25	4.53	1.36	2.75	0.09	16.1	21.0	1.32
	52.7	0.24	4.64	1.46	2.67	0.13	15.9	21.2	1.19
	52.5	0.25	4.43	1.30	2.65	0.08	16.1	21.3	1.23
	53.7	0.24	4.41	1.32	2.64	0.09	16.0	21.4	1.29
	52.6	0.24	4.49	1.44	2.62	0.09	16.0	21.3	1.24
	52.8	0.22	4.61	1.55	2.68	0.10	16.0	20.9	1.34
	52.3	0.23	4.51	1.28	2.63	0.10	16.0	21.4	1.17
	52.4	0.26	4.59	1.42	2.76	0.09	16.1	21.3	1.31
	52.7	0.20	4.19	1.23	2.64	0.08	16.2	21.5	1.31
	52.6	0.24	4.38	1.33	2.72	0.07	16.0	21.3	1.25
	53.6	0.23	4.26	1.16	2.76	0.10	16.4	21.4	1.18
	53.0	0.25	4.53	1.31	2.73	0.09	16.1	21.2	1.28
NME1116	52.7	0.28	5.58	1.01	2.63	0.08	15.8	21.0	1.49
	51.9	0.27	5.63	1.03	2.66	0.08	15.7	21.0	1.47
	52.2	0.27	5.71	1.00	2.69	0.10	15.7	21.0	1.48
	52.2	0.25	5.62	1.02	2.65	0.08	15.8	20.9	1.41
	52.3	0.28	5.88	1.15	2.63	0.07	15.6	20.9	1.46
	52.0	0.28	5.66	0.96	2.64	0.10	15.7	21.0	1.52
	52.4	0.29	5.77	1.08	2.62	0.09	15.6	21.0	1.40
	51.9	0.29	5.76	1.05	2.64	0.07	15.7	21.0	1.42
	52.5	0.28	5.82	1.04	2.65	0.08	15.7	21.0	1.44
	52.3	0.29	5.80	0.99	2.62	0.06	15.8	21.0	1.44
	51.7	0.30	5.85	1.15	2.69	0.10	15.7	20.9	1.42
	52.4	0.29	5.89	1.13	2.65	0.09	15.6	21.0	1.46
	52.3	0.30	5.73	1.07	2.63	0.09	15.8	21.0	1.39
NBN0302A	51.3	0.44	5.02	0.86	2.76	0.08	16.2	21.6	1.06
	51.1	0.40	5.09	0.88	2.72	0.09	16.1	21.5	1.08
	51.5	0.26	4.34	0.75	2.63	0.09	16.6	22.0	0.79
	51.5	0.29	4.99	0.65	2.73	0.05	16.6	22.1	0.87
	51.1	0.33	5.40	0.70	2.74	0.09	16.1	21.6	0.97
	51.1	0.29	5.46	0.66	2.78	0.09	16.3	21.9	0.96
	51.2	0.35	4.92	1.05	2.69	0.07	16.1	22.0	0.89
	51.3	0.37	4.56	0.88	2.77	0.08	16.6	21.9	0.91
	51.5	0.31	4.48	0.83	2.62	0.08	16.6	21.9	0.88
NBN0305	51.9	0.20	3.70	0.93	2.52	0.05	16.8	22.2	0.69
	52.0	0.18	3.65	0.76	2.56	0.12	17.1	22.1	0.71
	52.0	0.21	3.61	0.86	2.53	0.05	16.9	22.2	0.78
	51.9	0.21	3.81	0.91	2.64	0.08	16.8	22.1	0.62
	52.0	0.22	3.77	1.05	2.69	0.13	16.9	22.0	0.74
	51.8	0.19	3.92	1.01	2.65	0.06	16.9	21.9	0.72
	52.0	0.22	3.77	0.92	2.67	0.08	17.0	22.1	0.70
	52.0	0.23	3.75	0.98	2.75	0.08	16.9	22.3	0.74
	52.2	0.18	3.82	0.74	2.61	0.07	16.8	22.4	0.72
NBN0311	51.2	0.43	6.04	0.77	2.68	0.08	15.8	20.7	1.52
	50.7	0.48	6.41	0.74	2.65	0.09	15.8	20.6	1.56
	50.3	0.47	6.40	0.85	2.53	0.15	15.6	20.3	1.57
	50.3	0.42	6.23	0.75	2.77	0.07	15.7	20.7	1.68
	51.3	0.31	5.67	0.76	2.73	0.10	16.1	20.9	1.40
NBN0316	51.4	0.24	4.41	0.52	2.93	0.03	16.9	22.9	0.49
	51.4	0.24	4.34	0.45	2.97	0.06	16.7	22.8	0.39
	51.3	0.23	4.48	0.52	3.02	0.09	16.8	22.8	0.45
	51.3	0.25	4.48	0.50	3.11	0.10	16.8	22.8	0.45
	51.2	0.27	4.63	0.47	2.88	0.09	16.5	22.9	0.50
	50.2	0.86	6.49	0.54	3.34	0.11	16.6	20.0	1.03
	51.7	0.20	4.29	0.47	3.03	0.11	16.9	22.7	0.47

CLINOPYROXENE

Sample	SiO_2	TiO_2	Al_2O_3	Cr_2O_3	FeO	MnO	MgO	CaO	Na_2O
NBN0319	51.4	0.26	4.41	0.46	2.99	0.10	16.7	22.8	0.38
	51.2	0.28	4.37	0.54	3.05	0.05	16.7	22.6	0.39
	51.6	0.27	4.11	0.32	2.94	0.09	17.0	23.0	0.37
	51.5	0.25	4.19	0.41	2.90	0.06	16.8	22.8	0.38
	51.7	0.23	4.32	0.42	3.05	0.09	16.8	23.0	0.32
	51.3	0.24	4.39	0.48	3.02	0.07	16.8	22.8	0.39
	51.2	0.22	4.30	0.46	2.97	0.08	17.0	22.7	0.38
	51.0	0.20	4.22	0.40	2.84	0.10	16.9	22.6	0.39
	51.5	0.25	4.37	0.47	3.04	0.07	16.8	22.9	0.37
	51.4	0.24	4.35	0.48	3.14	0.10	16.9	23.1	0.34
NBN0321	50.9	0.49	5.54	0.84	2.84	0.08	15.9	21.5	1.17
	51.3	0.52	5.43	0.82	2.64	0.04	16.3	21.1	1.14
	50.8	0.49	5.33	0.91	2.76	0.10	16.1	21.4	1.08
	51.1	0.50	5.68	0.94	2.88	0.05	16.0	20.8	1.32
	51.0	0.47	5.43	0.92	2.75	0.06	16.2	21.3	1.22
	51.3	0.48	5.61	0.90	2.72	0.09	16.0	21.4	1.12
	51.0	0.50	5.59	0.92	2.89	0.08	16.1	21.0	1.31
	50.6	0.49	5.72	0.85	2.85	0.06	15.9	21.1	1.13
	50.2	0.51	5.62	0.84	2.68	0.10	15.8	21.5	1.12

SPINEL

Sample	TiO_2	Al_2O_3	Cr_2O_3	FeO	MnO	NiO	MgO
NMS1302A	0.05	32.4	36.9	13.2	0.12	0.19	16.8
	0.05	32.9	36.7	13.2	0.11	0.19	17.0
	0.06	34.9	34.5	12.8	0.12	0.20	17.4
	0.06	34.6	35.3	13.1	0.11	0.18	17.2
	0.06	34.4	35.5	12.9	0.13	0.21	17.4
	0.06	33.7	36.5	13.1	0.12	0.19	17.2
	0.06	33.3	36.8	13.1	0.13	0.18	17.1
	0.06	33.8	35.9	13.1	0.12	0.19	17.2
	0.06	33.7	36.2	13.1	0.11	0.17	17.2
	0.06	33.5	36.4	13.0	0.11	0.20	17.3
	0.06	34.5	35.9	12.9	0.13	0.20	17.5
NMS1304	0.14	44.4	23.2	12.6	0.10	0.29	19.1
	0.12	44.7	23.5	12.3	0.10	0.26	18.7
	0.13	44.8	23.2	12.5	0.13	0.28	18.6
	0.12	44.4	23.6	12.8	0.11	0.27	18.5
	0.14	42.3	25.4	12.9	0.13	0.22	18.3
	0.14	42.0	26.0	13.2	0.12	0.24	18.1
	0.14	41.4	26.5	12.9	0.11	0.18	18.1
NMS1305	0.04	56.6	11.0	10.8	0.11	0.38	20.7
	0.03	56.6	10.9	11.0	0.11	0.40	20.7
	0.04	56.5	11.2	10.2	0.12	0.39	21.4
	0.03	56.2	11.5	10.9	0.08	0.38	20.8
	0.04	54.9	12.8	11.1	0.09	0.36	20.6
	0.04	54.1	14.0	11.4	0.12	0.33	20.4
	0.03	57.2	10.0	10.7	0.09	0.43	21.1
	0.03	56.9	10.0	10.9	0.09	0.39	21.1
		55.5	12.0	11.2	0.09	0.38	20.6
	0.03	55.9	11.6	11.0	0.11	0.38	20.5
	0.03	56.5	10.7	10.8	0.08	0.41	21.2
		56.2	11.3	11.0	0.07	0.40	20.8
		57.0	10.4	10.9	0.10	0.37	20.8
		57.2	11.0	11.0	0.07	0.40	20.9
		57.9	9.9	10.4	0.12	0.42	21.6
NMS1308	0.08	51.1	16.9	11.3	0.10	0.33	20.1
	0.06	49.3	18.6	11.6	0.10	0.32	19.7
	0.07	51.4	16.5	11.3	0.11	0.33	19.9
	0.08	50.9	17.1	11.4	0.10	0.33	19.8
	0.08	50.9	16.7	11.3	0.10	0.30	20.0
	0.08	51.1	16.5	11.4	0.11	0.32	19.9
	0.08	50.9	16.9	11.3	0.09	0.31	19.7
	0.10	49.6	17.8	11.4	0.08	0.32	19.8
	0.10	49.8	17.8	11.3	0.10	0.32	19.8
	0.09	50.1	17.5	11.3	0.09	0.35	19.7
	0.09	50.7	17.2	11.5	0.10	0.32	19.8
	0.09	49.7	17.9	11.2	0.11	0.30	20.0
NMS1310	0.10	53.2	13.9	11.5	0.11	0.32	20.8
	0.10	53.0	14.0	11.4	0.09	0.38	20.6
	0.10	52.8	14.5	11.6	0.12	0.39	20.8
	0.10	51.5	15.9	12.0	0.06	0.37	20.2
	0.10	52.4	14.5	11.7	0.09	0.35	20.3
	0.09	53.4	14.0	11.6	0.10	0.37	20.8
	0.11	53.0	14.1	11.6	0.10	0.33	20.7
NJS1302	0.20	54.2	12.3	12.4	0.10	0.40	19.8
	0.20	53.7	12.6	12.6	0.09	0.35	19.7
	0.20	53.5	12.8	12.5	0.11	0.39	19.8
	0.19	54.0	12.3	12.3	0.09	0.38	19.7
	0.19	53.6	12.7	12.6	0.08	0.32	19.8
	0.19	53.9	12.5	12.6	0.08	0.35	19.7

SPINEL

Sample	TiO_2	Al_2O_3	Cr_2O_3	FeO	MnO	NiO	MgO
NJS1304	0.19	54.4	12.5	12.5	0.08	0.36	19.8
	0.18	55.3	11.9	12.4	0.09	0.35	20.1
	0.18	55.0	11.7	12.5	0.09	0.34	20.0
	0.18	55.2	11.8	12.7	0.10	0.33	20.2
	0.17	55.2	11.7	12.6	0.11	0.38	20.1
	0.19	55.4	11.5	12.4	0.09	0.42	20.1
	0.19	55.2	12.0	12.4	0.11	0.33	20.1
NJS1306	0.14	56.3	9.5	14.3	0.13	0.41	20.0
	0.13	56.4	9.2	14.3	0.10	0.39	19.7
	0.13	56.2	9.4	14.2	0.09	0.38	19.8
	0.13	56.3	9.1	14.1	0.14	0.45	19.9
	0.14	56.5	8.9	14.2	0.13	0.40	20.0
	0.14	56.5	8.8	14.2	0.11	0.41	19.8
NJS1307	0.15	58.2	8.8	10.9	0.07	0.39	21.3
	0.14	58.1	9.0	10.7	0.08	0.42	21.2
	0.15	58.1	8.8	10.6	0.08	0.37	21.1
	0.15	58.4	8.8	10.7	0.09	0.37	21.1
	0.15	58.3	8.8	10.8	0.10	0.37	21.2
	0.15	58.2	8.8	10.7	0.08	0.39	21.2
	0.15	58.3	8.8	10.9	0.09	0.39	21.2
	0.16	58.2	8.8	10.8	0.09	0.39	21.3
	0.16	58.1	8.6	10.8	0.09	0.42	21.3
NPY1301	0.10	57.3	9.8	10.9	0.08	0.38	20.7
	0.10	57.3	10.2	10.9	0.12	0.40	20.8
	0.11	57.6	9.3	10.9	0.11	0.37	20.8
	0.10	57.7	9.7	10.8	0.07	0.42	20.8
	0.10	57.9	9.3	10.9	0.11	0.39	20.8
	0.09	55.5	9.3	16.0	0.19	0.34	18.3
	0.10	56.7	9.7	13.2	0.19	0.38	19.7
	0.10	57.6	9.4	10.7	0.08	0.39	21.0
	0.11	57.4	10.0	10.9	0.11	0.39	20.5
	0.11	57.6	9.8	10.8	0.10	0.38	20.9
	0.10	58.2	9.3	10.6	0.09	0.41	21.0
NPY1310	0.12	61.3	5.3	10.9	0.11	0.34	21.3
	0.09	60.7	5.3	11.3	0.09	0.40	21.4
	0.10	60.8	5.3	11.3	0.10	0.42	21.5
	0.09	61.0	5.3	11.3	0.12	0.44	21.6
	0.08	61.0	5.5	11.3	0.07	0.41	21.5
	0.09	61.2	5.4	11.3	0.11	0.35	21.5
	0.09	61.0	5.2	11.4	0.10	0.42	21.4
	0.09	61.4	5.1	11.3	0.06	0.42	21.4
	0.09	61.0	5.4	11.3	0.09	0.41	21.4
NPY1311	0.09	61.0	5.2	11.2	0.08	0.39	21.5
	0.10	60.5	5.7	11.5	0.11	0.42	21.5
	0.08	61.1	5.2	11.3	0.07	0.39	21.6
	0.10	61.1	5.3	11.3	0.08	0.41	21.5
	0.09	60.6	5.1	11.3	0.11	0.44	21.5
	0.10	60.9	5.2	11.4	0.07	0.44	21.5
	0.10	61.0	5.1	11.4	0.10	0.38	21.5
	0.09	60.5	5.7	11.1	0.07	0.43	21.3
	0.10	61.2	5.4	11.3	0.09	0.42	21.2
NPY1314	0.05	57.2	8.9	11.4	0.09	0.45	21.6
	0.05	58.2	8.6	11.1	0.08	0.40	20.7
	0.05	58.3	8.5	11.3	0.08	0.45	20.8
	0.06	58.5	8.5	11.1	0.09	0.44	21.2
	0.06	58.0	9.0	11.1	0.10	0.39	21.1
	0.07	57.8	9.4	11.0	0.11	0.42	20.8

SPINEL

Sample	TiO_2	Al_2O_3	Cr_2O_3	FeO	MnO	NiO	MgO
NFL1302	0.07	53.2	14.3	10.9	0.08	0.35	20.4
	0.07	52.9	14.6	11.0	0.10	0.36	20.7
	0.07	53.1	14.3	11.0	0.09	0.37	20.5
	0.08	52.8	14.5	11.0	0.09	0.35	20.6
	0.08	53.0	14.1	11.0	0.11	0.38	20.5
	0.07	52.8	14.3	11.1	0.10	0.36	20.7
	0.07	52.6	14.7	11.1	0.11	0.34	20.6
	0.07	53.3	13.8	11.0	0.09	0.34	20.5
	0.07	52.9	14.2	10.9	0.09	0.35	20.5
	0.07	53.1	14.3	11.0	0.08	0.37	20.5
	0.07	53.0	13.9	10.9	0.12	0.37	20.6
NFL1305	0.03	52.7	15.3	11.5	0.09	0.33	20.3
	0.04	52.9	14.9	11.2	0.09	0.33	20.3
	0.03	52.0	15.8	11.3	0.09	0.32	20.2
	0.04	52.8	15.0	11.4	0.11	0.41	20.5
	0.03	52.5	15.3	11.2	0.08	0.32	20.2
	0.04	52.4	15.2	11.4	0.11	0.34	20.3
NFL1315A	0.25	27.1	40.5	17.3	0.16	0.14	15.0
	0.26	27.3	39.9	17.4	0.15	0.20	15.1
	0.27	26.4	41.0	17.4	0.18	0.15	14.7
	0.27	26.6	40.6	17.4	0.17	0.16	14.9
	0.27	27.1	39.7	17.4	0.17	0.17	15.0
	0.27	26.8	40.8	17.3	0.17	0.17	14.9
	0.32	27.1	40.0	17.5	0.16	0.18	15.0
NFL1316	0.11	33.4	34.6	14.6	0.12	0.25	17.2
	0.10	33.3	34.5	14.3	0.12	0.22	17.0
	0.10	33.7	33.5	14.1	0.09	0.24	17.0
	0.15	33.3	34.0	13.5	0.13	0.20	16.2
	0.19	33.1	34.0	14.2	0.15	0.21	16.9
	0.09	33.0	34.6	13.9	0.14	0.21	17.1
NFL1324	0.14	39.9	27.8	13.2	0.09	0.28	18.5
	0.12	40.9	27.1	13.0	0.12	0.26	18.5
	0.11	40.7	27.1	13.3	0.13	0.24	18.6
	0.12	41.3	26.8	12.9	0.10	0.26	18.8
	0.10	40.4	27.3	13.3	0.12	0.25	18.6
	0.11	41.7	26.5	13.1	0.10	0.27	18.6
	0.10	41.5	26.2	13.2	0.13	0.25	18.6
NFL1326	0.60	31.9	27.8	24.9	0.25	0.20	13.9
	0.48	34.6	25.3	24.6	0.24	0.23	14.3
	0.48	34.3	25.8	24.3	0.20	0.19	14.4
	0.49	34.2	25.8	24.2	0.26	0.22	14.4
	0.46	35.9	24.4	24.1	0.23	0.20	14.7
	0.45	36.0	24.3	23.9	0.20	0.25	14.7
NFL1327	0.39	33.7	28.6	22.6	0.19	0.23	15.0
	0.41	33.5	28.5	22.5	0.20	0.23	14.9
	0.29	32.8	29.9	21.8	0.19	0.24	14.6
	0.66	33.7	28.6	21.0	0.22	0.24	14.7
	0.28	33.7	29.4	21.0	0.21	0.19	15.1
NFL1329	0.06	57.7	10.3	10.8	0.10	0.40	21.1
	0.05	58.1	9.4	10.5	0.10	0.42	21.0
	0.05	57.2	10.4	10.6	0.10	0.41	21.1
	0.05	57.4	9.9	10.7	0.09	0.39	20.9
NTB0306	0.16	28.6	39.4	16.0	0.27	0.17	16.2
	0.12	28.1	39.8	15.8	0.29	0.17	15.6
	0.09	27.3	41.4	15.9	0.33	0.22	16.3

SPINEL

Sample	TiO_2	Al_2O_3	Cr_2O_3	FeO	MnO	NiO	MgO
NTB0307	0.12	53.9	14.0	11.5	0.00	0.44	20.5
	0.11	54.1	14.0	11.6	0.00	0.35	20.6
	0.17	53.5	14.4	11.7	0.00	0.39	20.5
	0.10	53.2	14.9	11.4	0.00	0.39	20.7
	0.10	53.6	14.8	11.7	0.00	0.37	20.4
NTB1124	0.20	49.8	17.4	11.7	0.12	0.29	20.4
	0.22	50.1	17.6	11.8	0.11	0.33	20.4
	0.21	49.8	17.4	11.6	0.12	0.37	20.5
	0.17	50.0	17.5	11.7	0.12	0.33	20.6
	0.19	49.7	18.0	11.6	0.12	0.32	20.6
	0.19	49.8	17.7	11.8	0.12	0.37	20.7
NTB1116	0.10	49.6	17.9	11.3	0.07	0.33	20.2
	0.09	49.6	18.0	11.3	0.10	0.29	20.2
	0.10	49.5	18.2	11.6	0.12	0.35	20.2
	0.09	49.4	17.6	11.5	0.07	0.34	20.1
	0.10	49.8	17.9	11.6	0.09	0.35	20.3
	0.12	49.7	17.8	11.4	0.11	0.36	20.3
	0.10	49.5	18.0	11.6	0.07	0.35	20.2
	0.10	49.4	18.2	11.5	0.07	0.36	20.2
	0.09	50.0	17.3	11.3	0.07	0.34	20.1
	0.08	50.3	17.4	11.2	0.13	0.33	20.3
	0.11	48.1	19.3	11.5	0.11	0.33	19.7
	0.10	49.5	18.3	11.6	0.09	0.32	20.3
	0.10	49.1	18.5	11.7	0.10	0.39	20.1
NTB1122	0.40	50.2	14.9	14.1	0.12	0.28	19.1
	0.44	50.3	15.2	14.0	0.09	0.33	18.7
	0.38	50.0	15.5	14.5	0.11	0.40	19.2
	0.39	49.9	15.0	14.5	0.09	0.37	19.1
	0.36	50.3	15.3	14.4	0.12	0.33	19.2
	0.40	50.0	15.3	14.3	0.12	0.32	19.2
	0.39	50.0	15.3	14.3	0.11	0.33	19.2
	0.39	49.8	15.4	14.3	0.12	0.35	19.0
	0.39	49.7	15.4	14.2	0.11	0.31	18.9
	0.37	50.0	15.2	14.2	0.12	0.30	19.1
NFK0301	0.14	44.8	24.1	13.3	0.52	0.30	18.5
	0.13	44.0	24.8	13.5	0.64	0.29	18.4
	0.13	43.8	24.9	13.7	0.61	0.26	18.2
	0.12	44.7	24.2	13.4	0.55	0.25	18.5
	0.06	45.2	23.2	14.3	0.58	0.30	18.1
	0.06	45.3	23.2	13.7	0.53	0.27	18.4
	0.10	45.6	23.3	13.2	0.59	0.25	18.7
	0.13	44.6	24.0	13.6	0.60	0.30	18.4
	0.07	44.5	23.7	14.0	0.54	0.30	18.3
	0.11	43.8	23.3	15.1	0.48	0.27	17.2
	0.08	43.2	23.5	16.9	0.50	0.27	16.8
	0.26	42.5	23.4	18.5	0.46	0.27	16.0
NFK1123	0.25	37.5	31.4	13.6	0.15	0.22	18.1
	0.26	37.4	30.7	14.0	0.18	0.21	17.4
	0.15	43.3	24.0	13.0	0.11	0.31	19.3
	0.18	43.2	24.6	12.8	0.12	0.37	19.5
	0.45	30.3	34.4	20.3	0.27	0.21	14.6
	0.42	28.3	35.8	20.3	0.24	0.26	14.5

SPINEL

Sample	TiO_2	Al_2O_3	Cr_2O_3	FeO	MnO	NiO	MgO
NFK1108	0.49	40.9	17.9	13.0	0.09	0.28	17.4
	0.47	37.8	24.9	15.4	0.12	0.25	17.0
	0.51	42.4	23.9	15.7	0.15	0.26	18.3
	0.51	44.4	23.2	16.4	0.10	0.32	18.6
	0.47	42.3	23.9	15.8	0.12	0.27	18.2
	0.47	42.7	23.8	16.1	0.13	0.27	18.1
	0.50	42.3	23.7	15.4	0.11	0.26	18.3
	0.46	31.2	33.6	17.4	0.17	0.15	15.6
	0.47	30.4	34.5	17.2	0.15	0.18	15.7
	0.45	30.5	34.2	18.2	0.15	0.19	15.1
NFK1115	0.10	24.0	39.1	20.7	0.22	0.24	13.7
	0.10	24.0	39.1	21.1	0.20	0.13	13.5
	0.10	23.9	39.5	20.7	0.24	0.17	13.6
	0.09	25.3	38.0	19.9	0.21	0.15	14.2
	0.09	24.4	39.5	20.1	0.20	0.17	13.9
	0.09	24.9	38.9	20.0	0.19	0.21	13.9
	0.09	24.5	39.3	20.1	0.25	0.17	13.8
	0.09	24.4	39.0	19.7	0.20	0.21	14.0
	0.09	23.9	39.6	20.0	0.21	0.13	13.8
NFR0306	1.04	33.0	28.1	21.9	0.00	0.23	14.1
	1.16	33.5	27.4	22.4	0.00	0.22	14.0
	0.96	34.6	27.1	21.9	0.00	0.24	14.6
	0.57	33.4	29.2	21.9	0.00	0.26	14.1
	0.39	33.6	29.2	22.0	0.00	0.23	14.1
NFR0307	0.03	44.0	22.1	16.2	0.00	0.29	16.7
	0.09	43.2	22.0	16.2	0.00	0.29	16.5
	0.03	45.2	21.5	16.0	0.00	0.25	16.8
	0.03	44.6	22.0	16.0	0.00	0.27	16.7
	0.24	49.7	15.4	15.5	0.00	0.32	17.8
	0.24	49.7	15.4	15.5	0.00	0.32	17.8
NFR1109	0.45	22.6	40.0	24.1	0.35	0.17	12.1
	0.41	23.4	39.6	23.8	0.31	0.12	12.2
	0.41	23.1	39.7	23.6	0.23	0.11	12.1
	0.39	23.5	39.9	23.8	0.34	0.12	12.3
	0.52	22.1	40.5	24.7	0.34	0.14	11.9
NMC1301	0.11	35.1	32.6	15.2	0.09	0.27	17.1
	0.11	35.0	32.6	15.1	0.12	0.25	17.1
	0.11	34.7	33.0	14.8	0.15	0.25	17.1
	0.11	35.0	32.9	14.8	0.14	0.20	17.1
	0.11	34.9	33.1	14.9	0.14	0.25	17.0
	0.11	34.8	33.1	14.9	0.15	0.26	17.2
	0.10	34.9	33.0	15.1	0.11	0.24	17.2
NMC1309	0.06	49.6	16.7	14.1	0.13	0.35	18.8
	0.07	49.9	16.4	14.0	0.10	0.36	18.9
	0.07	50.8	16.8	12.3	0.14	0.29	18.9
	0.07	50.0	16.5	13.9	0.09	0.36	18.9
	0.07	49.6	16.7	14.1	0.12	0.34	18.8
	0.07	48.7	17.3	14.1	0.13	0.32	18.6
	0.07	49.3	16.7	13.7	0.12	0.31	18.9
	0.07	49.4	17.0	13.7	0.12	0.32	18.9
NMC1322	0.07	50.7	16.8	11.3	0.10	0.33	20.0
	0.05	50.9	16.8	11.3	0.12	0.39	20.1
	0.05	50.9	16.6	11.6	0.10	0.33	20.1
	0.05	50.7	16.9	11.5	0.10	0.36	20.0
	0.06	51.1	16.6	11.1	0.11	0.38	20.1
	0.05	50.7	16.9	11.3	0.10	0.34	20.2
	0.04	50.9	17.2	11.3	0.11	0.33	20.1
	0.06	50.7	17.0	11.4	0.12	0.34	20.2

SPINEL

Sample	TiO_2	Al_2O_3	Cr_2O_3	FeO	MnO	NiO	MgO
NMC1336A	0.13	48.5	19.0	12.1	0.11	0.32	20.0
	0.13	48.6	19.1	12.0	0.12	0.35	19.8
	0.13	48.3	19.3	12.2	0.08	0.32	19.9
	0.11	48.7	19.0	12.0	0.10	0.34	19.8
	0.12	48.4	19.2	12.1	0.08	0.36	19.8
	0.11	48.4	19.3	12.1	0.09	0.36	19.8
	0.13	48.6	19.0	12.2	0.11	0.33	19.9
	0.13	48.5	18.8	12.0	0.11	0.38	20.0
	0.12	49.2	18.3	11.9	0.09	0.35	20.1
	0.13	48.8	18.8	11.9	0.11	0.35	20.1
	0.14	48.2	19.3	12.0	0.13	0.33	19.8
	0.14	48.2	19.3	12.0	0.08	0.33	19.8
NMM1126	0.08	51.5	15.9	11.5	0.10	0.38	20.7
	0.08	51.7	16.2	11.2	0.13	0.37	20.7
	0.11	51.3	16.1	11.2	0.04	0.40	20.7
	0.07	51.0	16.5	11.5	0.09	0.35	20.7
	0.08	51.7	16.1	11.3	0.11	0.35	20.5
	0.08	51.5	16.5	11.3	0.15	0.37	20.6
NMM0318	0.07	55.8	11.2	12.7	0.12	0.35	19.8
	0.08	55.7	11.2	12.9	0.09	0.37	19.8
	0.08	55.8	11.2	12.7	0.11	0.36	19.9
	0.09	55.6	11.5	12.1	0.09	0.32	20.0
	0.07	56.1	11.4	12.5	0.11	0.33	20.1
	0.07	56.1	10.8	12.8	0.11	0.40	20.0
	0.08	56.1	11.1	12.5	0.11	0.34	19.9
	0.07	56.2	11.4	12.5	0.14	0.35	20.1
	0.07	56.3	11.0	12.5	0.07	0.34	20.2
	0.06	56.9	10.4	12.5	0.10	0.36	20.1
	0.07	57.2	10.3	12.3	0.10	0.38	20.0
	0.06	57.4	9.9	12.4	0.11	0.37	20.3
NMM1115	0.11	47.8	20.0	11.9	0.10	0.31	19.6
	0.11	47.7	20.4	11.6	0.09	0.34	19.5
	0.11	47.5	19.9	11.9	0.12	0.32	19.6
	0.12	45.9	22.0	12.2	0.07	0.32	19.3
	0.11	47.5	20.6	11.9	0.09	0.32	19.6
	0.12	47.4	20.5	12.1	0.12	0.32	19.8
	0.10	48.7	19.3	11.7	0.09	0.35	19.9
	0.10	48.7	19.5	11.5	0.12	0.28	19.9
	0.12	47.0	21.0	12.1	0.08	0.29	19.6
	0.12	46.4	21.7	12.1	0.11	0.31	19.5
	0.14	47.4	20.0	12.1	0.08	0.34	19.7
	0.12	46.6	21.4	12.0	0.11	0.29	19.4
	0.11	46.3	21.6	12.0	0.07	0.31	19.4
	0.12	46.8	21.3	12.0	0.10	0.33	19.4
	0.11	47.5	20.2	12.0	0.12	0.32	19.6
	0.12	47.6	20.2	11.9	0.08	0.33	19.7
NME1122	0.15	47.2	19.9	12.3	0.11	0.32	19.8
	0.11	47.4	20.1	12.1	0.11	0.34	19.8
	0.15	47.3	19.7	12.5	0.11	0.29	19.9
	0.11	47.8	19.8	12.2	0.11	0.30	19.9
	0.17	47.2	20.2	12.4	0.11	0.32	19.5
	0.19	43.2	24.4	13.4	0.14	0.29	18.6
	0.17	47.4	20.3	12.7	0.15	0.37	19.8

SPINEL

Sample	TiO_2	Al_2O_3	Cr_2O_3	FeO	MnO	NiO	MgO
NME0528	0.16	38.3	29.5	14.2	0.11	0.22	17.5
	0.17	37.9	30.3	14.4	0.12	0.25	17.5
	0.17	37.6	30.3	14.6	0.12	0.28	17.4
	0.17	37.6	30.4	14.7	0.12	0.28	17.6
	0.18	37.0	30.7	14.6	0.12	0.25	17.6
	0.19	38.4	30.0	14.2	0.13	0.25	17.7
	0.17	38.5	29.5	14.4	0.12	0.25	17.8
	0.16	38.0	29.6	14.3	0.12	0.20	17.6
	0.16	38.0	29.8	14.4	0.11	0.28	17.5
	0.17	37.6	30.9	14.6	0.15	0.24	17.4
	0.17	37.9	30.0	14.5	0.11	0.22	17.5
NME1116	0.09	50.9	17.0	11.8	0.09	0.38	20.2
	0.09	50.5	17.4	11.8	0.10	0.32	20.1
	0.09	50.2	18.0	12.0	0.10	0.34	20.2
	0.09	50.4	17.4	12.0	0.09	0.27	20.1
	0.09	49.9	18.0	11.7	0.10	0.29	20.0
	0.09	50.6	17.8	11.7	0.09	0.32	20.2
	0.09	49.3	18.8	12.1	0.10	0.30	20.0
NBN0302A	0.10	51.1	15.8	12.1	0.07	0.33	20.0
	0.13	51.9	16.0	10.8	0.12	0.33	20.4
	0.11	51.0	15.4	12.2	0.11	0.35	20.6
	0.08	54.3	12.1	11.1	0.08	0.37	21.4
	0.14	54.4	12.3	10.8	0.15	0.36	21.5
	0.16	54.0	12.5	11.3	0.08	0.39	21.4
	0.12	49.5	16.9	12.0	0.15	0.30	20.4
	0.12	49.5	16.7	12.4	0.15	0.33	20.3
	0.09	49.4	17.0	11.8	0.13	0.34	20.2
NBN0305	0.15	41.2	25.8	13.2	0.17	0.31	19.0
	0.14	40.7	26.0	13.5	0.13	0.23	18.7
	0.19	42.4	24.3	12.8	0.14	0.28	19.1
	0.13	42.7	25.0	12.8	0.15	0.29	18.7
	0.11	41.3	26.0	13.2	0.14	0.31	18.9
	0.14	41.6	25.8	13.1	0.10	0.25	18.7
	0.15	41.1	25.9	13.3	0.16	0.23	18.7
	0.16	42.0	24.3	13.6	0.18	0.30	18.9
NBN0311	0.75	40.7	26.2	12.9	0.16	0.21	18.5
	1.42	38.8	27.2	13.7	0.14	0.21	18.0
NBN0316	0.09	54.7	11.6	12.0	0.10	0.40	20.6
	0.05	55.2	11.0	12.4	0.17	0.34	20.7
	0.24	54.7	12.3	11.4	0.13	0.28	20.2
	0.28	56.0	10.1	10.6	0.13	0.35	20.5
	0.10	55.0	10.8	12.6	0.09	0.35	20.3
	0.10	55.6	11.0	11.5	0.10	0.43	20.7
	0.10	56.7	10.7	11.0	0.13	0.36	20.4
NBN0319	0.06	54.7	11.2	13.0	0.07	0.42	20.1
	0.09	55.0	11.3	12.7	0.16	0.34	19.8
	0.09	54.2	11.5	13.1	0.14	0.42	19.9
	0.22	56.6	11.4	10.4	0.11	0.34	20.4
	0.09	53.8	11.2	13.4	0.12	0.38	20.2
	0.04	53.3	12.7	13.2	0.10	0.38	20.1
	0.06	55.2	10.7	13.3	0.09	0.36	19.7
	0.07	54.5	11.0	13.0	0.07	0.41	20.1
	0.09	53.0	12.5	13.3	0.06	0.37	19.8
	0.09	52.1	13.3	13.7	0.12	0.42	19.8
	0.13	56.9	11.1	10.8	0.10	0.38	19.8
	0.76	54.5	10.9	9.9	0.11	0.17	20.1

SPINEL

Sample	TiO_2	Al_2O_3	Cr_2O_3	FeO	MnO	NiO	MgO
NBN0321	0.27	50.6	16.6	11.6	0.15	0.37	20.0
	0.33	51.5	16.2	11.3	0.16	0.35	20.1
	0.41	50.4	16.1	11.4	0.11	0.36	20.1
	0.42	50.3	16.0	11.8	0.15	0.34	20.2
	0.13	51.6	14.8	11.1	0.09	0.39	20.8
	0.12	51.6	15.2	11.4	0.09	0.38	21.0
	0.26	51.5	15.0	11.5	0.11	0.33	20.9
	0.17	51.7	15.3	11.4	0.11	0.38	20.8
	0.34	51.9	14.7	11.5	0.09	0.33	20.3
	0.39	52.4	14.4	11.4	0.14	0.34	20.6

AMPHIBOLE

Sample	SiO_2	TiO_2	Al_2O_3	Cr_2O_3	FeO	MnO	MgO	CaO	Na_2O	K_2O	NiO	Cl	F
NMS1304	40.9	1.32	13.8	1.77	3.59	0.06	18.2	11.8	3.00	1.10	0.13		
	40.9	1.31	13.6	1.75	3.61	0.06	18.0	11.9	3.18	1.16			
	41.7	1.34	13.5	1.75	3.47	0.06	18.1	12.0	2.60	1.26	0.14		
	41.6	1.34	13.5	1.72	3.56	0.05	18.1	11.9	2.99	1.11			
	41.8	1.39	13.4	1.65	3.48	0.07	18.0	11.9	3.01	1.12	0.12		
	41.7	1.37	13.4	1.66	3.48	0.05	18.1	11.9	3.01	1.17	0.18		
	41.3	1.30	13.6	1.77	3.48	0.05	18.0	11.9	3.05	1.07	0.09		
	42.0	1.67	12.8	1.74	3.66	0.05	15.9	14.3	4.51	1.07	0.09		
	40.9	1.36	13.5	1.97	3.56	0.05	18.0	11.9	2.83	1.14	0.15		
	41.6	1.36	13.4	1.81	3.54	0.05	18.0	11.8	2.89	1.05	0.12		0.06
NMS1308	41.0	2.62	14.3	1.36	3.91	0.08	17.7	10.8	3.69	0.33			
	41.5	1.98	14.0	1.99	3.51	0.06	17.6	11.1	3.52	0.39	0.10		
	41.2	2.02	14.0	2.00	3.59	0.07	17.6	11.2	4.07	0.43			
	40.9	3.12	14.0	1.37	3.98	0.07	17.8	10.8	3.92	0.34	0.12		
NJS1302_1	38.9	8.06	13.8	0.13	5.26	0.07	16.0	11.1	3.16				
	39.1	8.12	13.8	0.12	5.14	0.07	16.1	11.0	3.49				
NJS1302_2	41.2	4.21	13.6	1.24	4.72	0.08	16.7	10.5	3.75		0.10		
	41.3	4.26	13.5	1.18	4.65	0.07	16.8	10.5	3.97		0.13		
NFL1302	41.2	1.66	14.4	1.37	3.81	0.07	18.0	11.2	3.83	0.45	0.15	0.03	0.06
	42.0	1.69	14.4	1.39	3.76	0.06	18.0	11.3	3.81	0.50	0.17		
NFL1315A	42.0	2.03	11.7	1.37	3.94	0.07	18.0	11.1	3.39	1.07	0.11	0.03	0.10
	42.5	1.90	12.3	1.70	3.91	0.06	18.2	11.4	3.06	1.13	0.09	0.04	0.09
	42.5	1.67	12.2	2.42	4.05	0.06	18.1	11.3	3.28	1.23	0.09	0.05	0.09
	42.1	1.67	12.0	2.48	3.90	0.07	18.1	11.4	2.90	1.17	0.16	0.04	0.11
	42.1	1.72	12.3	2.56	4.09	0.06	18.3	11.5	3.09	1.22	0.13	0.04	0.11
	42.3	2.47	12.3	2.35	3.99	0.07	18.1	11.4	3.25	0.84	0.13	0.03	0.07
	41.9	2.58	12.4	2.41	4.21	0.06	18.0	11.4	3.38	0.96		0.05	0.07
NFL1324	41.4	1.72	13.6	2.12	3.70	0.06	18.2	11.5	3.15	1.21	0.12	0.05	
	41.3	1.72	13.5	1.96	3.70	0.05	18.1	11.6	3.20	1.28	0.13	0.06	0.07
	42.1	1.71	13.5	1.99	3.71	0.04	18.1	11.5	3.28	1.20	0.10	0.05	
	41.7	1.77	13.6	1.97	3.72	0.05	18.3	11.5	3.11	1.24	0.14	0.06	
	42.0	1.54	13.4	2.16	3.61	0.05	18.0	11.4	3.04	1.19	0.10	0.05	
	41.8	1.54	13.5	2.08	3.80	0.06	17.9	11.3	3.15	1.18	0.10	0.06	
	42.0	1.26	13.4	2.04	3.71	0.06	18.0	11.5	3.11	1.07	0.12	0.05	
	42.0	1.26	13.4	2.06	3.61	0.06	18.1	11.5	3.23	1.06	0.19	0.05	0.05
	42.3	1.22	13.5	1.88	3.66	0.05	18.1	11.4	3.16	1.08		0.05	
NFL1326	40.7	1.85	13.0	1.71	6.08	0.09	16.7	11.5	3.14	1.18		0.04	0.20
	41.0	1.80	12.9	1.45	6.15	0.11	16.7	11.5	2.98	1.08		0.04	0.20
	40.7	1.84	13.0	1.56	5.99	0.09	16.8	11.4	3.14	1.10			0.20
	41.2	1.82	12.7	1.51	6.31	0.09	16.8	11.5	3.07	1.10			0.20
	41.1	1.70	12.9	1.66	6.01	0.09	16.7	11.6	3.30	0.99	0.11		0.25
	40.9	1.68	13.0	1.61	6.15	0.09	16.6	11.4	3.32	0.98			0.17
	40.9	1.59	13.1	1.50	6.20	0.09	16.8	11.5	3.37	0.74	0.11	0.03	0.20
	40.9	1.66	13.2	1.61	6.32	0.10	16.8	11.6	3.58	0.70	0.12	0.03	0.20
	40.9	1.70	12.8	1.60	6.00	0.08	16.9	11.6	3.42	0.77	0.11		0.18
NFL1329	41.8	1.66	14.5	1.14	4.04	0.07	17.9	11.2	3.99	0.10	0.14		
	42.0	1.67	14.3	1.16	4.09	0.06	17.9	11.2	3.85	0.11	0.13		
	41.8	1.72	14.4	1.20	3.99	0.08	17.8	11.2	4.02	0.15	0.17		
	41.9	1.70	14.3	1.16	4.05	0.07	17.9	11.2	3.99	0.14	0.11		

Appendix B2 - Trace-Element Compositions of Pyroxenes and Amphibole

ORTHOPYROXENE

Sample	Rb	Th	U	Ba	Nb	Ta	La	Ce	Pb	Sr	Pr	Nd	Hf	Zr	Sm
NMS1302A			0.001	0.040	0.030					0.09			0.022	0.38	0.005
			0.004	0.023	0.012					0.04			0.017	0.38	
	0.070	0.015		0.192	0.065		0.007		0.052	0.14	0.006	0.054		0.41	
					0.048	0.006		0.011		0.10	0.002	0.034	0.027	0.38	0.024
		0.006		0.233	0.030	0.003				0.02	0.007			0.30	0.005
				0.031	0.025		0.002		0.028	0.02				0.41	0.026
	0.106			0.111	0.063				3.060	0.07			0.015	0.33	0.005
	0.050				0.052			0.075		0.21	0.006		0.025	0.37	
	0.123		0.006	0.038	0.028			0.030		0.34		0.038		0.42	
				0.047	0.124		0.012	0.017	0.070	0.36		0.045		0.60	
		0.002		0.025	0.072	0.001	0.007	0.046	0.041	0.63	0.001	0.031		7.07	
NMS1304				0.003				0.019		0.12				0.86	
		0.006	0.009	0.013			0.005	0.027		0.20	0.007	0.052	0.030	0.84	0.049
								0.022		0.17	0.009	0.037	0.030	1.07	
								0.027		0.09		0.035	0.057	0.91	0.035
							0.006	0.019		0.13			0.057	1.04	
				0.010				0.029		0.19	0.005	0.058	0.048	0.91	
								0.016		0.10			0.028	0.96	
				0.003			0.011			0.15	0.011			0.98	
										0.14			0.072	0.81	
NMS1305								0.021		0.18	0.012	0.037	0.041	2.64	
		0.011	0.004	0.004	0.004	0.003	0.014	0.024		0.15	0.006	0.037	0.068	3.00	0.026
				0.025	0.018	0.006		0.029		0.19	0.003		0.072	3.22	
	0.232			0.528	0.078	0.005	0.020	0.072		1.33	0.018	0.097	0.111	4.58	0.033
			0.003	0.085	0.093		0.012	0.028		0.41			0.126	4.66	
	0.093		0.004	0.117	0.032		0.006	0.026		0.38	0.005		0.130	4.87	
NMS1308				0.403			0.009	0.018	0.056	0.44			0.062	1.38	
				0.101	0.008	0.009				0.18		0.030		1.32	
				0.036						0.18			0.038	1.40	
				0.525				0.017	0.181	0.14	0.008		0.037	1.22	
	0.063			0.185	0.088			0.012	0.062	0.26	0.008		0.032	1.26	
				0.157				0.008		0.08			0.026	1.19	
NMS1310	0.052						0.008	0.008		0.15	0.002		0.031	1.37	
								0.011		0.14	0.002		0.068	1.40	
			0.009		0.012	0.007	0.005	0.011		0.21			0.023	1.53	
										0.16			0.045	1.38	0.052
					0.005					0.16				1.47	0.024
						0.002				0.13			0.068	1.59	
								0.013		0.15			0.043	1.53	
		0.007	0.006							0.20			0.069	1.50	
NJS1302		0.002		0.003				0.018		0.13	0.007	0.089	0.098	5.26	
				0.004		0.002		0.024		0.11	0.006	0.060	0.138	5.63	
				0.004				0.025		0.08			0.254	7.06	
				0.200	0.031			0.025		0.21	0.011	0.061	0.175	5.88	0.050
								0.041		0.12	0.008	0.053	0.140	5.33	0.033
							0.008	0.025		0.08		0.048	0.091	4.75	0.035
								0.033		0.13	0.010	0.062	0.162	5.67	0.060
				0.004				0.018		0.09	0.019	0.048	0.120	4.53	
			0.003	0.011			0.006	0.020	0.051	0.11	0.007	0.129	0.071	3.94	

Eu	Gd	Tb	Ti	Dy	Ho	Y	Er	Tm	Yb	Lu	Sc	V	Cr	Co	Ni
		0.001	144		0.010	0.21	0.017	0.011	0.058	0.017	22.9	88	4806	63	781
0.003			135	0.035	0.008	0.22	0.043	0.004	0.077	0.017	22.0	79	3310	57	732
		0.007	140	0.027	0.010	0.24	0.027		0.075	0.022	22.9	82	3083	60	770
			133	0.047	0.012	0.25			0.085	0.007	22.2	80	3234	55	690
		0.004	131	0.029	0.011	0.19		0.008	0.054	0.012	21.0	76	2809	58	747
0.009	0.020		138		0.010	0.23		0.009	0.072	0.021	23.0	81	3063	62	805
			145	0.058	0.010	0.23	0.038	0.012	0.048	0.014	22.5	80	3093	61	778
	0.010		142	0.036	0.016	0.25	0.046	0.006	0.036	0.022	22.2	80	3077	60	772
0.008			150	0.015	0.007	0.23	0.048		0.068		22.5	83	3187	62	794
0.005			144			0.26	0.053	0.008	0.071		21.5	80	2945	60	770
	0.033		126	0.067		0.23	0.031		0.087	0.020	18.6	67	2601	52	661
	0.053	0.003	409	0.052	0.016	0.44	0.051	0.007	0.109	0.031	20.6	100	2617	59	729
	0.051	0.010	403	0.078	0.017	0.49	0.098	0.011	0.160	0.038	20.4	97	2533	58	714
0.021	0.050		459	0.103	0.024	0.52	0.077	0.015	0.160	0.024	22.2	108	2981	62	755
			467	0.062	0.025	0.49	0.078	0.016	0.096	0.025	21.1	102	3076	58	721
	0.029	0.008	480	0.047	0.021	0.52	0.090	0.017	0.072	0.030	22.9	110	3025	61	752
	0.043	0.011	457	0.046	0.017	0.53	0.076	0.020	0.141	0.028	21.0	101	2846	60	736
0.010		0.012	439	0.069	0.023	0.58	0.053	0.025	0.113	0.022	22.2	108	2894	62	760
			463	0.085	0.025	0.56	0.060		0.138	0.020	22.6	109	2989	62	763
0.013	0.039	0.005	455	0.110	0.016	0.49	0.078	0.015		0.035	20.7	104	2952	61	756
0.022		0.008	582	0.118	0.032	1.03	0.140	0.023	0.276	0.044	16.1	77	2877	57	697
0.022	0.060	0.017	354	0.117	0.028	0.90	0.121	0.029	0.352	0.046	16.7	73	2343	63	785
0.017	0.078	0.017	618	0.086	0.032	1.04	0.128	0.036	0.283	0.055	17.6	85	2700	65	803
0.018	0.073	0.012	182	0.062	0.028	0.94	0.128	0.037	0.319	0.030	16.5	62	2219	62	779
		0.012	155	0.090	0.033	0.83	0.132	0.030	0.306	0.046	15.3	58	1784	62	773
0.011		0.012	164	0.132	0.030	0.98	0.081	0.031	0.289	0.047	16.4	62	1982	65	804
		0.006	416	0.077	0.024	0.73	0.067	0.022	0.216	0.033	15.9	80	2712	64	795
		0.012	478	0.126	0.028	0.68	0.094	0.012	0.176	0.024	15.1	82	2910	57	720
	0.059	0.006	585	0.096	0.027	0.77	0.095	0.012	0.210	0.037	15.4	85	3266	59	749
	0.036	0.011	450	0.076	0.024	0.71	0.111	0.024	0.147	0.030	16.2	84	2877	61	768
	0.042	0.011	414	0.076	0.022	0.77	0.110	0.020	0.173	0.026	15.7	82	2556	61	778
			588	0.077	0.019	0.77	0.084		0.131	0.026	15.8	91	3274	59	731
0.006		0.010	658	0.109	0.040	1.05	0.130	0.034	0.237	0.046	18.1	95	2738	66	785
	0.050	0.012	689	0.133	0.033	1.04	0.134	0.025	0.259	0.061	18.9	102	3161	63	768
	0.065	0.017	638	0.129	0.048	1.04	0.133	0.042	0.297	0.056	18.3	98	2741	65	796
0.013		0.019	684	0.119	0.037	1.04	0.130	0.028	0.287	0.055	17.6	98	3145	65	798
		0.010	699	0.149	0.036	1.00	0.165	0.023	0.260	0.041	17.4	98	3140	60	729
		0.015	715	0.105	0.027	1.14	0.167	0.033	0.287	0.050	19.3	109	3538	67	827
	0.083		668	0.124	0.045	1.07	0.102	0.034	0.299	0.050	18.7	103	3512	66	815
0.017		0.019	668	0.151	0.037	1.06	0.161	0.028	0.176	0.037	18.3	98	3019	63	804
0.026	0.072	0.014	1192	0.254	0.060	1.67	0.226	0.045	0.378	0.059	18.2	97	2261	69	805
0.019	0.083	0.017	1377	0.133	0.049	1.62	0.212	0.048	0.380	0.068	17.6	97	2293	64	735
0.028	0.136	0.034	1648	0.170	0.055	1.61	0.303	0.046	0.365	0.070	18.9	110	2852	68	779
	0.061	0.018	1247	0.265	0.053	1.70	0.236	0.030	0.391	0.064	18.2	100	2353	66	757
0.027	0.114	0.020	1388	0.112	0.059	1.44	0.143	0.037	0.313	0.054	16.2	87	2423	59	681
0.015	0.066	0.021	1065	0.171	0.059	1.43	0.182	0.018	0.341	0.063	16.0	83	2149	64	747
0.032	0.057	0.016	1308	0.233	0.052	1.51	0.183	0.046	0.292	0.062	17.7	97	2563	67	766
		0.013	1276	0.118	0.037	1.32	0.180	0.035	0.248	0.043	17.2	92	2645	67	776
	0.067	0.012	1124	0.157	0.032	1.21	0.185	0.037	0.289	0.059	15.8	84	2477	65	751

ORTHOPYROXENE

Sample	Rb	Th	U	Ba	Nb	Ta	La	Ce	Pb	Sr	Pr	Nd	Hf	Zr	Sm
NJS1304			0.003		0.007	0.004		0.029	0.029	0.08	0.009	0.045	0.101	4.47	0.057
						0.003		0.015		0.09		0.050	0.064	3.86	
	0.165				0.002			0.025		0.11	0.007		0.052	3.82	
				0.003		0.002		0.019		0.13	0.009		0.103	3.92	
		0.003						0.026		0.09			0.133	4.34	0.033
			0.002					0.031	0.071	0.09	0.011	0.075	0.092	4.17	0.075
				0.728	0.135	0.007		0.017		0.40		0.064	0.138	4.28	0.062
				0.597	0.032		0.007	0.028		0.31	0.011	0.106	0.110	3.78	0.053
		0.004				0.003		0.029	1.526	0.09	0.010	0.083	0.078	4.14	
					0.008		0.012	0.017		0.09	0.011	0.090	0.105	4.23	0.062
NJS1306			0.009				0.013	0.035		0.28			0.088	2.52	0.035
		0.005	0.004	0.034		0.002		0.042		0.26	0.010	0.046	0.081	2.52	0.063
							0.007	0.030		0.24	0.007		0.092	2.48	
		0.005			0.003		0.013	0.034		0.28	0.007	0.046	0.084	2.23	0.042
			0.004	0.035	0.013		0.016	0.032		0.22			0.052	2.55	
			0.009		0.008	0.001		0.037		0.22	0.011	0.046	0.077	2.57	
		0.016	0.007	0.001	0.009	0.002	0.015	0.035		0.24		0.050	0.129	3.20	0.057
NJS1307					0.010			0.018	0.039	0.32		0.062	0.061	2.07	
							0.009			0.27			0.087	2.07	
						0.007	0.005	0.020		0.26			0.096	2.43	0.081
								0.019		0.20	0.013	0.054	0.065	2.32	0.102
							0.009	0.017		0.30			0.085	2.39	
								0.014		0.32		0.084	0.074	2.44	
			0.012					0.016		0.22			0.083	2.55	0.046
				0.007	0.008	0.003	0.015	0.018		0.36	0.014		0.090	2.58	0.018
NPY1301				0.003	0.012	0.007		0.018	0.036	0.20		0.033	0.051	1.31	
					0.006		0.007			0.14				1.54	
		0.007	0.005		0.013		0.007			0.27			0.074	1.38	
		0.005			0.006		0.007			0.14		0.029	0.045	1.82	
	0.049			0.165			0.051		0.075	0.14	0.007		0.059	1.85	
							0.005			0.14		0.042	0.042	1.36	
						0.007			0.046	0.13	0.007		0.087	1.64	0.054
							0.005			0.17		0.038	0.039	1.40	
NPY1310				0.624	0.004	0.005			1.519	0.18				1.01	
	0.143			0.680	0.011			0.017		0.75		0.074	0.037	0.99	0.012
		0.009						0.011		0.15		0.073		0.87	0.026
				0.009				0.018	0.160	0.09			0.045	1.03	
				0.021		0.002		0.012	0.459	0.08		0.040	0.031	1.11	
	0.139		0.096	0.340	0.010		0.004		0.057	0.18	0.011	0.034	0.038	1.13	0.017
				0.012	0.008			0.012	0.168	0.25				1.13	
NPY1311					0.005					0.09		0.038	0.062	0.93	
						0.002				0.05			0.047	0.94	
						0.004		0.012		0.07	0.003	0.050		1.07	
		0.004		0.005				0.020		0.06			0.039	0.94	
		0.011	0.004							0.08	0.004	0.030	0.035	0.84	
				0.137		0.004				0.23	0.008	0.067		1.07	
				0.005		0.006	0.011	0.021		0.21		0.029	0.029	0.92	0.033
								0.018		0.21	0.010		0.065	1.07	
				0.015	0.008			0.016		0.12		0.018	0.067	1.13	0.026
NPY1314			0.013							0.07			0.108	1.93	
			0.008		0.003			0.018		0.08			0.043	1.75	0.038
			0.014	0.008						0.07		0.053		1.63	0.045
			0.009	0.008			0.007	0.011		0.10		0.035	0.054	1.92	
			0.009		0.004			0.018		0.55	0.012	0.049	0.088	1.82	
			0.004	0.029	0.008		0.007			0.08		0.037	0.090	2.06	
				0.001		0.002		0.020		0.22		0.037	0.078	1.79	0.069

Eu	Gd	Tb	Ti	Dy	Ho	Y	Er	Tm	Yb	Lu	Sc	V	Cr	Co	Ni
	0.059	0.016	1194	0.213	0.052	1.35	0.210	0.036	0.271	0.051	16.5	94	2392	69	794
0.012	0.082	0.018	1094	0.097	0.044	1.23	0.170	0.035	0.271	0.059	15.3	86	2211	70	813
	0.166	0.016	1187	0.205	0.059	1.29	0.166	0.039	0.254	0.054	16.5	91	2267	70	813
	0.084	0.011	1311	0.188	0.042	1.35	0.204	0.042	0.252	0.047	16.0	92	2526	70	801
0.024	0.072	0.021	1196	0.187	0.049	1.28	0.166	0.034	0.298	0.042	16.0	90	2332	68	780
0.025	0.081	0.015	1356	0.132	0.047	1.22	0.165	0.042	0.261	0.050	16.7	94	2577	67	769
0.010	0.090	0.013	1064	0.151	0.047	1.22	0.163	0.028	0.373	0.041	14.9	84	2129	67	770
0.028	0.108	0.016	1024	0.167	0.036	1.24	0.150	0.024	0.258	0.053	14.5	81	2073	63	731
	0.056	0.016	1146	0.174	0.044	1.35	0.193	0.036	0.348	0.068	16.2	91	2404	69	793
0.013	0.090	0.016	1134	0.175	0.046	1.32	0.181	0.020	0.320	0.069	16.1	91	2406	70	799
0.021	0.110	0.010	797	0.171	0.052	1.64	0.213	0.049	0.408	0.064	21.9	108	2493	71	879
0.018	0.119	0.017	712	0.165	0.055	1.44	0.189	0.036	0.346	0.058	19.9	97	2213	65	803
0.018	0.076	0.018	657	0.172	0.054	1.52	0.181	0.028	0.318	0.044	19.3	94	2115	63	773
0.018		0.018	695	0.182	0.037	1.49	0.215	0.034	0.230	0.057	19.8	99	2194	64	790
		0.030	723	0.104	0.048	1.48	0.199	0.037	0.339	0.044	19.6	101	2265	65	812
0.015	0.122	0.023	787	0.225	0.064	1.65	0.207	0.034	0.280	0.046	22.3	110	2510	70	875
0.017	0.094	0.019	715	0.167	0.060	1.40	0.227	0.042	0.256	0.065	19.9	100	2269	63	795
0.018	0.114	0.021	975	0.199	0.056	1.54	0.194	0.039	0.375	0.045	18.6	107	2282	64	777
	0.073	0.018	939	0.193	0.047	1.35	0.171	0.030	0.322	0.057	17.8	101	2120	61	755
0.015	0.066	0.020	1029	0.220	0.050	1.53	0.195	0.049	0.401	0.070	18.7	109	2342	65	792
0.020		0.019	1044	0.161	0.042	1.45	0.194	0.048	0.266	0.066	18.9	110	2366	65	799
0.021	0.075	0.025	1013	0.131	0.055	1.49	0.196	0.036	0.276	0.054	19.3	111	2374	65	796
0.030	0.054	0.018	930	0.170	0.050	1.46	0.208	0.021	0.371	0.068	18.0	100	2074	60	735
		0.017	1033	0.136	0.052	1.47	0.176	0.046	0.353	0.076	20.1	114	2336	67	829
	0.106	0.030	1105	0.179	0.056	1.66	0.246	0.038	0.402	0.068	20.6	117	2468	66	825
		0.010	718	0.103	0.021	0.98	0.146	0.031	0.339	0.053	15.4	95	2512	57	679
0.010			755	0.124	0.041	1.21	0.170	0.025	0.389	0.054	18.2	103	2360	66	825
0.018	0.051		766	0.134	0.039	1.18	0.164	0.027	0.289	0.068	17.6	102	2358	64	777
0.015		0.010	881	0.139	0.038	1.15	0.164	0.027	0.320	0.056	17.9	108	2600	65	775
		0.013	839	0.133	0.028	1.12	0.169	0.024	0.371	0.065	17.1	103	2368	63	778
0.008			721	0.083	0.031	1.14	0.134	0.037	0.311	0.059	16.4	96	2140	63	777
0.016	0.051	0.013	799	0.140	0.056	1.15	0.114	0.024	0.296	0.060	17.2	105	2798	63	758
			765	0.158	0.043	1.15	0.175	0.033	0.294	0.039	16.6	100	2558	64	775
0.014	0.057	0.012	833	0.143	0.044	1.33	0.242	0.049	0.265	0.044	20.6	145	1766	68	766
0.003	0.057	0.021	725	0.122	0.050	1.20	0.180	0.032	0.280	0.042	18.5	127	1524	61	717
	0.025	0.009	755	0.130	0.045	1.27	0.190	0.041	0.327	0.065	19.2	132	1397	63	715
		0.018	795	0.110	0.049	1.32	0.168	0.032	0.333	0.057	20.2	136	1437	67	757
		0.018	818	0.144	0.042	1.26	0.175	0.027	0.342	0.052	20.6	141	1478	68	771
0.012	0.090	0.017	734	0.142	0.050	1.15	0.145	0.034	0.283	0.043	18.7	126	1326	65	745
0.014	0.058		774	0.132	0.040	1.22	0.206	0.035	0.315	0.070	19.1	128	1506	65	738
0.025		0.023	757	0.136	0.049	1.24	0.173	0.052	0.320	0.068	20.1	132	1500	64	737
0.015		0.013	753	0.147	0.040	1.27	0.184	0.033	0.310	0.070	20.3	131	1377	66	759
0.015		0.005	757	0.216	0.031	1.20	0.143	0.030	0.350	0.059	20.0	132	1354	67	757
0.018		0.011	723	0.140	0.050	1.24	0.188	0.032	0.243	0.052	19.7	127	1341	65	744
		0.015	778	0.146	0.044	1.24	0.190	0.031	0.365	0.066	20.7	135	1386	68	779
0.007	0.041	0.013	694	0.122	0.042	1.18	0.149	0.033	0.304	0.066	18.6	125	1330	63	710
0.015	0.053	0.008	718	0.150	0.029	1.15	0.145	0.021	0.249	0.055	17.8	121	1417	55	631
0.009	0.064	0.012	697	0.091	0.045	1.03	0.160	0.023	0.282	0.056	17.6	120	1473	53	605
0.013	0.068	0.013	702	0.133	0.040	1.21	0.196	0.070	0.270	0.048	18.8	131	1583	60	682
	0.036		898	0.139	0.046	1.15	0.191	0.037	0.279	0.038	19.8	119	2668	70	852
0.015	0.081	0.018	558	0.184	0.036	1.03	0.162	0.035	0.327	0.051	18.4	103	2300	69	854
0.013	0.053	0.011	601	0.152	0.034	1.22	0.161	0.038	0.308	0.053	19.9	107	2371	72	888
	0.074	0.023	529	0.136	0.046	1.15	0.132	0.038	0.310	0.058	18.2	99	2285	64	785
	0.086	0.013	643	0.126	0.045	1.19	0.175	0.027	0.301	0.063	18.5	98	2138	63	779
0.017	0.051	0.012	872	0.202	0.066	1.19	0.139	0.037	0.306	0.045	18.7	105	2326	62	769
	0.020	0.009	632	0.162	0.043	1.17	0.155	0.023	0.271	0.055	18.6	95	1923	63	793

ORTHOPYROXENE

Sample	Rb	Th	U	Ba	Nb	Ta	La	Ce	Pb	Sr	Pr	Nd	Hf	Zr	Sm
NFL1302		0.007	0.003	0.009		0.003	0.008	0.015		0.09	0.003		0.029	1.21	0.022
					0.007			0.026		0.13	0.012	0.060	0.023	1.26	
		0.007	0.006	0.418	0.042			0.018		0.53	0.007		0.052	1.25	0.015
		0.005						0.024		0.10			0.051	1.17	
								0.022		0.10			0.031	1.04	
NFL1305							0.010	0.023		0.09	0.002		0.093	1.75	
				0.135	0.027		0.008	0.020		0.46			0.068	1.73	0.017
					0.009	0.007		0.025		0.09	0.002			1.72	0.011
				0.004	0.011					0.10	0.005	0.042	0.051	1.85	
		0.006			0.017	0.001	0.007	0.027		0.08		0.024		1.97	
		0.007			0.017			0.022		0.07		0.035	0.063	2.26	
NFL1315A		0.003			0.013	0.001		0.048		0.36	0.011	0.081	0.072	2.62	
		0.004		0.106	0.013			0.048		0.29	0.021	0.088	0.061	2.56	0.040
				0.001	0.011			0.053		0.31		0.113	0.050	2.80	0.021
							0.014	0.051		0.33	0.014	0.074	0.091	3.11	
					0.019			0.059		0.29	0.009		0.073	2.84	0.042
			0.006		0.010		0.018	0.034	0.028	0.30		0.084	0.061	2.52	0.040
		0.010		0.019	0.023			0.057		0.34	0.008	0.120	0.049	2.23	0.046
				0.011				0.051		0.39	0.010	0.087	0.053	2.61	
NFL1316				0.040	0.014	0.002	0.006			0.10	0.005	0.038		0.73	0.022
		0.007					0.007			0.09				0.78	
					0.011		0.006			0.11	0.004	0.011	0.035	0.78	0.004
		0.003		0.038		0.005	0.009	0.010		0.10		0.021	0.036	0.85	
			0.005		0.009					0.07	0.001	0.008	0.037	0.86	0.048
			0.005			0.006		0.014		0.08			0.031	0.83	
				2.345	0.065		0.008			0.69			0.021	1.20	
NFL1324				0.063	0.043	0.003	0.033	0.088		0.31	0.032	0.151	0.144	6.63	
		0.010		0.040			0.014	0.106	0.034	0.29	0.021	0.101	0.192	6.88	
		0.009	0.017		0.024		0.023	0.130		0.31	0.032	0.184	0.044	3.97	0.091
					0.014	0.007	0.021	0.107		0.31	0.026	0.206	0.081	5.71	
NFL1327					0.019	0.003	0.018	0.096		0.34		0.117	0.036	1.36	
				0.001			0.010	0.080		0.23		0.143	0.044	1.40	0.080
		0.007			0.017		0.009	0.062	0.034	0.27	0.019	0.064		1.16	0.058
		0.007				0.001	0.008	0.058		0.28	0.022	0.120	0.085	2.36	0.021
			0.003	0.024	0.037	0.003		0.071		0.24	0.019	0.162		1.17	0.043
					0.013		0.019	0.061		0.30	0.019	0.117	0.021	1.18	
					0.009		0.010	0.076		0.26	0.014	0.071		1.31	0.022
NFL1329			0.009	0.003	0.009	0.002				0.09			0.069	1.53	0.011
		0.013								0.09	0.007	0.051	0.074	1.42	
			0.006					0.009		0.05	0.007		0.046	1.23	
			0.006					0.006		0.08			0.065	1.45	
					0.008			0.006		0.11	0.011		0.025	1.32	
								0.010		0.08				1.18	
				0.019		0.001		0.009		0.11		0.024		1.38	0.011
		0.009		0.038	0.010			0.009	0.035	0.12			0.082	1.46	
							0.004	0.009		0.10		0.036	0.030	1.26	
		0.011		0.005				0.011		0.09			0.054	1.46	
NTB0306								0.008		0.09				0.07	
	0.014			2.950	0.006		0.008	0.007		0.08				0.07	
				0.050	0.010			0.007		0.11				0.07	
					0.006		0.008	0.014		0.11				0.06	0.015
					0.012		0.006	0.009		0.08				0.06	
	0.011			0.029				0.012		0.08				0.05	
								0.011	0.048	0.07	0.010			0.05	
	0.217			0.429			0.006	0.014		0.08				0.06	
		0.003			0.007			0.012		0.11	0.003			0.08	
				0.131	0.006		0.007	0.010		0.07				0.08	
								0.009		0.08				0.06	

Eu	Gd	Tb	Ti	Dy	Ho	Y	Er	Tm	Yb	Lu	Sc	V	Cr	Co	Ni
	0.063		427	0.181	0.029	1.09	0.195	0.030	0.267	0.056	20.8	102	2879	66	815
	0.060	0.021	420	0.100	0.053	1.03	0.131	0.030	0.306	0.042	20.5	99	2734	61	775
0.008		0.009	425	0.117	0.030	1.02	0.167	0.017	0.237	0.048	19.2	94	2656	58	727
0.007	0.030	0.019	453	0.076	0.042	1.03	0.126	0.034	0.265	0.055	20.4	98	2806	62	777
			439	0.087	0.031	1.04	0.186	0.033	0.280	0.046	20.9	102	2793	63	784
		0.012	212	0.151	0.030	0.77	0.115	0.025	0.242	0.047	19.3	91	3034	60	769
0.010	0.042	0.014	181	0.038	0.023	0.74	0.078	0.016	0.213	0.036	18.9	87	2892	62	792
			209	0.071	0.023	0.74	0.128	0.028	0.260	0.027	19.7	91	3233	63	806
0.009			202	0.081	0.026	0.86	0.107	0.030	0.217	0.048	20.2	97	3184	64	817
		0.014	202	0.144	0.027	0.78	0.089	0.027	0.205	0.044	19.0	91	3086	61	783
			227	0.097	0.025	0.79	0.147	0.030	0.182	0.046	19.9	94	3210	62	784
0.015	0.092	0.017	337	0.150	0.042	1.03	0.144	0.026	0.207	0.035	15.9	53	3251	60	701
0.027	0.062	0.014	345	0.124	0.025	0.88	0.147	0.020	0.224	0.035	15.3	52	3238	60	691
	0.087	0.017	368	0.165	0.039	0.99	0.117	0.027	0.194	0.051	15.8	54	3628	61	716
0.017	0.070	0.018	392	0.165	0.034	0.94	0.108	0.024	0.203	0.045	15.4	64	6374	64	711
0.016	0.079	0.010	400	0.141	0.037	0.97	0.160	0.021	0.194	0.031	15.4	61	5544	63	711
0.019	0.052	0.015	375	0.124	0.038	0.95	0.110	0.025	0.212	0.029	13.8	48	3246	58	668
0.019	0.095	0.015	378	0.136	0.033	0.85	0.085	0.022	0.121	0.032	13.1	47	3227	60	670
	0.070		362	0.125	0.024	0.89	0.098	0.023	0.138	0.020	12.9	47	3129	57	642
	0.037		283	0.033	0.007	0.26	0.045	0.008	0.067	0.013	24.0	92	3391	60	760
0.012		0.001	295	0.057	0.014	0.24	0.042	0.009	0.054	0.012	23.2	90	3359	57	717
0.004			294		0.008	0.17			0.107	0.018	22.6	88	3240	55	701
0.011			296	0.028	0.019	0.28	0.031	0.009	0.120	0.015	25.9	102	3740	63	795
			288		0.014	0.26	0.030	0.010	0.130	0.022	25.3	98	3701	62	782
		0.005	297	0.032	0.008	0.28		0.006	0.052	0.019	23.3	89	3285	57	726
		0.004	296		0.012	0.24	0.049	0.008	0.088	0.022	24.5	96	3457	60	774
0.020	0.086	0.016	343	0.176	0.024	1.09	0.129	0.031	0.254	0.043	15.5	60	3599	58	759
0.031	0.122	0.014	346	0.183	0.062	1.23	0.141	0.032	0.208	0.047	16.7	66	3885	63	820
		0.015	281	0.156	0.037	1.16	0.180	0.032	0.274	0.048	15.9	78	5962	62	830
0.022	0.087	0.010	373	0.140	0.040	1.18	0.118	0.032	0.232	0.053	16.7	72	5418	65	838
	0.056	0.019	405	0.132	0.041	1.18	0.141	0.026	0.257	0.046	13.1	63	3225	59	671
0.027	0.100	0.017	385	0.207	0.052	1.05	0.147	0.022	0.268	0.047	14.2	67	3338	62	686
		0.013	344	0.126	0.042	1.07	0.141	0.042	0.263	0.032	13.9	64	3159	61	696
0.033	0.085	0.020	390	0.195	0.034	1.14	0.152	0.031	0.256	0.052	14.1	69	3351	60	693
0.016	0.040	0.021	342	0.116	0.038	1.04	0.121	0.020	0.287	0.037	14.2	68	3179	60	692
	0.143	0.016	351	0.114	0.039	1.04	0.136	0.025	0.194	0.042	14.9	74	3545	61	695
0.034	0.072	0.018	373	0.097	0.044	1.09	0.124	0.029	0.273	0.053	15.0	73	3401	60	698
0.019	0.040	0.012	426	0.095	0.032	1.03	0.118	0.028	0.283	0.056	19.9	98	2228	62	783
		0.006	384	0.131	0.034	0.94	0.184	0.033	0.274	0.055	18.8	93	2189	62	790
0.024		0.008	348	0.086	0.030	0.97	0.142	0.037	0.224	0.044	18.7	91	2217	64	810
	0.069	0.014	398	0.099	0.042	1.03	0.161	0.034	0.260	0.054	19.2	96	2377	64	792
		0.016	395	0.084	0.027	0.97	0.099	0.031	0.222	0.050	18.7	94	2344	63	796
0.007		0.010	369	0.152	0.032	0.92	0.110	0.021	0.173	0.061	18.2	90	2191	63	783
0.014	0.051	0.011	433	0.133	0.034	1.01	0.106	0.036	0.248	0.056	19.3	94	2548	63	792
0.010		0.012	383	0.132	0.033	1.01	0.135	0.032	0.210	0.045	19.2	95	2495	64	802
		0.017	430	0.089	0.032	0.94	0.136	0.020	0.289	0.041	17.8	88	2427	60	763
		0.005	444	0.128	0.026	1.00	0.119	0.037	0.210	0.043	18.3	90	2443	61	762
			214	0.024	0.010	0.22	0.027	0.007	0.054	0.019	15.0	65	3130	56	692
			224	0.040	0.006	0.22	0.049		0.081	0.011	15.6	68	3320	55	679
0.004	0.026		263	0.021	0.011	0.26	0.028	0.008	0.090	0.013	16.8	76	3760	56	679
		0.004	306	0.022	0.008	0.25	0.044	0.006	0.092	0.017	15.5	71	3640	55	647
		0.005	273	0.038	0.007	0.23	0.018	0.008	0.071	0.015	15.0	70	3460	54	649
			287	0.026	0.010	0.24	0.032	0.008	0.066	0.013	15.0	70	3520	54	653
			182	0.015		0.19	0.030	0.008	0.063	0.015	13.2	63	2890	51	618
			215	0.033	0.008	0.21	0.040		0.053	0.009	14.9	70	3350	54	645
		0.003	296	0.020	0.005	0.21	0.039	0.009	0.054	0.012	15.3	75	3410	55	642
		0.002	249	0.025	0.008	0.21	0.033		0.062	0.012	14.2	65	3200	54	628
		0.003	221	0.038	0.008	0.23	0.037		0.079	0.012	14.9	68	3230	55	669

ORTHOPYROXENE

Sample	Rb	Th	U	Ba	Nb	Ta	La	Ce	Pb	Sr	Pr	Nd	Hf	Zr	Sm
NTB0307				0.068	0.006			0.012		0.06		0.034		0.52	
		0.005			0.005			0.009		0.16	0.003		0.044	0.52	
								0.006		0.05				0.50	
			0.003		0.008			0.006		0.03	0.002		0.019	0.55	0.031
					0.012			0.045		0.18	0.007	0.056	0.027	0.48	
NTB1124			0.004					0.008		0.08			0.044	1.04	
								0.007		0.09	0.004		0.045	1.02	
					0.010			0.007		0.09				0.92	
								0.009		0.08		0.030	0.035	1.02	
								0.010		0.14	0.007			1.13	
					0.009			0.008		0.09	0.005			1.12	0.033
							0.003	0.012		0.12	0.003		0.035	1.06	
								0.011		0.11				0.96	
					0.007			0.008		0.11			0.046	1.01	
	0.085			0.039		0.004		0.011		0.22			0.047	0.99	
								0.009	0.045	0.09				1.08	
		0.006			0.012			0.009		0.08		0.050	0.047	1.14	
					0.008			0.007		0.09		0.035		1.04	
					0.009			0.008		0.07			0.029	1.07	
										0.07	0.003		0.054	1.14	0.043
					0.005			0.007		0.10			0.045	1.05	
NTB1116				0.003	0.004			0.013		0.14		0.060	0.037	1.24	
			0.006	0.966	0.028		0.017			1.01		0.062	0.035	1.20	0.066
		0.003		0.009			0.009	0.011		0.13	0.007			0.88	
						0.003		0.011		0.14	0.002		0.059	0.90	
	0.136	0.009		0.062		0.007		0.016		0.44	0.006	0.036		0.98	
					0.003	0.007	0.007	0.021		0.19		0.027	0.036	1.17	
					0.009					0.17				1.13	
NTB1122				0.004		0.003	0.014	0.062		0.18	0.014	0.107	0.076	3.25	0.066
				0.004			0.010	0.052		0.19	0.013	0.109	0.095	2.90	
					0.007			0.058		0.27	0.022	0.091	0.094	3.26	0.043
			0.006	0.002	0.006			0.069		0.18		0.067	0.134	3.01	0.093
			0.059			0.005		0.066		0.20	0.013	0.117	0.068	3.56	0.041
					0.006		0.007	0.052		0.18	0.012	0.064	0.127	3.28	0.070
NFK0301					0.020		0.038	0.170		0.50	0.026	0.155	0.034	1.83	
	0.034				0.025		0.028	0.124		0.48	0.025	0.102	0.038	1.72	0.048
					0.011		0.018	0.100		0.26	0.019	0.164	0.026	1.70	
			0.004		0.017		0.019	0.088		0.27	0.015	0.116		1.86	0.044
					0.021		0.019	0.097		0.28	0.022	0.139	0.032	1.69	0.068
					0.014		0.018	0.083		0.25	0.018	0.098	0.033	1.74	0.055
					0.012		0.015	0.093		0.24	0.018		0.048	1.74	0.050
					0.012		0.025	0.094		0.24	0.014	0.094		1.55	0.043
					0.022		0.019	0.078		0.26	0.016	0.090	0.025	1.56	0.043
					0.016		0.016	0.091		0.21	0.019		0.027	1.42	0.048
					0.013		0.022	0.085		0.25	0.017		0.035	1.49	0.041
					0.013		0.013	0.087		0.22	0.012	0.097		1.53	
					0.024		0.015	0.079	0.037	0.22	0.017	0.061	0.020	1.39	0.035
		0.026		0.016	0.029	0.004	0.166	0.567		1.90	0.085	0.451	0.057	2.87	0.068
		0.013			0.025		0.125	0.432		1.57	0.104	0.275	0.031	2.60	0.099
				0.255	0.022		0.022	0.111		0.30	0.023	0.181	0.033	1.94	0.045
					0.020		0.021	0.100		0.28	0.021	0.075	0.040	1.92	0.048
				0.149	0.017		0.018	0.088	0.022	0.26	0.019	0.090	0.039	2.01	0.043

Eu	Gd	Tb	Ti	Dy	Ho	Y	Er	Tm	Yb	Lu	Sc	V	Cr	Co	Ni
		0.008	290	0.091	0.020	0.66	0.110	0.025	0.184	0.031	16.6	84	2790	60	829
		0.007	344	0.059	0.024	0.58	0.089	0.021	0.187	0.033	15.8	86	2840	59	771
		0.007	327	0.060	0.015	0.62	0.098	0.020	0.189	0.033	15.6	82	2760	60	785
		0.006	358	0.068	0.022	0.65	0.091	0.019	0.214	0.037	16.1	86	2810	59	764
		0.008	269	0.069	0.025	0.73	0.095	0.024	0.171	0.036	16.0	80	2720	58	782
0.009	0.057	0.016	828	0.118	0.027	0.89	0.135	0.020	0.230	0.045	18.7	100	3690	57	732
	0.041	0.011	878	0.122	0.025	0.91	0.138	0.027	0.215	0.038	18.7	102	3750	58	734
	0.030	0.008	831	0.126	0.035	0.90	0.121	0.033	0.204	0.037	18.5	101	3640	58	755
0.007	0.058	0.008	828	0.104	0.027	0.90	0.119	0.027	0.239	0.049	18.6	101	3640	57	741
	0.057	0.012	890	0.124	0.035	1.05	0.145	0.031	0.194	0.039	19.4	104	3950	59	775
	0.057	0.011	953	0.118	0.035	0.94	0.149	0.024	0.232	0.038	19.4	107	3900	60	768
	0.052	0.009	860	0.102	0.034	0.88	0.130	0.023	0.210	0.043	18.4	103	3630	60	732
0.012		0.011	829	0.120	0.030	0.89	0.129	0.024	0.217	0.040	18.6	99	3530	57	716
0.015	0.050	0.010	822	0.140	0.033	0.94	0.140	0.028	0.237	0.038	19.0	100	3520	58	749
	0.051	0.012	811	0.124	0.032	0.91	0.142	0.027	0.231	0.044	18.4	101	3500	59	733
0.009	0.056	0.012	829	0.122	0.033	0.93	0.117	0.024	0.233	0.039	18.4	101	3780	57	757
0.014	0.056	0.010	975	0.128	0.039	0.98	0.126	0.030	0.279	0.046	20.1	109	4070	60	758
		0.011	877	0.111	0.036	0.90	0.161	0.028	0.231	0.035	18.9	104	3670	58	733
	0.034	0.011	857	0.098	0.032	0.98	0.144	0.022	0.241	0.048	19.1	103	3600	56	730
0.010	0.033	0.011	851	0.129	0.034	0.89	0.142	0.029	0.218	0.039	19.2	103	3680	58	766
		0.010	813	0.141	0.038	0.93	0.109	0.033	0.190	0.037	18.8	101	3440	60	759
		0.017	550	0.150	0.035	0.97	0.177	0.029	0.165	0.027	20.4	104	3598	63	800
0.012		0.017	545	0.115	0.049	1.03	0.155	0.037	0.244	0.048	20.5	103	3485	61	793
		0.013	522	0.085	0.024	0.87	0.122	0.029	0.218	0.055	18.4	96	3337	61	777
0.016	0.081	0.018	484	0.084	0.040	0.82	0.128	0.027	0.189	0.031	19.5	98	3546	64	805
	0.062	0.013	467	0.111	0.040	0.90	0.109	0.023	0.312	0.024	18.8	95	3309	62	811
		0.013	531	0.121	0.048	0.97	0.081	0.031	0.208	0.049	20.9	105	3702	63	813
0.021	0.041	0.014	511	0.122	0.034	0.89	0.123	0.022	0.209	0.037	20.2	101	3488	63	822
0.037	0.087	0.024	1501	0.243	0.062	1.76	0.204	0.044	0.372	0.065	27.7	146	3142	62	735
0.026	0.091	0.025	1597	0.231	0.048	1.81	0.262	0.045	0.364	0.061	27.3	143	3222	64	757
0.029	0.100	0.031	1544	0.228	0.056	1.81	0.226	0.052	0.449	0.069	27.0	144	3213	61	733
0.030	0.089	0.015	1503	0.250	0.061	1.76	0.222	0.046	0.364	0.079	26.9	140	3120	63	744
0.018	0.155	0.026	1372	0.265	0.072	1.83	0.214	0.051	0.390	0.071	27.7	143	3307	63	742
0.021	0.117	0.027	1453	0.273	0.078	1.81	0.235	0.044	0.478	0.058	27.7	142	3198	64	758
0.025	0.060	0.019	485	0.144	0.043	1.16	0.166	0.039	0.311	0.055	15.8	80	4440	59	742
0.013		0.015	476	0.153	0.044	1.20	0.171	0.034	0.281	0.051	15.5	79	4220	59	738
0.022	0.059	0.013	466	0.156	0.035	1.11	0.155	0.034	0.343	0.048	14.9	75	3910	57	737
0.024	0.080	0.019	477	0.174	0.037	1.19	0.181	0.033	0.287	0.052	15.5	78	4040	59	762
0.033	0.068	0.014	467	0.139	0.038	1.09	0.152	0.033	0.270	0.050	14.9	76	4260	58	742
0.020	0.068	0.013	470	0.117	0.045	1.12	0.157	0.028	0.279	0.061	15.5	77	4150	57	733
0.019	0.071	0.019	499	0.138	0.037	1.15	0.152	0.034	0.292	0.056	15.7	79	4060	58	735
0.014	0.059	0.014	477	0.148	0.046	1.12	0.121	0.029	0.297	0.052	15.2	75	3690	57	735
0.019	0.058	0.020	478	0.123	0.039	1.10	0.152	0.026	0.232	0.039	15.1	75	3740	57	739
	0.044	0.013	430	0.155	0.029	0.98	0.155	0.033	0.212	0.047	12.9	72	3510	57	721
0.020	0.059	0.011	413	0.112	0.031	0.93	0.118	0.027	0.260	0.042	12.9	72	3470	57	735
0.011	0.085	0.015	427	0.141	0.038	0.99	0.154	0.021	0.223	0.045	13.1	74	3560	56	730
0.022	0.045	0.016	415	0.117	0.030	0.94	0.123	0.027	0.231	0.038	12.6	73	3520	57	724
0.045	0.146	0.027	525	0.226	0.055	1.58	0.203	0.035	0.335	0.067	16.2	84	5240	56	713
0.040	0.120	0.029	511	0.200	0.058	1.51	0.186	0.041	0.350	0.069	16.0	80	4950	56	727
0.022	0.075	0.015	499	0.150	0.042	1.28	0.165	0.032	0.297	0.053	15.4	77	4510	57	726
0.024	0.074	0.020	493	0.168	0.043	1.30	0.195	0.038	0.366	0.049	15.4	78	4550	58	752
0.018	0.080	0.014	494	0.171	0.042	1.25	0.174	0.037	0.259	0.059	15.1	74	4190	57	735

ORTHOPYROXENE

Sample	Rb	Th	U	Ba	Nb	Ta	La	Ce	Pb	Sr	Pr	Nd	Hf	Zr	Sm
NFK1123			0.003		0.011		0.018	0.080		0.15	0.013	0.066	0.027	1.14	
			0.003		0.010	0.003	0.017	0.084		0.16	0.015	0.093	0.034	1.13	
				0.024	0.014		0.018	0.090		0.16	0.017	0.064		1.14	0.029
		0.018	0.006		0.023	0.003	0.350	1.020	0.053	2.63	0.112	0.492	0.034	1.85	0.085
		0.004			0.016		0.013	0.086		0.19	0.014	0.063	0.035	1.16	0.022
					0.012		0.015	0.079		0.18	0.013	0.088	0.035	1.19	0.038
			0.003		0.007		0.022	0.088		0.21	0.015	0.068		1.16	0.034
	0.059			0.044	0.009		0.052	0.171		0.49	0.024	0.093	0.028	1.55	
					0.011		0.017	0.095		0.17	0.014	0.069		1.14	0.037
NFK1108				0.012		0.005	0.005	0.026		0.24	0.015		0.068	1.56	
							0.011	0.044		0.27		0.092		1.42	
					0.013			0.043		0.32		0.088	0.010	0.64	
								0.049	0.040	0.23		0.077	0.033	1.35	
		0.005		0.003	0.014	0.008	0.006	0.043	0.040	0.39		0.085	0.067	1.42	0.007
				0.005	0.016		0.015	0.033		0.28				1.49	
NFK1115	0.147	0.004		0.522	0.192	0.003		0.063		1.21		0.047	0.045	1.98	0.071
					0.010			0.033		0.32	0.013	0.066	0.043	1.65	
		0.004			0.009		0.012	0.031	0.015	0.27	0.013	0.081	0.021	1.63	
					0.010			0.047		0.24	0.020	0.072	0.037	1.70	
								0.043		0.31	0.016	0.091	0.033	1.40	
			0.007	0.006	0.006		0.008	0.041		0.26	0.023	0.098		1.66	0.042
NFR0306		0.004					0.011	0.035		0.18	0.009		0.060	1.05	
							0.008	0.038		0.19			0.049	1.18	
				0.022	0.014			0.031		0.16	0.007		0.034	1.08	0.036
					0.009			0.041		0.15	0.009	0.049	0.044	0.94	
								0.039		0.17	0.007	0.056	0.035	1.12	0.024
					0.007			0.034		0.18	0.009	0.042	0.041	1.11	
					0.008			0.034		0.22	0.007		0.030	1.02	
							0.007	0.047		0.18	0.005	0.069	0.044	1.06	
NFR0307					0.017			0.008		0.08				0.49	
	0.085							0.008		0.08	0.004			0.47	
					0.006			0.008		0.04				0.49	
					0.008			0.007		0.04			0.019	0.46	0.015
					0.009		0.004	0.006		0.04				0.46	0.029
										0.04	0.002	0.038	0.020	0.45	
					0.007			0.007		0.04				0.47	
	0.023				0.040			0.007		0.07	0.004			0.43	
								0.010		0.10			0.031	0.46	
		0.007						0.010		0.07			0.046	0.46	
								0.005		0.04			0.025	0.49	0.018
								0.005		0.04			0.025	0.46	
					0.005			0.006		0.05				0.48	
NFR1109					0.011			0.045		0.31	0.008	0.062		0.62	0.022
					0.009			0.048		0.25	0.012	0.132		0.66	
					0.010		0.008	0.050		0.25	0.014	0.104		0.67	
							0.009	0.044	0.030	0.24	0.010	0.053	0.022	0.62	
							0.009	0.050		0.25	0.010		0.016	0.76	0.037
					0.014		0.010	0.045		0.25	0.014			0.71	
					0.012		0.008	0.049		0.27	0.011	0.087		0.71	0.030
		0.005			0.011		0.008	0.041		0.26	0.009		0.021	0.73	0.039
							0.022	0.077		0.59	0.017	0.079	0.019	0.65	0.053
	0.023			0.088	0.022			0.049	0.047	0.37	0.011	0.098	0.027	0.63	
					0.015		0.045	0.137		0.89	0.026	0.081		0.75	0.046
					0.011	0.003	0.012	0.053		0.30	0.010		0.037	0.69	

Eu	Gd	Tb	Ti	Dy	Ho	Y	Er	Tm	Yb	Lu	Sc	V	Cr	Co	Ni
	0.045	0.007	512	0.083	0.018	0.58	0.055	0.020	0.125	0.026	18.5	80	4190	59	792
	0.024	0.009	477	0.083	0.021	0.58	0.073	0.015	0.135	0.021	18.1	79	4140	59	776
		0.010	517	0.099	0.023	0.61	0.077	0.016	0.155	0.020	18.6	80	4100	59	810
0.024	0.089	0.016	535	0.122	0.026	0.85	0.085	0.019	0.137	0.032	19.8	84	4810	57	770
0.009	0.035	0.008	529	0.085	0.019	0.60	0.073	0.016	0.151	0.021	18.5	78	4250	59	787
0.013	0.051	0.009	542	0.088	0.019	0.58	0.080	0.011	0.149	0.030	18.5	79	4110	59	772
0.010	0.054	0.011	540	0.095	0.019	0.56	0.071	0.013	0.136	0.025	17.2	71	3730	56	759
0.010	0.056	0.011	562	0.092	0.022	0.62	0.093	0.017	0.157	0.027	17.6	74	3850	58	785
0.012	0.032	0.010	542	0.075	0.024	0.61	0.070	0.019	0.131	0.025	17.1	73	3820	58	791
		0.031	667	0.175	0.047	1.37	0.179	0.041	0.357	0.050	24.5	119	4310	70	820
0.017	0.063		606	0.122	0.049	1.26	0.186	0.027	0.267	0.036	22.9	107	3961	70	840
	0.107	0.018	667	0.143	0.047	0.97	0.123	0.027	0.201	0.028	13.8	71	2477	44	530
0.018	0.059	0.014	578	0.098	0.052	1.29	0.188	0.051	0.277	0.040	24.0	113	4041	73	865
	0.086	0.017	591	0.194	0.052	1.43	0.221	0.038	0.344	0.051	24.5	114	4215	69	835
	0.070	0.025	616	0.154	0.045	1.26	0.179	0.027	0.345	0.065	23.7	113	4183	71	846
0.026	0.046	0.010	123	0.153	0.030	0.83	0.095	0.023	0.164	0.040	18.2	58	3227	63	777
0.018	0.052	0.013	120	0.153	0.020	0.83	0.108	0.024	0.227	0.034	18.4	61	3280	59	741
0.014	0.049		120	0.083	0.033	0.80	0.129	0.031	0.184	0.027	18.2	59	3103	61	768
		0.012	123	0.101	0.032	0.82	0.104	0.029	0.177	0.035	18.6	63	3257	62	776
		0.015	121	0.123	0.020	0.69	0.085	0.023	0.149	0.034	18.7	64	3322	57	723
0.023	0.042	0.012	118	0.102	0.021	0.70	0.095	0.021	0.180	0.036	20.3	71	3325	62	777
0.013	0.044	0.008	550	0.137	0.036	1.05	0.141	0.037	0.193	0.047	15.5	84	3590	59	633
0.012	0.043	0.017	591	0.127	0.041	1.04	0.175	0.031	0.248	0.051	16.1	85	3580	59	638
0.016	0.039	0.015	581	0.118	0.037	1.00	0.165	0.029	0.241	0.044	15.6	86	3710	58	624
0.014	0.041	0.012	478	0.104	0.037	0.94	0.130	0.024	0.247	0.040	14.7	80	3260	57	617
0.014	0.076	0.016	536	0.138	0.037	1.06	0.159	0.030	0.310	0.043	16.5	86	3630	59	640
	0.039	0.009	509	0.142	0.039	1.01	0.130	0.034	0.244	0.044	15.2	83	3450	59	641
0.015	0.048	0.014	505	0.121	0.039	1.00	0.108	0.025	0.242	0.040	15.5	81	3400	60	638
0.011	0.078	0.015	559	0.119	0.039	1.03	0.147	0.032	0.260	0.050	15.9	85	3520	62	654
	0.023	0.004	424	0.056	0.013	0.47	0.059	0.014	0.169	0.029	16.1	93	2940	60	788
			423	0.054	0.015	0.46	0.064		0.134	0.029	15.8	92	2920	60	778
0.008	0.028		405	0.060	0.013	0.48	0.063	0.017	0.151	0.030	16.2	93	2960	61	778
0.006			431	0.041	0.015	0.48	0.073	0.016	0.149	0.028	16.2	90	2880	58	752
0.006	0.021		435	0.040	0.011	0.42	0.069	0.014	0.138	0.026	15.5	92	2860	62	765
0.006	0.017	0.005	435	0.063	0.014	0.46	0.055	0.018	0.126	0.021	15.2	88	2900	60	757
0.006		0.006	388	0.053	0.018	0.44	0.058	0.011	0.127	0.028	15.4	89	2920	59	752
	0.036	0.005	363	0.048	0.014	0.45	0.064	0.014	0.112	0.026	15.1	85	2540	58	722
		0.005	388	0.037	0.014	0.45	0.058	0.018	0.130	0.028	16.0	89	2700	57	754
0.006			390	0.048	0.013	0.45	0.079	0.016	0.122	0.029	16.0	89	2700	57	731
		0.004	417	0.047	0.013	0.46	0.074	0.018	0.148	0.027	16.2	92	2820	57	742
	0.020	0.005	434	0.061	0.015	0.49	0.083	0.019	0.131	0.032	16.8	91	2840	60	763
0.008			407	0.051	0.020	0.46	0.089	0.020	0.150	0.030	16.1	91	2780	60	756
0.015	0.057	0.007	351	0.077	0.015	0.59	0.077	0.017	0.136	0.028	11.9	60	3500	60	640
0.014		0.007	368	0.087	0.024	0.64	0.082	0.014	0.144	0.022	12.5	67	3770	61	661
0.013	0.066	0.015	375	0.089	0.023	0.64	0.071	0.019	0.140	0.026	12.0	65	3660	60	641
0.016		0.010	410	0.097	0.024	0.67	0.083	0.018	0.166	0.023	11.5	63	3720	61	628
0.022	0.051	0.014	432	0.078	0.024	0.66	0.072	0.019	0.123	0.026	11.3	64	3760	60	622
0.013	0.060	0.015	419	0.106	0.026	0.68	0.092	0.021	0.102	0.026	11.7	64	3820	61	631
0.017	0.044	0.007	426	0.109	0.023	0.71	0.103	0.018	0.169	0.029	11.6	62	3730	63	645
0.011	0.029	0.011	438	0.071	0.023	0.71	0.105	0.022	0.153	0.031	12.0	63	3660	62	636
0.014	0.043	0.015	383	0.098	0.025	0.68	0.079	0.018	0.151	0.025	11.9	62	3490	62	641
0.017		0.015	414	0.075	0.019	0.60	0.081	0.015	0.180	0.027	9.2	54	3290	59	591
0.019	0.048	0.016	434	0.110	0.026	0.76	0.095	0.021	0.116	0.039	10.2	52	3440	60	621
0.009	0.055	0.012	448	0.113	0.030	0.69	0.097	0.022	0.157	0.031	9.9	53	3430	62	625

ORTHOPYROXENE

Sample	Rb	Th	U	Ba	Nb	Ta	La	Ce	Pb	Sr	Pr	Nd	Hf	Zr	Sm
NFR0309								0.018		0.08		0.032	0.070	2.06	
							0.009	0.022		0.05	0.005	0.033	0.072	2.07	0.004
					0.009			0.022		0.30	0.005		0.084	1.96	
				0.417				0.023		0.12	0.008		0.051	2.18	
			0.004	0.013	0.009			0.017		0.11	0.011		0.049	2.01	0.020
					0.008		0.006	0.017	0.024	0.10	0.005		0.082	2.12	0.038
NFR1107		0.002		0.128	0.013			0.013		0.16	0.007		0.053	1.38	0.074
						0.005	0.007	0.025	0.043	0.17	0.010		0.050	1.32	0.037
		0.011						0.019		0.22	0.007		0.026	1.12	
				0.012	0.004					0.17	0.007			1.23	
		0.001					0.005	0.012		0.20			0.039	1.15	0.037
	0.096			0.034	0.135			0.013	0.070	0.39			0.053	1.76	0.045
					0.011					0.18		0.051	0.062	1.17	
NMC1301					0.014		0.026	0.079		0.34	0.013	0.117	0.060	3.37	0.036
			0.004	0.002	0.023		0.019	0.072		0.38	0.028	0.123	0.092	3.47	0.019
		0.003			0.041		0.018	0.093		0.34	0.011	0.108	0.063	3.19	
				0.001	0.018	0.005	0.011	0.098		0.33	0.018	0.114	0.055	3.00	
			0.005	0.025	0.026		0.016	0.078		0.41	0.017	0.116	0.058	3.14	
					0.043		0.018	0.076		0.31	0.014	0.081	0.045	2.67	
					0.046		0.014	0.062		0.46	0.017	0.095	0.031	2.80	
NMC1309							0.004	0.013		0.11	0.006		0.032	0.74	
		0.001	0.005		0.014			0.019		0.13	0.006	0.042		0.76	
				0.004			0.006	0.015		0.13		0.055	0.045	0.87	
						0.002	0.006	0.021		0.10	0.006	0.051	0.023	0.82	
				0.005			0.006	0.011		0.11		0.014	0.026	0.79	0.021
						0.005		0.016		0.16	0.006	0.043		0.75	
NMC1322				0.043				0.017		0.10		0.041	0.020	0.55	
	0.240			0.097			0.020	0.060		0.64	0.008	0.040	0.027	0.59	
	0.122			0.037				0.022	0.134	0.10				0.47	
				0.413			0.020	0.017	0.219	0.69	0.023		0.020	0.44	
				0.656				0.014		0.15	0.012		0.018	0.51	
			0.007	0.063				0.029	0.202	0.16	0.006		0.046	0.43	
	0.174	0.040		1.818	0.011			0.033		0.94				0.48	0.044
NMC1336A			0.003						0.033	0.08	0.009		0.053	1.89	0.041
							0.002	0.012		0.10		0.053	0.051	1.26	
		0.004		0.070		0.003		0.010		0.06			0.051	1.13	
		0.007				0.004	0.006	0.011	0.033	0.11		0.032		1.24	0.032
			0.006		0.008	0.002				0.07	0.006		0.068	1.21	
	0.063		0.007	0.603	0.031			0.038	0.830	0.44		0.058	0.034	1.19	0.026
					0.003		0.010		0.043	0.08	0.010		0.075	1.25	
NMM1126								0.004		0.03	0.003			0.25	
	0.011	0.005			0.008					0.04				0.29	
										0.03				0.29	
		0.003						0.005		0.04			0.016	0.33	
	0.039			0.050	0.020		0.005			0.11			0.018	0.35	
		0.007			0.012	0.002		0.017		0.32	0.006			0.49	0.038
					0.010		0.007	0.017		0.28	0.004		0.033	0.42	
	0.092				0.007					0.08		0.020		0.31	
					0.004			0.005		0.05			0.024	0.28	
					0.007		0.002	0.004		0.04			0.017	0.28	0.017
					0.007			0.006		0.04	0.002			0.29	
NMM0318				0.011	0.008	0.002	0.014	0.043		0.16	0.016	0.062		2.44	0.030
		0.006	0.009	0.003				0.058		0.15	0.012	0.042	0.043	2.74	
	0.078	0.011					0.015	0.052		0.17	0.008	0.115	0.057	2.87	
	0.149			0.022	0.023		0.016	0.061		0.34	0.023	0.056	0.042	2.94	0.037
					0.011	0.007	0.010	0.069		0.18	0.018	0.107	0.071	3.10	0.048
			0.012	0.002			0.015	0.059		0.21	0.010	0.064	0.068	2.72	0.074
		0.011	0.005	0.005	0.005	0.007	0.004	0.049		0.17	0.014	0.090	0.064	2.76	
		0.007	0.011	0.004	0.001			0.047		0.13	0.009	0.062	0.087	2.14	

Eu	Gd	Tb	Ti	Dy	Ho	Y	Er	Tm	Yb	Lu	Sc	V	Cr	Co	Ni
0.012	0.071	0.015	845	0.138	0.053	1.24	0.207	0.037	0.252	0.052	20.4	99	2366	59	701
0.009	0.079	0.014	859	0.171	0.038	1.30	0.181	0.037	0.277	0.057	21.2	100	2358	60	708
0.011	0.029	0.014	814	0.174	0.045	1.23	0.158	0.033	0.281	0.056	21.3	102	2174	62	739
0.014	0.037	0.021	835	0.184	0.043	1.34	0.190	0.034	0.307	0.068	20.6	101	2152	61	736
0.010		0.013	844	0.176	0.047	1.32	0.167	0.031	0.349	0.051	21.3	106	2303	68	820
0.009	0.090	0.019	792	0.200	0.044	1.39	0.213	0.029	0.363	0.047	20.9	103	2071	65	792
0.008		0.010	531	0.095	0.034	0.90	0.113	0.018	0.163	0.026	23.1	104	3859	62	800
0.017	0.087	0.010	515	0.094	0.027	0.86	0.090	0.015	0.174	0.039	22.8	102	3844	62	796
	0.063		502	0.131	0.025	0.72	0.099	0.022	0.153	0.038	20.9	99	3745	61	786
0.016	0.076		541	0.099	0.037	0.79	0.091	0.016	0.196	0.019	21.6	100	3625	58	740
0.014	0.059	0.013	549	0.167	0.024	0.78	0.131	0.024	0.142	0.030	22.0	98	3677	58	744
		0.019	516	0.085	0.019	0.84	0.084	0.028	0.139	0.024	22.3	100	3655	60	766
	0.074	0.013	531	0.070	0.027	0.86	0.090	0.015	0.136	0.028	22.2	101	3843	61	786
	0.040	0.015	268	0.122	0.025	0.76	0.110	0.014	0.122	0.026	22.2	99	4167	66	838
0.020	0.055	0.011	275		0.029	0.76	0.106	0.021	0.130	0.028	23.4	101	4195	65	833
	0.074	0.011	258	0.111	0.029	0.70	0.098	0.012	0.145	0.032	22.4	97	4002	66	831
	0.049	0.014	216	0.059	0.017	0.57	0.094	0.027	0.073	0.022	20.4	89	3895	59	751
0.014		0.011	248	0.077	0.027	0.68	0.083	0.011	0.118	0.028	21.9	94	3920	65	827
	0.051	0.012	241	0.053	0.023	0.64	0.080	0.013	0.168	0.020	21.8	96	4159	67	837
		0.007	252	0.073	0.023	0.52	0.065	0.012	0.148	0.026	22.3	97	4111	65	821
	0.088	0.013	330	0.139	0.034	0.94	0.132	0.029	0.303	0.054	20.8	99	3038	58	743
	0.040	0.009	321	0.107	0.025	0.96	0.170	0.021	0.241	0.039	21.5	101	3058	63	786
	0.054	0.012	330	0.084	0.033	1.00	0.140	0.033	0.246	0.026	20.7	100	3020	60	763
		0.010	329	0.102	0.038	0.93	0.148	0.030	0.294	0.056	21.8	102	3089	63	783
	0.030	0.014	325	0.104	0.024	0.92	0.130	0.030	0.202	0.046	21.5	101	3117	63	795
0.010		0.009	322	0.124	0.043	0.93	0.119	0.040	0.244	0.050	19.7	95	2928	58	723
		0.009	321	0.071	0.044	0.95	0.150	0.027	0.150	0.049	20.0	91	3332	61	796
		0.009	283	0.083	0.028	0.87	0.098	0.016	0.203	0.042	16.4	78	3022	47	618
0.013			326	0.084	0.019	0.91	0.138	0.017	0.211	0.039	19.7	93	3371	60	793
0.024		0.016	289	0.083	0.033	0.96	0.132	0.025	0.213	0.045	18.5	86	3088	58	766
			295	0.080	0.027	0.79	0.147	0.019	0.167	0.058	17.8	83	3122	56	748
		0.016	281	0.124	0.030	0.96	0.051	0.020	0.193	0.039	18.9	87	3009	61	805
		0.010	272	0.101	0.017	0.85	0.114	0.025	0.157	0.040	17.7	81	3065	59	782
0.021	0.081	0.028	965	0.139	0.065	1.41	0.146	0.042	0.291	0.065	19.1	105	5425	63	828
0.015		0.016	802	0.195	0.051	1.24	0.174	0.034	0.238	0.052	17.4	92	4155	62	831
	0.082	0.014	716	0.123	0.039	1.33	0.167	0.025	0.291	0.052	18.1	92	3546	67	878
	0.078	0.012	636	0.140	0.047	1.18	0.209	0.032	0.335	0.044	17.3	86	3451	64	836
	0.046	0.016	714	0.162	0.039	1.19	0.161	0.023	0.168	0.053	17.2	85	3440	63	837
0.017		0.021	687	0.141	0.064	1.22	0.178	0.038	0.318	0.046	17.4	86	3407	64	854
0.012	0.039	0.014	728	0.149	0.047	1.30	0.157	0.030	0.301	0.054	17.4	88	3487	64	844
		0.005	368	0.061	0.023	0.59	0.080	0.015	0.156	0.028	16.4	93	3520	59	772
	0.023		376	0.070	0.020	0.63	0.114	0.021	0.177	0.036	16.1	92	3570	59	772
0.010		0.007	388	0.070	0.024	0.62	0.092	0.019	0.149	0.027	16.4	93	3660	59	764
		0.006	357	0.078	0.022	0.73	0.113	0.022	0.199	0.043	18.4	89	3200	59	759
0.009		0.005	359	0.059	0.027	0.75	0.102	0.019	0.202	0.038	18.6	90	3190	60	781
	0.042	0.015	485	0.114	0.035	0.96	0.155	0.027	0.258	0.047	21.1	107	4510	62	803
0.010	0.037	0.012	446	0.100	0.027	0.89	0.117	0.027	0.233	0.043	19.9	100	4180	59	767
0.009			357	0.110	0.025	0.73	0.102	0.025	0.193	0.038	17.6	87	3040	60	792
	0.022	0.006	339	0.060	0.022	0.66	0.085	0.023	0.204	0.030	16.6	86	3040	56	737
0.005	0.020	0.008	351	0.089	0.024	0.67	0.086	0.020	0.198	0.035	17.4	90	3130	58	749
0.006		0.008	345	0.068	0.023	0.67	0.094	0.022	0.204	0.040	17.2	91	3180	58	762
		0.021	491	0.165	0.042	1.33	0.209	0.030	0.358	0.042	19.1	90	2439	63	724
0.021	0.123	0.019	538	0.116	0.031	1.32	0.215	0.045	0.389	0.053	19.3	93	2753	65	754
	0.101	0.017	489	0.156	0.043	1.28	0.152	0.026	0.354	0.049	19.1	90	2446	65	733
0.019	0.077	0.019	529	0.226	0.027	1.32	0.179	0.045	0.319	0.069	18.9	90	2516	64	733
	0.071	0.019	548	0.114	0.041	1.35	0.162	0.038	0.382	0.057	18.3	91	2660	61	718
0.020	0.080	0.019	471	0.156	0.043	1.21	0.141	0.047	0.306	0.071	18.1	86	2206	60	696
0.015	0.089	0.015	525	0.117	0.036	1.25	0.121	0.046	0.300	0.055	17.8	88	2268	62	719
0.014	0.068	0.019	716	0.129	0.037	1.17	0.241	0.035	0.323	0.060	18.4	99	2719	60	709

ORTHOPYROXENE

Sample	Rb	Th	U	Ba	Nb	Ta	La	Ce	Pb	Sr	Pr	Nd	Hf	Zr	Sm
NMM1115		0.011	0.017				0.002	0.006		0.09			0.043	1.01	
		0.015	0.017	0.002	0.005					0.09			0.019	1.15	
		0.021	0.019		0.004			0.010		0.05			0.026	1.01	0.029
		0.019	0.016	0.002				0.008		0.07		0.045		1.02	
		0.021				0.001		0.009		0.07		0.044	0.028	0.95	
		0.036	0.018		0.010		0.007	0.010		0.09			0.023	1.10	0.035
		0.031	0.023							0.06	0.005	0.023	0.029	0.93	0.027
NME1122				0.098				0.009		0.09	0.002		0.020	0.51	
	0.038							0.010		0.05	0.002			0.56	
					0.005			0.009		0.07		0.031	0.023	0.54	
					0.006		0.007	0.017		0.16			0.023	0.59	
					0.006			0.012		0.08	0.003	0.038		0.58	
					0.006			0.007		0.09			0.026	0.58	
								0.009		0.06				0.64	
				0.016			0.010	0.018		0.22	0.005			0.60	
	0.010	0.003			0.007		0.005	0.014		0.08				0.64	
					0.009			0.013		0.07			0.023	0.58	
NME0528				0.671			0.016	0.064		0.33	0.013	0.082	0.043	2.32	0.059
			0.003	0.001	0.010		0.005	0.025		0.23			0.048	2.11	
				0.003				0.067		0.19		0.105	0.047	2.31	
		0.014		0.028			0.012	0.037		0.22	0.014	0.056		2.27	0.046
		0.006	0.006		0.013	0.003	0.016	0.043	0.037	0.25	0.015	0.053		1.91	
				0.086	0.028		0.019	0.023		0.39	0.008		0.038	2.19	0.051
NME1116		0.008					0.001	0.006		0.14		0.028	0.033	0.74	0.032
			0.010	0.011		0.002		0.006		0.18		0.034	0.033	0.88	0.031
			0.003					0.010	0.011	0.15	0.006	0.021		0.74	0.019
			0.003					0.012		0.12			0.033	0.90	
				0.003						0.14		0.035	0.029	0.89	0.024
		0.002			0.009					0.16	0.005	0.032	0.023	0.76	
			0.018	0.087	0.011			0.015	0.029	0.30		0.026		0.97	
NBN0302A										0.05			0.063	1.50	
										0.18		0.068	0.074	1.91	
					0.022			0.011		0.14	0.006		0.080	1.76	
													0.076	1.22	
													0.071	1.42	
										0.09	0.010		0.050	1.16	
										0.12		0.080		1.28	
											0.013			0.99	
								0.033					0.074	1.25	
										0.12			0.035	1.22	
													0.075	1.79	
									0.028				0.047	1.34	0.062
		0.008		0.038			0.005	0.012		0.22		0.029	0.044	1.61	
	0.024				0.021			0.015		0.09			0.090	1.62	0.033
		0.008					0.005			0.07			0.030	1.50	
NBN0305										0.12	0.014		0.026	0.47	
	0.110			0.109	0.032		0.009			0.16				0.57	
										0.06			0.056	0.48	0.054
				0.067	0.018		0.013			0.12			0.049	0.50	
										0.07			0.030	0.41	
					0.019			0.019	0.030	0.11				0.44	0.059
								0.023		0.11	0.015			0.38	
										0.24				0.44	
										0.17				0.50	

Eu	Gd	Tb	Ti	Dy	Ho	Y	Er	Tm	Yb	Lu	Sc	V	Cr	Co	Ni
	0.062	0.012	461	0.067	0.028	0.85	0.149	0.015	0.199	0.056	20.4	93	3075	60	753
	0.042	0.013	499	0.122	0.019	0.95	0.111	0.029	0.249	0.040	21.9	100	3205	62	783
0.011	0.039	0.010	501	0.139	0.034	0.98	0.123	0.016	0.186	0.042	21.8	100	3212	63	801
			480	0.065	0.036	0.85	0.148	0.024	0.194	0.045	21.2	95	3118	64	810
	0.047		488	0.096	0.032	0.86	0.138	0.027	0.213	0.034	21.3	96	3285	63	806
	0.057	0.010	490	0.104	0.027	0.97	0.143	0.023	0.178	0.044	22.0	100	3737	65	807
0.011		0.018	474	0.060	0.024	0.87	0.123	0.026	0.219	0.034	21.6	99	4142	64	805
		0.008	415	0.044	0.013	0.44	0.043	0.014	0.109	0.018	14.3	82	2970	52	667
0.008		0.004	444	0.044	0.016	0.41	0.075	0.011	0.138	0.023	15.1	86	3070	55	694
	0.019		418	0.056	0.014	0.43	0.066	0.011	0.102	0.022	14.8	83	3100	54	696
0.008		0.006	447	0.075	0.018	0.51	0.057	0.015	0.118	0.018	15.3	81	3130	54	690
0.005	0.029	0.007	487	0.063	0.018	0.44	0.065	0.017	0.094	0.019	15.1	86	3150	54	691
0.008		0.006	493	0.055	0.014	0.44	0.067	0.011	0.112	0.021	14.8	87	3160	54	717
0.008		0.005	477	0.072	0.018	0.44	0.076	0.012	0.107	0.026	15.3	86	3150	53	694
	0.039	0.005	457	0.070	0.022	0.47	0.070	0.013	0.111	0.015	14.5	84	3090	53	695
0.009		0.006	473	0.052	0.018	0.46	0.074	0.012	0.107	0.022	15.2	87	3160	53	697
		0.007	458	0.049	0.017	0.44	0.080	0.016	0.106	0.024	14.6	88	3230	55	711
0.020	0.078	0.015	438	0.125	0.036	0.82	0.094	0.029	0.231	0.036	18.6	91	4431	61	744
0.011	0.089	0.010	421	0.080	0.027	0.76	0.079	0.028	0.203	0.025	17.0	82	3595	58	703
	0.046		438	0.108	0.033	0.83	0.133	0.013	0.192	0.050	19.4	92	3782	65	803
0.020	0.086	0.013	441	0.112	0.051	0.79	0.104	0.028	0.194	0.041	19.6	96	3908	65	799
0.023	0.075	0.016	407	0.090	0.029	0.86	0.107	0.027	0.184	0.029	19.2	90	3696	63	775
		0.006	403	0.136	0.035	0.81	0.115	0.024	0.184	0.027	19.3	88	3609	62	777
0.008			410	0.072	0.026	0.74	0.122	0.022	0.184	0.032	21.2	94	3152	59	744
	0.057	0.014	441		0.023	0.82	0.125	0.028	0.179	0.039	23.1	105	3401	64	801
0.010	0.041		418	0.086	0.040	0.83	0.126	0.025	0.225	0.040	21.7	99	3311	61	783
0.012		0.011	447	0.115	0.045	0.80	0.113	0.028	0.195	0.036	22.2	103	3579	61	773
	0.044	0.018	452	0.107	0.036	0.83	0.136	0.017	0.213	0.042	22.1	103	3499	61	763
		0.010	449	0.079	0.034	0.82	0.087	0.018	0.198	0.047	22.6	103	3242	61	768
		0.014	449	0.110	0.021	0.90	0.122	0.027	0.225	0.035	23.2	108	3519	64	819
	0.058	0.017	557	0.073	0.024	0.78	0.074	0.026	0.194	0.026	14.8	84	2996	60	716
			681	0.102	0.031	0.82	0.111	0.021	0.195	0.040	16.6	109	3001	60	730
0.007	0.049	0.011	689	0.120	0.035	0.87	0.065	0.028	0.257	0.026	16.7	108	3094	61	728
	0.061		395			0.79	0.149	0.016		0.009	15.1	79	2592	64	752
0.031			383	0.077		0.82		0.034	0.271	0.060	15.0	79	2585	62	766
		0.022	403	0.107		0.79	0.182	0.022	0.267	0.044	15.2	78	2404	63	755
0.017		0.012	365	0.133	0.017	0.77		0.021	0.222		15.5	80	2435	62	761
			359	0.069	0.058	0.73	0.156		0.230	0.032	15.3	78	2353	63	797
0.041		0.010	329	0.159	0.025	0.85	0.090	0.035	0.332	0.039	15.8	84	2139	63	752
			309			0.89			0.219	0.036	17.0	82	2146	64	740
0.021	0.076	0.010	298		0.051	0.80	0.241	0.050	0.408	0.045	16.8	80	2105	59	731
		0.012	305	0.051	0.038	0.92	0.154	0.025	0.228	0.032	14.9	79	2078	63	757
0.009	0.056	0.008	591	0.092	0.022	0.85	0.135	0.024	0.200	0.041	15.6	95	2681	59	718
0.006		0.009	636	0.078	0.034	0.85	0.187	0.026	0.265	0.048	16.5	102	2975	59	742
0.020	0.048	0.009	435	0.090	0.016	0.82	0.124	0.016	0.206	0.040	16.8	87	2380	61	732
0.014	0.053		308		0.014	0.53	0.074	0.013	0.095	0.036	18.3	91	2770	60	752
	0.043		311	0.078	0.025	0.44	0.153	0.028	0.208	0.012	18.9	93	2884	60	753
			328	0.118	0.007	0.51	0.067	0.015	0.161	0.017	19.2	93	2923	61	763
			318	0.062	0.008	0.54	0.094	0.021	0.070	0.040	19.4	95	2950	60	765
			305	0.105	0.013	0.52	0.131	0.008	0.137		17.8	91	2911	61	759
0.011	0.042		344	0.076	0.027	0.53		0.016	0.142	0.021	19.6	98	3102	61	756
			303	0.052	0.013	0.44			0.088	0.014	18.2	99	3142	61	770
		0.010	308	0.097	0.021	0.33	0.142	0.017	0.234		18.4	101	3242	62	790
		0.019	309			0.48	0.116		0.153	0.017	18.0	97	3103	62	770

ORTHOPYROXENE

Sample	Rb	Th	U	Ba	Nb	Ta	La	Ce	Pb	Sr	Pr	Nd	Hf	Zr	Sm
NBN0311	0.025	0.005			0.037					0.10	0.004	0.068	0.040	1.28	
								0.006		0.09			0.045	1.15	
										0.09			0.041	1.13	0.053
					0.024				0.025	0.07	0.011	0.036	0.070	1.03	
				0.043						0.07				1.10	
								0.005		0.09	0.007		0.035	0.94	
	0.018							0.021		0.08				0.97	
	0.006			0.035					0.019	0.12			0.034	0.86	
					0.042			0.022		0.07		0.019	0.031	0.95	
										0.09				1.16	
										0.09	0.003		0.036	1.05	
					0.015					0.10			0.023	0.98	0.023
	0.386	0.089								0.75			0.077	1.09	
					0.018					0.13			0.029	1.00	0.083
	0.141									0.33			0.030	0.98	
NBN0316				0.043	0.008					0.03			0.060	1.55	
					0.022			0.010		0.03		0.039	0.054	1.53	
	0.316	0.036						0.025		0.32	0.012			1.55	
							0.031						0.102	1.08	
								0.023					0.034	1.13	
											0.012	0.067		1.27	0.113
														1.65	
														1.04	
													0.124	1.05	
NBN0319				0.080	0.023			0.024		0.04			0.109	1.57	
										0.02	0.005		0.051	1.59	
					0.017			0.008		0.03			0.057	1.52	
					0.029					0.03			0.047	1.33	
	0.042									0.03			0.055	1.32	
								0.023		0.01			0.057	1.21	
					0.011			0.009					0.093	1.21	
								0.012		0.03			0.088	1.45	
					0.032			0.017					0.073	1.31	
NBN0321					0.017		0.005			0.15			0.066	1.17	
					0.013		0.004			0.08		0.026	0.056	1.18	
	0.018				0.033					0.05			0.042	1.06	0.023
					0.014					0.06				0.98	
					0.027				0.012	0.07	0.005	0.019	0.060	1.14	
	0.394	0.014							0.458	0.20			0.060	1.38	
		0.012		0.173					0.140	0.18		0.043		1.25	
					0.018					0.08			0.031	1.21	0.040
				0.040				0.015		0.06	0.004		0.063	1.13	0.034
								0.012		0.07	0.005		0.050	1.32	
		0.007			0.015					0.08			0.043	1.18	
					0.025			0.011		0.06	0.004		0.060	1.26	0.023
				0.040	0.010					0.08	0.005	0.040	0.040	1.12	0.022

Eu	Gd	Tb	Ti	Dy	Ho	Y	Er	Tm	Yb	Lu	Sc	V	Cr	Co	Ni
0.020	0.039	0.023	548	0.073	0.022	0.85	0.147	0.025	0.299	0.051	16.2	94	2866		
0.010		0.010	529	0.097	0.024	0.88		0.027	0.202	0.059	15.7	93	2875		
	0.094	0.013	560	0.050	0.039	0.86	0.173	0.025	0.217	0.045	15.5	93	2900		
	0.097	0.011	456	0.053	0.021	0.80	0.085	0.030	0.377	0.027	14.9	82	2485		
		0.010	463	0.149	0.029	0.79	0.124	0.022	0.336	0.044	15.2	85	2406		
0.013	0.035	0.012	438	0.140	0.024	0.70	0.086	0.014	0.201	0.035	14.9	85	2442		
	0.020		413	0.120	0.029	0.80	0.132	0.023	0.204	0.036	14.5	84	2379		
	0.030	0.012	398	0.072	0.038	0.74	0.097	0.019	0.249	0.044	15.0	85	2389		
0.009		0.011	429	0.093	0.034	0.70	0.090	0.026	0.223	0.030	14.8	85	2518		
0.015	0.021	0.012	462	0.087	0.020	0.82	0.135	0.027	0.226	0.040	15.2	89	2860		
		0.008	459	0.122	0.030	0.84	0.128	0.026	0.248	0.048	14.9	86	2629		
0.019		0.009	465	0.044	0.037	0.75	0.134	0.019	0.297	0.047	14.2	84	2478		
		0.013	396	0.091	0.021	0.89	0.249	0.017	0.301	0.063	15.0	84	2282		
			397			0.79	0.133	0.029		0.034	15.2	86	2300		
		0.016	409	0.147	0.037	0.95	0.240	0.028	0.137	0.041	15.3	85	2259		
0.017		0.017	366	0.081	0.038	0.94	0.152	0.014	0.258	0.059	18.7	85	2024	61	730
0.012	0.046	0.004	367	0.065	0.035	0.93	0.130	0.035	0.231	0.050	19.3	85	2013	63	736
			354	0.081	0.026	0.98	0.159	0.025	0.171	0.057	17.1	84	2065	65	783
0.028		0.013	332	0.072	0.045	0.81	0.124	0.023	0.215	0.045	17.0	86	2031	65	752
		0.013	340	0.145	0.027	0.83	0.083	0.018	0.307	0.036	16.0	85	2139	65	765
		0.015	355	0.088		0.68	0.142	0.052	0.212	0.035	17.4	86	2198	66	766
0.019	0.073		328	0.153		0.73	0.261		0.227	0.032	15.7	81	2125	66	766
			360	0.156	0.040	0.71	0.203	0.039	0.199	0.049	15.7	81	2105	67	784
		0.009	353	0.112	0.028	0.82		0.032	0.254	0.010	15.8	85	2187	64	782
0.013		0.011	371	0.081	0.030	0.82	0.098	0.038	0.206	0.053	18.0	84	1945		
0.009	0.046		381	0.085	0.025	0.68	0.135	0.024	0.284	0.047	18.3	87	2094		
		0.011	365	0.085	0.032	0.74	0.155	0.023	0.265	0.057	18.0	84	1969		
0.016	0.038	0.012	319	0.080	0.030	0.70	0.103	0.035	0.186	0.022	16.0	87	2079		
		0.009	324	0.070	0.026	0.66	0.060	0.028	0.177	0.031	16.3	87	2050		
0.016		0.008	319	0.137	0.021	0.66	0.132		0.372	0.017	15.3	84	1979		
		0.024	366	0.079	0.027	0.72	0.075		0.215	0.030	17.1	86	2181		
		0.012	348	0.093	0.025	0.67	0.093	0.030	0.236	0.036	16.4	85	2234		
		0.010	371	0.078	0.039	0.69	0.151	0.024	0.082	0.048	16.2	86	2218		
0.010	0.080		665	0.097	0.024	0.72	0.131	0.027	0.154	0.024	17.7	98	2696	56	679
		0.010	614	0.089	0.027	0.69	0.126	0.017	0.156	0.040	16.9	94	2657	56	676
0.010	0.023	0.006	576	0.052	0.029	0.64	0.090	0.021	0.118	0.033	17.1	93	2634	54	683
		0.012	445	0.089	0.028	0.62	0.150	0.021	0.117	0.025	16.8	91	2352	59	724
0.009	0.033	0.012	455	0.144	0.031	0.75	0.164	0.016	0.194	0.026	17.2	92	2416	58	719
0.016		0.022	443	0.160	0.052	0.73		0.012	0.216	0.031	17.2	90	2552	63	764
0.041		0.013	468	0.081	0.071	0.82		0.013	0.183	0.068	18.3	89	2521	66	798
		0.013	607	0.120	0.036	0.82	0.074	0.030	0.267	0.032	19.2	96	2762	60	719
	0.058	0.011	754	0.081	0.032	0.79	0.154	0.029	0.219	0.040	19.2	103	3301	60	730
	0.101	0.012	744	0.151	0.035	0.79	0.102	0.027	0.233	0.040	18.4	104	3438	60	731
	0.101	0.015	539	0.096	0.031	0.82	0.123	0.021	0.201	0.020	18.4	98	2836	60	717
	0.084	0.017	619	0.102	0.035	0.83	0.102	0.019	0.250	0.064	18.9	104	3054	62	731
0.013	0.046	0.009	570	0.081	0.025	0.77	0.113	0.014	0.125	0.036	17.9	96	2839	61	742

CLINOPYROXENE

Sample	Rb	Th	U	Ba	Nb	Ta	La	Ce	Pb	Sr	Pr	Nd	Hf	Zr	Sm
NMS1302A	0.178	0.063	1.67	0.096	0.537	0.072	1.11	3.06	0.12	36.4	0.52	2.69	0.20	5.80	0.54
		0.035	0.018	0.972	0.486	0.074	1.11	3.08	0.06	34.9	0.51	2.43	0.19	5.46	0.56
	0.045	0.081	0.025	0.042	0.540	0.081	1.18	3.39		39.6	0.57	3.21	0.14	4.74	0.52
		0.050	0.025	0.031	0.469	0.073	1.17	3.19		34.8	0.55	2.67	0.19	6.06	0.68
NMS1304		0.061	0.009	0.062	0.022	0.015	3.14	8.63	0.19	124	1.30	5.71	0.60	17.0	1.40
		0.038		0.085	0.029	0.011	2.66	7.31	0.22	116	1.07	5.44	0.51	14.9	1.28
		0.030	0.019	0.051	0.034	0.009	2.93	7.73	0.18	110	1.20	5.32	0.73	17.3	1.26
		0.051	0.012	0.052	0.023	0.012	3.09	8.68	0.21	122	1.28	6.44	0.58	16.9	1.63
		0.046	0.011	0.047	0.017		2.70	7.52	0.22	111	1.14	5.58	0.64	17.1	1.47
		0.019	0.012	0.036		0.011	2.78	7.54	0.19	113	1.20	5.34	0.65	16.0	1.16
		0.040		0.058			2.85	7.82	0.22	114	1.19	5.35	0.65	16.6	1.46
		0.044	0.013	0.078	0.019	0.016	3.20	8.44	0.19	123	1.24	5.89	0.66	16.7	1.43
		0.031		0.067		0.008	2.65	7.41	0.16	113	1.08	5.34	0.49	15.1	1.38
	0.731	0.095	0.027	0.362	0.184		2.93	7.74	1.32	130	1.16	4.90	0.75	16.2	1.29
		0.033	0.011	0.058			2.84	7.74	0.15	119	1.14	5.33	0.56	15.2	1.36
NMS1305		0.249	0.076	0.098	0.158	0.013	4.87	14.52		102	2.21	9.42	1.13	56.3	2.50
		0.208	0.050	0.084	0.146	0.014	4.28	12.48		95.5	1.94	8.33	1.28	66.6	1.92
		0.230	0.063	0.083	0.113	0.026	4.56	13.65	0.12	99.2	2.09	9.40	1.30	70.3	2.20
	0.080	0.214	0.053	0.255	0.395	0.089	4.80	14.68		99.4	2.29	10.40	1.86	102	2.56
	0.372	0.224	0.053	0.813	0.629	0.103	4.58	14.32		102	2.33	10.91	2.75	116	2.73
		0.243	0.082	0.103	0.545	0.092	5.30	16.47		105	2.62	12.59	2.02	104	2.90
NMS1308	0.062	0.042	0.027	0.084	0.048	0.016	1.05	3.35	0.56	57.6	0.65	3.59	1.15	38.9	1.34
		0.050	0.013	0.249	0.084	0.043	1.21	3.91	0.11	65.1	0.72	4.22	1.18	39.8	1.47
		0.038	0.025	0.025	0.113	0.042	1.31	4.17		70.7	0.75	4.49	0.93	35.5	1.84
	0.056	0.058	0.024	0.214	0.055	0.023	1.06	3.60		59.2	0.69	4.16	1.23	41.5	1.57
		0.055	0.017	0.187	0.064	0.023	1.11	3.49	0.09	59.4	0.67	4.17	1.26	40.2	1.56
		0.037	0.025	0.022	0.040	0.021	1.03	3.40		57.3	0.67	3.60	0.80	29.1	1.32
		0.043	0.015		0.072	0.029	1.18	3.76		61.5	0.69	4.44	0.75	30.7	1.57
NMS1310				0.065	0.052	0.023	0.99	3.57		71.6	0.67	4.19	0.89	32.0	1.71
		0.032	0.009	0.015	0.043	0.018	1.01	3.60		71.4	0.67	4.01	0.82	30.6	1.71
	0.049	0.021		0.060	0.060	0.011	1.08	3.39		71.4	0.65	4.04	0.93	30.4	1.73
				0.020	0.199	0.038	1.11	3.67		82.0	0.74	3.98	0.93	30.0	1.80
		0.021	0.010	0.050	0.054	0.019	0.98	3.53		72.4	0.65	3.94	1.02	30.4	1.71
		0.013	0.013	0.066	0.077	0.019	1.06	3.60		71.2	0.72	3.96	1.01	31.6	1.38
		0.025		0.013	0.159	0.023	1.04	3.60		80.1	0.68	4.27	0.97	29.3	1.69
		0.026		0.013	0.103	0.021	0.99	3.56		73.7	0.73	4.27	0.94	29.7	1.43
NJS1302			0.011	0.039	0.014	0.013	1.84	8.78		43.1	1.94	11.46	3.65	135	4.05
		0.022	0.014	0.046		0.018	1.79	9.53		46.0	2.05	12.46	3.47	136	4.22
		0.028		0.253	0.031	0.020	1.89	8.91		42.4	1.91	11.44	3.57	133	3.58
	0.038	0.019	0.014	0.040	0.027	0.024	1.96	9.68		47.9	2.10	12.26	3.44	130	3.73
		0.019	0.012	0.038	0.035	0.032	1.92	9.56		48.5	2.09	12.27	3.34	129	3.88
			0.016	0.045	0.030	0.039	2.20	10.18		51.7	2.19	12.30	3.20	127	4.23
		0.012	0.009	0.297	0.094	0.012	2.02	9.57		48.6	2.08	11.52	3.11	128	4.04
		0.026		0.043	0.029	0.026	2.10	9.95		51.7	2.13	11.92	2.83	112	3.61
		0.037		0.052	0.022	0.021	2.03	9.45		47.2	2.03	11.29	2.86	111	3.49
NJS1304		0.015	0.003	0.059	0.062	0.035	2.21	10.66		62.0	2.20	12.02	2.43	104	3.75
	0.086	0.028	0.015	0.792	0.212	0.025	2.16	9.48	0.06	52.0	1.92	10.79	2.46	100	3.32
		0.059	0.012	0.122	0.020	0.067	2.02	9.21		54.1	1.97	10.98	2.53	98.8	3.04
		0.027		0.098	0.039	0.017	2.12	9.56		57.5	1.99	11.37	2.55	98.1	3.03
NJS1306		0.039	0.027	0.070	0.022	0.009	2.80	7.23		76.1	1.08	5.52	1.15	36.5	1.98
		0.070	0.015	0.032		0.008	2.36	5.78		69.1	0.92	5.05	1.13	37.2	1.67
		0.051	0.014	0.034	0.025	0.005	2.73	7.16	0.05	73.5	1.02	5.39	1.12	36.2	1.69
		0.057	0.017	0.067			1.90	5.05		68.2	0.87	4.94	1.08	36.5	1.75
		0.060	0.013	0.021	0.010		1.42	4.03		67.4	0.82	4.70	1.12	38.0	1.88
		0.067	0.015	0.030	0.026		1.92	5.27	0.08	66.5	0.95	5.06	1.21	37.4	1.89
		0.040	0.018	0.038	0.015		1.87	5.08		66.6	0.88	5.34	1.15	38.6	2.08

Eu	Gd	Tb	Ti	Dy	Ho	Y	Er	Tm	Yb	Lu	Sc	V	Cr	Co	Ni
0.19	0.53	0.079	307	0.65	0.089	2.97	0.30	0.04	0.28	0.05	77	188	5141	23	375
0.20	0.66	0.093	297	0.53	0.12	2.96	0.34	0.05	0.32	0.05	72	182	5864	20	338
0.22	0.40	0.092	269	0.55	0.10	2.77	0.25	0.05	0.31	0.05	60	173	7174	22	344
0.21	0.65	0.10	324	0.57	0.12	3.20	0.35	0.05	0.35	0.06	66	184	6804	20	342
0.50	1.60	0.25	1525	1.65	0.31	7.72	0.69	0.10	0.67	0.10	68	255	6396	20	331
0.46	1.37	0.21	1335	1.44	0.27	6.78	0.62	0.12	0.68	0.09	70	241	5030	20	330
0.47	1.37	0.23	1538	1.60	0.29	7.20	0.69	0.10	0.78	0.09	72	258	6504	21	336
0.58	1.69	0.28	1520	1.65	0.30	7.79	0.83	0.11	0.77	0.12	66	257	6597	21	329
0.48	1.48	0.22	1517	1.42	0.27	7.04	0.75	0.09	0.72	0.09	71	257	5933	21	335
0.43	1.33	0.22	1433	1.43	0.31	7.02	0.77	0.11	0.66	0.08	71	250	5913	21	336
0.48	1.48	0.22	1483	1.40	0.29	7.30	0.64	0.11	0.60	0.09	71	253	6604	20	328
0.49	1.68	0.26	1464	1.53	0.29	7.81	0.76	0.09	0.84	0.12	68	253	6462	21	329
0.42	1.38	0.19	1236	1.44	0.25	6.57	0.69	0.10	0.61	0.09	71	241	4973	21	337
0.48	1.41	0.20	1269	1.35	0.27	6.82	0.70	0.10	0.69	0.11	71	241	4912	25	445
0.47	1.48	0.21	1285	1.41	0.27	6.95	0.69	0.09	0.62	0.08	70	242	4967	20	328
0.93	3.05	0.48	2494	3.38	0.79	19.5	2.14	0.32	2.11	0.31	64	258	5103	21	330
0.79	2.14	0.37	1186	2.78	0.66	16.1	1.79	0.24	1.76	0.25	62	193	4553	21	340
0.83	2.43	0.44	1512	3.07	0.71	17.9	2.10	0.30	1.71	0.27	64	239	5111	21	326
0.88	2.38	0.43	1417	3.19	0.67	17.6	1.83	0.27	1.89	0.28	61	217	5091	21	331
0.87	2.55	0.44	857	3.13	0.70	17.2	1.83	0.31	2.01	0.28	59	183	4698	21	328
1.00	2.97	0.46	1820	3.40	0.76	19.4	2.14	0.29	2.11	0.30	61	227	4923	21	332
0.56	1.92	0.35	1929	2.49	0.48	13.2	1.37	0.19	1.19	0.20	66	240	6572	20	319
0.69	2.15	0.39	2569	2.59	0.57	14.6	1.42	0.21	1.37	0.20	56	241	9607	20	321
0.69	2.08	0.38	2541	2.66	0.53	14.9	1.63	0.23	1.43	0.17	51	235	9700	20	326
0.55	2.19	0.37	2232	2.51	0.51	13.7	1.61	0.19	1.27	0.17	61	243	8073	20	318
0.62	1.93	0.31	2118	2.52	0.53	13.8	1.64	0.21	1.24	0.20	64	244	7156	20	325
0.50	1.68	0.31	2077	2.07	0.52	12.6	1.36	0.20	1.23	0.17	67	263	6659	20	327
0.59	1.92	0.36	2623	2.61	0.48	14.0	1.46	0.21	1.35	0.18	61	267	8277	20	326
0.68	2.29	0.41	3166	2.97	0.65	17.5	1.90	0.29	1.80	0.25	71	281	6837	22	327
0.71	2.27	0.41	3022	2.92	0.67	17.3	1.99	0.25	1.81	0.26	68	272	6943	21	326
0.64	1.96	0.39	2731	3.02	0.65	17.0	1.86	0.26	1.75	0.25	71	274	6496	21	331
0.67	2.54	0.44	3054	3.19	0.69	17.5	1.85	0.28	1.88	0.27	64	269	7543	22	332
0.64	2.22	0.40	2958	3.06	0.68	17.2	1.92	0.27	1.76	0.27	70	273	6500	22	335
0.73	2.35	0.44	2854	2.78	0.66	17.1	1.91	0.30	1.78	0.27	71	272	6678	22	337
0.62	2.25	0.42	2967	3.07	0.65	17.1	1.94	0.27	1.73	0.28	67	271	6774	21	343
0.66	2.38	0.44	2963	2.91	0.66	16.8	2.07	0.26	1.87	0.27	64	261	7685	21	335
1.45	4.59	0.75	6568	5.33	1.14	27.6	2.98	0.39	2.84	0.38	63	277	5200	22	320
1.43	4.99	0.81	7060	5.63	1.16	29.6	3.14	0.45	2.78	0.38	61	280	5375	22	323
1.30	4.74	0.78	5856	5.13	1.04	26.8	2.92	0.41	2.67	0.32	66	273	4628	22	324
1.39	4.47	0.72	6777	5.00	1.01	27.0	2.77	0.39	2.38	0.34	61	272	5989	21	319
1.39	4.61	0.81	6681	5.20	1.04	26.9	2.71	0.37	2.61	0.33	63	273	5872	22	320
1.47	4.85	0.81	7362	5.41	1.10	27.7	2.84	0.39	2.69	0.38	61	275	6081	21	325
1.36	4.68	0.77	6502	5.04	1.00	26.2	2.94	0.40	2.57	0.37	63	269	5535	21	318
1.31	3.99	0.62	6654	4.47	0.86	23.3	2.43	0.36	2.44	0.32	62	265	6634	22	322
1.11	3.79	0.60	6181	4.15	0.92	22.1	2.34	0.32	2.24	0.28	63	265	6738	22	315
1.32	3.93	0.68	6902	4.13	0.90	23.0	2.58	0.33	2.36	0.31	65	272	6331	22	333
1.08	3.74	0.55	5745	3.85	0.80	21.2	2.24	0.34	2.26	0.31	67	268	5622	23	331
1.17	3.65	0.57	5466	4.10	0.82	21.0	2.20	0.32	2.30	0.28	67	266	5343	22	323
1.07	3.57	0.61	5748	3.96	0.79	21.4	2.26	0.32	2.06	0.30	67	265	5453	22	328
0.84	2.78	0.43	2676	3.42	0.67	18.4	2.10	0.27	1.91	0.26	58	240	4635	24	357
0.74	2.39	0.43	2934	3.43	0.68	18.1	1.99	0.28	1.77	0.24	61	256	4570	24	348
0.81	2.69	0.48	2669	3.10	0.73	18.1	2.03	0.27	1.85	0.24	58	245	4630	24	352
0.77	2.36	0.42	2832	2.97	0.72	18.4	1.93	0.28	1.86	0.26	58	249	4566	24	355
0.77	2.57	0.48	3580	3.51	0.74	19.1	2.03	0.28	1.94	0.26	62	270	4630	23	356
0.77	2.67	0.46	3135	3.21	0.72	18.4	2.09	0.24	1.88	0.31	60	259	4789	24	358
0.81	2.56	0.49	3527	3.41	0.73	19.4	2.03	0.28	2.13	0.30	58	261	5006	24	352

CLINOPYROXENE

Sample	Rb	Th	U	Ba	Nb	Ta	La	Ce	Pb	Sr	Pr	Nd	Hf	Zr	Sm
NJS1307		0.036		0.037	0.096	0.036	1.18	4.32		78.7	0.82	5.16	1.21	43.4	1.81
		0.014	0.006	0.021	0.106	0.017	1.14	4.21		79.3	0.86	5.37	1.25	41.8	2.01
	0.059	0.013	0.012	0.019	0.124	0.014	1.20	4.24		79.8	0.82	4.99	1.32	43.5	1.85
		0.014		0.020	0.113	0.018	1.12	4.34		79.0	0.88	5.19	1.29	42.8	1.94
		0.014		0.024	0.078	0.014	1.16	4.25	0.04	79.4	0.86	4.69	1.19	42.2	1.97
			0.011	0.029	0.083	0.024	1.24	4.26		80.3	0.80	5.02	1.38	42.3	1.82
		0.015	0.012	0.025	0.110	0.021	1.18	4.27		78.5	0.80	5.04	1.28	41.5	2.12
			0.011	0.017	0.113	0.019	1.09	4.20		80.2	0.78	5.01	1.32	40.9	2.04
NPY1301			0.014		0.186	0.049	1.14	3.75		78.8	0.64	3.90	0.94	30.3	1.53
		0.030	0.012	0.017	0.161	0.045	1.16	3.80		78.5	0.67	4.04	0.86	30.9	1.73
		0.026	0.013	0.096	0.115	0.035	1.11	3.71		77.0	0.67	4.19	1.11	30.9	1.49
		0.023	0.010		0.114	0.025	1.19	3.68		75.9	0.69	3.89	1.03	31.9	1.51
		0.030	0.011	0.017	0.165	0.042	1.20	3.82		79.7	0.71	4.13	0.89	29.8	1.84
	0.136	0.034	0.015	0.132	0.108	0.031	1.13	3.89	0.08	73.3	0.77	4.37	0.93	35.7	1.64
		0.025	0.011	0.045	0.240	0.038	1.18	3.90		78.8	0.72	4.52	1.11	35.5	1.56
	1.777	0.025	0.008	0.408	0.296	0.046	1.17	3.92	0.08	75.7	0.71	4.26	1.01	32.5	1.75
		0.021	0.017	0.020	0.236	0.048	1.21	3.90		80.3	0.66	4.15	1.00	31.8	1.91
NPY1310	0.053	0.010		0.111	0.026	0.009	1.04	3.55	0.11	40.0	0.69	3.66	0.78	17.6	1.47
		0.009		1.203	0.034	0.009	1.00	3.51	0.05	40.2	0.68	3.80	0.77	16.8	1.51
				0.483	0.037	0.010	0.98	3.55		40.2	0.62	3.76	0.76	17.6	1.60
	0.055			0.035	0.016	0.032	1.10	3.59	0.10	40.0	0.68	3.84	0.89	18.1	1.32
			0.006	0.025	0.042	0.012	0.99	3.44		39.5	0.63	3.57	0.80	17.2	1.61
		0.008		0.020	0.026	0.007	0.98	3.56		39.6	0.64	3.80	0.75	17.5	1.57
				0.036	0.062	0.010	1.09	3.52		40.7	0.65	3.92	0.73	16.7	1.72
NPY1311		0.005		0.038	0.054	0.018	1.06	3.70	0.04	40.8	0.64	3.86	0.63	15.7	1.49
		0.011	0.012	0.347	0.064	0.007	1.00	3.51		39.2	0.63	3.83	0.66	16.2	1.45
			0.004		0.044	0.014	1.00	3.61		40.0	0.68	3.94	0.83	17.5	1.39
		0.011		0.030	0.062	0.010	0.94	3.39		40.0	0.69	3.73	0.69	16.3	1.55
		0.011		0.034	0.044	0.006	1.05	3.68	0.05	39.3	0.68	3.96	0.61	17.1	1.51
				0.012	0.030	0.011	1.06	3.55	0.04	39.9	0.66	3.74	0.79	17.0	1.55
		0.020		0.014	0.039		1.05	3.61		39.4	0.64	3.76	0.84	17.1	1.57
	0.145			0.279	0.025	0.015	1.04	3.55		39.8	0.66	4.01	0.81	17.5	1.65
			0.009	0.030	0.039	0.007	0.97	3.67		40.9	0.64	3.53	0.70	17.2	1.49
				0.024	0.042	0.017	1.02	3.51		40.2	0.71	3.74	0.75	17.6	1.52
NPY1314		0.381	0.285	0.022	0.054	0.031	1.31	3.72	0.06	51.9	0.67	4.42	1.07	37.1	1.78
		0.467	0.280	0.021	0.019	0.008	1.12	3.36	0.04	41.9	0.57	3.70	1.09	35.1	1.61
		0.353	0.264	0.012	0.046	0.025	1.32	3.91	0.05	50.9	0.71	4.42	1.03	36.6	2.26
		0.265	0.196	0.012	0.045	0.024	1.27	3.99	0.05	53.9	0.73	4.63	1.13	36.6	1.89
		0.158	0.108	0.045	0.030	0.017	1.05	3.63	0.13	45.8	0.72	4.34	1.19	39.0	1.91
		0.118	0.100	0.028	0.024	0.011	0.95	3.24	0.23	39.1	0.66	4.01	1.17	36.6	1.58
NFL1302		0.093	0.035	1.519	0.199	0.013	1.63	3.38		48.6	0.53	2.66	0.65	20.6	1.31
		0.118	0.021	0.034	0.123	0.012	1.80	3.75		47.3	0.52	2.97	0.70	19.9	1.19
	0.052	0.131	0.033	0.530	0.182	0.014	2.80	6.68	0.05	52.7	0.91	4.15	0.67	21.8	1.44
		0.099	0.029	1.176	0.202	0.008	2.44	6.11		53.4	0.83	3.99	0.71	21.3	1.38
	0.076	0.115	0.027	0.063	0.337	0.006	2.48	5.89		51.1	0.82	3.82	0.66	20.7	1.26
	0.074	0.102	0.036	0.393	0.178	0.009	2.30	5.56	0.08	51.6	0.72	3.57	0.60	19.2	1.39
		0.137	0.043	0.042	0.135	0.018	1.99	4.14	0.07	48.2	0.66	3.04	0.74	20.1	1.06
NFL1305		0.206	0.051	0.035	0.334	0.067	3.97	8.68	0.06	70.6	1.08	4.70	0.33	28.5	1.09
		0.196	0.060	0.034	0.202	0.054	3.19	7.37		52.6	0.98	3.92	0.44	29.2	0.97
		0.181	0.052	0.027	0.268	0.100	3.22	7.25	0.04	50.7	0.95	4.10	1.00	37.2	0.91
	0.111	0.169	0.043	0.054	0.233	0.064	2.94	6.88	0.04	48.9	0.96	3.82	0.90	40.2	1.15
		0.195	0.059	0.046	0.350	0.126	3.35	7.95	0.05	53.1	1.07	4.20	1.14	39.7	0.85
		0.210	0.072	0.076	0.290	0.085	3.40	8.23	0.04	58.5	1.18	4.41	1.04	44.4	1.13

Eu	Gd	Tb	Ti	Dy	Ho	Y	Er	Tm	Yb	Lu	Sc	V	Cr	Co	Ni
0.77	2.88	0.48	4349	3.78	0.80	21.1	2.46	0.32	2.21	0.31	64	275	5133	23	342
0.74	2.75	0.51	4207	3.41	0.78	20.9	2.09	0.30	2.21	0.32	67	280	4847	23	344
0.80	2.98	0.48	4389	3.68	0.79	21.2	2.36	0.32	2.39	0.32	65	275	5150	23	349
0.71	2.78	0.48	4332	3.69	0.82	20.8	2.18	0.32	2.06	0.32	63	273	5017	23	343
0.81	2.84	0.49	4221	3.99	0.85	21.1	2.25	0.34	2.15	0.29	68	282	4706	23	344
0.80	2.64	0.53	4191	3.57	0.81	20.6	2.41	0.33	2.17	0.30	68	284	4651	23	349
0.81	2.83	0.51	4244	3.57	0.80	21.3	2.26	0.33	2.16	0.35	63	275	4875	22	341
0.84	2.93	0.49	4188	3.55	0.80	21.4	2.25	0.30	2.26	0.33	65	277	4917	22	343
0.74	2.38	0.43	3266	3.29	0.65	18.4	2.20	0.26	2.00	0.29	66	274	5623	21	334
0.68	2.43	0.43	3269	3.21	0.73	18.8	2.06	0.30	2.01	0.27	65	275	5602	21	329
0.67	2.48	0.47	3268	3.30	0.75	18.4	1.95	0.32	2.03	0.28	67	274	5337	21	334
0.65	2.32	0.45	3360	3.15	0.72	18.9	2.11	0.29	2.30	0.31	68	275	5688	21	330
0.74	2.43	0.46	3173	3.49	0.74	19.2	2.05	0.31	2.17	0.30	58	255	6096	21	324
0.70	2.40	0.45	3629	3.36	0.72	19.6	2.10	0.31	2.13	0.27	63	264	5551	21	327
0.71	2.31	0.41	3579	3.11	0.75	19.3	2.17	0.30	2.01	0.34	67	277	5107	21	330
0.70	2.45	0.43	3326	3.06	0.71	18.5	2.04	0.28	1.97	0.27	63	273	5464	22	329
0.76	2.72	0.42	3327	3.19	0.74	19.0	2.07	0.33	1.97	0.29	61	263	5458	21	326
0.65	2.37	0.43	3323	3.11	0.72	18.3	2.00	0.27	1.85	0.27	68	329	2726	23	328
0.58	2.31	0.43	3340	3.10	0.77	18.2	1.94	0.28	1.91	0.29	67	325	2704	22	324
0.57	2.46	0.48	3392	3.13	0.62	18.2	1.81	0.29	2.02	0.28	68	328	2785	23	325
0.63	2.48	0.48	3544	3.33	0.71	18.5	1.99	0.28	1.88	0.28	68	335	2998	24	444
0.61	2.24	0.45	3338	3.44	0.73	17.9	1.99	0.29	1.88	0.28	67	326	2934	23	324
0.64	2.33	0.45	3330	3.13	0.68	18.8	2.08	0.26	1.88	0.27	66	326	2854	22	331
0.66	2.33	0.45	3205	3.28	0.75	18.1	1.94	0.28	1.86	0.30	64	317	2863	22	326
0.65	2.30	0.40	3154	3.13	0.75	19.1	2.16	0.28	2.17	0.30	56	306	3455	23	313
0.69	2.08	0.41	3165	3.11	0.70	17.8	1.90	0.25	2.11	0.25	65	317	2660	22	334
0.62	2.32	0.44	3402	3.24	0.69	19.2	2.17	0.29	1.97	0.27	61	319	3251	22	319
0.60	2.16	0.42	3138	3.31	0.70	17.8	1.90	0.29	1.71	0.25	65	320	2821	22	319
0.68	2.63	0.48	3303	3.49	0.71	18.8	2.02	0.32	2.02	0.29	61	316	3086	22	316
0.64	2.37	0.49	3293	3.29	0.72	19.0	2.17	0.28	1.98	0.30	62	318	3042	22	318
0.63	2.20	0.44	3266	3.05	0.66	18.2	2.01	0.29	1.86	0.26	66	326	2842	23	326
0.64	2.53	0.49	3336	3.27	0.72	18.6	2.15	0.29	1.90	0.26	63	322	2958	22	325
0.60	2.48	0.41	3229	3.24	0.69	18.3	2.08	0.30	1.97	0.30	64	321	2758	22	320
0.60	2.54	0.43	3326	3.45	0.69	18.7	2.15	0.29	1.87	0.28	64	327	2819	22	318
0.68	2.87	0.50	3834	3.67	0.81	21.6	2.27	0.31	2.20	0.28	62	270	5059	21	330
0.66	2.40	0.43	2716	3.15	0.72	18.5	2.00	0.28	1.86	0.32	66	261	4346	22	344
0.79	2.80	0.53	3756	3.94	0.84	21.7	2.44	0.39	2.23	0.28	58	258	5290	21	334
0.79	2.88	0.52	3830	3.55	0.78	21.6	2.34	0.33	2.43	0.31	60	268	5287	21	333
0.76	2.69	0.52	3670	3.78	0.85	21.4	2.50	0.33	2.30	0.32	62	262	5015	31	537
0.67	2.52	0.48	2773	3.16	0.76	18.8	1.92	0.32	1.99	0.26	64	260	4742	21	334
0.49	2.09	0.39	2128	2.85	0.58	16.1	1.87	0.23	1.78	0.23	69	263	5864	22	346
0.46	2.15	0.32	1983	2.62	0.59	15.6	1.72	0.22	1.70	0.28	69	262	5512	22	342
0.55	1.95	0.37	2051	2.87	0.66	16.3	1.77	0.25	1.81	0.25	66	258	6621	21	336
0.53	1.76	0.33	1646	2.62	0.60	14.9	1.68	0.24	1.54	0.20	67	251	5543	21	352
0.54	1.89	0.37	1772	2.49	0.62	15.2	1.76	0.25	1.84	0.24	66	250	5374	21	336
0.59	1.78	0.35	1868	2.47	0.61	15.2	1.76	0.22	1.70	0.23	68	256	5218	21	342
0.52	1.75	0.35	1979	2.62	0.59	15.5	1.72	0.25	1.74	0.26	70	263	5710	21	333
0.40	1.22	0.24	892	1.90	0.48	11.8	1.44	0.17	1.30	0.18	65	234	5452	22	338
0.38	1.40	0.24	961	1.90	0.47	11.8	1.35	0.22	1.35	0.20	64	242	6403	21	331
0.38	1.25	0.24	879	1.97	0.43	11.7	1.31	0.19	1.36	0.19	65	239	5808	21	332
0.37	1.37	0.23	766	1.94	0.45	11.6	1.46	0.20	1.39	0.21	63	228	5613	21	336
0.41	1.41	0.28	906	1.97	0.47	12.1	1.34	0.20	1.44	0.19	65	246	5932	21	344
0.40	1.54	0.26	815	1.77	0.48	11.9	1.37	0.19	1.32	0.19	64	227	6032	21	329

CLINOPYROXENE

Sample	Rb	Th	U	Ba	Nb	Ta	La	Ce	Pb	Sr	Pr	Nd	Hf	Zr	Sm
NFL1315A		0.154	0.031	0.168	0.342	0.051	8.73	26.10	0.13	195	4.23	19.39	2.37	83.2	4.22
		0.166	0.022	0.129	0.341	0.056	8.08	24.53	0.15	191	4.19	19.34	2.18	76.6	4.17
		0.165	0.035	0.144	0.335	0.082	8.24	25.15	0.19	188	4.10	19.74	2.61	79.3	4.12
		0.128	0.015	0.140	0.265	0.066	7.66	23.06	0.18	175	3.59	15.34	3.29	91.5	3.09
		0.180	0.033	0.134	0.351	0.050	7.05	22.68	0.14	184	3.78	18.26	2.12	77.2	4.21
		0.129	0.026	0.818	0.272	0.016	6.70	20.78	0.15	183	3.50	16.88	1.78	66.2	3.85
		0.122	0.034	0.169	0.233	0.030	6.54	20.76	0.13	181	3.52	16.68	1.98	71.8	4.02
NFL1316		0.088	0.012	0.035	0.038	0.036	2.67	5.17	0.09	62.5	0.62	2.81	0.54	18.7	0.70
		0.083	0.028	2.282	0.056	0.017	2.39	4.65	0.07	58.3	0.59	2.89	0.58	19.9	0.87
		0.108	0.021	0.042	0.047	0.012	2.33	4.74	0.08	56.1	0.62	2.86	0.58	20.2	0.77
	0.116	0.093	0.023	4.550	0.155	0.016	2.29	4.53	0.08	55.8	0.59	2.80	0.52	19.1	0.79
		0.105	0.028	0.107	0.058	0.024	2.11	4.38	0.04	58.9	0.59	3.06	0.48	18.4	0.72
		0.106	0.017	0.025	0.030	0.011	2.36	4.70	0.08	55.9	0.62	2.55	0.47	18.5	0.74
	0.071	0.104	0.023	2.054	0.088	0.034	2.29	4.50	0.08	58.6	0.56	2.77	0.50	19.0	0.76
NFL1324		0.434	0.139	0.220	0.532	0.124	13.73	39.76	0.47	166	6.15	27.72	3.40	142	5.48
		0.380	0.111	0.280	0.506	0.114	12.58	37.49	0.39	162	5.81	25.36	3.24	134	5.11
		0.414	0.115	0.224	0.477	0.126	13.84	39.71	0.39	173	6.04	26.46	1.81	113	5.27
		0.396	0.108	0.217	0.479	0.124	13.92	40.86	0.43	179	6.19	26.43	1.39	106	5.19
	0.051	0.430	0.113	0.209	0.501	0.096	13.23	38.73	0.45	164	5.87	26.16	2.20	119	4.96
		0.423	0.150	0.229	0.484	0.091	13.01	37.48	0.45	162	5.65	24.61	2.34	117	4.96
	0.050	0.416	0.152	0.243	0.657	0.151	13.94	40.68	0.42	179	6.14	27.83	2.44	119	5.13
NFL1326		0.080	0.021	0.110	0.220	0.040	4.10	12.28	0.06	98.2	2.04	9.34	1.03	30.5	2.48
		0.083	0.021	0.065	0.214	0.038	4.20	12.43	0.06	103	1.92	9.62	0.93	28.0	2.68
		0.078	0.025	0.103	0.235	0.023	4.56	12.81	0.05	99.3	2.08	9.58	1.05	30.4	2.55
		0.084	0.020	0.106	0.203	0.022	3.96	11.81		97.2	1.94	8.84	1.05	26.9	2.33
		0.118	0.025	0.083	0.240	0.039	4.87	13.84	0.07	88.4	2.22	10.29	0.93	31.0	2.53
		0.136	0.022	0.087	0.333	0.044	4.99	14.21	0.07	92.1	2.25	10.46	1.02	31.7	2.56
		0.144	0.018	0.081	0.227	0.035	5.04	14.20	0.07	98.2	2.26	10.53	1.14	31.7	2.69
NFL1327		0.073	0.013	0.165	0.383	0.046	6.71	21.49	0.08	119	3.59	17.52	0.34	29.1	3.76
		0.067	0.018	0.091	0.238	0.050	6.42	20.54		119	3.31	16.01	0.38	23.9	3.58
		0.073	0.011	0.152	0.270	0.036	6.55	20.63	0.06	119	3.34	15.62	0.35	23.0	3.54
		0.054	0.010	0.142	0.315	0.045	6.55	20.33		121	3.20	14.54	0.24	20.9	3.21
		0.071	0.021	0.164	0.289	0.038	6.56	20.22	0.04	116	3.29	15.10	0.29	22.7	3.44
		0.077	0.031	0.114	0.276	0.036	5.94	18.48	0.06	118	2.88	13.33	0.37	19.6	3.03
		0.068	0.019	0.128	0.240	0.028	5.92	19.11	0.07	114	2.96	13.26	0.34	18.6	2.92
NFL1329		0.172	0.066		0.019	0.010	1.15	3.18	0.16	43.1	0.60	3.08	0.89	24.6	1.24
		0.215	0.084	0.017		0.015	1.20	3.22	0.08	47.6	0.60	3.57	0.79	25.9	1.44
		0.191	0.082	0.014	0.025		1.12	3.20	0.11	44.6	0.61	3.12	0.82	24.3	1.12
		0.213	0.074		0.051	0.017	1.20	3.25	0.12	47.3	0.58	3.42	0.77	25.9	1.23
		0.200	0.072	0.042	0.065		1.13	3.24	0.08	48.5	0.61	3.45	0.89	26.3	1.44
		0.195	0.107		0.050		1.10	3.17	0.08	48.3	0.60	3.45	0.97	25.5	1.39
		0.190	0.072	0.064	0.050	0.015	1.15	3.23	0.10	48.1	0.57	3.55	1.02	26.6	1.34
NTB0306		0.268	0.050		0.201		3.44	4.50	0.08	71.4	0.32	0.95	0.09	1.59	0.28
		0.307	0.053		0.013		3.52	4.59	0.08	71.3	0.34	0.96	0.08	1.55	0.33
		0.311	0.051	0.040	0.012		3.48	4.63	0.12	73.1	0.33	0.89	0.07	1.65	0.35
		0.295	0.054		0.023		3.30	4.74	0.16	76.8	0.33	0.98	0.12	1.71	0.36
		0.333	0.063		0.018		3.82	5.46	0.13	77.5	0.37	1.17	0.11	1.97	0.39
	0.319	0.295	0.060		0.020		3.75	5.48	0.10	76.1	0.40	1.13	0.10	1.79	0.36
	0.034	0.312	0.056	0.820	0.017		3.77	5.56	0.19	76.4	0.43	1.13	0.07	1.76	0.29
	0.025	0.264	0.046	0.377	0.019		3.72	5.61	0.13	75.2	0.42	1.25	0.08	1.76	0.32
NTB0307	0.031	0.059	0.018		0.070	0.017	0.80	2.56	0.03	36.7	0.42	2.37	0.41	9.77	0.88
	0.028	0.046	0.022	0.081	0.062	0.021	0.77	2.48	0.04	35.8	0.40	2.36	0.37	9.45	0.82
		0.054	0.021		0.053	0.019	0.83	2.61	0.03	37.2	0.42	2.21	0.42	10.1	0.82
	0.047	0.062	0.024	0.050	0.117	0.020	0.88	2.77	0.09	40.2	0.43	2.52	0.41	10.3	0.89
		0.068	0.026	0.069	0.082	0.017	0.86	2.69	0.03	40.8	0.44	2.31	0.43	10.2	0.99
		0.113	0.029		0.054	0.020	0.86	2.72		36.5	0.45	2.16	0.42	10.6	0.91
		0.058	0.022		0.058	0.016	0.81	2.64		36.7	0.43	2.31	0.43	10.2	0.96

Eu	Gd	Tb	Ti	Dy	Ho	Y	Er	Tm	Yb	Lu	Sc	V	Cr	Co	Ni
1.36	3.92	0.53	802	3.10	0.64	15.8	1.65	0.21	1.32	0.19	73	191	9053	21	308
1.41	3.65	0.57	892	3.37	0.58	15.1	1.52	0.21	1.24	0.19	67	180	8439	20	306
1.39	3.70	0.51	629	3.21	0.56	15.1	1.57	0.18	1.21	0.19	71	206	8750	20	304
1.11	2.57	0.37	460	2.36	0.42	11.8	1.17	0.17	1.06	0.16	95	230	9041	21	309
1.40	3.92	0.57	1219	3.29	0.64	15.6	1.59	0.19	1.34	0.19	56	170	8908	20	291
1.22	3.28	0.48	1006	3.01	0.55	13.5	1.44	0.17	1.13	0.17	56	164	7710	20	303
1.32	3.26	0.52	1015	2.99	0.54	14.0	1.54	0.20	1.29	0.18	60	176	8340	20	294
0.30	0.82	0.11	826	0.74	0.15	3.98	0.41	0.05	0.45	0.07	81	249	7280	21	332
0.29	0.75	0.13	848	0.71	0.16	3.94	0.46	0.07	0.52	0.08	95	280	6772	20	342
0.28	0.76	0.13	854	0.77	0.16	4.07	0.57	0.07	0.51	0.08	98	283	7321	20	331
0.23	0.65	0.13	780	0.72	0.17	3.85	0.44	0.07	0.60	0.08	97	278	7249	20	336
0.27	0.68	0.11	801	0.74	0.13	3.86	0.44	0.07	0.46	0.07	89	266	6292	20	335
0.31	0.92	0.13	788	0.78	0.13	3.65	0.35	0.06	0.56	0.08	89	263	6612	20	326
0.26	0.75	0.11	796	0.63	0.15	3.87	0.51	0.05	0.45	0.08	83	252	7266	20	339
1.66	4.65	0.63	1271	3.78	0.70	17.8	1.71	0.24	1.35	0.18	59	169	8144	21	348
1.61	4.57	0.58	1198	3.56	0.72	16.7	1.62	0.22	1.50	0.17	59	171	9180	21	345
1.58	4.13	0.54	1181	3.51	0.64	16.8	1.69	0.22	1.53	0.19	60	185	8867	22	361
1.59	4.10	0.54	1090	3.40	0.64	16.6	1.69	0.24	1.37	0.18	60	186	9357	22	354
1.59	4.14	0.60	1196	3.42	0.62	16.6	1.77	0.24	1.31	0.20	61	182	8544	20	349
1.40	3.87	0.57	1172	3.19	0.61	16.0	1.63	0.22	1.27	0.18	62	179	8094	20	346
1.70	4.38	0.57	1201	3.43	0.68	17.1	1.77	0.23	1.37	0.22	62	184	8232	21	355
0.86	2.79	0.40	2267	2.88	0.59	14.5	1.34	0.22	1.47	0.19	56	234	5591	21	253
0.92	2.50	0.41	2065	2.74	0.52	13.7	1.46	0.22	1.43	0.22	55	227	5552	21	261
0.91	2.90	0.43	2131	2.90	0.57	15.0	1.66	0.24	1.50	0.22	56	241	6089	21	266
0.84	2.51	0.40	1919	2.58	0.56	13.9	1.41	0.21	1.41	0.19	53	224	5456	22	259
1.00	2.76	0.49	2376	3.05	0.64	17.1	1.94	0.27	1.83	0.25	61	264	6344	21	257
0.90	3.29	0.42	2417	3.20	0.69	17.2	1.90	0.25	1.93	0.24	60	264	6203	21	256
1.03	2.92	0.46	2366	3.26	0.63	16.0	1.66	0.26	1.62	0.21	59	256	5986	21	265
1.25	3.18	0.49	1583	2.92	0.55	14.3	1.53	0.20	1.15	0.19	44	176	6610	21	290
1.23	3.12	0.44	1265	2.83	0.51	13.8	1.40	0.22	1.45	0.19	45	175	6822	21	304
1.16	2.97	0.42	1212	2.64	0.50	13.5	1.48	0.20	1.32	0.21	47	189	7286	22	303
1.11	2.86	0.41	1150	2.39	0.47	13.5	1.35	0.20	1.55	0.21	52	210	7066	22	305
1.20	2.87	0.43	1140	2.60	0.52	13.5	1.32	0.19	1.34	0.19	50	193	6833	22	311
1.04	2.17	0.38	1044	2.18	0.48	12.4	1.47	0.18	1.49	0.17	53	214	6843	22	314
1.02	2.45	0.37	1069	2.20	0.45	12.5	1.27	0.21	1.29	0.18	56	218	7029	22	315
0.52	1.69	0.34	1604	2.48	0.54	14.1	1.60	0.22	1.54	0.22	63	237	4166	21	342
0.62	2.04	0.35	1843	2.90	0.60	15.6	1.67	0.24	1.52	0.24	62	244	4306	22	342
0.53	1.99	0.33	1632	2.33	0.57	14.3	1.54	0.20	1.45	0.20	63	233	3900	21	344
0.60	1.99	0.37	1816	2.70	0.56	15.0	1.74	0.23	1.70	0.23	64	240	4500	21	341
0.68	1.86	0.38	1866	2.68	0.59	15.2	1.63	0.22	1.58	0.23	63	240	4401	21	335
0.57	1.91	0.39	1962	2.68	0.59	15.5	1.62	0.24	1.62	0.22	66	247	4915	22	347
0.58	2.11	0.37	1980	2.80	0.64	15.3	1.78	0.23	1.59	0.23	65	241	5049	21	340
0.16	0.48	0.10	661	0.77	0.18	4.12	0.53	0.07	0.53	0.08	73	257	6270	21	336
0.15	0.57	0.10	686	0.79	0.18	4.35	0.55	0.08	0.49	0.08	74	259	5420	21	338
0.14	0.53	0.11	792	0.84	0.18	4.39	0.59	0.08	0.55	0.08	73	264	7370	21	333
0.15	0.58	0.11	801	0.76	0.19	4.17	0.52	0.07	0.53	0.07	73	273	9320	21	327
0.17	0.77	0.10	1030	0.89	0.21	4.99	0.60	0.08	0.55	0.09	75	267	6880	22	347
0.16	0.56	0.12	997	0.90	0.18	4.61	0.64	0.08	0.54	0.08	76	274	7620	21	339
0.14	0.50	0.11	904	0.89	0.19	4.57	0.56	0.08	0.63	0.09	72	257	6890	22	344
0.13	0.55	0.10	596	0.72	0.17	3.89	0.49	0.07	0.53	0.07	73	247	8250	22	342
0.34	1.38	0.26	1440	1.88	0.42	10.9	1.25	0.18	1.31	0.17	61	241	6100	22	368
0.37	1.34	0.25	1450	1.84	0.40	10.7	1.25	0.17	1.22	0.17	58	241	5830	21	353
0.38	1.35	0.26	1490	2.07	0.46	11.1	1.21	0.18	1.24	0.17	60	252	6260	23	385
0.40	1.36	0.25	1650	2.11	0.48	12.0	1.36	0.19	1.35	0.17	62	264	6030	22	385
0.39	1.47	0.27	1720	2.07	0.46	12.0	1.42	0.19	1.30	0.20	61	265	6180	22	372
0.39	1.30	0.25	1520	2.02	0.44	11.6	1.36	0.19	1.28	0.18	62	263	6170	22	380
0.40	1.29	0.26	1600	2.07	0.45	11.8	1.34	0.18	1.29	0.19	63	257	6330	22	361

CLINOPYROXENE

Sample	Rb	Th	U	Ba	Nb	Ta	La	Ce	Pb	Sr	Pr	Nd	Hf	Zr	Sm
NTB1124	0.038	0.010	0.005	0.062	0.039		0.79	2.53	0.07	45.2	0.45	2.73	0.72	17.2	1.18
					0.027		0.75	2.48	0.05	45.3	0.45	2.95	0.79	17.8	1.20
		0.019	0.005		0.020		0.78	2.48	0.05	45.7	0.44	2.71	0.71	18.1	1.18
		0.009	0.004		0.035		0.72	2.50	0.05	45.1	0.42	2.89	0.66	17.8	1.20
		0.007			0.035		0.73	2.54	0.03	51.8	0.46	3.12	0.78	17.8	1.38
		0.009	0.006		0.030		0.73	2.40	0.06	53.0	0.48	2.87	0.63	17.2	1.27
		0.018			0.032		0.74	2.54	0.06	50.2	0.46	3.06	0.72	18.1	1.33
		0.018			0.036		0.77	2.43	0.06	45.8	0.48	2.85	0.77	18.1	1.21
		0.009	0.005		0.032		0.68	2.41	0.04	46.0	0.43	2.59	0.73	16.8	1.17
		0.012			0.032	0.006	0.78	2.48	0.03	47.2	0.45	2.78	0.71	18.0	1.26
		0.011	0.003		0.037	0.007	0.75	2.53	0.06	50.5	0.46	2.91	0.71	18.6	1.30
		0.015	0.005		0.047	0.005	0.75	2.53	0.32	50.8	0.46	2.97	0.72	18.2	1.26
		0.015	0.006		0.045	0.005	0.81	2.62	0.05	48.2	0.47	3.16	0.76	19.3	1.32
NTB1116	0.212	0.031	0.032	0.486	0.101	0.010	0.81	3.00	0.10	64.3	0.58	3.33	0.81	22.0	1.43
		0.029	0.021	0.033	0.123	0.017	0.83	3.15	0.04	66.2	0.66	3.64	0.79	23.2	1.41
	0.064	0.021	0.033	0.012	0.085	0.018	0.82	2.95		62.8	0.59	3.85	0.78	22.3	1.41
		0.028	0.014	0.024	0.063	0.015	0.89	3.07		64.8	0.60	3.64	0.72	22.5	1.40
	0.064		0.037	0.074	0.092	0.023	0.82	2.97		65.1	0.57	3.51	0.63	22.2	1.09
		0.023	0.021	0.018	0.036	0.016	0.80	2.91		61.3	0.59	3.23	0.68	22.6	1.45
NTB1122		0.100	0.038	0.071	0.133	0.060	3.59	12.69	0.07	70.9	2.26	12.38	1.34	39.8	3.59
		0.155	0.041	0.065	0.150	0.088	3.68	12.89	0.08	69.5	2.29	12.60	1.36	39.3	3.44
		0.119	0.042	0.053	0.138	0.064	3.71	12.70	0.06	70.0	2.33	12.10	1.38	40.5	3.70
		0.146	0.037	0.222	0.154	0.037	3.56	12.41	0.07	66.7	2.23	12.22	1.45	39.8	3.41
		0.117	0.043	0.084	0.156	0.055	3.59	12.38	0.06	67.8	2.25	12.21	1.39	39.7	3.61
		0.105	0.055	0.053	0.126	0.042	3.58	12.66	0.07	65.6	2.31	12.52	1.24	39.3	3.29
NFK0301	0.600	0.080	0.020	6.600	0.658	0.037	0.65	1.68	0.15	19.9	0.25	1.25	0.28	10.5	0.41
		0.187	0.037		0.452	0.083	11.90	34.60	0.08	145	4.81	19.90	0.55	34.1	3.85
	0.024	0.154	0.034	0.039	0.468	0.084	11.70	34.40	0.06	138	4.68	19.10	0.53	30.5	3.60
		0.145	0.032		0.375	0.079	11.20	32.90	0.07	144	4.45	18.70	0.58	29.7	3.50
		0.163	0.028		0.440	0.086	11.30	32.80	0.07	142	4.20	16.10	0.48	24.8	2.89
	0.031	0.137	0.039	0.060	0.406	0.079	10.90	36.20	0.08	151	4.73	19.10	0.55	31.2	3.60
	0.106	0.142	0.040		0.404	0.058	10.60	34.90	0.08	144	4.55	17.90	0.55	29.7	3.51
		0.149	0.034	0.060	0.396	0.075	10.40	34.20	0.12	144	4.44	17.30	0.54	29.0	3.40
		0.145	0.037		0.441	0.085	11.40	36.80	0.08	151	4.89	20.20	0.48	28.5	3.50
		0.140	0.040	0.068	0.341	0.061	10.80	35.10	0.07	149	4.54	19.10	0.61	32.6	3.74
		0.149	0.036	0.066	0.427	0.077	10.80	35.60	0.07	147	4.59	19.00	0.59	30.6	3.55
		0.123	0.033	0.058	0.367	0.066	10.60	33.70	0.05	143	4.42	17.80	0.52	30.7	3.45
		0.172	0.037	0.082	0.415	0.080	11.80	35.00	0.08	149	4.91	20.60	0.63	38.5	4.11
		0.157	0.036	0.039	0.453	0.080	11.90	35.20	0.08	150	4.99	21.40	0.66	39.1	4.32
		0.167	0.031	0.048	0.398	0.066	11.90	34.80	0.08	151	4.92	21.80	0.68	42.2	4.28
		0.166	0.039	0.049	0.715	0.116	12.50	35.10	0.06	152	4.96	20.70	0.69	37.6	4.26
	0.024	0.167	0.038	0.076	0.470	0.075	11.80	34.10	0.08	147	4.82	20.80	0.64	37.4	4.06
NFK1123		0.155	0.075	0.161	0.268	0.051	14.30	38.00	1.47	116	4.31	15.70	0.53	21.8	2.28
		0.157	0.074	0.110	0.259	0.051	13.80	37.40	1.39	117	4.36	15.50	0.51	21.9	2.17
		0.165	0.079	0.088	0.268	0.057	14.30	38.20	1.48	117	4.42	15.90	0.53	22.9	2.15
		0.183	0.081	0.095	0.229	0.053	13.80	37.60	1.42	114	4.40	15.70	0.53	23.1	2.38
		0.171	0.079		0.216	0.042	13.70	36.50	1.48	111	4.32	15.70	0.51	22.1	2.27
		0.189	0.075	0.232	0.220	0.038	13.40	36.20	1.44	112	4.29	15.70	0.54	23.0	2.09
		0.179	0.080	0.120	0.230	0.046	13.60	37.70	1.57	110	4.42	16.50	0.66	24.3	2.38
		0.156	0.071	0.090	0.209	0.033	12.40	34.80	1.47	108	4.09	14.60	0.61	23.4	2.12
		0.182	0.077	0.090	0.230	0.034	13.20	36.70	1.53	109	4.33	15.80	0.65	24.3	2.36
NFK1108	0.078	0.057	0.016	0.344	0.195	0.025	2.99	9.30	0.13	90.9	1.39	6.98	0.65	19.4	1.68
		0.013	0.005	0.057	0.180	0.014	2.31	7.73		81.8	1.36	6.55	0.52	14.2	1.77
		0.035		0.897	0.231	0.021	2.76	8.91		86.6	1.44	6.89	0.59	18.4	1.90
		0.059	0.017	0.067	0.146	0.031	3.32	9.95	0.06	87.3	1.59	7.61	0.74	20.2	1.92
		0.058	0.021	0.042	0.076		3.25	9.40	0.05	89.0	1.54	6.93	0.52	18.6	1.67
		0.058	0.021	0.064	0.089	0.012	3.11	9.46		87.4	1.48	6.60	0.52	18.6	1.83

Eu	Gd	Tb	Ti	Dy	Ho	Y	Er	Tm	Yb	Lu	Sc	V	Cr	Co	Ni
0.48	1.72	0.32	3410	2.31	0.51	13.1	1.52	0.24	1.26	0.18	65	284	7860	23	379
0.51	1.81	0.34	3420	2.48	0.52	13.6	1.40	0.20	1.38	0.20	68	283	8350	23	379
0.48	1.81	0.33	3470	2.49	0.53	13.5	1.50	0.22	1.39	0.19	66	287	8420	24	373
0.49	1.84	0.29	3300	2.37	0.50	13.0	1.49	0.20	1.36	0.19	66	285	8220	23	375
0.52	1.76	0.35	3670	2.55	0.54	14.1	1.62	0.23	1.53	0.21	63	291	8060	24	368
0.55	1.89	0.34	3680	2.38	0.54	13.8	1.52	0.21	1.49	0.19	64	290	7970	23	373
0.51	1.95	0.36	3840	2.58	0.56	14.5	1.62	0.24	1.61	0.20	64	290	8270	24	382
0.51	1.96	0.34	3480	2.56	0.54	13.9	1.60	0.22	1.49	0.19	65	288	8240	23	375
0.47	1.65	0.33	3200	2.35	0.50	12.7	1.45	0.18	1.36	0.18	64	285	7450	22	363
0.51	1.81	0.33	3690	2.63	0.54	13.8	1.59	0.23	1.44	0.19	66	287	8030	24	378
0.51	1.84	0.34	3840	2.66	0.56	14.1	1.56	0.22	1.47	0.20	65	288	7980	23	378
0.57	1.94	0.35	3820	2.70	0.59	14.1	1.63	0.23	1.42	0.21	66	285	8180	23	366
0.56	1.93	0.36	3940	2.50	0.59	15.0	1.70	0.25	1.61	0.22	63	282	9270	23	378
0.53	1.75	0.33	1999	2.39	0.56	14.2	1.42	0.22	1.44	0.19	72	274	7562	21	338
0.53	1.81	0.40	2124	2.40	0.56	14.6	1.54	0.22	1.41	0.20	69	273	7598	20	322
0.59	1.94	0.34	2085	2.36	0.55	14.6	1.56	0.23	1.57	0.17	69	271	7496	20	320
0.56	1.90	0.36	2099	2.74	0.60	14.5	1.50	0.23	1.40	0.21	72	279	8082	21	333
0.56	2.15	0.36	2065	2.80	0.60	14.5	1.40	0.20	1.47	0.20	70	269	7494	20	329
0.53	1.81	0.31	2045	2.46	0.56	14.7	1.63	0.22	1.56	0.19	72	272	7421	21	330
1.18	3.76	0.62	5891	4.00	0.82	20.8	2.18	0.32	1.89	0.27	67	319	5648	23	334
1.28	3.83	0.61	5807	4.03	0.80	21.0	2.29	0.31	2.05	0.28	66	304	5327	23	331
1.22	3.79	0.58	5949	4.10	0.81	20.9	2.34	0.30	2.12	0.30	67	321	5685	23	331
1.15	3.79	0.62	5569	3.97	0.79	20.0	2.07	0.30	1.96	0.28	69	324	5739	23	340
1.13	3.74	0.57	5777	3.89	0.79	20.3	2.17	0.28	1.94	0.26	67	323	5669	23	329
1.19	3.98	0.62	5702	3.93	0.80	20.7	2.24	0.30	1.96	0.28	65	297	5633	23	327
0.15	0.54	0.10	1205	0.67	0.15	4.30	0.44	0.07	0.44	0.07	16	82	2625	105	1960
1.32	3.21	0.48	1850	3.20	0.65	16.7	1.82	0.27	1.73	0.26	66	231	9750	21	337
1.22	3.18	0.44	1790	3.12	0.57	16.2	1.75	0.27	1.79	0.25	63	235	9550	21	342
1.11	2.98	0.44	1730	2.95	0.59	15.4	1.59	0.24	1.62	0.23	63	230	8080	21	348
1.02	2.65	0.40	1800	2.69	0.53	13.8	1.43	0.22	1.36	0.22	66	242	9470	22	343
1.17	3.01	0.43	1760	3.00	0.60	15.2	1.50	0.23	1.63	0.23	57	240	9010	23	383
1.15	2.90	0.42	1710	2.81	0.54	14.3	1.57	0.21	1.43	0.22	56	236	8790	22	365
1.16	2.88	0.42	1630	2.79	0.53	14.0	1.37	0.22	1.50	0.20	54	234	8440	22	371
1.32	3.10	0.45	1740	2.89	0.57	14.9	1.53	0.22	1.42	0.24	57	248	9820	23	371
1.22	3.01	0.44	1650	2.98	0.57	14.9	1.57	0.23	1.49	0.22	54	238	9350	22	358
1.21	2.87	0.44	1740	2.86	0.58	14.6	1.61	0.21	1.53	0.20	55	238	9230	22	363
1.20	2.95	0.43	1650	2.72	0.54	14.3	1.52	0.23	1.57	0.21	55	233	8430	21	346
1.37	3.52	0.50	1780	3.38	0.66	17.8	1.84	0.27	1.76	0.26	60	217	8590	21	342
1.38	3.65	0.54	1780	3.56	0.67	17.9	1.92	0.29	1.87	0.26	60	220	8910	20	336
1.44	3.69	0.52	1730	3.61	0.70	18.5	2.01	0.29	1.95	0.26	61	213	8790	21	346
1.33	3.49	0.55	1810	3.46	0.66	17.7	1.94	0.27	1.69	0.24	61	217	8600	21	337
1.36	3.42	0.49	1740	3.37	0.69	17.6	1.86	0.25	1.80	0.26	59	213	8740	21	339
0.63	2.03	0.28	1940	1.67	0.37	8.89	0.93	0.14	0.92	0.12	58	235	9200	24	387
0.66	1.82	0.26	1940	1.72	0.36	9.04	0.90	0.14	0.85	0.12	59	236	9090	23	389
0.66	1.86	0.28	1960	1.76	0.34	9.02	0.99	0.13	0.87	0.12	60	237	9440	24	405
0.64	1.95	0.28	2040	1.82	0.35	9.38	0.97	0.13	0.94	0.12	60	231	9030	23	385
0.61	1.91	0.28	1940	1.80	0.34	8.87	0.90	0.12	0.84	0.12	57	226	8600	23	381
0.65	1.85	0.27	1990	1.73	0.35	9.07	0.92	0.13	0.83	0.13	59	229	8840	23	385
0.66	2.03	0.30	2140	1.77	0.35	9.37	0.94	0.13	0.90	0.12	57	228	9260	22	380
0.62	1.93	0.27	2040	1.68	0.36	8.57	0.98	0.12	0.92	0.10	57	227	8860	23	378
0.67	2.05	0.29	2110	1.84	0.35	9.09	1.00	0.14	0.90	0.12	59	231	8940	22	378
0.69	2.17	0.36	1944	2.38	0.55	14.3	1.60	0.22	1.57	0.21	67	260	7320	21	316
0.74	2.02	0.37	2462	2.60	0.53	13.6	1.43	0.20	1.50	0.20	64	274	7747	25	363
0.75	2.03	0.37	2010	2.51	0.50	13.1	1.33	0.21	1.29	0.18	64	244	6708	24	345
0.79	2.40	0.40	1953	2.62	0.56	13.9	1.61	0.19	1.44	0.24	59	240	7730	21	309
0.75	2.16	0.35	1833	2.67	0.57	14.4	1.56	0.19	1.59	0.20	68	266	7399	21	313
0.75	2.06	0.42	1855	2.72	0.53	14.5	1.71	0.25	1.54	0.23	68	265	7542	21	314

CLINOPYROXENE

Sample	Rb	Th	U	Ba	Nb	Ta	La	Ce	Pb	Sr	Pr	Nd	Hf	Zr	Sm
NFK1115		0.067	0.008	0.118	0.208	0.028	6.74	21.64	0.08	181	3.58	16.59	1.14	52.4	3.63
		0.069	0.012	0.129	0.176	0.016	6.64	21.86	0.08	179	3.61	16.59	0.94	50.6	3.46
		0.073	0.012	0.095	0.153	0.017	6.41	20.76	0.09	173	3.35	15.55	0.85	48.4	3.00
		0.068		0.118	0.139	0.023	6.04	19.86	0.06	158	3.25	14.45	0.65	42.0	3.07
		0.053	0.014	0.103	0.128	0.014	6.06	19.17	0.08	157	3.00	13.71	0.70	41.9	2.91
NFR0306		0.057	0.011		0.116	0.011	3.44	11.10	0.04	83.4	1.63	7.44	0.80	20.8	1.96
	0.119	0.073	0.013	1.410	0.218	0.016	3.42	11.50	0.06	83.1	1.64	7.83	0.76	21.4	2.06
		0.056	0.014	0.033	0.125	0.014	3.45	11.50	0.04	83.8	1.70	7.77	0.83	22.2	1.96
		0.059	0.012		0.110	0.018	3.35	11.70	0.05	83.8	1.73	7.61	0.78	20.5	2.08
		0.088	0.018		0.159	0.024	3.77	12.50	0.05	85.5	1.88	8.57	0.89	24.3	2.42
		0.097	0.018		0.180	0.029	3.80	12.80	0.06	82.8	1.92	8.79	0.88	26.1	2.34
	0.015	0.050	0.009	0.042	0.099	0.020	3.28	10.80	0.04	81.2	1.56	7.50	0.68	20.1	2.03
		0.045	0.012		0.123	0.013	3.34	11.60	0.04	80.8	1.69	7.97	0.74	20.3	1.83
		0.068	0.016		0.113	0.016	3.44	11.40	0.04	78.7	1.74	7.91	0.78	22.1	2.01
		0.072	0.012	0.041	0.125	0.015	3.44	11.60	0.04	79.1	1.68	7.92	0.76	22.2	2.10
		0.085	0.014		0.156	0.023	3.73	12.50	0.03	91.4	1.86	8.44	0.83	22.9	2.09
		0.073	0.016		0.140	0.022	3.65	12.40	0.04	88.5	1.79	8.38	0.73	22.2	2.12
		0.055	0.013		0.131	0.029	3.46	11.50	0.05	84.6	1.76	8.18	0.78	22.2	2.10
NFR0307		0.154	0.073		0.103	0.014	1.19	3.61	0.06	41.9	0.52	2.55	0.36	9.61	0.68
	0.028	0.159	0.079	0.033	0.073	0.015	1.22	3.72	0.05	40.2	0.52	2.43	0.34	9.78	0.59
		0.154	0.077		0.054	0.015	1.19	3.63		39.9	0.54	2.65	0.36	9.77	0.61
		0.158	0.072		0.082	0.019	1.19	3.87	0.05	44.8	0.56	2.76	0.34	10.1	0.73
		0.143	0.080	0.028	0.083	0.017	1.13	3.88	0.07	44.0	0.53	2.35	0.41	10.1	0.66
		0.170	0.072		0.096	0.019	1.22	3.89		45.6	0.56	2.87	0.40	10.2	0.73
		0.145	0.078		0.086	0.019	1.21	3.75	0.06	43.5	0.54	2.57	0.38	9.84	0.70
		0.147	0.076		0.068	0.019	1.19	3.67		43.8	0.54	2.74	0.33	9.66	0.68
		0.146	0.064		0.073	0.022	1.22	3.72	0.06	44.0	0.54	2.56	0.38	9.48	0.65
	0.085	0.152	0.070		0.090	0.013	1.21	3.55	0.16	39.6	0.50	2.37	0.36	9.49	0.67
		0.159	0.077		0.080	0.020	1.17	3.74	0.05	43.1	0.55	2.58	0.37	9.29	0.63
		0.177	0.082		0.064	0.018	1.23	3.83	0.08	42.9	0.56	2.69	0.35	9.59	0.66
		0.186	0.074		0.063	0.023	1.29	3.93		44.3	0.56	2.62	0.41	10.4	0.67
		0.169	0.078		0.057	0.013	1.20	3.71	0.04	39.1	0.50	2.53	0.38	9.84	0.68
	0.232	0.169	0.078	0.119	0.158	0.015	1.26	3.75	0.16	41.0	0.54	2.59	0.36	9.76	0.70
NFR1109		0.088	0.027		0.121	0.028	4.80	16.00	0.06	128	2.37	10.20	0.31	15.8	2.29
		0.117	0.033	0.052	0.143	0.029	4.67	15.30	0.06	122	2.17	10.10	0.37	15.2	2.11
		0.083	0.025	0.027	0.135	0.017	4.80	15.90		128	2.29	10.40	0.34	16.3	2.25
		0.091	0.024	0.046	0.131	0.009	4.83	15.60	0.07	135	2.25	10.40	0.34	16.9	2.43
		0.105	0.030	0.031	0.114	0.009	4.86	16.00	0.04	137	2.39	10.90	0.36	17.4	2.46
		0.086	0.034		0.228	0.018	4.89	16.00	0.07	131	2.35	10.80	0.42	17.6	2.44
		0.093	0.027		0.106	0.009	4.99	16.80	0.05	134	2.50	10.80	0.43	18.6	2.60
	0.033	0.090	0.028		0.131	0.017	4.97	16.90	0.11	133	2.41	11.10	0.41	18.5	2.66
		0.088	0.023		0.122	0.016	4.94	16.60	0.08	132	2.53	11.60	0.47	18.8	2.50
		0.091	0.022	0.040	0.131	0.015	4.91	16.10	0.10	135	2.42	11.50	0.39	18.5	2.52
NFR0309		0.468	0.105	0.051	0.338	0.052	3.40	8.04	0.17	34.2	1.07	5.38	1.16	41.3	2.01
		0.536	0.146	0.036	0.522	0.024	2.43	5.55	0.04	58.9	0.89	4.43	1.15	39.4	1.63
		0.498	0.142	0.052	0.477	0.043	3.15	7.10	0.02	45.0	0.99	4.81	1.08	37.7	1.76
		0.610	0.154	0.030	0.612	0.023	2.99	6.31	0.03	49.7	0.98	5.20	0.94	35.5	1.99
		0.530	0.152	0.038	0.363	0.038	3.03	6.83		46.8	1.05	5.16	1.14	38.7	1.91
		0.508	0.140	0.086	0.483	0.041	3.00	6.76	0.06	48.6	1.00	4.96	1.25	41.8	1.97
NFR1107		0.098	0.040	0.071	0.253		1.35	5.34		111	1.03	5.68	0.81	27.5	1.56
		0.081	0.033	0.029	0.090		1.27	5.23	0.04	112	0.99	5.95	0.74	26.3	1.79
		0.110	0.049	0.025	0.062	0.013	1.71	5.66	0.09	105	1.09	5.57	0.75	27.6	1.39
		0.152	0.046	0.022	0.077	0.013	1.45	5.43		111	1.10	6.12	0.86	27.5	1.85
		0.128	0.063	0.029	0.068		1.58	5.36	0.07	101	1.02	5.75	0.90	27.7	1.57
		0.140	0.054	0.030	0.071		1.66	5.37	0.08	101	1.06	5.60	0.85	27.6	1.51

Eu	Gd	Tb	Ti	Dy	Ho	Y	Er	Tm	Yb	Lu	Sc	V	Cr	Co	Ni
1.11	2.97	0.42	338	2.52	0.49	12.2	1.31	0.18	1.19	0.16	81	226	9353	20	330
1.13	2.92	0.39	329	2.43	0.48	12.1	1.20	0.19	1.34	0.17	82	235	8221	21	332
0.95	2.68	0.34	335	2.18	0.43	10.9	1.04	0.17	1.11	0.15	87	255	9440	20	334
0.98	2.36	0.35	304	1.82	0.38	10.0	1.06	0.14	1.10	0.14	87	238	8227	21	332
0.96	2.41	0.34	290	1.88	0.41	9.95	1.06	0.15	0.99	0.12	87	237	8782	21	341
0.76	2.13	0.36	1750	2.50	0.53	13.1	1.51	0.21	1.49	0.20	61	268	7200	23	323
0.79	2.17	0.35	1800	2.50	0.52	12.9	1.56	0.23	1.47	0.21	61	263	7150	23	309
0.80	2.26	0.37	1970	2.72	0.55	13.8	1.57	0.22	1.48		62	271	6470	23	320
0.80	2.25	0.38	1840	2.56	0.54	13.2	1.57	0.23	1.60	0.19	61	260	7810	23	317
0.97	2.56	0.44	2640	2.91	0.61	15.5	1.80	0.26	1.74	0.25	65	303	7160	24	317
0.98	2.66	0.45	2660	2.98	0.63	15.9	1.86	0.26	1.78	0.26	63	292	6050	24	309
0.78	2.20	0.37	1660	2.49	0.53	13.2	1.53	0.22	1.44	0.20	64	265	8560	24	324
0.74	2.27	0.38	1680	2.44	0.54	13.3	1.53	0.20	1.49	0.22	63	276	7890	24	330
0.78	2.33	0.36	1930	2.67	0.52	13.8	1.63	0.23	1.49	0.22	64	283	7580	23	305
0.79	2.18	0.38	1850	2.70	0.55	14.0	1.58	0.22	1.60	0.23	64	272	8450	24	313
0.97	2.52	0.42	2360	3.00	0.62	15.9	1.86	0.27	1.86	0.25	70	310	9080	25	324
0.86	2.54	0.40	2290	2.82	0.60	15.8	1.72	0.27	1.67	0.25	69	305	8780	25	323
0.84	2.49	0.41	2090	2.76	0.56	14.6	1.67	0.24	1.64	0.21	65	283	8220	23	316
0.25	0.86	0.17	1850	1.30	0.30	7.86	0.91	0.13	0.99	0.14	61	264	6190	23	378
0.25	0.86	0.15	1720	1.29	0.31	7.69	0.91	0.13	0.92	0.14	62	262	6210	23	390
0.25	0.89	0.17	1820	1.33	0.31	7.81	0.94	0.13	0.93	0.14	62	268	6230	24	388
0.28	0.90	0.16	1990	1.31	0.30	8.11	0.97	0.14	0.94	0.14	62	280	6220	24	396
0.25	0.90	0.18	2090	1.41	0.32	8.14	0.98	0.14	1.13	0.13	63	283	6180	25	404
0.26	0.94	0.17	2050	1.40	0.31	8.32	0.95	0.15	0.97	0.15	62	275	6660	24	402
0.25	0.90	0.16	1880	1.39	0.30	7.94	0.93	0.14	0.97	0.14	62	274	6860	23	387
0.25	0.93	0.16	1900	1.36	0.31	8.07	0.98	0.14	1.03	0.14	64	271	6830	23	393
0.27	0.86	0.16	1880	1.35	0.32	7.99	0.96	0.13	0.96	0.14	64	271	6260	24	390
0.23	0.77	0.16	1710	1.26	0.29	7.71	0.89	0.15	0.97	0.14	62	271	6420	24	414
0.25	0.88	0.18	1860	1.25	0.31	7.70	0.93	0.16	1.05	0.14	62	269	6340	24	378
0.25	0.93	0.18	1850	1.22	0.32	7.91	0.90	0.14	0.98	0.14	61	275	6380	24	392
0.27	0.88	0.17	2030	1.42	0.31	8.43	0.97	0.15	1.05	0.15	62	294	7560	25	398
0.25	0.87	0.17	1800	1.33	0.31	7.77	0.90	0.14	1.05	0.15	61	272	6650	23	385
0.24	0.78	0.16	1770	1.35	0.30	7.76	0.91	0.14	1.02	0.14	60	284	6750	26	501
0.92	1.98	0.29	1100	1.76	0.33	8.49	0.95	0.13	0.92	0.12	70	266	9890	24	339
0.84	1.73	0.25	1040	1.61	0.30	7.89	0.74	0.12	0.88	0.12	73	291	10400	24	326
0.86	2.18	0.29	1100	1.76	0.34	8.66	0.91	0.13	0.86	0.13	64	255	10200	26	355
0.88	2.18	0.31	1080	1.84	0.34	9.14	0.92	0.14	0.94	0.13	60	236	10200	25	327
0.90	2.31	0.32	1090	1.93	0.36	9.10	0.90	0.14	0.99	0.12	63	248	10600	25	327
0.96	2.23	0.32	1170	2.04	0.35	9.29	1.00	0.16	0.94	0.13	67	257	10700	24	322
0.95	2.40	0.34	1260	2.11	0.38	9.71	1.01	0.14	0.95	0.13	52	220	10800	25	321
0.92	2.32	0.34	1320	2.01	0.39	9.66	1.08	0.16	0.96	0.14	54	222	11100	26	326
0.94	2.34	0.35	1410	2.12	0.40	10.3	1.07	0.15	1.04	0.14	57	224	11000	26	334
0.95	2.30	0.35	1270	2.05	0.37	9.79	0.96	0.15	0.97	0.15	53	214	10700	25	324
0.76	2.66	0.47	3711	3.64	0.76	20.6	2.26	0.31	1.93	0.30	65	269	5026	21	309
0.67	2.56	0.51	3885	3.46	0.73	20.0	2.06	0.27	1.99	0.29	67	280	5183	22	319
0.78	2.81	0.48	3755	3.35	0.76	20.0	2.26	0.29	1.91	0.29	65	273	5079	21	315
0.80	2.62	0.51	3660	3.88	0.76	21.1	2.26	0.30	2.20	0.31	55	246	5607	21	314
0.80	2.65	0.52	3828	3.79	0.77	20.8	2.21	0.32	2.26	0.32	60	257	5272	21	310
0.80	2.70	0.50	4113	3.85	0.84	21.5	2.34	0.32	2.10	0.32	64	268	4664	21	317
0.66	2.04	0.35	1865	2.27	0.51	11.8	1.17	0.18	1.02	0.15	83	285	8477	21	340
0.67	1.93	0.32	1779	2.17	0.45	11.3	1.11	0.17	1.06	0.16	79	282	9692	22	334
0.69	1.86	0.33	1844	2.24	0.47	11.9	1.19	0.17	0.94	0.11	83	285	8332	20	328
0.65	2.14	0.31	1903	2.18	0.49	11.8	1.30	0.17	0.97	0.15	83	287	8198	20	334
0.59	2.08	0.33	1860	2.11	0.46	11.8	1.23	0.17	1.04	0.13	82	282	8375	20	328
0.66	1.98	0.31	1755	2.09	0.44	11.5	1.38	0.17	1.09	0.13	86	283	8163	21	332

CLINOPYROXENE

Sample	Rb	Th	U	Ba	Nb	Ta	La	Ce	Pb	Sr	Pr	Nd	Hf	Zr	Sm
NMC1301		0.191	0.039	0.160	1.292	0.261	10.95	30.29	0.07	196	4.13	15.93	1.71	70.2	2.79
		0.207	0.042	0.168	1.265	0.295	10.27	29.30	0.07	188	4.09	15.81	1.28	62.0	2.55
		0.227	0.039	0.154	0.872	0.278	9.82	27.20	0.08	182	3.92	14.99	1.31	62.5	2.39
		0.217	0.039	0.184	1.660	0.238	11.84	31.18	0.10	210	4.06	15.76	1.22	62.9	2.49
		0.216	0.049	0.147	0.921	0.289	9.61	28.03	0.07	179	3.91	15.90	1.24	62.0	2.54
		0.184	0.039	0.111	0.781	0.255	8.86	24.74	0.07	169	3.49	13.43	0.45	43.1	1.86
		0.172	0.036	0.155	1.356	0.265	10.16	26.69	0.08	192	3.52	11.71	0.40	38.4	1.81
		0.161	0.043	0.092	0.783	0.214	8.61	24.61	0.10	167	3.39	13.48	0.44	44.2	1.82
NMC1309		0.046	0.010	0.037	0.058	0.014	1.97	5.75	0.03	56.1	0.80	3.61	0.51	13.1	1.03
		0.028	0.011	0.038	0.053	0.013	2.09	5.86	0.07	56.2	0.80	3.88	0.47	13.5	1.11
		0.046	0.017	0.045	0.088	0.014	2.16	6.24		59.4	0.87	3.74	0.35	13.2	1.13
		0.045		0.417	0.080	0.012	2.15	5.97	0.09	58.7	0.90	3.67	0.41	12.6	1.01
		0.023		0.169	0.069	0.015	1.93	5.61	0.05	55.0	0.80	3.49	0.32	13.7	1.09
		0.035		0.027	0.071	0.009	2.01	5.49	0.05	59.4	0.79	3.56	0.39	12.7	0.92
		0.029	0.010	0.409	0.145	0.025	2.08	5.73	0.04	55.9	0.80	3.67	0.40	13.1	0.99
		0.027	0.008	0.028	0.061		2.04	5.88	0.03	56.1	0.81	3.93	0.40	13.8	1.03
NMC1322	0.101	0.127	0.035	0.153	0.269	0.057	2.41	6.24	0.04	47.6	0.97	4.71	0.40	10.7	1.14
		0.146	0.031	1.824	0.246	0.062	2.50	6.52	0.06	48.4	1.07	4.72	0.35	10.4	1.25
	0.054	0.144	0.044	0.119	0.298	0.069	2.60	6.54	0.11	50.1	1.00	4.77	0.32	10.6	1.33
	0.064	0.170	0.030	0.250	0.225	0.048	2.74	6.94	0.17	53.8	0.92	4.87	0.35	10.4	1.31
	0.347	0.154	0.035	0.127	0.372	0.089	2.47	6.67	0.51	52.2	1.07	4.93	0.32	10.2	1.10
	0.067	0.144	0.043	0.885	0.332	0.077	2.71	6.74	0.08	54.8	1.03	4.80	0.34	10.1	1.20
		0.139	0.040	0.061	0.348	0.089	2.60	6.45	0.09	51.1	1.03	4.87	0.34	10.0	1.18
		0.160	0.036	0.907	0.204	0.058	2.70	6.77	0.07	53.5	0.99	4.80	0.37	10.1	1.15
NMC1336A		0.033	0.016	0.017		0.007	0.34	2.22		45.4	0.56	4.26	1.06	27.1	1.87
	0.050	0.093	0.063	0.047	0.011		0.48	2.14	0.05	37.7	0.51	3.62	0.96	26.8	1.75
		0.061	0.038		0.002		0.42	2.11	0.57	41.0	0.53	3.61	0.97	26.3	1.80
				0.011	0.008		0.38	2.27		45.7	0.58	4.03	0.93	26.0	1.80
		0.121	0.055	0.020			0.56	2.16	0.04	40.2	0.55	3.91	0.91	24.8	1.72
		0.097	0.050	0.081	0.010		0.51	2.19	0.06	40.4	0.55	4.17	0.89	25.8	1.62
		0.113	0.049	0.014		0.003	0.53	2.27	0.09	41.9	0.55	4.04	0.90	25.7	1.81
NMM1126	0.011	0.029	0.014		0.108	0.006	0.45	1.43		26.9	0.24	1.70	0.28	5.85	0.67
		0.032	0.014		0.097	0.011	0.48	1.40		27.3	0.24	1.48	0.25	6.04	0.66
		0.036	0.017	0.028	0.073	0.012	0.45	1.49		27.2	0.25	1.44	0.28	6.01	0.61
		0.037	0.017		0.053	0.009	0.46	1.38		26.3	0.26	1.53	0.30	6.20	0.66
	0.051	0.031	0.016	0.163	0.081	0.007	0.47	1.40	0.05	25.7	0.24	1.51	0.25	6.24	0.64
	1.060	0.034	0.019	0.473	0.110	0.010	0.44	1.37	0.20	26.8	0.24	1.50	0.23	6.04	0.67
		0.024	0.015		0.055	0.010	0.48	1.55	0.04	26.4	0.26	1.61	0.20	5.53	0.66
		0.030	0.019		0.051	0.014	0.51	1.65		25.8	0.25	1.53	0.26	5.72	0.68
		0.025	0.015		0.054	0.008	0.50	1.65		26.8	0.25	1.63	0.24	5.91	0.67
NMM0318		0.467	0.147	0.082	0.185	0.017	6.03	17.37	0.08	86.1	2.68	11.39	0.98	41.8	2.78
		0.502	0.135	0.113	0.197	0.016	6.41	18.61	0.24	88.5	2.85	12.06	1.11	43.0	2.84
		0.561	0.140	0.093	0.168	0.011	6.55	18.95	0.05	89.8	2.79	12.84	1.11	45.7	2.95
		0.540	0.135	0.101	0.198	0.008	6.30	19.02	0.06	88.5	2.98	13.21	1.12	51.7	2.80
		0.509	0.160	0.109	0.180		6.20	17.79		83.4	2.65	12.66	1.15	50.4	2.87
		0.428	0.130	0.085	0.217	0.021	6.13	18.61	0.06	87.9	2.84	12.60	1.16	54.7	3.24
NMM1115		3.420	1.011	0.019	0.036		1.24	2.50	0.04	46.6	0.46	2.89	0.63	20.4	1.08
		3.410	1.053	0.025	0.034	0.008	1.28	2.58	0.03	46.6	0.46	3.11	0.59	21.5	1.24
		3.460	1.106	0.060	0.070		1.14	2.43	0.05	48.0	0.46	3.17	0.60	19.3	1.11
		3.490	1.086	0.027	0.026		1.48	2.58	0.06	42.9	0.49	2.89	0.55	20.2	1.08
		3.630	1.065	0.186	0.183	0.008	1.43	2.60	0.10	43.0	0.47	2.85	0.53	19.4	1.37

Eu	Gd	Tb	Ti	Dy	Ho	Y	Er	Tm	Yb	Lu	Sc	V	Cr	Co	Ni
0.87	2.01	0.29	734	1.81	0.37	9.25	0.78	0.12	0.81	0.10	83	268	9151	22	355
0.83	1.87	0.27	674	1.74	0.31	8.58	0.86	0.12	0.63	0.11	84	270	8991	22	356
0.81	1.84	0.29	702	1.68	0.33	8.98	0.93	0.13	0.71	0.12	85	268	8908	22	358
0.85	1.85	0.29	688	1.76	0.35	8.80	0.87	0.10	0.80	0.09	82	266	8856	22	360
0.87	1.89	0.27	719	1.77	0.35	8.83	0.91	0.13	0.81	0.12	83	265	8871	22	358
0.62	1.55	0.25	669	1.31	0.27	7.31	0.82	0.10	0.67	0.08	83	268	8854	22	364
0.64	1.16	0.21	649	1.20	0.25	7.17	0.72	0.12	0.60	0.09	80	264	8852	22	360
0.69	1.41	0.22	682	1.26	0.28	7.60	0.72	0.11	0.75	0.09	83	267	8794	22	360
0.51	1.50	0.27	1223	2.12	0.52	13.4	1.50	0.24	1.57	0.21	66	256	6471	21	327
0.40	1.38	0.29	1191	2.05	0.50	13.3	1.50	0.20	1.41	0.23	68	256	5887	21	330
0.51	1.47	0.33	1387	2.41	0.51	14.2	1.61	0.19	1.53	0.21	67	263	6125	21	331
0.51	1.55	0.29	1273	2.10	0.49	13.6	1.70	0.23	1.48	0.20	65	252	6851	21	331
0.43	1.56	0.27	1250	2.23	0.50	13.1	1.34	0.23	1.41	0.23	66	253	6359	21	329
0.42	1.52	0.29	1274	2.02	0.43	13.5	1.38	0.20	1.53	0.21	67	255	5876	21	335
0.43	1.46	0.27	1119	2.04	0.43	12.2	1.40	0.21	1.40	0.20	67	244	5539	22	338
0.47	1.53	0.31	1164	2.02	0.47	12.6	1.38	0.19	1.56	0.20	67	253	6139	21	335
0.44	1.58	0.27	1215	2.18	0.48	13.5	1.48	0.25	1.55	0.17	71	241	7220	20	334
0.39	1.62	0.29	1201	2.37	0.52	13.7	1.53	0.20	1.68	0.21	72	244	6767	20	335
0.39	1.53	0.26	1216	2.26	0.54	13.9	1.56	0.20	1.38	0.22	73	243	6566	20	331
0.42	1.48	0.27	1173	2.20	0.53	13.6	1.44	0.24	1.77	0.21	72	239	7370	20	333
0.44	1.43	0.29	1170	2.25	0.49	13.5	1.53	0.23	1.43	0.22	71	242	6637	20	337
0.44	1.60	0.28	1100	2.09	0.51	13.7	1.48	0.21	1.58	0.23	70	240	7245	21	343
0.42	1.59	0.29	1213	2.07	0.48	13.9	1.48	0.23	1.63	0.23	74	246	6583	21	350
0.37	1.42	0.27	1145	2.18	0.48	13.5	1.53	0.19	1.48	0.23	71	240	6754	20	342
0.76	2.77	0.50	3121	3.65	0.75	20.3	2.26	0.27	1.86	0.24	66	252	8126	22	357
0.67	2.70	0.43	2763	3.24	0.72	19.3	2.01	0.27	1.86	0.26	68	246	7233	21	349
0.75	2.53	0.52	3017	3.62	0.75	19.9	2.06	0.27	1.77	0.25	65	248	7254	21	348
0.76	2.79	0.49	3024	3.62	0.80	20.1	2.10	0.26	1.83	0.23	65	250	7789	21	358
0.71	2.53	0.50	2741	3.58	0.77	19.4	2.16	0.29	1.85	0.23	63	243	7300	21	346
0.80	2.70	0.50	3042	3.64	0.76	20.2	2.16	0.28	1.81	0.25	64	245	8036	21	349
0.72	2.71	0.51	2972	3.56	0.77	20.2	2.17	0.27	1.64	0.27	64	245	7215	21	353
0.32	1.20	0.23	1590	1.93	0.44	11.7	1.33	0.21	1.48	0.19	65	263	7310	23	375
0.30	1.23	0.24	1620	1.97	0.45	11.9	1.46	0.20	1.41	0.19	67	264	7610	24	381
0.29	1.20	0.24	1610	1.94	0.46	11.8	1.33	0.19	1.35	0.20	66	264	7470	23	382
0.28	1.13	0.22	1580	1.91	0.46	11.7	1.38	0.20	1.33	0.19	67	257	7130	23	375
0.31	1.21	0.23	1570	1.96	0.44	11.6	1.35	0.20	1.37	0.19	68	260	7300	23	373
0.27	1.20	0.22	1620	1.90	0.42	11.1	1.28	0.20	1.34	0.19	69	267	7380	29	459
0.28	1.17	0.22	1540	1.73	0.40	10.7	1.24	0.18	1.25	0.18	64	270	7060	24	385
0.29	1.11	0.23	1640	1.82	0.44	11.2	1.31	0.18	1.31	0.18	64	271	8240	23	391
0.31	1.08	0.24	1680	1.95	0.46	11.3	1.41	0.21	1.35	0.20	65	273	7470	23	388
1.00	2.79	0.46	2117	3.27	0.72	18.3	1.86	0.29	1.88	0.25	57	229	4625	22	317
1.08	2.98	0.53	2149	3.35	0.73	18.8	2.20	0.26	1.96	0.27	57	229	4898	22	325
1.11	3.03	0.52	2122	3.39	0.72	18.6	2.02	0.27	1.93	0.32	56	225	5039	23	314
1.13	3.06	0.51	2064	3.55	0.72	19.0	2.04	0.26	1.92	0.25	56	220	4579	22	321
1.11	3.09	0.47	2018	3.48	0.74	18.6	2.01	0.30	1.98	0.26	55	227	5124	22	316
1.21	3.39	0.54	1960	3.55	0.70	18.5	2.16	0.30	1.92	0.28	54	222	4627	22	316
0.50	1.53	0.35	1820	2.31	0.51	13.1	1.50	0.20	1.20	0.20	73	270	6695	21	335
0.50	1.69	0.31	1865	2.23	0.52	13.5	1.43	0.23	1.35	0.18	72	270	6865	21	332
0.49	1.84	0.31	1751	2.27	0.48	12.9	1.48	0.23	1.29	0.19	73	267	7124	21	339
0.49	1.81	0.31	1788	2.16	0.51	12.9	1.49	0.19	1.37	0.20	74	271	7524	20	323
0.45	1.77	0.30	1666	2.32	0.49	12.5	1.37	0.20	1.21	0.20	71	259	7235	20	326

CLINOPYROXENE

Sample	Rb	Th	U	Ba	Nb	Ta	La	Ce	Pb	Sr	Pr	Nd	Hf	Zr	Sm
NME1122	0.668	0.289	0.075	0.155	0.046	0.006	2.30	4.49		49.0	0.53	2.53	0.50	13.7	0.93
	0.019	0.282	0.075		0.048		2.28	4.68	0.07	46.0	0.53	2.62	0.47	13.2	0.88
	0.053	0.320	0.092	0.062	0.143	0.007	2.27	4.47		45.7	0.49	2.51	0.44	13.5	0.90
		0.319	0.083	0.040	0.050	0.006	2.31	4.40		45.0	0.50	2.49	0.41	13.0	0.95
		0.299	0.075		0.060	0.006	2.36	4.50		44.7	0.52	2.44	0.45	13.3	0.90
		0.309	0.073		0.057	0.005	2.27	4.21	0.06	44.7	0.51	2.39	0.50	14.4	0.99
	0.054	0.308	0.075	0.037	0.094		2.24	4.25		46.3	0.49	2.50	0.47	14.0	0.93
		0.311	0.069		0.053	0.005	2.25	4.06		43.4	0.49	2.54	0.45	14.0	0.92
		0.296	0.079		0.057	0.005	1.81	3.65	0.06	45.0	0.46	2.60	0.44	13.8	0.94
		0.305	0.079		0.052	0.004	1.91	3.65	0.07	43.8	0.42	2.53	0.51	13.7	0.94
	0.036	0.312	0.076	0.049	0.060	0.007	1.87	3.47	0.13	44.4	0.45	2.54	0.53	14.4	1.02
NME0528		0.299	0.076		0.053	0.006	1.95	3.85	0.03	42.3	0.46	2.43	0.47	14.2	1.01
		0.115	0.022	0.125	0.207	0.057	4.26	12.68	0.06	107	1.97	8.31	0.96	41.7	1.96
		0.133	0.019	0.093	0.199	0.038	4.45	12.74	0.13	105	2.08	9.77	0.99	46.0	2.26
		0.131	0.029	0.070	0.200	0.075	4.53	13.04	0.13	110	1.90	8.32	1.14	42.1	2.20
	0.080	0.155	0.016	0.101	0.181	0.070	4.54	12.53	0.19	106	1.97	7.96	0.97	40.4	2.04
		0.142	0.030	0.106	0.166	0.036	4.25	12.19	0.05	104	1.82	7.86	0.98	39.7	2.02
		0.121	0.024	0.076	0.177	0.054	4.08	11.15	0.08	100	1.58	7.66	0.94	38.9	2.11
NME1116			0.009	0.030	0.059	0.007	0.70	2.71	0.02	63.7	0.51	2.80	0.37	16.1	0.98
				0.023	0.074	0.014	0.75	2.81	0.02	64.7	0.53	2.90	0.43	15.6	1.04
			0.007	0.020	0.054		0.75	2.77		62.8	0.51	2.83	0.40	16.4	0.87
					0.055	0.008	0.74	2.71	0.04	63.6	0.53	2.74	0.42	16.8	0.97
		0.014	0.015	0.024	0.065	0.010	0.74	2.78	0.03	63.6	0.52	3.16	0.47	17.4	1.12
		0.008	0.008	0.016	0.038	0.008	0.76	2.82	0.04	63.8	0.56	2.80	0.49	17.1	0.91
NBN0302A		0.066		0.101	0.069		1.00	3.26	0.07	46.9	0.54	3.73	0.92	28.0	1.78
		0.054	0.011	0.183	0.055		0.94	3.45	0.08	46.9	0.61	3.87	0.96	28.4	1.33
	0.286	0.045	0.012		0.068		0.85	3.27	0.11	48.6	0.65	4.21	1.09	28.6	1.26
	0.514	0.039	0.018	0.339			1.05	3.76	0.10	59.7	0.66	4.19	0.89	30.4	1.82
	0.612			0.718	0.036		0.66	3.14		45.8	0.56	3.41	0.91	24.6	1.45
		0.071	0.042		0.025		1.08	4.04	0.13	55.9	0.71	4.76	1.15	33.7	1.52
		0.088	0.019				1.06	3.92		50.5	0.64	4.06	1.01	31.0	2.00
		0.023			0.082		1.11	3.65	0.11	55.4	0.73	4.19	1.25	33.5	2.04
		0.042	0.014		0.048	0.008	1.09	4.33	0.07	50.8	0.79	4.06	0.89	26.6	1.50
		0.029	0.011		0.051		0.95	3.88	0.07	43.8	0.69	3.95	0.70	26.6	1.52
		0.035	0.030		0.050	0.013	0.94	3.94	0.09	48.4	0.74	4.23	0.71	26.3	1.60
		0.054	0.024		0.042	0.013	0.98	4.24	0.09	52.0	0.71	4.46	0.83	24.8	1.51
NBN0305		0.039	0.011		0.051		1.55	4.17	0.21	94.4	0.63	3.58	0.43	8.67	1.12
		0.018	0.010				1.60	4.34	0.14	90.4	0.60	3.32	0.39	8.54	1.17
		0.020			0.057		1.54	4.07	0.14	94.9	0.70	3.50	0.38	9.14	1.18
	0.198	0.027		0.805			1.57	4.03	0.19	91.7	0.70	3.39	0.41	8.28	1.11
		0.039		0.127	0.039		1.57	4.37	0.15	93.5	0.74	3.35	0.56	8.93	1.05
	0.533	0.014		0.866			1.61	3.91	0.15	91.1	0.65	3.64	0.32	8.03	1.23
	0.054			0.258	0.055		1.01	3.76	0.12	86.6	0.71	3.70	0.37	6.01	1.45
			0.011		0.046		1.51	4.06	0.11	98.5	0.66	3.53	0.38	7.78	0.96
		0.018			0.046		1.48	4.18	0.18	92.6	0.68	3.19	0.27	7.72	0.82

Eu	Gd	Tb	Ti	Dy	Ho	Y	Er	Tm	Yb	Lu	Sc	V	Cr	Co	Ni
0.42	1.38	0.24	2230	1.63	0.32	8.26	0.90	0.13	0.86	0.11	58	293	8630	24	379
0.41	1.28	0.23	2050	1.53	0.31	8.07	0.86	0.12	0.82	0.12	57	292	8230	24	376
0.37	1.31	0.22	2200	1.56	0.30	8.10	0.92	0.12	0.84	0.12	58	293	8400	24	408
0.40	1.26	0.23	2250	1.56	0.31	8.28	0.86	0.13	0.82	0.13	55	288	8160	23	364
0.39	1.38	0.23	2270	1.64	0.31	8.28	0.92	0.14	0.93	0.12	56	287	8300	22	354
0.39	1.32	0.23	2280	1.60	0.32	8.58	0.88	0.13	0.92	0.12	60	290	8270	22	362
0.39	1.35	0.23	2110	1.51	0.32	8.44	0.96	0.13	0.86	0.13	59	279	8120	24	449
0.38	1.37	0.23	2210	1.65	0.33	8.38	0.89	0.12	0.84	0.13	58	277	8330	22	358
0.41	1.30	0.22	2390	1.58	0.32	8.20	0.87	0.14	0.91	0.13	59	295	8440	24	384
0.36	1.27	0.23	2250	1.58	0.32	8.13	0.86	0.12	0.88	0.13	59	290	8190	23	379
0.39	1.33	0.22	2450	1.63	0.32	8.62	0.87	0.14	0.93	0.12	59	300	8450	23	384
0.36	1.20	0.22	2390	1.55	0.33	8.24	0.95	0.14	0.86	0.12	58	305	8870	24	387
0.70	2.05	0.33	1403	1.96	0.43	10.9	1.17	0.16	1.15	0.13	80	270	8486	21	323
0.83	2.14	0.32	1430	2.42	0.46	11.4	1.25	0.18	1.06	0.16	77	263	9692	21	319
0.68	1.92	0.35	1450	2.17	0.47	10.9	1.14	0.15	0.95	0.16	81	273	10780	21	322
0.74	2.04	0.28	1388	2.11	0.42	11.1	1.17	0.14	1.20	0.13	77	267	9146	21	326
0.70	2.01	0.31	1368	2.07	0.44	10.9	1.25	0.15	1.13	0.15	75	267	8637	20	324
0.66	2.04	0.34	1331	2.17	0.42	10.6	1.09	0.18	0.99	0.13	77	259	8078	21	328
0.37	1.15	0.25	1625	1.91	0.43	11.5	1.26	0.17	1.32	0.21	69	268	6966	20	329
0.37	1.53	0.25	1535	1.98	0.47	11.5	1.27	0.21	1.30	0.19	68	262	7057	21	329
0.38	1.44	0.24	1611	1.97	0.43	11.6	1.32	0.19	1.25	0.19	71	269	7091	21	332
0.39	1.36	0.27	1682	1.99	0.43	11.8	1.24	0.21	1.37	0.19	71	269	7476	21	329
0.43	1.62	0.26	1706	2.06	0.44	12.0	1.42	0.18	1.32	0.18	72	271	6860	21	332
0.42	1.46	0.26	1732	1.94	0.46	12.0	1.27	0.16	1.28	0.19	69	266	7777	21	327
0.62	1.95	0.37	1729	2.39	0.44	12.0	1.49	0.21	1.55	0.17	56	224	6408	22	352
0.44	2.54	0.39	1908	2.57	0.52	13.3	1.66	0.22	1.65	0.20	59	239	7181	22	360
0.66	2.18	0.39	1883	2.42	0.57	12.6	1.34	0.15	1.73	0.21	60	232	6018	22	363
0.72	2.27	0.35	2089	2.65	0.51	13.9	1.77	0.19	1.34	0.20	63	243	6033	23	348
0.46	1.95	0.31	1643	2.10	0.43	11.4	1.08	0.19	1.30	0.16	56	212	5112	25	397
0.62	2.42	0.47	1799	2.65	0.60	16.2	1.72	0.27	1.69	0.27	63	245	4464	22	343
0.57	1.88	0.43	1652	2.94	0.70	15.2	1.46	0.21	1.66	0.19	62	236	4386	21	352
0.73	2.10	0.39	1813	2.78	0.57	15.8	1.64	0.24	1.52	0.21	67	250	4444	22	345
0.77	2.35	0.37	2735	2.53	0.51	13.8	1.47	0.24	1.54	0.23	52	256	7261	22	345
0.67	2.10	0.35	2185	2.25	0.49	12.8	1.40	0.17	1.34	0.17	54	255	7103	22	343
0.66	1.79	0.37	2658	2.81	0.51	13.6	1.56	0.18	1.55	0.18	50	251	7248	22	338
0.75	2.39	0.38	2712	2.57	0.52	14.1	1.60	0.22	1.49	0.21	51	253	7338	22	345
0.31	1.19	0.17	1059	1.21	0.29	6.84	0.77	0.10	0.75	0.13	67	245	5923	23	362
0.40	1.58	0.23	1103	1.46	0.24	6.71	0.72	0.12	0.62	0.11	68	246	5852	22	364
0.33	1.02	0.22	1057	1.31	0.31	6.84	0.79	0.12	0.80	0.11	66	246	6742	22	361
0.38	1.01	0.23	1071	1.38	0.23	6.89	0.73	0.10	0.73	0.10	68	242	5398	23	361
0.39	1.15	0.22	1071	1.29	0.31	6.91	0.75	0.09	0.80	0.09	67	247	5449	22	360
0.37	1.28	0.26	1084	1.35	0.23	6.96	0.78	0.13	0.74	0.10	66	246	5685	24	369
0.36	1.40	0.19	1953	1.03	0.28	6.44	0.81	0.09	0.89	0.11	66	315	6562	24	396
0.31	1.44	0.16	1071	1.32	0.23	5.49	0.73	0.12	0.61	0.10	62	256	6214	22	382
0.39	1.00	0.15	1026	1.22	0.20	5.69	0.72	0.08	0.47	0.07	63	258	6172	23	373

CLINOPYROXENE

Sample	Rb	Th	U	Ba	Nb	Ta	La	Ce	Pb	Sr	Pr	Nd	Hf	Zr	Sm
NBN0311	0.008	0.111	0.017	0.047	0.108	0.014	1.06	3.66	0.03	66.2	0.63	3.92	0.96	27.4	1.73
	0.029	0.083	0.005		0.092	0.018	1.08	3.56	0.04	64.7	0.69	3.84	0.96	27.7	1.34
		0.033	0.010		0.117	0.012	0.95	3.67		64.2	0.68	3.70	0.99	28.1	1.68
		0.034	0.006		0.115	0.020	1.03	3.67		59.3	0.59	4.16	0.79	25.4	1.43
		0.047	0.010		0.092	0.018	0.95	3.66	0.03	58.6	0.64	3.71	0.76	25.8	1.34
		0.033	0.010	0.050	0.103	0.022	1.00	3.76	0.04	62.4	0.65	3.65	0.74	24.3	1.33
		0.020	0.023		0.155	0.024	1.11	3.68	0.04	61.2	0.64	3.77	0.75	24.2	1.59
		0.033	0.019		0.126	0.024	1.04	3.58	0.03	62.8	0.57	3.92	0.65	22.8	1.39
	0.576	0.034	0.014	0.364	0.076	0.013	0.99	3.60		56.8	0.60	3.64	0.73	25.5	1.65
		0.026	0.013		0.081	0.016	1.02	3.72	0.02	59.7	0.60	3.81	0.79	25.1	1.47
		0.022	0.018		0.082	0.009	1.07	3.64	0.03	57.9	0.63	3.70	0.77	26.5	1.59
		0.023	0.005		0.050	0.010	0.93	3.43	0.03	61.5	0.58	3.53	0.78	24.8	1.30
							1.02	3.47		58.4	0.58	3.50	0.80	26.8	1.42
					0.071		0.98	3.18		58.6	0.65	4.01	0.82	25.4	1.56
		0.035	0.016			0.020	0.96	3.37		57.0	0.64	3.45	0.94	26.2	1.43
			0.011				0.90	3.51		58.5	0.52	3.77	0.67	27.2	1.37
		0.032	0.020				1.01	3.77		60.6	0.61	3.53	0.78	27.1	1.91
		0.035	0.011				1.02	3.58		62.4	0.56	3.46	0.84	26.2	1.53
NBN0316		0.104	0.020				0.67	2.29	0.23	19.3	0.44	2.58	0.69	17.8	1.05
		0.052	0.013				0.64	2.46	0.25	18.9	0.47	2.92	0.73	18.9	1.24
		0.060	0.015		0.073		0.72	2.57	0.25	21.0	0.48	3.13	0.68	18.4	1.09
		0.039	0.014		0.077		0.59	2.46	0.32	20.7	0.41	2.58	0.78	16.4	1.16
	0.055	0.083	0.020		0.057		0.77	2.46	0.22	18.7	0.50	2.70	0.80	17.5	1.22
		0.072	0.021		0.060		0.67	2.62	0.19	18.2	0.42	2.89	0.36	16.2	1.03
		0.096	0.014		0.060		0.69	2.47	0.22	19.2	0.43	2.43	0.51	15.9	1.26
		0.066		0.296			0.64	2.91	0.22	19.1	0.41	2.84	0.49	15.8	1.30
		0.063	0.014				0.52	2.39	0.31	21.5	0.52	2.96	0.66	15.4	0.92
		0.079	0.019	0.104	0.055		0.55	2.52	0.55	19.6	0.45	3.15	0.56	15.8	0.72
		0.055	0.019		0.053		0.65	2.32	0.21	20.7	0.45	3.28	0.67	15.7	1.39
NBN1309		0.025					0.62	2.48	0.26	22.0	0.42	2.70	0.66	19.0	1.08
		0.023	0.010		0.013		0.66	2.54	0.22	22.2	0.46	2.76	0.78	18.7	1.07
	0.017	0.025	0.006		0.026	0.004	0.64	2.47	0.23	22.2	0.48	2.79	0.73	19.3	1.13
	0.017				0.023		0.62	2.53	0.27	23.3	0.49	2.73	0.58	14.3	0.95
		0.018			0.066		0.57	2.57	0.25	23.2	0.44	2.91	0.65	15.5	0.81
		0.014			0.053		0.61	2.91	0.19	23.2	0.56	3.00	0.66	15.5	1.12
							0.67	2.69	0.23	23.0	0.48	2.86	0.46	15.1	0.94
		0.038	0.010		0.020		0.58	2.45	0.23	22.3	0.46	2.52	0.51	16.0	1.13
		0.024					0.58	2.32	0.22	21.6	0.44	2.30	0.60	15.3	0.87
		0.020				0.008	0.60	2.53	0.25	21.9	0.56	2.61	0.48	16.1	1.12
		0.015	0.014				0.63	2.63	0.22	22.2	0.52	2.72	0.58	15.7	1.33
		0.026	0.007				0.60	2.82	0.23	21.9	0.48	2.85	0.56	16.7	1.11

Eu	Gd	Tb	Ti	Dy	Ho	Y	Er	Tm	Yb	Lu	Sc	V	Cr	Co	Ni
0.56	2.55	0.41	2353	3.03	0.64	16.1	1.79	0.26	1.57	0.24	67	275	5298		
0.68	2.29	0.35	2439	2.66	0.67	16.6	1.93	0.27	1.78	0.26	68	277	5563		
0.65	2.51	0.45	2473	3.14	0.59	16.3	2.06	0.25	1.63	0.27	66	279	5556		
0.74	2.28	0.39	2591	2.82	0.56	15.7	1.71	0.23	1.77	0.23	53	249	6528		
0.64	2.30	0.37	2484	2.74	0.62	15.6	1.79	0.21	1.78	0.25	56	256	6487		
0.63	2.11	0.46	2594	2.97	0.63	15.6	1.78	0.27	1.82	0.23	51	247	6587		
0.61	2.02	0.41	2592	2.91	0.59	15.8	1.67	0.26	1.66	0.24	51	246	6668		
0.71	2.27	0.38	2644	2.81	0.57	15.3	1.84	0.25	1.70	0.20	53	249	6767		
0.68	1.84	0.38	2364	2.65	0.60	14.8	1.62	0.21	1.64	0.26	58	266	6347		
0.64	2.15	0.45	2540	3.06	0.54	15.2	1.68	0.25	1.77	0.22	56	258	6522		
0.63	1.82	0.41	2470	2.88	0.61	15.5	1.83	0.23	1.66	0.22	61	265	6203		
0.63	2.00	0.35	2121	2.82	0.58	14.9	1.63	0.23	1.54	0.22	64	264	5335		
0.50	1.90	0.39	2150	3.01	0.43	14.9	1.70	0.27	1.35	0.23	64	273	5402		
0.69	2.31	0.46	2100	2.68	0.53	14.9	1.73	0.22	1.28	0.25	64	273	5310		
0.52	1.88	0.44	2137	2.78	0.54	15.1	1.76	0.21	1.79	0.28	64	275	5644		
0.62	2.49	0.43	2296	3.03	0.69	15.9	2.01	0.24	1.83	0.21	64	275	5906		
0.61	2.23	0.44	2350	2.57	0.62	16.1	1.97	0.21	1.78	0.24	64	276	5871		
0.62	2.02	0.40	2169	3.30	0.62	15.0	1.77	0.31	1.42	0.24	64	273	5392		
0.53	1.46	0.33	1340	2.26	0.44	11.0	1.15	0.13	1.12	0.15	48	177	3348	23	367
0.44	1.47	0.29	1333	2.20	0.44	11.1	1.44	0.19	1.17	0.17	48	178	3409	23	371
0.55	1.79	0.32	1334	1.99	0.45	11.0	1.21	0.20	1.17	0.19	48	179	3404	24	369
0.37	1.46	0.30	1252	1.94	0.39	10.9	1.34	0.12	0.86	0.15	45	172	3092	24	372
0.44	1.26	0.27	1286	2.24	0.44	10.2	1.09	0.15	1.14	0.13	44	172	3249	25	371
0.39	2.14	0.27	1214	1.63	0.42	9.71	1.08	0.16	1.15	0.15	42	176	3232	24	357
0.50	1.39	0.28	1289	2.04	0.35	9.92	1.25	0.15	0.91	0.17	44	179	3349	23	369
0.47	1.93	0.32	1259	1.90	0.37	9.67	0.97	0.16	1.16	0.14	42	180	3297	23	364
0.54	1.39	0.26	1295	2.01	0.41	9.07	1.05	0.17	1.01	0.17	45	183	3146	24	368
0.39	1.53	0.29	1278	1.78	0.41	8.78	1.09	0.14	0.54	0.14	43	178	3320	22	373
0.60	1.25	0.30	1312	1.72	0.43	9.49	1.10	0.17	1.10	0.13	42	182	3309	23	359
0.49	1.44	0.28	1352	2.07	0.36	10.9	1.13	0.17	1.18	0.16	45	175	3044		
0.44	1.44	0.29	1340	1.78	0.39	10.2	1.13	0.16	1.13	0.17	46	169	2903		
0.44	1.47	0.29	1351	1.88	0.41	10.3	1.17	0.13	1.10	0.16	46	169	2870		
0.33	1.10	0.22	1133	1.59	0.30	7.58	0.95	0.12	0.84	0.14	39	170	3018		
0.37	1.38	0.22	1194	1.64	0.33	8.06	0.99	0.16	0.96	0.12	40	173	3150		
0.48	1.08	0.24	1161	1.58	0.30	8.31	0.83	0.11	1.04	0.13	41	175	3040		
0.42	1.13	0.25	1121	1.70	0.31	7.88	0.98	0.11	0.83	0.13	38	172	2985		
0.35	1.51	0.27	1277	1.60	0.28	8.71	0.89	0.12	0.86	0.13	41	174	3147		
0.44	1.52	0.26	1251	1.80	0.33	8.46	1.10	0.13	1.09	0.16	42	172	3185		
0.46	1.66	0.22	1275	1.59	0.36	9.06	1.01	0.19	0.88	0.13	41	175	3091		
0.44	1.57	0.22	1271	1.68	0.33	8.53	1.18	0.13	0.97	0.15	41	174	3070		
0.47	1.55	0.30	1278	1.66	0.33	9.14	1.11	0.14	1.14	0.14	41	176	3225		

CLINOPYROXENE

Sample	Rb	Th	U	Ba	Nb	Ta	La	Ce	Pb	Sr	Pr	Nd	Hf	Zr	Sm
NBN0321	0.049	0.012	0.023		0.104		1.03	4.05	0.06	66.5	0.67	4.98	1.00	27.5	1.88
							0.46	2.47	0.15	35.3	0.54	3.88	0.74	16.5	1.51
	0.102			0.473	0.193		0.46	2.61		43.6	0.56	3.93	0.71	16.7	1.94
		0.062	0.012	0.210	0.075		1.02	4.06		67.3	0.72	4.47	1.05	27.8	1.92
		0.034					0.89	3.96	0.05	64.4	0.68	3.84	1.01	26.1	1.46
		0.016	0.011	0.038	0.085	0.016	0.96	3.63	0.03	63.4	0.64	3.95	1.07	26.1	1.93
	0.384		0.008	1.612	0.260	0.026	0.85	3.44	0.15	62.9	0.65	4.46	0.79	24.5	2.22
	0.378			0.531	0.101		0.41	2.14	1.08	37.2	0.50	3.62	0.69	14.5	1.95
		0.048			0.071		1.03	3.96	0.04	63.5	0.68	4.29	1.05	27.5	1.78
	0.127	0.007		0.193	0.120	0.015	0.40	1.93	0.14	35.3	0.52	3.49	0.84	13.7	2.03
		0.045	0.010		0.034	0.012	1.07	3.86	0.03	56.7	0.69	4.17	0.96	28.6	1.88
		0.029	0.022	0.055	0.063	0.015	1.17	3.96	0.03	61.7	0.77	3.92	0.97	28.7	1.69
		0.036		0.055	0.079		0.99	3.58		53.9	0.67	3.77	0.91	26.1	1.81
					0.084		0.35	1.96	0.13	32.9	0.50	3.48	0.84	15.7	2.04
							0.64	2.78		43.4	0.59	3.77	0.83	20.6	1.83
						0.017	0.50	2.45		38.0	0.51	4.26	0.83	19.3	2.24
		0.014			0.073		1.10	3.77		56.1	0.66	3.99	1.21	28.9	2.10
					0.051		1.06	3.90		59.0	0.68	3.73	0.75	28.8	1.73
		0.020			0.026		1.01	3.78		57.7	0.66	3.47	1.11	29.5	1.81
							1.12	3.53		53.1	0.67	3.79	1.01	28.0	1.85
		0.026	0.012		0.099		0.91	3.85		53.4	0.66	3.90	0.64	29.0	1.83
		0.015			0.058		1.10	3.62		54.1	0.69	3.29	1.04	29.5	1.69
		0.038		0.173		0.021	1.03	3.69		72.7	0.63	3.91	1.01	28.9	1.40

Eu	Gd	Tb	Ti	Dy	Ho	Y	Er	Tm	Yb	Lu	Sc	V	Cr	Co	Ni
0.64	2.59	0.40	2467	3.25	0.64	14.3	1.71	0.26	1.51	0.19	70	289	5243	20	333
0.71	2.96	0.58	4393	3.02	0.66	15.0	1.83	0.26	1.80	0.19	64	298	4690	27	393
0.88	3.26	0.54	6282	3.73	0.70	17.6	1.95	0.21	1.62	0.25	85	460	8221	24	382
0.76	2.73	0.54	2494	3.22	0.66	13.8	2.04	0.21	1.47	0.23	70	292	5536	21	337
0.75	2.26	0.51	2329	3.09	0.62	13.5	1.68	0.18	1.67	0.18	70	279	5461	21	341
0.76	3.09	0.54	4042	3.47	0.73	16.9	2.00	0.24	1.66	0.23	81	358	6882	21	352
0.87	3.75	0.55	5402	3.97	0.76	19.1	2.46	0.29	1.84	0.25	85	377	6711	23	365
0.87	4.13	0.64	7028	4.35	0.87	20.9	2.70	0.29	1.99	0.26	92	475	8382	29	483
0.75	2.30	0.46	2261	2.92	0.59	13.8	1.45	0.23	1.21	0.21	72	274	5506	21	338
0.91	3.89	0.71	7341	4.35	0.91	22.2	2.55	0.30	2.11	0.26	96	521	9659	26	411
0.79	2.78	0.45	2739	3.03	0.56	14.7	1.65	0.19	1.18	0.20	73	296	6269	21	342
0.79	2.89	0.50	2953	3.33	0.59	15.5	1.75	0.23	1.38	0.19	72	296	6441	21	336
0.73	2.38	0.40	2105	2.74	0.51	12.9	1.44	0.19	1.02	0.19	70	279	5819	21	344
0.68	2.84	0.51	5304	3.00	0.66	16.7	1.99	0.26	1.56	0.25	70	346	6362	29	424
0.79	2.61	0.53	4164	3.32	0.65	16.0	1.83	0.24	1.18	0.17	73	321	6120	26	397
0.82	2.70	0.50	4733	3.48	0.66	15.9	1.84	0.28	1.23	0.22	70	330	6063	28	416
0.74	2.37	0.45	2412	2.84	0.64	14.5	1.34	0.19	1.18	0.20	75	300	5713	22	355
0.69	2.84	0.40	2592	2.56	0.61	14.5	1.39	0.21	1.32	0.23	75	299	5619	21	349
0.56	2.84	0.48	2507	2.75	0.52	14.8	1.50	0.22	1.38	0.19	76	296	5668	22	353
0.74	2.52	0.47	2177	2.77	0.50	13.3	1.46	0.20	1.10	0.18	72	290	6603	22	362
0.66	2.37	0.42	2460	2.80	0.57	13.9	1.63	0.16	1.61	0.24	71	298	6842	21	348
0.67	1.68	0.41	2287	2.94	0.57	13.5	1.50	0.22	1.50	0.18	73	289	6545	21	352
0.67	2.98	0.42	2656	3.25	0.61	15.3	1.45	0.23	1.31	0.16	76	305	5790	22	348

AMPHIBOLE

Sample	Rb	Th	U	Ba	Nb	Ta	La	Ce	Pb	Sr	Pr	Nd	Hf	Zr	Sm
NMS1304	5.71	0.085		247	3.39	0.39	5.94	15.2	0.87	351	2.17	9.47	0.80	26.2	2.37
	5.96	0.10	0.015	251	3.53	0.39	5.89	14.8	0.90	358	2.09	9.44	0.83	26.9	1.98
	11.9	0.12	0.017	118	3.82	0.43	6.40	16.3	0.11	329	2.23	10.9	0.99	29.3	2.87
	12.6	0.093	0.010	137	3.54	0.41	5.78	15.2	0.42	372	2.20	9.44	0.74	28.0	2.22
	5.80	0.067	0.017	252	3.39	0.42	5.94	15.2	0.87	352	2.21	10.3	0.97	27.5	2.37
	5.86	0.085	0.022	248	3.46	0.40	5.96	15.4	0.93	355	2.12	10.0	0.87	26.9	2.08
	4.85	0.10		219	3.75	0.45	5.78	14.5	0.88	363	2.05	9.31	0.91	26.8	2.25
NMS1308	4.62	0.021	0.014	34.8	6.55	0.49	0.81	3.72	0.25	145	0.89	5.25	0.89	26.5	2.40
	6.74	0.027	0.020	36.6	5.38	0.23	1.26	3.39	0.08	125	0.60	2.88	0.92	33.5	1.30
	2.18			29.3	6.70	0.50	0.55	3.04	0.05	136	0.67	5.05	0.77	20.2	2.20
NJS1302			0.017	0.94	1.04	0.07	1.26	7.15		208	1.72	12.0	1.74	64.7	4.38
	0.22		0.027	1.44	1.85	0.28	2.65	12.1		197	2.42	14.0	2.28	87.6	4.27
NFL1302	6.06	0.11	0.020	77.9	14.0	0.43	3.38	7.89	0.13	139	1.04	4.93	0.66	24.6	1.79
	6.63	0.10	0.036	88.8	12.3	0.34	2.96	7.06	0.12	135	0.94	4.08	0.66	22.5	1.39
NFL1315A	7.23	0.36	0.058	178	98.6	5.34	17.2	49.4	0.40	475	7.60	34.1	4.28	150	7.42
	7.39	0.35	0.082	178	94.5	5.14	17.1	49.5	0.43	465	7.66	35.6	3.74	144	7.27
	9.05	0.27	0.062	140	56.6	2.17	11.3	34.6	0.41	392	5.52	25.5	2.92	117	5.84
	9.68	0.21	0.048	134	56.3	2.19	11.4	34.1	0.43	388	5.31	25.2	2.72	114	5.58
	3.83	0.23	0.044	151	56.4	2.44	10.3	31.8	0.61	445	5.09	25.2	2.60	110	5.91
NFL1324	11.3	0.51	0.169	316	74.0	4.92	20.0	55.6	1.50	399	7.86	36.1	3.84	169	6.99
	11.0	0.55	0.157	336	70.5	3.72	20.6	56.8	1.57	400	8.20	36.7	3.81	170	6.98
	10.9	0.62	0.178	281	73.4	3.50	21.0	57.8	1.65	400	8.52	36.4	3.53	171	7.01
	13.1	0.61	0.187	343	84.4	4.76	23.2	63.1	1.74	433	9.20	40.9	4.33	176	7.84
	13.4	0.60	0.178	318	85.9	4.85	23.3	62.8	1.61	438	9.31	41.3	4.13	178	7.88
	13.0	0.56	0.163	337	87.6	4.99	23.3	63.3	1.63	439	9.24	41.5	4.62	176	7.48
	13.5	0.63	0.199	318	90.6	5.15	23.4	65.3	1.83	456	9.23	41.1	4.41	178	7.88
NFL1326	8.61	0.11	0.020	139	17.7	0.70	5.47	15.6	0.20	256	2.40	11.5	1.09	33.6	3.06
	8.56	0.12	0.029	139	18.3	0.72	5.50	15.7	0.25	256	2.39	11.5	1.09	33.0	3.11
	8.87	0.10	0.016	145	19.1	0.76	5.71	16.2	0.25	262	2.44	11.5	1.05	34.9	2.64
	7.54	0.11	0.027	145	17.6	0.59	6.00	16.6	0.25	267	2.44	12.1	0.99	32.7	2.79
	7.45	0.11	0.031	118	16.3	0.67	5.73	16.0	0.23	259	2.53	11.5	1.00	33.5	3.13
	5.45	0.085	0.032	108	15.4	0.98	4.86	14.1	0.24	210	2.25	11.3	0.88	32.0	2.90
NFL1329	2.15	0.18	0.079	8.98	2.89	0.20	1.21	3.59	0.33	131	0.64	3.72	0.87	26.5	1.58
	3.19	0.22	0.096	29.4	2.76	0.20	1.55	3.81	0.28	126	0.76	3.97	0.87	26.9	1.93
	2.80	0.19	0.098	22.1	2.60	0.16	1.39	3.96	0.30	123	0.67	4.00	0.85	27.2	1.70

Eu	Gd	Tb	Ti	Dy	Ho	Y	Er	Tm	Yb	Lu	Sc	V	Cr	Co	Ni
0.89	2.99	0.38	7891	2.32	0.49	13.0	1.23	0.17	1.03	0.20	80	522	10778	38	852
0.81	2.35	0.39	8038	2.51	0.45	12.1	1.27	0.15	1.01	0.15	81	534	11390	39	880
0.85	2.74	0.37	8648	2.60	0.55	13.2	1.40	0.18	1.12	0.18	88	578	12092	42	962
0.83	2.53	0.41	8260	2.40	0.47	12.9	1.25	0.17	1.21	0.16	82	535	10976	38	855
0.91	2.30	0.40	7975	2.63	0.53	13.2	1.37	0.19	0.95	0.15	83	539	11130	39	884
0.85	2.62	0.40	8085	2.72	0.47	12.4	1.22	0.17	1.21	0.17	80	546	11704	40	885
0.75	2.45	0.33	8079	2.45	0.51	11.8	1.16	0.16	0.97	0.15	80	544	12436	39	875
1.00	3.10	0.52	14611	3.70	0.79	20.0	2.15	0.29	1.74	0.26	45	370	8822	43	819
0.56	1.64	0.31	10154	2.42	0.54	14.5	1.56	0.22	1.33	0.22	43	320	11137	34	759
0.87	2.99	0.54	18709	3.61	0.76	20.3	1.97	0.27	1.86	0.25	47	398	8858	42	858
1.58	5.96	1.03	37920	6.85	1.36	34.7	3.41	0.43	2.48	0.39	54	539	4201	46	799
1.46	4.59	0.78	25602	4.95	1.06	27.7	2.82	0.34	2.58	0.30	45	372	7806	48	928
0.72	2.28	0.43	9087	3.18	0.71	19.4	2.17	0.27	1.99	0.27	54	411	8458	38	827
0.70	2.17	0.45	9322	3.25	0.74	19.3	2.24	0.30	1.89	0.28	53	416	9204	40	845
2.51	6.47	0.90	11955	5.12	0.93	24.0	2.46	0.28	1.76	0.22	62	319	9180	37	780
2.34	6.37	0.85	11022	4.97	0.95	23.0	2.26	0.31	1.77	0.22	61	314	10693	37	773
1.79	5.03	0.69	9564	4.09	0.78	19.3	1.86	0.24	1.62	0.21	48	316	15677	37	728
1.82	4.51	0.65	9438	3.92	0.72	18.4	2.00	0.21	1.44	0.22	48	317	15883	37	735
2.02	5.08	0.72	14409	4.36	0.76	19.9	1.92	0.27	1.63	0.22	40	283	14113	37	724
2.12	5.59	0.79	8000	4.52	0.83	21.5	2.04	0.28	1.80	0.25	53	326	13596	39	916
2.13	5.43	0.77	7580	4.62	0.86	21.2	2.00	0.27	1.60	0.22	54	330	13166	39	910
2.20	5.67	0.70	7469	4.38	0.85	22.0	2.08	0.29	1.53	0.27	56	332	11624	40	911
2.32	6.31	0.84	9337	4.67	0.94	22.9	2.05	0.27	1.72	0.19	54	330	13802	40	912
2.37	6.42	0.80	9274	5.07	0.86	23.0	2.27	0.26	1.63	0.23	54	325	13689	40	916
2.29	6.06	0.84	9439	4.79	0.84	23.0	2.11	0.30	1.77	0.23	53	325	13562	39	914
2.45	6.54	0.82	9680	4.69	0.92	23.6	2.24	0.27	1.89	0.21	53	325	13759	40	917
1.03	3.24	0.52	10736	3.10	0.65	16.5	1.72	0.24	1.59	0.24	46	401	11247	40	622
0.97	2.90	0.47	10730	3.15	0.59	16.7	1.66	0.24	1.42	0.21	45	409	12255	42	629
1.08	3.14	0.46	10843	3.21	0.62	16.6	1.81	0.23	1.58	0.20	46	392	9308	39	609
1.10	3.23	0.49	9845	3.41	0.71	17.5	1.75	0.22	1.72	0.23	45	409	13200	42	646
1.05	3.19	0.48	9629	3.23	0.71	17.9	1.81	0.26	1.62	0.22	46	394	10162	39	612
0.97	3.04	0.54	9673	3.52	0.76	18.5	2.10	0.30	1.79	0.27	48	409	9798	39	633
0.74	2.20	0.44	10042	3.17	0.70	18.6	2.02	0.27	1.86	0.25	51	403	7581	41	897
0.65	2.72	0.47	10002	3.21	0.74	19.7	2.22	0.36	2.07	0.25	51	414	7554	45	990
0.66	2.53	0.41	9610	3.45	0.71	19.2	2.06	0.29	2.07	0.29	50	400	6897	41	898

Appendix B3 - Multielement Patterns of Individual Samples

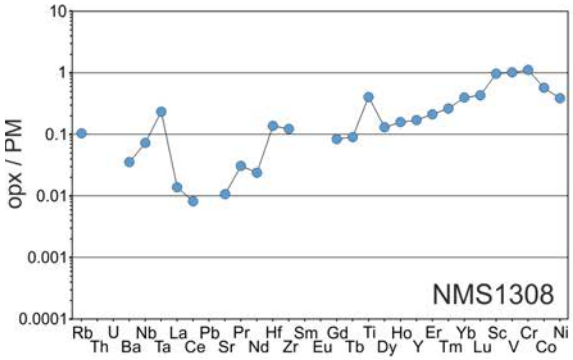

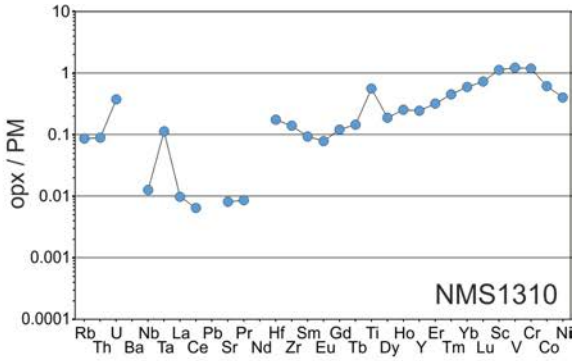

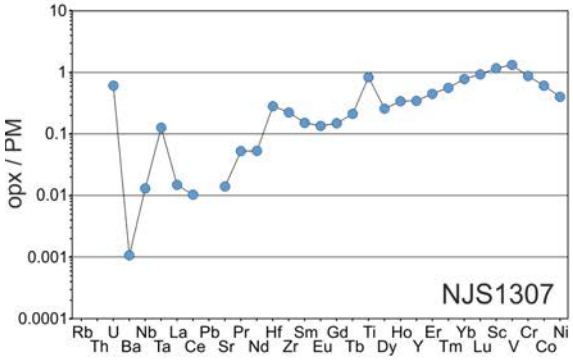

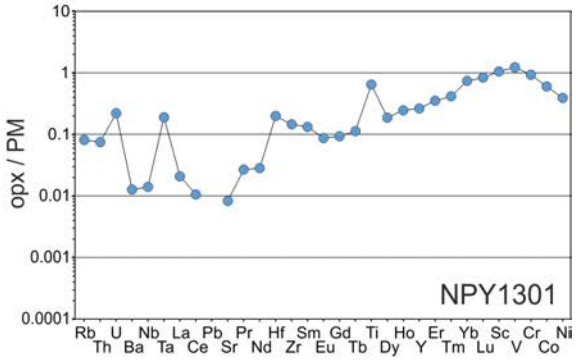

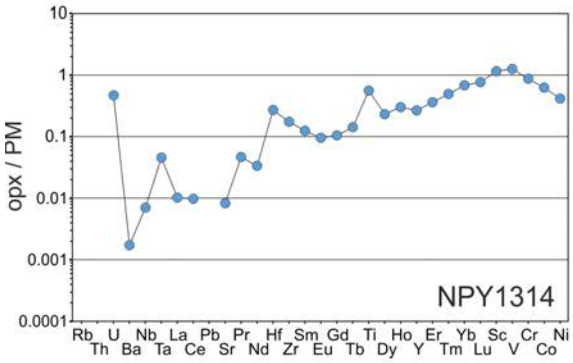

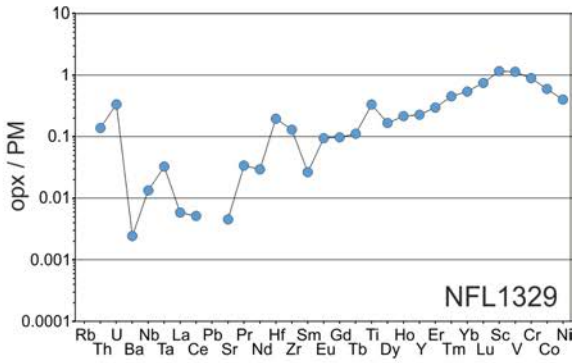

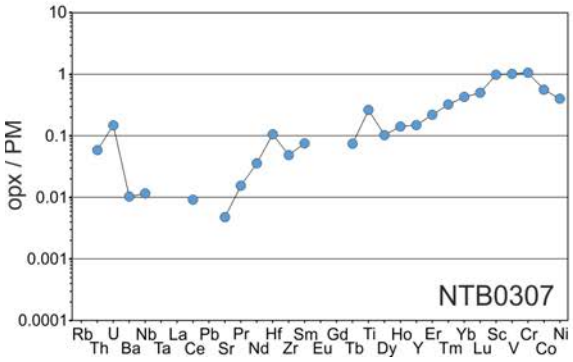

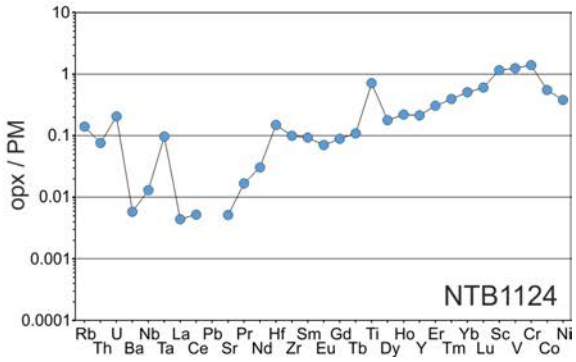

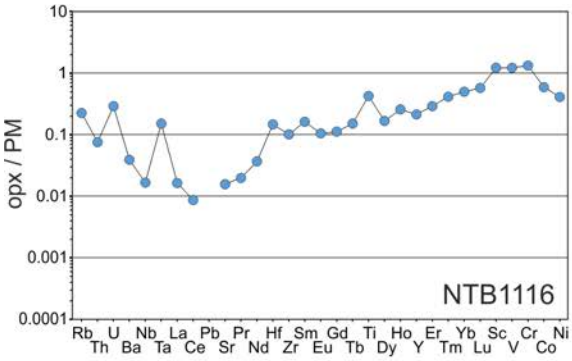
NTB1116
opx / PM
10
1
0.1
0.01
0.001
0.0001
Rb U Nb La Pb Pr Hf Sm Gd Ti Ho Er Yb Sc Cr Ni
Th Ba Ta Ce Sr Nd Zr Eu Tb Dy Y Tm Lu V Co

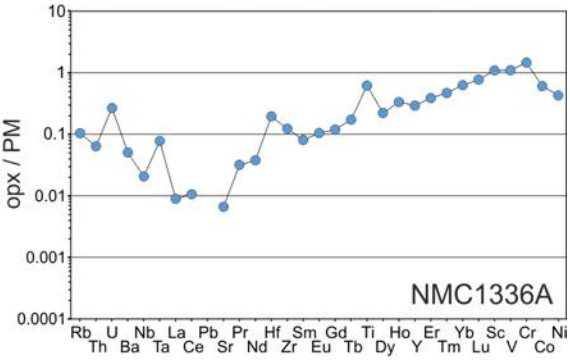
NMC1336A
opx / PM
10
1
0.1
0.01
0.001
0.0001
Rb U Nb La Pb Pr Hf Sm Gd Ti Ho Er Yb Sc Cr Ni
Th Ba Ta Ce Sr Nd Zr Eu Tb Dy Y Tm Lu V Co

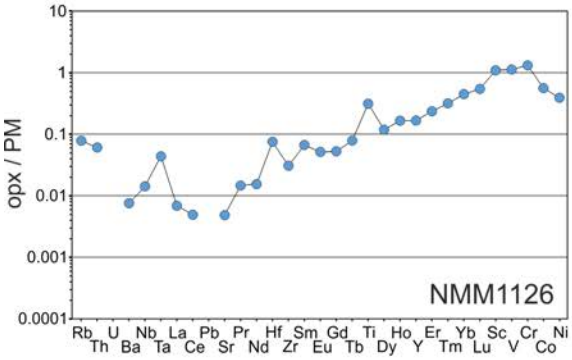
NMM1126
opx / PM
10
1
0.1
0.01
0.001
0.0001
Rb U Nb La Pb Pr Hf Sm Gd Ti Ho Er Yb Sc Cr Ni
Th Ba Ta Ce Sr Nd Zr Eu Tb Dy Y Tm Lu V Co

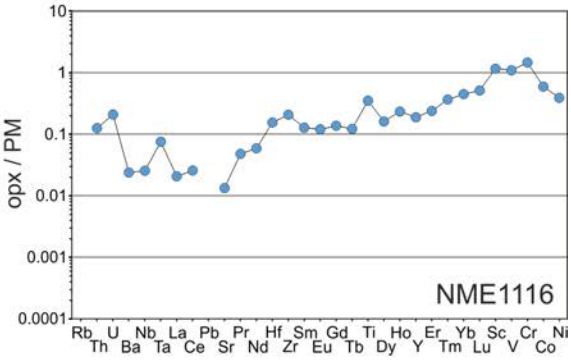
NME1116
opx / PM
10
1
0.1
0.01
0.001
0.0001
Rb U Nb La Pb Pr Hf Sm Gd Ti Ho Er Yb Sc Cr Ni
Th Ba Ta Ce Sr Nd Zr Eu Tb Dy Y Tm Lu V Co

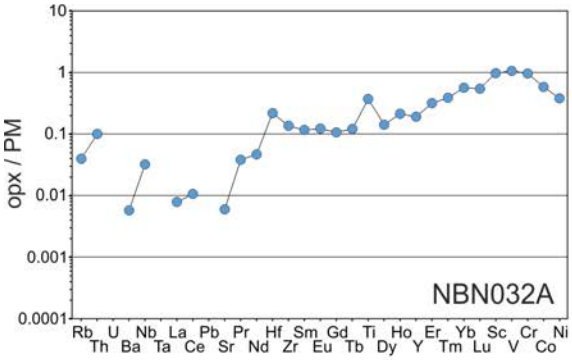
NBN032A
opx / PM
10
1
0.1
0.01
0.001
0.0001
Rb U Nb La Pb Pr Hf Sm Gd Ti Ho Er Yb Sc Cr Ni
Th Ba Ta Ce Sr Nd Zr Eu Tb Dy Y Tm Lu V Co

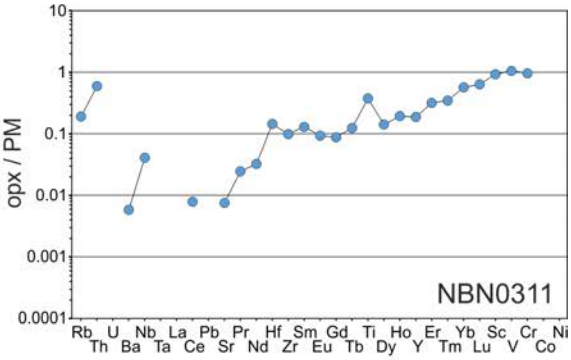
NBN0311
opx / PM
10
1
0.1
0.01
0.001
0.0001
Rb U Nb La Pb Pr Hf Sm Gd Ti Ho Er Yb Sc Cr Ni
Th Ba Ta Ce Sr Nd Zr Eu Tb Dy Y Tm Lu V Co

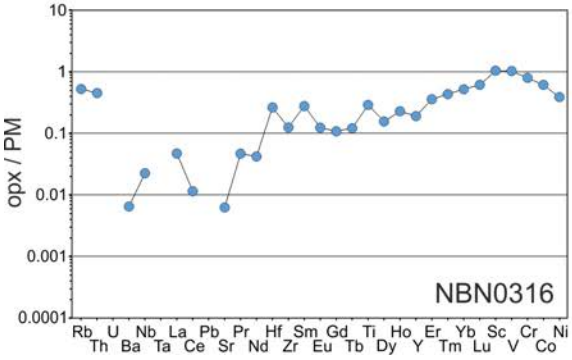
NBN0316
opx / PM
10
1
0.1
0.01
0.001
0.0001
Rb U Nb La Pb Pr Hf Sm Gd Ti Ho Er Yb Sc Cr Ni
Th Ba Ta Ce Sr Nd Zr Eu Tb Dy Y Tm Lu V Co

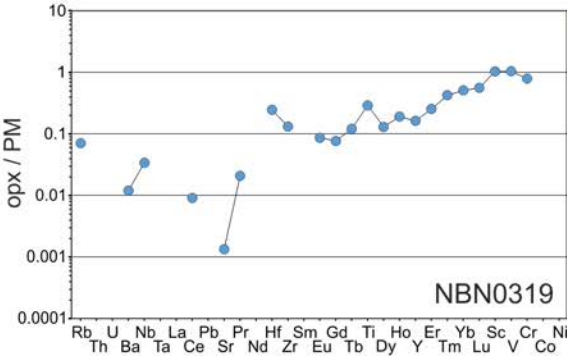
NBN0319
opx / PM
10
1
0.1
0.01
0.001
0.0001
Rb U Nb La Pb Pr Hf Sm Gd Ti Ho Er Yb Sc Cr Ni
Th Ba Ta Ce Sr Nd Zr Eu Tb Dy Y Tm Lu V Co

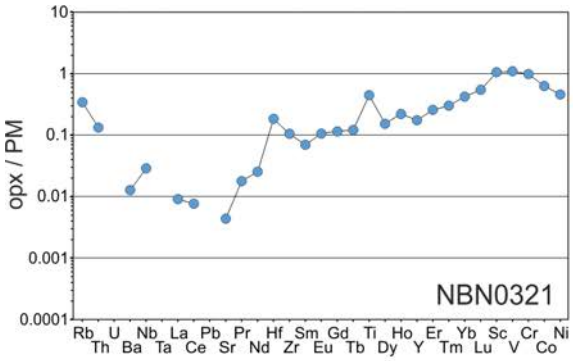
opx / PM
10
1
0.1
0.01
0.001
0.0001
NBN0321
Rb U Nb La Pb Pr Hf Sm Gd Ti Ho Er Yb Sc Cr Ni
Th Ba Ta Ce Sr Nd Zr Eu Tb Dy Y Tm Lu V Co

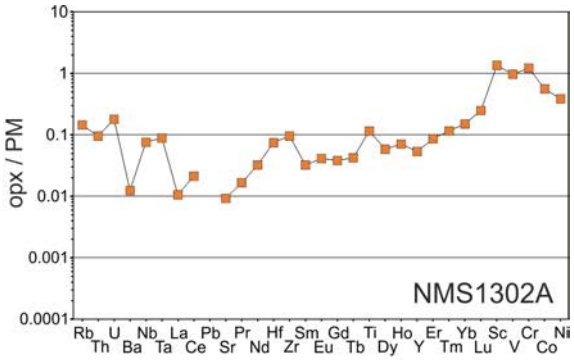
opx / PM
10
1
0.1
0.01
0.001
0.0001
NMS1302A
Rb U Nb La Pb Pr Hf Sm Gd Ti Ho Er Yb Sc Cr Ni
Th Ba Ta Ce Sr Nd Zr Eu Tb Dy Y Tm Lu V Co

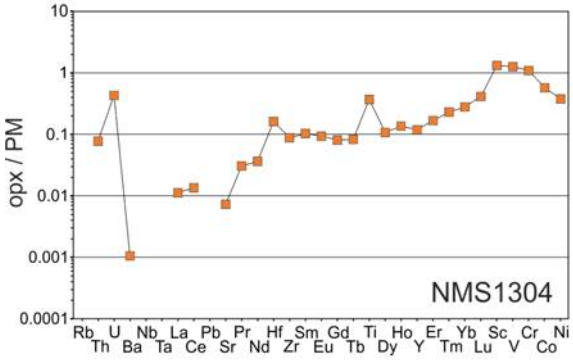
opx / PM
10
1
0.1
0.01
0.001
0.0001
NMS1304
Rb U Nb La Pb Pr Hf Sm Gd Ti Ho Er Yb Sc Cr Ni
Th Ba Ta Ce Sr Nd Zr Eu Tb Dy Y Tm Lu V Co

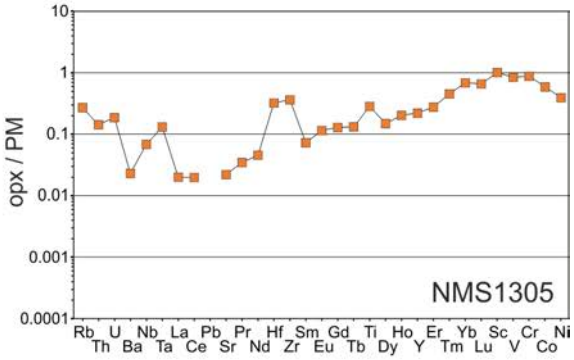
opx / PM
10
1
0.1
0.01
0.001
0.0001
NMS1305
Rb U Nb La Pb Pr Hf Sm Gd Ti Ho Er Yb Sc Cr Ni
Th Ba Ta Ce Sr Nd Zr Eu Tb Dy Y Tm Lu V Co

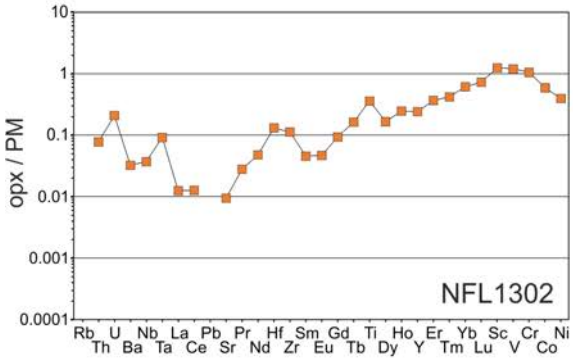
opx / PM
10
1
0.1
0.01
0.001
0.0001
NFL1302
Rb U Nb La Pb Pr Hf Sm Gd Ti Ho Er Yb Sc Cr Ni
Th Ba Ta Ce Sr Nd Zr Eu Tb Dy Y Tm Lu V Co

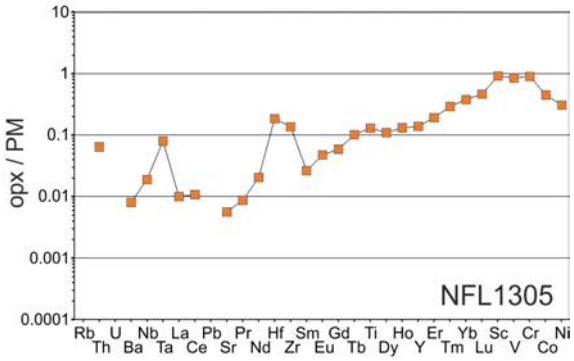
opx / PM
10
1
0.1
0.01
0.001
0.0001
NFL1305
Rb U Nb La Pb Pr Hf Sm Gd Ti Ho Er Yb Sc Cr Ni
Th Ba Ta Ce Sr Nd Zr Eu Tb Dy Y Tm Lu V Co

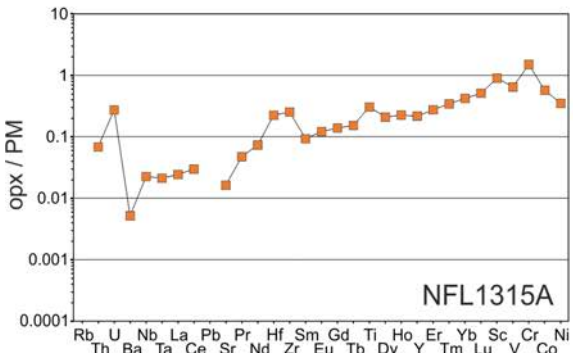
opx / PM
10
1
0.1
0.01
0.001
0.0001
NFL1315A
Rb U Nb La Pb Pr Hf Sm Gd Ti Ho Er Yb Sc Cr Ni

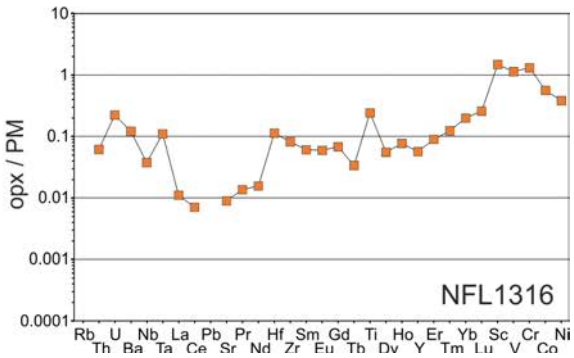
opx / PM
10
1
0.1
0.01
0.001
0.0001
NFL1316
Rb U Nb La Pb Pr Hf Sm Gd Ti Ho Er Yb Sc Cr Ni

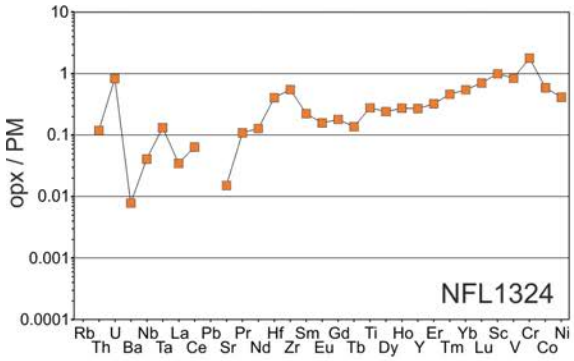
opx / PM
10
1
0.1
0.01
0.001
0.0001
NFL1324
Rb U Nb La Pb Pr Hf Sm Gd Ti Ho Er Yb Sc Cr Ni
Th Ba Ta Ce Sr Nd Zr Eu Tb Dy Y Tm Lu V Co

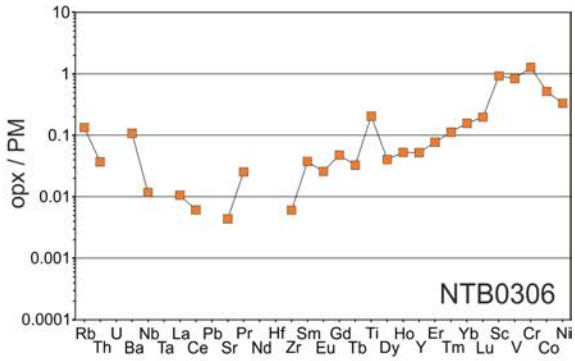
opx / PM
10
1
0.1
0.01
0.001
0.0001
NTB0306
Rb U Nb La Pb Pr Hf Sm Gd Ti Ho Er Yb Sc Cr Ni
Th Ba Ta Ce Sr Nd Zr Eu Tb Dy Y Tm Lu V Co

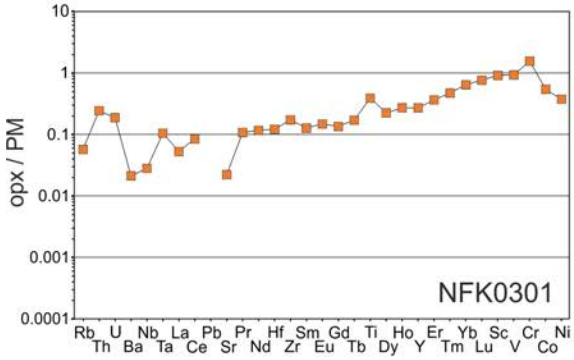
opx / PM
10
1
0.1
0.01
0.001
0.0001
NFK0301
Rb U Nb La Pb Pr Hf Sm Gd Ti Ho Er Yb Sc Cr Ni
Th Ba Ta Ce Sr Nd Zr Eu Tb Dy Y Tm Lu V Co

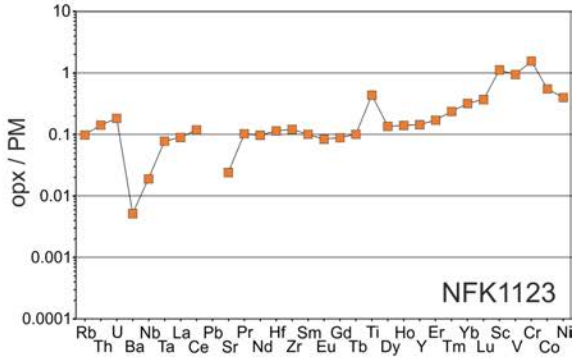
opx / PM
10
1
0.1
0.01
0.001
0.0001
NFK1123
Rb U Nb La Pb Pr Hf Sm Gd Ti Ho Er Yb Sc Cr Ni
Th Ba Ta Ce Sr Nd Zr Eu Tb Dy Y Tm Lu V Co

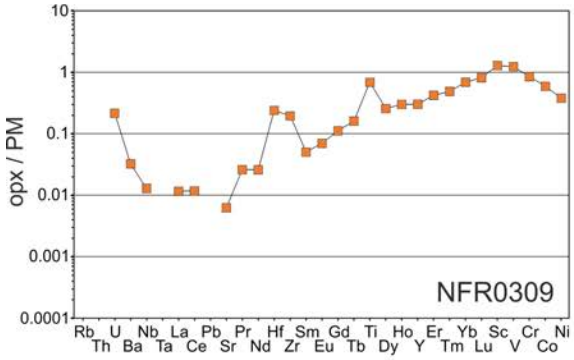
opx / PM
10
1
0.1
0.01
0.001
0.0001
NFR0309
Rb U Nb La Pb Pr Hf Sm Gd Ti Ho Er Yb Sc Cr Ni
Th Ba Ta Ce Sr Nd Zr Eu Tb Dy Y Tm Lu V Co

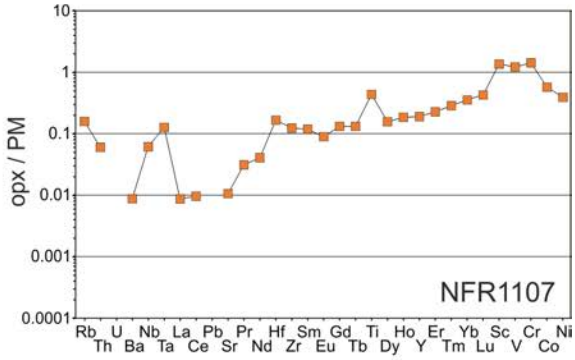
opx / PM
10
1
0.1
0.01
0.001
0.0001
NFR1107
Rb U Nb La Pb Pr Hf Sm Gd Ti Ho Er Yb Sc Cr Ni
Th Ba Ta Ce Sr Nd Zr Eu Tb Dy Y Tm Lu V Co

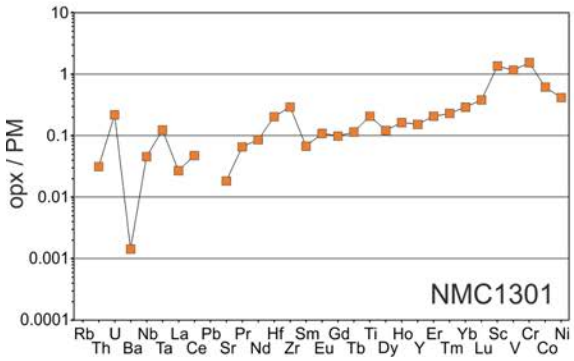
opx / PM
10
1
0.1
0.01
0.001
0.0001
NMC1301
Rb U Nb La Pb Pr Hf Sm Gd Ti Ho Er Yb Sc Cr Ni
Th Ba Ta Ce Sr Nd Zr Eu Tb Dy Y Tm Lu V Co

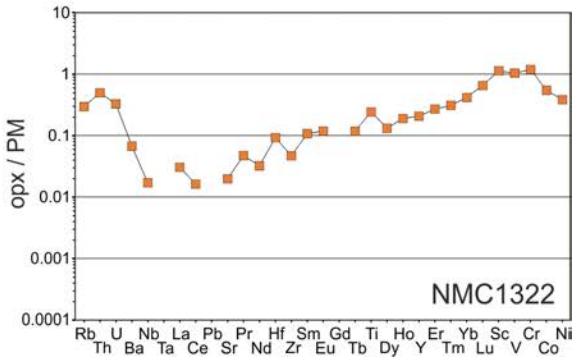
opx / PM
10
1
0.1
0.01
0.001
0.0001
NMC1322
Rb U Nb La Pb Pr Hf Sm Gd Ti Ho Er Yb Sc Cr Ni
Th Ba Ta Ce Sr Nd Zr Eu Tb Dy Y Tm Lu V Co

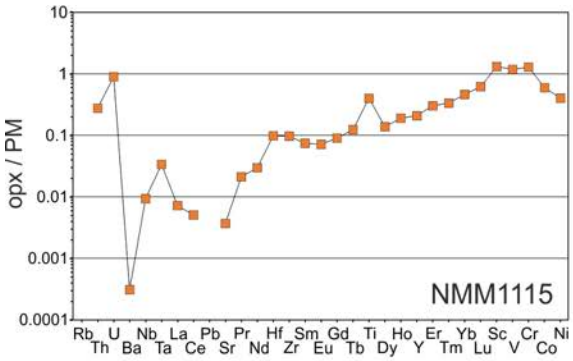
opx / PM
10
1
0.1
0.01
0.001
0.0001
NMM1115
Rb U Nb La Pb Pr Hf Sm Gd Ti Ho Er Yb Sc Cr Ni
Th Ba Ta Ce Sr Nd Zr Eu Tb Dy Y Tm Lu V Co

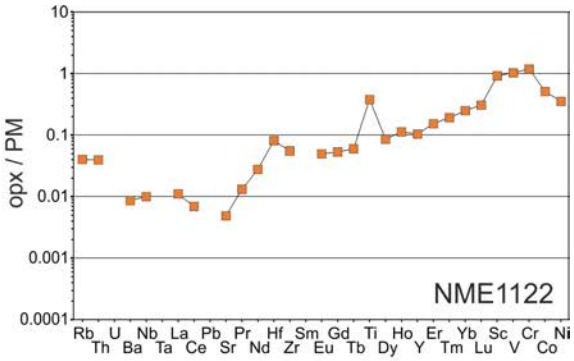
opx / PM
10
1
0.1
0.01
0.001
0.0001
NME1122
Rb U Nb La Pb Pr Hf Sm Gd Ti Ho Er Yb Sc Cr Ni
Th Ba Ta Ce Sr Nd Zr Eu Tb Dy Y Tm Lu V Co

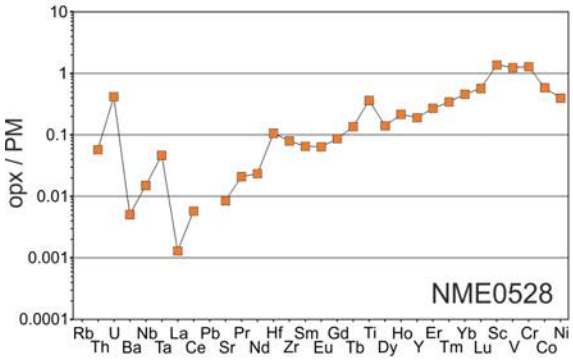
opx / PM
10
1
0.1
0.01
0.001
0.0001
NME0528
Rb U Nb La Pb Pr Hf Sm Gd Ti Ho Er Yb Sc Cr Ni
Th Ba Ta Ce Sr Nd Zr Eu Tb Dy Y Tm Lu V Co

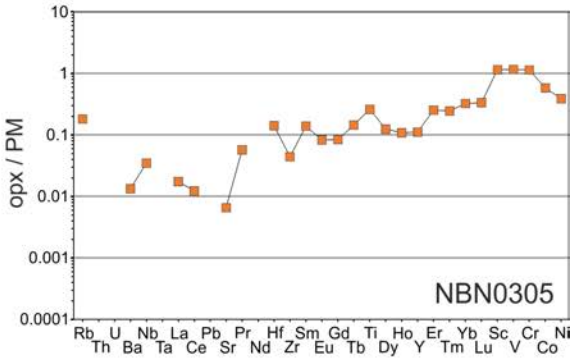
opx / PM
10
1
0.1
0.01
0.001
0.0001
NBN0305
Rb U Nb La Pb Pr Hf Sm Gd Ti Ho Er Yb Sc Cr Ni
Th Ba Ta Ce Sr Nd Zr Eu Tb Dy Y Tm Lu V Co

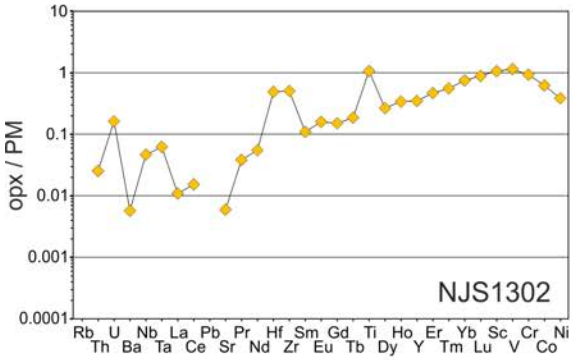
opx / PM
10
1
0.1
0.01
0.001
0.0001
NJS1302
Rb U Nb La Pb Pr Hf Sm Gd Ti Ho Er Yb Sc Cr Ni
Th Ba Ta Ce Sr Nd Zr Eu Tb Dy Y Tm Lu V Co

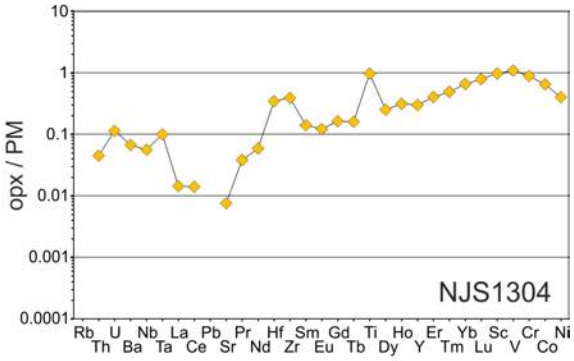
opx / PM
10
1
0.1
0.01
0.001
0.0001
NJS1304
Rb U Nb La Pb Pr Hf Sm Gd Ti Ho Er Yb Sc Cr Ni
Th Ba Ta Ce Sr Nd Zr Eu Tb Dy Y Tm Lu V Co

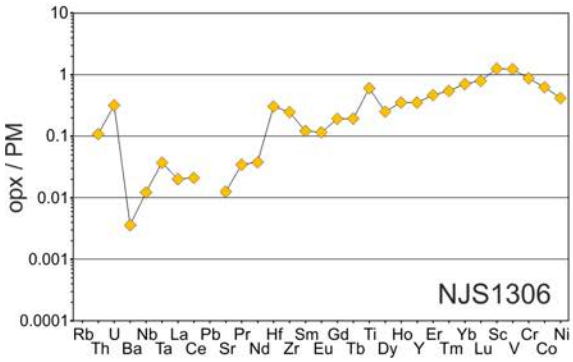
opx / PM
10
1
0.1
0.01
0.001
0.0001
NJS1306
Rb U Nb La Pb Pr Hf Sm Gd Ti Ho Er Yb Sc Cr Ni
Th Ba Ta Ce Sr Nd Zr Eu Tb Dy Y Tm Lu V Co

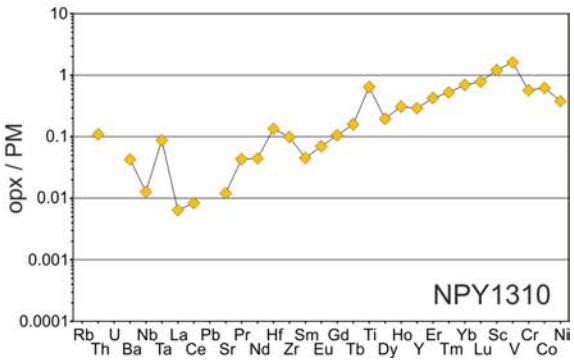
opx / PM
10
1
0.1
0.01
0.001
0.0001
NPY1310
Rb U Nb La Pb Pr Hf Sm Gd Ti Ho Er Yb Sc Cr Ni
Th Ba Ta Ce Sr Nd Zr Eu Tb Dy Y Tm Lu V Co

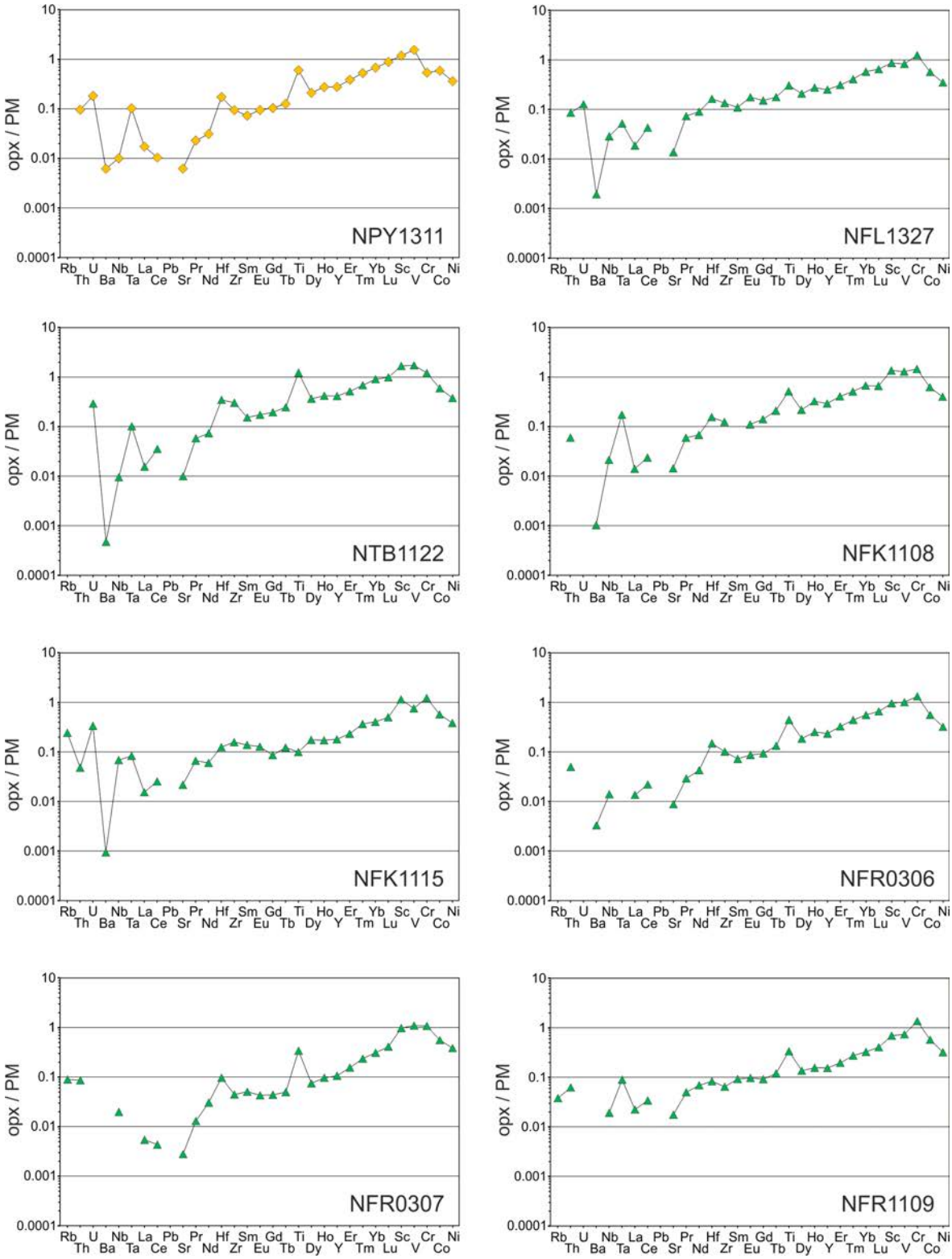
NPY1311
NFL1327
NTB1122
NFK1108
NFK1115
NFR0306
NFR0307
NFR1109
opx / PM
10
1
0.1
0.01
0.001
0.0001
Rb U Nb La Pb Pr Hf Sm Gd Ti Ho Er Yb Sc Cr Ni
Th Ba Ta Ce Sr Nd Zr Eu Tb Dy Y Tm Lu V Co

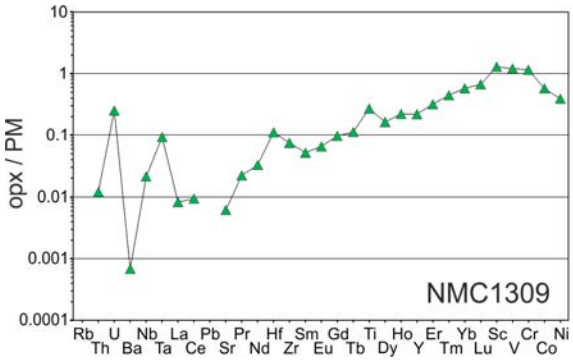
opx / PM
10
1
0.1
0.01
0.001
0.0001
NMC1309
Rb U Nb La Pb Pr Hf Sm Gd Ti Ho Er Yb Sc Cr Ni
Th Ba Ta Ce Sr Nd Zr Eu Tb Dy Y Tm Lu V Co

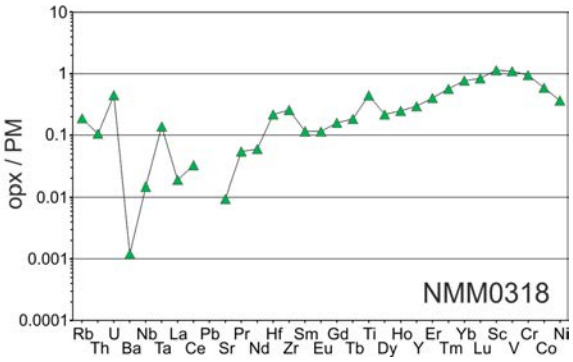
opx / PM
10
1
0.1
0.01
0.001
0.0001
NMM0318
Rb U Nb La Pb Pr Hf Sm Gd Ti Ho Er Yb Sc Cr Ni
Th Ba Ta Ce Sr Nd Zr Eu Tb Dy Y Tm Lu V Co

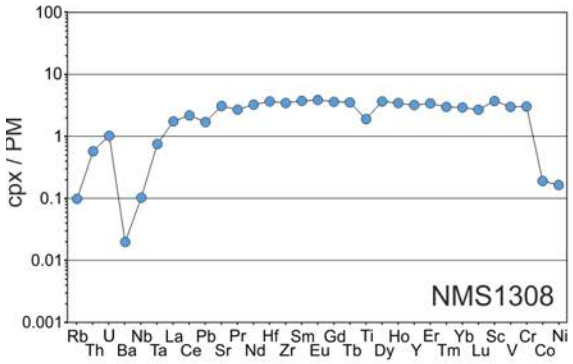
cpx / PM
100
10
1
0.1
0.01
0.001
NMS1308
Rb U Nb La Pb Pr Hf Sm Gd Ti Ho Er Yb Sc Cr Ni
Th Ba Ta Ce Sr Nd Zr Eu Tb Dy Y Tm Lu V Co

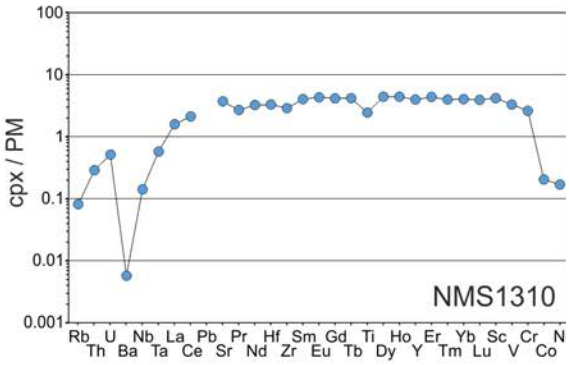
cpx / PM
100
10
1
0.1
0.01
0.001
NMS1310
Rb U Nb La Pb Pr Hf Sm Gd Ti Ho Er Yb Sc Cr N
Th Ba Ta Ce Sr Nd Zr Eu Tb Dy Y Tm Lu V Co

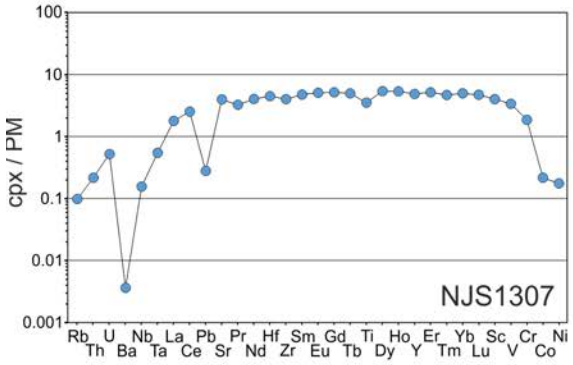
cpx / PM
100
10
1
0.1
0.01
0.001
NJS1307
Rb U Nb La Pb Pr Hf Sm Gd Ti Ho Er Yb Sc Cr Ni
Th Ba Ta Ce Sr Nd Zr Eu Tb Dy Y Tm Lu V Co

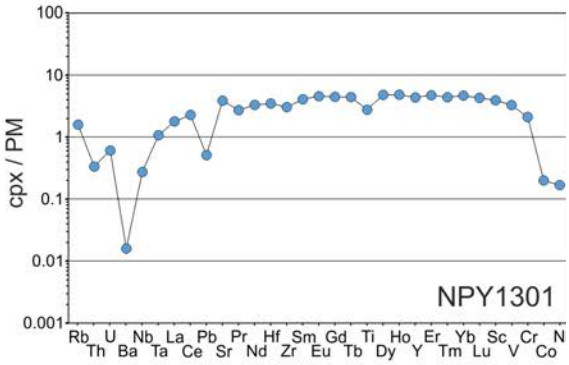
cpx / PM
100
10
1
0.1
0.01
0.001
NPY1301
Rb U Nb La Pb Pr Hf Sm Gd Ti Ho Er Yb Sc Cr N
Th Ba Ta Ce Sr Nd Zr Eu Tb Dy Y Tm Lu V Co

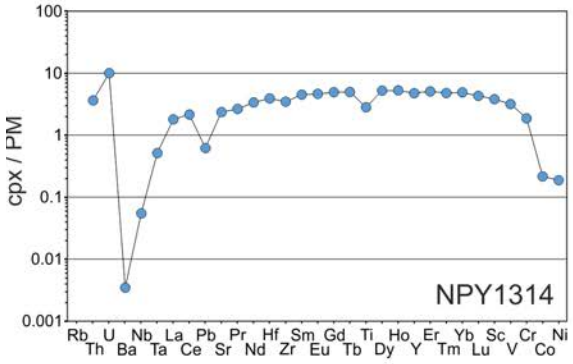
cpx / PM
100
10
1
0.1
0.01
0.001
NPY1314
Rb U Nb La Pb Pr Hf Sm Gd Ti Ho Er Yb Sc Cr Ni
Th Ba Ta Ce Sr Nd Zr Eu Tb Dy Y Tm Lu V Co

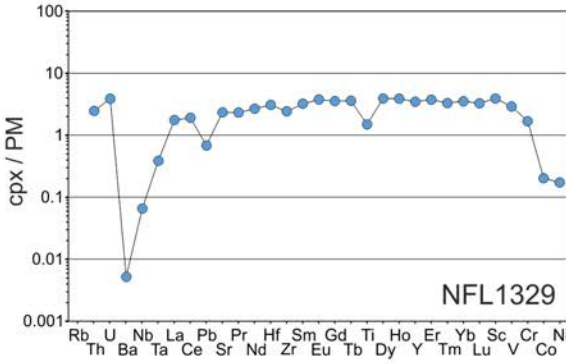
cpx / PM
100
10
1
0.1
0.01
0.001
NFL1329
Rb U Nb La Pb Pr Hf Sm Gd Ti Ho Er Yb Sc Cr N
Th Ba Ta Ce Sr Nd Zr Eu Tb Dy Y Tm Lu V Co

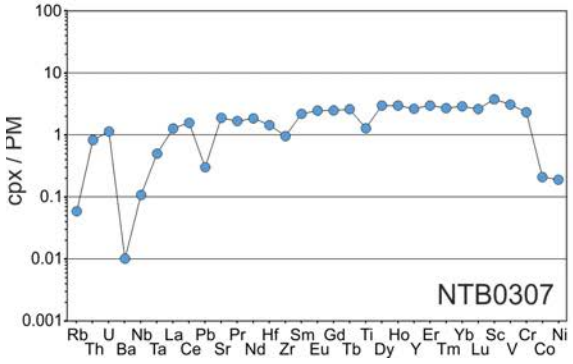
cpx / PM
100
10
1
0.1
0.01
0.001
NTB0307
Rb U Nb La Pb Pr Hf Sm Gd Ti Ho Er Yb Sc Cr Ni
Th Ba Ta Ce Sr Nd Zr Eu Tb Dy Y Tm Lu V Co

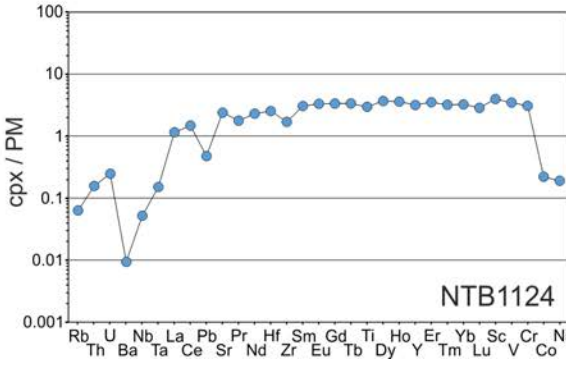
cpx / PM
100
10
1
0.1
0.01
0.001
NTB1124
Rb U Nb La Pb Pr Hf Sm Gd Ti Ho Er Yb Sc Cr N
Th Ba Ta Ce Sr Nd Zr Eu Tb Dy Y Tm Lu V Co

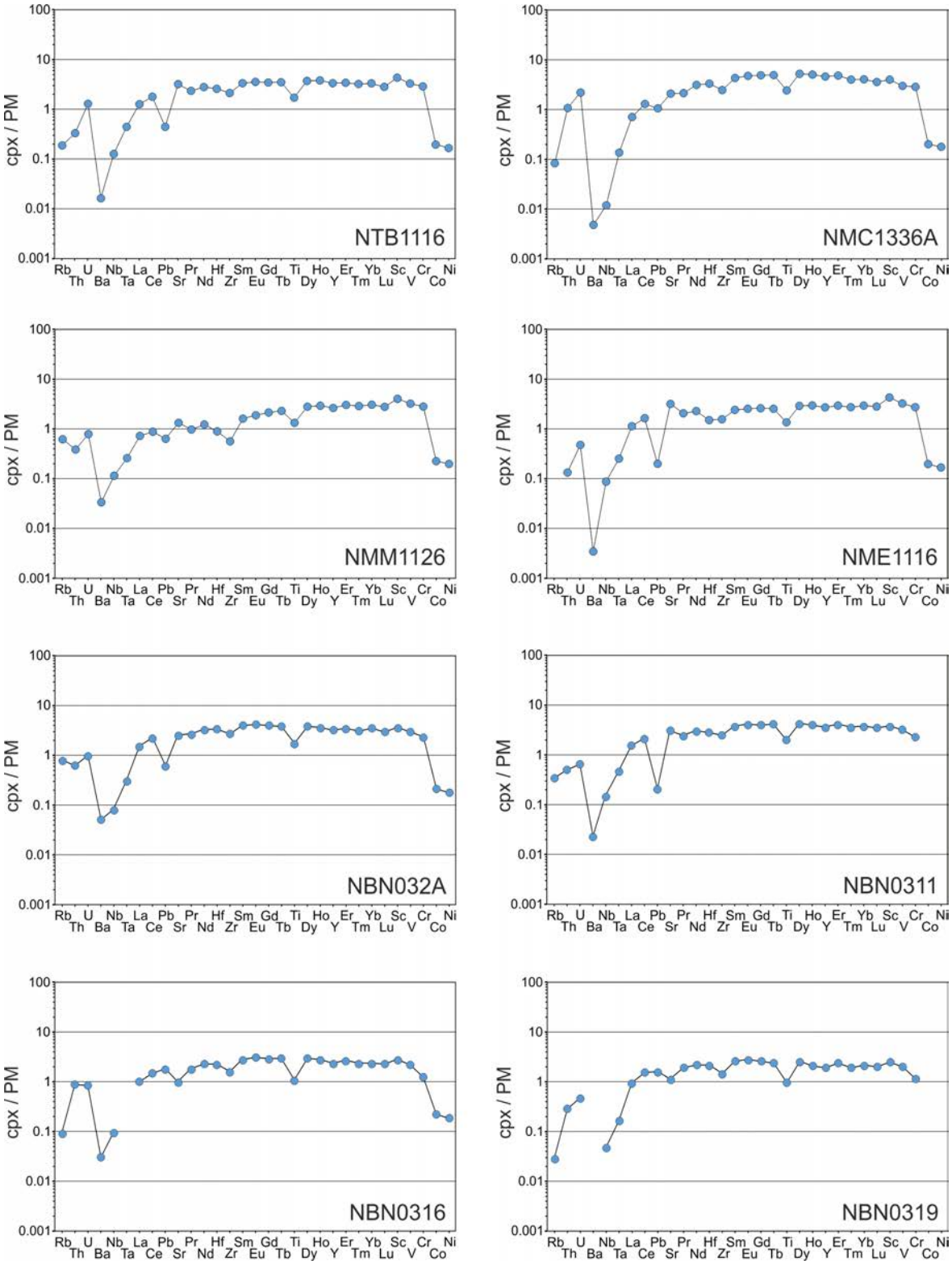
cpx / PM
100
10
1
0.1
0.01
0.001
Rb U Nb La Pb Pr Hf Sm Gd Ti Ho Er Yb Sc Cr Ni
Th Ba Ta Ce Sr Nd Zr Eu Tb Dy Y Tm Lu V Co
NTB1116
NMC1336A
NMM1126
NME1116
NBN032A
NBN0311
NBN0316
NBN0319

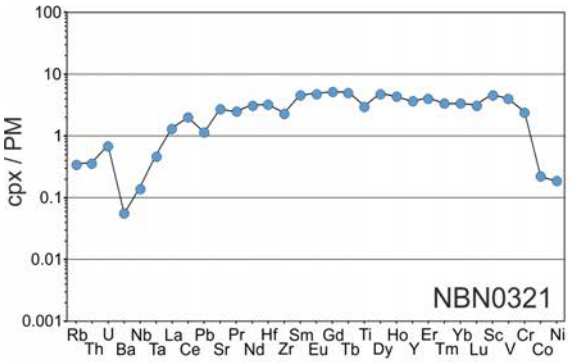
cpx / PM
100
10
1
0.1
0.01
0.001
NBN0321
Rb U Nb La Pb Pr Hf Sm Gd Ti Ho Er Yb Sc Cr Ni
Th Ba Ta Ce Sr Nd Zr Eu Tb Dy Y Tm Lu V Co

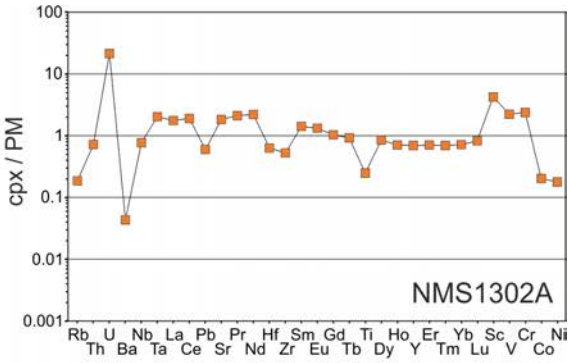
cpx / PM
100
10
1
0.1
0.01
0.001
NMS1302A
Rb U Nb La Pb Pr Hf Sm Gd Ti Ho Er Yb Sc Cr Ni
Th Ba Ta Ce Sr Nd Zr Eu Tb Dy Y Tm Lu V Co

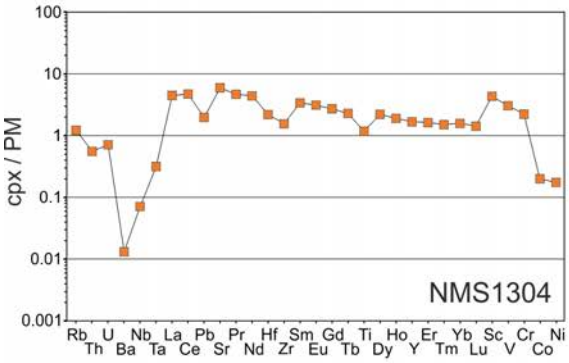
cpx / PM
100
10
1
0.1
0.01
0.001
NMS1304
Rb U Nb La Pb Pr Hf Sm Gd Ti Ho Er Yb Sc Cr Ni
Th Ba Ta Ce Sr Nd Zr Eu Tb Dy Y Tm Lu V Co

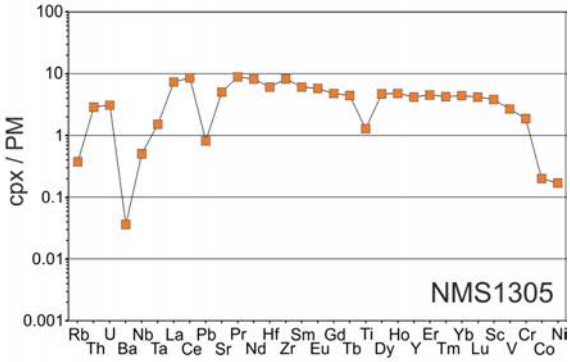
cpx / PM
100
10
1
0.1
0.01
0.001
NMS1305
Rb U Nb La Pb Pr Hf Sm Gd Ti Ho Er Yb Sc Cr Ni
Th Ba Ta Ce Sr Nd Zr Eu Tb Dy Y Tm Lu V Co

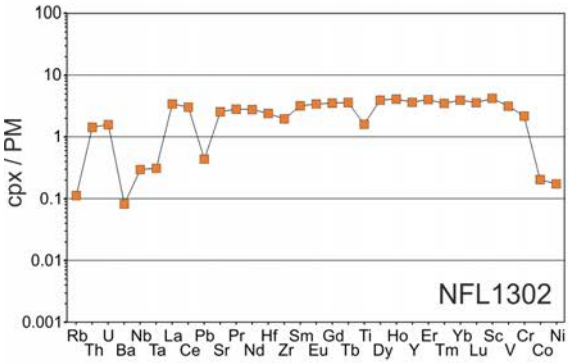
cpx / PM
100
10
1
0.1
0.01
0.001
NFL1302
Rb U Nb La Pb Pr Hf Sm Gd Ti Ho Er Yb Sc Cr Ni
Th Ba Ta Ce Sr Nd Zr Eu Tb Dy Y Tm Lu V Co

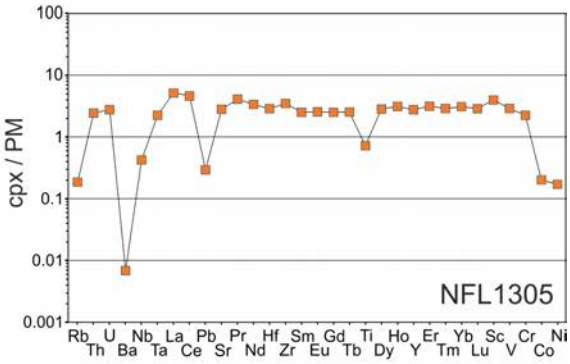
cpx / PM
100
10
1
0.1
0.01
0.001
NFL1305
Rb U Nb La Pb Pr Hf Sm Gd Ti Ho Er Yb Sc Cr Ni
Th Ba Ta Ce Sr Nd Zr Eu Tb Dy Y Tm Lu V Co

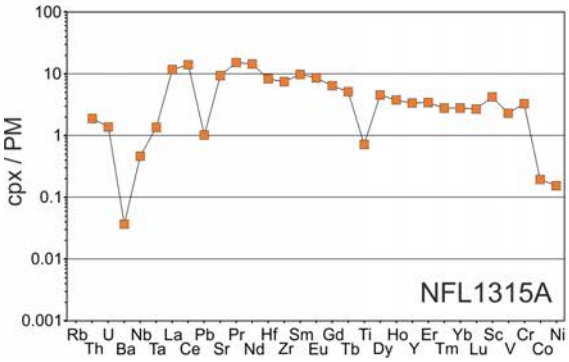
cpx / PM
100
10
1
0.1
0.01
0.001
NFL1315A
Rb U Nb La Pb Pr Hf Sm Gd Ti Ho Er Yb Sc Cr Ni
Th Ba Ta Ce Sr Nd Zr Eu Tb Dy Y Tm Lu V Co

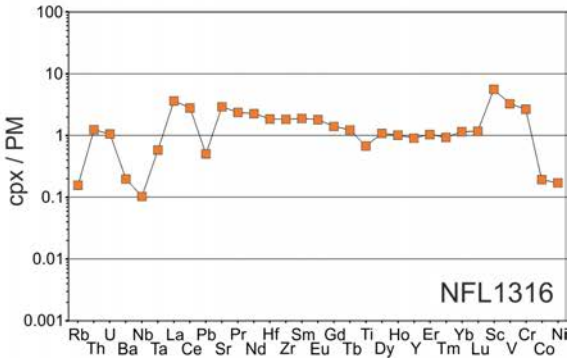
cpx / PM
100
10
1
0.1
0.01
0.001
NFL1316
Rb U Nb La Pb Pr Hf Sm Gd Ti Ho Er Yb Sc Cr Ni
Th Ba Ta Ce Sr Nd Zr Eu Tb Dy Y Tm Lu V Co

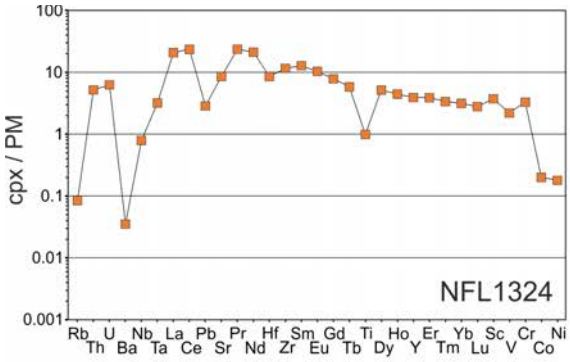
cpx / PM
100
10
1
0.1
0.01
0.001
NFL1324
Rb U Nb La Pb Pr Hf Sm Gd Ti Ho Er Yb Sc Cr Ni
Th Ba Ta Ce Sr Nd Zr Eu Tb Dy Y Tm Lu V Co

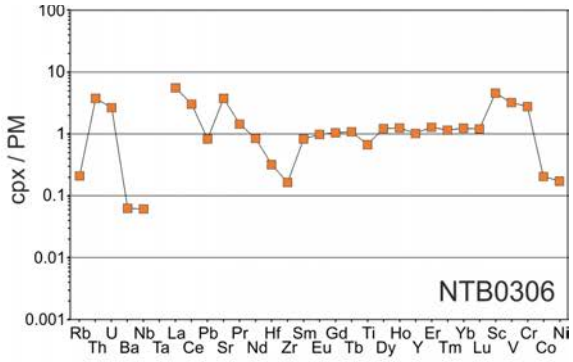
cpx / PM
100
10
1
0.1
0.01
0.001
NTB0306
Rb U Nb La Pb Pr Hf Sm Gd Ti Ho Er Yb Sc Cr Ni
Th Ba Ta Ce Sr Nd Zr Eu Tb Dy Y Tm Lu V Co

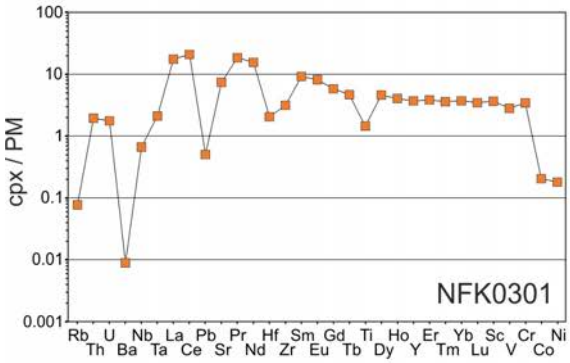
cpx / PM
100
10
1
0.1
0.01
0.001
NFK0301
Rb U Nb La Pb Pr Hf Sm Gd Ti Ho Er Yb Sc Cr Ni
Th Ba Ta Ce Sr Nd Zr Eu Tb Dy Y Tm Lu V Co

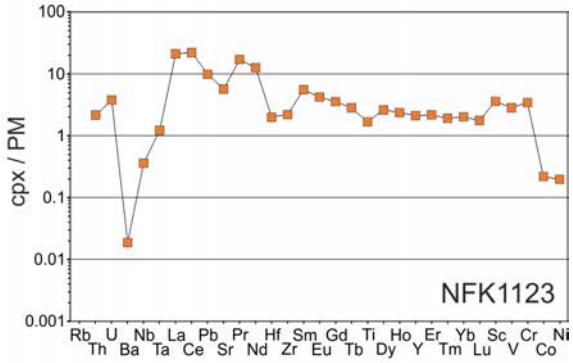
cpx / PM
100
10
1
0.1
0.01
0.001
NFK1123
Rb U Nb La Pb Pr Hf Sm Gd Ti Ho Er Yb Sc Cr Ni
Th Ba Ta Ce Sr Nd Zr Eu Tb Dy Y Tm Lu V Co

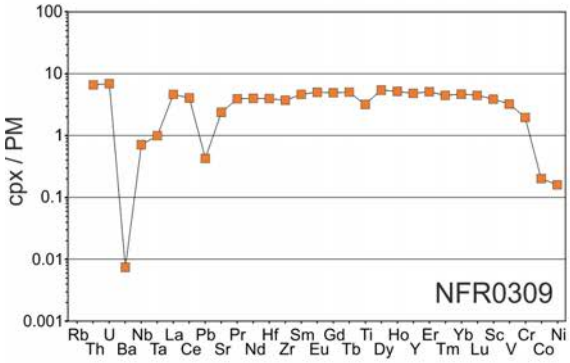
cpx / PM
100
10
1
0.1
0.01
0.001
NFR0309
Rb U Nb La Pb Pr Hf Sm Gd Ti Ho Er Yb Sc Cr Ni
Th Ba Ta Ce Sr Nd Zr Eu Tb Dy Y Tm Lu V Co

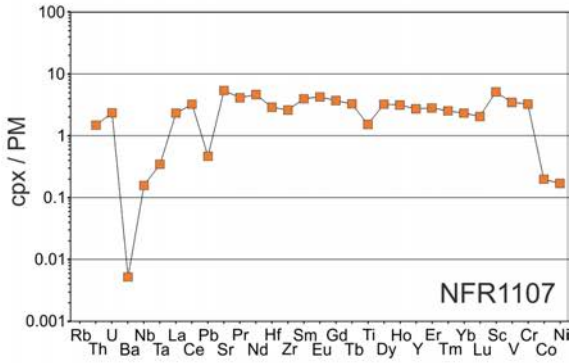
cpx / PM
100
10
1
0.1
0.01
0.001
NFR1107
Rb U Nb La Pb Pr Hf Sm Gd Ti Ho Er Yb Sc Cr Ni
Th Ba Ta Ce Sr Nd Zr Eu Tb Dy Y Tm Lu V Co

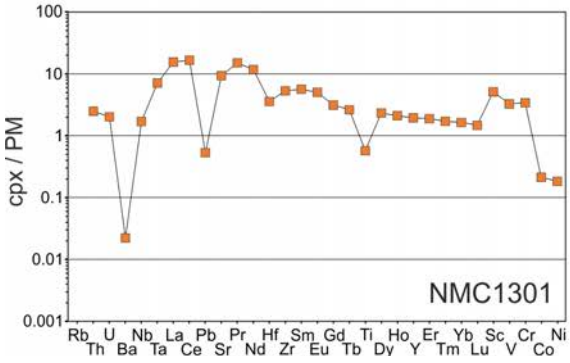
cpx / PM
100
10
1
0.1
0.01
0.001
NMC1301
Rb U Nb La Pb Pr Hf Sm Gd Ti Ho Er Yb Sc Cr Ni
Th Ba Ta Ce Sr Nd Zr Eu Tb Dy Y Tm Lu V Co

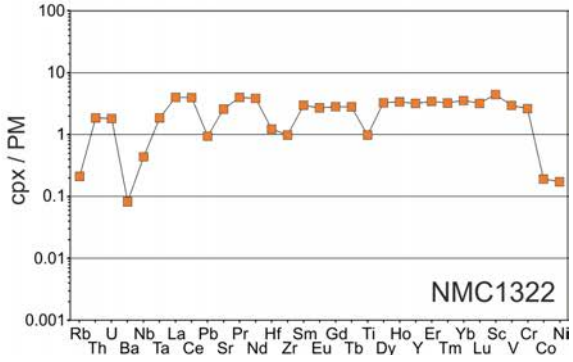
cpx / PM
100
10
1
0.1
0.01
0.001
NMC1322
Rb U Nb La Pb Pr Hf Sm Gd Ti Ho Er Yb Sc Cr Ni
Th Ba Ta Ce Sr Nd Zr Eu Tb Dy Y Tm Lu V Co

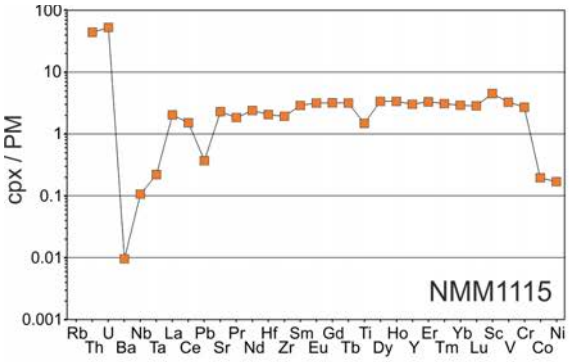
cpx / PM
100
10
1
0.1
0.01
0.001
NMM1115
Rb U Nb La Pb Pr Hf Sm Gd Ti Ho Er Yb Sc Cr Ni
Th Ba Ta Ce Sr Nd Zr Eu Tb Dy Y Tm Lu V Co

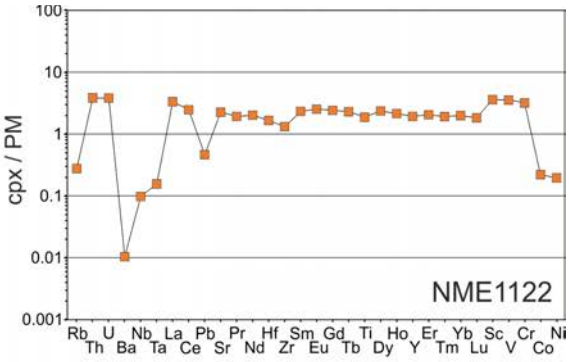
cpx / PM
100
10
1
0.1
0.01
0.001
NME1122
Rb U Nb La Pb Pr Hf Sm Gd Ti Ho Er Yb Sc Cr Ni
Th Ba Ta Ce Sr Nd Zr Eu Tb Dy Y Tm Lu V Co

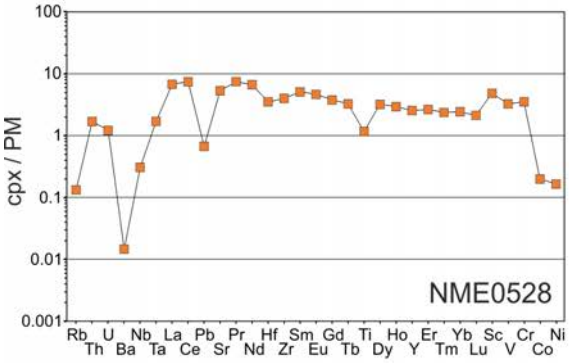
cpx / PM
100
10
1
0.1
0.01
0.001
NME0528
Rb U Nb La Pb Pr Hf Sm Gd Ti Ho Er Yb Sc Cr Ni
Th Ba Ta Ce Sr Nd Zr Eu Tb Dy Y Tm Lu V Co

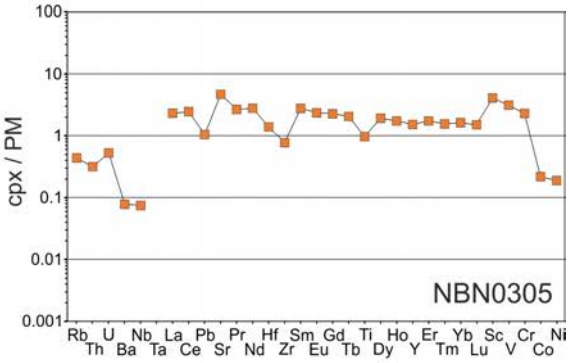
cpx / PM
100
10
1
0.1
0.01
0.001
NBN0305
Rb U Nb La Pb Pr Hf Sm Gd Ti Ho Er Yb Sc Cr Ni
Th Ba Ta Ce Sr Nd Zr Eu Tb Dy Y Tm Lu V Co

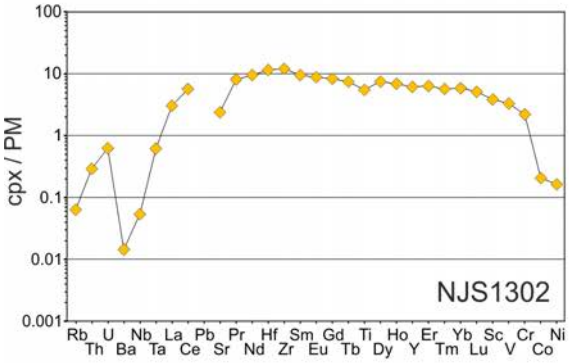
cpx / PM
100
10
1
0.1
0.01
0.001
NJS1302
Rb U Nb La Pb Pr Hf Sm Gd Ti Ho Er Yb Sc Cr Ni
Th Ba Ta Ce Sr Nd Zr Eu Tb Dy Y Tm Lu V Co

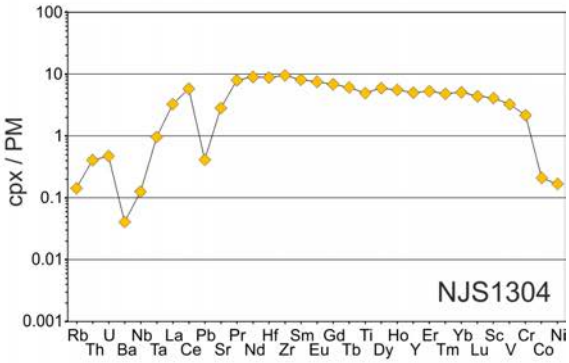
cpx / PM
100
10
1
0.1
0.01
0.001
NJS1304
Rb U Nb La Pb Pr Hf Sm Gd Ti Ho Er Yb Sc Cr Ni
Th Ba Ta Ce Sr Nd Zr Eu Tb Dy Y Tm Lu V Co

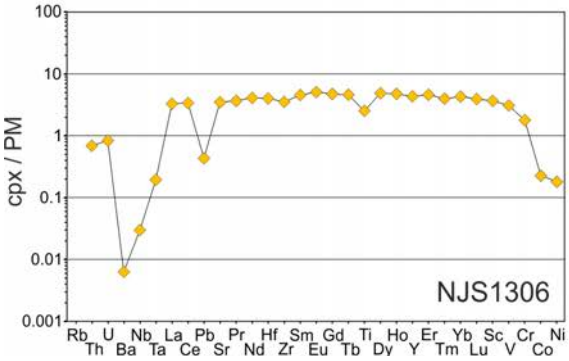
cpx / PM
100
10
1
0.1
0.01
0.001
NJS1306
Rb U Nb La Pb Pr Hf Sm Gd Ti Ho Er Yb Sc Cr Ni
Th Ba Ta Ce Sr Nd Zr Eu Tb Dy Y Tm Lu V Co

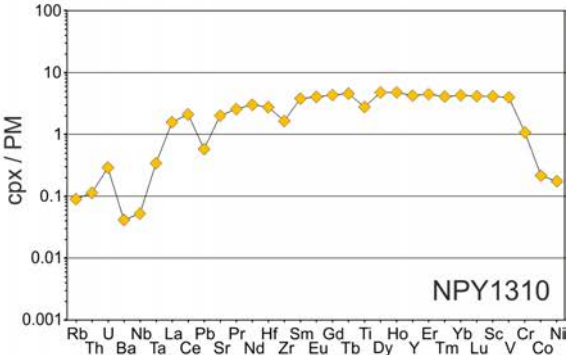
cpx / PM
100
10
1
0.1
0.01
0.001
NPY1310
Rb U Nb La Pb Pr Hf Sm Gd Ti Ho Er Yb Sc Cr Ni
Th Ba Ta Ce Sr Nd Zr Eu Tb Dy Y Tm Lu V Co

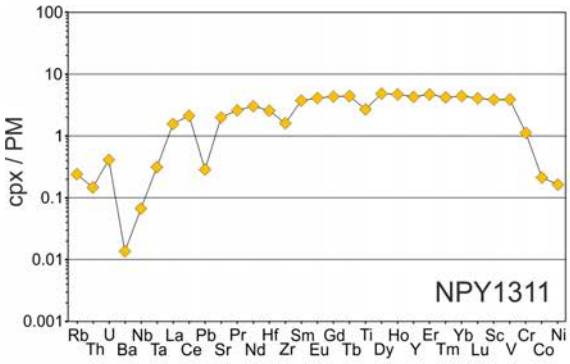
cpx / PM
100
10
1
0.1
0.01
0.001
NPY1311
Rb U Nb La Pb Pr Hf Sm Gd Ti Ho Er Yb Sc Cr Ni
Th Ba Ta Ce Sr Nd Zr Eu Tb Dy Y Tm Lu V Co

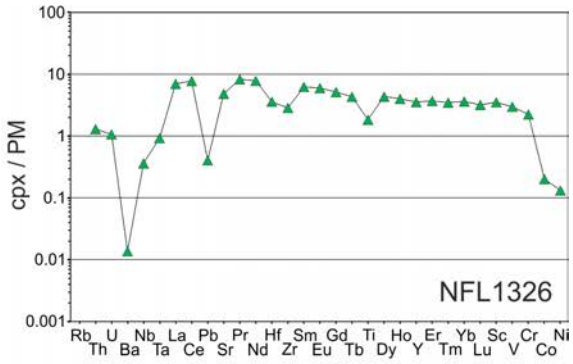
cpx / PM
100
10
1
0.1
0.01
0.001
NFL1326
Rb U Nb La Pb Pr Hf Sm Gd Ti Ho Er Yb Sc Cr Ni
Th Ba Ta Ce Sr Nd Zr Eu Tb Dy Y Tm Lu V Co

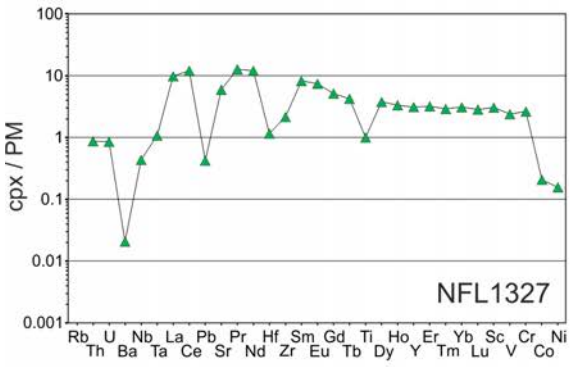
cpx / PM
100
10
1
0.1
0.01
0.001
NFL1327
Rb U Nb La Pb Pr Hf Sm Gd Ti Ho Er Yb Sc Cr Ni
Th Ba Ta Ce Sr Nd Zr Eu Tb Dy Y Tm Lu V Co

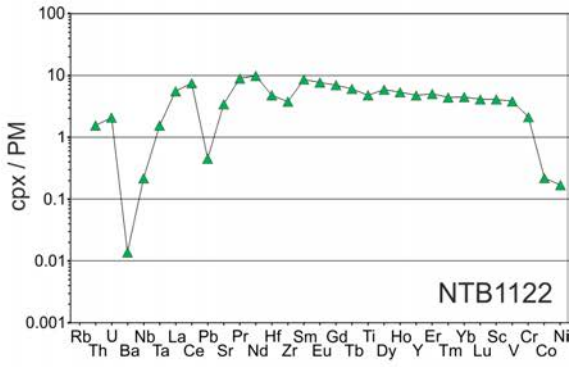
cpx / PM
100
10
1
0.1
0.01
0.001
NTB1122
Rb U Nb La Pb Pr Hf Sm Gd Ti Ho Er Yb Sc Cr Ni
Th Ba Ta Ce Sr Nd Zr Eu Tb Dy Y Tm Lu V Co

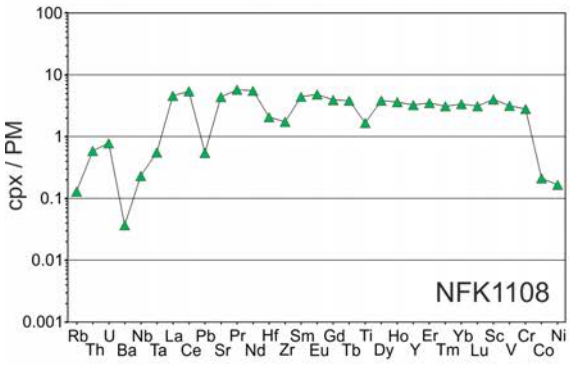
cpx / PM
100
10
1
0.1
0.01
0.001
NFK1108
Rb U Nb La Pb Pr Hf Sm Gd Ti Ho Er Yb Sc Cr Ni
Th Ba Ta Ce Sr Nd Zr Eu Tb Dy Y Tm Lu V Co

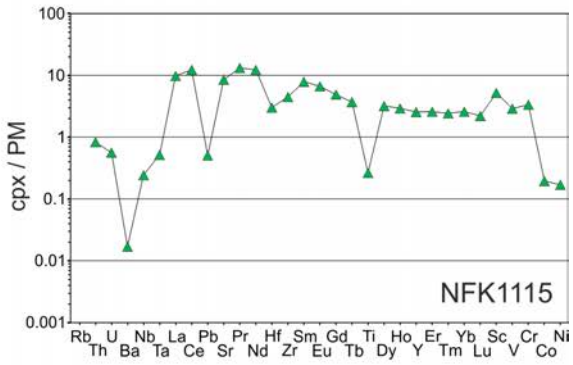
cpx / PM
100
10
1
0.1
0.01
0.001
NFK1115
Rb U Nb La Pb Pr Hf Sm Gd Ti Ho Er Yb Sc Cr Ni
Th Ba Ta Ce Sr Nd Zr Eu Tb Dy Y Tm Lu V Co

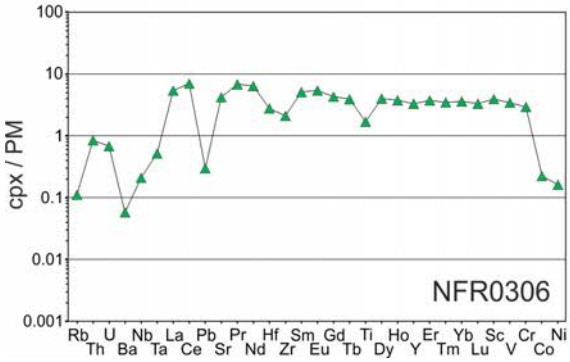
cpx / PM
100
10
1
0.1
0.01
0.001
NFR0306
Rb U Nb La Pb Pr Hf Sm Gd Ti Ho Er Yb Sc Cr Ni
Th Ba Ta Ce Sr Nd Zr Eu Tb Dy Y Tm Lu V Co

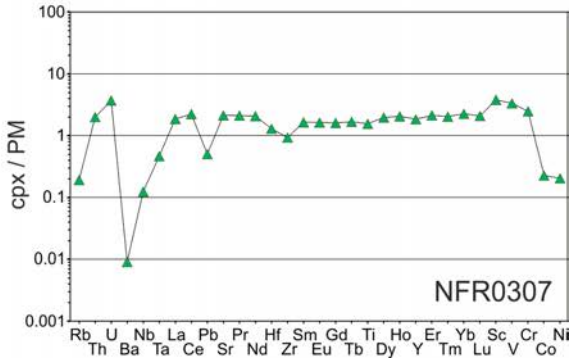
cpx / PM
100
10
1
0.1
0.01
0.001
NFR0307
Rb U Nb La Pb Pr Hf Sm Gd Ti Ho Er Yb Sc Cr Ni
Th Ba Ta Ce Sr Nd Zr Eu Tb Dy Y Tm Lu V Co

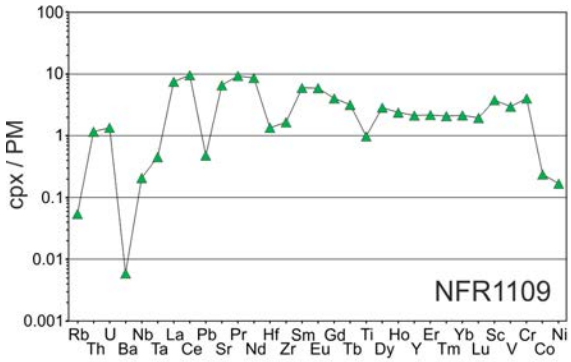
cpx / PM
100
10
1
0.1
0.01
0.001
NFR1109
Rb U Nb La Pb Pr Hf Sm Gd Ti Ho Er Yb Sc Cr Ni
Th Ba Ta Ce Sr Nd Zr Eu Tb Dy Y Tm Lu V Co

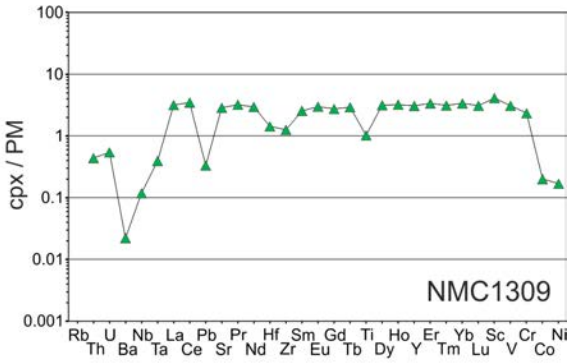
cpx / PM
100
10
1
0.1
0.01
0.001
NMC1309
Rb U Nb La Pb Pr Hf Sm Gd Ti Ho Er Yb Sc Cr Ni
Th Ba Ta Ce Sr Nd Zr Eu Tb Dy Y Tm Lu V Co

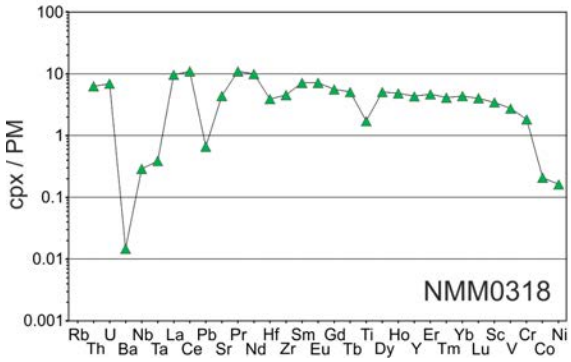
cpx / PM
100
10
1
0.1
0.01
0.001
NMM0318
Rb U Nb La Pb Pr Hf Sm Gd Ti Ho Er Yb Sc Cr Ni
Th Ba Ta Ce Sr Nd Zr Eu Tb Dy Y Tm Lu V Co

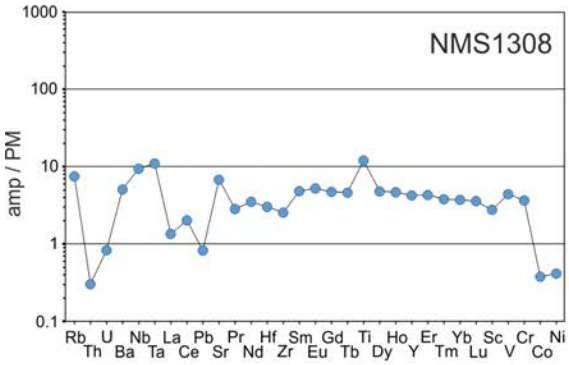
NMS1308
amp / PM
1000
100
10
1
0.1
Rb U Nb La Pb Pr Hf Sm Gd Ti Ho Er Yb Sc Cr Ni
Th Ba Ta Ce Sr Nd Zr Eu Tb Dy Y Tm Lu V Co

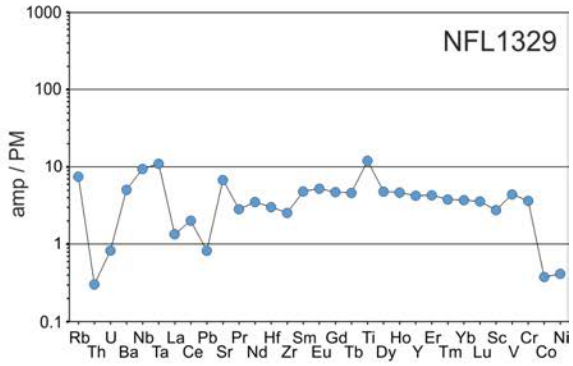
NFL1329
amp / PM
1000
100
10
1
0.1
Rb U Nb La Pb Pr Hf Sm Gd Ti Ho Er Yb Sc Cr Ni
Th Ba Ta Ce Sr Nd Zr Eu Tb Dy Y Tm Lu V Co

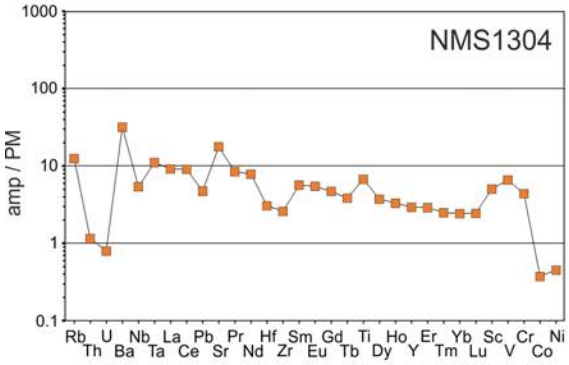
NMS1304
amp / PM
1000
100
10
1
0.1
Rb U Nb La Pb Pr Hf Sm Gd Ti Ho Er Yb Sc Cr Ni
Th Ba Ta Ce Sr Nd Zr Eu Tb Dy Y Tm Lu V Co

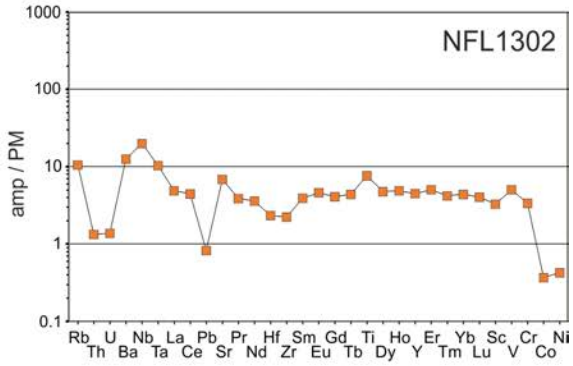
NFL1302
amp / PM
1000
100
10
1
0.1
Rb U Nb La Pb Pr Hf Sm Gd Ti Ho Er Yb Sc Cr Ni
Th Ba Ta Ce Sr Nd Zr Eu Tb Dy Y Tm Lu V Co

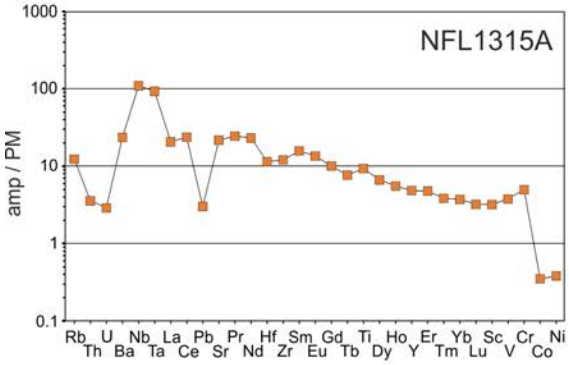
NFL1315A
amp / PM
1000
100
10
1
0.1
Rb U Nb La Pb Pr Hf Sm Gd Ti Ho Er Yb Sc Cr Ni
Th Ba Ta Ce Sr Nd Zr Eu Tb Dy Y Tm Lu V Co

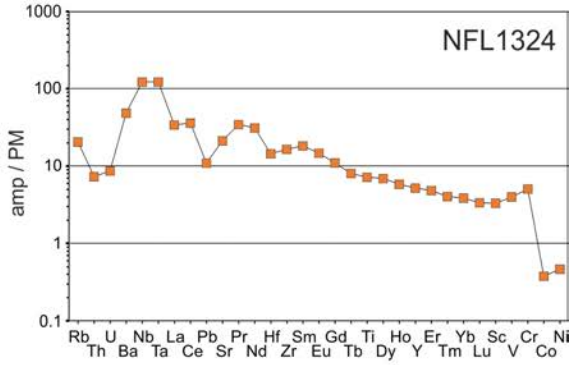
NFL1324
amp / PM
1000
100
10
1
0.1
Rb U Nb La Pb Pr Hf Sm Gd Ti Ho Er Yb Sc Cr Ni
Th Ba Ta Ce Sr Nd Zr Eu Tb Dy Y Tm Lu V Co

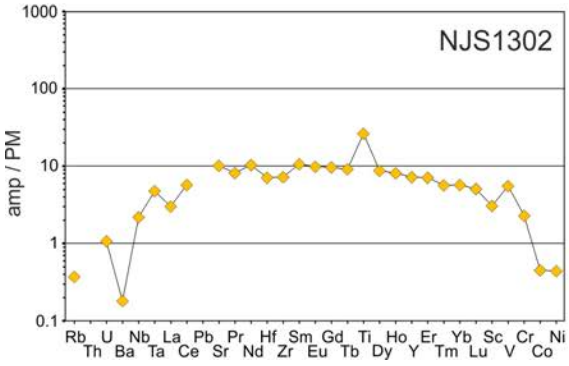
NJS1302
amp / PM
1000
100
10
1
0.1
Rb U Nb La Pb Pr Hf Sm Gd Ti Ho Er Yb Sc Cr Ni
Th Ba Ta Ce Sr Nd Zr Eu Tb Dy Y Tm Lu V Co

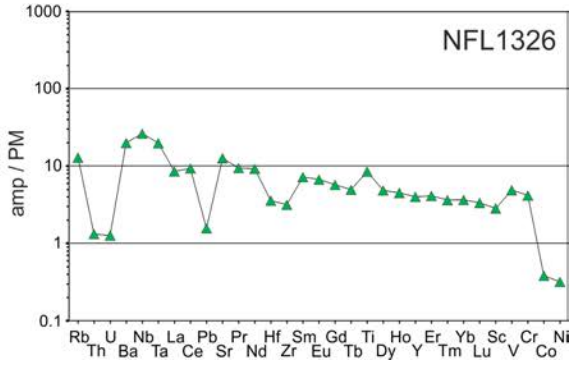
NFL1326
amp / PM
1000
100
10
1
0.1
Rb U Nb La Pb Pr Hf Sm Gd Ti Ho Er Yb Sc Cr Ni
Th Ba Ta Ce Sr Nd Zr Eu Tb Dy Y Tm Lu V Co

Appendix B4 - Calculated Orthopyroxene Rare-Earth Element Contents

Sample	Group	La	Ce	Pr	Nd	Sm	Eu	Gd	Tb	Dy	Ho	Er	Tm	Yb	Lu
NMS1302A	Group IB	0.004	0.015	0.002	0.015	0.006	0.002	0.018	0.004	0.034	0.009	0.033	0.007	0.058	0.013
NMS1304	Group IB	0.011	0.037	0.005	0.029	0.014	0.005	0.047	0.010	0.088	0.023	0.077	0.015	0.13	0.022
NMS1305	Group IB	0.018	0.067	0.010	0.054	0.025	0.010	0.083	0.019	0.19	0.058	0.21	0.041	0.35	0.065
NMS1308	Group IB	0.004	0.017	0.003	0.022	0.016	0.007	0.063	0.015	0.15	0.042	0.16	0.029	0.24	0.042
NMS1310	Group IB	0.004	0.017	0.003	0.022	0.017	0.008	0.073	0.018	0.18	0.054	0.21	0.039	0.33	0.062
NJS1302	Group IIA	0.007	0.044	0.009	0.064	0.040	0.016	0.145	0.032	0.30	0.083	0.30	0.055	0.47	0.080
NJS1304	Group IIA	0.008	0.045	0.009	0.060	0.034	0.013	0.119	0.026	0.24	0.067	0.25	0.047	0.41	0.069
NJS1306	Group IIA	0.008	0.026	0.004	0.028	0.019	0.009	0.082	0.020	0.19	0.058	0.22	0.039	0.35	0.061
NJS1307	Group IA	0.004	0.020	0.004	0.027	0.020	0.009	0.091	0.021	0.22	0.065	0.25	0.046	0.40	0.074
NPY1301	Group IA	0.004	0.018	0.003	0.022	0.017	0.008	0.078	0.019	0.19	0.059	0.23	0.043	0.38	0.067
NPY1310	Group IIA	0.004	0.016	0.003	0.020	0.016	0.007	0.076	0.020	0.19	0.058	0.21	0.040	0.35	0.065
NPY1311	Group IIA	0.004	0.017	0.003	0.020	0.016	0.007	0.076	0.019	0.19	0.057	0.22	0.041	0.36	0.064
NPY1314	Group IIA	0.004	0.017	0.003	0.023	0.019	0.008	0.086	0.022	0.21	0.064	0.24	0.047	0.40	0.068
NFL1302	Group IB	0.008	0.024	0.003	0.018	0.013	0.006	0.061	0.015	0.16	0.049	0.19	0.034	0.32	0.056
NFL1305	Group IB	0.012	0.036	0.004	0.022	0.010	0.004	0.044	0.011	0.11	0.038	0.15	0.028	0.25	0.045
NFL1315A	Group IB	0.028	0.108	0.017	0.096	0.041	0.015	0.111	0.022	0.18	0.045	0.16	0.027	0.22	0.042
NFL1316	Group IB	0.009	0.022	0.003	0.015	0.008	0.003	0.024	0.005	0.043	0.012	0.05	0.009	0.092	0.018
NFL1324	Group IB	0.050	0.183	0.026	0.141	0.053	0.018	0.136	0.025	0.20	0.053	0.18	0.033	0.25	0.043
NFL1326	Group IIB	0.017	0.061	0.009	0.052	0.026	0.011	0.090	0.019	0.17	0.049	0.18	0.034	0.29	0.050
NFL1327	Group IIB	0.024	0.094	0.014	0.081	0.035	0.013	0.090	0.018	0.15	0.040	0.15	0.028	0.25	0.044
NFL1329	Group IB	0.004	0.015	0.003	0.018	0.014	0.007	0.062	0.016	0.16	0.047	0.18	0.032	0.29	0.051
NTB0306	Group IB	0.013	0.024	0.002	0.006	0.003	0.002	0.018	0.005	0.048	0.015	0.06	0.011	0.10	0.019
NTB0307	Group IB	0.003	0.012	0.002	0.012	0.009	0.004	0.043	0.011	0.12	0.036	0.14	0.026	0.24	0.041
NTB1124	Group IA	0.003	0.012	0.002	0.015	0.013	0.006	0.059	0.015	0.15	0.044	0.17	0.031	0.26	0.045
NTB1116	Group IA	0.003	0.014	0.003	0.019	0.014	0.006	0.061	0.015	0.15	0.046	0.16	0.031	0.27	0.044
NTB1122	Group IIB	0.013	0.059	0.010	0.066	0.036	0.014	0.122	0.026	0.24	0.065	0.24	0.043	0.36	0.064
NFK0301	Group IB	0.042	0.161	0.020	0.103	0.038	0.014	0.101	0.020	0.18	0.049	0.18	0.035	0.30	0.054
NFK1123	Group IB	0.050	0.172	0.019	0.084	0.023	0.007	0.062	0.012	0.10	0.029	0.10	0.019	0.16	0.027
NFK1108	Group IIB	0.011	0.042	0.006	0.037	0.019	0.009	0.068	0.016	0.15	0.044	0.17	0.030	0.27	0.049
NFK1115	Group IIB	0.024	0.096	0.014	0.082	0.033	0.012	0.085	0.016	0.13	0.035	0.12	0.024	0.21	0.034
NFR0306	Group IIB	0.013	0.055	0.007	0.043	0.021	0.010	0.075	0.017	0.16	0.046	0.18	0.034	0.29	0.052
NFR0307	Group IIB	0.004	0.017	0.002	0.014	0.007	0.003	0.028	0.007	0.079	0.025	0.10	0.020	0.18	0.033
NFR1109	Group IIB	0.018	0.075	0.010	0.058	0.025	0.010	0.070	0.014	0.11	0.029	0.10	0.020	0.17	0.030
NFR0309	Group IB	0.011	0.031	0.004	0.027	0.019	0.009	0.085	0.022	0.22	0.063	0.24	0.043	0.38	0.070
NFR1107	Group IB	0.006	0.025	0.005	0.031	0.017	0.007	0.064	0.014	0.13	0.038	0.13	0.024	0.19	0.032
NMC1301	Group IB	0.037	0.129	0.016	0.078	0.024	0.009	0.054	0.011	0.092	0.025	0.090	0.017	0.13	0.023
NMC1309	Group IIB	0.008	0.027	0.004	0.020	0.011	0.005	0.048	0.013	0.13	0.039	0.16	0.030	0.27	0.048
NMC1322	Group IB	0.010	0.031	0.004	0.026	0.012	0.005	0.049	0.012	0.13	0.041	0.16	0.031	0.29	0.050
NMC1336A	Group IA	0.002	0.010	0.002	0.021	0.018	0.008	0.086	0.021	0.21	0.062	0.23	0.039	0.33	0.056
NMM1126	Group IA	0.002	0.007	0.001	0.008	0.007	0.003	0.037	0.010	0.11	0.036	0.15	0.028	0.25	0.044
NMM0318	Group IIB	0.023	0.086	0.012	0.067	0.030	0.013	0.098	0.022	0.20	0.059	0.22	0.040	0.35	0.063
NMM1115	Group IB	0.005	0.012	0.002	0.016	0.012	0.006	0.055	0.014	0.13	0.041	0.16	0.030	0.23	0.044
NME1122	Group IB	0.008	0.019	0.002	0.013	0.010	0.004	0.042	0.010	0.094	0.026	0.10	0.019	0.16	0.028
NME0528	Group IB	0.016	0.058	0.008	0.044	0.021	0.008	0.065	0.014	0.13	0.035	0.13	0.023	0.20	0.033
NME1116	Group IA	0.003	0.013	0.002	0.015	0.010	0.005	0.046	0.011	0.12	0.036	0.14	0.027	0.24	0.044
NBN0302A	Group IA	0.004	0.017	0.003	0.022	0.017	0.007	0.069	0.017	0.15	0.043	0.16	0.030	0.28	0.046
NBN0305	Group IB	0.006	0.019	0.003	0.019	0.012	0.004	0.039	0.009	0.076	0.021	0.082	0.015	0.13	0.023
NBN0311	Group IA	0.004	0.017	0.003	0.020	0.015	0.007	0.069	0.018	0.17	0.048	0.19	0.035	0.30	0.055
NBN0316	Group IA	0.002	0.012	0.002	0.015	0.012	0.005	0.050	0.013	0.12	0.033	0.13	0.022	0.19	0.035
NBN0319	Group IA	0.002	0.012	0.002	0.015	0.011	0.005	0.045	0.010	0.10	0.025	0.11	0.019	0.17	0.031
NBN0321	Group IA	0.003	0.016	0.003	0.021	0.019	0.009	0.090	0.021	0.19	0.052	0.19	0.033	0.27	0.049

Appendix C: Crystal Preferred Orientation - Pole Figures

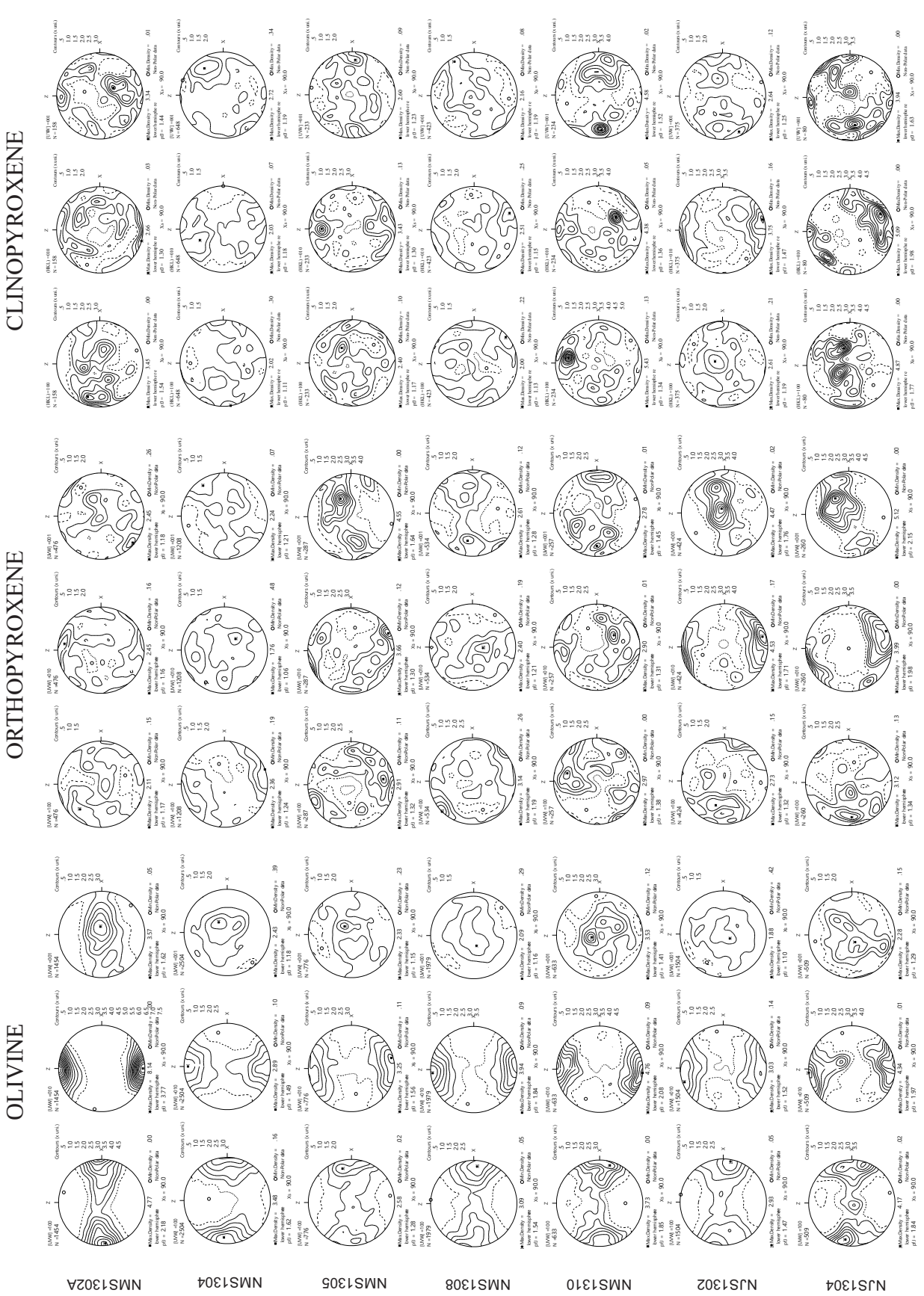
OLIVINE
ORTHOPYROXENE
CLINOPYROXENE
NMS1302A
NMS1304
NMS1305
NMS1308
NMS1310
NJS1302
NJS1304

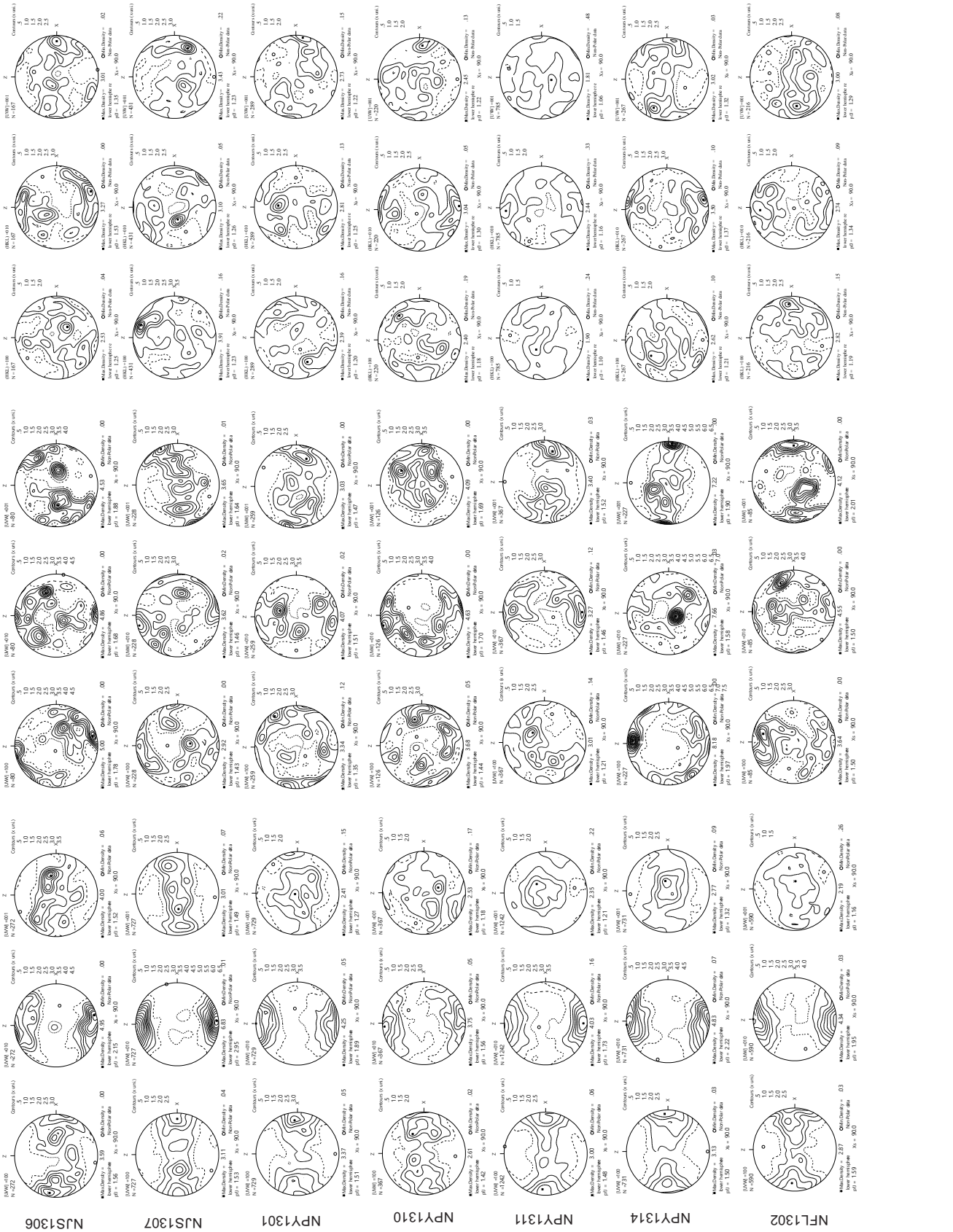
NJS1306
NJS1307
NPY1301
NPY1310
NPY1311
NPY1314
NFL1302

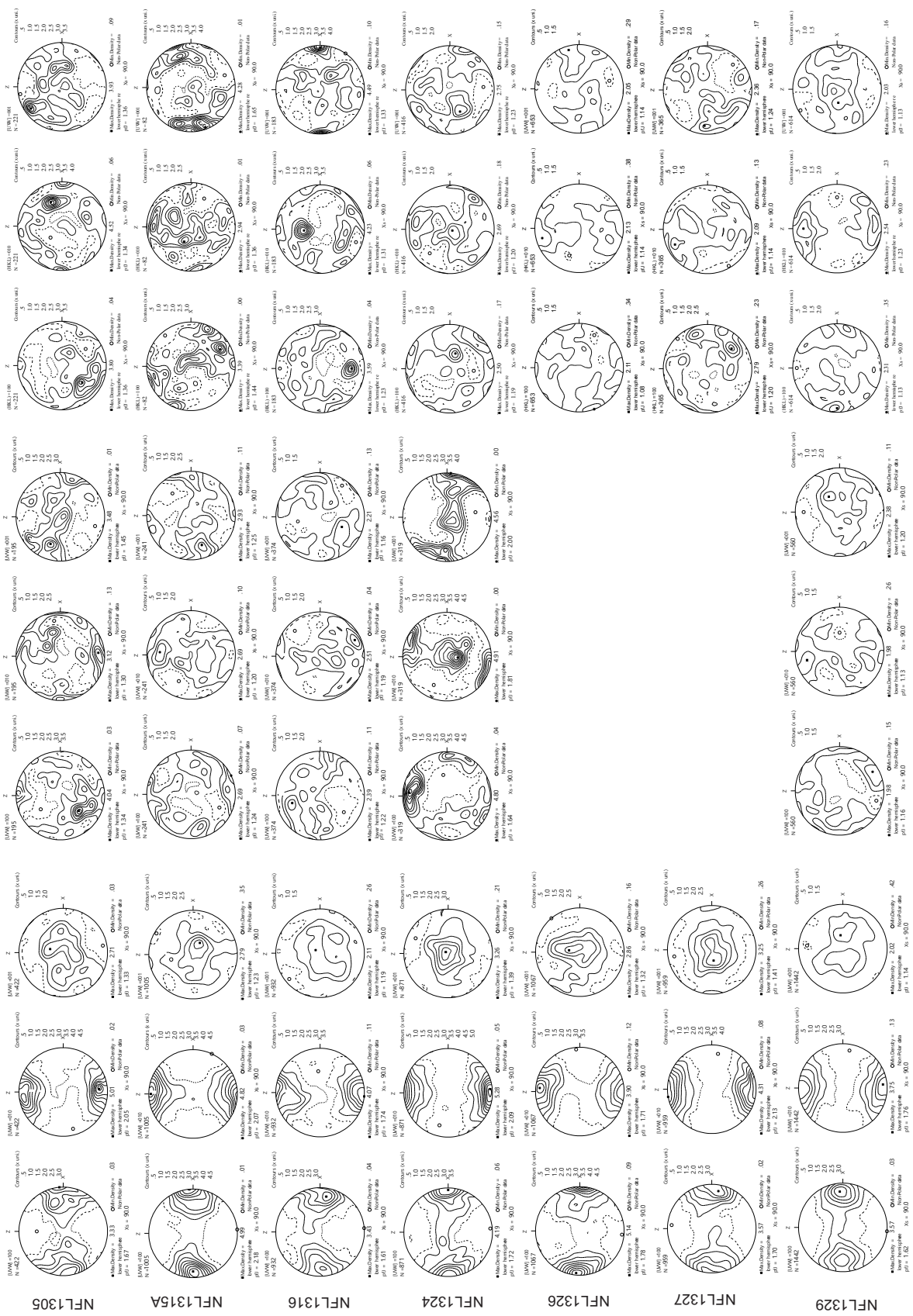
NFL1305
NFL1315A
NFL1316
NFL1324
NFL1326
NFL1327
NFL1329

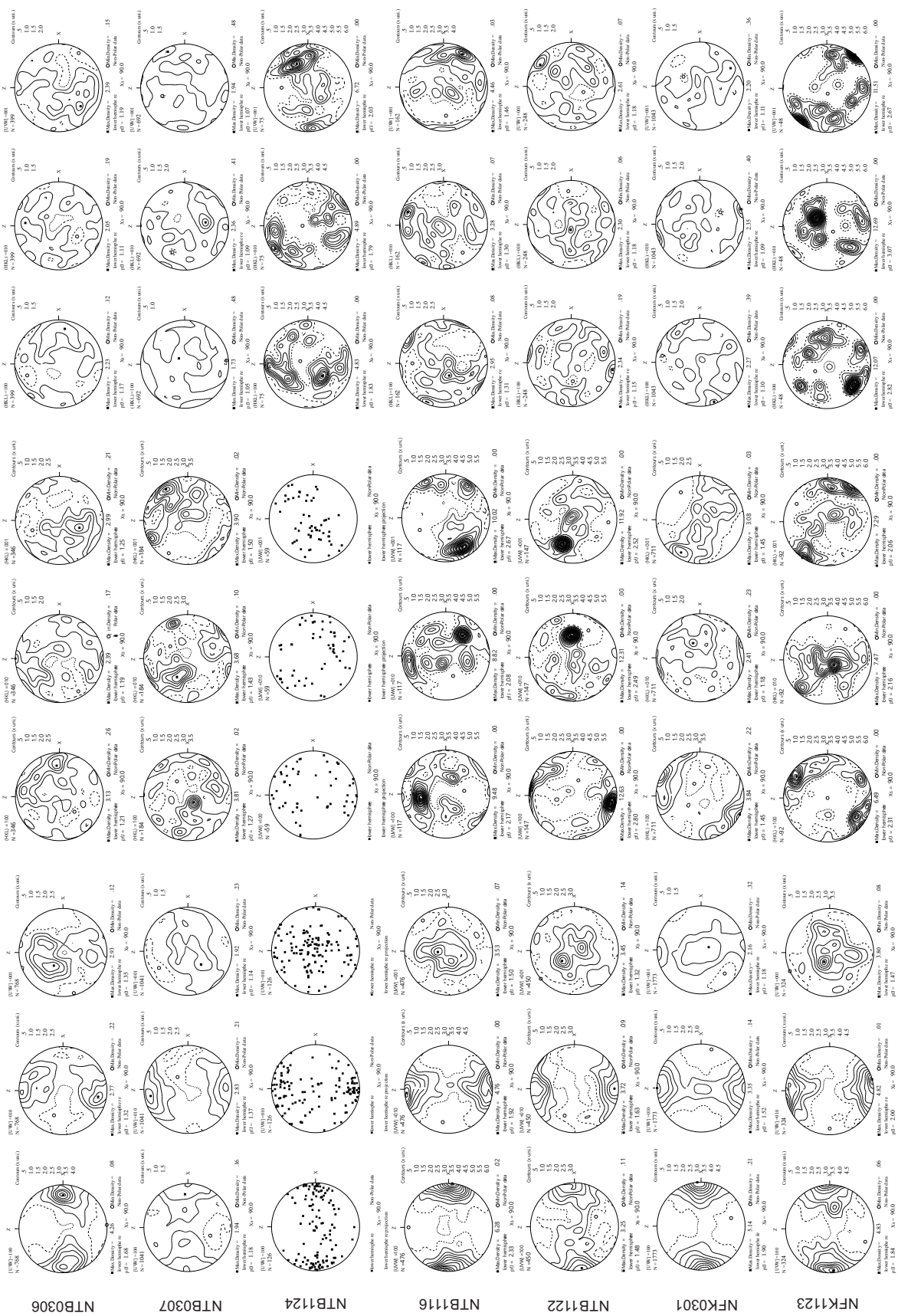
NTB0306
NTB0307
NTB1124
NTB1116
NTB1122
NFK0301
NFK1123

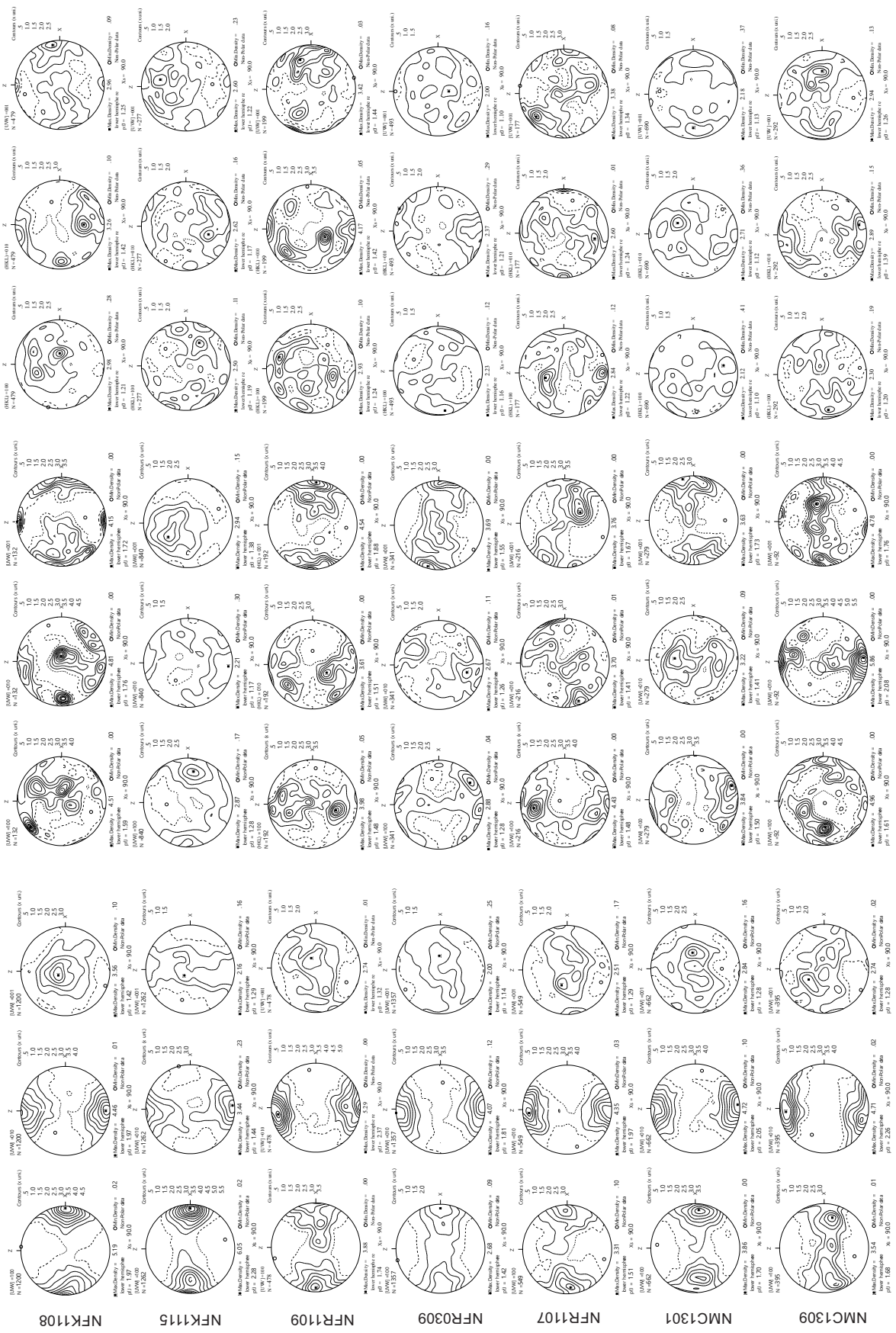
NFK1108
NFK1115
NFR1109
NFR0309
NFR1107
NMC1301
NMC1309

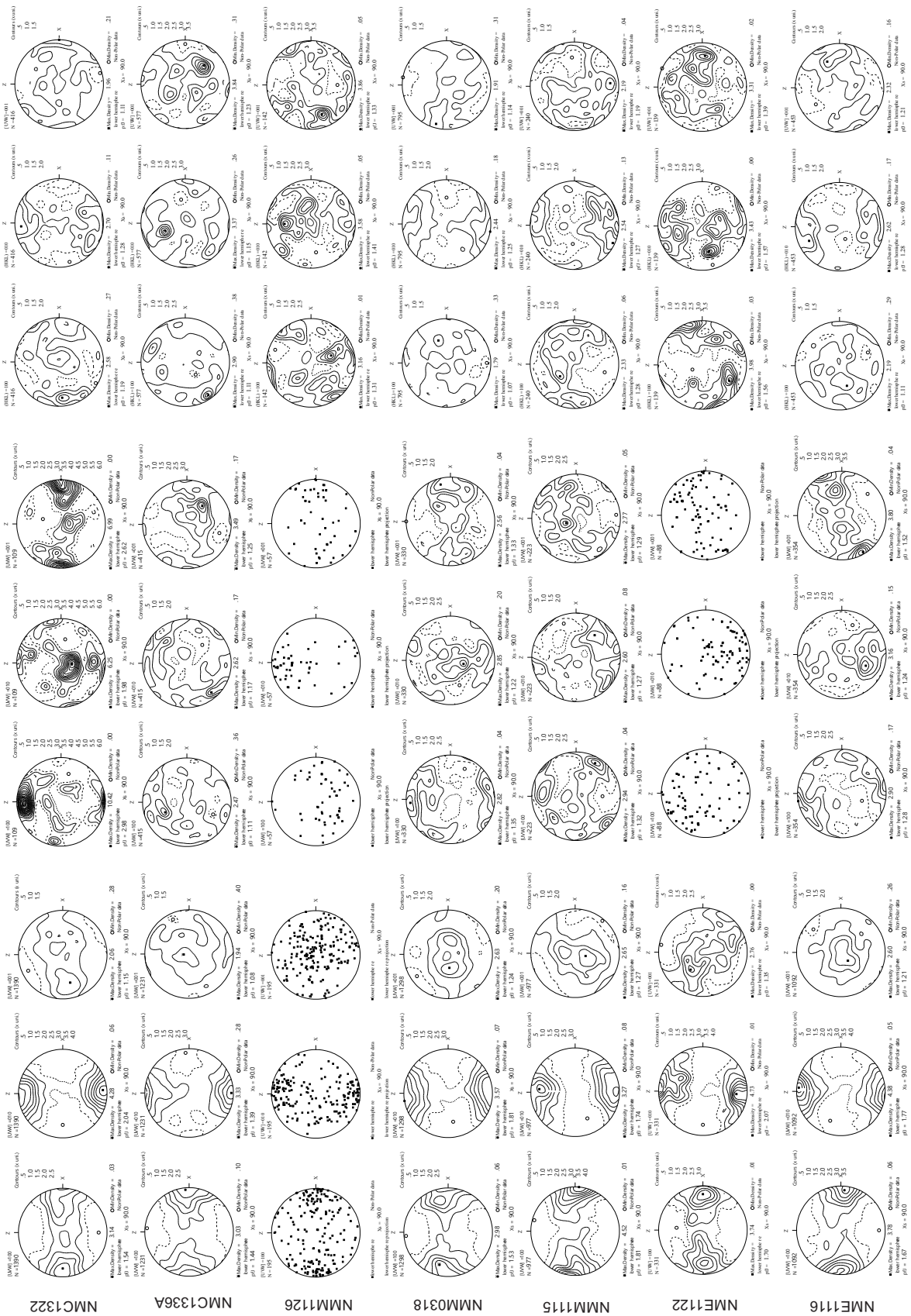
NMC1322
NMC1336A
NMM1126
NMM0318
NMM1115
NME1122
NME1116

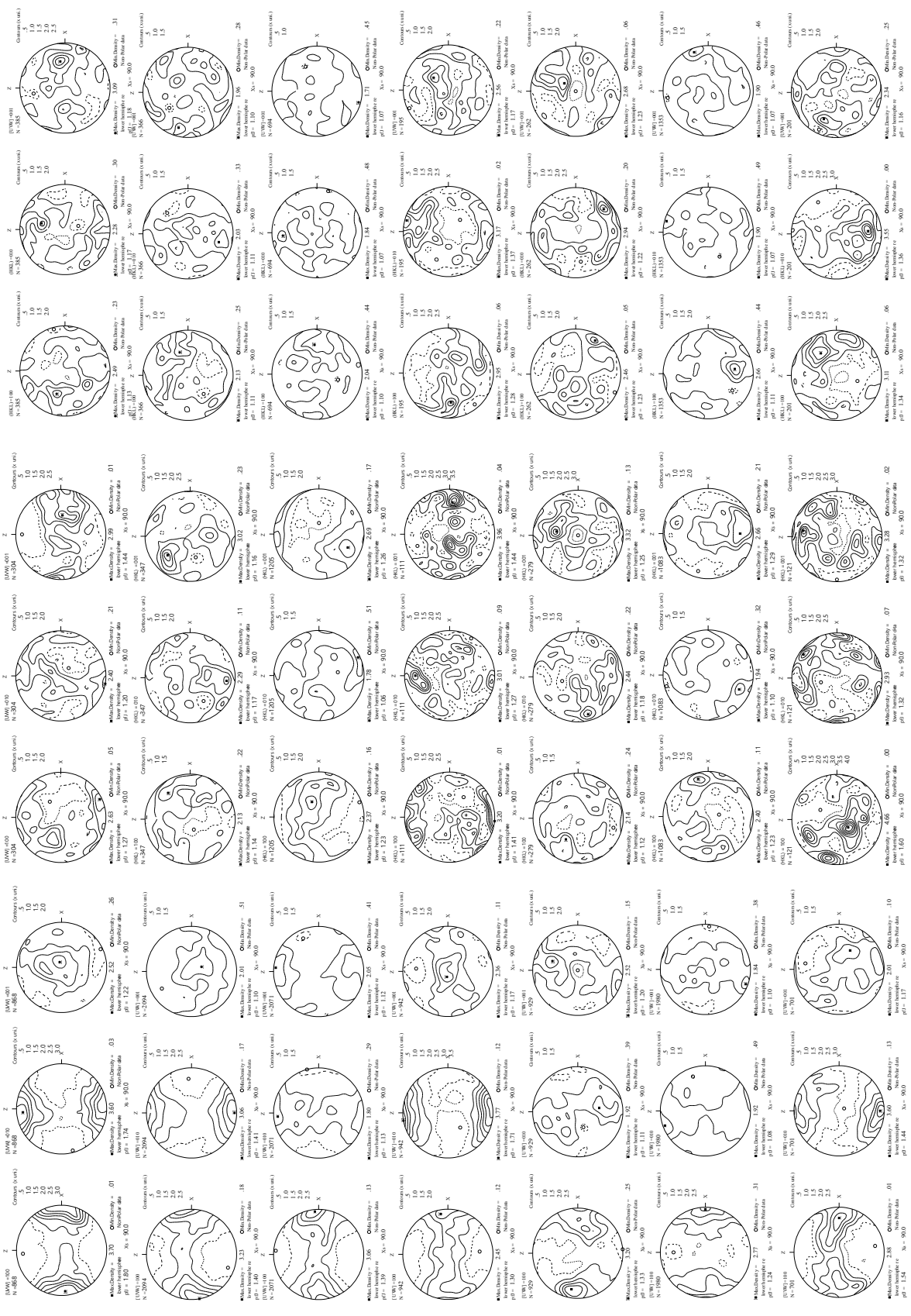
NME0528
NBN0302A
NBN0305
NBN0311
NBN0316
NBN0319
NBN0321

Appendix D: Publication: Liptai et al., 2017. Journal of Petrology, 58, 1107-1144. doi:10.1093/petrology/egx048

Pages A136-A173 of this thesis have been removed as they contain published material under copyright. Removed contents published as:

Nóra Liptai, Levente Patkó, István J. Kovács, Károly Hidas, Zsanett Pintér, Teresa Jeffries, Zoltán Zajacz, Suzanne Y. O'Reilly, William L. Griffin, Norman J. Pearson, Csaba Szabó (2017) Multiple Metasomatism beneath the Nógrád–Gömör Volcanic Field (Northern Pannonian Basin) Revealed by Upper Mantle Peridotite Xenoliths, Journal of Petrology, Vol. 58, Iss. 6, pp. 1107–1144.

https://doi.org/10.1093/petrology/egx048